



University of HUDDERSFIELD

University of Huddersfield Repository

Otamonga, Jean Paul

Stopped-Flow Kinetic Investigation of Manganese-based Chemiluminescence Oxidation Reactions

Original Citation

Otamonga, Jean Paul (2013) Stopped-Flow Kinetic Investigation of Manganese-based Chemiluminescence Oxidation Reactions. Doctoral thesis, University of Huddersfield.

This version is available at <http://eprints.hud.ac.uk/id/eprint/18054/>

The University Repository is a digital collection of the research output of the University, available on Open Access. Copyright and Moral Rights for the items on this site are retained by the individual author and/or other copyright owners. Users may access full items free of charge; copies of full text items generally can be reproduced, displayed or performed and given to third parties in any format or medium for personal research or study, educational or not-for-profit purposes without prior permission or charge, provided:

- The authors, title and full bibliographic details is credited in any copy;
- A hyperlink and/or URL is included for the original metadata page; and
- The content is not changed in any way.

For more information, including our policy and submission procedure, please contact the Repository Team at: E.mailbox@hud.ac.uk.

<http://eprints.hud.ac.uk/>

Stopped-Flow Kinetic Investigation of Manganese-based Chemiluminescence Oxidation Reactions

By

Jean Paul Otamonga BSc. MSc. PGCE



A thesis submitted to the University of Huddersfield in fulfilment of the
thesis requirement for the award of Doctor of Philosophy in Chemistry

Department of Chemical and Biological Sciences
School of Applied Sciences
The University of Huddersfield
Queensgate
Huddersfield
West Yorkshire
HD1 3DH
England (UK)

*** 21st May 2013 ***

Acknowledgments

It takes the help of many people involved to carry out an original and approved research programme, which is documented and published by producing a thesis. I would like to express my deep appreciation and sincere gratitude to people who helped me in this process, including:

Dr Roger Jewsbury, advisor and supervisor, who generously and patiently guided and provided me with his expertise, professional and personal support throughout this work,

all academic and technical staff of the Department of Chemical and Biological Sciences for their help during this work and fellow graduate students for their friendship and assistance,

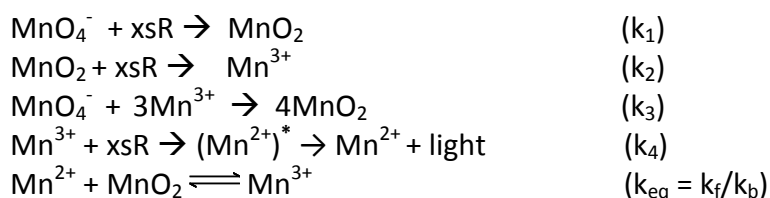
the University of Huddersfield and the Department of Chemical and Biological Sciences for funding this research.

Finally, I would like to express my special appreciation to my dear wife Jacky T Muamba and my lovely sons Jude, Enoch, Jean Marc, and Roger Otamonga for sharing it all with me and for their love and encouragement. Words are not enough.

Abstract

In order to better understand the mechanism of solution manganese-based chemiluminescence, the kinetics of a number of chemiluminescent oxidations by manganese species were studied using stopped-flow spectrophotometry. Both the kinetics of the decay of the oxidant and the chemiluminescence emission were followed for oxidations by permanganate, manganese dioxide sol and $\text{Mn}^{3+}_{(\text{aq})}$ of a range of organic compounds.

The most detailed studies were carried out on the oxidation of the relatively simple compounds including glyoxylic acid and glyoxal under pseudo first order conditions and an acidic medium at 25°C. For permanganate under these conditions, the decay is sigmoidal consistent with autocatalysis and for manganese dioxide sol and Mn^{3+} pseudo first order. Simple mechanisms are suggested and compared with the experimental kinetic data. For permanganate CL system, the following chemical kinetic model was considered:



The feedback mechanism in this model does not involve Mn^{2+} directly but Mn^{3+} . The accuracy of the kinetics model predictions for manganese-based chemiluminescence systems were tested and validated against a variety of experimental data sets and in varying the reaction conditions for permanganate oxidation of glyoxylic acid and glyoxal and good agreement was found. Under conditions of a large excess of glyoxal over permanganate concentration, the rate constants are approximately estimated as follows: $k_1=0.02 \text{ s}^{-1}$; $k_2=4.78 \text{ s}^{-1}$; $k_3=7.20 \text{ s}^{-1}$; $k_4=1.98 \text{ s}^{-1}$; $k_f=9.24 \times 10^{-4} \text{ s}^{-1}$ and $k_b=9.52 \times 10^{-4} \text{ s}^{-1}$.

These are then applied to the chemiluminescence in the presence of known enhancers such as aqueous formaldehyde and added $\text{Mn}^{2+}_{(\text{aq})}$ confirming that the enhancement is a kinetic phenomenon, consistent with faster formation of $\text{Mn}^{3+}_{(\text{aq})}$ intermediate which has been shown to be involved in the chemiluminescence process. For permanganate oxidation of glyoxal, the addition of formaldehyde and Mn^{2+} showed simple pseudo first order decay with no induction period. Also, it increases the reaction rates of the relevant steps and of the chemiluminescence signal intensity in predictable manner, and both predicted profiles for permanganate consumption and chemiluminescence emission agreed with measured profiles. The rate constants in the presence of 0.80M formaldehyde are determined as follows: $k_1=0.25 \text{ s}^{-1}$; $k_2=5.66 \text{ s}^{-1}$; $k_3=17.3 \text{ s}^{-1}$; $k_4=7.32 \text{ s}^{-1}$; $k_f=1.10 \times 10^{-4} \text{ s}^{-1}$ and $k_b=2.96 \times 10^{-4} \text{ s}^{-1}$. With the addition of 0.20M Mn^{2+} , the rate constants are estimated as follows: $k_1=0.26 \text{ s}^{-1}$; $k_2=34.5 \text{ s}^{-1}$; $k_3=17.0 \text{ s}^{-1}$; $k_4=7.93 \text{ s}^{-1}$; $k_f=2.60 \text{ s}^{-1}$ and $k_b=1.16 \text{ s}^{-1}$.

The model has been applied to other reductants including oxalic acid, malic acid, metronidazole, tetracycline and pyridoxine and enhancers such as glyoxal, pyrogallol and gallic acid. The application of these results to the optimisation of known and potential analytical methods is discussed.

Table of Contents

Acknowledgements	ii
Abstract	iii
Table of Contents	iv
Chapter 1 Introduction to the research	1
1.1 Background and Significance of this study	1
1.2 Research Objectives	4
1.3 Thesis Organization	4
Chapter 2 Introduction to the analytical methods	5
2.1 Chemiluminescence	5
2.1.1 Historical Overview	5
2.1.2 Types of Luminescence	14
2.1.2.1 Luminescence associated with heating	14
2.1.2.2 Luminescence associated with prior irradiation	14
2.1.2.3 Luminescence associated with electrical phenomena	14
2.1.2.4 Luminescence associated with structural rearrangement in solid	15
2.1.2.5 Luminescence associated with chemical reactions	15
2.1.3 Photoluminescence	15
2.1.4 Generation of chemiluminescence	17
2.1.4.1 Gas-phase Chemiluminescence reactions	21
2.1.4.2 Liquid-Phase Chemiluminescence – Biochemiluminescence Reaction	22
2.1.4.3 Liquid-Phase Chemiluminescence – Chemiluminescence Reactions	23
2.1.4.4 Liquid-Phase Chemiluminescence – Electrochemiluminescence Reactions	25
2.1.4.4.1 Annihilation ECL	26
2.1.4.4.2 Oxidative-reduction mechanism	27
2.1.4.4.3 Reductive-oxidation mechanism	27
2.2 Flow Analysis (FA)	28
2.2.1 Flow Injection Analysis (FIA)	29
2.2.2 Sequential Injection Analysis (SIA)	32
2.2.3 Bead Injection Analysis (BIA)	34
2.2.4 Advantages of Flow-based analysis	35
2.2.5 Components of a Flow Injection Analysis System	36
2.2.5.1 Pumps	36
2.2.5.2 Injection valve	37
2.2.5.3 Manifold design	38
2.2.5.4 Detection Systems	39
2.2.5.4.1 Flow Injection Analysis and Chemiluminescence Detection	41
2.2.5.4.2 Photomultiplier Tube (PMT)	42
2.2.5.4.3 Photodiode Systems	44
2.2.5.4.4 Charge-Coupled Devices (CCD)	46

2.2.6 Miniaturization through lab-on-a-chip (LOC)	47
2.3 Stopped-flow Technique	49
2.3.1 Principle of Stopped-flow technique	49
2.3.2 Application of Stopped-flow technique in Spectrophotometry	51
2.3.3 Application of Stopped-flow technique to Chemiluminescence	53
2.4 Permanganate (MnO_4^-) Oxidations	54
2.4.1 Potassium Permanganate Chemistry	55
2.4.2 Potassium Permanganate Applications	67
2.4.3 Cautions	68
2.4.4 Chemiluminescence from manganese-based oxidation reactions	68
2.4.4.1 Chemiluminescence from potassium permanganate	69
2.4.4.2 Chemiluminescence from manganese(IV)	70
2.4.4.3 Chemiluminescence from manganese(III)	73
Chapter 3 Materials and Methods	102
3.1 Chemicals	102
3.2 Preparation of solutions	103
3.2.1 Potassium permanganate solutions	103
3.2.2 Manganese (II) sulphate	104
3.2.3 Manganese (III) reagent	104
3.2.4 Manganese (IV) reagent	104
3.3 Instrumentation and Equipment	105
3.3.1 Volumetric equipment	105
3.3.2 Weighing	105
3.3.3 pH measurement	105
3.3.4 UV-visible spectrophotometry	106
3.3.5 Stopped flow measurements	106
3.3.6 Validation of stopped-flow instrumentation	108
3.3.6.1 Reaction of acid hydrolysis of tri (ethylamine) nickel (II) ion	108
3.3.6.2 Determination of the dead-time	110
3.4 Experimental procedures	113
3.4.1 Stopped-flow absorbance kinetics	113
3.4.2 Stopped-flow chemiluminescence kinetics	114
3.5 Significance of the following experiments	115
Chapter 4 Kinetics Study of the Chemiluminescence Reactions in the Manganese-based Oxidation of Various Organic Substances.	117
4.1 Introduction	117
4.2 Chemiluminescence in glyoxal oxidation reactions	118
4.2.1 Permanganate oxidation of glyoxal	119
4.2.1.1 Effect of glyoxal concentration	122
4.2.1.2 Effect of MnO_4^- concentration	124

4.2.1.3 Effect of manganese(II)	125
4.2.1.4 Effect of formaldehyde as enhancer	128
4.2.2 Manganese(III) oxidation of glyoxal	129
4.2.3 Manganese(IV) oxidation of glyoxal	134
4.2.4 Dichromate oxidation of glyoxal	141
4.3 Glyoxylic acid chemiluminescence oxidation reactions	142
4.3.1 Permanganate oxidation of glyoxylic acid	142
4.3.1.1 Effect of glyoxylic acid concentration	143
4.3.1.2 Effect of permanganate concentration	144
4.3.2 Manganese(III) oxidation of glyoxylic acid	145
4.3.2.1 Effect of Mn(III) concentration	145
4.3.2.2 Effect of glyoxylic acid concentration	147
4.3.3 Manganese(IV) oxidation of glyoxylic acid	147
4.3.3.1 Effect of Mn(IV) concentration	148
4.3.3.2 Effect of glyoxylic acid concentration	149
4.4 Oxalic acid chemiluminescence oxidation reactions	150
4.4.1 Permanganate oxidation of oxalic acid	150
4.4.2 Manganese(III) oxidation of oxalic acid	151
4.4.3 Manganese(IV) oxidation of oxalic acid	152
4.5 Malic acid chemiluminescence oxidation reactions	154
4.5.1 Permanganate oxidation of malic acid	154
4.5.1.1 Effect of malic acid concentration	154
4.5.1.2 Influence of formaldehyde on malic acid chemiluminescence	155
4.5.1.3 Influence of added Mn(II) on malic acid chemiluminescence	157
4.5.1.4 Influence of glyoxal on malic acid chemiluminescence	157
4.5.2 Manganese(III) oxidation of malic acid	159
4.5.3 Manganese(IV) oxidation of malic acid	162
4.6 Metronidazole chemiluminescence oxidation reactions	163
4.6.1 Permanganate oxidation reaction of Metronidazole	163
4.6.1.1 Effect of formaldehyde concentration on the Chemiluminescence	164
4.6.1.2 Influence of glyoxal concentration on the Chemiluminescence	165
4.6.1.3 Influence of pyrogallol concentration on the Chemiluminescence	167
4.6.1.4 Influence of gallic acid concentration on the Chemiluminescence	169
4.6.2 Manganese(III) oxidation of metronidazole	171
4.6.3 Manganese(IV) oxidation of metronidazole	172
4.7 Tetracycline chemiluminescence oxidation reactions	173
4.7.1 Permanganate oxidation of tetracycline	174
4.7.1.1 Effect of manganese(II) as catalyst	175
4.7.1.2 Effect of formaldehyde as enhancer	176
4.7.1.3 Effect of glyoxal as enhancer	177
4.7.2 Manganese(IV) oxidation of tetracycline	178

4.7.3 Manganese(III) oxidation of tetracycline	180
4.8 Pyridoxine chemiluminescence oxidation reactions	181
4.8.1 Permanganate oxidation of pyridoxine	181
4.8.1.1 Effect of manganese(II)	183
4.8.1.2 Effect of formaldehyde	184
4.8.2 Manganese(III) oxidation of pyridoxine	185
4.8.3 Manganese(IV) oxidation of pyridoxine	186
4.9 Summary	187
Chapter 5 Modelling and Mechanism for Mn-based CL Reactions	189
5.1 Introduction	189
5.2 Modelling Permanganate Chemiluminescence System	191
5.2.1 Rate constants dependence on [glyoxal] and [glyoxylic acid]	194
5.2.2 Rate constants dependence on formaldehyde concentration	197
5.2.3 Rate constants dependence on manganese(II) concentration	205
5.2.4 Complex (alternative) mechanism	208
5.2.4.1 Rate Constant Dependence on Glyoxylic Acid Concentration	210
5.2.4.2 Rate Constant Dependence on Glyoxal Concentration	213
5.2.4.3 Rate Constant Dependence on Formaldehyde Concentration	216
5.2.4.4 Rate Constant Dependence on Manganese(II) Concentration	222
5.3 Modelling Mn(IV) Chemiluminescence System	229
5.4 Modelling the Mn(III) Chemiluminescence System	232
5.5 Reaction Mechanism for Manganese-based CL System	236
Chapter 6 Conclusions	243
Bibliographic References	245

Chapter 1

Introduction to the research

1.1 Background and Significance of this study

Chemiluminescence (CL) is light emission produced through a chemical reaction exciting a compound to a high-energy state which then rapidly loses its excess energy to produce photon usually of visible light¹⁻¹⁰, although chemiluminescence in IR region is also analytically important. Chemiluminescence reactions are encountered in a number of biological systems, where the process is often termed bioluminescence. The number of distinct chemical reactions that produce chemiluminescence is small, thus limiting the procedure to a relatively small number of species. Nevertheless, some of the compounds that do react to give chemiluminescence are important components of the environment⁷.

Chemiluminescence has found widespread use in analytical chemistry^{11, 12} and biochemistry^{11, 13}. Examples include widely used chemiluminescent immunoassay for a peroxidase label involving a mixture of luminol, hydrogen peroxide, and p-iodophenol¹⁴ and the routine industrial monitoring of morphine in process streams by chemiluminescent permanganate oxidation¹⁵. The CL technique is now well established as a powerful analytical technique for its inherent potential high levels of sensitivity with minimum background noise, selectivity, and wide linear detection range with inexpensive instrumentation^{3, 16-19}.

Advances in molecular biology and an increased need for more sensitive assays have prompted the development of novel chemiluminescence systems for a wide variety of applications in clinical science²⁰, the pharmaceutical industry^{6, 7, 15, 21-53}, agricultural and environmental monitoring⁵⁴⁻⁸¹, food technology⁸²⁻⁹⁹, and forensic investigations^{6, 7, 100}. This is true even though chemiluminescence is not as widely applicable as absorption, emission, or even fluorescence methods of detection since so few molecules undergo native CL with common reagents such as potassium permanganate^{6, 7}.

To promote the development of the chemiluminescence technique, it is essential to discover new chemiluminescent reactions, mainly, direct chemiluminescent reactions^{9, 10, 85, 101-107} in order to increase the number of analytes accessible through the technique. Most analytically useful chemiluminescent reactions have been discovered by trial and error or are modifications of existing reactions^{9, 10}. The latter often make use of additional reagents described as "enhancers or sensitizers"^{21, 24, 36, 38, 49, 51, 67, 68, 70, 89, 100, 108-141}.

A previous work undertaken by Abdel-Mageed¹⁰ has shown for the first time that for manganese oxidations "reaction kinetics can be used to explain the effect of enhancers". This is important, as it enables a more systematic approach to be taken to the phenomenon of solution chemiluminescence.

Therefore, further knowledge and understanding of the kinetics and reaction mechanisms should allow the prediction of analytically useful compounds or combinations of compounds. The results of these studies are expected to lead to suggestions for new analytical methods.

Kinetic data should enable the comparison of chemiluminescence characteristics with the kinetic laws of the chemical reaction in order to establish quantitative connections between kinetics of the reaction and chemiluminescence generated.

Efforts in this study are concentrated on the liquid-phase chemiluminescence in organic substance oxidations using manganese species as oxidizing agents. Manganese oxidations have been chosen for this study because of (i) the range of reductants for which chemiluminescence has been reported, (ii) the potential choice of three oxidants MnO_4^- , MnO_2 and Mn^{3+} , and (iii) the diversity of reported enhancers, such as low molecular weight aldehydes and metal ions.

There are, however, a number of disadvantages and difficulties in using manganese oxidants, of which by far the most popular is permanganate. They include (i) the potential involvement of five oxidation states of manganese, (ii) the lack of any consensus on the mechanism of these oxidations, despite the use of permanganate for around 150 years and (iii) the possibility of several reductant species that are difficult to identify.

Manganese-based chemiluminescence systems refer to reactions between manganese-based oxidants, such as permanganate(Mn(VII)), manganese(IV) and manganese(III) ions with a variety of organic compounds in acidic solution to generate light.

Since the chemiluminescence process is time dependent, optimizing manganese-based chemiluminescence systems to improve its analytical sensitivity relies on an adequate model for the dependence of the reaction kinetics and chemiluminescence on each of the reagents.

Of manganese-based oxidants, acidic potassium permanganate has been most widely used in analytical chemistry^{6, 7}. Although the application of acidic permanganate chemiluminescent reaction is widespread for its sensitive detection and determination of wide variety of substances (such as pharmaceuticals, illicit drugs, biomolecules, antioxidants, pollutants, etc.), the details of the reaction mechanism, including the number and identity of the intermediate(s) responsible for the chemiluminescence signal production are poorly understood^{7, 142, 143}.

Again the in-depth understanding of the reaction mechanism may improve the chemiluminescence response and the limits of detection and lead to the development of new analytical chemiluminescence systems.

Moreover, work on sensitized CL reactions has shown that the use of enhancers (or sensitizers), such as low molecular weight aldehydes^{68, 88, 119-122, 124-126, 144} and metal ions^{77, 110, 125, 126, 145-148}, in MnO_4^- CL, to increase the signal intensity from the analyte, has been reported, but the regulatory mechanism of enhancement has, as yet, not been completely elucidated.

As mentioned above, the mechanism of enhancement by formaldehyde and related compounds has, as yet, not been fully clarified⁷. In a number of papers, the influence of formaldehyde as enhancer on CL has been explained by their capacity to react with permanganate to form excited carbon dioxide^{7, 120, 149, 150}, singlet oxygen^{7, 131, 150, 151} or unknown intermediates^{7, 121, 124} that either emit light or transfer energy to other emitters. However, the experimental evidence for a Mn(II) emitter^{7, 112, 151, 152} and the identical spectral distribution in the presence and absence of formaldehyde^{7, 151, 153} do not support these pathways¹¹⁹. The first hypothesis of the existence of a quantitative link between the activity of enhancers and their capacity for increasing CL response was put forward by Tsaplev^{7, 154}. He proposed that Mn(II) inhibits a direct non-irradiative reaction, in favour of the light-producing pathway via manganese(III)^{7, 154}. Zhu et al. found that the time required to reach the maximum emission intensity from the oxidation of butane-2,3-dione with permanganate was considerably reduced by the addition of Mn(II), which they exploited to quantify the metal ion^{7, 155}.

Others have suggested that these enhancers increase the rate of analyte oxidation^{7, 119, 130}. For instance, Abdel-Mageed¹⁰ work suggested that these enhancers increase the rate of analyte oxidation and chemiluminescence, and showed that for manganese-based chemiluminescence oxidations, reaction kinetics can be used to explain the effect of enhancers. However, no concrete mechanisms of the effect of enhancers on the CL of permanganate have been confirmed, since up to the present time the reason why a change in the concentration of enhancers affects the intensity of the CL of permanganate is unknown.

This study aimed to address the following general questions:

- What data do we need to design a chemiluminescence system?
- What is the mechanism controlling a chemiluminescence reaction and the enhancement of chemiluminescence signal responses?
- Is there any strategy for improving the limit of detection (LoD)?
- Can new chemiluminescence assays be designed?

To address the mechanisms of manganese-based chemiluminescence reactions and of the CL enhancement, the study of the kinetics of manganese-based CL reactions using the stopped-flow technique was considered, to determine the dependence of the CL intensity on the concentration of enhancer, organic substrate and oxidant, and the connection between CL and the mechanism of the reaction and the action of various enhancers.

We hope to conclude with a concrete kinetic mechanism for the action of enhancers on manganese-based chemiluminescence system.

To simplify the kinetic study, where possible, experiments were carried out under pseudo-first order reaction conditions with either organic substrate or oxidant in large excess, as this forms the basis of chemiluminescence analytical methods for the detection of reactants.

The chemiluminescence step of the reaction will be determined by comparing the time courses of the resulting chemiluminescence emission with changes in the absorbance spectrum for the oxidants.

1.2 Research Objectives

To summarize the following specific objectives were defined:

- Measure kinetics of chemiluminescence output and oxidizing reagent consumption of oxidation reactions of a variety target molecules.
- Carry out extensive kinetic studies to determine the first and second-order rate constants for the oxidation of selected simple model system.
- Identify and quantify the controlling factors related to oxidant consumption that affect the rate constants of the reaction and chemiluminescence response.
- Based on the data collected, identify mechanisms of CL reaction and mechanism of enhancement for selected simple model chemiluminescent systems.

1.3 Thesis Organization

The overall structure of the study takes the form of six themed chapters, including this introductory chapter.

Chapter 2 presents a review of the chemiluminescence technique as a mode of detection, flow analysis and manganese compound oxidants as chemiluminescent reagents.

Chapter 3 describes the handling, preparation of materials, methods, instrumentation and equipment used in this research.

Chapter 4 addresses research activities dealing with the study and assessment of the rates of chemiluminescent oxidation of a range of organic compounds of analytical interest.

Chapter 5 attempts to develop a general model for manganese CL emission using the kinetic data collected and mechanisms developed from the previous chapter.

Chapter 6, finally, provides a summary and conclusions and significant contributions from this research.

Chapter 2

Introduction to the analytical method

Chemiluminescence analytical method is a variation of the standard photoluminescent spectroscopy techniques. A substrate is converted to a reaction product that emits photons of light instead of developing a heat or visible color. Luminescence is described as the emission of light from a substance as it returns from an electronically excited state to ground state. Chemiluminescence is the principle of light generation or glow produced in certain chemical reactions without external energy input from sources such as light or heat. The chemiluminescent substance is excited by the oxidation and catalysis forming intermediates. When the excited intermediates return back to their stable ground state, a photon is released, which is detected using a suitable spectroscopic probe. The detector yields a calibration curve to quantify the target analyte.

Since the resulting chemiluminescence emission, which is the rate of emission of photons/sec from a chemical reaction, is the product of the oxidation turnover of analyte, the intensity of the chemiluminescence emission is determined by the kinetics of the oxidation reaction, and the light output is directly proportional to the concentration of the limiting reactant in the system, catalyst, or additives to enhance the native chemiluminescence signal intensity. This forms the basis of chemiluminescence analytical methods for the detection of reactants, catalyst, or any additives.

The applications of chemiluminescence techniques, as a mode of detection, are widespread in analytical chemistry and biochemistry for its simplicity of detection, high sensitivity with minimum background signal, linearity over a broad concentration range, selectivity, unexpensive instrumentation with moderate running costs. The simple requirements of chemiluminescent methods make them robust and easy to use for determination of trace ultra-trace levels of environment pollutants, industrial chemicals and clinical assays. However, the chemiluminescence techniques provide limited structural information and limited number of chemiluminescent reactions, thus limited samples throughput.

The purpose of this chapter is to present an overview of the chemiluminescence analytical method, permanganate chemiluminescence and the reaction conditions and mechanisms that are involved in the oxidation of organic compounds with manganese-based oxidants.

2.1 Chemiluminescence

2.1.1 Historical Overview^{2, 6, 9}

The first true luminescence observed was bioluminescence in luminous organisms including insects, fungi and bacteria on rotting wood and flesh.

Electroluminescence was observed as the aurora borealis and ignis lambens, a silent electric discharge observed under some atmospheric conditions. The earliest written reference to luminescent animals is in Chinese poetry of around 1500BC and there are other references in ancient writings from Japan and India.

The Greek philosopher Aristotle (384-322BC) gave the first recorded detailed description of luminescent animals and other luminescence phenomena in *De Anima*. This discussed the differences between luminescence and items which have colour and are seen in daylight. In the first century AD Caius Plinius Secundus, Pliny the Elder, described luminous glow-worms, fungus, lantern fish and jellyfish in *Historia Naturalis*.

During the Middle Ages various authors including St Isidore of Seville, in the 6th century, Rabanus Maurus, archbishop of Mainz in the 9th century and Hildegard of Bingen in the 12th century made references to luminous insects and other luminescence phenomena.

The first book totally devoted to luminescence was published at Zurich, in 1555, by Conrad Gesner. Generally referred to as *De luminarii* it was titled, in translation, a short commentary on rare and marvellous plants that are called lunar either because they shine at night or for other reasons; and also on other things that shine in darkness. It drew on the ancient authors, describing luminous plants and animals also luminous stones, and included Gesner's own ideas on the subject.

Ancient and medieval authors on luminescence had been mainly concerned with describing luminescent objects. From the beginning of the 17th century more attempts were being made to explain these phenomena. Francis Bacon (1561-1626) wrote several works on light and luminescence including "The Advancement of Learning (1605), *Topica Inquisitionis de Luce at Lumine* (published before 1612) and *Sylva Sylvarum* or *A Natural History in Ten Centuries* (published 1627)".

The last describes sixteen experiments with shining wood, fish and flesh. At about the same time an Italian, Vincenzo Cascariolo of Bologna, found that a local mineral consisting of native barium sulphate could be made to phosphoresce; this was the Bologna phosphor or lapis bononiensis. Other examples of inorganic luminescence were then discovered; the most important being that of phosphorus, first prepared in 1669 by Hennig Brandt.

The late 17th century also saw the discovery of artificial electroluminescence in tubes, by Jean Picard in 1675. Thermoluminescence in certain types of fluorspar, which emit light when warmed slightly, was recognised as a separated form of luminescence in 1676 by Johan Sigmund Elsholtz.

Robert Boyle made an extended study of the properties of luminescent materials. His first studies were into diamond and were reported in 1663.

Diamond can display phosphorescence, thermoluminescence, electroluminescence and also triboluminescence, which is the property of emitting light for a short while when bonds are broken.

Preparing phosphorus independently of Brandt, Boyle's work on the element was published in 1680 as "The Aerial Noticula". His best known studies into luminescence related to shining flesh and wood and the effects of air on these. These experiments were made possible by the vacuum pump invented by Otto von Guericke in 1650 and improved by Boyle and Hooke in the 1660s. The results were reported in the Philosophical Transactions, on December 16/1672 as "Some Observations about Shining Flesh".

Reports of these experiments appear to have circulated widely. In the play "The Virtuoso", a satire on the Royal Society, written in 1676 by Thomas Shadwell for the Duke's Company, a character described the essential features of these experiments: "There was a lucid sirloin of beef in the Strand.

Foolish people thought it burned when it only became lucid and crystalline by the coagulation of the aqueous juice of the beef by the corruption that invaded it. Tis frequent. I myself have read a Geneva Bible by a leg of pork tis the finest light in the world. But for all that, I could eclipse the leg of pork in my receiver by pumping out the air. But immediately upon the appulse of the air let in again, it becomes lucid as before".

At this time many philosophers, including Isaac Newton(1642-1727) and Robert Hooke (1635-1702), were considering that the emission of light was connected with vibrations in the emitting object. Newton considered that the light was propagated in the form of a stream of particles while Hooke and Christian Huygens(1629-1695) supported the wave theory of propagation. Hooke also made a number a number of studies of luminescence phenomena.

During the 18th century many materials were found to be luminescent, including several observed by Jacopo Bartolommeo Beccari and co-workers in Bologna. These workers developed a classification of luminescence by the method of excitation. They did not use modern terminology, but otherwise the classification is very similar to those in current use.

By the early 19th century the wave theory of light became more widely supported due to the work on diffraction by Thomas Young(1773-1829) and Augustin Fresnel(1778-1827). In 1802 the first spectrometer to use a slit was proposed by Hyde Wollaston enabling the first good spectra of phosphors to be observed.

In the 1850s, publications by Edmond Becquerel(1820-1891) described the composition of the exciting light, and later the emitted light of fluorescent materials. In the latter part of the

19th century it was found that rather simple organic (non-biological) compounds could give rise to chemiluminescence.

It was found in 1877 by Bronislaus Radziszewski that a synthesised lophine (2,4,5 triphenylimidazole) emitted green light when it reacted with oxygen in alkaline solution of alcohol. This discovery essentially founded the science of solution chemiluminescence.

In 1888 the term CL was proposed for the first time by Eilhard Wiedeman(1852-1928) to describe light emission occurring as a result of chemical processes.

The next major discovery in solution chemiluminescence was of pyrogallol, described by J.M. Eder in 1887, and studied in detail by Trautz and Shorigin in 1905. In 1887 Raphael Dubois demonstrated that light is emitted from the mixture of a luciferin and luciferase in the presence of oxygen and discovered the chemiluminescence from aesculin, a glucosidic compound present in horse-chestnut bark.

Several more chemiluminescent compounds were discovered in the early part of this century. These included lucigenin by K. Gleu and P. Petsch in 1935 and luminol, which was discovered by H.O. Albrecht in 1928.

Luminol is still the most widely used chemiluminescent compound for analytical applications. Currently many CL systems are known, biological as well as non-biological, but despite intensive studies the detailed mechanisms involved are largely unknown¹⁵⁶.

Also, several new inorganic luminescent systems were reported in the 18th century, including the white flash observed when lime is mixed with a strong acid.

Phosphorescence is the persistent emission of light by a substance as a result of having absorbed energy from a form of electromagnetic radiation, such as visible light or x-rays. Unlike fluorescence, phosphorescence continues for a short while after the source of radiation is removed. Glow-in-the-dark products are phosphorescent.

Natural examples of CL include the male firefly, but many other organisms can also emit light. When in search of a mate, the male firefly will emit flashes of light. This light is produced by the reaction of luciferin with molecular oxygen, which is catalyzed by the enzyme luciferase.

Bioluminescence differs from species to species, but the general mechanism begins with the oxidation of a luciferin catalysed by luciferase as shown in the figure 2.1, which depicts a schematic representation of the luciferin bioluminescent reaction^{4, 157-163}.

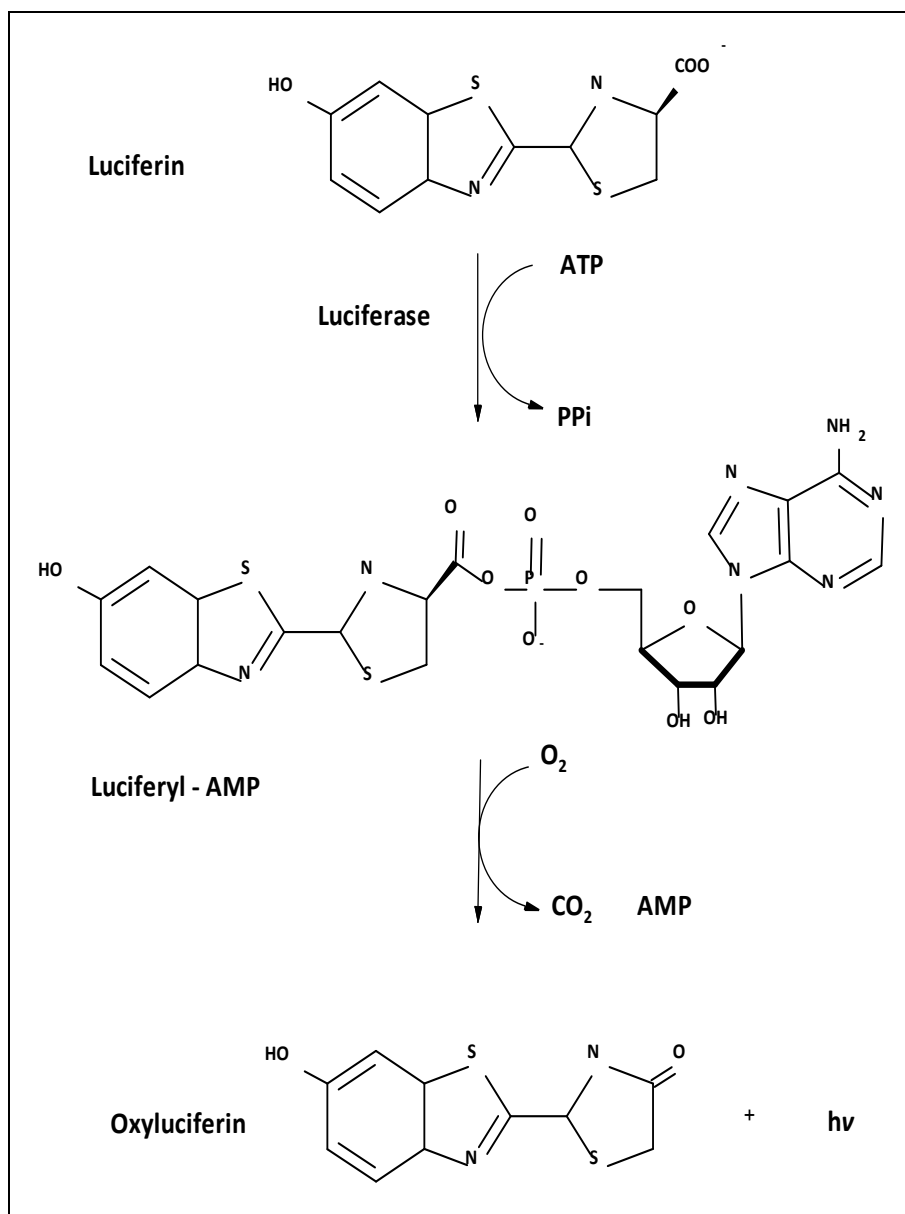


Figure 2.1 Light-emission mechanisms of Luciferin substrates¹⁶⁴

The most popular and probably well-known and studied chemiluminescent systems in liquid-phase studies include luminol¹⁶⁵⁻¹⁷² and lucigenin¹⁷³⁻¹⁹², which illustrate the process of direct and indirect chemiluminescence, respectively.

Lucigenin (10-Methyl-9-(10-methylacridin-10-ium-9-yl)acridin-10-ium dinitrate) is one of the more efficient CL substances which emits an intense green emission when oxidised in an alkaline medium¹⁶⁴. Other acridinium derivatives¹⁹³ have been shown to produce CL emission upon hydrogen peroxide oxidation of aqueous alkaline solutions. The main reaction product is N-methylacridone, acting as an active intermediate in the mechanism proposed by Rauhut et al^{194, 195}. The application of this reaction has permitted the determination of several ions, oxidants or reductors, such as ascorbic acid¹⁹⁶.

Lucigenin undergoes a reaction with hydrogen peroxide to form an unstable dioxetane whose decomposition leads to N-methylacridone in an electronically excited state. The excited acridone emits light as it relaxes to a stable state¹⁷³. Sensitizers, such as rhodamine B and fluorescein are used as energy transfer reagents for enhancing the CL. The proposed mechanism of reaction of lucigenin with H₂O₂ is shown in Figure 2.2.

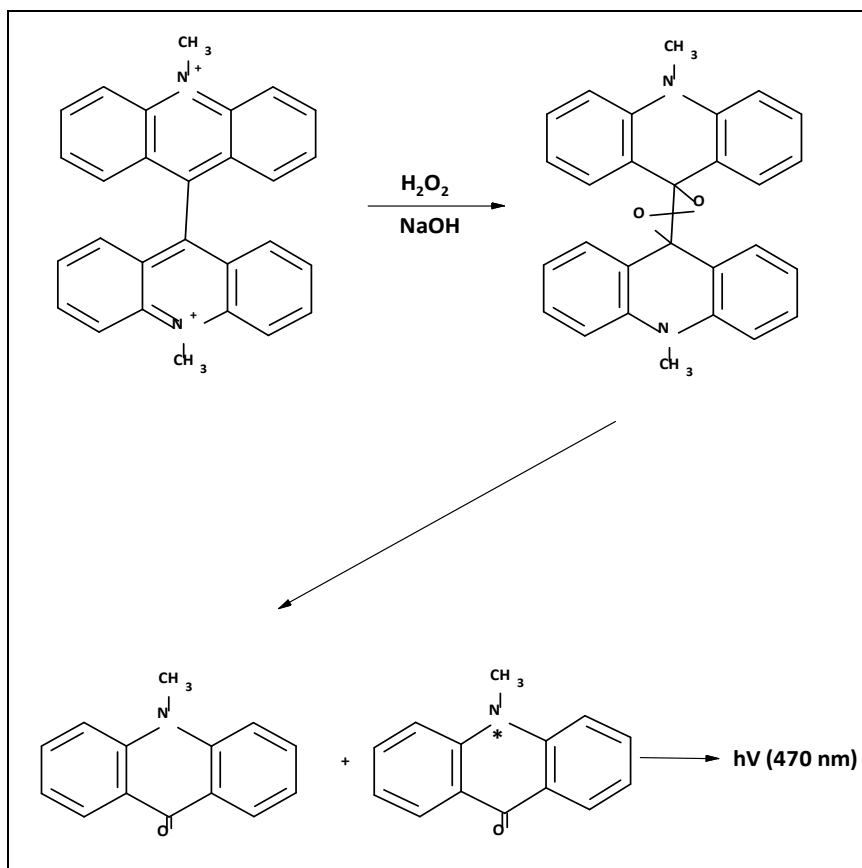


Figure 2.2 Proposed Mechanism for the Lucigenin CL reaction¹⁷³

Luminol (5-Amino-2,3-dihydro-1,4-phthalazinedione) is a chemical that exhibits blue chemiluminescence^{166, 197}, when mixed with an appropriate oxidizing agent. It is a white to slightly yellow crystalline solid that is soluble in water and most polar organic solvents. Luminol is used by forensic investigators to detect trace amounts of blood left at crime scenes. It is also used as an assay label and in cellular assays for the detection of copper, iron, and cyanides.

Probably the most useful oxidant is hydrogen peroxide^{166, 197}, however, other oxidants have been used such as permanganate¹⁹⁸, hypochlorite¹⁹⁹, and iodine²⁰⁰. The oxidation is catalyzed by, cobalt(II), iron(II), hexacyanoferrate(III), hemoglobin components hemin and hema-tine²⁰¹, and Cu²⁺. The decomposition of peroxide produces an excited carboxylate anion which emits a photon (bright blue colour) in returning to the ground state. However, the mechanism of the luminol light emitting reaction in aqueous solution, though widely studied, is not fully understood.

It is thought to involve peroxide, which then decays to form 3-diaminophthalate in an electronically excited triplet state (two unpaired electrons of the same spin). This then slowly undergoes an intersystem crossing to the singlet state (two unpaired electrons of different spin). The excited singlet state product then decays to the ground state, which results in the emission of blue-green light, a process which is called fluorescence. A schematic representation of the luminol chemiluminescent reaction is shown in Figure 2.3.

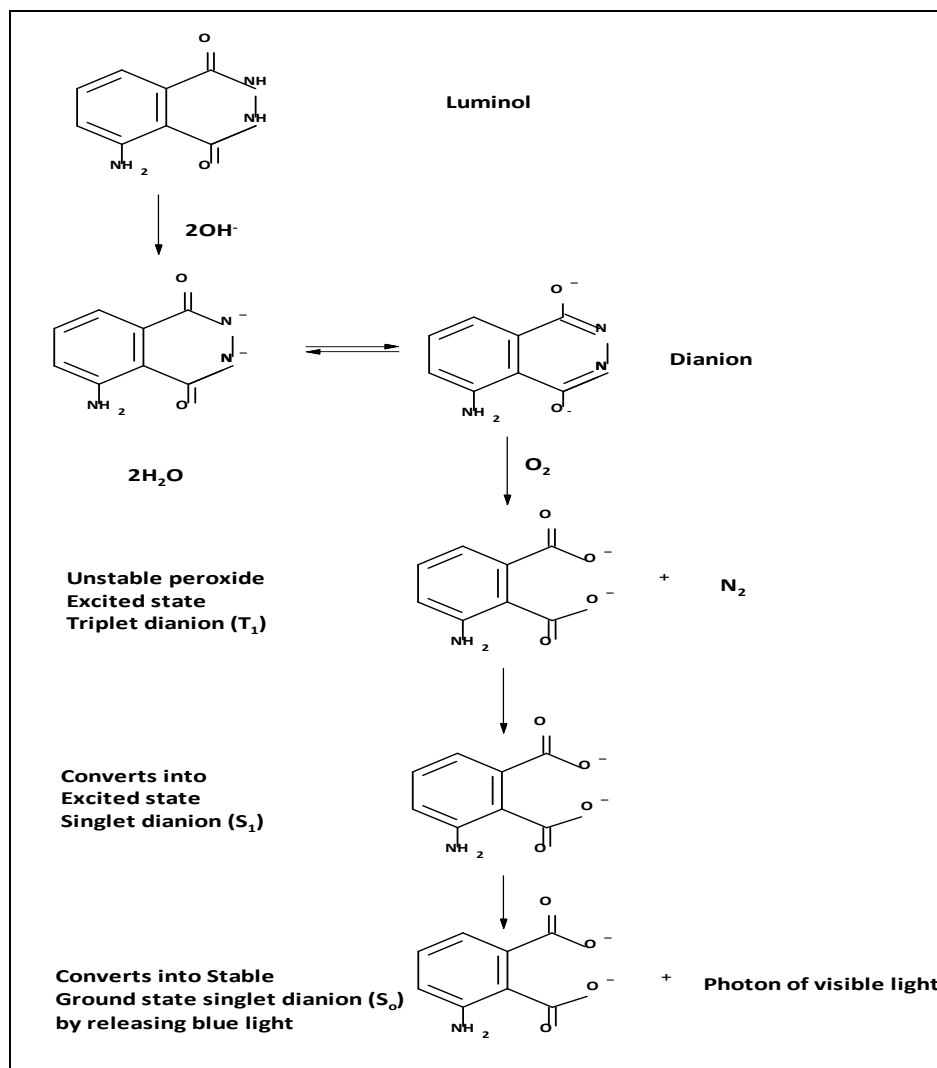


Figure 2.3 Proposed light-emission mechanism of Luminol oxidation¹⁶⁶

The chemiluminescence phenomenon, often referred to as “cold light”, is relatively uncommon because, in most chemical reactions, there are several ways for an electronically excited state to lose its extra energy, either by reacting with another molecule, molecular dissociation, collision with its surrounding molecules, or luminescence. In the latter case, it can react to release sufficient energy to produce photon of visible light, and the visible spectrum extends from 400 to 750 nm. More than a hundred years ago, chemiluminescence emission from the reaction between acidified potassium permanganate and pyrogallol (and also in the presence of hydrogen peroxide) was first reported by Grinberg²⁰² in 1920.

Numerous more manganese-based (mainly permanganate) chemiluminescent reactions have been discovered since then, notably that with siloxene²⁰³, glucose²⁰⁴ and oxalic acid²⁰⁵.

In 1972, Nikolaevsky and Miroshnikova studied chemiluminescence detection for the diagnosis of gas resistance in plants using potassium permanganate in sulphuric acid²⁰⁶.

Stauff and Bergmann²⁰⁷ found that the oxidation reaction of oxalic acid by potassium permanganate in the presence of Mn(II) sulphate generated chemiluminescence emission, which could last for 200 s with maximum intensity reached after 90 s.

A book published by Stauff et al.²⁰⁸ discussed further some of the results of this paper and proposed excited triplet dimer of carbon dioxide as the emitting species. In 1975, Stauff and Jaeschke⁵⁴ reported for the chemiluminescence determination of sulphur dioxide using acidic potassium permanganate as chemiluminescence reagent.

Veselovskii et al.²⁰⁹ observed the emission of chemiluminescence when *Escherichia coli* cells were exposed to acid potassium permanganate. From further studies on whole bacterial cells, lipids, proteins, amino acids, and other cell components they determined that the luminescence observed from whole cells was due to protein oxidation by permanganate⁶.

In 1977, Lebedev and Tsibanova²¹⁰ studied the CL from the potassium permanganate oxidation of 12 amino acids; whilst all reactions were found to emit light, the greatest intensities were observed for glutamic acid and aspartic acid. In the presence of sodium fluoride, the luminescence intensity was reduced, and they subsequently speculated that Mn (III) ions formed during the reaction caused decarboxylation of the amino acid thus producing carbon dioxide radical anions thence luminescence. Later that year, Lebedev and Tsibanova studied the kinetics of the CL from aspartic acid oxidation.

Whilst complicated behaviour was observed, the authors concluded that the chemiluminescence was limited by the decomposition of a Mn (III) aspartic acid complex, then inferred that the emission may have arisen during this rate limiting step from a triplet state of the transition metal complex.

Using the emission from the oxidation of *Escherichia coli* cells, Lebedev and Veselovskii²¹¹ acquired a chemiluminescence spectrum which revealed a broad band from 600 up to 800 nm with a maximum lying between 700 and 750 nm.

From kinetic studies with various cell fractions they determined that the emission was associated with the oxidation of cell membrane proteins, and that other cell constituents elicited no chemiluminescence. Ushakova and Parkhomenko²¹² studied the chemiluminescence oxidation of proteins, including albumin, peptone and peroxidase, by potassium permanganate and noted that in the presence of pyocyanin, the response was decreased by approximately 40%.

In contrast, the emission from the oxidation of alcohol dehydrogenase, cytochrome c and lysozyme showed little or no effect from the presence of pyocyanin. The same group²¹³ extended their chemiluminescence study to other cell types.

In fact, almost all liquid phase reactions involving permanganate oxidant are chemiluminescent under some circumstances. The chemiluminescent reactions between permanganate and organic analytes are probably the most sensitive and have found the broadest applications. The first analytical application – the determination of sulphur dioxide – was published in 1975⁵⁴, but it was not until the mid-1980s that applications involving organic analytes were reported^{110, 111, 214}.

Over the past decade, there has been a significant rise in the number of applications, particularly those involving organic analytes. Chemical and spectroscopic evidence for the species responsible for the characteristic red emission observed from many reactions with acidic potassium permanganate has emerged^{9, 127} and several researchers have continued to explore the relationship between chemiluminescence intensity and analyte structure^{73, 151, 215, 216}.

The use of acidic potassium permanganate as a chemiluminescence reagent and its analytical applications has been reviewed by various authors. For further details of the early development of this chemiluminescence reagent, the reader is referred to the previous review and recent reviews on CL detection^{6, 7, 11, 215, 217}.

Manganese(IV) and manganese(III) CL have been reviewed in a number of articles^{9, 127, 218, 219}. For instance, in 1984 and again in 1993, Jaky²²⁰ dissolved manganese dioxide in aqueous phosphoric acid (3 M) and investigated the kinetics of the oxidation of various simple organic compounds *e.g.* propane-1,2-diol, formaldehyde, formic acid, oxalic acid.

Using FIA methodology, Zhang and co-workers developed a method based on the CL reaction with a manganese(III) reagent that was generated on-line by constant-current electrolysis of manganese(II) sulphate in acidic solution, for the determination of numerous organic compounds such as isoniazid²²¹, adreson (cortisone acetate)²²², Chlorpromazine²²³, aminopyrine(amidopyrine)²²⁴, captopril²²⁵, cephradine²²⁶, cephalexin²²⁷, Chlorpromazine²²³, dexamethasone 21-phosphate²²⁸, quinine²²⁹, reserpine²³⁰, sulfite²³¹, tryptophan²³².

2.1.2 Types of Luminescence

Luminescence is concerned primarily with the emission of visible or near-visible radiation (200-1500 nm) when electrons in excited orbital decay to their ground state, the light arising from the potential energy of electronic transitions within atoms or molecules. Chemiluminescence is one of a number of luminescent phenomena. Conventionally, these phenomena have been distinguished by a prefix which identifies the energy source responsible for generating and initiating emission of electromagnetic radiation.

Wiedemann^{4, 233} defined the term “luminescence” (Greek: Lucifer, light bearer) in order to distinguish between light emission from thermally excited substances and CL emission from molecules excited by other mechanisms without increasing their average kinetic energy.

He classified luminescence phenomena into six different kinds, according to the way of excitation: photoluminescence caused by the absorption of light, electroluminescence produced in gases by an electric discharge, thermoluminescence produced by slight heating, triboluminescence as a result of friction, cristalloluminescence as a result of crystallization, and chemiluminescence caused by a chemical reaction. Based on Harvey², the luminescence phenomena can be classified according to the source of excitation into:

2.1.2.1 Luminescence associated with heating

- **Thermoluminescence:** refers to the luminescence of solids and crystals on mild heating i.e., well below that necessary to produce incandescence. It is observed when certain minerals, having previously been exposed to high-energy radiation, release energy in the form of visible light when heated. For example the heating of diamond. Thermoluminescence has been used as a means of archaeological dating.
- **Candoluminescence:** luminescence of incandescent solids emitting light at shorter wavelengths than expected. For example the heating of ZnO.
- **Pyroluminescence:** refers to the luminescence of metal atoms in flames. For example the yellow sodium (Na) flame.

2.1.2.2 Luminescence associated with prior irradiation

- **Photoluminescence:** luminescence caused by UV or visible light irradiation. For example, the Bologna stone (BaSO_4).
- **Cathodoluminescence:** luminescence produced in a material by ionizing radiation such beta particles irradiation or electron beam bombardment. Example a cathode television screen.
- **Anodoluminescence:** refers to the luminescence produced in a material by ionizing radiation such alpha particles (He nuclei) or He nuclei bombardment. Example zinc sulphide phosphor.
- **Radioluminescence:** refers to the luminescence caused in material by ionizing radiation such as gamma-rays or X-rays. Ground state molecules are excited by collisions with high energy particles. Example luminous paint.

2.1.2.3 Luminescence associated with electrical phenomena

- **Electroluminescence and piezoluminescence:** refers to luminescence associated with electric discharges and fields. Example fluorescent strip light.

- **Galvanoluminescence:** relates to luminescence produced during electrolysis. Example electrolysis of NaBr.
- **Sonoluminescence:** refers to the emission of light by tiny bubbles in a liquid excited by sound (intense sound waves in solution). Example ultrasonic probe in glycerol.

2.1.2.4 Luminescence associated with structural rearrangement in solids

- **Triboluminescence:** is the emission of light energy when a mechanical stress is applied to a crystal, the crystal stressed by applying pressure or torque. Luminescence on shaking, rubbing, or crushing. Example gentle agitation of uranyl nitrate, $\text{UO}_2(\text{NO}_3)_2 \cdot 6\text{H}_2\text{O}$.
- **Crystalloluminescence:** luminescence on crystallisation. Example HCl or ethanol addition to saturated alkali metal halide solutions (NaCl, KCl).
- **Lyoluminescence:** luminescence on dissolving crystals. Example LiCl or KCl coloured by irradiation by cathode rays.

2.1.2.5 Luminescence associated with chemical reactions

- **Chemiluminescence:** refers to the light energy emitted results from a chemical reaction. Ground state molecules are excited by certain chemical reactions. Example oxidation reaction of glyoxal by acid permanganate.
- **Bioluminescence:** when the luminescent chemical reaction occurs in a living organism. Example $\text{O}_2 + \text{Luciferin-Luciferase}$ (firefly).
- **Electrogenerated chemiluminescence:** when the emission of light results from the formation of excited species at the electrode surface.

2.1.3 Photoluminescence

Photoluminescence is the spontaneous emission of light which is caused by the irradiation of a substance with other light (light from a material under optical excitation)^{9, 10, 234}. Photoluminescence spectroscopy is a contactless, non-destructive method of probing the electronic structure of materials.

Light is directed onto a sample, where it is absorbed and imparts excess energy into the material in a process called photo-excitation. One way this excess energy can be dissipated by the sample is through the emission of light, or luminescence.

The intensity and spectral content of this photoluminescence is a direct measure of various important material properties. The excitation energy and intensity are chosen to probe different regions and excitation concentrations in the sample.

Quantum mechanically, this can be described as the photo-excitation causing electrons within the material to move into permissible excited states.

When these electrons return to their equilibrium states, the excess energy is released and may include the emission of light (a radiative process) or may not (a nonradioactive process). The energy of the emitted light (photoluminescence) relates to the difference in energy levels between the two electron states involved in the transition between the excited state and the equilibrium state. The quantity of the emitted light is related to the relative contribution of the irradiative process.

The emission of light or luminescence through this process is photoluminescence. Figure 2.4 shows Jablonski energy-level diagram²³⁵ that best illustrates the electronic energy levels (and their relative positions) of a molecule. A Jablonski diagram enables radiative transitions between energy levels in molecules, as well as such phenomena as internal conversion. The vertical axis measures energy, with the electronic energy levels in their lowest vibrational states being short horizontal lines. The horizontal axis represents wavelength.

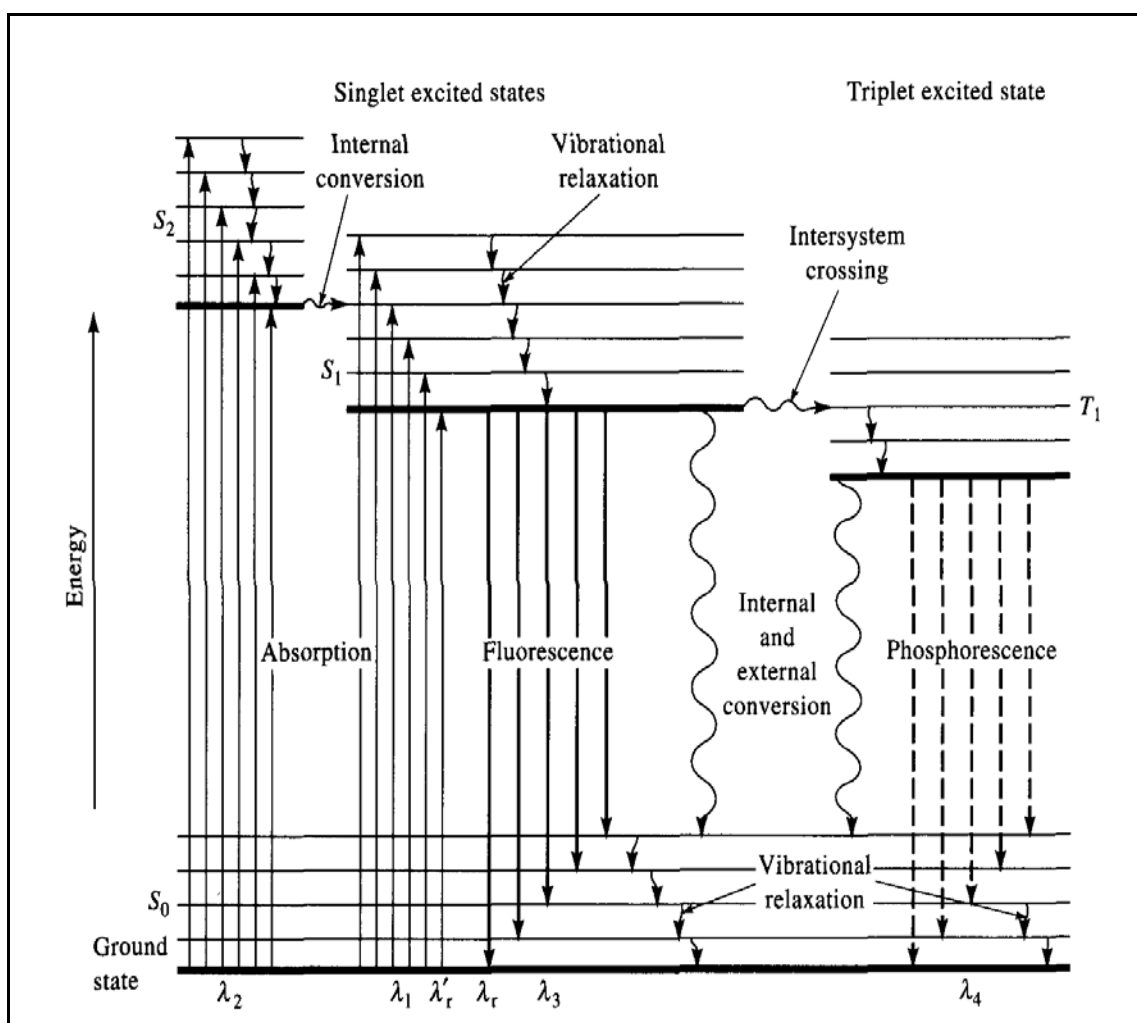


Figure 2.4 Energy Levels for Luminescence Transitions (Jablonski energy-level diagram).

As mentioned above, this is one of many forms of luminescence and is distinguished by photoexcitation (excitation by photons), hence the prefix photo-. The period between absorption and emission is typically extremely short, in the order of 10 nanoseconds. Under special circumstances, however, this period can be extended into minutes or hours.

The term embraces both molecular fluorescence and phosphorescence, which differ in the time after irradiation over which the luminescence occurs.

The simplest photoluminescent processes are resonant radiations, in which a photon of a particular wavelength is absorbed and an equivalent photon is immediately emitted – absorbed radiation is reemitted without alteration.

This process involves no significant internal energy transitions of the chemical substrate between absorption and emission and is extremely fast, of the order of 10 nanoseconds.

More interesting processes occur when the chemical substance undergoes internal energy transitions before re-emitting the energy from the absorption event.

The most familiar such effect is fluorescence – short-lived with luminescence ending almost immediately. Fluorescence is also typically a fast process, but in which some of the original energy is dissipated so that the emitted light photons are of lower energy than those absorbed. The generated photon in this case is said to be red shifted, referring to the loss of energy as Jablonski diagram shows.

An even more specialized form of photoluminescence is phosphorescence – this involves change in electron spin and may endure for several seconds. In phosphorescence process, the energy from absorbed photons undergoes intersystem crossing into a state of higher spin multiplicity, usually a triplet state.

Once the energy is trapped in the triplet state, transition back to the lower singlet energy states is quantum mechanically forbidden, meaning that it happens much more slowly than other transitions.

The result is a slow process of radioactive transition to back to the singlet state, sometimes lasting minutes or hours. This is the basis for "glow in the dark" substances.

2.1.4 Generation of chemiluminescence

The generation of light by a chemical process in solution may be divided into two steps. The first step of the CL process is the conversion of reactants to an electronically excited state. It is this excitation step that distinguishes reactions that generate visible light from all other chemical transformations.

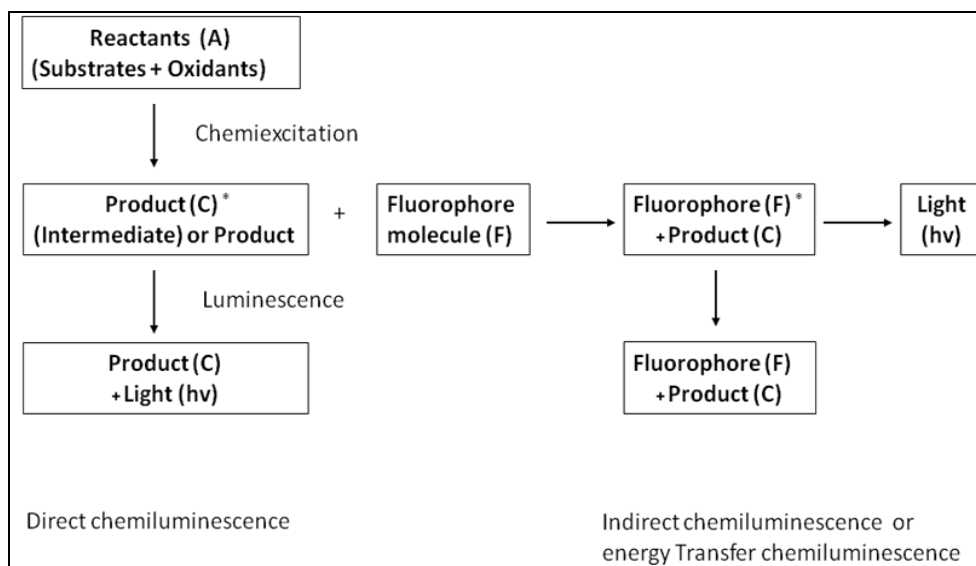


Figure 2.5 Basic mechanisms of chemiluminescent reactions³

Where C^* represents the excited state of the species C. F and F^* denote acceptor or fluorophore molecules in the ground state and the electronically excited state, respectively.

The excitation step provides the mechanism whereby the energy released during the conversion of reactants to products is diverted from heat to light. There has been considerable diversity of opinions regarding the details of this transformation.

The second step in all chem. - and bioluminescent reactions is the emission of light from an electronically excited state.

The ultimate emitter may be the excited state formed as a direct consequence of the excitation step or it may be a state formed indirectly by energy transfer from the first formed excited state.

The first circumstance is referred to as direct chemiluminescence and the second as indirect chemiluminescence. To provide a better understanding of CL process, the figure 2.5 above gives a schematic representation of this process.

Chemiluminescence yield of the above reactions is considered to be the product of the efficiency for generation of C^* and the efficiency of its radiative decay to the ground state. Efficiency of chemiluminescence is measured in terms of the chemiluminescence quantum yield. The quantum yield is equal to the ratio of number of photons emitted during a reaction divided by the number of molecules which reacted. Thus, two main factors affect the light intensity; the rate of reaction and the efficiency for producing C^* .

Therefore, the efficiency of a chemiluminescent reaction (CL quantum yield) is determined according to the following mathematical relation:

$$\Phi_{\text{CL}} = \Phi_{\text{C}} \times \Phi_{\text{Ex}} \times \Phi_{\text{e}} \text{ (Equation 2.1)}$$

Where Φ_{CL} , Φ_{C} , Φ_{Ex} , and Φ_{e} denote the overall quantum yield, chemical yield (fraction of molecules going through the chemiluminescence pathway), excited state molecules yield (the efficiency of population of the excited state), and excited state quantum yield – efficiency of emission (fraction of excited state molecules which produce a photon), respectively. In the case of indirect chemiluminescence, where there has been energy transfer between fluorescing species and acceptor species, further terms; Φ_{T} and $\Phi_{\text{e}}^{\text{A}}$ are added, and the equation 2.1 can be rewritten as follows;

$$\Phi_{\text{CL}} = \Phi_{\text{C}} \times \Phi_{\text{E}} \times \Phi_{\text{T}} \times \Phi_{\text{e}}^{\text{A}} \text{ (Equation 2.2)}$$

where Φ_{T} describes the efficiency of energy transfer and $\Phi_{\text{e}}^{\text{A}}$ relates to efficiency of emission from the acceptor molecule. Quantum efficiencies of many chemiluminescent reactions are low and those used in analytical chemistry are typically in the range 0.001 to 0.1 and up to 0.5 for peroxyoxalate systems.

Reactions with lower quantum efficiencies down to 10^{-15} , often called ultra-weak can be used analytically, particularly when the time of emission is relatively long.

Some reactions have particularly high quantum efficiencies, approaching unity. These reactions are mainly bioluminescent reactions, where the presence of other biological molecules such as proteins is believed to protect emitting species from loss of energy by interaction with surrounding molecules.

The most efficient luminescence systems, resulting in the high quantum efficient species and spectral characteristics, are dictated by the environment in which the species live. Thus, in marine environments, luminescent species typically emit green light, whereas terrestrial species emit blue light to enabling them to be seen from a maximum distance.

There are several ways for an electronically excited state to lose its extra energy, either by reacting with another molecule, molecular dissociation, collision with its surrounding molecules, or luminescence. In the latter case, it can react to liberate sufficient energy to produce photon of visible light. The overall quantum yield can be measured down to 10^{-15} .

The rate of production of light and concentration of chemiluminescent molecule, often coupled to concentration of a catalytic reagent, imposes limits on the amount of time that the luminescence can be analytically useful from a sample volume.

Some samples will generate a relatively bright signal for a short period of time (until all of chemiluminescent reagent is completely used up); others will produce a weaker signal over a longer period of time.

To be chemiluminescent the reaction must fulfil three essential features:

- It must be an exothermic (energetic) reaction, at least one product must be excited into the electronically excited state,
- And the excited product must lose its energy by light emission or transfer it to a fluorophore.

For a reaction to be chemiluminescent in visible region (400 -750 nm), the energy required is in the range $160 - 300 \text{ kJmol}^{-1}$, as derived from the combination of Planck and Einstein equations:

$$E = hc/\lambda \text{ (Equation 2.3)}$$

It is obvious that if the energy generated in the reaction of the excited state is lost as vibrational and rotational energy (or heat), chemiluminescence will not occur. The change in free energy (ΔG) is that determines whether a reaction can occur;

$$\Delta G = \Delta H - T\Delta S \text{ (Equation 2.4)}$$

For many chemiluminescence reactions ΔS is small, so ΔG and ΔH are similar in magnitude. The difference between the activation energy ΔH_A and the reaction energy ΔH_R must be at least equal to the energy required to generate the excited state ΔH_{Ex} , as mathematically illustrated below.

$$\text{Energy available} = \Delta H_A - \Delta H_R \geq \Delta H_{Ex} \text{ (Equation 2.5)}$$

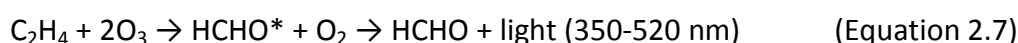
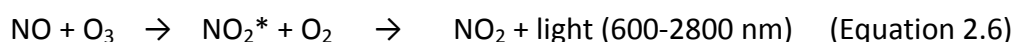
There are many inorganic and organic chemical reactions that are known to produce light. The most popular and probably well-known and studied chemiluminescent systems in liquid-phase studies include luminol and lucigenin (see Figures 2.2 and 2.3), which, also illustrate the process of direct and indirect chemiluminescence, respectively.

Chemiluminescent reactions can also be classified according to the chemical nature of luminescent compound that is reacting, such as, organic or inorganic, or according to the phase in which the reaction occurs, that is liquid, solid and gas, or finally according to the mechanism of the light emitting reaction¹⁹⁷.

In direct CL reactions, the emitter is the product of the chemiexcitation step and is generated directly in an excited state. Whereas in indirect chemiluminescence reactions, usually called sensitised or energy transfer chemiluminescence, the excited species transfers its energy to a fluorophore(or acceptor), the sensitizer, which then emits light (Figure 2.5). Considering the phase in which the reaction occurs, many hundreds of chemical compounds are at the origin of chemiluminescence reactions which can occur in liquid or solid phases, or at solid-liquid or solid-gas interfaces¹⁵⁶.

2.1.4.1 Gas-phase Chemiluminescence reactions⁴

In gas phase chemiluminescence, the light emission is produced by the oxidation reaction between an inorganic analyte (e.g. nitrogen monoxide) and strongly oxidising reagent gas such as ozone²³⁶ or fluorine. The most widely used gas-phase chemiluminescence reagent is ozone. Some analytical methods have been proposed for the determination of NO, sulphur monoxide and unsaturated hydrocarbons, such as alkenes, alkynes, aromatics and alkanes at high temperatures, based on the chemiluminescence emission produced in their reaction with ozone. Several of these are as follows:



The development of chemiluminescent methods for determining components of a gas largely originated from the need to determine atmospheric pollutants, allowing the development of instruments for pollutant monitoring with sensitivities ranging to the ppb-level.

The production of chemiluminescence emission in the UV-visible spectral region requires highly exothermic reactions such as atomic or radical recombination, or reaction of reduced species such as hydrogen atoms, olefins, and several sulphur and phosphorous compounds with strong oxidants such as ozone, fluorine and chlorine dioxide.

Based on the principles of the reactions above, several commercial chemiluminescence portable analysers have been developed for the determination of sulphur, nitrogen or phosphorous compounds.

In atmospheric research, the most useful detectors are applied in the detection of oxides of nitrogen using the above-proposed reaction. The detector, named "NOx box" measures both NO and the sum of NO and NO₂ (i.e., NO_x), as well as NO_y (i.e. total reactive oxides of nitrogen)²³⁷. These reactions with NO and ethylene are the basis of the Fast Ozone Detector, used to measure ozone in the atmosphere.

In heterogeneous gas-solid phase, a fast-response detector allows a very sensitive and selective determination based on the chemiluminescence induced when rhodamine B, adsorbed on silica gel, is exposed to ozone^{238, 239}. This procedure has been used for the study of vertical distribution of ozone in the atmosphere using miniaturised probes²⁴⁰. The former reaction constitutes the basis of the named "pyroluminescence method", in which organic and inorganic nitrogen (including nitrate) are oxidised in air at 1000 °C to form nitrogen monoxide, which makes it possible to determine harmful nitrogen as a criterion of beet quality²⁴¹.

Sulphur-selective CL detection can also be achieved by converting sulphur-containing compounds to SO^{242} . This forms the basis of analytical methods for the detection of SO (if it could be sampled and brought into contact with ozone), or other reduced CL sulphur species that can react with ozone and be converted to SO as an intermediate before the final elementary CL reactions ($\text{SO} + \text{O}_3 \rightarrow \text{SO}_2^* + \text{O}_2$) and ($\text{SO}_2^* \rightarrow \text{SO}_2 + h\nu$).

Oxygen atoms have also been applied as strong oxidants when reacted with a wide range of analytes, although not so frequently used in analytical applications. The reaction with nitric oxide produces a yellow-green chemiluminescence emission that has been used for measuring concentration of oxygen atoms in kinetic experiments:



Also, fluorine is used in CL as the stronger oxidant to produce CL emission in gas-phase. F_2 reacts with certain reduced sulphur compounds such as thiols, sulphides, disulphides and trisulphides, phosphines, alkyl phosphine and monophosphinate esters to produce intense CL emission^{243, 244}.

Some chemiluminescence reactions are based on the light emission produced in a flame, rather than the “cold” chemiluminescence emission as mentioned above²⁴⁵. In this case, the high temperatures of the flame promote chemical reactions that form key reaction intermediates and provide additional thermal excitation of the emitting species.

This methodology has been used for selective detection of compounds containing sulphur, nitrogen, phosphorous, boron, antimony, arsenic and halogens. As example, the mechanism for the detection of organophosphorous compounds can be cited involving the formation of PO, which subsequently reacts with H atoms in a fuel-rich flame to produce the excited species²⁴⁶:



2.1.4.2 Liquid-Phase Chemiluminescence – Biochemiluminescence Reactions

Bioluminescence refers to the ability of living organisms to produce light. Not only is it of interest to study and record the bioluminescent emission of organisms in their natural environment (~90% of deep sea marine life is thought to exhibit bioluminescence), but several of the individual biomolecules that give rise to bioluminescence have been identified, isolated, studied, often genetically coded, and put to use across a range of applications.

These uses have penetrated a broad field of study, including intracellular physiology, pre-clinical research, micro titre and biochip-based assays.

The analytically most widely applied bioluminescence systems are based on the firefly luciferin-luciferase reaction and the systems derived from the firefly *Photinus pyralis* and certain marine bacteria (*Vibrio Harvey* and *Photobacterium Fischeri*).

For example, firefly luciferase emits light in the presence of its substrate luciferin and Adenosine Triphosphate (ATP) and is widely used for measuring ATP concentrations (refer to Figure 2.1). In enzyme-catalysed bioluminescence reactions, light is emitted according to the following scheme:



Since all living organisms contain ATP it finds principal use as a measure of bi-contamination, for example in the food industry. Importantly, luciferase has been coded and adopted as a gene reporter, routinely transfected into living organisms and cells to study, for example, expression levels and cell physiology.

2.1.4.3 Liquid-Phase Chemiluminescence – Chemiluminescence Reactions

There are many known chemiluminescent reactions; two most prominent examples are arguably luminol chemiluminescence and peroxyoxalate chemiluminescence. The first is the oxidation of luminol (5-aminophthalylhydrazide) in alkaline medium, to produce excited 3-aminophthalate ion (Figure 2.3). Oxidants such as permanganate, hypochlorite, or iodine can be used but the most useful is hydrogen peroxide. The reaction is catalysed by metal ions (Fe(II), Cu(II), Co(II) amongst others), ferricyanide or some metallocomplexes (hemin, haemoglobin and peroxidases).

In this sense, this reaction has been applied for the determination of catalysts such as metal ions or enzymes (peroxidases, haematic compounds, etc.), certain oxidants, inhibitors or substances that are easily oxidised and are determined indirectly by measuring the decreased chemiluminescence emission.

Also, luminol has been extensively used in medico-legal investigations in presumptive tests to detect trace quantities of blood, which are not visible to the naked eye, e.g., areas intentionally wiped clean of blood, washed clothes, dark surfaces²⁴⁷, etc.

The second involves the TCPO plus the oxidant (H₂O₂)²⁴⁸ reacting to produce a proposed intermediate, in this example shown as a dioxetane (see equation 2.15); although, this reaction probably produces many intermediates, and others, such as hydroperoxyoxalate, have been proposed^{249, 250}. The intermediate, shown here as 1,2-dioxetanedione(see equation 2.15), excites a fluorophore. In this reaction 9,10-diphenylanthracene acts as the fluorophore; its λ_{max} is 425 nm in the solvent used, tetrahydrofuran. Its reaction with the intermediate produces the excited state product which quickly emits light.

The process of transferring the energy of the initial reaction, the chemical reaction of hydrogen peroxide with TCPO, to light emission from the excited state fluorophore (fluorophore*) can be de-excited along the way by losses in each step of the process: the initial oxidation to produce the intermediate, the reaction of the intermediate with a fluorophore, and the reaction of the excited fluorophore to produce light²⁵¹.

The initial oxidation can yield the high energy intermediate or;

- TCPO can be hydrolysed instead or
- oxidation can occur that doesn't yield chemiluminescent products.

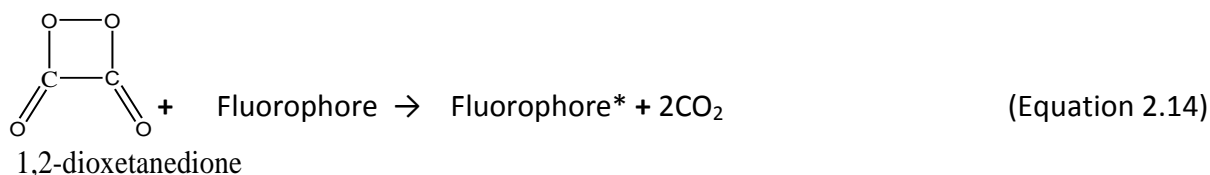
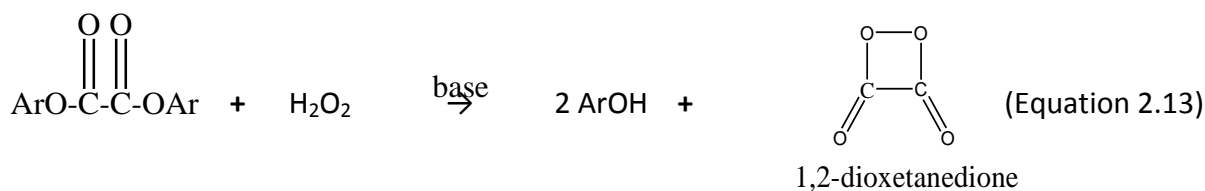
The high energy intermediate can react to excite the fluorophore or;

- the intermediate can react with a quencher more easily oxidized than the fluorophore
- the intermediate and fluorophore can react without yielding excited fluorophore
- the intermediate can decompose or be further oxidized by residual H₂O₂.

Finally the excited fluorophore can lose energy by emission of light or the excited fluorophore can de-excited by production of heat instead of light.

This reaction can be used to determine a great number of species such as hydrogen peroxide, compounds that are highly fluorescent (*e.g.* polycyclic aromatic hydrocarbons) or compounds that do not exhibit native fluorescence but can be derivatized chemically using dansyl chloride (amino acids, steroids, aliphatic amines, carboxylic acids, etc.) or fluorescamine (catecholamines)⁴.

The general reaction scheme can be represented by the following chemiluminescent mechanism:



where Ar is an electronegative aryl group such as 2,4-dinitrophenyl or 2,4,6-trichlorophenyl. In this work, efforts have been concentrated on liquid-phase chemiluminescence reactions because of their importance in analysis and development of sensors.

2.1.4.4 Liquid-Phase CL – Electrochemiluminescence Reactions

Electrochemiluminescence (ECL), also known as electro generated (CL), is the emission of light produced by an electrochemical reaction or from an electrolytic system and is known to be a useful phenomenon, especially in analytical chemistry²⁵²⁻²⁵⁴.

In electro generated, electrochemically generated intermediates undergo a highly exergonic reaction to produce an electronically excited state that then emits light²⁵⁵. Electrochemiluminescence excitation is caused by energetic electron transfer (redox) reactions between electrochemically generated species (e.g. anion and cation radicals). Such luminescence excitation is a form of chemiluminescence where one/all reactants are produced electrochemically on the electrodes²⁵⁶.

Electrochemiluminescence is usually observed during application of potential (several volts) to electrodes of electrochemical cell that contains solution of luminescent species (polycyclic aromatic hydrocarbons, metal complexes) in solvent (ECL composition).

Electrochemiluminescence proved to be very useful in analytical applications as a highly sensitive and selective method. It combines analytical advantages of chemiluminescent analysis (absence of background optical signal) with ease of reaction control by applying electrode potential.

Enhanced selectivity of electrochemiluminescence analysis is reached by variation of electrode potential thus controlling species that are oxidized or reduced at the electrode and take part in the electrochemiluminescence reaction.

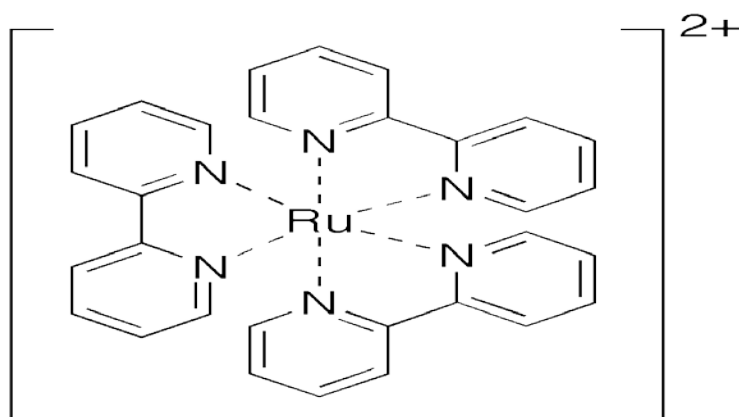


Figure 2.6 Tris (2,2'-bipyridyl)ruthenium(II) ($\text{Ru}(\text{bpy})_3^{2+}$).

Electrochemiluminescence (ECL) first became of interest for analytical assays with the discovery in the 1970's that tris(2,2'-bipyridyl)ruthenium(II) ($\text{Ru}(\text{bpy})_3^{2+}$) (Figure 2.6) emitted a photon near 620nm when excited by an electrode held at about +1.3V (relative to Ag/AgCl)^{257, 258}.

Furthermore, it was found that this reaction had fairly high quantum efficiency (2%) in water. Previous systems that were known to exhibit ECL were only useful in non-aqueous solutions, like acetonitrile.

The technology has been developed into a robust analytical chemistry technique by commercial vendors for use in clinical chemistry analyzers²⁵⁹ with $[\text{Ru}(\text{bpy})_3]^{2+}$ attached to antibodies or antigens.

The number of electrochemiluminescent reagents is also expanding rapidly. For instance, a commercial vendor, Roche, (formerly IGEN of Gaithersburg, MD), currently sells reagents for linking the $[\text{Ru}(\text{bpy})_3]^{2+}$ complex to oligonucleotides, thiols, carbohydrates and carboxyls.

In all mechanisms the light emitting species is excited state, $[\text{Ru}(\text{bpy})_3]^{2+*}$, produced when electrochemically generated $[\text{Ru}(\text{bpy})_3]^{3+}$ reacts with electrochemically generated $[\text{Ru}(\text{bpy})_3]^+$ (Annihilation ECL); when electrochemically generated $[\text{Ru}(\text{bpy})_3]^+$ is chemically reduced by a species other than $[\text{Ru}(\text{bpy})_3]^{3+}$ (Oxidative-reduction mechanism); and when electrochemically generated $[\text{Ru}(\text{bpy})_3]^+$ is chemically oxidized to $[\text{Ru}(\text{bpy})_3]^{3+}$ followed by annihilation ECL with $[\text{Ru}(\text{bpy})_3]^+$ (Reductive-oxidation mechanism).

2.1.4.4.1 Annihilation ECL^{257, 260}

Electrochemical oxidation of $[\text{Ru}(\text{bpy})_3]^{2+}$ at a positive potential (Reaction a) results in the formation of $[\text{Ru}(\text{bpy})_3]^{3+}$. Electrochemical reduction of $[\text{Ru}(\text{bpy})_3]^{2+}$ at a negative potential (Reaction b) results in the formation of $\text{Ru}(\text{I})(\text{bpy})_3$. $[\text{Ru}(\text{bpy})_3]^{3+}$ and $[\text{Ru}(\text{bpy})_3]^+$ react to yield $[\text{Ru}(\text{bpy})_3]^{2+}$ and electronically excited $[\text{Ru}(\text{bpy})_3]^{2+*}$ (Reaction c). The latter emits light at 617 nm when it relaxes to the ground state (Reaction d).

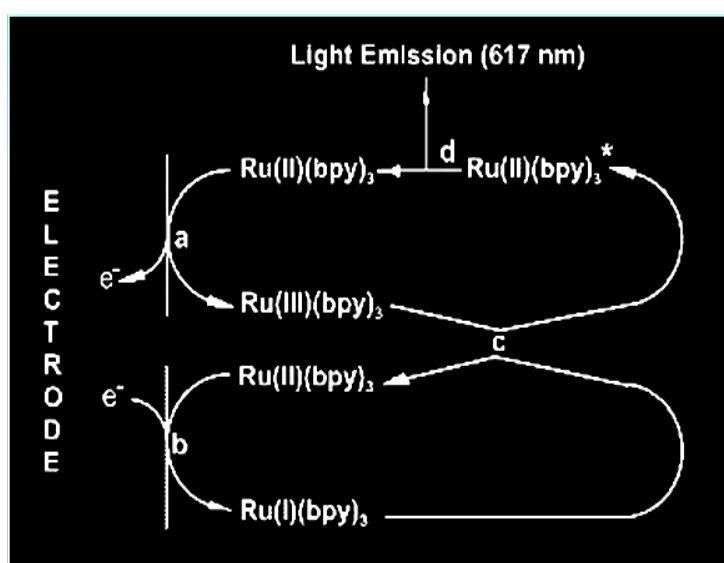


Figure 2.7 Basic mechanisms of Annihilation Electrochemiluminescence²⁵⁷

2.1.4.4.2 Oxidative-reduction mechanism^{257, 261}

Electrochemical oxidation of TPA (tripropylamine) (Reaction a) results in the formation of TPA^+ , which spontaneously loses a proton, forming a neutral TPA^\bullet radical (Reaction b).

Electrochemically generated $[\text{Ru}(\text{bpy})_3]^{3+}$ is reduced by TPA^\bullet to electronically excited $[\text{Ru}(\text{bpy})_3]^{2+*}$ (Reaction c), which emits light at 617 nm when it relaxes to the ground state (Reaction d). Reaction b results in the generation of a high concentration of protons and therefore a high capacity buffer is required to maintain the optimum pH of around 7.

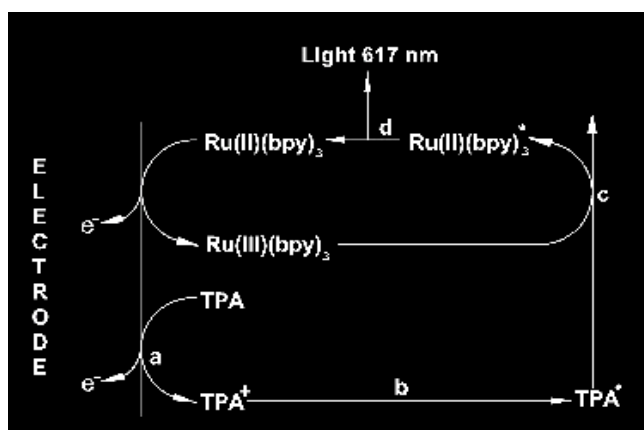


Figure 2.8 Basic mechanisms of Oxidative-reduction Electrochemiluminescence²⁵⁷

2.1.4.4.3 Reductive-oxidation mechanism^{257, 262}

Electrochemical reduction of $[\text{Ru}(\text{bpy})_3]^{2+}$ at a negative potential (Reactions a) results in the formation of $[\text{Ru}(\text{bpy})_3]^+$. Chemical oxidation of $[\text{Ru}(\text{bpy})_3]^+$ by peroxodisulfate ($\text{S}_2\text{O}_8^{2-}$) (Reaction b) yields $[\text{Ru}(\text{bpy})_3]^{3+}$. $[\text{Ru}(\text{bpy})_3]^{3+}$ and $[\text{Ru}(\text{bpy})_3]^+$ react to yield $[\text{Ru}(\text{bpy})_3]^{2+}$ and electronically excited $[\text{Ru}(\text{bpy})_3]^{2+*}$ (Reaction c). The latter emits light at 617 nm when it relaxes to the ground state (Reaction d).

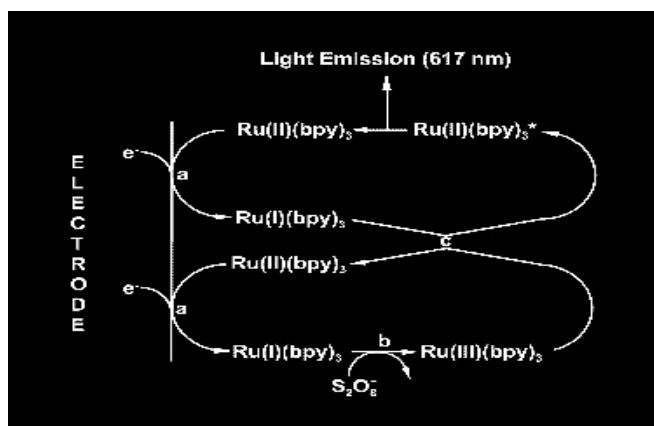
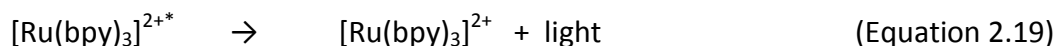
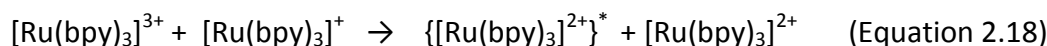
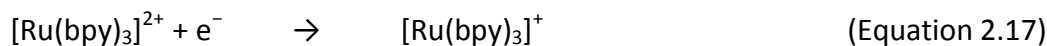
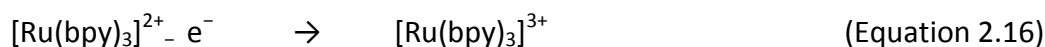


Figure 2.9 Basic mechanisms of Reductive-oxidation Electrochemiluminescence²⁵⁷.

In general terms, the $[\text{Ru}(\text{bpy})_3]^{2+}$ reaction mechanism is as follows^{257, 261}; note that $[\text{Ru}(\text{bpy})_3]^{2+}$ molecule is regenerated after the emission of each photon, enabling multiple cycles and many photons for each $[\text{Ru}(\text{bpy})_3]^{2+}$ molecule.



The advantages of CL are retained, but the electrochemical reaction allows the time and position of the light emitting reaction to be controlled. By controlling the time light emission can be delayed until events such as immune or enzyme catalysed reactions have taken place. Although similar control can be exercised over alternative detection methods such as fluorescence, the equipment is considerably more sophisticated and expensive.

2.2 Flow Analysis (FA)

Flow-based analysis²⁶³ is the generic term which describes a group of automated sample manipulation procedures that make use of unsegmented flowing streams in micro-conduits. Most common among these techniques is Flow Injection Analysis (FIA).

FIA is the process whereby a small segment of sample solution, is injected into a flowing carrier stream. This stream either contains a reagent, or the stream is merged with a reagent stream to produce a compound which can be determined in a flow-through detector.

These zones penetrate one another as they are carried to the detector by a suitable pump. Determination of the analyte of interest is analogous to FIA.

Flow Injection (FA) offers a very convenient and fast approach to enhance the automation and miniaturization of reagent based assays. The automation of this principle is done in the following way: a fluid flows continuously through a carrier.

In a simple realization this can be the reagent. Into this flow a precisely dosed amount of the solution that contains the detectable component (sample) is injected by a valve, therefore the term "flow injection"^{264, 265}.

Although there are many variations of flow injection methods, most can be assigned to one of three general categories: FIA, SIA, or bead injection analysis (BIA). This section briefly reviews flow based analytical techniques such as flow injection (FI), sequential injection (SI), bead injection analysis (BIA) and Stopped-Flow methods.

2.2.1 Flow Injection Analysis (FIA)

Flow injection analysis (FIA)^{263, 266} is a simple, rapid, and versatile technique for manipulation of the solution/sample/reagent followed by different detection methods.

It is an analytical technique based on microfluidic manipulation of samples and reagents. Samples are injected into a carrier/reagent solution which transports the sample zone into a detector while desired (bio) chemical reactions take place. Detector response (absorbance, fluorescence, mass spectra, etc.) yield a calibration curve quantifying the target analyte²⁶⁷.

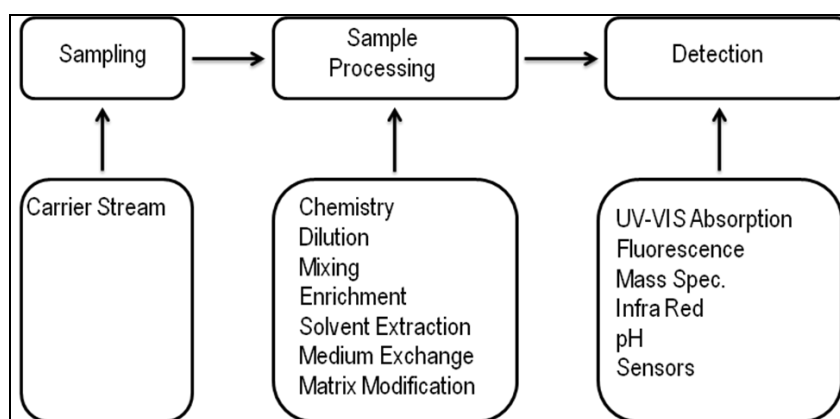


Figure 2.10 Generic description of Flow Injection Analysis (FIA)

Flow injection analysis (FIA) was first described in Denmark by Ruzicka and Hansen in 1975²⁶⁸. Since then the technique has grown into a discipline covered by 20 monographs and more than 20,000 research papers^{9, 10, 268}. The scope of the method has grown from serial assay of samples to a tool for enhancement of performance of spectroscopic and electrochemical instruments. The method has been widely adopted by researchers, and is gaining greater acceptance in industry as a fast approach to the analysis of waters, wastewaters, sediments and biota, clinical and biochemical samples, drugs, food and beverages, and agricultural products. Other fields include monitoring of chemical processes in real time, biotechnology, immunoassays including antibody/antigen reactions. Flow manifolds have become widely used in analytical chemistry with chemiluminescence detection.

There are different flow systems possible. One of these is a segmented flow system. A technique that uses air bubbles to create segments of fluid with air in between - it involves the separation of sample and a wash solution by air bubbles in order to avoid cross contamination between samples. In a segmented flow system, turbulent flow conditions apply, complete sample dispersion occurs, and a steady-state condition is attained prior to analyte detection. Sample throughput in segmented flow system is therefore generally slower than in flow injection analysis, although the former has until recently been more amenable to multi-channel, multi-parameter analysis. One segment now can be transported through the system like a mini reactor. The air bubbles have to be removed, just before the detector.

Flow injection analysis consists of a multichannel peristaltic pump that propels the carrier stream through a narrow tube, an injection valve by which a specific and reproducible volume of a sample solution is injected into the carrier stream, a coiled reactor where the sample zone disperses and reacts with the reagent from the carrier stream of which the product passes through a detector for CL such as a classical high voltage photomultiplier tube (PMT).

The assemblage of flow tubing, mixing coils, injection valve, etc., in a given configuration, used in a flow injection analysis system is referred to collectively as a manifold. A simple two line manifold is shown in figure 2.11^{269, 270} using the common symbolic notation.

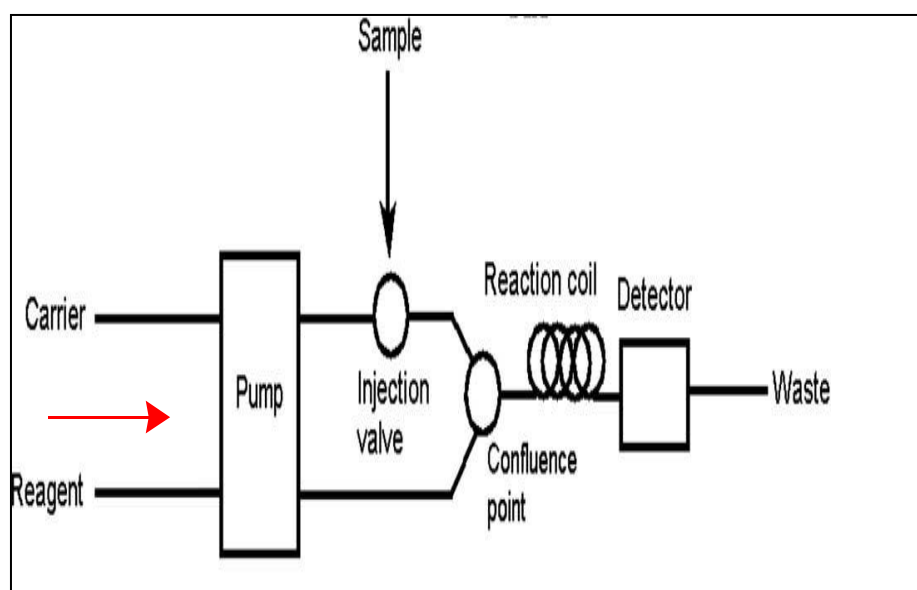


Figure 2.11 Schematic diagram of a typical Two Line Flow Injection Analysis Manifold

Some modern flow injection analysis systems may include additional components such as a flow through heater to increase the speed of chemical reactions, columns for sample reduction, debubblers, and filters for particulate removal.

Reagents may be added at various confluence points and these mix with the sample zone under the influence of radial dispersion, to produce reactive or detectable species which can be sensed by any one of a variety of flow-through detection devices.

The height or area of the peak-shaped signal thus obtained can be used to quantify the analyte after comparison with the peaks obtained for solutions containing known concentrations of the analyte²⁶⁵.

Figure 2.12 shows a typical detector output of flow injection analysis that is a plot of the response of the detector against time, a peak with height H , area A and width W , both of which carry key analytical information. The residence time T on the figure is the time during which the chemical reaction takes place and is related to peak height H ^{9, 10, 265}.

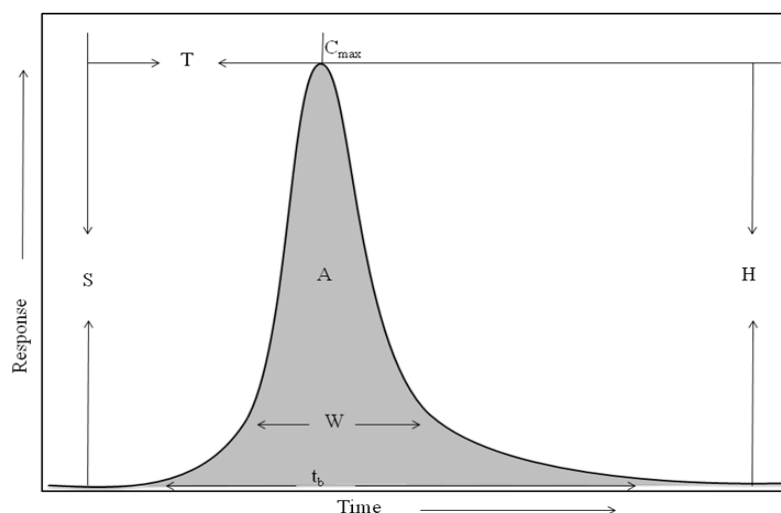


Figure 2.12 Typical Detector Output of a Flow Injection Analysis (FIA) System.

where A: Peak area; t_b : Peak width at baseline; C_{max} : Maximum Concentration of the analyte; W: Peak width; H: Peak Height; S: Injection Point.

However, the response curve and the ability for a FIA system to produce a high sample throughput depend on dispersion (or mixing) of the sample in a flow injection system, which is caused by two phenomena: convection and diffusion. The sample undergoes dispersion when it is transported through the flow system.

As stated previously, the control of dispersion is the most important aspect of flow injection system - it is defined as the dilution of a sample volume injected into a flowing stream. It is clear that a high dilution (large dispersion) reduces the sample throughput²⁷⁰. Ruzicka and Hansen defined dispersion as the amount that the chemical signal is reduced by injecting a sample plug to into a flow injection analysis (FIA). Mathematically, this can be represented as follows^{10, 265, 268}:

$$D = C_o/C_{max} \quad (\text{Equation 2.20})$$

where D is the dispersion coefficient at the peak maximum produced by the ratio between C_o (the initial concentration of the sample), and C_{max} (the peak concentration of the analyte). After the injection the carrier stream transports the injection plug to the detection cell. The sample zone is progressively dispersed into the carrier, initially by convection, and later by axial and radial diffusion, as it is transported along the conduit under laminar flow conditions^{10, 265, 267}.

Flow injection systems are categorized^{9, 10, 265, 267, 268} as high, medium, and low dispersion systems depending on the degree of dispersion of the injected zone at the read out point.

Except when preconcentration is performed, the dispersion value must always be greater than unity. Flow injection systems with $1 < D < 3$ are classified as having limited dispersion, and are used in conjunction with high sensitivity detection systems such as ion selective electrodes, atomic spectroscopy, CL detection, etc. where minimal sample dilution is necessary.

Flow injection systems with $3 < D < 10$ are classed as medium dispersion, and are most commonly used in systems where significant sample and reagent mixing is required, as is the case for methods involving spectrophotometric, fluorimetric, etc.

Large dispersion systems ($D > 10$) are used where extensive mixing between sample and reagent is required, such as for flow injection titrations.

The main experimental parameters influencing the dispersion of an injected fluid zone include sample volume, flow rate of carrier and merging fluid streams, geometrical dimensions and configuration of transport conduits and on line reactor.

The volume of the injected fluid zone, which most cases is the sample, is important factor influencing its dispersion. The dispersion decreases with an increase in sample volume^{265, 268}.

Flow injection analysis is based on three principles which are critical for its successful operation and application; (1) reproducible timing, (2) reproducible sample injection, (3) partial and controlled dispersion of the sample zone^{265, 268}.

Because the length of the manifold tubing remains constant and carrier and reagent flow rates vary little during transport of the sample zone from injection to the point of detection, the period for sample zone transport and mixing will be highly reproducible. Reproducible sample injection is achieved by the use of an injection valve with an injection loop of a defined volume.

Partial and controlled dispersion of the sample zone is critical for successful analysis - it provides the mechanism for mixing between sample and reagents, and prevents cross contamination between successive samples²⁶⁸. Chemiluminescence is usually detected in low dispersion systems. Under these conditions, response will be increased if the CL is produced over a shorter time period.

2.2.2 Sequential Injection Analysis (SIA)

Sequential Injection Analysis (SIA)²⁶³ is the second generation of FIA compatible assays – it was “born” in 1990 by J. Ruzicka and G.D. Marshall.²⁷¹ At that time, Flow Injection Analysis was becoming a widely accepted and rapidly evolving technique in most academic analytical chemistry laboratories. Sharing many characteristics with FIA, some would argue that it is simply an extension of FIA.

Nevertheless, more than 1000 journal articles have been published on SIA since the first paper in 1990. While, like FIA, it is fundamentally dependent on the dispersion of zones in a flowing stream, conceptually, the practice of SIA is different from FIA^{269, 270}.

Sequential Injection Analysis (SIA) is the recommended approach for online and remote site monitoring, where robustness and low reagent consumption is critical. Sequential Injection is also ideal for biomolecule assays such as Enzymatic Assays and Bioligand Interaction Assays^{269, 270, 272-277}.

This approach to automated sample manipulation arose from a need to simplify manifolds and address the unique requirements of the field of process analysis. In SIA, a selection valve and bi-directional pump is used to draw up small volumes of sample and reagents, and then propel them through a coil to a detector.

Again, the process causes mixing of the sample and reagent segments leading to chemistry that forms a detectable species before reaching the detector.

Sequential Injection Analysis (SIA) usually consists^{269, 270} of a single-channel high precision bi-directional pump, a holding coil, a multiposition valve, and a flow through detector. The system is initially filled with a carrier stream into which a zone of sample and a zone of reagent(s) are sequentially aspirated into a holding coil, forming a linear stack.

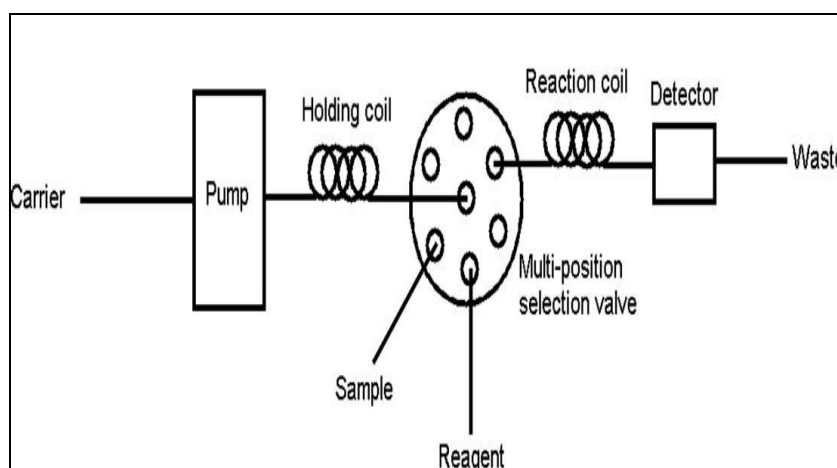


Figure 2.13 Schematic diagram of a Simple Sequential Injection Manifold

These zones become overlapped due the parabolic profile induced by differences between flow velocities of adjacent streamlines. Flow reversals and flow acceleration further promote mixing. The multiposition valve is then switched to the detector position, and the flow direction is reversed, propelling the sample/reagent zones through the flow cell. The advantage of SIA over the more traditional flow injection analysis (FIA) is that SIA typically consumes less than one-tenth the reagent and produces far less waste – an important feature when dealing with expensive chemicals, hazardous reagents, or online/remote site applications.

One disadvantage of SIA is that it tends to run slower than FIA^{269, 270}. The following diagram can be used to describe the basic components and principles of SIA (Figure 2.13).

2.2.3 Bead Injection Analysis (BIA)

The bead-injection (BI) technique²⁶³ is the combination of the use of beads with a flowing stream of solution in a FI system. Beads are utilized as solid surfaces to preconcentrate or extract the analyte or to accommodate a chemical reaction.

The use of beads for sample pre-treatment, such as preconcentration, isolation, and separation, and for accommodation of chemical reactions has attracted increasing interest. Beads can be used as a removable solid surface in many analytical applications. It is very practical to use beads in a flow-based system, where beads can easily be moved in and out of the system using a flowing stream of reagent(s).

The bead-injection technique was first introduced to be used with a sophisticated computer-controlled sequential injection analysis system. There is no need to regenerate the bead surfaces because they are discarded after each use and are replaced by fresh ones. This helps to reduce the risk of contamination, denaturation, and system fouling, and also makes it possible to operate BI in the continuous flow system even if no suitable eluent for bead cleaning is found possible^{278, 279}.

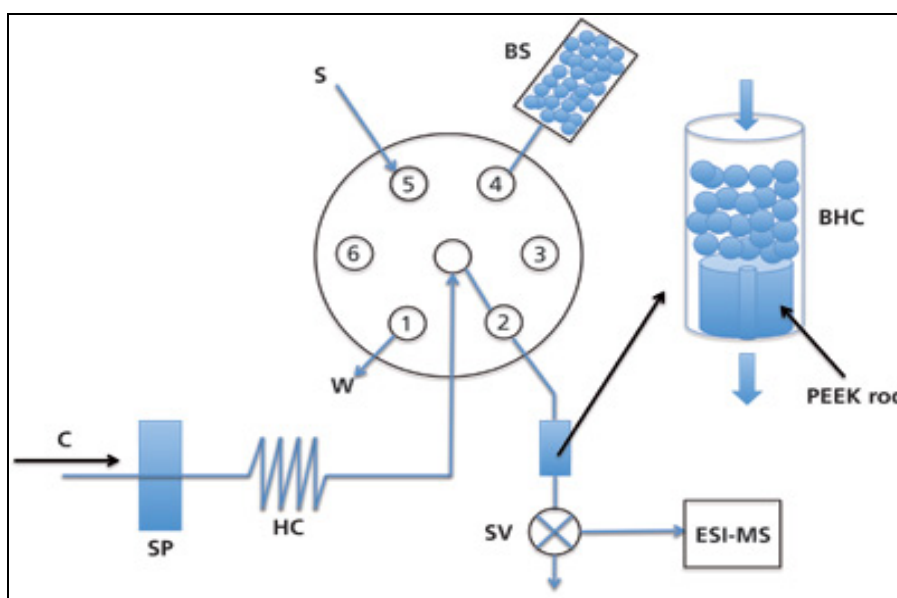


Figure 2.14 Illustration of a typical sequential injection lab-on-valve (SIA-LOV-BI) system. C = carrier, SP = syringe pump, HC = holding coil, SV = three-way solenoid valve, S = sample, BS = bead suspension, BHC = bead holding chamber, W = waste. Port 1: bead waste; port 2: bead-holding chamber; port 4: bead suspension; port 5, sample; ports 3 and 6 are not used in this particular setup.

Early BI techniques were coupled with the sequential injection analysis technique²⁸⁰. Beads were retained in a specially designed jet ring cell that lets only the solution pass through. There are two different forms normally employed. Micro-beads may first be trapped in a flow cell or column and then physically or chemically retain the analyte of interest. Upon eluting with a suitable solvent, the solution of the analyte is detected downstream.

There are examples of applications with this form of detection using ETAAS^{281, 282}. Another form is on-bead detection, where the change on the surface of the beads after interacting with the analyte is monitored directly using the detector located at the flow cell, or by transporting the beads into the detector. There are a number of examples of this form of detection using fibre-optic spectrofluorometry²⁸³, fluorescence microscopy²⁸⁴ and ETAAS²⁸⁵.

The SIA system has also been further developed into the lab-on-valve (LOV) system that comprises specially designed micro-channels on a piece of plastic integrated as a part of the multi-channel valve²⁸⁶.

The BI technique can be coupled to the SIA–LOV system and can be used in various applications, such as environmental studies, immunoassays²⁸⁷, and biological studies²⁸⁸. Beads can be trapped in an adjustable volume channel on the LOV.

Now, commercially available, LOV can be adjusted into two different volumes or path-lengths by moving the optical fiber. Detection can be done directly on the beads with the optical fibres that are made to fit the channel or can be done downstream via the eluted sample.

The main advantage of the SIA–LOV–BI system is that the micro-miniaturization of on-line sample pre-treatment and detection can be done automatically with various types of detectors^{108, 289, 290}.

2.2.4 Advantages of Flow-based analysis

- Applicable to a broad range of compounds by using a variety of simple photometric and electrochemical detectors.
- Low instrumentation costs.
- Low scheduled maintenance requirement.
- Unattended automated operation over an extended period of time provides a detailed picture of analyte profiles. This detailed information is not available when grab samples, or even composites, are taken and analysed at a later time and remote location. Unstable compounds can be measured in-situ.
- Accurate and precise sample manipulation.
- Quality control measures can be included to assure the integrity of the analytical results.

- A wide range of useful manifold components allow complex operations such as dilution, trace enrichment, gas permeation, dialysis, and several others to be incorporated into the analyser manifold.
- Constant flushing of the manifold lines minimizes the risk of fouling.

2.2.5 Components of a Flow Injection Analysis System

The assemblage of flow tubing, mixing coils, injection valve, etc., in a given configuration, used in a flow injection analysis system is referred to collectively as a manifold. The basic and major components of a flow injection analysis system are briefly described in this section.

Although there may be some variations design which can be acceptable, the common and essential characteristic for all components is that they can carry out their intended tasks reproducibly.

2.2.5.1 Pumps²⁶⁵

Pumps represent a propulsion system for delivery of carrier and reagent solutions. This is most frequently a peristaltic pump²⁶⁵, typically with the capacity to pump between four to eight carrier/reagent lines.

Reciprocating piston pumps used for liquid chromatography, and gas pressure or gravity-fed delivery systems may also be employed. Flow rates used in flow injection analysis systems typically vary from 0.5 - 4 ml.min⁻¹. Peristaltic pumps are a type of positive displacement pump used for pumping a variety of fluids. The fluid is contained within a flexible hose or tube fitted inside the pump casing. The actual pumping principle, called peristalsis, is based on alternating compression and relaxation of the hose or tube, drawing content in and propelling product away from the pump as shown in figure 2.14.

This process makes a peristaltic pump an accurate dosing pump or metering pump, with an equal amount of liquid dosed each time. The liquid being pumped never comes into contact with any moving parts because it is totally contained within the re-enforced hose or tube. A rotating shoe or roller passes along the length of the hose or tube creating a total seal between the suction and discharge sides of the pump. As the pump's rotor turns this sealing pressure moves along the tube or hose forcing product to move away from the pump and into the discharge line. Where the pressure has been released the hose or tube recovers creating a vacuum, which draws the product into the suction side of the pump, the priming mechanism.

Combining these suction and discharge actions results in a self-priming positive displacement pump, the peristaltic pump.

The perfect seal between the two sides of the pump means that there is no product slip, when coupled with the pump's linear speed-flow characteristic it makes peristaltic pumps ideal for dosing.

Additionally, as the pumped liquid is totally contained within the hose or tube, this makes a peristaltic pump a hygienic pumping solution with zero chance for contamination. This also reduces maintenance time as the hose or tube is the only wearing part.

Peristaltic pumps provide excellent problem solving pumping solutions especially when the product being pumped is particularly abrasive, corrosive or viscous. Their lack of valves, seals and glands makes them inexpensive to maintain the only maintenance item is the hose or tube. Peristaltic pumps also have a gentle pumping action, ideal for shear sensitive polymers and fragile cell cultures. Lastly, the only part of the pump in contact with the fluid being pumped is the interior of the tube or hose, making it easy to sterilise and clean the inside surfaces of the pump. Note that tubes need to be replaced regularly as they do become distorted.

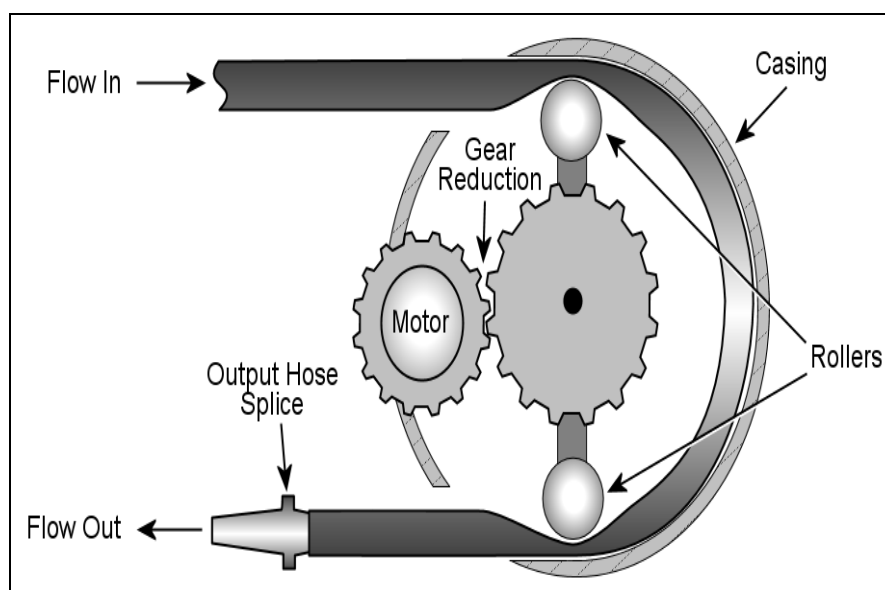


Figure 2.15 Peristaltic Pump Concept

2.2.5.2 Injection valve

Precision in FIA is dependent on accurate and reproducible injection. An injection valve is a sample injection device for reproducibly introducing a small volume of sample into the flowing carrier or reagent stream.

The most common injection device is a low pressure rotary 6-port injection valve (Figure 2.16)²⁹¹, the injection volume of which can be varied by changing the size of the attached injection loop. These may be operated manually, or actuated pneumatically or electrically.

Other injection systems used include the syringe flap-valve, solenoid-actuated commutator valves, coupled solenoid valves, or hydrodynamic injection achieved by a combination of intermittent pumping of carrier and sample. The injector may be connected to an autosampler for fully automated operation.

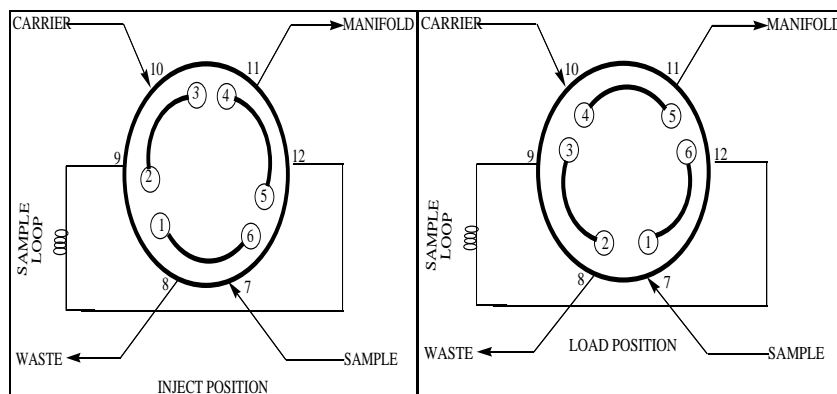


Figure 2.16 Six-Port Injection Valve. The valve configurations are shown in LOAD and INJECT positions.

2.2.5.3 Manifold design

As mentioned previously, a manifold is defined as an assemblage of flow tubing, mixing coils, injection valve, etc., in a given configuration, used in a flow injection analysis system. Flow Injection analysis systems can be configured in a wide variety of different modes, depending on the desired application. The simplest design is the single-stream manifold in which a stream containing reagent is pumped through the system. A volume of sample is injected into the stream and dispersion causes mixing of the reagent with the sample zone leading to chemistry between analyte and reagent as the zone passes through the reactor and detector. For situations where economy of reagent use is required, or there is an abundance of sample, such as oceanographic analysis, or continuous wastewater monitoring applications, reagent injection, or reverse flow injection analysis (Figure 2.17) may be employed. This entails the injection of reagent into a continuously pumped stream of sample, and results in economical use of reagents.

The tubing in which dispersion occurs is typically 0.5 to 1.0 mm internal diameter of a chemically inert material such as PTFE. Mixing of reagents is achieved using Y or T pieces of chemically stable material.

For chemiluminescence applications, where limited dispersion is required, the narrower tubing diameters, up to 0.5 mm id are preferred. Where delays are required, for slow reaction to take place, delay coils of dispersion tubing are used. Generally reactor tubing is wound in coils, however more complex formats such as knitted open tubular reactors have been recommended, in order to reduce dispersion while achieving adequate radial mixing^{9, 292}.

FIA systems are generally low pressure and push fittings are often sufficient for linking tubes, however, flanged and ferrule joints are also used. Joints must be smooth to avoid disturbances for laminar flow⁹.

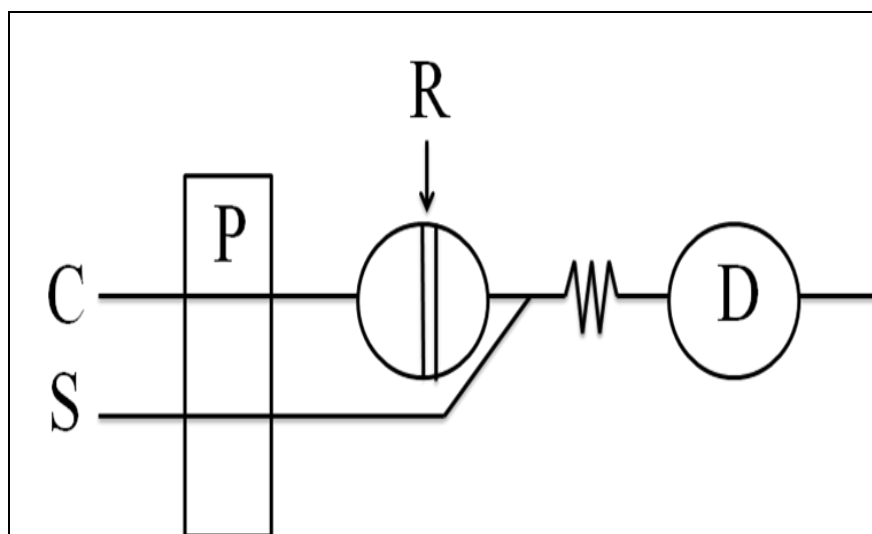


Figure 2.17 Schematic diagram of a reagent injection Manifold

where C, carrier solution; D, flow through detector; P, pump; R reagent solution; S, sample.

2.2.5.4 Detection Systems

The detection module in a FIA system depends on the product that has to be detected. FIA system can use whole arsenal of detection methods of modern analytical chemistry. While the interface between a flow injection system and a conventional detector is a commercial or laboratory-made flow cell, the interface to the high resolution detector has a decisive influence on the performance of the hyphenated system, as analytical quality parameters such as reproducibility, accuracy, sensitivity and selectivity are highly dependent on how the coupling is accomplished.

The complexity of the interface is very different depending on whether the measurement is performed in solution, plasma, or vacuum.

Optical detectors, including fluorescence and UV/VIS spectrophotometry, are the most common detection techniques, for biomolecular assays and for trace analysis of inorganic and organic molecules, used in FIA systems. And many reactions that convert the analyte (to suitable form for detection) to products which absorb light in visible or ultraviolet, or are fluorescent, have been automated in flow injection format.

Examples of analytes include cations^{9, 293}, anions^{9, 294} and organics species such as glucose^{9, 295}. Metals are also commonly detected by atomic absorption spectrometry^{9, 296}.

Spectrophotometric detector systems, including fluorometer which is optimal for very low level fluorometric and chemiluminescence assays, and the spectrometer which is optimal for absorbance assays from the UV through the NIR range are principal detectors of most of commercial FIA instrumentation.

Although FIA can be coupled to any detection system capable of flow-through operation covering a range that extends from simple LED-based optical systems to sophisticated mass spectrometers, UV–vis spectrophotometry seems to be the technique of choice for FI pharmaceutical applications. UV–vis spectrophotometry offers the advantages of simple, low cost instruments that are available at all laboratories.

Running costs are minimal and no highly-skilled personnel are required for their operation. Another significant advantage is that pre-existing batch instruments can be easily converted to flow-through by either home-made or commercially available cells²⁹⁷.

Although usually a photometric absorption detector is used, electrochemical detectors (potentiometry), atomic spectroscopy (AAS and AES) or mass detectors are also being used.

Electrochemical detectors in FIA systems, based on potentiometric, amperometric and conductimetric measurements, have been widely used for trace analysis of electroactive materials. The most common method is amperometric detection with a single disk (or plate) electrode maintained at constant potential²⁹⁸.

Recently, much attention has been focused on electrochemical flow-through voltammetric detection with scanning potentials in order to obtain three-dimensional information (such as time, potential and current)²⁹⁸.

Electroanalytical techniques are more prolific in innovations due to the wider possibilities for the design of probe-sensors that can easily be converted into flow-through sensors by insertion in the appropriate flow cell. Both voltammetric and amperometric measurements have been implemented in FI from the very beginning of the technique. Both conventional and new excitation modes have been applied to both commercial unmodified and chemically modified electrodes.

The conventional FI methods have been proposed for the determination of a number of analytes, such as trace metals, glycerol and acid phosphatase activity. Fast-scan and dual-pulse voltammetries have been used in FI for selective determination of methylmercury and ethanol in beer. Arrays of gold microelectrodes modified by electrodeposition of palladium for the determination of ascorbic and uric acids in urine or by electrocatalysis for carbohydrates and amino acids have also been reported. Stripping modes of electroanalysis have been coupled with FI as a means of preconcentrating the analyte, removing the sample matrix, and performing simultaneous determinations.

FI-stripping also gives other advantages, such as (a) in situ regeneration of film-mercury electrodes by passage through the flow cell of the appropriate dissolution of Hg(II) using a switching valve for introduction; (b) ability to exchange the stripping solution in order to avoid interferences during this step; and (c) ability to stop the flow during stripping for increasing reproducibility. In stripping voltammetry, mercury film electrodes have been the most commonly used due to their ability to regenerate the film in a continuous way.

Potentiometric stripping has most often used in situ formation of the amalgam by introducing the Hg(II) to the sample. Adsorptive stripping voltammetry with different types of electrodes depending on the analyte nature and different voltammetry modes has also been coupled with FI to produce significant integrating effects. An example of this phenomenon is a calibrationless determination of mercury based on FI stripping coulometry. Conductimetry and coulometry are less frequently coupled with FI.

Due to the short analysis time and feasibility for on-line system, flow-based systems have become one of the most powerful analytical tools in recent years. Various types of detection modes are applied to flow analytical techniques, and atomic absorption spectroscopy is one that is most commonly used sensors.

Flow analytical techniques coupled with AAS comprise those involving flow separation and/or preconcentration. For the ideal of on-line preconcentration, Cerutti and co-workers²⁹⁹ have described an on-line flow injection preconcentration-electrothermal AAS for the determination of traces of cobalt in drinking water.

2.2.5.4.1 Flow Injection Analysis and Chemiluminescence Detection

Chemiluminescence detection has been used extensively in procedures based on flow injection analysis (FIA) methodology¹¹, due in part to the excellent sensitivity and wide calibration ranges that have been obtained for diverse classes of analytes. Moreover, the instrumentation is simple, essentially comprising a reaction vessel or conduit with a transparent surface, mounted against a photodetector. The emission of photons from a chemiluminescence reaction is transient and occurs at a rate that is dependent on both the kinetics of the chemical reaction and the physical processes of solution mixing.

For the greatest sensitivity, the instrument manifold and the flow cell should be configured to maximize the emission and detection of light when the reacting mixture passes through the cell⁴.

For relatively fast chemiluminescence reactions, such as the oxidation of organic molecules by acidic potassium permanganate⁷ or tris(2,2'-bipyridine)ruthenium(III)³⁰⁰, the analyte and reagent solutions should merge at (or close to) the point of detection. In addition, the dead volume should be minimized to ensure rapid rinsing of the cell between analyses.

A variety of chemiluminescence detection cells have been described³⁰¹. The most commonly used configuration consists of a coil of glass or polymer tubing (normally 0.5-1.0 mm i.d.) mounted against a photomultiplier tube within a light-tight container. Solutions merge at a T- or Y-shaped junction shortly before entering the coil^{214, 301}.

As mentioned before, the most frequently used reagent for CL detection in FIA is luminol, which, when oxidised to 3-aminophthalate produces blue chemiluminescence. The luminol CL reactions coupled with flow injection analysis have been used to determine reducing agents, such as uric acid, ascorbic acid, cortisone, fructose and glucose¹⁰.

Some transition metal ions, and also a number of organic species, have a catalytic or an inhibiting effect on the luminol reaction with hydrogen peroxide, or oxygen, this is used for analytical determination. Luminol can be used for the very sensitive detection of hydrogen peroxide, in the presence of Cu(II) or Co(II). Several systems have been developed for the determination of transition metal ions. Determinations of Co(II) and Fe(II) are based on the catalytic effect these ions on luminol oxidation with hydrogen peroxide.

The same effect has been used in the determination of gold as tetrachloroaurate(III) in a reversed micellar system. Determinations of Zn and Cd have been based on their inhibition of the cobalt-catalysed generation of CL from luminol.

In addition to the use of luminol and peroxyoxalate, several applications in FIA CL have been reported for lucigenin. Luminescence is produced by the addition either hydrogen peroxide or an organic reducing agent to an alkaline solution of lucigenin. Chemiluminescence of acridinium esters (AE) was used for flow injection analysis of H₂O₂ in Natural Waters³⁰².

The most commonly used detectors in CL detection are the photomultiplier. Photodiode array (PDA) systems, charge-coupled devices (CCD) and photographic methods are also used. Systems available for detection of chemi- and bioluminescence have been reviewed^{9, 101}.

2.2.5.4.2 Photomultipliers Tube (PMT)

A PMT tube converts light into an electrical signal, and then amplifies that signal to a useful level by emission of secondary electrons. PMTs have traditionally been the workhorse detector in luminometers.

A typical photomultiplier consists of a photoemissive cathode (photocathode) which converts light flux into electron flux, an electro-optical input system which focuses and accelerates the electron flux, followed by an electron multiplier consisting of a series of secondary-emission electrodes (dynodes) and, finally an anode which collects the electron flux from the multiplier and supplies the output signal. The two phenomena fundamental to the operation of a photomultiplier are photoemission and secondary emission.

There are a number of factors that determine the performance level of PMT tubes. These include spectral response range, sensitivity, rise time, applied voltage, and gain.

The spectral response range of incident light the photomultiplier tube detects is also called the wavelength range. Sensitivity is a measure of the effectiveness of a detector in producing an electrical signal at the peak sensitivity wavelength. Rise time equates to the time necessary for the photomultiplier tubes' output to go from 10% to 90% of its final value. Applied voltage is the anode-to-cathode voltage of the photomultiplier tube. Gain is the factor by which the current generated by a photon is increased before the signal is detected, also known as current amplification.

As mentioned previously, PMTs have a high internal gain and are extremely highly sensitive detectors for low-intensity applications such as fluorescence spectroscopy.

In the photosensor field, photomultiplier tubes are known to have particularly high sensitivity, a broad dynamic range and applicability over a reasonably broad spectral range. PMT also have many advantages such as high-speed response time (1-15 ns), wavelength range (110-1100 nm), and quantum efficiency 1-10% (Q.E., number of electrons ejected by the photocathode/number of incident photons). Photomultiplier tubes have high bandwidth and noise-free gain on the order of a million. This makes them ideal for the detection of extremely low light or short pulses of light.

PMTs do have low dark currents leading to excellent signal to noise for low intensity samples. Some types of photomultipliers are designed to filter out some of the noise, which would negatively impact upon their ability to detect light. It is the dark current which limits instrumental contribution to the limit of detection.

Two types of filters include dark current protection and noise equivalent protection (NEP). Dark current is associated with a detector during operation in the dark with an applied voltage. Increased temperature and applied voltage will result in increased dark current. Also, larger active areas will generally have a higher dark current.

NEP deals with the power of incident light, at a specific wavelength, required to produce a signal on the detector that is equal to the noise.

PMT based systems operate in two basic modes, single photon counting and current sensing. There are examples of hybrid systems which are single photon counting to a light level in the low millions of photons/second and then switch to current sensing above that level.

PMT single photon counting systems are capable of exquisite sensitivity. Use of this type of detector is the method of choice for low light detection and quantitation as in, for example, detecting the ultra-weak luminescence associated with phagocytosis. The greater sensitivity comes at a cost however. Sample housings must be very light-tight. Moderate light levels saturate the detector; high levels can cause irreversible damage to the PMT.

PMT current sensing systems are also capable of excellent sensitivity and will often read higher light levels than single photon counting systems without damage.

There are differing opinions in the chemiluminescence instrumentation field regarding which system is "better", current sensing or single photon counting.

In a modern luminometer, both systems achieve excellent sensitivity and are easy to use. A proper understanding of the characteristics of each system should allow the user to choose the one best suited to the application.

There are two main types of PMT tubes, side-on photomultipliers and end-on Photomultipliers. Side-on detectors are more economical than end-on models, and have the faster rise times. They are ideal for photometry and spectrophotometry applications. The main disadvantage of these PMT tubes is their no uniform sensitivity. End-on photomultiplier tubes, sometimes known as head-on photomultipliers, offer better spatial uniformity and photosensitive areas from tens of square millimetres to hundreds of square centimetres.

Photomultipliers commonly used for chemiluminescence FIA systems have a good sensitivity in the range of 300 to 700 nm, which is appropriate for luminol λ_{\max} 425 nm and potassium permanganate λ_{\max} 680 nm. Many PMTs are supplied with two possible detectors. We do have the red sensitive PMTs which are better for manganese chemiluminescence systems.

2.2.5.4.3 Photodiode Systems

Photodiodes are solid state photodetectors, semiconductor light sensors that generate a current or voltage when illuminated by light. The term photodiode can be broadly defined to include even solar batteries, but it usually refers to sensors used to detect low levels intensity of light.

When a photon strikes a semiconductor, it can promote an electron from the valence band (filled orbitals) to the conduction band (unfilled orbitals) creating an electron(-) - hole(+) pair.

The concentration of these electron-hole pairs is dependent on the amount of light striking the semiconductor, making the semiconductor suitable as an optical detector. There are two ways to monitor the concentration of electron-hole pairs.

In photodiodes, a voltage bias is present and the concentration of light-induced electron-hole pairs determines the current through the semiconductor. Photovoltaic detectors contain a p-n junction that causes the electron-hole pairs to separate to produce a voltage that can be measured.

The photodiode spectral response can be in the X-ray, UV, visible, or IR regions. X-ray photodiodes are optimized for X-ray, gamma ray, and beta radiation detection. The photodiode spectral response can be measured in X-ray, UV, visible, or IR.

X-ray photodiodes are optimized for X-ray, gamma ray, and beta radiation detection. UV enhanced photodiodes are optimized for the UV and blue spectral regions. Visible photodiodes operate in the visible range without enhancement for operation in UV or IR. IR enhanced photodiodes are optimized for the near IR spectral region.

Photodiode arrays are packaged as multiples. Photodiode arrays will contain a certain number of elements (Photodiodes). Some photodiodes can be a position sensitive detector. Important photodiode performance specifications to consider include sensitivity, rise time, quantum efficiency, and operating temperature.

Sensitivity is a measure of the effectiveness of a detector in producing an electrical signal at the peak sensitivity wavelength. Rise time is the time necessary for a detector's output to go from 10% to 90% of its final value. A photodiode's capability to convert light energy to electrical energy, expressed as a percentage, is its quantum efficiency.

Photodiodes can have a noise factor. This is measured as the dark current and noise equivalent power. Noise equivalent power is the power of incident light, at a specific wavelength, required to produce a signal on the detector that is equal to the noise.

Common materials of construction for photodiodes include silicon, indium gallium arsenide, germanium, gallium nitride, and silicon carbide.

Photodiodes can be classified by function and construction as follows: PN photodiode, PIN photodiode, or APD (Avalanche photodiode). All of these types provide the following features and are widely used for the detection of the intensity, position, colour and presence of light. PN photodiodes feature a two-electrode, radiation-sensitive PN junction formed in a semiconductor material in which the reverse current varies with illumination.

PIN photodiodes are diodes with a large intrinsic region sandwiched between p-doped and n-doped semiconducting regions.

Photons absorbed in this region create electron-hole pairs that are then separated by an electric field, thus generating an electric current in a load circuit.

When the device's reverse-bias voltage nears breakdown level, the hole-electron pairs collide with ions to create additional hole-electron pairs, thus achieving a signal gain.

Silicon photodiodes convert light into an electrical signal. This conversion occurs when photons having more energy than the bandgap of the detector material are absorbed, exciting an electron from the valence band of the semiconductor to the conduction band, where it is read out as signal.

Silicon photodiodes are suitable for precision photometry, making them useful in medical instrumentation, analytical instruments, semiconductor tools and industrial measurement systems.

Avalanche photodiodes use the same process, but they generate internal gain using an avalanche multiplication process. An avalanche region is produced within the APD, creating an area of very high electric-field strength.

When a photogenerated (or thermally generated) electron in the conduction band moves into the avalanche region, the electric-field strength is sufficient to accelerate it to the point at which it can cause "impact ionization" and liberate another electron.

Both of these electrons can be accelerated as well, creating an avalanche multiplication. This process results in detector gain. Typical gains for an APD are in the range of ten to a few hundred.

Photodiodes are capable of recording higher light intensities than photomultiplier tube detectors. This facet makes them an excellent choice for applications where high light intensities are to be measured. However, the inherent dark current in solid state detectors is generally much higher than that of photomultiplier tubes.

One method of mitigating this problem is to cool the solid state detector via a thermoelectric cooler. Dark currents in solid state detectors drop dramatically with temperatures in the 0 to -30 degree Celsius range. Cooled detectors can then be used to integrate the light intensity for one to hundreds of seconds without the signal being overwhelmed by dark current.

Silicon photodiode detector has been used with chemiluminescence FIA systems. It has the advantages of being robust, stable, does not require a high voltage, and has a response over a wide range including red region. Although its sensitivity is less than that of a PMT, it has been used for the measurement of biocompounds in the industrial field^{10, 303}.

A miniaturised and integrated sensor accommodating both the electrodes and photodiode on the same silicon chip has been applied for the electrochemiluminescent measurements of codeine^{10, 304}.

2.2.5.4.4 Charge-Coupled Devices (CCD)

A CCD is best described as a semiconductor image chip, one face of which is sensitive to light, this is an array of light-sensitive pixels that are electrically biased so that they generate and store electrons - electric charge - when illuminated with light. The amount of charge trapped beneath each pixel directly relates to the number of photons illuminating the pixel. This charge is then "read out" by changing the electrical bias of an adjacent pixel so that the charge travels out of the sensor, is converted into a voltage and is then digitized into an intensity value. This action is performed for each pixel, to create an electronic image of the scene. The integrated-circuit chip contains an array of capacitors that store charge when light creates e-hole pairs. The charge accumulates and is read in a fixed time interval. In an imaging CCD the charge is generated by received photons, either optical or X-ray.

CCDs are used in similar applications to other array detectors such as photodiode arrays, although the CCD is much more sensitive for measurement of low light levels.

The principal advantages of CCDs are their sensitivity, dynamic range, linearity and good resolution but, are expensive and require extensive data handling capacity.

The sensitivity, or quantum efficiency, is simply the fraction of photons incident on the chip, which is detected. It is common for CCDs to achieve a quantum efficiency of about 80%. CCDs are also sensitive to a broad range of wavelengths and they are much more sensitive to red light than photomultiplier tubes used in photoelectric photometers. However, they have a poor response to blue and ultra-violet light. CCDs are sensitive to a wide range of light levels: a typical dynamic range (that is, the ratio of the brightest accurately detectable signal to the faintest) is about 10^5 , corresponding to a range of about 14.5 magnitudes.

The corresponding figure for a photographic plate is a range of less than about 1000 corresponding to 7.5 magnitudes. Furthermore, within this dynamic range the response is essentially linear: the size of the signal is simply proportional to the number of photons detected, which makes calibration straightforward.

2.2.6 Miniaturization through lab-on-a-chip (LOC)³⁰⁵⁻³⁰⁸

Lab-on-a-chip (LOC), also known as a "Micro Total Analysis Systems" (μ TAS) or microfluidics device is a term for devices that integrate and scale down (or miniaturized) all the stages of chemical analysis including sample pre-preparation, chemical reactions, analyte separation, analyte purification, analyte detection, and data analysis on a single microprocessor chip of only millimetres to a few square centimetres in size and that are capable of using extremely small fluid volumes on the order of nano to pico litres. Microfluidics is a broader term that describes also mechanical flow control devices like pumps and valves or sensors like flowmeters and viscometers.

However, strictly regarded "Lab-on-a-Chip" indicates generally the scaling of single or multiple laboratory processes down to chip-format, whereas " μ TAS" is dedicated to the integration of the total sequence of laboratory processes to perform chemical analysis. The term "Lab-on-a-Chip" was introduced later on when it turned out that μ TAS technologies were more widely applicable than only for analysis purposes.

The ability to perform laboratory operations on a small scale using miniaturized (lab on-a-chip) devices is very appealing. Recently, lab-on-a-chip devices have attracted great interest due to many advantages over conventional macro scale instruments, such as ease-of-use and portability, speed of analysis, low sample and reagent consumption, high reproducibility due to standardization and automation of chemical analysis, high-throughput screening, and online analysis.

Microfluidic systems have diverse and widespread applications. Lab-on-a-chip devices can be used to obtain a variety of interesting measurements including molecular diffusion coefficients, fluid viscosity, pH, chemical binding coefficients, enzyme reaction kinetics, etc. Other applications for microfluidic devices include capillary electrophoresis, immunoassays, and sample injection of proteins for analysis via mass spectrometry, DNA analysis, cell manipulation, cell separation, cell patterning and chemical gradient formation. Many of these applications have utility for clinical diagnostics.

Although the application of Lab-on-a-chip devices is still novel and modest, a growing interest of companies and applied research groups is observed in different fields such as chemical analysis including chemiluminescence.

Chemiluminescence as a detection method for micro sensing systems has the advantage of high sensitivity, low detection limits, and simple instrumentation compared with other spectrophotometric techniques, due to the exclusion of an external light source.

However, the drawback of this detection technique is the limited number of chemiluminescence reagents. Furthermore, since the chemiluminescence reagent needs to be mixed with the separated analytes before detection, a more complex microchip layout is required.

Miniaturization of detectors, such as CL detector, however, leads to problems due to the reduced analysis volumes mean a reduction in detection volumes, decreasing the number of analytes available for detection and making it more difficult to detect them.

Thus, the two main factors that affect the choice of the detection method for microfluidic devices are sensitivity and scalability to smaller dimensions. One solution is to interface the chip with a macro-scale detector such as a photomultiplier tube; this is called the “off-chip” approach.

This can be achieved, for example, by using optical fibres to carry light from the chip to the detector. An alternative solution – the “on-chip” approach - is to assemble a compact version of the detector and integrate this on the chip with the rest of the analytical system³⁰⁵.

Chemiluminescence detection offers high sensitivity, low detection limits and instrumental simplicity but requires a relatively complex manifold on the microchip, the details depending on the CL reaction system being used; for example, a Y-shaped channel junction works best when using peroxide-luminol chemiluminescence³⁰⁹, while a V-shaped junction yielded better results with the peroxalate–peroxide system³¹⁰. Reagent is delivered by a micro pump. The chip design must ensure that a high proportion of the emitted light enters the off-chip photomultiplier; this frequently involves coupling with an optical fibre.

Such an arrangement typically achieves micro molar detection limits and has been used for a range of analytes including catechol and dopamine²⁷, amino-acids³¹¹, cytochrome c and myoglobin³¹² as well as the determination of chip-separated chromium(III), cobalt(II) and copper(II).

Horseradish peroxidase can be determined at sub-nanomolar levels. Micro molar concentrations of ATP (adenosine triphosphate) can be measured by means of luciferin-luciferase bioluminescence.

The effect of antioxidants has been measured using a microfluidic system incorporating peroxy-oxalate CL, by injecting the antioxidants into the hydrogen peroxide stream³¹³. The method is simple and rapid and excellent analytical performance is obtained in terms of sensitivity, dynamic range and precision. Electrochemiluminescence detection has been applied for microchip separations using electrodes installed during fabrication.

Photodiodes have been fabricated into chips at the bottoms of the microfluidic channels and have been used for on-chip CL detection of DNA produced by the polymerase chain reaction and separated on the same chip by capillary electrophoresis³⁰⁵.

These devices have been used also to detect luminol CL for the micro molar determination of hydrogen peroxide generated by the oxidation of glucose with glucose oxidase.

Thin-film organic photodiodes can be fabricated by vacuum deposition and integrated into chips. Copper-phthalocyanine-fullerene small molecule diodes have high quantum efficiency and have been used to determine hydrogen peroxide by peroxy-oxalate chemiluminescence. Another example has been used for hydrogen peroxide determination by luminol chemiluminescence.

2.3 Stopped-flow Technique

Stopped-flow is a technique for studying the mechanisms and kinetics of fast, liquid-phase chemical and biochemical reactions initiated by the rapid mixing and stopping (stopped-flow) of the reactants and reagents.

A spectroscopic probe (absorbance or fluorescence) is employed to follow the course of the reaction by recording changes in the amplitude of the spectroscopic signal as a function of time. This section describes the principle and applications of stopped-flow technique in both spectrophotometry and chemiluminescence.

2.3.1 Principle of Stopped-flow technique

Stopped-flow technique was first introduced by Chance³¹⁴ and has been reviewed Crouch³¹⁵ and Gomez-Henz³¹⁶. Stopped-flow is one of a number of techniques used to study biomolecular interactions, kinetics and fast reaction mechanisms, typical of many reactions in chemical and biological systems. In the simplest form of the technique, two reactant solutions are rapidly mixed by being forced into a mixing chamber, and then through an observation cell. At some point in time, the flow is suddenly stopped, and the reaction monitored using a suitable spectroscopic probe, such as absorbance, fluorescence or chemiluminescence. The change in the spectroscopic signal as a function of time is recorded.

When measuring the kinetics of a reaction it would be ideal to be able to mix the reactants and periodically sample the mixture in order to analyse the reactant or product. Unfortunately, for some reactions the time required to mix the reactants together may be comparable to the reaction time. That is, the half-life of the reaction occurs on approximately the same timescale as the mixing. This results in an uncertainty in both initial concentration and initial time.

A stopped-flow method can be used when reactions occur under these conditions. Figure 2.18 is a diagram of the stopped-flow apparatus. In this method, the reactants are injected simultaneously into a mixing chamber, where they begin to react, then moved quickly through a spectrophotometer cell and finally to a stopping syringe. This stopping syringe fills and drives its plunger back against a stopping block. This stops the flow and triggers the activation of data acquisition on a computer. The progress of the reaction is followed by monitoring a change in absorbance of either a reactant or product in the spectrophotometer cell. The time that is required for the reactant and products to travel to the spectrophotometer cell is known as the “dead time.” In this method the mixing time plus the dead time is on the order of milliseconds, which allows for reactions with half-lives of milliseconds or tens of seconds to be measured.

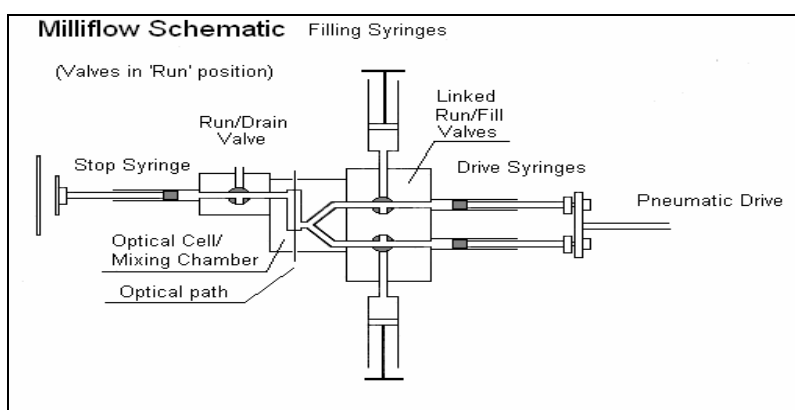


Figure 2.18 Schematic diagram of a stopped-flow system

Mixing options for stopped-flow include multi-mixing (also known as double mixing or sequential mixing) where more than two solutions are mixed together, variable ratio mixing using different size syringes and micro volume mixing for applications where only very small quantities of reactants are available. The performance of a stopped-flow instrument is determined to a large extent by the dead-time. This is defined as the minimum time after the reactant have mixed that the observation starts.

The dead-time is essentially the age of the reaction as it enters the observation cell. The limiting factor in the dead-time of a particular stopped-flow apparatus is determined by the distance between the mixer and the cell, and the final velocity of the flow at the instant the flow is stopped.

Another factor which can affect the dead-time is the efficiency of the mixer. Typically, dedicated stopped-flow instruments can achieve dead-times in the region of a millisecond. Using ultra-small observation cells, dead times of less than 0.5ms can be achieved. Typically however, the true experimental limitation is the rate of mixing of solutions of the two reactants.

Companies offering modern stopped-flow instruments that are sensitive, equipped with good user-friendly software, are Hi-Tech Scientific (Salisbury, UK), Applied Photophysics Ltd. (Leatherhead, UK), Bio-Logic-Science Instruments SA (Claix, France), Olis Incorporated (Bogart, GA, USA) and KinTek Corporation (Austin, TX, USA). This work has employed extensively the stopped-flow equipment from Applied Photophysics Ltd for the investigation of the oxidation reaction of potassium permanganate and other manganese oxidising agent with organic compounds.

2.3.2 Application of Stopped-flow technique in Spectrophotometry

The range of applications for stopped-flow spectroscopy is huge and many thousands of examples of its use can be found in the literature.

Stopped flow spectroscopy is an established technique for acquiring kinetic data on dynamic processes in chemical and biochemical reactions.

Spectrophotometry is the most widespread method for the detection of several compounds in stopped-flow technique because of its versatility and low cost. Stopped-flow has lent itself to UV/Vis detection methods – both by absorption and fluorescence spectroscopy and these are still the most common methods employed. The study of enzyme catalysis, protein refolding, signal transduction, ligand or drug binding to proteins or DNA and kinetics of coordination chemistry are numbered among the many applications of stopped-flow spectroscopy.

Stopped-flow spectrophotometers allow the following of reaction kinetics, initiated by the mixing of two (or more) reactants, from the millisecond time range onwards, using changes in various optical probes, like fluorescence and absorbance. This allows a very diverse range of mechanism of many different types of biochemical reactions to be studied in great depth.

Biochemical reactions carried out by enzymes are fundamental to the metabolic processes of catabolism, and anabolism. Similarly the binding events and signal modifications that are carried out by signalling and receptors proteins are important in the control functions of an organism. Studies of the mechanisms of these important biochemical agents allows insights into how an organisms functions at the molecular level.

The kinetics of biochemical reactions involves the study of rates of chemical processes involved in many processes. Measurements of the rates of reactions under different experimental conditions (for instance pH, solvent, concentration and temperature) allow the construction of models that describe the characteristics of a biochemical reaction.

This model provides insights into the reaction mechanisms involved in the reaction. The most important mechanistic reactions can be broadly classed as binding events, and enzymatic catalysis.

One area of particular interest at the moment is the study of protein folding/refolding. Protein folding is the physical process by which a polypeptide folds into a characteristic three dimensional structure. Formation of the 3D structure is essential for the protein's functions. Understanding these processes is essential for both academic and pharmaceutical research. Protein folding/refolding reactions have been the subject of detailed kinetic studies using stopped-flow method. The mechanism of folding/refolding is usually monitored by following changes in spectroscopic signals after stopped-flow mixing of denaturant unfolded protein into native solvent conditions.

For example, in an interesting application of stopped-flow spectroscopy technique, folding and assembly kinetics of procaspase-3 were studied by Sara L. et al³¹⁷.

In enzyme kinetics, enzymatic reactions catalyse the conversion of metabolites and are the agents that carry out the large variety of specific chemical reactions in biology.

As with all chemical kinetics, understanding of the number and rate of reactions, and the building of reactions models around this information can provide profound insights into the mechanism of actions at the chemical level for enzymatic reactions.

Stopped-flow has long been a key technique for understanding enzyme kinetics. Single and multi-substrate reactions can be followed with stopped flow techniques to study the catalytic mechanism of an enzyme, and to learn about its role in the cell.

Mechanisms can be investigated by changing reactant concentrations, and by adding fluorescent dyes to the protein to enable observation of movements during reactions.

For example William Cooper et al used stopped-flow spectroscopy for elucidation of the complete kinetic mechanism of a mammalian HSD using rat 3 α -HSD of the aldo-keto reductase superfamily (AKR1C9) with the substrate pairs androstane-3,17-dione and NADPH (reduction) and androsterone and NADP⁺ (oxidation) and identification of all enzyme forms on the reaction coordinate³¹⁸.

Ligand binding reactions, such a protein-ligand binding and release, are fundamental to all biochemistry, from signaling pathways to binding of reactants in enzymatic reactions. The stopped-flow spectrophotometer is particularly powerful tool to study the kinetics of binding reactions, using fluorescence and other optical probes.

This can provide information about the mechanisms of binding, and the energies involved. For example, stopped-flow spectroscopy technique was successively used to identify a new class of heme-binding oxygen sensors, reveal their unusual phylogenetic origin, and propose a sensing mode of a member of this class³¹⁹.

A common application of stopped-flow is fast tracking of transient kinetics of water (or solute) transport across the membranes of small (10-500 nm scale) vesicles. These reactions can be generated by mixing purified membrane vesicles with a hyperosmotic solution. The concentration gradient induces a fast flow of water out of the vesicles. The volume of vesicles is reduced in a kinetic reaction.

Although stopped-flow mixing technique is most frequently used to obtain fundamental information about rapid chemical reactions (rate law information, rate constants, activation energies, etc.), it has also been used for analytical purposes^{133, 320}.

For example, Pulgarin et al³²¹ used stopped-flow mixing technique to determine simultaneously morphine and naloxone by time-resolved chemiluminescence. There are several reasons why the stopped-flow technique has considerable potential in the analytical laboratory. First, with moderately rapid reactions, stopped-flow mixing can provide analytical information in a very short time, often in a few seconds or less.

A second reason why stopped-flow mixing should gain increasing acceptance in analytical chemistry is the extremely small solution volumes required to obtain analytical information. Often, reaction-rate or endpoint methods can be carried out with sample volumes as small as a few microliters. The stopped-flow technique can also be completely automated to eliminate manual manipulations of reagents and to provide rapid and reproducible mixing of reactants.

These latter features are, of course, desirable even for measurements on reactions which are normally considered slow. Finally, the increasing use of minicomputers and microprocessors with stopped-flow systems for control, data acquisition, and data processing should lead to a higher level of automation with significant increases in measurement throughput, accuracy, and precision.

2.3.3 Application of Stopped-flow technique to Chemiluminescence

Several fast reaction kinetics do not result in measurable changes in absorbance. Some of them, however, do exhibit a change in chemiluminescence as the reaction progresses. Examples include organic and inorganic oxidation and reductions.

The use of a stopped-flow system equipped with fluorescence measurement facilities can, therefore, considerably extend the scope of this already powerful technique.

The combination of stopped-flow mixing technique with chemiluminescence as a detection method was first used by Chance et al³²² to study the kinetics and mechanism of chemiluminescence light production from the reaction of luciferin-luciferase-oxygen system.

Advantages of chemiluminescence detection in relation to wide calibration ranges, the high sensitivity and its potential, when combined with advantages of stopped-flow, such as rapid

and highly efficient mixing of sample and reagents, immediate detection of chemiluminescence signal and the ability to record the whole CL intensity vs. time profile, make stopped-flow chemiluminescence technique a valuable analytical tool to the determination of reaction rates and mechanisms, which are essential for understanding chemical processes.

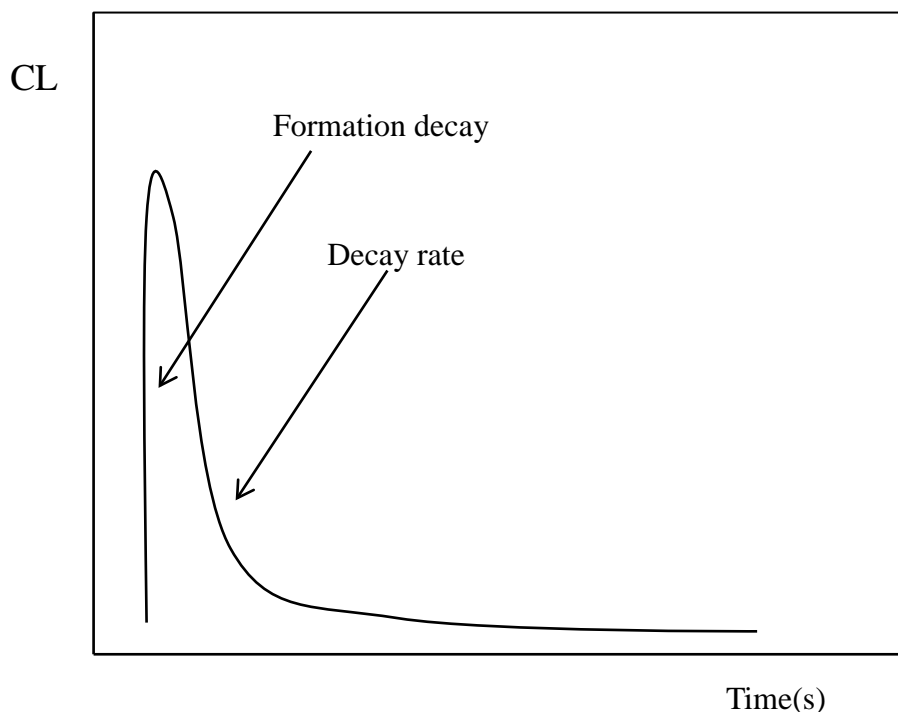


Figure 2.18 Intensity-Time profile for a stopped-flow signal output showing zones used for determination of rates of formation and decay

CL reactions involving acidic KMnO_4 ⁷, peroxyoxalates¹¹, firefly luciferase³²³⁻³²⁵, luminol³²⁶, acridinium esters¹⁹³ and tris(2,2'-bipyridine)ruthenium(III)³⁰⁰ are being used in stopped-flow technique to determine their kinetic parameters, such as formation and decay rates, and to identify the reaction mechanisms.

An example of stopped-flow chemiluminescence technique was used to investigate the temperature-dependent kinetics of the imidazole-catalysed peroxyoxalate reaction in order to further elucidate the reaction mechanism. Pseudo-first-order rate constants were obtained from the chemiluminescence intensity vs. time profiles³²⁷.

2.4 Permanganate Oxidations

This section focuses on the interaction of manganese-based oxidising agents with organic and inorganic materials and begins with a background discussion of the physical and chemical properties, relevant reactions, and application in chemiluminescence analysis.

The greatest advantage of this oxidant over others is that it is the source of the chemiluminescence produced in the reaction; with slight discrepancies, there is wide consensus that

the actual emitting agent is an intermediate product of the reduction of Mn(VII) rather than the oxidation product of the analyte or organic substrate.

However, the mechanism behind the emission remains controversial. The central role of this oxidant in the production of CL justifies its extensive analytical use; however, why it exhibits no emission under specific conditions where other oxidants do, remains unexplained.

2.4.1 Permanganate Chemistry

Potassium permanganate, KMnO_4 , is a purple crystalline compound with a metallic sheen. It is soluble in water, in acetone and in methanol, but it is decomposed by ethanol. Potassium permanganate is prepared by fusing manganese dioxide with potassium hydroxide to form the potassium manganate and then electrolyzing the manganate solution using iron electrodes at about 60 °C.

Acidic permanganate oxidation reactions have been known for a long time and reviewed³²⁸, as well as the reaction mechanisms put forward to account for the kinetic and other experimental data for oxidation by permanganate³²⁹.

However, the reaction stoichiometry, kinetics and mechanisms involving permanganate in chemiluminescence systems are quite complex and are not fully understood.

Manganese species have the potential valence states ranging from +1 and +7, of which the +2, +3, +4, and +7 states are the only ones that are relatively stable over a wide range of acidity. Manganese in permanganate has the highest oxidation state.

This VII-state occurs in the oxo compounds MnO_4^- , Mn_2O_7 and MnO_3F . Permanganate which is the most commonly used reagent in chemiluminescence analytical applications. It is relatively stable to thermal decomposition but not to photolytic decomposition (both in the solid form and in solution).

Manganese(VII) is reduced to Mn(II) during oxidation processes presumably via many manganese species having different oxidation states such as Mn(VI), Mn(V), Mn(IV) and Mn(III). The appearance of these intermediate oxidation states depends upon various reaction conditions, types of substrate and their stability.

A few compounds of Mn(V) species are frequently postulated as intermediates in the reduction of MnO_4^- . Although Mn(II) is the most stable oxidation state, it is quite readily oxidized to Mn(IV) in alkaline solution. The reactivity of these intermediates states depends on the nature of the substrate and on the pH of the medium.

The standard redox potentials in acidic media of Mn(VII)/Mn(II), Mn(VII)/Mn(IV), Mn(IV)/Mn(III) and Mn(III)/Mn(II)¹⁰ are presented in Figure 2.20.

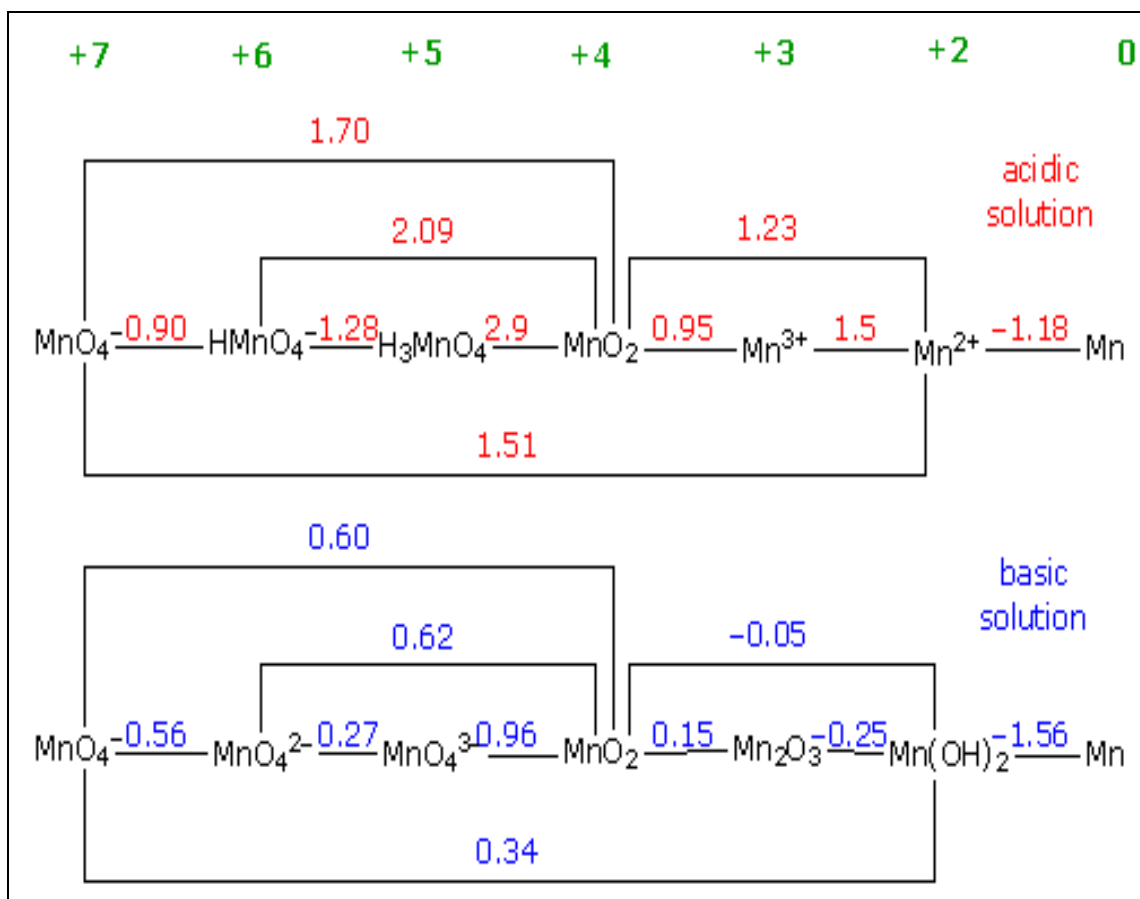


Figure 2.20 Standard Reduction Potentials (V) at 25 °C for Manganese Species³³⁰

Oxidation with permanganate may occur via several different mechanisms: electron exchange, hydrogen atom abstraction and direct donation of oxygen. The rate of permanganate oxidation, as well as, the reaction pathway that occurs may vary with the substrate and the reaction conditions, such as, the pH of the medium.

In alkaline, neutral, and weakly acid solution, permanganate is reduced to manganese dioxide, which precipitates out of solution³³¹.

In strongly acid solution, the permanganate ion is further reduced, and the valence of manganese changes from VII to II. All reactions are exothermic. Permanganate solutions in acidic condition are less stable than in neutral conditions, but unless the solutions are boiled, the decomposition is still relatively slow.

Concentrated permanganate solutions in alkaline conditions can also slowly decompose to produce oxygen and manganate, which is unstable and can slowly disproportionate to permanganate and manganese dioxide.

The general physical and chemical properties of permanganate are listed in Table 3.2.

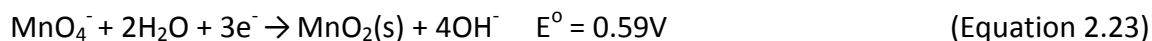
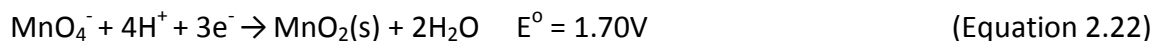
Table 2.1 Properties and characteristics of permanganate

Property	Descriptions
Chemical formula	KMnO ₄
Purity (% by weight)	Technical grade = 98%
Molecular weight	158.03 g/mol
Solid density	2.703 g/cm ³
Bulk density	~ 1605 kg/m ³
Form and features	Dark purple solid with metallic lustre, sweetest astringent taste, odourless, granular crystalline, oxidize
Solubility in distilled water:	
0°C	27.8 g/L
20°C	65.0 g/L
40°C	125.2 g/L
60°C	230.0 g/L
Aqueous solubility	S = 30.55 + 0.796T + 0.0392T ² (T in °C) S = 62.9 g/L at 20 °C
Aqueous specific gravity	Sg = 1.000 + 0.007C (C: the concentration of KMnO ₄ in %w/w)
Specific conductance	Sc (mS/cm) = 0.7002C + 0.0915 (C: the concentration of KMnO ₄ in %w/w)
Average Mn-O bond distance	0.1629 ± 0.0008 nm
Average O-Mn-O bond angle	109.4 ± 0.7°
Stability	Stable indefinitely if held in cool dry area in sealed containers
Incompatibilities	Avoid contact with acids, peroxides, and all combustible organics or readily oxidisable materials. In neutral or alkaline conditions, it is not corrosive to iron, mild steel or stainless steel. However, chloride corrosion may be accelerated.
Materials compatibility	Plastics such as polypropylene, PVC, epoxy resins, and Hypalon are suitable but Teflon FEP and fibbers are often incompatible.

In acidic solution, MnO₄⁻ is reduced to manganese(II) if excess of reducing agent is present (E° = 1.5V), whereas in the presence of excess permanganate, MnO₂ is formed as a result of the oxidation of Mn(II) by MnO₄⁻. The presence of Mn(V) could not be directly demonstrated, as it is too unstable in acid medium³³². Mn (IV) is directly reduced to Mn(II), and Mn(III) is formed by reaction between Mn(IV) and Mn(II).

MnO₄⁻ follows three overall redox reactions according to pH. The pH also has a significant effect on the kinetics of MnO₄⁻ oxidation. The reaction follows the half-reaction pathway represented by the equation 2.21 under acidic conditions (pH < 3.5) and in the typical environmental range (3.5 < pH < 12) the primary reaction follows equation 2.22 or equation 2.23 depending of the pH, and finally at high pH (pH >12) the reaction follows equation 2.24³²⁹.

The most common permanganate reaction employed in CL detection is the complete reduction of permanganate to manganese(II).

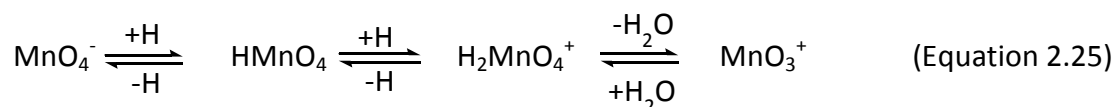


The reduction potential (E°) for the formation of MnO_2 in acid solution is much higher than in alkaline solution, +1.70V (Equation 2.23) compared with +0.59V (Equation 2.24). Although the redox potential of permanganate ion decreases with increasing pH, many organic compounds, such as alcohol and formic acids, are oxidised faster at higher pH.

With many organic substrates, mechanistic factors are of major importance in contrast to the overall free energy change of the oxidant³²⁸.

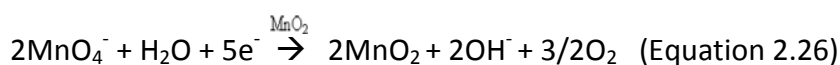
Rudakov, Lobachev and Zaichuk^{299, 333} have studied the oxidation of organic compounds with different permanganate species. Manganese(VII) in an aqueous solution can be present in the form of the permanganate anion, permanganic acid (HMnO_4), or permanganyl cation (MnO_3^+) depending on the pH of the medium.

It was determined through kinetic studies that the reaction with MnO_4^- dominates at a pH greater than 2.5, whereas at a pH less than 0.3 the reaction of HMnO_4 dominates. To study the reactivity of MnO_3^+ the reactions were carried out in very acidic perchloric acid solution ($\text{HClO}_4 = 3.5 \text{ M}$)³³³. The following scheme represents the different reactive species that can form depending on the pH,



The pK_a of HMnO_4 is -2.2. H_2MnO_4^+ is a hydrated species, which upon loss of water can form a perchloric complex ($\text{ClO}_3\text{OMnO}_3$)³³³. The rates of organic substrates oxidation by Mn(VII) species increases in the series $\text{MnO}_4^- < \text{HMnO}_4 < \text{MnO}_3^+$.

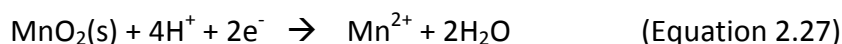
Permanganate can also react with water and auto decompose, but at very slow rates, resulting in manganate, which is unstable and can slowly disproportionate to manganese dioxide³²⁸ according to the Equation 2.26.



Permanganate solution in acidic condition is less stable than in neutral conditions, unless the solution is boiled; the decomposition is still relatively slow.

However, the presence of MnO_2 can catalyse the decomposition of permanganate solutions, though the extent of the catalysis is not known. Thus, traces of MnO_2 initially present in the permanganate solution, or formed by the reaction of permanganate with reducing agents, such as, organic matter may lead to a catalysed decomposition of permanganate.

In acidic solutions, the MnO_2 can be reduced slowly to Mn^{2+} :



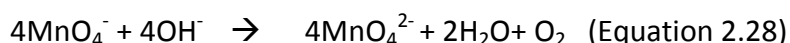
Permanganate can serve as a multiple equivalent oxidant depending on the characteristics of the substrate that is attacked. For example, under basic conditions, sulphide can be oxidized to sulphate by excess permanganate while sulphur and tetrathionate might also be produced due to incomplete oxidation of sulphide in neutral or acidic solutions³²⁸. Permanganate can also easily oxidize metal ions (e.g., ferrous iron, chromium ion, and vanadium ion) from reduced states to oxidized states.

Permanganate is a strong oxidant so only few oxidants (e.g., solid bismuthate in acid, ammonium persulfate, lead dioxide, potassium periodate, and ozone) are able to oxidize manganese ions to permanganate³²⁸.

Permanganate has a unique affinity for oxidizing organic compounds containing carbon-carbon double bonds, aldehyde groups or hydroxyl groups. It was also suggested by Stewart³²⁸ that "permanganate oxidation for organic compounds is often, but by no means always considerably faster in alkaline than in neutral solution" because a change of the organic substrate (e.g., ionization of alcohol) might occur in a basic solution. However, a general phenomenon is that the oxidation rate is accelerated in strongly acidic conditions due to a conversion of MnO_4^- ion to the more active oxidant, permanganate acid.

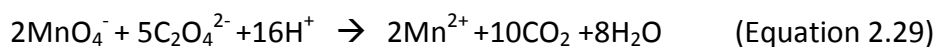
Permanganate may oxidize organic compounds via different reaction pathways^{328, 334}. The reaction pathway that occurs significantly depends on the structure of the substrates and the pH of the solutions. Other reaction conditions such as temperature and the concentrations of MnO_4^- and the target compound also influence the rate of the oxidation reaction.

It has been shown that alkaline permanganate solutions, in the absence of an oxidizable substrate, undergo decomposition and oxygen gas is evolved from solutions, according to the Equation 2.28, and further reduction of the manganate does not occur. The higher the pH of the solution, the greater is the rate of evolution of oxygen³³⁵.



The kinetics of acidic permanganate oxidation of oxalate was first studied by Harcourt and Esson^{329, 336}.

The effects of permanganate and oxalate concentrations were investigated, and as the stoichiometry is precise, the reaction is used to standardise volumetric permanganate solutions, according to the following reaction (Equation 2.29).



It was observed that the initial rate of this reaction is relatively slow (long induction period) but, the deliberate addition of manganese(II) sulphate considerably increases the reaction kinetics up to the $\text{MnO}_4^- : \text{Mn}^{2+}$ ratio of 2:3 and eliminates the initial slow reaction.

In neutral conditions or the presence of excess permanganate MnO_2 is formed as a result of oxidation of Mn(II) by permanganate and Guyard reaction becomes as following Equation (2.30):

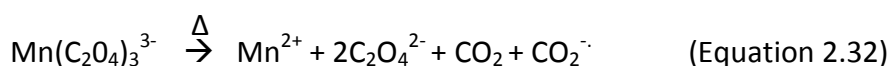


Under acidic conditions therefore, manganese(II) produced in most permanganate oxidations plays an autocatalytic role in many of these reactions. It is suggested that manganese(II) reacts with permanganate, whereby increases the reaction rate, to yield manganese(III) as an intermediate product, which is expected to react immediately with organic substrate or organic daughter products to form manganese(II).

Equation 2.30 is called Guyard reaction which describes the exchange between Mn(VII), Mn(IV), and Mn(II), and can be used for the volumetric determination of manganese. The relative amount of oxidation done by the two species depends on their concentrations, which are governed by the disproportionation reaction³³⁷ (Equation 2.31):



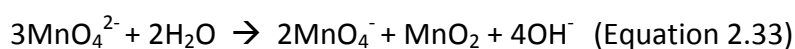
However, the disproportionation reaction can be stabilised in several ways, such as by, increasing the acidity of the medium, the addition of pyrophosphate³³⁸, azide³³⁹, a large excess of Mn(II) or fluoride ions³⁴⁰. The latter complexes Mn(III) in the form of MnF_4^- and this equilibrium is often used to identify or prove the presence of Mn(III) as oxidising intermediate entity during MnO_4^- oxidation reactions. Complexes are readily broken down on increasing the temperature of the reaction, for example the manganese(III)-trioxalato complex formed is readily broken down at 60 °C (Equation 2.32). A mechanism involving a radical anion intermediates has been proposed³⁴¹. The formation of this complex is one of the reasons that permanganate-oxalate titration are normally carried out at higher temperatures. The use of surfactants or crown ethers³⁴² has been proposed to prevent formation of trioxalato complex and so increase the rate of reaction in oxalate-permanganate titrations⁹.



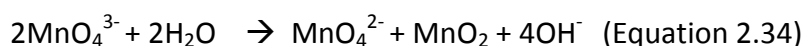
Koupparis and co-workers³⁴³ used stopped-flow injection to monitor the disappearance of permanganate ions at 525 nm, in the first step of the reaction. They found that the reaction is first order in permanganate and Mn(II) and second order in oxalate ions, and used this relationship as the basis of a kinetic measurement of manganese(II)⁹.

Manganese(VI) and manganese(V) are stable only in very alkaline solutions, although they are both formed as intermediates in the reduction of permanganate in moderately basic and acid solutions. Therefore, the study of Mn(VI) and Mn(V) could not be carried out in this work, as they are highly unstable in acid medium and very difficult to monitor.

Manganate ion Mn(VI), at concentrations less than 1.0M in solution of hydroxide ions, slowly undergoes the disproportionation reaction (Equation 2.33) to MnO_4^- and MnO_2 .



Manganate and hypomanganate Mn(V) oxidations are found to be much slower than permanganate oxidations. Hypomanganate Mn(V) solutions disproportionate (Equation 2.34) very slowly at lower concentrations than 4.0M in hydroxide ion solutions.

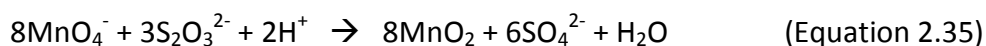


It was shown that manganese(V) is an intermediate in the oxidation reaction of hydrogen peroxide by basic permanganate solution, however no chemiluminescence light was observed and reported for permanganate oxidation in alkaline medium⁹. Despite the fact that Mn(VI) and Mn(V) in acidic medium disproportionate more rapidly than they react with organic substrates, a solution of acidic manganese(V) was generated by reduction of permanganate with arsenious acid^{10, 344}. Reactions of Mn(VI) have been studied by fast acidification of a stable alkaline manganate(VI) solution.

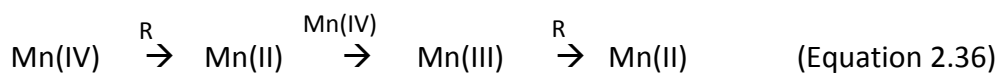
The short-lived manganese(V) produced is unstable due to disproportionation reaction, but would react rapidly with some reductants, such as alcohols and can be stabilised by phosphorous acid^{10, 344}.

As seen previously, manganese(IV), as manganese dioxide, is one of the compound produced by disproportionation reaction and is usually a blackish or brown insoluble solid. Manganese dioxide can be also produced by the oxidation reaction between permanganate and thiosulphate³⁴⁵ (Equation 2.35).

However, if diluted neutral solutions are mixed in stoichiometric ratio, colloidal sols can be prepared³⁴⁶. These can be used as oxidizing agents without the normal solubility problems associated with MnO_2 .

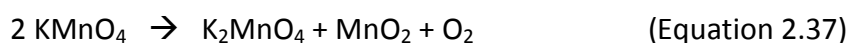


The colloidal sols are stable, probably due to anions on the surface of the colloidal particles. At pH four to five, manganese dioxide is reduced by oxalic acid and the following reduction sequence (Equation 2.36) has been proposed where R stands for the reductant⁹.



It has been suggested that manganese(II) is produced directly in the first step, and when sufficient formed, reacts with Mn(IV) to generate Mn(III), which then reacts with more reductant. Other workers have suggested that Mn(III) is formed directly^{9, 347} in the first step, rather than Mn(II). The formation and reduction of colloidal manganese dioxide have been used as an explanation³⁴⁸ for the apparent oscillatory kinetics in the permanganate-oxalate reaction^{349, 350}. Recently, soluble MnO₂ in orthophosphoric acid has been prepared and used as CL reagent for the determination of a variety of organic compounds^{9, 218, 351}.

Manganates(VII) are not very thermally stable. Thermal decomposition of KMnO₄ produces layered MnO₂ having characteristics for battery applications and it is also the material that stains one's skin when handling KMnO₄. For instance, potassium permanganate decomposes at 230 °C, according to equation (2.37) below:

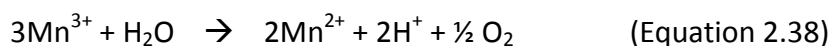


Although KMnO₄ is the form the most utilised in permanganate oxidation reactions, copper permanganate has been used to improve specificity of some oxidations^{352, 353}.

Aqueous MnO₄⁻ solutions are reasonably stable if kept in the dark room, but they undergo photochemical decomposition with evolution of oxygen and precipitation of manganese dioxide, under light influence, which accelerates the reaction of MnO₄⁻ decomposition⁹.

Manganese(III) has been obtained in solution via three routes; oxidation of Mn(II) by chemical and electrochemical methods, reduction of manganese(IV) or reduction of Mn(VII)³⁵⁴.

Mn(III) is slowly reduced by water, according to the following reaction (Equation 2.38):



Most organic compounds are degraded by aqueous permanganate to carbon dioxide on extended heating, however, in alkaline solutions, oxalate ions can be the major product of the degradation reactions. These oxidations are often faster in alkaline than in neutral solutions. In strongly acidic medium, permanganate is protonated to produce HMnO₄ (Equation 2.25).

The broad reactivity of permanganate with organic compounds is used in the preparation of pure and drinking water, where distillation from permanganate results in water free from organic contaminants.

The permanganate oxidation reaction is also used in methods for chemical oxygen demand or permanganate index in water³⁵⁵. Some regulatory authorities, including the EU, consider that the permanganate oxidation reaction is too general and prefer the use of methods based on dichromate oxidation reaction.

The mechanisms for different organic substrates suggested by various authors are not similar, depending upon the nature of the reactive manganese species, the reaction environment and the nature of the substrate. One of the principal aims of many workers in the field of acid permanganate oxidations has been the attempt to formulate modes of oxidation and to classify reactions between permanganate and organic compounds by the mechanism according to which the oxidation proceeds.

Tompkins and his collaborators³²⁹ have attempted to show that there are two principal mechanisms by which organic compounds are oxidized by acid permanganate; one mechanism proceeds by direct oxidation by the permanganate ions, and the second involves the prior formation of the MnO_2 ions and subsequent oxidation by hydroxyl radicals produced from these ions and water molecules.

It is postulated that the radical mechanism is characterized by an initial induction period, while the direct oxidation by the permanganate ions is of the second order throughout. Alcohols and olefinic compounds undergo oxidation by MnO_4^- ions through the formation of a substrate-Mn(VII) complex, which finally decomposes to give the desired products.

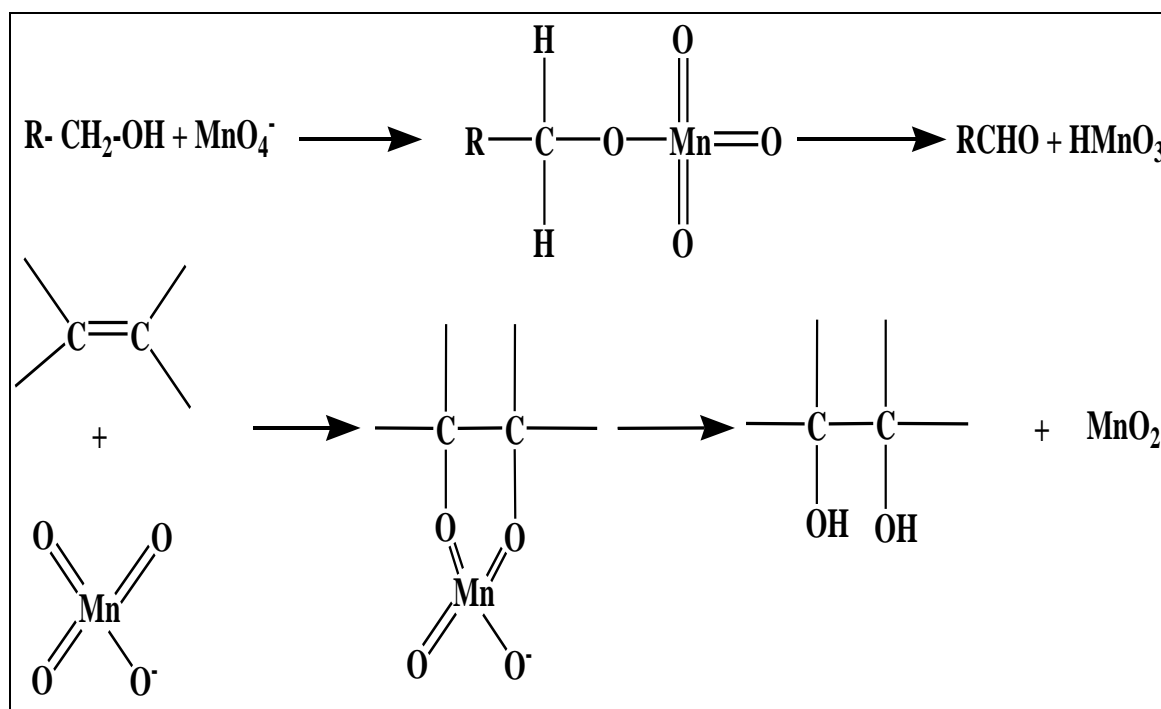
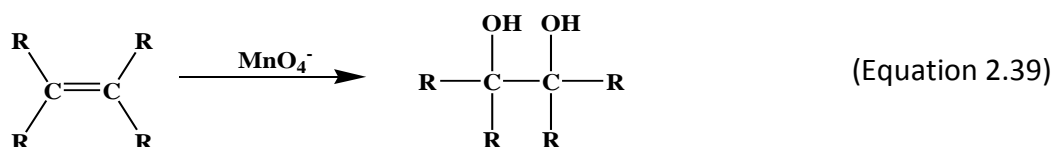


Figure 2.21 Proposed mechanism for permanganate oxidation of alcohols and olefinic compounds³⁵⁶

The oxidation of carbon–carbon double bonds by permanganate ions is an important, in a mechanistic as well as from a synthetic prospective. Under alkaline conditions, olefins are converted into the corresponding diols in good yield³⁵⁶⁻³⁵⁹, while in neutral or slightly basic solutions α -hydroxy ketones are produced³⁵⁹.

These reactions are always accompanied by a certain amount of C–C bond cleavage³⁶⁰ and, under acidic conditions, the cleavage products predominate^{361, 362}.

Aqueous permanganate was used originally for the conversion of alkenes into diols according to Wagner dihydroxylation reaction (Equation 2.39).



Owing to the rapidity and the complex mechanism of the permanganate oxidations, the mechanisms of oxidation of various olefinic derivatives are still poorly understood. Permanganate oxidations of alkenes and their derivatives have been suggested to be associated with a cyclic manganese(V) intermediate. In a kinetic study of the permanganate oxidation of maleic by a stopped-flow technique at acidic pH, Simandi et al³⁶² have found that the rate determining step is cis attack of permanganate on the double bond, resulting in the formation of a cyclic intermediate (1) containing manganese(V). A manganese(V) species could not, however, be detected and this is reduced in a fast process, which leads to a detectable intermediate, Mn(III), and formyl(hydroxy)acetic acid.

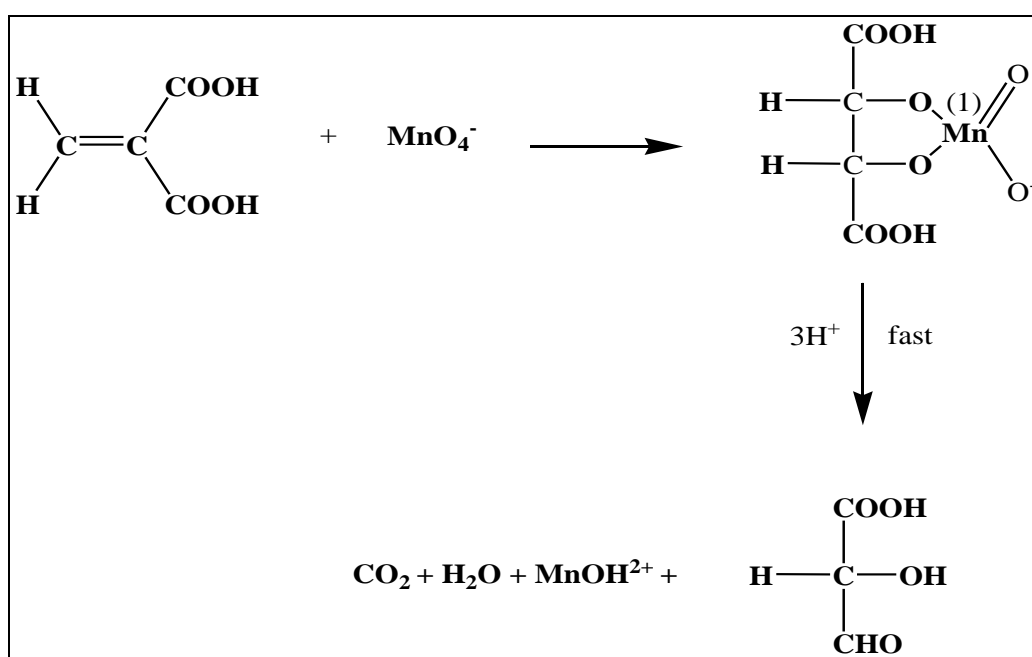


Figure 2.22 Proposed mechanism of permanganate oxidation of maleic acid³⁶¹⁻³⁶³

As mentioned previously, hypomanganate esters are formed as intermediates in the oxidation of alkenes by potassium permanganate.

The transition state for the second step (oxidative decomposition of the ester) probably contains a fairly well developed carbonyl group as evidenced by both isotope and substituent effects. Under these conditions, the latter step is much slower and it controls the overall rate of the reaction. Accepting that the hypomanganate esters are the initial intermediates in these reactions under all conditions, a mechanism has been proposed in Figure 2.23. The fate of the hypomanganate ester is entirely dependent upon the reaction conditions.

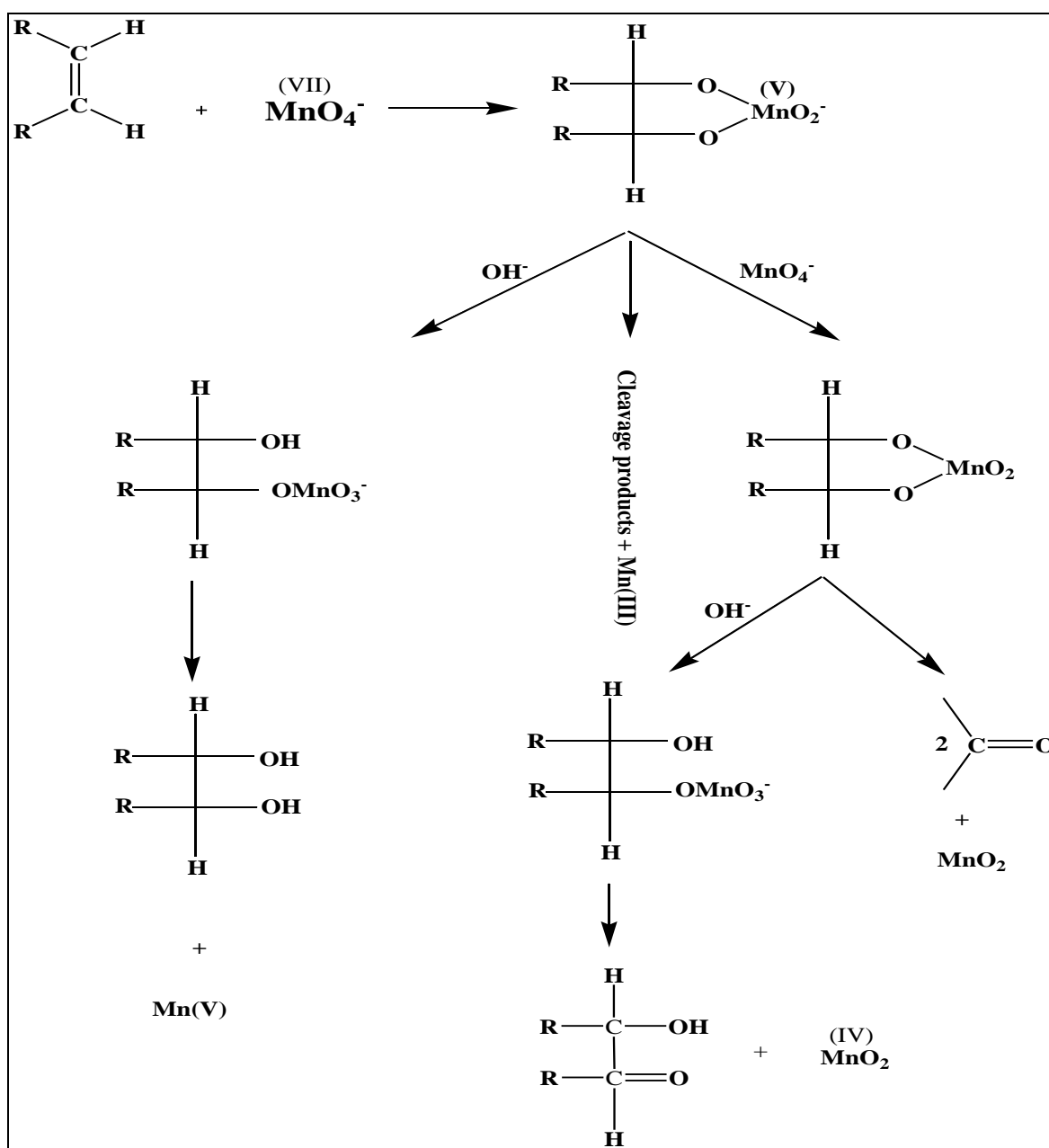


Figure 2.23 Proposed mechanism of the conversion of alkenes into diols and α -hydroxy ketones by permanganate³⁵⁶

Permanganate oxidations of many other classes of organic compounds have been studied including aromatic acids and polyphenols^{364, 365}, aldehydes³⁶⁶, amino acids^{367, 368} and carbohydrates^{367, 369, 370}. The oxidation of ascorbic acid by acidic permanganate has been investigated and a mechanism of the reaction has been proposed³⁷¹.

Mn(VII) was assumed to be the most probable oxidising species, as the addition of sulphate, pyrophosphate, fluoride and Mn(II) ions to the reaction mixture did not affect the rate of the reaction. The following is the proposed mechanism of the reaction.

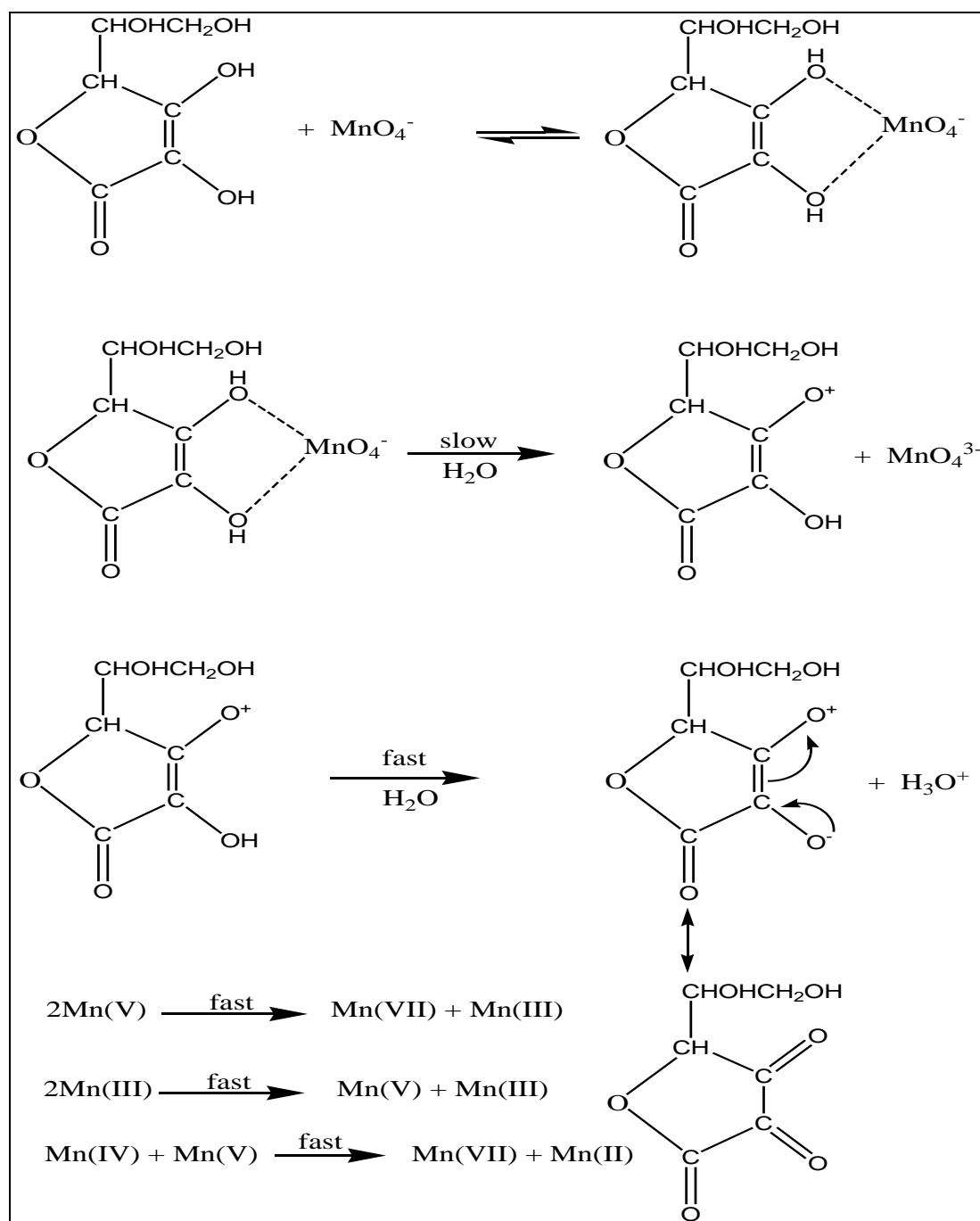


Figure 2.24 Proposed mechanism of permanganate oxidation of L-ascorbic acid^{9, 371}

2.4.2 Permanganate Applications

Permanganate ion has been for a long time one of the most versatile and widely employed oxidizing agents in diverse chemical reactions in the laboratory and in industry.

It is an oxidising agent with disinfectant, deodorising and astringent properties. Among its applications, it is primarily used for the purification of drinking water, cleaning of swimming pools, and treatment of industrial wastewater.

As mentioned previously, it acts as a general oxidant, attacking all organic material, converting them ultimately into carbon dioxide and water. It reacts over a wide range of pH and requires no additional catalyst. Potassium permanganate has long been a suitable oxidant to neutralize some of these pollutants and many studies are progressing in this direction.

In environment pollution, MnO_4^- has been successfully used for the *in situ* degradation of many organic contaminants. Potassium permanganate is a suitable oxidant to oxidise some of these pollutants and many studies are progressing in this direction.

For example a study was undertaken to understand fully the kinetics and mechanism of the oxidation of trichloroethylene (TCE)³⁷², an important pollutant present in ground water, using potassium permanganate. The study was undertaken to identify the reaction products, elucidate the reaction pathways and their pH dependence, develop a kinetic model and determine the rate constants for all of the major reactions in the $\text{KMnO}_4/\text{TCE}/\text{H}_2\text{O}$ system.

In analytical chemistry, acidic solutions of permanganate are used as a chemiluminescence reagent. During the oxidation of organic compounds, potassium permanganate is reduced, depending on the pH, to manganese(II) or dioxide and the reduced manganese dioxide can be recycled. The recycled manganese dioxide can be used as a mild oxidant, as catalysts in batteries, as pigments in paints and dyes, and as raw material for permanganate production. The recycling of manganese dioxide has made the usage of potassium permanganate environment friendly.

Most analytical methods based on direct CL measurements involve oxidizing the analyte with potassium permanganate in a strong (sulfuric) acid.

In fact, permanganate is the most common oxidant used in CL reactions; cephalosporin and penicillin class antibiotics appear among the drugs determined most frequently with this reagent by the FIA–CL technique. Within a comprehensive review by Hindson and Barnett⁶ concerning a wide range of analytical applications of permanganate in CL reactions, potassium permanganate in acidic media, with or without CL enhancers or promoters, has been used to determine a wide variety of compounds, including pharmaceuticals, biomolecules, antioxidants, illicit drugs, pesticides and pollutants⁷.

For example, the determination of amidopyrine, benzocaine, procaine and other local anesthetics, cefadroxil, codeine, imipramine, levodopa, medazepam, methotrexate, naltrexone, perphenazine, promethazine, reserpine, salicylamide, tetracyclines and tetrahydropalmatine in pharmaceutical preparations⁷. All gave good recoveries and agreement with official or standard analytical methods.

2.4.3 Cautions

As mentioned previously permanganate is a chemical used in various applications: topical antibacterial, photography, laboratory chemical, wood dye, water purification and bleaching processes. Ingestion and other exposures to the chemical can cause various symptoms.

The type and severity of symptoms varies depending on the amount of chemical involved and the nature of the exposure.

Solid KMnO_4 is a very strong oxidizer, which when mixed with pure glycerine, will cause a highly exothermic chemical reaction to take place. This reaction would turn red hot as a spontaneous "combustion" which would melt a glass or other container holding the reacting contents and could ignite anything flammable nearby. A reaction of this sort could take place when solid KMnO_4 is mixed with many kinds of organic materials. Aqueous solutions of KMnO_4 are much less dangerous, especially when diluted. Mixing solid KMnO_4 with concentrated sulphuric acid causes an explosion.

KMnO_4 stains the hand and clothing and should be handled with care. Clothing stains may be washed away using acetic acid or hydrochloric acid. Skin stains go off within 48 hours. It causes corrosive burns on the skin, while swallowing it may lead to gastroenteritis. In addition, mixing solid KMnO_4 with concentrated hydrochloric acid generates lethal chlorine gas.

Potassium Permanganate is reduced to MnO_2 when exposed to light. This reduction is noted by the formation of brown precipitate in the reagent container. Storage in an amber glass container is recommended.

2.4.4 Chemiluminescence from manganese-based oxidation reactions

As mentioned in the previously sections, manganese compounds have the potential valence states ranging from +1 and +7, and manganese in permanganate (Mn^{7+}) has the highest oxidation state. Many of these compounds have been proposed as the reactive oxidants responsible for oxidation by permanganate resulting in CL. Almost every oxidant intermediate has been suggested as participating at some stage of the reduction of permanganate.

A variety of manganese oxidants, as chemiluminescent reagents, in acidic or alkaline media have been investigated for various analyses using flow injection CL method.

As manganese(VI) and manganese(V) are regarded as short-lived undetectable intermediates, it is the purpose of this section to review exclusively the oxidation reactions resulting in chemiluminescence by Manganese-based oxidants, such as potassium permanganate[Mn(VII)], manganese(IV) and manganese(III).

2.4.4.1 Chemiluminescence from Permanganate

Potassium permanganate, in acidic media, with or without CL enhancers, has been widely used in analytical chemistry⁷.

The permanganate-based CL methods are mainly based on the direct oxidation of the analyte by KMnO_4 , or based on the enhancement of CL intensity of the permanganate-analyte system, using substances, such as formaldehyde, glyoxal, formic acid, surfactants, etc., as a sensitizer. For example, the reduction of acidic MnO_4^- has been used for the determination of morphine in biological fluids for forensic applications²⁴ and for process analysis during the extraction of opiate alkaloids from opium poppies using flow injection analysis³⁷³.

Based on the number of published articles, sulphuric acid and polyphosphoric acid are the most preferred medium for permanganate-based CL reactions. However, the suitability of sulphuric or polyphosphoric acid is also subject of controversy.

The optimization of the acidic medium mostly shows that the use of sulphuric acid leads to better reproducibility. The role of polyphosphoric acid is double: on one hand, it provides the required acidic medium for the oxidation, and on the other hand it acts as promoter of the CL since it most likely stabilizes reaction intermediates¹¹⁸. Similar role is played by polyphosphate (hexametaphosphate) in sulphuric acid medium³⁷⁴.

The presence of chemical additives such as sensitizers or media can increase the emission intensity even by several orders of magnitude. Surfactants such as; Tween 60¹¹⁸, benzalkonium chloride⁹⁸, protect the microenvironment of CL emitter through formation of micelles or they can facilitate energy transfer¹¹⁸. β -cyclodextrin also protect the emitter and minimize the non-electromagnetic emission pathway during relaxation of the excited species³⁷⁵.

As mentioned previously, many fluorophores have been tested and proposed in different drug determinations. Quinine^{374, 376, 377}, glutaraldehyde³⁵, formaldehyde^{121, 153, 378, 379} and formic acid¹¹⁹ were utilized as fluorophores where the energy from excited state of intermediate or products is transferred to this fluorescing compound which is the final emitter. Cephalosporines³⁷ were determined by MnO_4^- -induced CL enhanced by glyoxal as sensitizer.

Chemiluminescence detection was used for drug determination in complicated matrices, such as human serum by using on-line solid-phase extraction and SIA³⁷⁴. The authors determined salbutamol that was initially adsorbed from the matrix on a cartridge packed with sili-

ca-gel (modified with carboxylic acid) and then eluted by sulphuric acid; the CL determination of eluted salbutamol was performed by oxidation with permanganate in sulphuric acid medium.

The transformation of non-chemiluminescent compounds into CL intermediates by prior UV-irradiation is a real possibility how to achieve CL reaction. Photo-induced CL was employed for the determination of chloramphenicol³⁸⁰ and sulphonamides³⁸¹. A screening test for the development of photo-induced FIA-CL of pharmaceuticals has been also reported³⁸².

The use of acidic potassium permanganate CL to determine a wide variety of compounds (e.g. drug, biomolecules, antioxidants, illicit drugs, pesticides and pollutants) in pharmaceutical and clinical samples, agricultural and environmental matrices, food and consumer products and materials is reviewed in tables 2.2; 2.3; 2.4 below.

Despite its widespread use, as with other solution chemiluminescence reactions, the detailed mechanism is not unambiguously resolved.

Agater⁹ showed that the emission spectrum for permanganate oxidations does not depend upon the reductant and that permanganate, manganese dioxide (sol) and manganese(III) chemiluminescent oxidations also give the same emission spectrum. From this, it was deduced that the emitting species involved manganese presumably just prior to the last stage, that is formation of Mn(II). This is consistent with the earlier observation by Karavaev³⁹¹ that the emission spectrum for Mn(III) oxidation of malic acid matches that of photo-excited Mn(II). Despite these results, which have been independently confirmed recently³⁸³, some other authors have suggested singlet oxygen, sulphur dioxide, and fluorescent oxidation products of the analyte as the emitting species⁶.

Earlier work in these laboratories^{9,10}, which showed that Mn(III) is particularly important in the chemiluminescence, has provided one of the bases for this investigation.

2.4.4.2 Chemiluminescence from manganese(IV)

Like permanganate, the oxidation reaction of manganese(IV) with a variety of organic compounds and inorganic species in acid media is accompanied by CL emission that can be enhanced by some low molecular weight aldehydes such as formaldehyde, and which has been exploited for the development of a range of highly sensitive analytical procedures²¹⁹.

The excited species formed by the manganese(IV) oxidation is probably electronically excited manganese(II) species. Lu and co-workers³⁸⁴ proposed that singlet molecular oxygen is the emitter of the chemiluminescence emission accompanying the reaction between manganese(IV) and formaldehyde in the presence of various analytes. However, subsequent spectroscopic investigations lead by Barnett and co-workers^{7, 112, 219, 385} on the chemiluminescent reactions of manganese-based oxidants (e.g. permanganate, manganese(IV) and manga-

nese(III) with various organic compounds revealed striking similarity in the chemiluminescence spectra between these manganese oxidants.

These investigations into the light-producing pathways of these reactions have revealed that many lead to the same broad red emission with maximum intensity at 735 ± 5 nm, which has been attributed to an electronically excited manganese(II) species.

Calatayud and co-workers³⁸⁶ immobilised solid manganese dioxide in an on-line reaction column (using a polyester resin) for the chemiluminescence determination of isoniazid. The manganese oxidant did not directly participate in the light-producing reaction; detection was based on the inhibition of a luminol–H₂O₂–hexacyanoferrate(III) system by manganese(II) ions that were released when isoniazid reacted with the immobilised oxidant³⁸⁶.

In contrast, Lin and co-workers used the reaction between analgin, rhodamine B, and solid manganese dioxide immobilised on sponge rubber within a chemiluminescence flow cell for the determination of analgin³⁸⁷.

Using flow injection analysis (FIA) methodology, analytically useful chemiluminescence responses were obtained from the oxidation of twenty five organic and inorganic species^{218, 385}. As with many chemiluminescence reactions with permanganate, the addition of formaldehyde was found to significantly enhance the emission of light³⁸⁵.

Since this initial evaluation, a further fourteen publications^{127, 219, 384, 388} have emerged on the use of soluble manganese(IV) as a chemiluminescence reagent for the determination of various organic compounds. The majority of studies on chemiluminescence reactions with soluble manganese(IV) used formaldehyde as an enhancer^{127, 219, 384, 385, 388}, which can increase the emission intensity by over two orders of magnitude²¹⁹. In Barnett and co-workers investigations, formaldehyde was included in the carrier and/or sample solutions at concentrations between 0.2 M and 3.0 M^{127, 219, 385}, whereas Lu and co-workers have used formaldehyde concentrations of 3–4% (1.0–1.4 M)^{384, 388}.

A range of other potential enhancers (formic acid, polyphosphates, surfactants, β -cyclodextrin, sodium thiosulfate, sodium sulphite and quinine sulphate) have been tested^{127, 384, 385, 388} and although these species generally provided inferior or no enhancement, there were some circumstances where an alternative enhancer was more suitable^{127, 384}. A combination of 0.4 M formaldehyde and 1% (m/v) sodium hexametaphosphate was reported to provide the best signal-to-background response for the reaction of soluble manganese(IV) with ascorbic acid¹²⁷.

Lu and co-workers examined a range of potential enhancers for the reaction between soluble manganese(IV) and fluoroquinolone antibiotics and found that sodium sulphite (1×10^{-3} M) gave a fourfold increase in chemiluminescence intensity compared to the same reactions in the presence of formaldehyde³⁸⁴.

The rate of the light-producing reactions between the soluble manganese(IV) reagent, various analytes and formaldehyde have been examined with stopped-flow experiments^{219, 385}. In most cases, the chemiluminescence time courses reached a maximum between 0.5 s and 6.0 s after the reaction was initiated, and returned to baseline within 15–70 s²¹⁹. However, the light-producing reaction between the manganese(IV) reagent and potassium oxalate was found to persist for several minutes³⁸⁵.

A wide range of compounds have been found to elicit light upon reaction with soluble manganese(IV) and in many cases, limits of detection have been reported. There have been several studies in which the chemiluminescence responses from various analytes have been compared^{219, 385} but as yet, no discernable trend with respect to molecular structure and intensity has emerged. However, it is clear that the selectivity of the soluble manganese(IV) reagent is markedly different to that of acidic potassium permanganate^{219, 385}.

For example, limits of detection for morphine and codeine with permanganate in an aqueous polyphosphoric acid environment differ by over three orders of magnitude (1×10^{-10} M and 3×10^{-7} M, respectively)^{214, 389}, but their limits of detection with soluble manganese(IV) are quite similar (5×10^{-8} M and 1×10^{-8} M)²¹⁹.

Using FIA methodology, the soluble Mn(IV) reagent has been used to determine numerous pharmaceuticals in commercial formulations³⁸⁴. Similarly, vitamin C and tyrosine have been determined in tablets and injections using FIA and SIA¹²⁷.

Validation and interference studies using common excipients suggested that this reagent was sufficiently selective for accurate measurement of the target analytes in these relatively simple matrices. Limits of detection in these procedures were between 3×10^{-9} M and 1×10^{-6} M, and the dynamic ranges typically covered 1.5–2.5 orders of magnitude.

Lin and co-workers described a FIA system that incorporated a flow-through detector packed with solid manganese dioxide immobilised on sponge rubber, which they used to establish dissolution profiles of analgin tablets³⁸⁷.

The limit of detection (8×10^{-5} M) was over three orders of magnitude poorer than that reported in subsequent publications for the determination of analgin with soluble manganese(IV).

The detection of drugs and biomolecules in more complex matrices (such as biological fluids) with soluble manganese(IV) necessitates the separation of the analyte from interfering species^{219, 384, 388}. One approach, adopted by Lu and co-workers for the determination of analgin, indomethacin, indapamide, and tamoxifen in urine, involved the selective adsorption of the analyte in a glass column packed with a molecular-imprinted polymer.

Once the analyte was absorbed, the interferences were washed away and the chemiluminescence reaction was initiated by pumping the manganese(IV) reagent through the column.

In each case, a formaldehyde solution was used to both rinse the column and enhance the chemiluminescence reaction. The total analysis time (3–5 min) was significantly longer than that required for FIA, but the selectivity was much greater.

The responses for urine samples that did not contain the target analytes were only 1–5% higher than blank signals obtained with double-distilled water (compared to 230–450% higher using FIA)^{384, 388}.

The precision of the molecular imprinted polymer approach (2.4–4.1% RSD) was slightly poorer than that of the FIA procedures without isolation of the target analyte (1.1–3.4% RSD). Urine samples from volunteers who had consumed pharmaceutical formulations were analysed, but the results were not validated against conventional methodology. Good percentage recoveries were reported for urine spiked with the analyte. The lifetimes of the purpose-built columns were not discussed^{384, 388}.

The same research group has published several similar procedures for the determination of pharmaceuticals in urine based on acidic potassium permanganate CL^{388, 390, 391}.

Alternatively, CL detection can be coupled with chromatographic separations, for the determination of multiple analytes in complex samples containing interfering species.

Although post-column chemiluminescence detection with soluble manganese(IV) has not as yet been applied to real samples, Barnett and co-workers have demonstrated the determination of six opiate alkaloids using a commercially available monolithic column²¹⁹. The six analytes were separated in under 4 min using gradient elution, and detected by merging the column eluate with a formaldehyde solution and then with the soluble manganese(IV) reagent within a chemiluminescence detector. The relative standard deviation for retention time and peak area was <0.3% and <4%, respectively. The limit of detection for each of the six analytes was approximately 5×10^{-7} M (when an injection volume of 2 μ L was used).

The use of manganese dioxide sol chemiluminescence to determine a wide variety of compounds, including pharmaceuticals, pollutants, etc. is summarised in Table 2.5.

2.4.4.3 Chemiluminescence from manganese(III)

As mentioned above, manganese(III) has been shown to generate chemiluminescence. Junghänel and co-workers³⁹² reported that the oscillating manganese(II)-catalysed Belousov–Zhabotinskii system (i.e. the oxidation of malonic acid with bromate catalysed by the repeated interchange between manganese(II) and manganese(III)) evoked a periodic emission of light with a maximum intensity at 630 nm, which they attributed to excited molecular oxygen formed by the recombination of HO₂ radicals.

However, Karavaev et al. subsequently showed that this emission (which they found to be most intense at 680–720 nm) was a result of the reduction of manganese(III), and postulated that the emitter was electronically excited manganese(II)³⁹³, noting the similarity of the emission with the corresponding photoluminescence reported by Sveshnikova and Stroganov³⁹⁴.

Several research groups have developed analytical methods based upon chemiluminescence from reactions with manganese(III) species.

Watanabe et al. found that the oxidation of glyoxal in a tartrate buffer using either a manganese(III)–lactate complex or a combination of hydrogen peroxide and manganese peroxidase, produced an emission of light with maximum intensity at 700–710 nm^{218, 395}.

Using FIA methodology, Zhang and co-workers developed a method for the determination of isoniazid, based on the CL reaction with a manganese(III) reagent that was generated on-line by constant-current electrolysis of manganese(II) sulphate in acidic solution^{221, 393}.

Previous investigations by Barnett and co-workers in their laboratory have included an examination of chemiluminescence reactions with a manganese(III) reagent prepared by adding excess manganese(II) sulphate monohydrate to the soluble manganese(IV) solution, or by adding freshly precipitated manganese dioxide and manganese(II) sulphate monohydrate to a solution of sodium hexametaphosphate¹¹².

The chemiluminescence spectral distributions for the reaction of sodium tetrahydroborate with these reagents matched those recorded for reactions with either manganese(IV) or permanganate reagents¹¹², and were each attributed to an electronically excited manganese(II) species.

The on-line electrogeneration of manganese(III) from manganese(II) has been applied to the chemiluminescence determination of a wide range of analytes.

This approach is not limited to manganese(III); other oxidants such as hypochlorite, hypobromite, silver(II) and cobalt(II), which are either unstable in aqueous solution or undesirable to prepare off-line, have been generated for CL reactions in a similar manner³⁹⁶.

In several reports of the electrochemical generation of manganese(III) for chemiluminescence detection, the reagent was prepared by constant-current electrolysis of manganese(II) sulphate in acidic aqueous solution, within a flow-through electrochemical cell containing a platinum working electrode. The reagent solution then merged with the analyte/carrier stream (or column eluate) at a T-fitting, before the reacting mixture entered the detection cell^{221, 229}. A later approach involved merging the manganese(II) sulphate solution with the analyte/carrier stream (or column eluate) within a flow-through electrolytic cell that was located in front of the detector (photomultiplier tube)^{229, 231, 397}.

The optimum chemical conditions are in part dependent on the instrumental configuration and target analyte, but the most suitable solution for the electrogeneration of Mn(III) for CL detection has generally been found to consist of between 50 mM and 200 mM manganese(II) sulphate in 3.0 M to 5.0 M sulphuric acid^{221, 225, 229, 231, 397}.

A brown deposit, presumably manganese dioxide, was formed on the working electrode when sulphuric acid concentrations below 2.0 M were used^{218, 221, 397}. Other acids (such as nitric, phosphoric, perchloric and acetic) resulted in inferior chemiluminescence signals^{225, 229, 231}. As shown in Table 2.6, many of the organic compounds determined using chemiluminescence reactions involving manganese(III) are heterocyclic and/or polycyclic.

However, as the studies to date have each focussed on the detection of only one compound, the relationship between the chemical structure of the analytes and the CL intensity is yet to be elucidated. This reagent has also been applied to the detection of sulphite²³¹, and enhancers of the chemiluminescence reaction between manganese(III) and sulphite^{228, 229}.

To date, most analytical applications of manganese(III) involve the determination of pharmaceuticals in tablets and other formulations, using FIA methodology^{221, 225, 228, 229}.

As with the manganese(IV) reagent, validation and interference studies using common excipients suggest that manganese(III) is sufficiently selective to accurately analyse these simple samples^{221, 225}.

However, the use of these chemiluminescence reagents for the detection of drugs and biomolecules in more complex matrices such as serum and urine requires separation of the target analytes from interfering species³⁹⁷. For example, Zhang and co-workers³⁹⁷ reported a HPLC procedure for the determination of a non-steroidal anti-inflammatory drug, indomethacin, in human urine.

Sample components were separated using a C₁₈ column and a mobile phase consisting of methanol/water/acetic acid and a flow rate of 1 mL min⁻¹. Indomethacin was eluted within 8 min, and chemiluminescence detection (with manganese(III)) provided lower limits of detection than those achieved using UV-absorbance.

The indomethacin concentration in the urine of a healthy volunteer that had taken a 50 mg tablet of the drug was measured eight times over 24 h to demonstrate the potential for clinical monitoring. Percentage recoveries for urine samples spiked with 0.25–1.0 µg mL⁻¹ indomethacin were between 92% and 108%³⁹⁷.

In spite of the previously discussed studies supporting a manganese(II) emitter in chemiluminescence reactions with manganese-based oxidants^{112, 218, 219}, there has been very little discussion on the possible light-producing pathways for the reaction of electrogenerated manganese(III) with organic compounds.

In one paper, however, Zhang and co-workers²²⁵ proposed that the reaction of manganese(III) with captopril led to the well-known bimolecular emission from singlet oxygen, largely based on the observed increase and decrease of signal intensity when nitrogen and oxygen were bubbled through the solutions, respectively, however, the chemiluminescence spectral distribution was not presented.

Interestingly, Mogel and McFadden detected CL from the oxygenase activity of manganese(II)-activated d-ribulose-1,5-bisphosphate carboxylase-oxidase (Rubisco)³⁹⁸. Although initially attributed to the production of singlet oxygen³⁹⁸, Lilley et al. subsequently presented strong evidence that this luminescence emanated from the manganese(II) ion at the active site, due to an electron exchange process involving a transient manganese(III) intermediate³⁹⁹.

Table 2.2 Analytical applications of acidic potassium permanganate CL for the determination of organic molecules

Analyte	Acid/enhancers	Instrumentation/comments	Matrix	Limit of detection (LoD)	Reference
Acridine yellow	Sulphuric acid	FIA, some other acridines also produce CL	Natural waters	5 $\mu\text{g L}^{-1}$ (2×10^{-8} M)	R.O. Segarra Guerrero ⁴⁰⁰
Acriflavine and proflavin	Sulphuric acid	FIA, channels and injection loop heated to 68 °C	Wastewater	Acriflavine 10 ng mL ⁻¹ (4×10^{-8} M)	O. Rubio Pons ⁴⁰¹
Acrolein	Pyrophosphoric acid, ethanol	Multicommutation, on-line photoreactor, photodegradation prior to analysis	Natural and bottled waters, urine, soil	0.1 $\mu\text{g L}^{-1}$ (2×10^{-9} M)	T. Gamazo Climent ⁶⁷
Adrenergic amines	Sulphuric acid, polyphosphate	FIA and HPLC (monolithic C ₁₈), isocratic mobile phase: aqueous trifluoroacetic acid	Dietary supplements	Synephrine 1×10^{-8} M Octopamine 5×10^{-9} M Tyramine 1×10^{-8} M Hordenine 5×10^{-9} M	T. Slezak ⁹⁵
Albumin	Polyphosphoric acid	FIA	Serum	Bovine serum albumin 4 $\mu\text{g mL}^{-1}$ Human serum albumin 3 $\mu\text{g mL}^{-1}$ γ -Globulins 4 $\mu\text{g mL}^{-1}$	N.T.Deftereos ¹⁰⁹
Aldicarb	Sulphuric acid, quinine	Multicommutation, on-line photoreactor, photodegradation in SDS and Fe(III) solution prior to analysis	Granular formulation, mineral waters	0.07 $\mu\text{g L}^{-1}$ (4×10^{-10} M)	M. Palomeque ⁶⁸
Atenolol	Eu ³⁺ /H ₂ SO ₄ / Na ₂ SO ₃	Flow-injection chemiluminescence (FI-CL)	Biological liquid: human urine and plasma samples	Range 8.0×10^{-9} to 1.0×10^{-5} g mL ⁻¹ LoD: 3×10^{-9} g mL ⁻¹	Dongdong Li ⁴⁰²
Amidopyrine	Formaldehyde	FIA	Injection	3×10^{-5} g L ⁻¹ (1×10^{-7} M)	Y. He ^{403, 404}
<i>p</i> -Aminobenzoates	Sulphuric acid, formic acid	Batch procedure	Spray, ear drops (benzocaine and procaine)	Benzocaine 30 ng mL ⁻¹ (2×10^{-7} M) Butacaine 20 ng mL ⁻¹ (7×10^{-8} M) Butoform 30 ng mL ⁻¹ (2×10^{-7} M) Procaine 40 ng mL ⁻¹ (2×10^{-7} M) Tetracaine 3 ng mL ⁻¹ (1×10^{-8} M)	X.R. Zhang ⁴⁵
<i>p</i> -Aminobenzoates	Sulphuric acid, formic acid	SIA	Injection, teething solution (benzocaine and procaine)	Procaine 1×10^{-6} M Benzocaine 2×10^{-6} M Tetracaine 3×10^{-7} M	H. Paseková ⁴⁴
Amoxicillin	Sulphuric acid, quinine	FIA	Capsules	0.02 $\mu\text{g mL}^{-1}$ (6×10^{-8} M)	J. Du ³⁷⁶

Table 2.2 Continued

Analyte	Acid/enhancers	Instrumentation/comments	Matrix	Limit of detection (LoD)	Reference
Amoxicillin	Hydrochloric acid	FIA	Capsules	$6 \times 10^{-8} \text{ g mL}^{-1}$ ($2 \times 10^{-7} \text{ M}$)	J. Shi ⁴⁰⁵
Amoxicillin	Sulphuric acid, formaldehyde	FIA	Raw medicines, capsules	$4 \times 10^{-8} \text{ M}$	W. Cao ²⁹
Amoxicillin	Formaldehyde	FIA	Capsules	$3 \times 10^{-8} \text{ g mL}^{-1}$ ($8 \times 10^{-8} \text{ M}$)	J. Shi ⁴⁰⁶
Amoxicillin	Sulphuric acid	FIA	Pharmaceutical formulations	$2 \times 10^{-6} \text{ M}$	Y. Liang ³¹
Ampicillin	Formaldehyde	FIA, analyte degraded in NaOH solution prior to analysis	Capsules	$9 \times 10^{-9} \text{ g mL}^{-1}$ ($3 \times 10^{-8} \text{ M}$)	K. Zhao ³⁰
Analgin	-	FIA	Tablets, injections	$4 \times 10^{-8} \text{ g mL}^{-1}$ ($1 \times 10^{-7} \text{ M}$)	L. Li ⁴⁰⁷
Antu	H ₂ SO ₄ , formaldehyde	Stopped-flow procedure	Natural water, grains	$0.005 \mu\text{g mL}^{-1}$ ($3 \times 10^{-8} \text{ M}$)	S. Fan ⁴⁰⁸
Arbutin and l-ascorbic acid	Polyphosphoric acid, formaldehyde	HPLC (C ₁₈), isocratic mobile phase: methanol-phosphate buffer	Cosmetics	Arbutin $0.2 \mu\text{g mL}^{-1}$ ($7 \times 10^{-7} \text{ M}$) Ascorbic acid $0.3 \mu\text{g mL}^{-1}$ ($2 \times 10^{-6} \text{ M}$)	Y. Wei ⁹⁷
Aromatic ketone hydrazones	Formic acid, rhodamine B	FIA	Not applied	Benzil dihydrazone $2 \times 10^{-6} \text{ M}$ Benzophenone hydrazone $3 \times 10^{-6} \text{ M}$ Acetophenone hydrazone $3 \times 10^{-6} \text{ M}$ Benzoin hydrazone $4 \times 10^{-5} \text{ M}$	T.E.A. Ahmed ⁴⁰⁹
Ascorbic acid	Sulphuric acid	Batch procedure	Tablets, injections	$3 \times 10^{-7} \text{ M}$	C.Q. Zhu ⁴¹⁰
Ascorbic acid	Sulphuric acid	FIA	Fruit drinks, nutritional supplements	$5 \times 10^{-7} \text{ M}$	I.B. Agater ⁸⁵
Ascorbic acid	Sulphuric acid	Flow-through sensor, reagent electrostatically immobilized on anion-exchange resin, sensor lifetime of over 500 injections	Tablets, vegetables	5 ng mL^{-1} ($3 \times 10^{-8} \text{ M}$)	Y. Huang ⁸⁶
Ascorbic acid	Phosphoric acid, hexametaphosphate, formaldehyde	FIA and SIA	Tablets	$5 \times 10^{-8} \text{ M}$ (both methods)	N. Anastos ¹⁴⁴

Table 2.2 Continued

Analyte	Acid/enhancers	Instrumentation/comments	Matrix	Limit of detection (LoD)	Reference
Ascorbic acid	Formaldehyde	FIA	Pills, injections	1×10^{-8} M	C. Xie ⁴¹¹
Ascorbic acid	Hydrochloric acid, formaldehyde	SIA	Tablets, injections	5×10^{-10} M	X. Xu ⁴¹²
Asulam	Sulphuric acid	Multicommutation, on-line photoreactor, carrier heated to 80 °C, photodegradation in alkaline glycine buffer prior to analysis	Irrigation, tap and spring water	$40 \mu\text{g L}^{-1}$ (2×10^{-7} M)	A. Chivulescu ⁷¹
Baicalin	Nitric acid, formaldehyde	HPLC (C ₁₈), isocratic mobile phase: methanol-phosphoric acid	Pharmaceutical and herbal formulations	3×10^{-7} M ¹³⁰	E.B. Liu ¹³⁴
Berberine, palmatine and jatrorrhizine	H ₂ SO ₄	FIA	Cortex Phellodendri and Rhizoma Coptidis	Range: 0.038–7.27, 0.031–18.1 and 0.012–3.61 $\mu\text{g/mL}$ LoD: 0.005, 0.004 and 0.0007 $\mu\text{g/mL}$	Xueqin Xu ⁴¹³
Bromoxynil	Polyphosphoric acid	FIA, on-line photoreactor, photodegradation in ethanol and KOH solution prior to analysis	Synthetic formulation, tap water	$5 \mu\text{g L}^{-1}$ (2×10^{-8} M)	Z. Pawlicová ⁴¹⁴
Brucine, strychnine ephedrine and pseudoephedrine	Polyphosphoric acid	HPLC (C ₁₈), gradient elution: dihydrogen orthophosphate-methanol	Medicine	Brucine 1×10^{-10} g mL ⁻¹ (3×10^{-10} M) Strychnine 1×10^{-8} g mL ⁻¹ (3×10^{-8} M) Ephedrine 1×10^{-5} g mL ⁻¹ (6×10^{-5} M) Pseudoephedrine 1×10^{-5} g mL ⁻¹ (6×10^{-5} M)	L. Zhu ⁴¹⁵
Brucine	Tetraphosphoric acid	FIA	Nux vomica	2×10^{-9} g mL ⁻¹ (4×10^{-9} M)	H. Qi ⁴¹⁶
Buprenorphine	Polyphosphoric acid	FIA	Tablets	1×10^{-8} M	A.A. Alwarthan ⁴¹⁷
Captopril	Sulphuric acid, formaldehyde	Stopped-flow procedure	Tablets	$0.01 \mu\text{g mL}^{-1}$ (5×10^{-8} M)	J.A. Murillo Pulgarín ¹³³
Carbaryl	Sulphuric acid	FIA	Natural waters	15 ng mL^{-1} (7×10^{-8} M)	G. Tsogas ⁷²
Carbohydrates	Sulphuric acid, manganese(II)	FIA	Not applied	Glucose, galactose, fructose, arabinose, xylose, lactose, sucrose, mannitol, glycerol and ascorbic acid 1×10^{-4} M	I.B. Agater, ¹⁴⁵

Table 2.2 Continued

Analyte	Acid/enhancers	Instrumentation/comments	Matrix	Limit of detection (LoD)	Reference
5-(4-Carboxyphenylazo)-8-salicyldeneaminoquinoline	Sulphuric acid	-	-	4×10^{-7} M	Y. Zhu ⁴¹⁸
Carbamate pesticides	Pyrophosphoric acid	Multicommutation, on-line photo-reactor, oxidant line heated to 60 °C, photodegradation in NaOH solution prior to analysis	Urine, surface, tap and bottled water	Karbutilate $10 \mu\text{g L}^{-1}$ (4×10^{-8} M) Isoproc carb $30 \mu\text{g L}^{-1}$ (2×10^{-7} M) Fenobucarb $50 \mu\text{g L}^{-1}$ (2.4×10^{-7} M)	C.M.P.G. Amorim ⁴¹⁹
Carbonyl compounds	Sulphuric acid, formic acid	FIA, off-line derivatisation with 2,4 dinitrophenylhydrazine, inhibition of chemiluminescence, samples in aqueous propan-2-ol	Oxidative deterioration of linoleic acid	Hexanal 2×10^{-7} M	A. Townshend ⁴²⁰
Catechol	Formaldehyde	FIA	Tap water	1×10^{-8} M	H. Li ⁴²¹
Catechol and dopamine	Sulphuric acid	Microchip capillary electrophoresis, boric acid electrophoresis buffer	Not applied	Dopamine 2×10^{-5} M Catechol 1×10^{-5} M	J.M. Lin ⁴²² and R. Su ²⁷
Catecholamines	Sulphuric acid	FIA, other polyhydroxybenzenes also produce chemiluminescence	Theoretical study	Epinephrine (adrenaline) 1×10^{-7} M Dopamine 1×10^{-7} M Norepinephrine 1×10^{-7} M	H. Ikkai ⁴²³
Catecholamines	Formaldehyde/ H_2SO_4	ion chromatography (IC) with chemiluminescence (CL) detection	human urine	Range: 0.02–0.5 $\mu\text{g/mL}$ LoD: 0.6 and 5.1 $\mu\text{g/L}$	HongWei Wu ⁴²⁴
Catecholamines	Formaldehyde, Sulphuric acid	FIA and continuous flow, see also table entry 'Dihydroxybenzenes and <i>o</i> -phenylenediamine'	Pharmaceutical formulations (epinephrine and l-dopa)	Epinephrine $0.03 \mu\text{g mL}^{-1}$ (2×10^{-7} M) Norepinephrine $0.05 \mu\text{g mL}^{-1}$ (3×10^{-7} M) l-Dopa $0.03 \mu\text{g mL}^{-1}$ (2×10^{-7} M) Dopamine $0.04 \mu\text{g mL}^{-1}$ (3×10^{-7} M)	N. Deftereos ¹²²
Catechols, catecholamines, triphenols and indoles	Sulphuric acid, cerium(IV) or copper(II)	FIA, screened a number of organic molecules using a number of chemiluminescence systems	Theoretical study	4-Methylpyrocatechol 1×10^{-5} M	T. Nakagama ⁴²⁵
Cefadroxil monohydrate	Sulphuric acid, quinine	FIA	Pharmaceutical formulations, plasma, urine	$0.05 \mu\text{g mL}^{-1}$ (1×10^{-7} M)	F.A. Aly ³⁹

Table 2.2 Continued

Analyte	Acid/enhancers	Instrumentation/comments	Matrix	Limit of detection (LoD)	Reference
Cefadroxil	Sulphuric acid, formaldehyde	FIA, other cephalosporins and some antibiotics also produce chemiluminescence	Capsules	25 ng mL ⁻¹ (7×10^{-8} M)	C. Thongpoon ¹⁴⁶
Cefazolin sodium	Polyphosphoric acid	FIA	Pharmaceutical formulations	2 mg L ⁻¹ (4×10^{-6} M)	D. Zhang ⁴³
Cefoperazone sodium	SDBS	FIA	Urine	4×10^{-9} g mL ⁻¹ (6×10^{-9} M)	Z. Chen ⁴⁰
Cefotaxime sodium	Polyphosphoric acid	Sample hydrolysed in basic medium prior to analysis	Pharmaceutical formulations	2 ng mL ⁻¹ (4×10^{-9} M)	D. Zhang ⁴³
Ceftriaxone sodium	Polyphosphoric acid	FIA, sample hydrolysed in NaOH prior to analysis	Pharmaceutical formulations	25 ng mL ⁻¹ (5×10^{-8} M)	D. Zhang ³⁶
Cephalexin and cephradine	Formaldehyde	FIA	Pharmaceutical formulations	Cephalexin 0.1 µg mL ⁻¹ (3×10^{-7} M) Cephadrine 0.1 µg mL ⁻¹ (3×10^{-7} M)	J. Wang ⁴¹
Cephalosporin antibiotics	Sulphuric acid, glyoxal	FIA	Tablets, capsules, solutions	Cefalexin 10 ng mL ⁻¹ (3×10^{-8} M) Cefadroxil 2 ng mL ⁻¹ (5×10^{-9} M) Cefazolin sodium 2 ng mL ⁻¹ (4×10^{-9} M)	Y. Sun ³⁷
Cephadrine	Polyphosphoric acid, fluorescein	FIA	Urine	3×10^{-9} g mL ⁻¹ (9×10^{-9} M)	Z. Chen ⁴²
Chloramphenicol	Sulphuric acid	FIA, on-line photochemical reactor, all lines heated to 70 °C, photodegradation in glycine buffer prior to analysis	Pharmaceutical formulations	30 ng mL ⁻¹ (9×10^{-8} M)	M. Catalá Icardo ⁴²⁶
Chlorogenic acid	Hydrochloric acid, formaldehyde	FIA	Frozen and dried fruit	6×10^{-9} g mL ⁻¹ (2×10^{-8} M)	X. Wang ⁸⁸
Chlorpheniramine	Formaldehyde	FIA	Pharmaceutical formulations	0.2 µg mL ⁻¹ (7×10^{-7} M)	L. Shen ⁴²⁷
Chlorpheniramine maleate	Formaldehyde	FIA	Tablets	5×10^{-8} g mL ⁻¹ (1×10^{-7} M)	J. Shi ⁴²⁸
Cinnarizine	Polyphosphoric acid, Tween 60	FIA, sample in ethanol	Tablets	18 ng mL ⁻¹ (5×10^{-8} M)	A. Townshend ¹¹⁸

Table 2.2 Continued

Analyte	Acid/enhancers	Instrumentation/comments	Matrix	Limit of detection (LoD)	Reference
Citric acid	-	FIA	Aerated water	$3 \times 10^{-6} \text{ g mL}^{-1}$ ($2 \times 10^{-5} \text{ M}$)	H. Yang ⁴²⁹
Clenbuterol	Polyphosphate, formaldehyde, Tween 20	Flow analysis, molecular imprinted polymer within detection cell, applied to microchip ⁴³⁰	Urine	$3 \times 10^{-10} \text{ g mL}^{-1}$ ($1 \times 10^{-9} \text{ M}$)	H. Zhou ¹³⁸ and Z. Zhang ⁴³⁰
Clomipramine	Formic acid/ H ₂ SO ₄	flow-injection analysis (FIA) technique		Range: 0.04–4 $\mu\text{g/mL}$ LoD: 0.008 $\mu\text{g/mL}$	Zhongling Ji ⁴³¹
Codeine	Polyphosphoric acid	FIA	Not applied	$3 \times 10^{-7} \text{ M}$	T.J. Christie ³⁸⁹
Dihydralazine sulphate	Sulphuric acid, rhodamine B	FIA	Tablets	2 ng mL^{-1} ($7 \times 10^{-9} \text{ M}$)	X. Yang ⁴³² and D. Wu ⁴³³
2,4-Dinitrochlorobenzene	Sulphuric acid	Batch procedure, analyte reacted with hydrazine at 100 °C for 90 min prior to analysis	Synthetic	$5 \times 10^{-8} \text{ g mL}^{-1}$ ($3 \times 10^{-7} \text{ M}$)	X. Liu ⁴³⁴
2,4-Dinitrophenylhydrazine	Sulphuric acid, formic acid	FIA, all lines heated to 40 °C, samples in aqueous propan-2-ol	Not applied	$1 \times 10^{-7} \text{ M}$	A. Townshend ⁴²⁰
Dipyridamole	Sulphuric acid, hydrogen peroxide	FIA	Tablets, injections	$6 \times 10^{-8} \text{ g mL}^{-1}$ ($1 \times 10^{-7} \text{ M}$)	M. Yang ⁴³⁵
Dipyridamole	Rhodamine B, Tween 80	FIA	-	$2 \times 10^{-8} \text{ g mL}^{-1}$ ($3 \times 10^{-8} \text{ M}$)	Z. Rao ⁴³⁶
Dobutamine	Hydrochloric acid, formaldehyde	FIA	Injections	0.07 mg L^{-1} ($2 \times 10^{-7} \text{ M}$)	S. Fan ⁴³⁷
l-Dopa	-	FIA	Tablets	$6 \times 10^{-5} \text{ g L}^{-1}$ ($3 \times 10^{-7} \text{ M}$)	M. Yang ⁴³⁸
Dopamine	Formaldehyde/ H ₂ SO ₄	Flow-injection chemiluminescence (FI-CL)	pharmaceutical preparation	Range: 3.1×10^{-8} - $1.7 \times 10^{-5} \text{ mol/L}$ LoD: $1.0 \times 10^{-8} \text{ mol/L}$	Saikh Mohammad Wabaidur ⁴³⁹
Erythromycin	Polyphosphoric acid or sulphuric acid	Batch procedure, other macrolide antibiotics also produce CL	Not applied	$0.2 \mu\text{g mL}^{-1}$ ($2 \times 10^{-7} \text{ M}$)	A. Mitsana-Papazoglou ¹¹⁴
Estradiol, estriol and estrone	sodium hexametaphosphate and CdTe NCs	Flow injection nanocrystals (NCs) chemiluminescence (CL) analysis	Estrogens in tap water samples	estriol $5.8 \times 10^{-11} \text{ mol/L}$ estrone $4.3 \times 10^{-12} \text{ mol/L}$ estradiol, $1.4 \times 10^{-11} \text{ mol/L}$	Lun Wang ⁴⁴⁰

Table 2.2 Continued

Analyte	Acid/enhancers	Instrumentation/comments	Matrix	Limit of detection (LoD)	Reference
Estrogens	Sulphuric acid, formaldehyde	FIA	Tablets, tap water	Dienestrol 3×10^{-9} g mL ⁻¹ (1×10^{-8} M) Diethylstilbestrol 1×10^{-9} g mL ⁻¹ (4×10^{-9} M) Hexestrol 6×10^{-9} g mL ⁻¹ (2×10^{-8} M)	J. Du ¹¹⁹
Ethacridine lactic acid	Hydrochloric acid, formic acid	FIA	Pharmaceutical formulations	3×10^{-8} g mL ⁻¹ (8×10^{-8} M)	L. Fang ⁴⁴¹
Ethamsylate	Sulphuric acid, formic acid	FIA	Pharmaceutical formulations	5×10^{-9} g mL ⁻¹ (2×10^{-8} M)	J. Pan ¹⁵³
Ethanol	Nitric acid	Batch procedure	Alcoholic beverages (gin)	0.3% (v/v) (5×10^{-2} M)	S.I. Montalvo ⁸²
Etoposide	Sulphuric acid	Batch procedure	Capsules	2 ng mL ⁻¹ (3×10^{-9} M)	A. Campiglio ^{442, 443}
Eugenol, isoeugenol, caffeic acid and cimetidine	Acidic solution (acid type not reported)	FIA and batch procedure, analyte in ethanol, NaOH or water	Pharmaceutical formulation (cimetidine)	Eugenol 1×10^{-5} M Isoeugenol 1×10^{-5} M Caffeic acid 1×10^{-4} M Cimetidine $20 \mu\text{g mL}^{-1}$ (8×10^{-5} M)	A. Mitsana-Papazoglou ⁴⁴⁴
Ferulic acid	Nitric acid	FIA	Beauty essence	1×10^{-7} M	L.N. Li ⁴⁴⁵
Fenfluramine	Calcein/ H ₂ SO ₄	IFFM-D flow injection CL analyser	weight-reducing tonic	Range: 1.0×10^{-7} to 6.0×10^{-6} g mL ⁻¹ LoD: 6×10^{-8} g mL ⁻¹	Fei Nie ⁴⁴⁶
Fluorouracil (5-FU)	Formaldehyde/ H ₂ SO ₄	Flow-injection chemiluminescence (FI-CL)	pharmaceutical preparations and biological fluids	LoD: 3×10^{-8} g mL ⁻¹	Hanwen Sun ⁴⁴⁷
Folic acid	Sulphuric acid, formaldehyde	FIA	Tablets	2×10^{-8} M	C. Sun ⁴⁴⁸
Folic acid	Formic acid	FIA	Tablets	1×10^{-8} g mL ⁻¹ (3×10^{-8} M)	Y. Li ⁴⁴⁹
Glyoxal	Sulphuric acid	FIA	Synthetic	7×10^{-6} g mL ⁻¹ (1×10^{-4} M)	L. Fang ⁴⁵⁰
Glutathione (GSH) and glutathione disulphide (GSSG)	H ₂ SO ₄	FIA / high performance liquid chromatography (HPLC)	cultured muscle cells treated for 24 h with glucose oxidase	Range: 7.5×10^{-7} to 1×10^{-5} M, and 5×10^{-7} M LoD:-	Geoffrey P. McDermott ⁴⁵¹
Heroin	Sulphuric acid, polyphosphate	FIA, sample hydrolysed with NaOH to morphine prior to analysis	Seizure samples	Not reported	K.M. Agg ⁴⁵²

Table 2.2 Continued

Analyte	Acid/enhancers	Instrumentation/comments	Matrix	Limit of detection (LoD)	Reference
Human DNA	Nitric acid	FIA	Serum	6 µg mL ⁻¹	X. Zhu ⁴⁵³
Hydralazine	Phosphoric acid, formaldehyde	Stopped-flow procedure	Tablets, injections	0.07 µg mL ⁻¹ (4 × 10 ⁻⁷ M)	J.A. Murillo Pulgarín ¹²⁸
Hydroquinone	-	FIA	Wastewater	2 × 10 ⁻⁷ g mL ⁻¹ (2 × 10 ⁻⁶ M)	L. Li ⁴⁵⁴
Imipramine and chlorpromazine	Sulphuric acid	FIA	Urine	Impramine 5 × 10 ⁻⁷ M Chlorpromazine 2 × 10 ⁻⁶ M	J.L. Lopez Paz ⁴⁵⁵
Imipramine	Glyoxal	FIA	Tablets	1 × 10 ⁻⁸ g mL ⁻¹ (4 × 10 ⁻⁸ M)	Y. Xue ⁴⁵⁶
Indole-2,3-dione (isatin) and indole-3-acetic acid(IAA)	Formaldehyde/ H ₂ SO ₄	Flow-injection chemiluminescence (FI-CL)	biological samples and soil extracts	Range: 0.1–100.0 µM (isatin) and 0.01–10.0 µM IAA. LoD: 10.0 nM for isatin and 1.0 nM for IAA.	Suqin Han ⁴⁵⁷
Isoprenaline	Sulphuric acid	FIA	Not applied	1 µg mL ⁻¹ (5 × 10 ⁻⁶ M)	S.A. Al-Tamrah ⁴⁵⁸
Isoprenaline	-	FIA	-	2 × 10 ⁻⁸ g mL ⁻¹ (1 × 10 ⁻⁷ M)	L. Li ⁴⁵⁹
Ketoprofen	Sulphite/ H ₂ SO ₄	FIA	ketoprofen in capsules and human urine sample.	LoD: 2.0 × 10 ⁻⁸ mol/L Range: 5.0 × 10 ⁻⁸ - 3.0 × 10 ⁻⁶ mol/L	Yafeng Zhuang ⁴⁶⁰
Lasiocarpine	Orthophosphoric acid, polyphosphate	FIA, some other pyrrolizidine alkaloids produced chemiluminescence	Not applied	1 × 10 ⁻⁷ M	B.A. Gorman ⁴⁶¹
Leucogen	Sulphuric acid, rhodamine B	FIA, sample prepared in 0.5% NaOH	Not applied	2 × 10 ⁻⁸ g mL ⁻¹ (7 × 10 ⁻⁸ M)	Z. Rao ⁴⁶²
α-Lipoic acid	Formaldehyde/ sodium hexametaphosphate medium (pH 3)	FIA / high performance liquid chromatography (HPLC)	Alfa-lipoic acid" capsules and in food products	LoD: 4 × 10 ⁻³ µg mL ⁻¹ Range: 0.5–20 µg mL ⁻¹	E. Wolyniec ⁴⁶³
Loprazolam	Hydrochloric acid, formic acid	FIA, six other benzodiazepines did not give significant emission	Tablets	7 × 10 ⁻⁶ M	A.R.J. Andrews ^{147, 464}
Malic acid	Sulphuric acid	Batch procedure	Apple juice, drink	1 × 10 ⁻⁹ M	K. Luo ⁸⁷
Maltol	Sulphuric acid, formic acid, hexadecylpyridinium chloride	FIA, all lines heated to 80 °C	Bread	10 µg L ⁻¹ (8 × 10 ⁻⁸ M)	M.C. Sanfeliu Alonso ⁴⁶⁵

Table 2.2 Continued

Analyte	Acid/enhancers	Instrumentation/comments	Matrix	Limit of detection (LoD)	Reference
Medazepam	Sulphuric acid	FIA	Not applied	2×10^{-5} M	S.M. Sultan ⁴⁶⁶
5-Methoxytryptophol	Perchloric acid, formaldehyde	FIA	Cerebrospinal fluid	8×10^{-9} M	X. Wu ⁴⁶⁷
Melamine	H ₂ SO ₄ /formaldehyde/sodium dodecyl sulphate micelles and Au/Ag NPs	FIA	powdered milk samples	Range: 0.01–35 ng mL ⁻¹ LoD: 8 pg mL ⁻¹	Jamshid L. Manzoori ⁴⁶⁸
Melatonin and related indoles	Sulphuric acid, formaldehyde	FIA	Tablets	Melatonin 2×10^{-8} M <i>N</i> -acetyl-5-hydroxytryptamine 1×10^{-8} M 5-Methoxyindolyl acetic acid 2×10^{-6} M 5-Methoxytryptamine 5×10^{-8} M <i>N</i> -acetyl-5-methoxy-6-hydroxytryptamine 5×10^{-9} M	G.N. Chen ¹⁵¹
6-mercaptopurine	/thioacetamide–sodium hexametaphosphate	Flow-injection chemiluminescence (FI-CL)	human serum samples	Range: 7.0×10^{-10} to 1.0×10^{-7} g/mL. LoD: 1.9×10^{-11} g/mL	Lun Wang ⁴⁶⁹
Methotrexate	Sulphuric acid, formaldehyde	FIA	Injection, tablet	3×10^{-9} g mL ⁻¹ (8×10^{-9} M)	C. Thongpoon ¹⁴⁶
Methylene Blue	Formaldehyde	FIA	Injection, biological fluid	$0.04 \mu\text{g mL}^{-1}$ (1×10^{-7} M)	C. Fan ⁴⁷⁰
Methylthiouracil and propylthiouracil	Sulphuric acid, formaldehyde	HPLC (C ₁₈), isocratic mobile phase: aqueous methanol	Serum	Methylthiouracil $0.03 \mu\text{g mL}^{-1}$ (2×10^{-7} M) Propylthiouracil $0.03 \mu\text{g mL}^{-1}$ (2×10^{-7} M)	Y. Wei ⁴⁷¹
Metoclopramide	Hydrochloric acid, formaldehyde	FIA	Tablets, injections	$0.03 \mu\text{g mL}^{-1}$ (1×10^{-7} M) ¹²¹	S. Fan ^{121, 472} Z. Wu ⁴⁷³
Mitoxantrone	Formaldehyde	FIA	Injections	$6 \mu\text{g L}^{-1}$ (1×10^{-8} M)	S. He ⁴⁷⁴
Morphine	Polyphosphoric acid	FIA	Not applied	1×10^{-10} M	R.W. Abbott ^{110, 214}
Morphine	Polyphosphoric acid	HPLC (polystyrene-divinylbenzene packing), isocratic mobile phase: polyphosphoric acid–methanol, <i>N</i> -ethylmorphine internal standard	Forensic samples (blood and urine)	25 ng mL^{-1} (9×10^{-8} M)	R.W. Abbott ⁴⁹

Table 2.2 Continued

Analyte	Acid/enhancers	Instrumentation/comments	Matrix	Limit of detection (LoD)	Reference
Morphine	Phosphoric acid	FIA, screened over 100 compounds	Not applied	$1 \times 10^{-8} \text{ g } 50 \mu\text{L}^{-1}$ ($7 \times 10^{-7} \text{ M}$)	Y.B. Tsaplev ¹⁵⁴
Morphine	Sulphuric acid, tetraphosphoric acid or hexametaphosphate	FIA	Process streams	$5 \times 10^{-8} \text{ M}$	N.W. Barnett ¹⁵
Morphine	Tetraphosphoric acid	-	Urine	3 ng mL^{-1} ($1 \times 10^{-8} \text{ M}$)	W. Chang ⁴⁷⁵
Morphine and related derivatives	Polyphosphoric acid	HPLC	Opium, urine	Morphine $1 \times 10^{-13} \text{ g L}^{-1}$ ($4 \times 10^{-16} \text{ M}$) Codeine $1 \times 10^{-9} \text{ g L}^{-1}$ ($3 \times 10^{-12} \text{ M}$) O^3 -Monoacetylmorphine $1 \times 10^{-11} \text{ g L}^{-1}$ ($3 \times 10^{-14} \text{ M}$) Heroin $1 \times 10^{-10} \text{ g L}^{-1}$ ($3 \times 10^{-13} \text{ M}$)	L. Zhu ⁵⁰
Morphine	Orthophosphoric acid, hexametaphosphate	SIA	Process streams	$1 \times 10^{-8} \text{ M}$	N.W. Barnett ²³
Morphine and monoacetylmorphine	Polyphosphoric acid, hexametaphosphate	HPLC (C ₁₈), isocratic mobile phase: sodium hexametaphosphate–methanol–TFA, nalorphine internal standard	Not applied	Morphine 1 ng mL^{-1} ($4 \times 10^{-9} \text{ M}$) Monoacetylmorphine 15 ng mL^{-1} ($5 \times 10^{-8} \text{ M}$)	E. Amiott ⁵¹
Morphine	Orthophosphoric acid, hexametaphosphate	SIA, heterogeneous reaction conditions	Non-aqueous, water immiscible, process streams	$1 \times 10^{-6} \text{ M}$	N.W. Barnett ²²
Morphine, 6-monoacetylmorphine and heroin	Polyphosphoric acid	CE, separation medium: borate and β -cyclodextrin	Not applied	Morphine 23 fmol 6-Monoacetylmorphine 66 fmol Heroin 115 fmol	Z. Gong ²¹
Morphine, oripavine and pseudomorphine	Sulphuric acid, polyphosphate	CE separation medium: 6-aminocaproic acid–hexadimethrine bromide– α -cyclodextrin,	Process liquor	Morphine $3 \times 10^{-7} \text{ M}$ Oripavine $3 \times 10^{-7} \text{ M}$ Pseudomorphine $5 \times 10^{-7} \text{ M}$	N.W. Barnett ²⁴
Morphine	Orthophosphoric acid, polyphosphate	Stopped-flow procedure	Process liquor	$2 \times 10^{-8} \text{ M}$	S.W. Lewis ⁴⁷⁶
Morphine	Sulphuric acid, polyphosphate	SIA	Not applied	$5 \times 10^{-11} \text{ M}$	C.E. Lenehan ⁴⁷⁷

Table 2.2 Continued

Analyte	Acid/enhancers	Instrumentation/comments	Matrix	Limit of detection (LoD)	Reference
Morphine and oripavine	Sulphuric acid, polyphosphate	HPLC (C ₈ ion-pairing), Gradient elution: acetonitrile–octane sulfonic acid, KMnO ₄ also used to oxidise Ru(bipy) ₃ ²⁺ reagent to detect codeine and thebaine	Process liquor	Morphine 1 × 10 ⁻⁶ M Oripavine 3 × 10 ⁻⁶ M	C.E. Lenehan ²⁶
Morphine	Phosphoric acid, polyphosphate	HPLC (monolithic C ₁₈), separation conditions not reported	Maggots reared on morphine spiked mince meat	Not reported	J.A. Gunn ⁴⁷⁸
Morphine and oripavine	Orthophosphoric acid, polyphosphate	HPLC (monolithic C ₁₈), gradient elution: methanol-trifluoroacetic acid	Process liquor	Morphine 1 × 10 ⁻¹⁰ M Oripavine 5 × 10 ⁻¹⁰ M	J.W. Costin ⁴⁷⁹
Naftopidil	Sulphuric acid, formaldehyde or formic acid	FIA	Not applied	14 ng mL ⁻¹ (4 × 10 ⁻⁸ M)	A. Townshend ¹²⁵
Naloxone	Phosphoric acid	Stopped-flow procedure	Pharmaceutical formulations	0.01 µg mL ⁻¹ (3 × 10 ⁻⁸ M)	J.A. Murillo Pulgarín ³²⁰
Naltrexone	Sulphuric acid	Batch procedure	Tablets, capsules	2 ng mL ⁻¹ (6 × 10 ⁻⁹ M)	A. Campiglio ⁴⁸⁰
Naphazoline and oxymetazoline	Formaldehyde/ H ₂ SO ₄	Flow-injection chemiluminescence (FI-CL)	pharmaceuticals	8.69 × 10 ⁻³ mg/L for naphazoline and 3.47 × 10 ⁻² mg/L for oxymetazoline	Nan-Nan Wang ⁴⁸¹
Naphthols	Sulphuric acid, rhodamine B	FIA, other naphthols also produced chemiluminescence	Not applied	2-Naphthol 1 × 10 ⁻⁶ M (no sensitizer) 1-Naphthol 5 × 10 ⁻⁷ M (sensitizer used)	S.A. Al-Tamrah ⁴⁸²
Neurotransmitters metabolites	Orthophosphoric acid, polyphosphate	FIA and HPLC (monolithic C ₁₈), gradient elution: methanol–trifluoroacetic acid	Urine (homovanilic acid and 5-hydroxyindole-3-acetic acid)	Homovanilic acid 3 × 10 ⁻⁸ M 3,4-Dihydroxyphenylacetic acid 2 × 10 ⁻⁸ M 5-Hydroxyindole-3-acetic acid 5 × 10 ⁻⁹ M Vanilmandelic acid 4 × 10 ⁻⁸ M 4-Hydroxy-3-methoxyphenylglycol 1 × 10 ⁻⁸ M (established using FIA)	J.L. Adcock ⁵

Table 2.2 Continued

Analyte	Acid/enhancers	Instrumentation/comments	Matrix	Limit of detection (LoD)	Reference
Neurotransmitters and metabolites, and opiate alkaloids	Sulphuric acid, polyphosphate	Hybrid FIA/HPLC (monolithic C ₁₈) system, gradient elution: methanol-trifluoroacetic acid	Urine (neurotransmitters and metabolites)	Homovanilic acid 3×10^{-7} M Serotonin 2×10^{-8} M 5-Hydroxyindole-3-acetic acid 1×10^{-7} M Vanilmandelic acid 5×10^{-7} M Morphine 3×10^{-9} M Pseudomorphine 1×10^{-8} M Oripavine 3×10^{-9} M	J.L. Adcock ⁴⁸³
Octopamine, synephrine, tyramine, <i>N</i> -methyltyramine and hordenine	sodium polyphosphate/H ₂ SO ₄	FIA / high performance liquid chromatography (HPLC)	weight-loss products	Range: 1×10^{-5} to 1×10^{-3} M LoD: 1×10^{-9} and 1×10^{-8} M	Dane W. Percy ⁴⁸⁴
Octyl dimethyl PABA	Sulphuric acid	FIA, ethanol in carrier stream	Sunscreen	25 ng mL ⁻¹ (9×10^{-8} M)	A. Townshend ⁹⁶
Organic pollutants	Sulphuric acid, ferrous ions	Continuous flow	Natural waters	Gallic acid 8×10^{-7} M	K. Fujimori ⁷⁵
Organic pollutants	Sulphuric acid, ferrous ions	FIA	Seawater	Not reported	K. Fujimori ⁷⁷
Oxalate	Formaldehyde	-	Urine	5×10^{-3} g mL ⁻¹ (5×10^{-2} M)	Y. He ⁴⁸⁵
Oxytetracycline	Sulphuric acid, formaldehyde	FIA	Binding of oxytetracycline to albumin	5×10^{-7} M	L. Wang ⁴⁸⁶
Penicillin G potassium	Sulphuric acid, formaldehyde	FIA, analyte degraded in NaOH solution prior to analysis	Raw medicines	7×10^{-8} g mL ⁻¹ (2×10^{-7} M) ⁴⁸⁷	W. Cao and Z. Zhang ³²
Penicillins	Sulphuric acid, glyoxal	FIA	Tablets, capsules, injections	Phenoxymethylpenicillin 0.05 µg mL ⁻¹ (1×10^{-7} M) Amoxicillin 0.03 µg mL ⁻¹ (8×10^{-8} M) Ampicillin 0.03 µg mL ⁻¹ (9×10^{-8} M) Ampicillin sodium 0.05 µg mL ⁻¹ (1×10^{-7} M)	Y. Sun ²⁸
Perphenazine	Sulphuric acid	FIA	Synthetic sample	50 ppm (1×10^{-4} M)	S.M. Sultan ⁴⁶
Phenacetin	formaldehyde	Flow analysis, molecular imprinted polymer within detection cell	Pharmaceutical formulations, urine	2×10^{-7} g mL ⁻¹ (1×10^{-6} M)	H. Zhang ⁴⁸⁸

Table 2.2 Continued

Analyte	Acid/enhancers	Instrumentation/comments	Matrix	Limit of detection (LoD)	Reference
Phenol	Sulphuric acid, formic acid	FIA, all lines heated to 80 °C, on-line pre-concentration on solid-phase column	Waste and ground water	1 ng mL ⁻¹ (1 × 10 ⁻⁸ M)	B. Gómez-Taylor Corominas ¹³⁵
Phenol	Hydrogen peroxide	FIA	Wastewater	3 × 10 ⁻⁸ g mL ⁻¹ (3 × 10 ⁻⁷ M)	L. Li ⁴⁸⁹
Phenol	Hydrochloric acid, formaldehyde	FIA	Wastewater	3 × 10 ⁻⁹ g mL ⁻¹ (3 × 10 ⁻⁸ M)	W. Cao ⁷⁴
Phenols	Sulphuric acid	Flow analysis, on-line pre-concentration column (if needed)	Natural waters	Phenol 5 ng mL ⁻¹ (5 × 10 ⁻⁸ M)	J. Michałowski ⁷³
Phenols	Sulphuric acid	-	Wastewater	1 × 10 ⁻⁶ M	Y. Li ⁴⁹⁰
Phenols (antioxidants)	Orthophosphoric acid, polyphosphate	FIA, correlation of antioxidant activity to chemiluminescence response	Total phenolic content of wine samples	Catechin 5 × 10 ⁻⁹ M Epicatechin 1 × 10 ⁻⁸ M Quercetin 4 × 10 ⁻¹⁰ M Rutin 7 × 10 ⁻⁸ M Caffeic acid 2 × 10 ⁻⁸ M Ferulic acid 3 × 10 ⁻⁸ M Gallic acid 5 × 10 ⁻⁸ M Vanillin 7 × 10 ⁻⁷ M 4-Hydroxycinnamic acid 2 × 10 ⁻⁸ M	J.W. Costin ⁴⁹¹
Phenols and amines	Sulphuric acid, polyphosphate, formaldehyde	FIA, see also table entry 'Serotonin, related indoles and morphine'	Not applied	8-Quinololinol 5 × 10 ⁻⁷ M 2,3-Diaminonaphthalene 1 × 10 ⁻⁶ M Eriochrome black T 4 × 10 ⁻⁶ M Calmagite 2 × 10 ⁻⁶ M Pyrocatechol violet 6 × 10 ⁻⁷ M Tryptamine 1 × 10 ⁻⁷ M I-Tryptophan 1 × 10 ⁻⁷ M	N.W. Barnett ⁴⁹²
Phenols, dihydroxybenzenes and polyphenols	Sulphuric acid, quinine, benzalkonium chloride	Multicommutation, all lines heated to 60 °C	Pharmaceutical formulations, photographic solution, natural waters (hydroquinone)	Hydroquinone 30 µg L ⁻¹ (3 × 10 ⁻⁷ M) Resorcinol 10 µg L ⁻¹ (9 × 10 ⁻⁸ M) Phloroglucinol 10 µg L ⁻¹ (8 × 10 ⁻⁸ M) Pyrocatechol 40 µg L ⁻¹ (4 × 10 ⁻⁷ M) 4-Hydroxybenzoic acid 20 µg L ⁻¹ (1 × 10 ⁻⁷ M) Quercetin 20 µg L ⁻¹ (7 × 10 ⁻⁸ M) Eugenol 80 µg L ⁻¹ (5 × 10 ⁻⁷ M)	B. Gómez-Taylor Corominas ⁹⁸

Table 2.2 Continued

Analyte	Acid/enhancers	Instrumentation/comments	Matrix	Limit of detection (LoD)	Reference
Phenols (polyphenols)	Glyoxal	FIA, inhibition of chemiluminescence from reaction of KMnO_4 with glyoxal	-	1×10^{-7} M	C. Yu ⁴⁹³
Phenylhydrazines, hexanal oxime, hydroxylamine and dimethylglyoxime	Sulphuric acid, formic acid, rhodamine B	FIA, some analytes in aqueous propan-2-ol	Not applied	2,4-Dinitrophenylhydrazine 5×10^{-10} M Hexanal oxime 1×10^{-5} M Hydroxylamine 1×10^{-4} M Dimethylglyoxime 1×10^{-4} M	A. Townshend ¹²⁰
Phentolamine	Sulphuric acid, formaldehyde	FIA	Injections, plasma, urine	5 ng mL^{-1} (2×10^{-8} M)	J. Pan ¹⁵³
Phentolamine mesylate	-	FIA	Injections, urine, plasma	$0.01 \text{ } \mu\text{g mL}^{-1}$ (3×10^{-8} M)	W. Liu ⁴⁹⁴
Phenylephrine hydrochloride	Sulphuric acid	FIA, all lines heated to 80°C	Pharmaceutical formulations	20 ppb (1×10^{-7} M)	Y. Fuster Mestre ⁴⁹⁵
Phloroglucinol	Formaldehyde	FIA	-	3×10^{-9} M	C. Xie ⁴⁹⁶
Polyhydroxybenzenes and <i>o</i> -phenylenediamine	Sulphuric acid	FIA, see also table entry 'Catecholamines'	Not applied	Epinephrine 8×10^{-6} M Norepinephrine 1×10^{-5} M Dopamine 2×10^{-5} M L-Dopa 6×10^{-6} M Hydroquinone 1×10^{-5} M Pyrogallol 1×10^{-5} M Phloroglucinol 8×10^{-6} M Pyrocatechol 5×10^{-6} M Resorcinol 6×10^{-6} M <i>o</i> -Phenylenediamine 9×10^{-6} M Gallic acid 5×10^{-6} M	N. Deftereos ¹²²
Polyhydroxybenzenes	Sulphuric acid, hexametaphosphate	FIA	Bulk	Catechol 2×10^{-6} M Resorcinol 1×10^{-6} M Hydroquinone 1×10^{-6} M	J. Dolejšová ⁴⁹⁷
Polyhydroxybenzenes	Sulphuric acid, formic acid	HPLC (C_{18}), isocratic mobile phase: methanol-phosphoric acid	Natural water	Catechol $5 \times 10^{-3} \text{ mg L}^{-1}$ (5×10^{-8} M) Resorcinol $5 \times 10^{-3} \text{ mg L}^{-1}$ (4×10^{-8} M) Hydroquinone $3 \times 10^{-3} \text{ mg L}^{-1}$ (3×10^{-8} M) 1,2,4-benzenetriol $4 \times 10^{-3} \text{ mg L}^{-1}$ (3×10^{-8} M)	S. Fan ^{124, 498}
Polyhydroxybenzenes	Sulphuric acid, hexametaphosphate	FIA	Bulk	Pyrogallol 7×10^{-6} M Phloroglucinol 1×10^{-6} M 1,2,4-Trihydroxybenzene 5×10^{-7} M	J. Dolejšová ⁴⁹⁷
Promethazine hydrochloride	Glyoxal	FIA	Tablets, injections	$4 \times 10^{-8} \text{ g mL}^{-1}$ (1×10^{-7} M)	Y. Xue ⁴⁹⁹

Table 2.2 Continued

Analyte	Acid/enhancers	Instrumentation/comments	Matrix	Limit of detection (LoD)	Reference
Promethazine hydrochloride	Sulphuric acid	FIA	Pharmaceutical formulations	2×10^{-5} M	S.M. Sultan ⁴⁷
Propanil and other anilide pesticides	Sulphuric acid	Multicommutation, on-line photoreactor, photodegradation in acetate buffer prior to analysis	Synthetic formulation, natural waters	Propanil $8 \mu\text{g L}^{-1}$ (4×10^{-8} M) Alachlor $41 \mu\text{g L}^{-1}$ (2×10^{-7} M) Flumetsulam $25 \mu\text{g L}^{-1}$ (8×10^{-8} M) Furalaxyl $34 \mu\text{g L}^{-1}$ (1×10^{-7} M) Ofurace $58 \mu\text{g L}^{-1}$ (2×10^{-7} M)	J.R. Albert-García ⁶⁹
Propranolol	Sulphuric acid	FIA	Tablets	70 ng mL^{-1} (3×10^{-7} M)	A. Townshend ¹²⁶
Propranolol hydrochloride	Polyphosphoric acid, ferrous ions	FIA	Tablets	$1 \times 10^{-7} \text{ g mL}^{-1}$ (3×10^{-7} M)	W. Liu ⁵⁰⁰
Propranolol	Sulphuric acid	Multicommutation	Tablets, injection	20 mg L^{-1} (8×10^{-5} M)	Marques ⁵⁰¹
Psilocin	Orthophosphoric acid, hexametaphosphate	FIA	Mushrooms	9×10^{-10} M	N. Anastos ¹⁰⁰
Psilocin	Orthophosphoric acid, polyphosphate	HPLC (C ₁₂), isocratic mobile phase: methanol-ammonium formate, 4-hydroxyindole internal standard and MnO ₄ ⁻	Mushrooms	Psilocin 1×10^{-8} M	N. Anastos ⁴⁵²
Pyruvate	Sulphuric acid, quinine	FIA	Serum	$0.8 \mu\text{g mL}^{-1}$ (9×10^{-6} M)	M.L. Feng ⁴⁹⁹
Reserpine	Polyphosphoric acid, hydrogen peroxide	FIA	Pharmaceutical formulations	$3 \times 10^{-7} \text{ g mL}^{-1}$ (5×10^{-7} M)	L. Li ⁵⁰²
Resorcinol	-	FIA	Wastewater	$0.06 \mu\text{g mL}^{-1}$ (5×10^{-7} M)	L. Li ⁵⁰³
Reserpine, rescinnamine and yohimbine	Polyphosphoric acid (pH adjusted with NaOH)	Batch procedure and FIA, sample in glacial acetic acid	Tablets	Reserpine $0.04 \mu\text{g mL}^{-1}$ (7×10^{-8} M) (FIA) Rescinnamine $0.04 \mu\text{g mL}^{-1}$ (6×10^{-8} M) (Batch) Yohimbine $0.03 \mu\text{g mL}^{-1}$ (9×10^{-8} M) (FIA)	N. Pinotsis ¹¹³
Resorcinol	Formaldehyde	FIA	-	3×10^{-9} M	C. Xie ⁵⁰⁴
RNA	Hydrochloric acid, ethidium bromide	-	Synthetic	$0.06 \mu\text{g mL}^{-1}$	H. Zhuang ⁵⁰⁵
Rutin	Sulphuric acid, hexmetaphosphate	FIA	Tablets	5×10^{-6} M	J. Dolejšová ⁵⁰⁶

Table 2.2 Continued

Analyte	Acid/enhancers	Instrumentation/comments	Matrix	Limit of detection (LoD)	Reference
Salbutamol	Sulphuric acid, polyphosphate	FIA	Capsules, syrup	3×10^{-8} M	N.W. Barnett ⁵⁰⁷
Salbutamol	Sulphuric acid, polyphosphate	SIA, on-line solid-phase extraction	Urine	$0.03 \mu\text{g mL}^{-1}$ (1×10^{-7} M)	J. Huclová ³⁷⁴
Salbutamol	-	FIA	Tablets, aerosol	60 ng mL^{-1} (3×10^{-7} M)	L. Lj ⁵⁰⁸
Salicylamide	Sulphuric acid	FIA, all lines heated to 80°C	Capsules, urine	20 ng mL^{-1} (2×10^{-7} M)	Y. Fuster Mestre ⁵⁰⁹
Salicylic acid	Glyoxal	-	Benzoic acid	8×10^{-6} M	Y. Lj ⁵¹⁰
Salicylic acid	Formaldehyde	FIA	Pharmaceutical formulations	3×10^{-7} M	C. Xie ⁵¹¹
Salicylic acid	Sulphuric acid	Multicommutation, anion-exchange gel in detection cell retains permanganate	Pharmaceutical formulations	$0.3 \mu\text{g mL}^{-1}$ (2×10^{-6} M)	E.J. Llorent-Martinez ⁵¹²
Serotonin, related indoles and morphine	Sulphuric acid, polyphosphate	FIA, see also table entry 'Phenols and amines'	Not applied	Serotonin 5×10^{-10} M 5-Hydroxytryptophan 3×10^{-9} M 5-Hydroxyindole-3-acetic acid 2×10^{-8} M Morphine 1×10^{-10} M	N.W. Barnett ⁴⁹²
Serotonin, dopamine, norepinephrine and catechol	Sulphuric acid	CE, sodium tetraborate electrophoresis buffer	Not applied	1×10^{-4} M for each analyte	Y. Lee ⁵¹³
Sulfadiazine	Polyphosphoric acid, formaldehyde	FIA	Pharmaceutical formulation	2×10^{-7} M	H. Liu ³⁴
Sulfadiazine	Formaldehyde/polyphosphate acid	Flow-injection chemiluminescence (FI-CL)	compound naristillae	Range: 8.0×10^{-7} to 2.0×10^{-4} mol/L. LoD: 2.0×10^{-7} mol/L	Haiyan Liu ³⁴
Sulphonamides	Sulphuric acid, glutaraldehyde	SIA	Eye drops, tablets (sulfacetamide and sulfafurazole)	Sulphanilamide 1×10^{-5} M Sulphacetamide 1×10^{-5} M Sulphathiazole 9×10^{-6} M Sulphadimidine 3×10^{-5} M Sulphafurazole 9×10^{-6} M Sulphamethoxypyridazine 2×10^{-5} M Sulphaguanidine 9×10^{-6} M	H. Paseková ³⁵

Table 2.2 Continued

Analyte	Acid/enhancers	Instrumentation/comments	Matrix	Limit of detection (LoD)	Reference
Sulphonamides	Sulphuric acid, hexadecylpyridinium	FIA, on-line photoreactor, sample heated to 70 °C before injection, photodegradation in water or sulphuric acid prior to analysis	Dissolution profiles of sulfamethoxazole pharmaceuticals	Sulphacetamide 60 µg L ⁻¹ (3 × 10 ⁻⁷ M) Sulphadiazine 80 µg L ⁻¹ (3 × 10 ⁻⁷ M) Sulphadimidine 80 µg L ⁻¹ (3 × 10 ⁻⁷ M) Sulphaguanidine 80 µg L ⁻¹ (4 × 10 ⁻⁷ M) Sulphamerazine 60 µg L ⁻¹ (2 × 10 ⁻⁷ M) Sulphamethoxazole 60 µg L ⁻¹ (2 × 10 ⁻⁷ M) Sulphamethoxypyridazine 80 µg L ⁻¹ (3 × 10 ⁻⁷ M) Sulphanilamide 30 µg L ⁻¹ (2 × 10 ⁻⁷ M) Sulphathiazole 60 µg L ⁻¹ (2 × 10 ⁻⁷ M)	M. Catalá Icardo ³⁸¹
Sympathomimetic drugs	Sulphuric acid, formic acid	FIA	Tablets, drops, plasma, urine	Etilefrine 0.2 µg mL ⁻¹ (9 × 10 ⁻⁷ M) Isoxsuprine 0.2 µg mL ⁻¹ (7 × 10 ⁻⁷ M) Prenalterol 0.03 µg mL ⁻¹ (1 × 10 ⁻⁷ M)	F.A. Aly ¹⁴⁹
Tannic acid	Perchloric acid, quinine	FIA, all lines heated to 60 °C	Pharmaceutical and galenic formulations, urine, natural waters	100 µg L ⁻¹	B. Gómez-Taylor Corominas ⁷⁶
Terbutaline sulphate	Sulphuric acid, formaldehyde	FIA	Binding of terbutaline to albumin	3 × 10 ⁻⁸ M	Z. Wang ³⁷⁹
Tetracyclines	Hydrochloric acid, octylphenyl polyglycol ether	FIA	Tablets	Tetracycline 0.4 µg mL ⁻¹ (9 × 10 ⁻⁷ M) Oxytetracycline 0.5 µg mL ⁻¹ (1 × 10 ⁻⁶ M) Chlortetracycline 0.6 µg mL ⁻¹ (1 × 10 ⁻⁶ M)	Z. Li ⁵¹⁴
Tetrahydrobenzothiazolyl imine	Formic acid	FIA	-	5 × 10 ⁻⁸ M	S. Zhang ⁵¹⁵
2,3,5,4'-Tetrahydroxystilbene-2-O-β-d-glucoside	Nitric acid, formaldehyde	HPLC (C ₁₈), isocratic mobile phase: acetonitrile–phosphoric acid	Chinese medicines	12 µg mL ⁻¹ (3 × 10 ⁻⁵ M)	H. Wei ⁵¹⁶
Thiamine	Sulphuric acid	FIA, on-line photoreactor, photodegradation in sulphuric acid prior to analysis	Tablets, ampoules	0.05 mg L ⁻¹ (2 × 10 ⁻⁷ M)	A. Wasiełczuk ⁵¹⁷

Table 2.2 Continued

Analyte	Acid/enhancers	Instrumentation/comments	Matrix	Limit of detection (LoD)	Reference
Thiazides	Sulphuric acid	FIA, on-line photoreactor, photodegradation in NaOH solution prior to analysis, Ce(IV) gave greater emission	Not applied	Not reported using KMnO ₄	M. Ci-borowski ⁵¹⁸
Thiol-containing drugs	Sulphuric acid, quinine	FIA	Pharmaceutical formulations (cysteine and captopril)	Cysteine 0.01 µg mL ⁻¹ (8 × 10 ⁻⁸ M) Glutathione 0.02 µg mL ⁻¹ (7 × 10 ⁻⁸ M) <i>N</i> -Acetylcysteine 0.02 µg mL ⁻¹ (1 × 10 ⁻⁷ M) Captopril 0.006 µg mL ⁻¹ (3 × 10 ⁻⁸ M)	Y. Li ³⁷⁴
Thioridazine hydrochloride	Sulphuric acid	FIA, other phenothiazine derivatives produced chemiluminescence	Tablets	1 × 10 ⁻⁶ M	A. Kojlo ⁵¹⁹
Trimetazidine	Polyphosphoric acid	Batch procedure	Serum, urine	2 ng mL ⁻¹ (8 × 10 ⁻⁹ M)	L.P. Palilis ⁵²⁰
Trimethoprim	Sulphuric acid, hexameta-phosphate	SIA	Tablets	0.1 µg mL ⁻¹ (3 × 10 ⁻⁷ M)	M. Polášek ¹¹⁶
Tryptophan	Galangin/polyphosphoric acid (PPA)	Flow-injection chemiluminescence (FI-CL)	-	Range 0.05–10 µg/mL LoD: 5.0 × 10 ⁻³ µg/mL	Hui Chen ⁵²¹
<i>l</i> -Tryptophan	-	FIA	Mixture of 18 amino acids	2 × 10 ⁻⁷ g mL ⁻¹ (1 × 10 ⁻⁶ M)	M. Yang ⁵²²
Tsumacide	Nitric acid, rhodamine 6G	FIA, sample degraded in KOH solution prior to analysis	Vegetables	7 × 10 ⁻⁴ mg L ⁻¹ (4 × 10 ⁻⁹ M)	H. Liu ⁵²³
<i>l</i> -Tyrosine	Hydrogen peroxide	FIA	-	4 × 10 ⁻⁷ g mL ⁻¹ (2 × 10 ⁻⁶ M)	L. Li ⁵²⁴
<i>l</i> -Tyrosine	Sulphuric acid	-	Amino acid injection	9 × 10 ⁻⁷ M	C. Zhu ⁵²⁵
Tyrosine	Formaldehyde	FIA	-	3 × 10 ⁻⁸ g mL ⁻¹ (2 × 10 ⁻⁷ M)	Y. He ⁵²⁶
Tyrosine and tryptophan	Orthophosphoric acid, polyphosphate	FIA, on-line C ₁₈ guard column separation, tyrosine	Mixture of 20 amino acids	Tyrosine 5 × 10 ⁻⁸ M Tryptophan 3 × 10 ⁻⁸ M Tyrosine at pH 6.75 1 × 10 ⁻⁸ M	J.W. Costin ⁴⁹¹
Uric acid	Nitric acid, octylphenyl polyglycol ether	FIA	Urine	0.06 µg mL ⁻¹ (3 × 10 ⁻⁷ M)	Z. Li ⁵²⁷
Uric acid	Hydrochloric acid, formaldehyde	FIA	Urine	6 × 10 ⁻⁶ g L ⁻¹ (4 × 10 ⁻⁸ M)	M. Liu ³⁸⁸
Vanillin and related compounds	Sulphuric acid or polyphosphoric acid	Batch procedure	Commercial vanilla products	Vanillin 0.05 µg mL ⁻¹ (3 × 10 ⁻⁷ M) Ethylvanillin 0.003 µg mL ⁻¹ (2 × 10 ⁻⁸ M) 4-Hydroxy-3-methoxybenzylalcohol 0.0009 µg mL ⁻¹ 6 × 10 ⁻⁹ M	M. Timotheou-Potamia ⁵²⁸
Vitamin E	Sulphuric acid, formaldehyde	FIA, inhibition of chemiluminescence, acetone medium	Tablets	3.0 × 10 ⁻⁶ M	L. Li ⁵²⁹

Table 2.3 Determination of inorganic compounds with acidic potassium permanganate⁷

Analyte	Acid/enhancers	Instrumentation/comments	Matrix	Limit of detection (LoD)	Reference
Arsenic(III)	Sulphuric acid, hexametaphosphate	FIA	Not applied	0.3 µg L ⁻¹ (4 × 10 ⁻⁹ M)	S. Sa-tienperaku ¹¹⁷
Copper(I)	Formaldehyde	FIA	-	6 × 10 ⁻⁸ g mL ⁻¹ (1 × 10 ⁻⁶ M)	Y. He ⁵³⁰
Gold nanoparticles	Sulphuric acid	FIA	Not applied	5 × 10 ⁻⁶ M	Z. Zhang ⁵³¹
Hydrazine	Sulphuric acid	Batch procedure, gas sampling device with hydrazine trap, hydrazine derivatives also produce light	Workroom air	2 × 10 ⁻⁸ g mL ⁻¹ (6 × 10 ⁻⁷ M)	Z. He ⁵³²
Hydrogen peroxide	H ₂ SO ₄ , octylphenyl polyglycol ether	FIA, compounds that affect micelle formation interfered	Rain water	6 × 10 ⁻⁹ M	M.L. Feng ⁷⁸
Hydrogen sulphide	Sulphuric acid, riboflavin phosphate	Flow analysis, reagent nebulised to react directly with gas	-	0.5 ppm	N. Omi ⁵³³
Iodide	Formaldehyde	-	Food	2 × 10 ⁻⁸ g mL ⁻¹ (1 × 10 ⁻⁷ M)	Y. He ⁵¹⁰ and Q. Gao ^{90, 534}
Iodide	Formaldehyde	Inhibition of chemiluminescence	Food	8 × 10 ⁻⁷ M	E. Liu ⁹¹
Iodide	Formaldehyde	SIA	Food	1 × 10 ⁻⁸ M	C. Gao ⁹²
Iodide	Hydrochloric acid, formaldehyde	FIA	Iodized salt	1 × 10 ⁻⁷ M	M. Yaqoob ⁸⁹
Iron(II)	Hydrochloric acid, formaldehyde	FIA	Natural water	4 × 10 ⁻¹⁰ g mL ⁻¹ (8 × 10 ⁻⁹ M)	Y. He ⁴⁰⁴
Iron(II)	Hydrochloric acid, formaldehyde	FIA	Natural water	0.6 µg L ⁻¹ (1 × 10 ⁻⁸ M)	W. Li ⁵³⁵
Iron(II)	Hydrochloric acid, formaldehyde	FIA, total iron determined after reduction of iron(III) to iron(II)	Natural water	1 × 10 ⁻⁹ M	M. Yaqoob ¹³⁷
Manganese(II)	Butane-2,3-dione (diacetyl)	Quantitation based on the effect on the reaction rate of acidic permanganate with butane-2,3-dione	Alloys	6 × 10 ⁻⁸ M	C. Zhu ¹⁵⁵
Nitrite	Sulphuric acid, acriflavine	FIA, on-line pre-concentration with solid-phase reactor, inhibition of CL.	Natural waters, industrial formulations, soil samples	10 µg L ⁻¹ (2 × 10 ⁻⁷ M) (without pre-concentration)	M. Catalá Icardo ⁷⁹
Permanganate index (COD _{Mn})	H ₂ SO ₄	Flow-injection chemiluminescence (FI-CL)	-	Range: 0.3–200 mg/L LoD: 0.3 mg/L COD _{Mn}	Jinjun TIAN ⁵³⁶

Table 2.3 Continued

Analyte	Acid/enhancers	Instrumentation/comments	Matrix	Limit of detection (LoD)	Reference
Reductants: iron(II), sulphide, iodide, Cu(I)	Formaldehyde	FIA	-	-	Y. He ⁵³⁷
Sulphite	Sulphuric acid, riboflavin phosphate or brilliant sulfaflavine	FIA, sulphide and thiosulfate also produce chemiluminescence	Not applied	0.9 ng 10 μL^{-1} (1×10^{-6} M)	M. Yamada ⁵³⁸
Sulphite	Sulphuric acid, riboflavin or CAPS	FIA, other cyclohexanes tested for enhancing effect	Not applied	1 ng 20 μL^{-1} (8×10^{-7} M)	S.A. Al-Tamrah ⁵³⁹
Sulphite	Riboflavin	Flow sensor, reagents electrostatically immobilised on anion-exchange resin, sensor lifetime of ~ 1000 injections	Beer, wine	0.06 mg L^{-1} (8×10^{-7} M)	W. Qin ⁸⁴
Sulphite and sulphur dioxide	Sulphuric acid, SDBS, tris(1,10-phenanthroline)ruthenium(II)	Batch procedure, sulphur dioxide sampled by bubbling air through triethanolamine solution	Air (sulphur dioxide)	Sulphite 5×10^{-9} M	H. Meng ⁶⁴
Sulphite and sulphur dioxide	Sulphuric acid, SDBS, tris(2,2'-bipyridyl)ruthenium(II)	Batch procedure, sulphur dioxide sampled by bubbling air through triethanolamine solution	Sugar (sulphite), air (sulphur dioxide)	Sulphite 3×10^{-8} M	H. Meng ⁶⁵
Sulphite	Quinine	FIA, permanganate immobilized on anion exchange resin, sensor lifetime of over 200 injections	Beer	5×10^{-8} g mL^{-1} (6×10^{-7} M)	P. Qu ⁵⁴⁰
Sulphite	Sodium hexametaphosphate / rhodamine B in 0.02 M H_3PO_4	pervaporation flow injection chemiluminescence (PFI-CL)	Food samples	Range of 0.5–10.0 mg L^{-1} LoD: 0.2 mg L^{-1}	Sakchai Sattienperakul ⁵⁴¹
Sulphur dioxide	Sulphuric acid	Batch procedure, analyte sampled by bubbling air through aqueous tetrachloromercurate	Not applied	20 ng cm^{-3}	J. Stauff ⁵⁴
Sulphur dioxide	Sulphuric acid	Batch procedure, analyte trapped on filter impregnated with tetrachloromercurate	Atmospheric air	0.03 $\mu\text{g m}^{-3}$ ^{58, 59}	W. Jaeschke ^{55, 57-59}
Sulphur dioxide	Sulphuric acid	Batch procedure, analyte trapped on filter impregnated with tetrachloromercurate	Atmospheric air	8 pptv ⁶⁰	F. Meixner ^{56, 60, 542, 543}
Sulphur dioxide	Sulphuric acid, flavin mononucleotide, Tween 85	Continuous flow, reagent nebulised to react directly with gas	Not applied	3 ppbv	M. Kato ⁶⁶
Sulphur dioxide	Sulphuric acid	Continuous flow, analyte stabilised in alkaline solution with sodium formate	Rain water	0.8 ng mL^{-1} (1×10^{-8} M)	K. Takeuchi ^{80, 544}
Sulphur dioxide and hydrogen sulphide	Riboflavin phosphate	Continuous flow, on-line gas trap, successive determination of two analytes, thiosulfate also produces light	Atmospheric air	Sulphur dioxide 2×10^{-7} M Hydrogen sulphide 9×10^{-7} M	M. Ishii ⁶³
Tin(II)	Hydrochloric acid, HCOH	FIA, sulfhydryl cotton separation	Natural waters	0.04 $\mu\text{g L}^{-1}$ (3×10^{-10} M)	S. Fan ⁴⁰⁸

Table 2.4 Determination of compounds that enhance of the CL from acidic potassium permanganate and sulphite⁷

Analyte	Acid/enhancers	Instrumentation/comments	Matrix	Limit of detection (LoD)	Reference
Acemetacin	Phosphoric acid, sulphite	FIA	-	7×10^{-8} M	X. Li ⁵⁴⁵
Aminopyrine	Dithionite	FIA	Tablets	6×10^{-8} g mL ⁻¹ (3×10^{-7} M)	L. Li ⁵⁴⁶
Bile acids	Sulphuric acid, sulphite	FIA, Ce(IV) gave greater intensity	Not applied	Not reported with KMnO ₄	I.M. Psarellis ⁵⁴⁷
Brucine	Polyphosphoric acid, sulphite	Flow analysis, molecular imprinted polymer within the detection cell	Urine	2×10^{-9} g mL ⁻¹ (5×10^{-9} M)	M. Liu ³⁹¹
Carbamates and other pesticides	Sulphuric acid, sulphite	FIA	Natural waters (carbaryl and carbofuran)	Carbaryl 10 ng mL ⁻¹ (5×10^{-8} M) Carbofuran 50 ng mL ⁻¹ (2×10^{-7} M) Dinoseb 100 ng mL ⁻¹ (4×10^{-7} M) Diazinon 100 ng mL ⁻¹ (3×10^{-7} M) Malathion 300 ng mL ⁻¹ (9×10^{-7} M)	A. Waseem ⁵⁴⁸
Ciprofloxacin	Sulphuric acid, thiosulfate	FIA	Tablets, injections, blood, urine	4×10^{-9} g mL ⁻¹ (1×10^{-8} M)	H. Sun ⁵⁴⁹
Ciprofloxacin	Sulphuric acid, dithionite	FIA, terbium(III) used as enhancer	Tablets, urine, serum	4×10^{-9} M	Z. Zhang ⁵⁵⁰
Enoxacin and ofloxacin	Hydrochloric acid or sulphuric acid, sulphite	FIA, terbium(III) used as enhancer	Pharmaceutical formulation, urine	Enoxacin 2×10^{-10} M Ofloxacin 6×10^{-10} M	L. Yi ⁵⁵¹
Ibuprofen	Sulphuric acid, sulphite	FIA	Tablets, urine	0.02 mg L ⁻¹ (1×10^{-7} M)	Y. Li ⁵⁵²
Ketoprofen	Sulphuric acid, sulphite	FIA	Tablets, urine	2×10^{-8} M	Y. Zhuang ⁴⁶⁰
Methyltestosterone	Sulphuric acid, thiosulfate	FIA, sample in aqueous acetone	Fish	1×10^{-8} g mL ⁻¹ (3×10^{-8} M)	Z. Xie ⁹³
Morphine	Polyphosphoric acid, sulphite	Flow analysis, molecular imprinted polymer within the detection cell	Urine	2×10^{-9} g mL ⁻¹ (7×10^{-9} M)	Y. He ³⁹⁰
Naproxen	Sulphite	FIA	Capsules	2×10^{-9} g mL ⁻¹ (9×10^{-9} M)	Y. Li ⁵²⁹
Noscapine (narcotine)	Sulphuric acid, sulphite	FIA	Synthetic	8×10^{-9} M	Y. Zhuang ⁵⁵³
Papaverine	Sulphuric acid, sulphite	FIA	Injections, compound liquorice tablets	1×10^{-7} M	Y. Zhuang ⁵⁵⁴

Table 2.4 Continued

Analyte	Acid/enhancers	Instrumentation/comments	Matrix	Limit of detection (LoD)	Reference
Paracetamol	Sulphuric acid, sulphite	FIA	Tablets	$2 \times 10^{-9} \text{ g mL}^{-1}$ ($1 \times 10^{-8} \text{ M}$)	X. Xiong ⁵⁵⁵
Pazufloxacin mesylate	NaOH (but final reaction mixture was pH 6), dithionite	FIA, europium(III) used as enhancer	Serum, urine	$3 \times 10^{-9} \text{ M}$	X.L. Wang ⁵⁵⁶
Pipemidic acid	Sulphuric acid, sulphite	FIA	Binding of pipemidic acid to albumin	$2 \times 10^{-7} \text{ M}$	B. Li ⁵⁵⁷
Pipemidic acid	Sulphite	FIA	Pharmaceutical formulations	$3 \times 10^{-8} \text{ g mL}^{-1}$ ($1 \times 10^{-7} \text{ M}$)	L. Li ⁵⁵⁸
Pipemidic acid	Tetraphosphoric acid, dithionite	FIA	Tablets, capsules	$3 \times 10^{-6} \text{ g L}^{-1}$ ($1 \times 10^{-8} \text{ M}$)	M. Yang ⁵⁵⁹
Pipemidic acid	Dithionite	FIA, europium(III) used as enhancer	Tablet, urine	$4 \times 10^{-9} \text{ M}$	X. Li ⁵⁴⁵
Riboflavin	Polyphosphoric acid, dithionite	FIA	Tablets, injections	$6 \times 10^{-8} \text{ g mL}^{-1}$ ($2 \times 10^{-7} \text{ M}$)	L. Li ⁵⁶⁰
Riboflavin	Polyphosphoric acid, sulphite	FIA	Pharmaceutical formulations	$3 \times 10^{-8} \text{ g mL}^{-1}$ ($8 \times 10^{-8} \text{ M}$)	L. Li ⁵⁶¹
Sinomenine hydrochloride	Thiosulfate	HPLC	Serum, urine	$8 \times 10^{-8} \text{ g mL}^{-1}$ ($2 \times 10^{-7} \text{ M}$)	Y. Sun ⁵⁶²
Sulfamethoxazole	Sulphite	FIA	Bulk	$3 \times 10^{-7} \text{ g mL}^{-1}$ ($1 \times 10^{-6} \text{ M}$)	L. Li ⁵⁶³
Tetracyclines	Phosphoric acid, sulphite	HPLC (C ₁₈), isocratic mobile phase: acetonitrile–phosphoric acid, β -cyclodextrin used as enhancer	Honey	Oxytetracycline 3 ng mL^{-1} ($7 \times 10^{-9} \text{ M}$) Tetracycline 5 ng mL^{-1} ($1 \times 10^{-8} \text{ M}$) Metacycline 0.9 ng mL^{-1} ($2 \times 10^{-9} \text{ M}$)	G. Wan ⁵⁶⁴
Tetrahydropalmatine	Dithionite ⁵⁶⁵ , thiosulfate ⁵⁶⁶ or sulphite ⁵⁶⁷	FIA	Tablets	$3 \times 10^{-9} \text{ g mL}^{-1}$ ($9 \times 10^{-9} \text{ M}$) ⁵⁶⁵	L. Li ⁵⁶⁵⁻⁵⁶⁷
Trimethoprim	Thiosulfate	FIA	Tablets	$4 \times 10^{-8} \text{ g mL}^{-1}$ ($1 \times 10^{-7} \text{ M}$)	M. Yang ⁵⁴⁶
Trimethoprim	Sulphuric acid, thiosulfate	Flow analysis, molecular imprinted polymer within the detection cell	Tablets, urine	$2 \times 10^{-8} \text{ g mL}^{-1}$ ($7 \times 10^{-8} \text{ M}$)	M. Yang ⁵⁴⁶
Vitamin B6	Polyphosphoric acid, dithionite	FIA	Tablet, injection	$6 \times 10^{-5} \text{ g L}^{-1}$ ($3 \times 10^{-7} \text{ M}$)	L. Li ⁵⁶⁸

Table 2.5 Analytical applications of manganese(IV) as a CL reagent²¹⁸

Analyte	Instrumentation & comments	Sample Matrix	Limit of detection (LoD)	Reference
Ascorbic acid	FIA	Tablets, injections	2×10^{-8} M	Zhu ⁵⁶⁹
Ascorbic acid	FIA/SIA	Vitamin C tablets	5×10^{-8} M	Anastos ¹²⁷
Atropine	FIA	–	5×10^{-6} M	Brown ²¹⁹
Cefazolin	FIA	–	4×10^{-7} M	Brown ²¹⁸
Cefoperazone	FIA	–	3×10^{-7} M	Brown ²¹⁸
Cefradine	FIA	Pharmaceuticals	3×10^{-8} M	Brown ²¹⁸
Ceftriaxone	FIA	–	3×10^{-9} M	Brown ²¹⁸
Ciprofloxacin	FIA	–	3×10^{-8} M	Du ³⁸⁴
Ciprofloxacin	FIA	–	1×10^{-7} M	Li ⁵⁷⁰
Codeine	FIA	–	5×10^{-8} M	Barnett ³⁸⁵
Codeine	FIA/HPLC	–	1×10^{-8} M	Brown ²¹⁹
Dipyron (analgin)	FIA	Tablets	8×10^{-5} M	Zhao ³⁸⁷
Dipyron (metamizol)	FIA	Injections	2×10^{-7} M	Brown ²¹⁸
Dipyron (analgin)	FA(MIP)	Urine	4×10^{-8} M	He ⁵⁷¹
Fenoterol	FIA	–	1×10^{-8} M	Brown ²¹⁹
Heroin	FIA	–	1×10^{-6} M	Brown ²¹⁹
5-Hydroxyindole-3-acetic acid	FIA	–	1×10^{-8} M	Brown ²¹⁹
5-Hydroxytryptophan	FIA	–	1×10^{-8} M	Brown ²¹⁹
Indapamide	FA(MIP)	Urine	2×10^{-8} M	Nie ³⁸⁸
Indomethacin	FA(MIP)	Urine	1×10^{-7} M	Nie ³⁸⁴
Iron(II)	FIA	–	3×10^{-7} M	Barnett ³⁸⁵
Manganese(II)	FIA	–	5×10^{-8} M	Barnett ³⁸⁵
Morphine	FIA	–	8×10^{-8} M	Barnett ³⁸⁵
Morphine	FIA/HPLC	–	5×10^{-8} M	Brown ²¹⁹

Table 2.5 Continued

Analyte	Instrumentation & comments	Sample Matrix	Limit of detection (LoD)	Reference
Norfloxacin	FIA	Capsules	3×10^{-8} M	Du ³⁸⁴
Norfloxacin	FIA	Capsules	3×10^{-8} M	Brown ²¹⁹
Ofloxacin	FIA	–	5×10^{-8} M	Du ³⁸⁴
Ofloxacin	FIA	–	3×10^{-8} M	Brown ²¹⁹
Oripavine	FIA/HPLC	–	5×10^{-9} M	Brown ²¹⁹
Papaverine	FIA/HPLC	–	1×10^{-9} M	Brown ²¹⁹
Pseudomorphine	FIA/HPLC	–	1×10^{-9} M	Brown ²¹⁹
Pyrogallol	FIA	–	5×10^{-9} M	Brown ²¹⁹
Serotonin	FIA	–	1×10^{-8} M	Brown ²¹⁹
Sulfadiazine	FIA	–	1×10^{-7} M	Brown ²¹⁸
Sulfaguanidine	FIA	–	9×10^{-8} M	Brown ²¹⁸
Sulfamethoxazole	FIA	Tablets	8×10^{-8} M	Brown ²¹⁸
Tamoxifen	FA(MIP)	Urine	1×10^{-7} M	Nie ³⁸⁸
Thebaine	FIA/HPLC	–	5×10^{-9} M	Brown ²¹⁹
2-Thiobarbituric acid	FIA	–	5×10^{-9} M	Brown ²¹⁹
Timolol maleate	FIA	Eye drops	7×10^{-7} M	Brown ²¹⁸
Tryptamine	FIA	–	5×10^{-9} M	Brown ²¹⁹
Tryptophan	FIA	–	1×10^{-8} M	Brown ²¹⁹
Tyrosine	FIA	Amino acid injection	1×10^{-6} M	Nie ⁵⁷²

Table 2.6 Analytical applications of electrogenerated Mn(III) as a CL reagent²¹⁸

Analyte	Instrumentation & comments	Sample Matrix	Limit of detection (LoD)	Reference
Adreson (cortisone acetate)	FIA	Tablets and injections	1×10^{-8} M	Brown ²¹⁸
Aminopyrine (amidopyrine)	FIA	Tablets and injections	9×10^{-7} M	Brown ²¹⁸
Ascorbic acid	HPLC	Beer, serum, urine	2×10^{-7} M	Yang ⁵⁷³
Captopril	FIA	Tablets	8×10^{-8} M	Zheng ²²⁵
Cephradine	FIA	Tablets and injections	6×10^{-8} M	Brown ²¹⁸
Chlorpromazine	FIA	Tablets	2×10^{-7} M	Brown ²¹⁸
Dexamethasone 21-phosphate	FIA	Pharmaceutical	1×10^{-7} M	Chen ²²⁸
Indomethacin	HPLC	Tablets and urine	2×10^{-8} M	Zhang ³⁹⁷
Quinine	FIA	Tablets	4×10^{-8} M	Zheng ²²⁹
Reserpine	FIA	Injections	8×10^{-9} M	Brown ²¹⁸
Sulfite	FIA	SO ₂ in air	8×10^{-8} M	Zheng ²³¹
Tryptophan	FIA	-	2×10^{-6} M	Brown ²¹⁸
Adreson (cortisone acetate)	FIA	Tablets and injections	1×10^{-8} M	Brown ²¹⁸

This review surveys a broad range of applications and shows a comprehensive picture of the current status of the manganese-based chemiluminescence in analytical chemistry. The most commonly used manganese reagent in the chemiluminescence analytical applications is undoubtedly the permanganate chemiluminescence detector thanks to its unique features. Permanganate is a strong oxidant with a unique affinity for oxidizing a range of reductants with potential chemiluminescence emission, particularly in acidic conditions due to a conversion of MnO_4^- ion to the more active oxidants and the potential involvement of five oxidation states of manganese. In addition, permanganate has the ability to react with divers chemiluminescence enhancers, such as low molecular weight aldehydes and metal ions than manganese(III) and manganese(IV). These characteristics have made permanganate suitable and a first choice manganese-based reagent for analytical applications. Mn(III) and Mn(IV) reagents also possess characteristics that provide new CL detections, such as the immobilisation of solid manganese dioxide, the production of colloidal manganese(IV) nanoparticles and the electrochemical generation of manganese(III). However, Mn(III) and Mn(IV) reagents are not very appropriate for the less acidic media because of their stability and preparation conditions. For example manganese(III) is readily disproportionates into the manganese(II) or reduction of manganese(IV) but can be stabilised by acidification, by complexation with anions or by adding manganese(II). Stable solution of manganese(IV) can be prepared by dissolving freshly precipitated manganese dioxide in 3M orthophosphoric acid.

Chapter 3

Materials and Methods

3.1 Chemicals

All the chemicals used in the research were of analytical grade unless stated otherwise and purchased from diverse suppliers as follows:

Acros Organics, Loughborough, UK

- N-acetyl-tryptophanamide (NATA), 98%, 245.28 g/mole, $C_{13}H_{15}N_3O_2$
- α -D(+)-Glucose anhydrous, 99%, 180.16 g/mole, $C_6H_{12}O_6$
- Glyoxal (1,2-ethanedione), 40%, 58.04 g/mol, $C_2H_2O_2$
- Manganese(III) acetate dihydrate, 98%, 268.09 g/mol, $C_6H_9MnO_6 \cdot 2(H_2O)$
- Glyoxylic acid (Formylformic Acid), 50% aqueous solution, 74.04 g/mol, $C_2H_2O_3$

Sigma-Aldrich Chemical Co Ltd, Gillingham, Dorset, England

- N-Bromosuccinimide (NBS), 99%, 177.99 g/mole, $C_4H_4BrNO_2$
- 2,6-Dichloroindophenol sodium salt hydrate (2,6-Dichlorophenolindophenol sodium salt), 90 - 100%, 290.08 g/mol, $C_{12}H_6Cl_2NNaO_2$
- Gallic acid(3,4,5-trihydroxybenzoate) 99.0% min, 170.12 g/mol, $C_7H_6O_5$
- Pyridoxine hydrochloride (Vitamin 6), 99%, 205.64 g/mol, $C_8H_{12}ClNO_3$
- Metronidazole, 99%, 171.15 g/mol, $C_6H_9N_3O_3$
- Tetracycline hydrochloride, 99%, 480.9 g/mol, $C_{22}H_{25}ClN_2O_8$

BDH Chemicals (VWR Chemicals), West Chester, United Kingdom

- Ascorbic acid (Vitamin C), 100%, 176.12 g/mol, $C_6H_8O_6$
- Manganese(II) sulfate tetrahydrate, 98 - 100%, 223.07 g/mole, $MnSO_4 \cdot 4H_2O$
- Oxalic acid dehydrate, 99.8%, 126.07 g/mol, $C_2H_2O_4 \cdot 2H_2O$
- Potassium permanganate, 90 - 100%, 158.034 g/mol, $KMnO_4$
- Pyrogallol(1,2,3-Trihydroxybenzene), 126.11 g/mol, $C_6H_6O_3$

Cambrian Chemicals Inc., Oakville, Ontario, Canada

- Malic acid (hydroxysuccinic acid), 99% minimum, 134.09 g/mol, $C_4H_6O_5$

Rohm and Haas (UK) Ltd, Dewsbury, West Yorkshire, England

- Ethylenediamine (1,2-Diaminoethane - EDA), 99%, 60.103 g/mol, $C_2H_8N_2$

Fisher Scientific, Loughborough, Leicestershire, England

- Formaldehyde(methanal) 37-41%, 30.026 g/mol, CH_2O

May and Baker Ltd (Rhone-Poulenc Group), Dagenham, Essex, England, United Kingdom

- Nickel(II) nitrate hexahydrate (1:2:6), 90 - 100%, 290.79 g/mol, $Ni(NO_3)_2 \cdot 6H_2O$.

3.2 Preparation of solutions

All reagents were of analytical grade unless stated otherwise and their solutions were prepared by dissolving the appropriate amount in deionised water, as for the examples below. The pH was adjusted prior to bringing the solution to final volume. NaOH or HCl were utilized to adjust the required acidity. Storage conditions depended on the solution. Most of solutions were stored at room temperature ($\sim 15 - 25$ °C) or in the refrigerator at 4°C. If needed, the solutions were protected from light by storage in dark bottles.

3.2.1 Potassium permanganate solutions

A stock 0.02 mol/L permanganate standard solution was prepared, using the method of Vogel⁵⁷⁴, by dissolving about 3.2g of KMnO_4 in 1 L of deionised water using a large beaker. The obtained permanganate solution was then gently boiled using a hot plate in the hood to destroy reducible substances (traces of organics remaining in deionised water). The solution was cooled down and stood overnight before it can be filtered through a glass filtering crucible to remove manganese dioxide impurities and stored in amber coloured bottle in a refrigerator. KMnO_4 was standardized by titration against oxalate. The concentration of the solution that was not acidified remained stable for several weeks. Working solutions were daily prepared by dilution of the stock standard solution.

Calibration standards were measured over entire UV-Vis region to determine max absorption. KMnO_4 absorbed best at ≈ 525 nm and the peak maxima measured for dilute aqueous permanganate solutions agreed well with published data^{10, 575}.

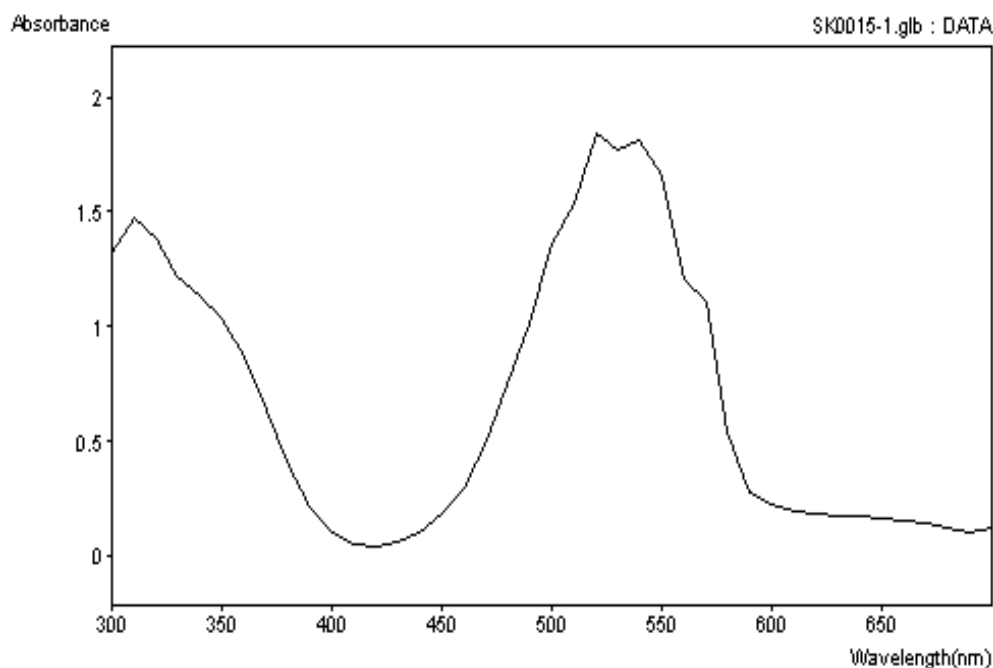


Figure 3.1 2D UV-visible spectra of solutions of KMnO_4 at 0.005M

3.2.2 Manganese(II) sulfate

Manganese(II) sulfate tetrahydrate was dissolved in the required strength of deionised water.

3.2.3 Manganese(III) reagent

A stock 0.05 mol/L Mn(III) reagent solution was prepared either by dissolving about 1.16g of Mn(III) acetate dehydrate in 100 ml of 2 mol/L H₂SO₄, or by dissolving about 1.98g of Mn(II) sulfate tetrahydrate in 60 ml of deionised water and adding with constant stirring 20 ml of concentrated sulphuric acid. The mixture was then cooled down in an ice bath to below 10 °C. Separately, 0.158g of potassium permanganate was dissolved in 20 ml of deionised water with stirring.

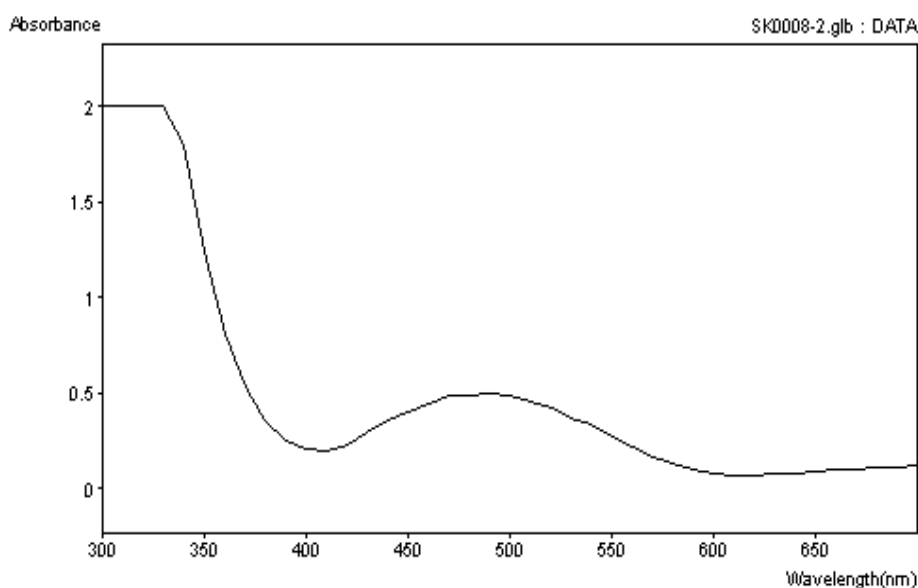


Figure 3.2 2D absorbance spectra of solutions of Mn(III) at 0.05M

The permanganate solution obtained was slowly added to the Mn(II) sulfate solution with constant stirring. Stirring was continued for 10 minutes to complete the reaction and the solution was kept in ice during the preparation to maintain the temperature below 10 °C. The Mn(III) reagent solution obtained was stored in amber coloured bottle in a refrigerator and its concentration remained stable for several weeks. Mn(III) absorbed best at \approx 500nm and the peak maxima measured for dilute aqueous Mn(III) solutions agreed well with published data¹⁰.

3.2.4 Manganese(IV) reagent

A stock 0.05 mol/L manganese(IV) reagent solution was prepared by slowly adding about 200 ml of aqueous reducing agent (0.35 – 0.70 g of hydrazine sulphate or 0.60 – 0.75 g of hydroxylamine sulphate) to a solution of KMnO₄ (7.90g KMnO₄ in 600 ml of 12 mol/L H₂SO₄) with stirring.

After the addition of reducing agent, the solution was stirred for another 15 minutes and then transferred to a 1000 ml volumetric flask and filled to the mark with 9 mol/L H₂SO₄ solution. Mn(IV) absorbed light at \approx 400nm, which is very different from that of Mn(III) and MnO₄⁻ and was used for Mn(IV) measurements in these experiments. The spectrum of Mn(IV) measured for dilute aqueous Mn(IV) solutions agreed well with published data¹⁰.

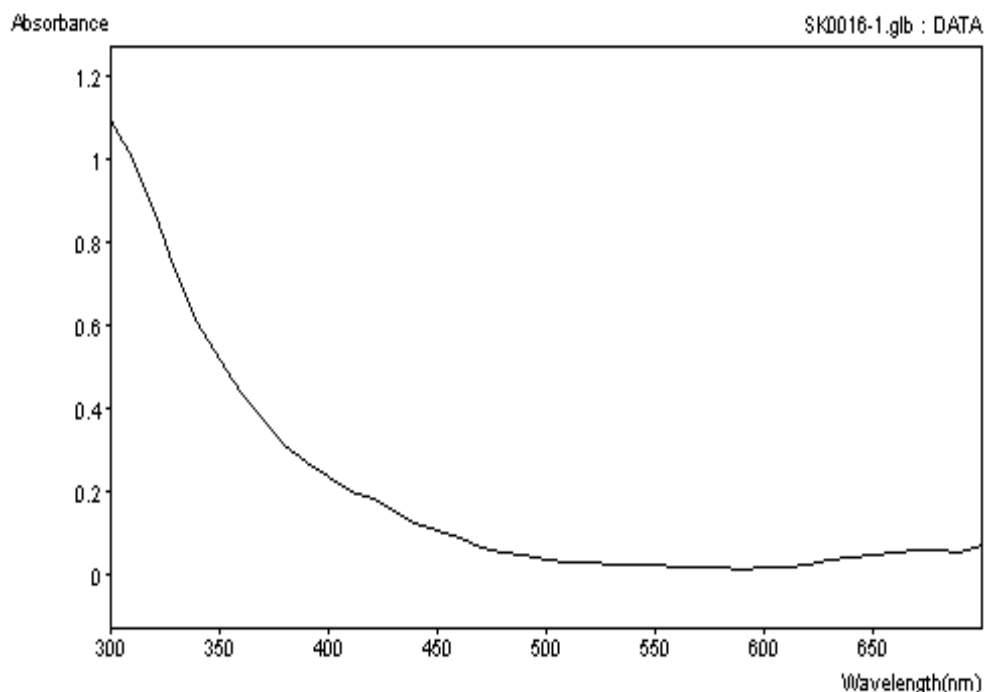


Figure 3.3 2D UV-visible spectra of solutions of manganese (IV) at 0.05M

3.3 Instrumentation and Equipment

3.3.1 Volumetric equipment

Standard laboratory grade B glassware, volumetric flasks, one mark and graduated pipettes, cylinders, burettes and air displacement pipettes (Gilson, Anachem) were used without further calibration.

3.3.2 Weighing

Weighing was carried out using 2 decimal place top pan (Salter BP2200) and 4 decimal place or 4/5 place (Precisa 405 M-200A) analytical balances as appropriate.

3.3.3 pH measurement

pH meter model Mettler Toledo MP 220 was used and calibrated with pH 4, 7 and 9.2 buffer solutions prepared from buffer tables (BDH). Relative accuracy: \pm 0.01. Fisher Scientific, Loughborough, UK.

3.3.4 UV-visible spectrophotometry

UV-visible spectra were obtained using a Shimadzu model 160A scanning UV/vis spectrophotometers, (Shimadzu corporation, Japan).

Silica and optical glass cuvettes with a 10 mm path length were used. These UV/vis spectrophotometers were used to scan and measure the decrease in absorbance at 525 nm, 500 nm, 400 nm, and absorption maxima for MnO_4^- , Mn(III) and Mn(IV), respectively.

3.3.5 Stopped flow measurements

Absorbance and chemiluminescence kinetics measurements were carried out using an electronics upgraded SX.18 to match an SX.20 stopped-flow reaction analyzer instrument, thermostated ($\pm 1^\circ\text{C}$) by circulating water bath, fitted with a 20 μl volume removable cell cartridge, 1.1ms dead-time, cell with optical path lengths of 10mm and 2mm and equipped with a sequential mixing capability, a rapid-scanning detection system (Applied Photophysics) and a dual detection accessory that allows the user to simultaneously acquire single wavelength absorbance and fluorescence data. A Fisher Scientific Isotemp 3016 water bath was used to maintain the temperature of the reaction mixtures within $\pm 0.1^\circ\text{C}$. Data analysis was performed using either by Pro-Kineticist software interfaced to the instrument or Microcal Origin software version 4.1 and Microsoft Office Excel 2007, by importing data into spreadsheets of data analysis.

The SX.20 was controlled by a Pro-Data instrument software and electronics running under WindowsTM, which provided comprehensive tools for data acquisition, display and analysis, Standard features included: wavelength scanning, repeat drives for signal averaging, acquisition of time-resolved spectra (Spectra Kinetic technique), linear- logarithmic- and splittime-base, digital oversampling, temperature-dependent scanning and kinetics capability. In addition, PC ProK and ProKII software packages as global analysis tools for multiwavelength data analysis.

SX.20 stopped-flow system components including 150W Xenon lamp power supply and igniter unit, lamp housing (lamp fitted) that provides easier alignment procedures and operation fitted with a non-ozone producing xenon arc lamp.

Monochromator (Mono1), optical rail for mounting of the lamp housing and monochromator and fibre optic light guide.

Single (with option sequential) mixing sample handling unit (SHU) fitted with cell cartridge chambers for fast and convenient stopped flow cell exchange and a side mounted autostop assembly, fitted with the latest design of autostop mechanism. Electronics unit fitted with single detection channel and computer fitted with fibre optic interface card.

Hamamatsu R6095 red extended photomultiplier tube that provides high sensitivity for UV to near IR in the spectral response range of 185-900nm for absorbance detection and a Hamamatsu R6095 photomultiplier tube (extended red tube), suitable for a wide detection range 300-900nm for fluorescence and chemiluminescence detection.

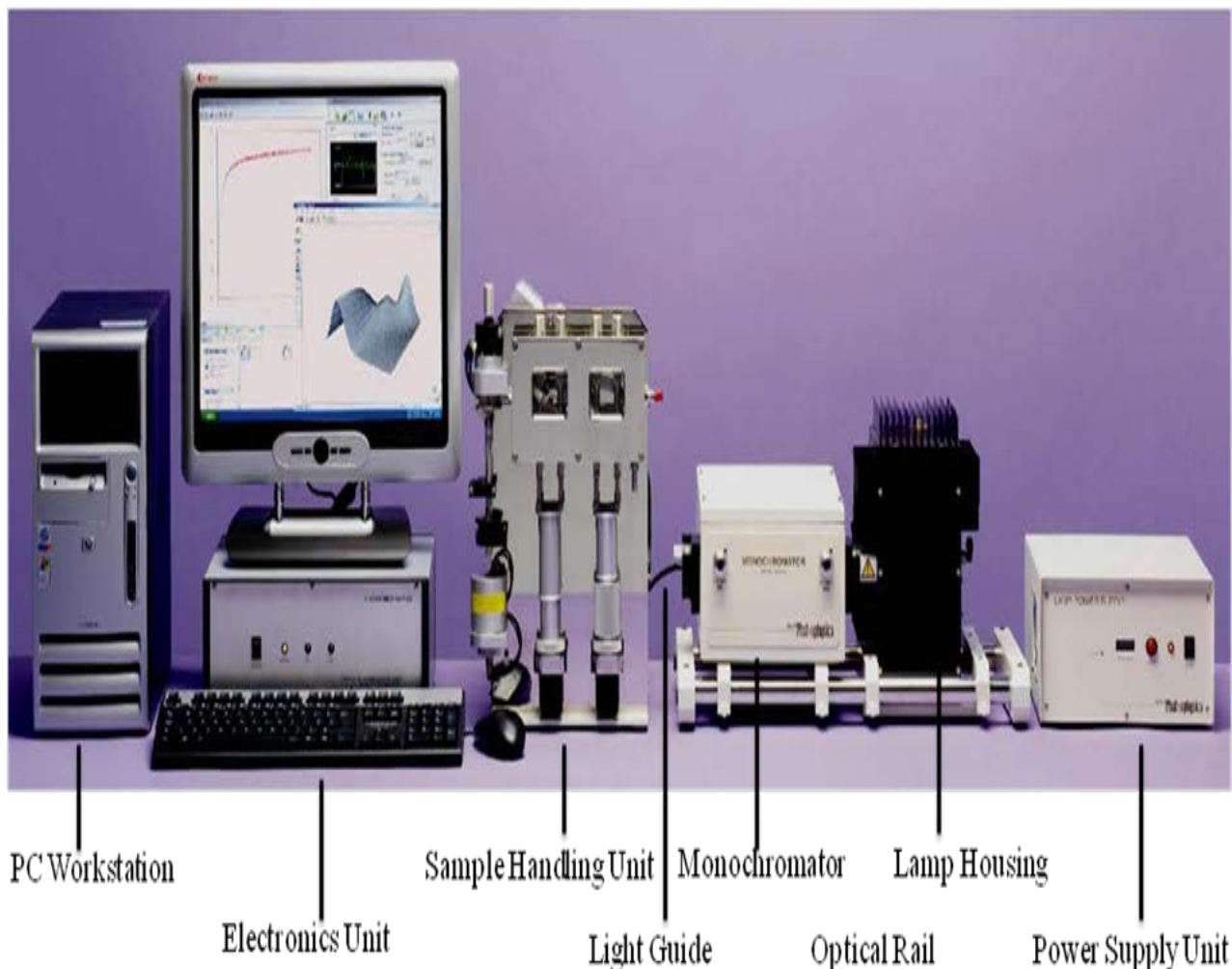


Figure 3.4 SX.20 Stopped-Flow Spectrometer (with option sequential mixing)

2.5 mL Kloehn or Hamilton drive and stop syringes are the standard type fitted to SX instruments. These syringes feature PEEK (Polyetheretherketone) pistons for corrosion free operation over the temperature range 0-60°C.

The micro-volume flow lines were constructed from PEEK or Teflon (PTFE) material, however, under acidic experimental conditions of the oxidation reactions investigated, PEEK tubing were replaced by Teflon (PTFE) ones, which turned out to be more robust, resistant to chemical corrosion and less oxygen permeable.

Flangeless ferrule compression terminals result in few leaks and longer life of the lines. All these accessories were supplied by Applied Photophysics.

3.3.6 Validation of stopped-flow instrumentation

To ensure that the system fulfills the quality requirements and is still operating satisfactorily and analytical measurements are reliable and accurate, two important reaction tests recommended by the manufacturer were performed.

3.3.6.1 Reaction of acid hydrolysis of tri (ethylamine) nickel (II) ion

The reaction of acid hydrolysis of tri (ethylamine) nickel (II) ion was used to check the general performance of the spectrometer. The reaction has several isosbestic points, for demonstrating the generation of time-resolved spectra from kinetic data acquired over a broad wavelength range.

The overall reaction has more than one step with the first being completed in about 10 to 20 ms. The final stage of the reaction is still taking place after several seconds. Figure 3.5 below shows the time resolved spectra constructed from data acquired and those which highlighted the isosbestic points were plotted. The time resolved spectra obtained are quite typical for the SX.20 stopped-flow spectrometer.

Figures 3.6 to 3.9 show the time profiles of data collected at the isosbestic wavelengths i.e. 330, 350, 570, 710 nm.

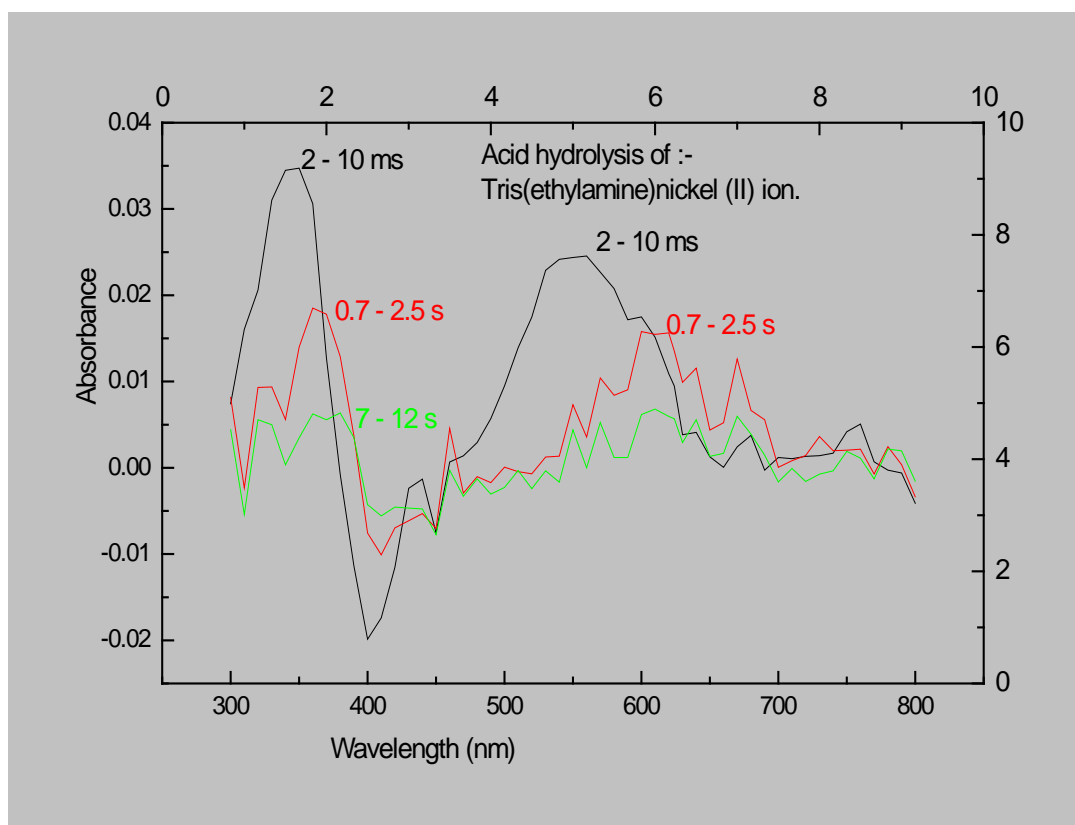


Figure 3.5 Time resolved spectra for the SX.20 stopped-flow spectrometer

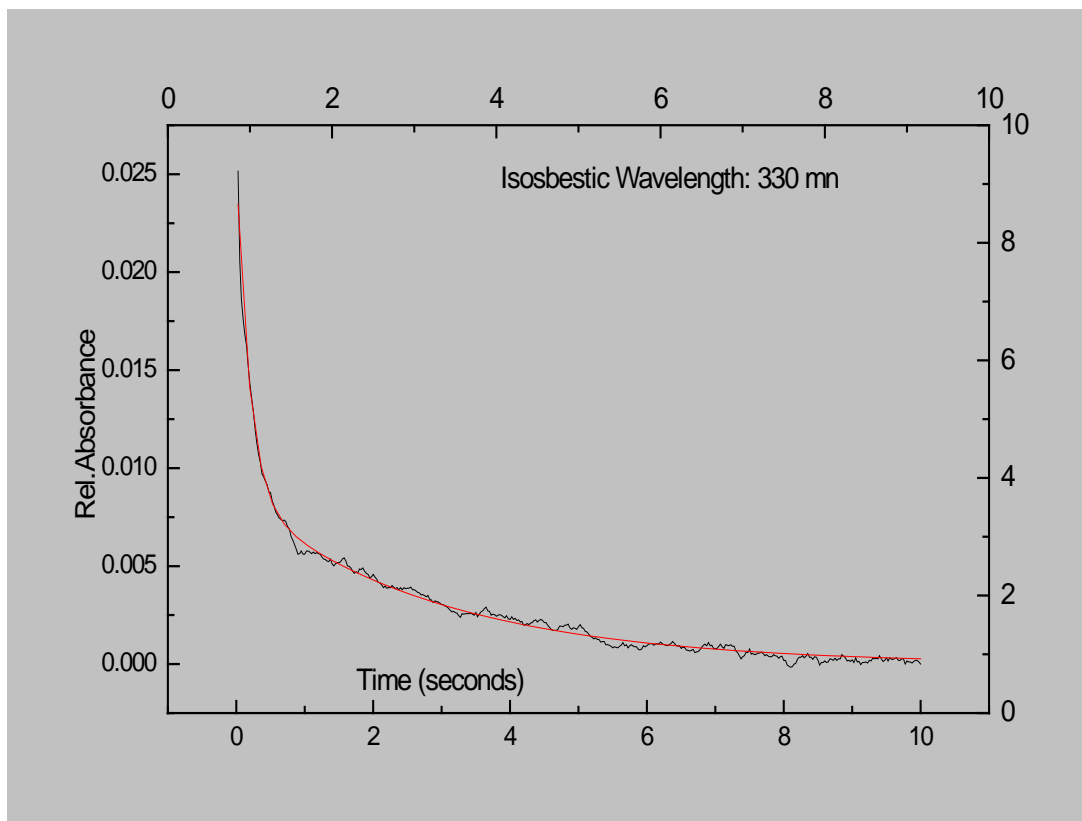


Figure 3.6 Time profile of data collected at the isosbestic $\lambda_{330 \text{ nm}}$

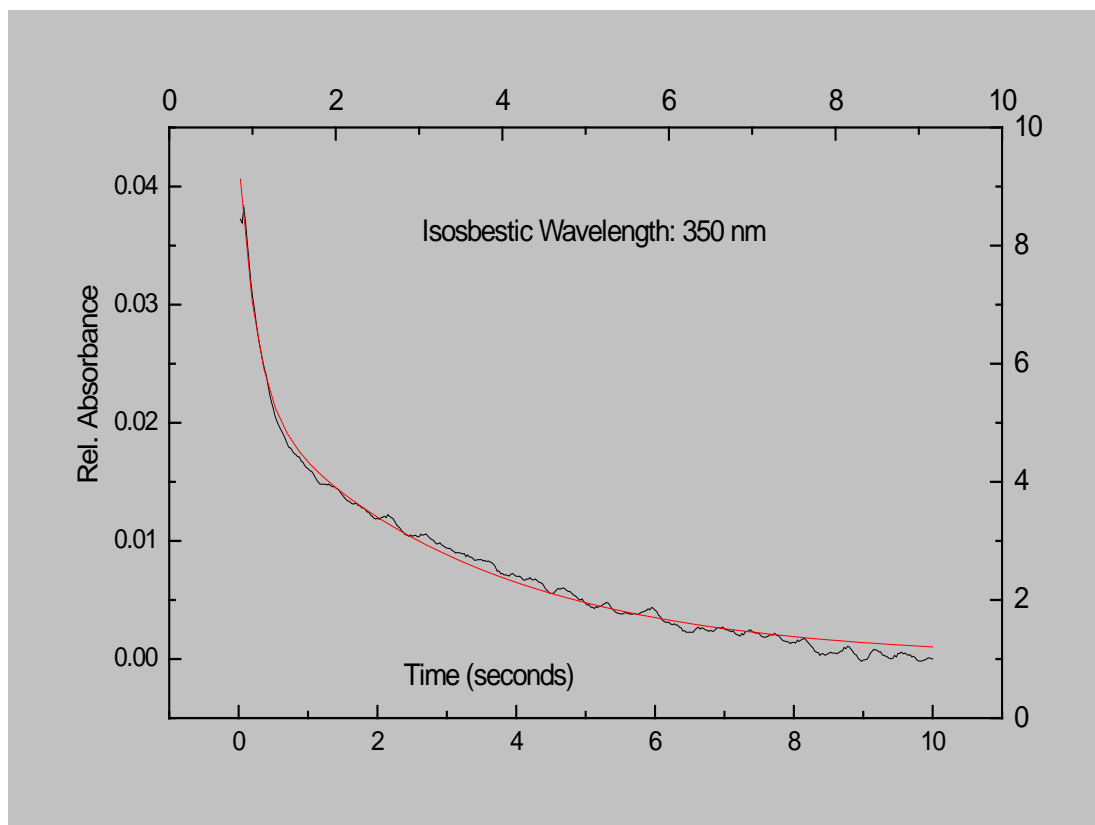


Figure 3.7 Time profile of data collected at the isosbestic $\lambda_{350 \text{ nm}}$

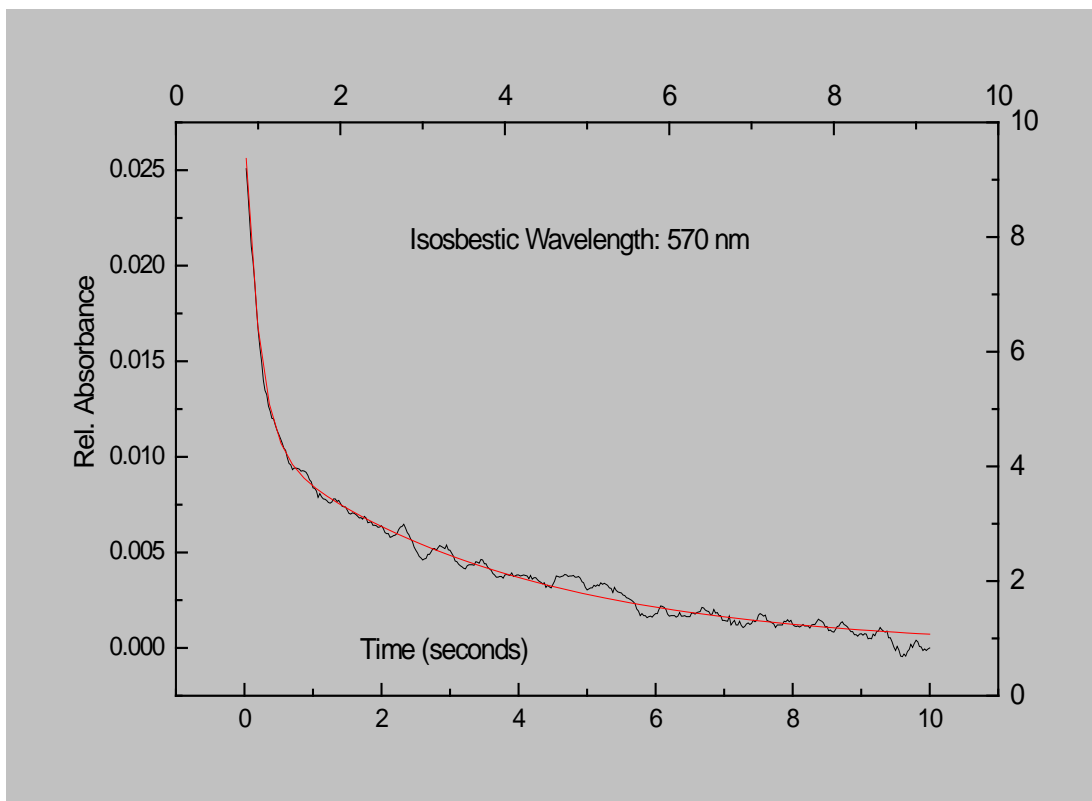


Figure 3.8 Time profile of data collected at the isosbestic $\lambda_{570 \text{ nm}}$

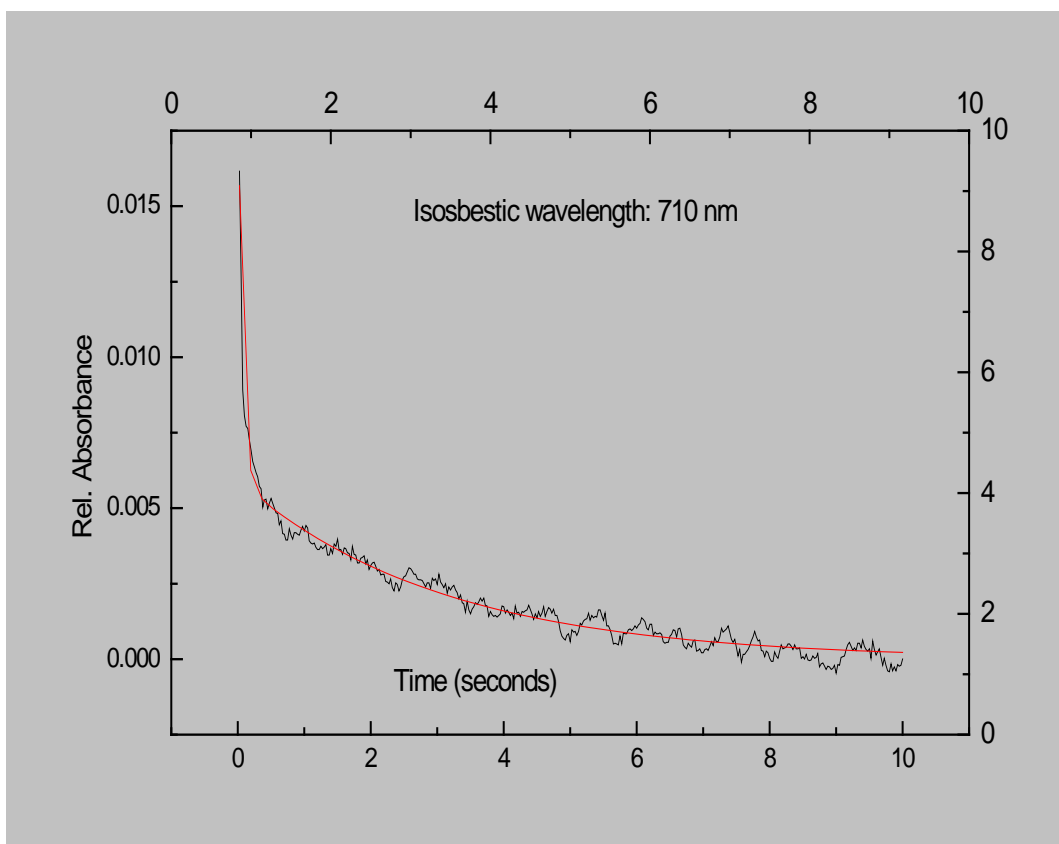


Figure 3.9 Time profile of data collected at the isosbestic $\lambda_{710 \text{ nm}}$

3.3.6.2 Determination of the dead-time

Dead time is the main factor that governs the performance of a stopped flow. It is defined as the time required for the solution to flow from the centre of the mixer to the centre of the observation cell.

The determination of the dead-time performance of the SX.20 stopped-flow spectrometer has been performed according to the methodology as published by Tonomura⁵⁷⁶. The reduction of 2, 6-Dichlorophenolindophenol (DCIP) by L-ascorbic acid is discussed in considerable detail in that paper (including the effect of pH) with respect to its use as a test reaction for dead-time determinations on stopped-flow instrumentation. From the stock ascorbic solution, the following concentrations were prepared using the HCl/NaCl solution for dilution: 2 mM, 5 mM, 10 mM, 15 mM, 20 mM, 30 mM, 40 mM, 60 mM, 80 mM, 100 mM, and the concentration of DCIP was 500 μ M to reproduce the conditions of pseudo-first reactions. Kinetic data collected for each of the ascorbic acid concentration, and after overlaying the kinetic traces (Figure 3.10) for each of ascorbic acid concentrations together with their appropriate kinetic fits (using a single exponential equation $A=A_0 e^{-(k_{obs}t)}$, each of the fitted curves was extrapolated and found to intersect at a common point which is considered as the starting time of the reaction and this point was taken to be zero time (t_0).

Figure 3.11 is a plot of the absorbance intensities from the experiment as a function of the measured rate constants (k_{obs}). The data were fitted to the exponential equation $A=A_0 e^{-(k_{obs}t)}$, where t represents the dead-time, k_{obs} is the measured rate constant, A and A_0 represent the absorbance intensity of the reaction and initial absorbance intensity, respectively. When data were fitted to the above equation, the dead-time (t) was calculated to be 1.54 ms (\pm 0.05 ms). The typical result for the SX.20 spectrometer with 10 mm path length (regular light guide) is 1.18 ms to 1.37 ms. The results obtained are slightly different from those given by the manufacturer but it is far better than the Hi-Tech Scientific Stopped-flow instrumentation used for preliminary work.

Graph 3.12 shows a fit defining the rate constants observed (k_{obs}) determined from the experiment plotted as a function of ascorbic concentration. This graph shows the increasing rate of the reaction is linear as a function of ascorbic concentration within the concentrations range of 2 to 40 mM. The measured rate constant (k_{obs}) was also plotted against the final ascorbic acid concentration (mM) in order to establish at which rate constant, deviation starts to occur ($k_{obs} = 833.3 \text{ S}^{-1}$).

The results show that SX.20 stopped-flow reaction analyser can be used to study rapid reactions in solution. The range of reactions accessible is limited only by the dead time, response time and resolution of the instrument. Sophisticated data processing facilities are also available which allow reaction mechanisms to be determined and component spectra, concentration profiles and rate constants to be calculated.

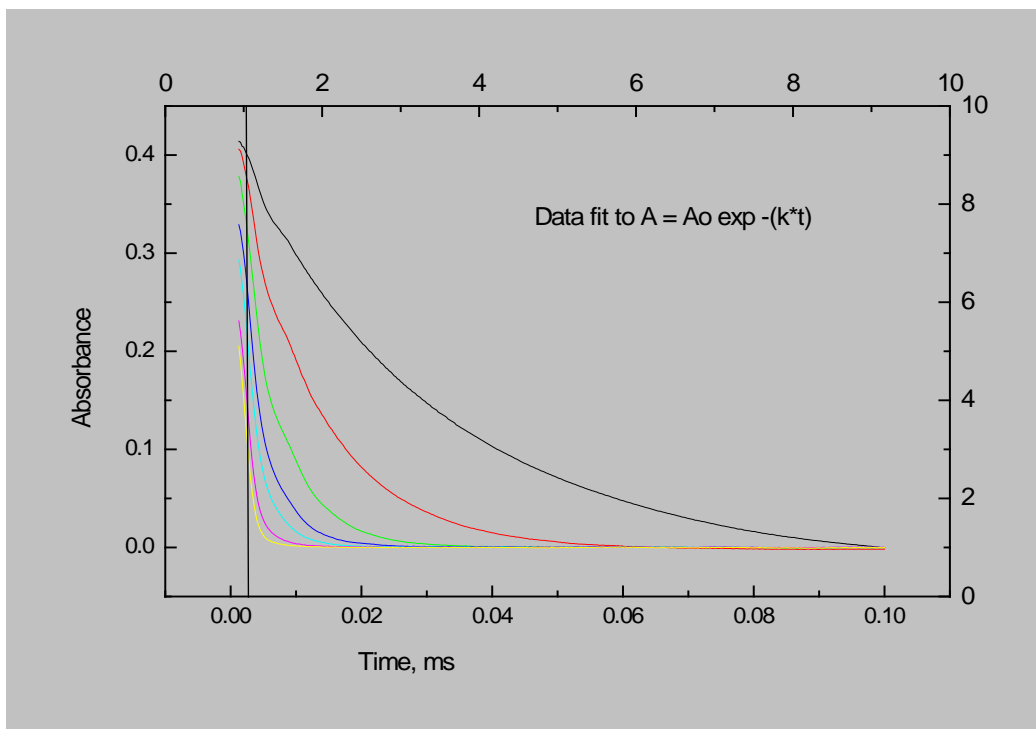


Figure 3.10 The reduction of 2,6 – dichlorophenolindophenol (DCIP) by L- ascorbic acid of concentrations: 2.0, 5.0, 10.0, 15.0, 20.0, 30.0, and 40.0 mM

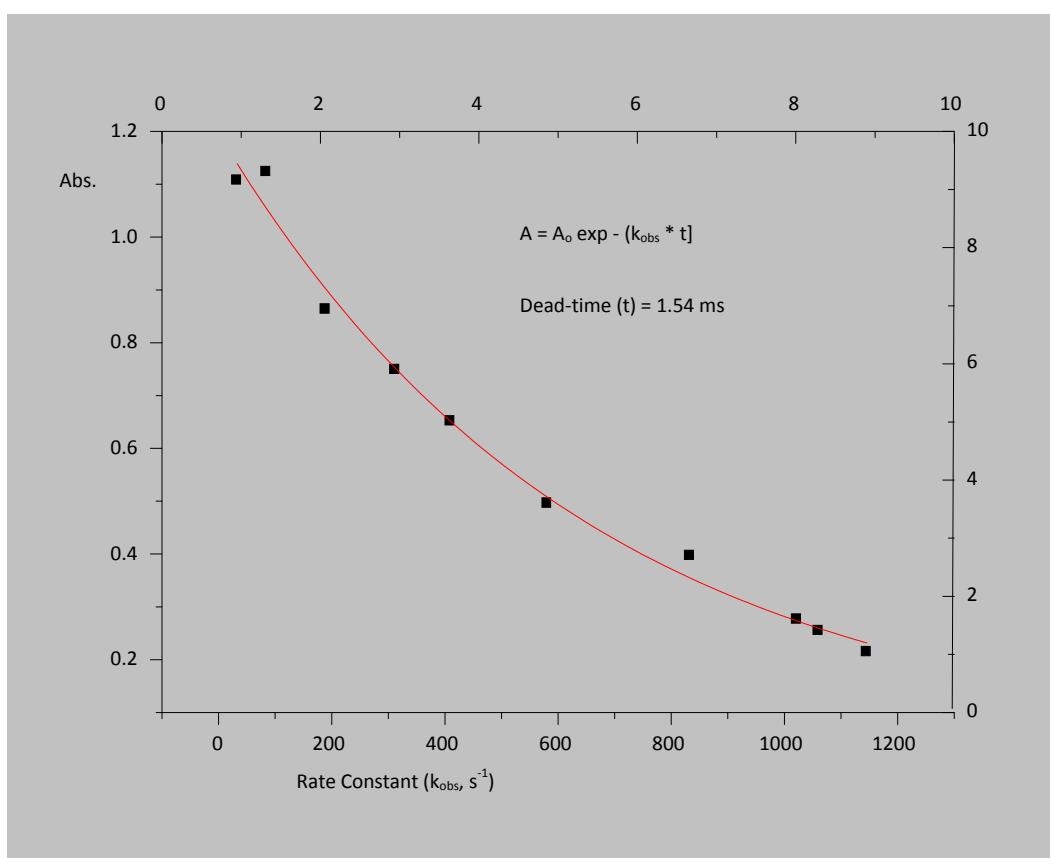


Figure 3.11 Absorbance plotted vs. rate constants to determine the dead-time (t)

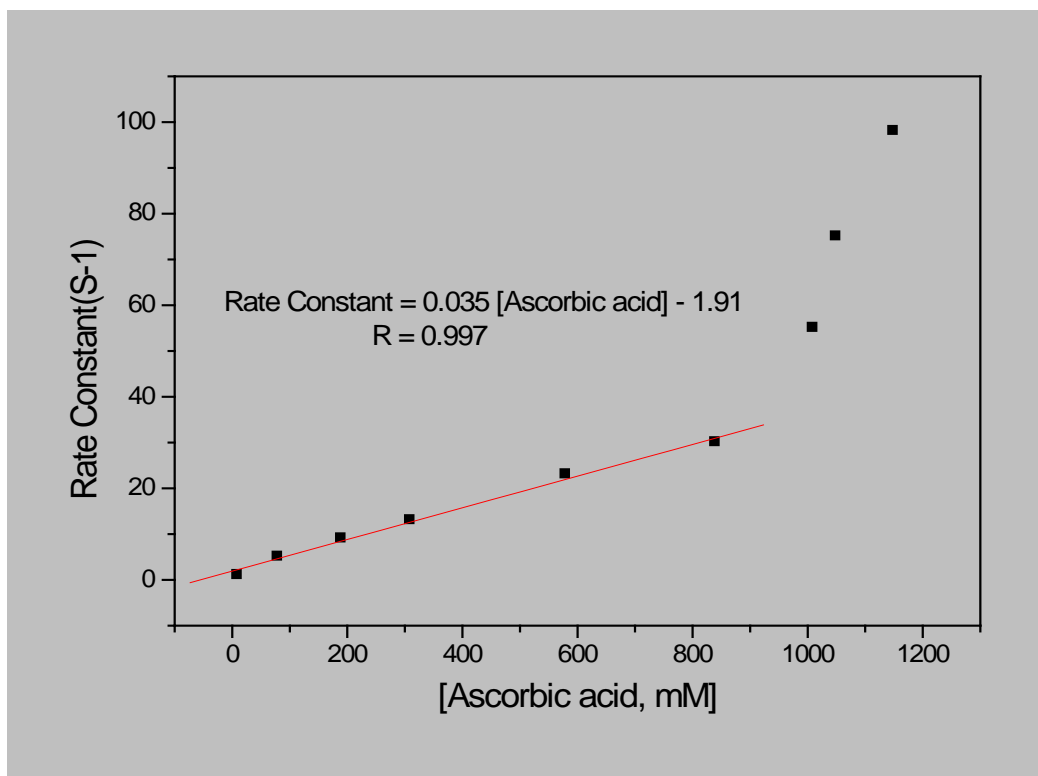


Figure 3.12 Plot of rate constants vs. ascorbic acid concentrations

3.4 Experimental procedures

This section provides detailed information relating to experimental operation of the SX.20 stopped-flow reaction analyser hardware.

3.4.1 Stopped-flow absorbance kinetics

The kinetics of manganese oxidants (e.g. MnO_4^-) reactions with the organic substrate (S) (e.g. glyoxal) was carried out using a stopped-flow spectrophotometer (SX.20, Applied Photophysics, UK). The kinetic measurements were conducted under pseudo-first-order conditions, where substrate concentrations (S) were present in a large excess over that of oxidant concentration, at least ten times that of the oxidant to allow determination of pseudo first-order rate constants, and at constants of temperature 25 ± 0.1 °C, $[\text{H}^+] = 2.0$ mol/L, unless otherwise is mentioned.

The reaction was started by mixing the requisite amounts of the manganese oxidant with the substrate. The progress of the reaction was monitored by following the rate of disappearance of manganese oxidants by measuring its absorbance during the reaction at appropriate absorption maximum (example 525 nm for MnO_4^- , 500 nm for Mn(III) and 400 nm for Mn(IV)).

A range of important parameters was adjusted to control the input signal:

Detection mode in the signal panel of the Pro-Data:	Absorbance mode
Sequencer panel:	Kinetics mode
Trigger panel:	External Trigger
Timebase panel:	Set appropriate acquisition time based on the timescale of the reaction and points:1000
Monochromator panel:	Set wavelength
Slit widths:	0.5 mm
Water as reference material:	Set baseline to zero the absorbance detector.

In a typical experiment, one syringe of the stopped-flow instrument was filled with 0.02M MnO_4^- and the other syringe filled with 0.20M, 0.40M, 0.80M, 1.60M or 3.20M Glyoxal solution, at the appropriate pH. After 1:1 volume ratio mixing of the reagents, the absorbance of MnO_4^- as a function of time data were collected at 520 nm over 10 minutes. The pseudo-first-order rate constants were obtained from the plots of $\log[\text{MnO}_4^-]$ versus time; the plots were linear up to 75% completion of the reaction and k_{obs} values were reproducible within $\pm 5\%$. During the progress of the reaction, the colour of the solution changed from violet to uncoloured.

The pseudo-first-order rate constants, k_1 , were obtained by nonlinear least-squares fits of A_t versus time(t) according to equation $A_t = A_\infty + (A_0 - A_\infty) e^{-(k_{\text{obs}}*t)}$, where A_0 and A_∞ are the initial and final absorbance, respectively.

The rate constants of the reaction represent an average of 10 replicates. Second-order rate constants, k_2 , were calculated from the slope of the linear plot of the pseudo first-order rate constants versus substrate concentration.

Three-dimensional plots of absorbance, wavelength and time were analysed using a global nonlinear regression fitting program, PC ProK and ProKII software packages, available from Applied Photophysics. All reported rate constants are tabulated using post mixing reagent concentrations. Reported rate constants are an average of at least three independent measurements and were determined by nonlinear regression fits to a minimum of 400 data points.

3.4.2 Stopped-flow chemiluminescence kinetics

Stopped-flow chemiluminescence measurements were also made using the Applied Photophysics SX.20 stopped-flow spectrophotometer (Applied Photophysics, Leatherhead, UK). In a typical experiment, the same concentrations of solutions used for the absorbance measurements were used for chemiluminescence measurements by changing only the detection mode into fluorescence mode in the signal panel of the Pro-Data.

The procedure for measurements was the same as described above. The reagents were mixed and profiles of chemiluminescence intensity versus time obtained over 10 minutes, as for absorbance kinetics, were recorded at its maximum emission. Chemiluminescence signal follows rise-fall kinetics with a fast increase in the signal followed by a similar decrease. Non-linear least-squares fit of the chemiluminescence profiles from the reaction to single exponential decay equation provided the measured rate constant (k_{obs}). The kinetics of the CL system profiles were analyzed using the following sequential-reaction model;



where A reactants; B, intermediates; and C, products; and k_1 and k_2 , are rate constants. Using this model, the chemiluminescence intensity is proportional to the concentration of [B], and all reactions steps are first order, and irreversible reactions. The rate constant k_1 and k_2 , were measured independently in separate experiments in which, only the disappearance of the oxidizing agent (KMnO_4 , and Mn(III)) is monitored by UV absorption. Reported rate constants are an average of at least three independent measurements and were determined by nonlinear regression fits to a minimum of 400 data points.

3.5 Significance of the following experiments

Manganese oxidants in acidic media are powerful, but selective, oxidizing agents that have great potential of producing an analytically detectable chemiluminescence emission. They are presented as the most efficient oxidants for direct liquid phase chemiluminescence processes. The chemiluminescence reactions between, particularly, acidic permanganate and organic analytes are probably the most sensitive and have found the broadest applications.

However, some of these analytes found as chemiluminescent are, in reality, very weak chemiluminescence compounds, as they do not react directly or react very slowly under the reaction conditions with permanganate and produce insufficient chemiluminescence signal for developing suitable analytical CL-procedures. Therefore, strategies such as the use of reactants (e.g. formaldehyde) or catalytic (e.g. Mn^{2+}) additives to enhance the native chemiluminescence signal intensity of such a compound are developed¹⁴⁰.

It was postulated that the resulting chemiluminescence intensity, which is the rate of emission of photons/sec from a chemiluminescence reaction, is the product of the oxidation turnover of analyte. And that the chemiluminescence emission is transient and occurs at a rate that is dependent on both the chemical processes and the physical processes of solution mixing⁴.

In fact, almost all liquid phase reactions involving manganese-based oxidants are potentially chemiluminescent. However, it is thought that the intensity of the chemiluminescence emission is determined by the kinetics of the oxidation reaction.

If the oxidation process is too slow or extremely fast then the chemiluminescence emission will not be observed. Thus, it was hypothesized in this study that as the rate of the oxidation reaction increases, the intensity of the chemiluminescence emission increases and the chemiluminescence process is entirely chemical kinetics dependent rather than a physical process of solution mixing.

The purpose of the following experiments was to test this hypothesis by changing the rates of reactions using reactants (e.g. formaldehyde) or catalytic (e.g. Mn^{2+}) additives or simply by varying the concentration of the organic analyte or the oxidant.

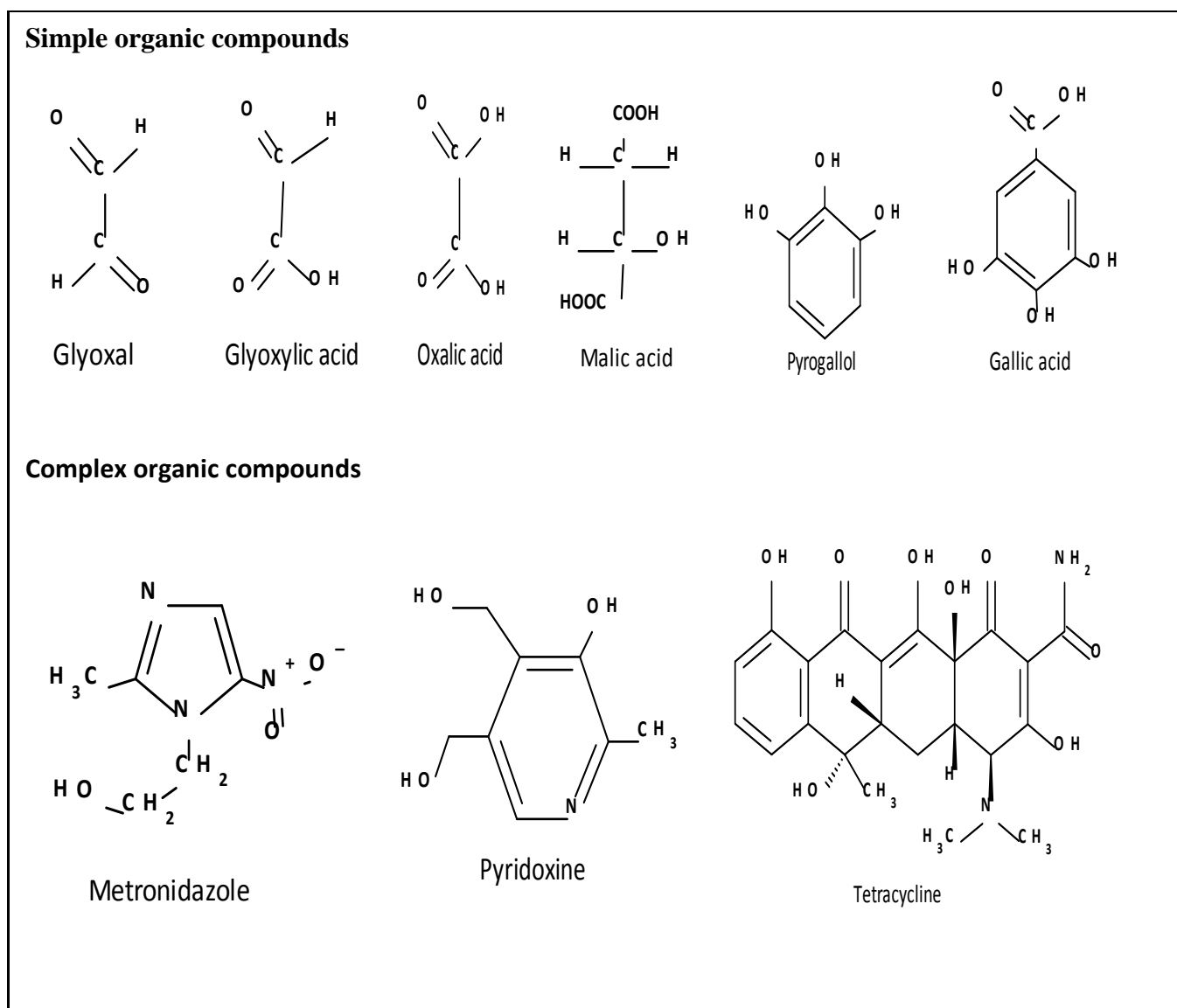


Figure 3.13 List of chemical structures of target molecules examined in this study

Chapter 4

Kinetics Study of Chemiluminescence Reactions in the Manganese-based Oxidation of Various Organic Substances

4.1 Introduction

Abdel-Mageed¹⁰ showed that the rate of MnO_4^- oxidation reaction of gallic acid ($\text{C}_7\text{H}_6\text{O}_5$) is faster ($t_{1/2} \sim 10$ ms) compared to the rate of MnO_4^- oxidation reaction of glyoxal (OCHCHO) ($t_{1/2} \sim 1000$ ms). However, on mixing glyoxal and gallic acid, the MnO_4^- oxidation reaction of the resulting solution becomes faster ($t_{1/2} \sim 25$ ms) and at the same time the intensity of CL emission signal is increased about tenfold (even by several orders of magnitude in some cases) compared to the individual CL emission signals measured separately (Figure 4.1).

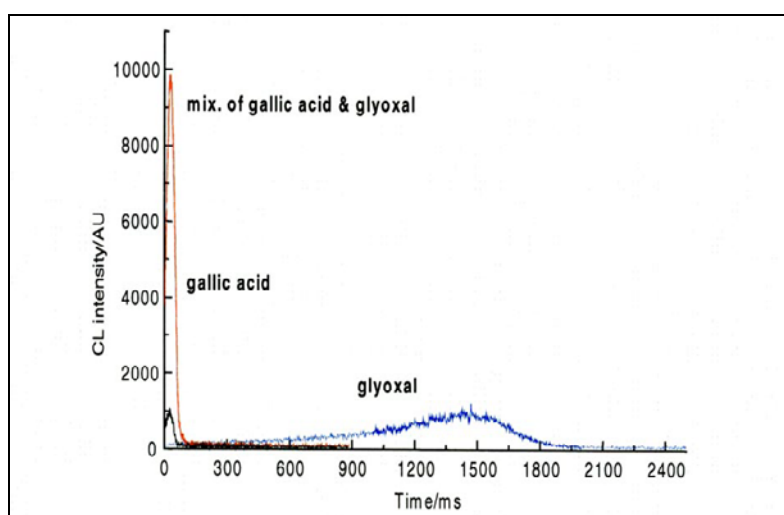


Figure 4.1 CL time courses for the oxidation of glyoxal and gallic acid in mixture by MnO_4^- . Reaction conditions: $[\text{OCHCHO}] = 0.1\text{M}$; $[\text{C}_7\text{H}_6\text{O}_5] = 0.0025\text{M}$; $[\text{MnO}_4^-] = 0.0015\text{M}$ ¹⁰.

Therefore the primary aim of this section is to extend Abdel-Mageed's work to a range of analytes of interest in process analysis, chemical, biological and pharmaceutical industries, clinical diagnostics, environmental and forensic sciences, etc. The second aim is to characterise the oxidation processes of these substances by permanganate, Mn (IV) and Mn (III) with a focus on characterizing the kinetics curves of the CL and light-producing reactions.

Indeed, a large number and type of compounds were tested, according either to their inhibiting, enhancing or catalytic effect on the chemiluminescent oxidation reaction. The results of these studies are expected to lead to the prediction of new analytical methods.

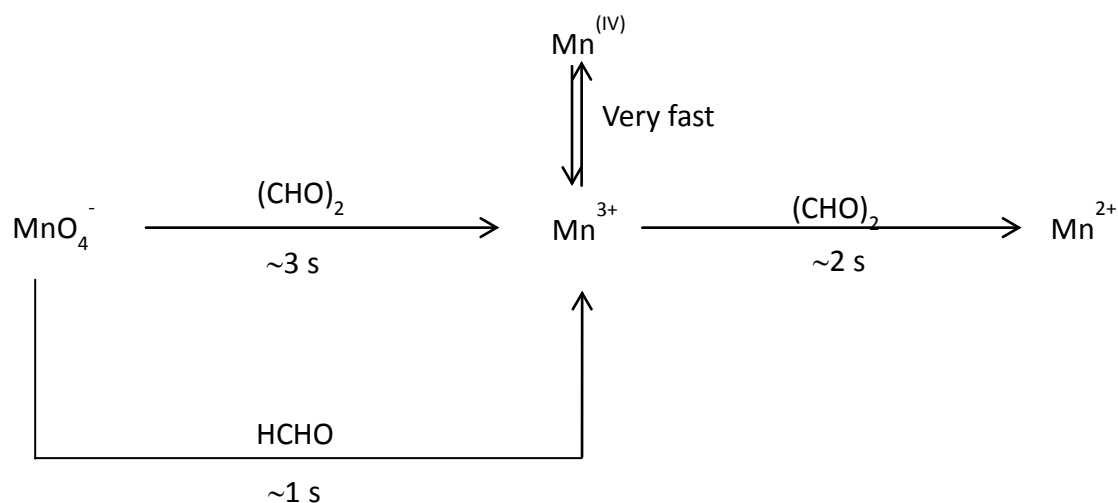
In the first set of experiments we tried to limit the potential intermediates by focusing on simple compounds such as glyoxal, glyoxyl acid and oxalic acid.

These compounds showed high reactivity with all three manganese oxidants, generated fairly intensity CL emission and the dependence of the intensity of the CL on various parameters could be measured with complete reliability. In the next set of experiments we chose organic compounds which reacted with permanganate at different rates. In comparison with glyoxal; compounds chosen were of - similar rate (e.g. malic acid, tetracycline, etc.); faster rate (pyrogallol, gallic acid, etc.); and slower rate (metronidazole). Under the conditions employed, most of these chemical systems generated with all three manganese oxidizing agents, significant CL signal and predictably analytically useful CL under acidic conditions.

4.2 Chemiluminescence in glyoxal (OCHCHO) oxidation reactions

It has been shown that if we consider the oxidation of glyoxal with permanganate and the enhancement of chemiluminescence with formaldehyde, then, using the observation that Mn(III) oxidations exhibit the same chemiluminescence as permanganate and manganese dioxide oxidations and based on the known chemistry of aqueous manganese solutions, it is possible to postulate a mechanism.

The suggested main steps involved in a glyoxal-permanganate-formaldehyde chemiluminescence system is as follows (Scheme 4. 1):



Scheme 4.1 The hypothetical mechanism for the enhancement of the observed CL emission during the oxidation reaction of glyoxal by MnO_4^-

Primary reactions of MnO_4^- with glyoxal and formaldehyde involving a four (or three) electron reduction of MnO_4^- - the reduction of MnO_4^- leads to Mn(III) intermediate which then rapidly react with glyoxal to form excited Mn(II) species (Mn(II)^*) that emits light.

Thus formaldehyde increases the CL signal intensity by increasing the concentration of the intermediate Mn^{3+} . In this case Mn(IV) seems to react at a similar rate so it may be that it is in rapid equilibrium with Mn^{3+} . In this section the chemiluminescence reaction of MnO_4^- and

glyoxal in sulphuric acid medium and the mechanism of formaldehyde enhancement are examined.

4.2.1 Permanganate oxidation of glyoxal

Glyoxal ($C_2H_2O_2$), also known as ethanedial or ethanedione, is a simple organic compound and the smallest dialdehyde (two aldehyde groups). As a low molecular weight and difunctional aldehyde, glyoxal provides high reactivity and fairly intensity CL emission when reacted with permanganate. Thus, the oxidation of glyoxal was selected as a substance test for a model chemiluminescent reaction to start this work.

Preliminary experiments on glyoxal oxidations by permanganate indicated that the kinetics of the reaction and chemiluminescence curves are of such rates that they can conveniently be measured using an SX.20 stopped-flow reaction analyzer instrument with both absorbance and fluorescence detection.

Further understanding of the reaction mechanism may enable the enhancement of the sensitivity and lead to the development of new chemiluminescence systems.

The kinetics of manganese oxidant disappearance and of the chemiluminescence production were investigated.

The oxidation of glyoxal by permanganate in sulphuric acid medium has been previously reported to elicit analytically useful chemiluminescence. Using flow injection analysis procedure, Fang⁴⁵⁰ reported the analytical application of acidic potassium permanganate as a chemiluminescence reagent for the chemiluminescence detection of glyoxal in synthetic matrix with detection limit of 1×10^{-4} M. Also, glyoxal has been used as enhancer for acidic permanganate chemiluminescence detection⁷. Therefore, it was decided to look at the CL of glyoxal oxidation by permanganate in sulphuric acid medium.

Kinetic experiments of oxidation of glyoxal with MnO_4^- were conducted at a constant temperature of 25 °C under the reaction conditions relevant to CL emission signal exhibition. Figures 4.2 and 4.3 give typical examples of the MnO_4^- absorbance time course and the CL emission time course obtained for the oxidation of glyoxal by MnO_4^- .

It is evident from Figure 4.2 that glyoxal is rapidly oxidized by MnO_4^- in sulphuric acid medium and the absorbance time course indicates half-life ($t_{1/2}$) reaction of 10 seconds and the MnO_4^- reduction efficiency is up to 99.5% within 20 seconds.

The reaction-time curve is found to be of inverted S-shape (sigmoidal) throughout the entire range of reaction and both kinetic curves and log – time profile in figure 4.2 show an inflection, which indicates that the oxidation of glyoxal by MnO_4^- proceeds in two stages.

The initial rate is relatively slow in the early stage, followed by an increase in the reaction rate over longer time periods.

This is consistent with an autocatalytic reaction, the initial rate (no catalytic) is relatively slower in the early and first stage, followed by the second stage (auto acceleration) in which an increase in the reaction rate over longer time period is observed.

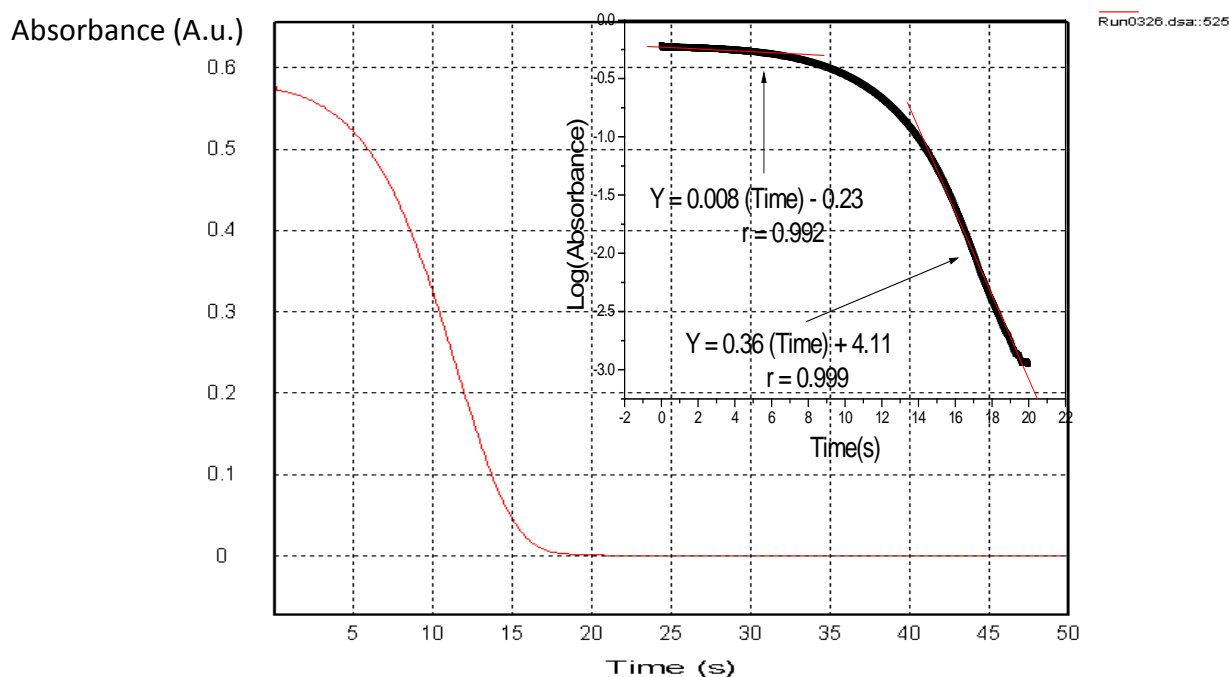


Figure 4.2 Plot of absorbance time course for MnO_4^- oxidation reaction of glyoxal. Experimental conditions: $[\text{MnO}_4^-] = 0.0025\text{M}$; $[\text{OCHCHO}] = 0.025\text{M}$; $[\text{H}_2\text{SO}_4] = 2\text{M}$; Wavelength = 525 nm; Temperature = 25°C.

It is possible that the shoulder in the CL corresponds to the first and slower early stage (no catalytic stage) during which MnO_4^- slowly interacts with glyoxal to generate Mn(III). In presence of large amount of glyoxal, Mn(III) is rapidly converted into Mn(II) and light.

The maximum intensity in the CL is believed to be the result of the predominant and faster second stage of the reaction (autocatalytic stage), during which manganese(II), the final product rapidly reacts with permanganate to produce Mn(III), which in the presence of a large amount of glyoxal, is quickly reduced to Mn(II) along with CL emission.

This is why the added Mn(II) increases the rate of the oxidation reactions and hence changes the chemiluminescence emission.

As can be seen from Figure 4.3 below, it is reasonable to believe that the CL emission observed is as a result of chemical reaction between glyoxal and MnO_4^- . The CL intensity reached a maximum between 10 and 20 seconds (at 15s) after the reaction was initiated and returned to baseline within 20s. Steady decay rates were observed, but a reproducible

shoulder was present on the rise portion of the intensity-time profile. This form of the CL indicates the complex nature of the MnO_4^- reaction.

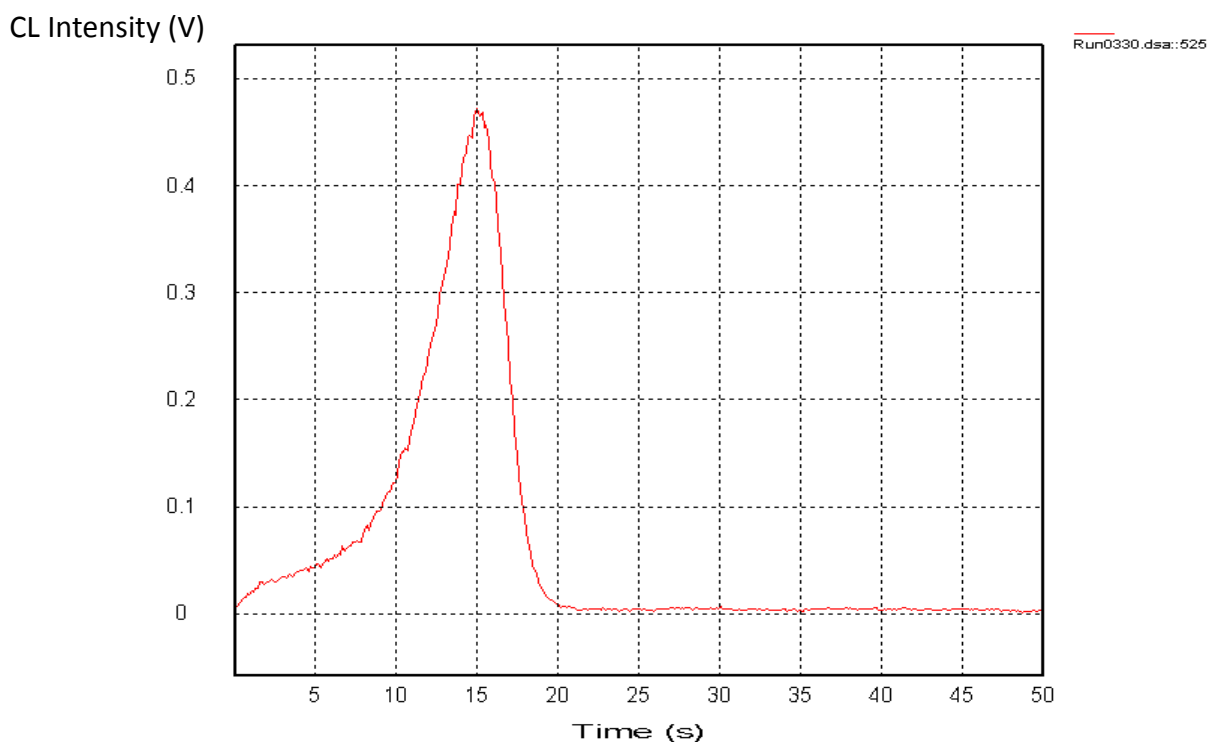


Figure 4.3 Example of stopped-flow CL intensity vs. time profiles for MnO_4^- oxidation reaction of glyoxal. Experimental conditions: $[\text{MnO}_4^-] = 0.0025\text{M}$; $[\text{OCHCHO}] = 0.025\text{M}$; $[\text{H}_2\text{SO}_4] = 2\text{M}$; Temperature = 25°C and HT (Fluorescence channel): 800V.

It is suggested that a net four-electron-transfer process occurs rapidly, followed by reactions between manganese(III) and glyoxal or its organic intermediates. Therefore, it is reasonable to model that the oxidation of glyoxal by permanganate by two consecutive steps, the first being a manganese(III) generation of an intermediate and the second of the manganese(III) oxidation of glyoxal to produce the chemiluminescence emission.

A comparison of the kinetics curve of the chemiluminescence emission (Figure 4.3) and the kinetic curve of the consumption of permanganate in Figure 4.2 shows a relationship between chemiluminescence and consumption of permanganate. As permanganate reagent is consumed, the intensity of the chemiluminescence rises and reaches the maximum intensity approximately at the same point that permanganate is used up from the reaction mixture.

In general, chemiluminescence intensities of organic substrates are known to greatly depend on the concentrations of the analyte (e.g. glyoxal), oxidant (e.g. MnO_4^- , Mn(III) and Mn(IV)), catalyst (e.g. enhancer or sensitizer), pH, etc. To evaluate the characteristics of the chemiluminescence process associated with change in concentration of the organic substrates, enhancers and oxidants concentrations, a series of unvaried experiments were carried out in

which all parameters and reaction conditions were held constant while the parameter of interest varies. The variables investigated included the concentrations of glyoxal, MnO_4^- enhancers such as formaldehyde and manganese(II) as catalyst.

There are two characteristics of CL peaks, the intensity of CL which is the total area under the peak and the maximum height of the peak. The former is important in some clinical assays which measure the total luminescence whereas the latter is important in many analytical determinations which use flow systems.

It is not expected that the total CL produced will change much with conditions unless the amount of manganese oxidant changes. Increasing the rate of emission of luminescence will increase the maximum height of the peak rather than area under the peak. It is to be expected that there will be some increase in total intensity with rate as the faster the luminescence is produced the less time there is for quenching from competing reactions.

4.2.1.1 Effect of glyoxal concentration

A set of experiments, in which the initial MnO_4^- concentration was held constant at 0.0025M and the initial glyoxal concentration was varied from 0.025 to 0.20M, was carried out.

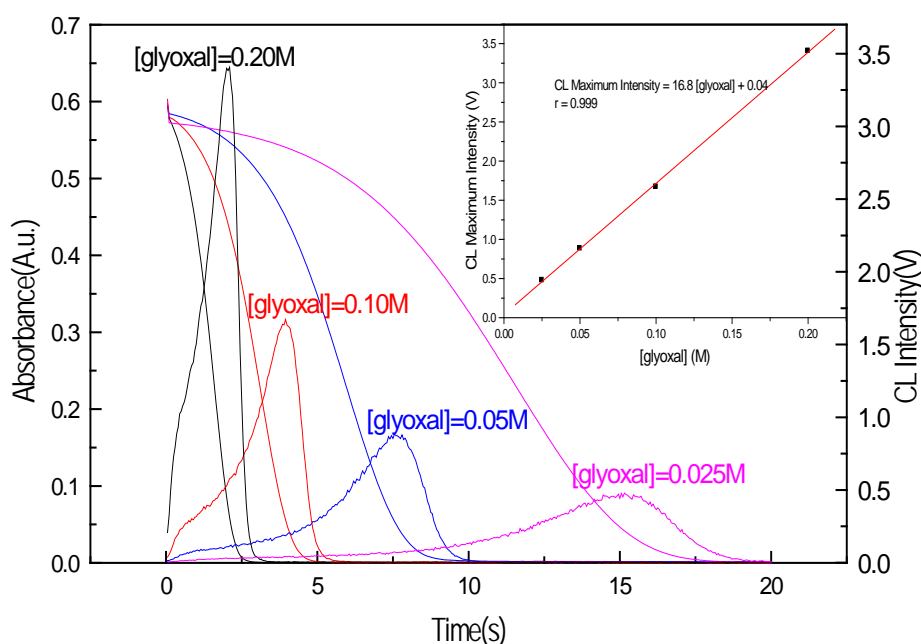


Figure 4.4 Plot comparing CL time course versus absorbance time course for MnO_4^- oxidation reaction of glyoxal. Experimental conditions: $[\text{MnO}_4^-] = 0.0025\text{M}$, $[\text{OCHCHO}] = 0.025, 0.05, 0.10$ and 0.2M , Temperature = 25°C , $[\text{H}_2\text{SO}_4] = 2\text{M}$; Wavelength = 525 nm and HT (Fluorescence channel): 600V.

As expected, the results from experiments demonstrate that the shape of each CL profile is similar and as the glyoxal concentration increased, the maximum of CL signal intensity increased, and the time to reach the maximum signal decreased with increasing [glyoxal], as can be seen in Figure 4.4. A plot of the maximum intensity versus [glyoxal] (inset of Figure 4.4) produced a straight line having a correlation coefficient of $R = 0.998$.

In Figure 4.4 the peak areas and maximum peak heights are as follows:

Table 4.1 Variation of profile areas and peak heights with glyoxal concentration

Variable factor: [OCHCHO] (M)	Intensity (area)	Approx. Peak height
0.025	3.60	0.50
0.05	4.65	0.90
0.10	5.46	1.70
0.20	7.04	3.40

As it can be seen from the Table 4.1, the obtained results match the prediction. Both peak areas and peak heights increased with increase in the glyoxal concentration. However, there is a small increase in areas whereas the height is directly proportional to the glyoxal concentration. Over a 2-fold increase in glyoxal concentration, only the profile height increased linearly by approximately 2-fold, the profile area increased but gradually by 1.2-fold. This would be the basis of an analytical method.

As the glyoxal is in excess, we predict that the rate of formation of the chemiluminescent emitter increases so the chemiluminescence is observed earlier.

In theory the total chemiluminescence should be constant as, with the glyoxal in excess, it depends on the amount of permanganate. The area does increase because if chemiluminescence is produced more rapidly, there is less loss of energy through competing processes.

As the rates of the reactions increase the peak becomes sharper and so the peak height increase more rapidly than the area and is found to be in direct proportion to the glyoxal concentration.

The MnO_4^- concentration for all four reactions, monitored at 525 nm, shows a similar shape of absorbance profiles with different rate constants. All the CL signals follow a relatively fast increase in the signal followed by a fast decrease. Qualitatively, the rate of CL signal decay is in good correlation with the rate of MnO_4^- disappearance as measured by UV absorption.

This result indicates that the fast step of the CL reaction corresponds to the oxidation reaction of glyoxal by Mn(III) intermediate for conditions of $[\text{OCHCHO}] \gg [\text{MnO}_4^-]$.

4.2.1.2 Effect of MnO_4^- concentration

The effect of increasing permanganate concentration from 0.0025 to 0.020M on chemiluminescence signal was evaluated, while the initial glyoxal concentration was held constant at 0.2M. The results from experiments demonstrate that, under the reaction conditions of $[\text{OCHCHO}] \gg [\text{MnO}_4^-]$, change in MnO_4^- concentration has little effect on the time of the chemiluminescence, but does increase the CL intensity. As expected, as the permanganate concentration increased, the maximum intensity of the CL response increased.

However, the time to reach the maximum CL proved to be independent on permanganate within the experimental range of permanganate concentration, as it can be seen in Figure 4.5. It is difficult to explain this behaviour, but it might be attributed to autocatalysis reaction between Mn(II) product and permanganate.

A plot of the profile intensity versus permanganate concentration (inset of Figure 4.5) produced a straight line having a correlation coefficient of $R = 0.998$.

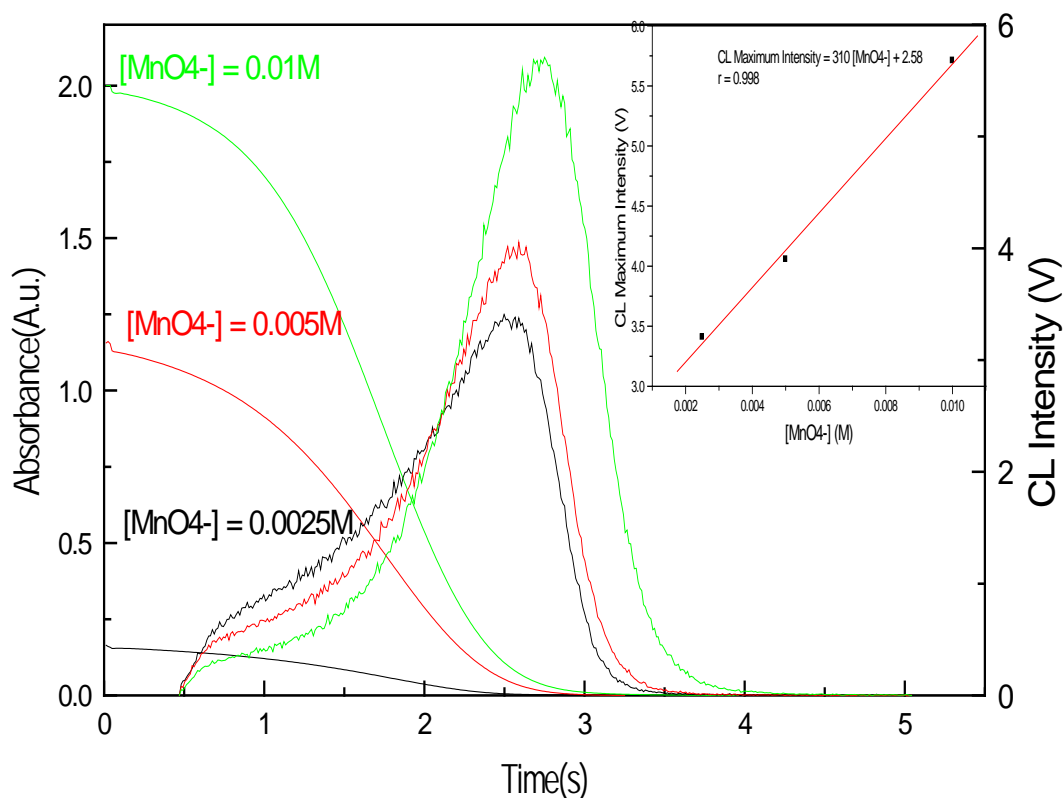


Figure 4.5 Plot comparing CL time course versus absorbance time course for MnO_4^- oxidation reaction of glyoxal. Experimental conditions: $[\text{OCHCHO}] = 0.2\text{M}$, $[\text{MnO}_4^-] = 0.0025, 0.005, 0.010\text{M}$, Temperature = 25°C , Wavelength = 525 nm ; HT (Fluorescence channel): 800V .

In Figure 4.5 the peak areas and maximum peak heights are as follows:

Table 4.2 Variation of profile areas and peak heights with MnO_4^- concentration

Variable factor: [MnO_4^-] (M)	Intensity (area)	Approx. Peak height
0.0025	6.80	3.41
0.005	6.64	4.02
0.010	9.64	5.71
0.020	-	-

As expected both chemiluminescence signal peak areas and peak heights increased with increase in the glyoxal concentration. However, there is a small increase in areas whereas the height is directly proportional to the permanganate concentration.

Again, this result confirms the conclusion that the observed CL emission is associated with the glyoxal oxidation. The first-order dependence of the intensity of the CL on permanganate concentration at low [MnO_4^-] and under the reaction conditions of [OCHCHO] \gg [MnO_4^-] is consistent with Mn(III) oxidant role of intermediate in subsequent reactions.

4.2.1.3 Effect of manganese(II)

It has been established that, under acidic conditions, Mn(II) generated plays an autocatalytic role in many of these reactions. It is suggested that Mn(II) reacts with MnO_4^- to yield Mn(III) intermediate, which reacts with organic substrate and increases the rate of the reaction.

Manganese(II), as well as other metal ions^{77, 96, 110, 125, 126, 145-147, 464, 519} has been used as an enhancer in analytical applications. Agater et al.¹⁴⁵ reported the successive determination of carbohydrates (glucose, galactose, fructose, arabinose, xylose, lactose, sucrose, mannitol, glycerol and ascorbic acid with a limit of detection of 1×10^{-4} M), based on the CL reaction with acidic permanganate enhanced by Mn(II) ions, using a flow-injection analysis system.

It was also shown that the addition of Mn(II) salts increased the rate of the chemiluminescent oxidation of butane-2,3-dione (diacetyl) with acidic potassium permanganate and manganese ions have been determined in alloys with a limit of detection of 6×10^{-8} M¹⁵⁵.

Therefore, it is essential to clarify the role of manganese(II) catalysis in permanganate chemiluminescence. The effect of added manganese(II) was studied in presence of 0.02M KMnO_4 , 0.1M glyoxal, and 2M H_2SO_4 at 25°C. The results are shown in the Figure 4.6.

This shows that the oxidation of glyoxal by permanganate in the presence of added Mn(II) produced a significant CL emission, and the resultant intensity versus time profiles (Figure 4.6) showed significant differences in the kinetics of emission with and without Mn(II). As it can be seen, under the reaction conditions, both the intensity of the chemilumines-

cence emission and the rate of permanganate disappearance increased as manganese(II) concentration increased, tending to some limiting value.

Manganese(II) provided a 2-10 fold increase compared to maximum chemiluminescence response from the reaction without Mn(II). The relevance of manganese(II) is clearly supported by the current findings. The added Mn(II) leads to the prediction that Mn^{2+} plays an important role in the kinetics.

A plot of the profile intensity versus glyoxal concentration (inset of Figure 4.6) produced a straight line having a correlation coefficient of $R = 0.997$.

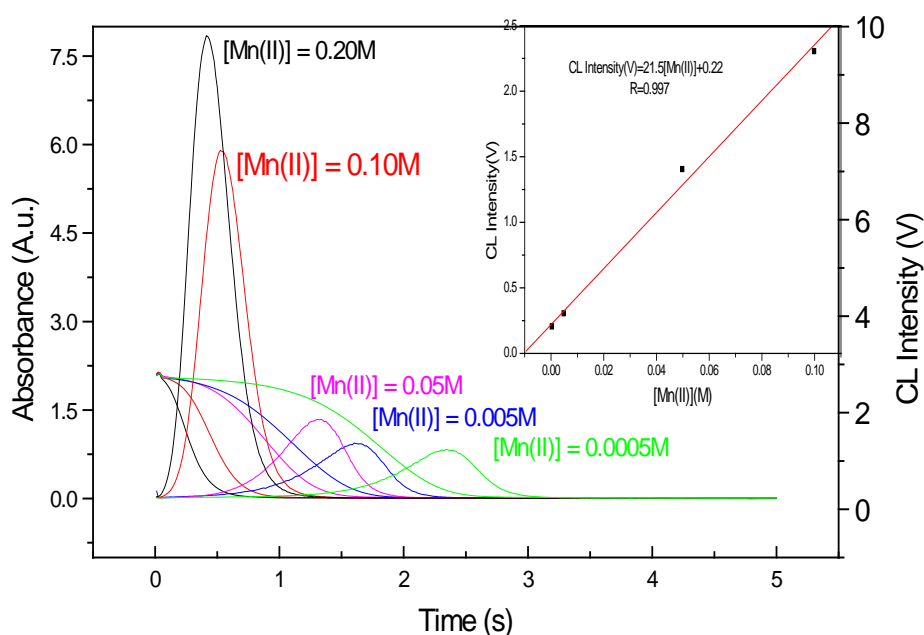


Figure 4.6 Effect of Mn(II) concentration on the kinetic of the reaction and CL. Experimental conditions: $[OCHCHO] = 0.2M$, $[MnO_4^-] = 0.01M$, $[Mn(II)] = 0.0005 - 0.2M$, Temperature = $25^\circ C$, $[H_2SO_4] = 2M$, Wavelength = 525 nm ; HT (Fluorescence channel): $600V$.

In Figure 4.6 the peak areas and maximum peak heights are as follows:

Table 4.3 Variation of profile areas and peak heights with Mn^{2+} concentration

Variable factor: $[Mn^{2+}] (M)$	Intensity (area)	Approx. Peak height
0.00	0.91	0.88
0.0005	0.95	0.93
0.005	1.20	1.34
0.010	3.90	5.90
0.020	5.86	7.85

The results in Table 4.3 illustrate some of the established main characteristics of the permanganate CL reaction such as the linear enhancement effect of the added manganese(II) on the CL signal intensity.

Accordingly to expectations, the results in Table 4.3 illustrate some of the established main characteristics of the permanganate chemiluminescence reaction such as the linear enhancement effect of the added manganese(II) on the chemiluminescence signal intensity. Accordingly to expectations, the profiles area and height increased significantly 6.5-fold and 10.6-fold, respectively in the manganese(II) concentration range of 0.0 - 0.2M.

A plot (Figure not shown) of both peak area and peak height confirmed linear dependence of manganese(II) concentrations with positive intercepts and slopes.

The reaction of manganese(II) with permanganate is often written as the Guyard reaction;



However, in acid solution, the main product may be Mn^{3+} (aq);



The reaction between MnO_4^- and excess of Mn(II) was followed by using the stopped-flow technique over five minutes. Figure 4.7 depicts the reaction of 0.002M permanganate with 0.2 Mn(II) in 2M sulphuric acid medium.

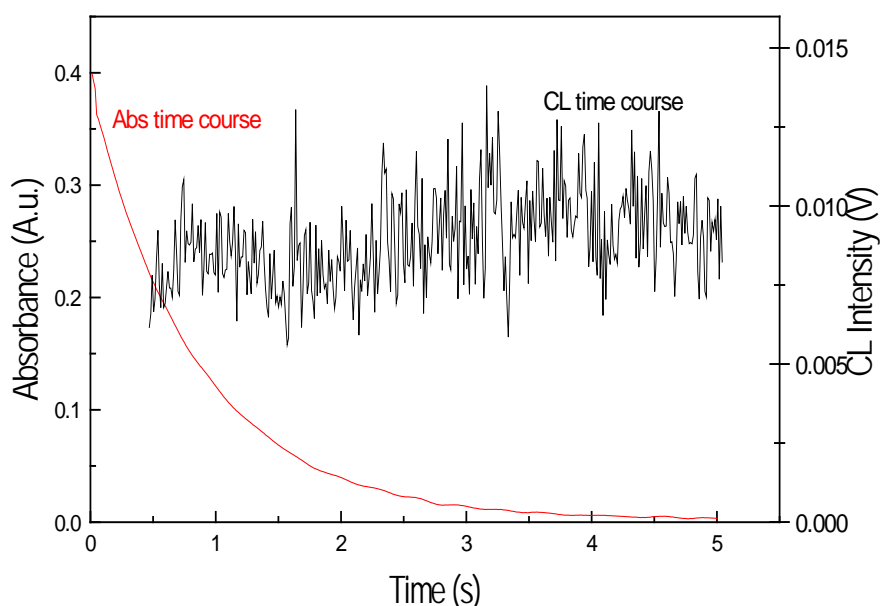


Figure 4.7 Plot comparing CL time course versus absorbance time course for MnO_4^- oxidation reaction of Mn(II). Experimental conditions: $[\text{Mn(II)}] = 0.2\text{M}$, $[\text{MnO}_4^-] = 0.002\text{M}$, Temperature = 25°C , $[\text{H}_2\text{SO}_4] = 2\text{M}$, Wavelength = 500 nm; HT (Fluorescence channel): 800V.

Whilst this reaction is demonstrated, it is significantly slower than in the presence of an organic reductant and as expected no CL emission is observed. The greater the chance of the reaction to occur quickly, the faster the emitting species is produced, the larger the chemiluminescence emission, as CL emission competes with other form of energy loss.

4.2.1.4 Effect of formaldehyde (HCHO)

As mentioned previously, it is well known that the addition of formaldehyde in the reaction mixture increases the CL response from oxidation reaction of many analytes with acidic potassium permanganate^{38, 77, 96, 110, 125, 126, 145-147, 464, 519}.

In order to visualize how formaldehyde participate in the permanganate oxidation of glyoxal to enhance CL, a series of kinetics runs were carried out by increasing the formaldehyde concentration from 0.0 – 1.6 mol dm⁻³ at constant concentrations of other reactants and parameters.

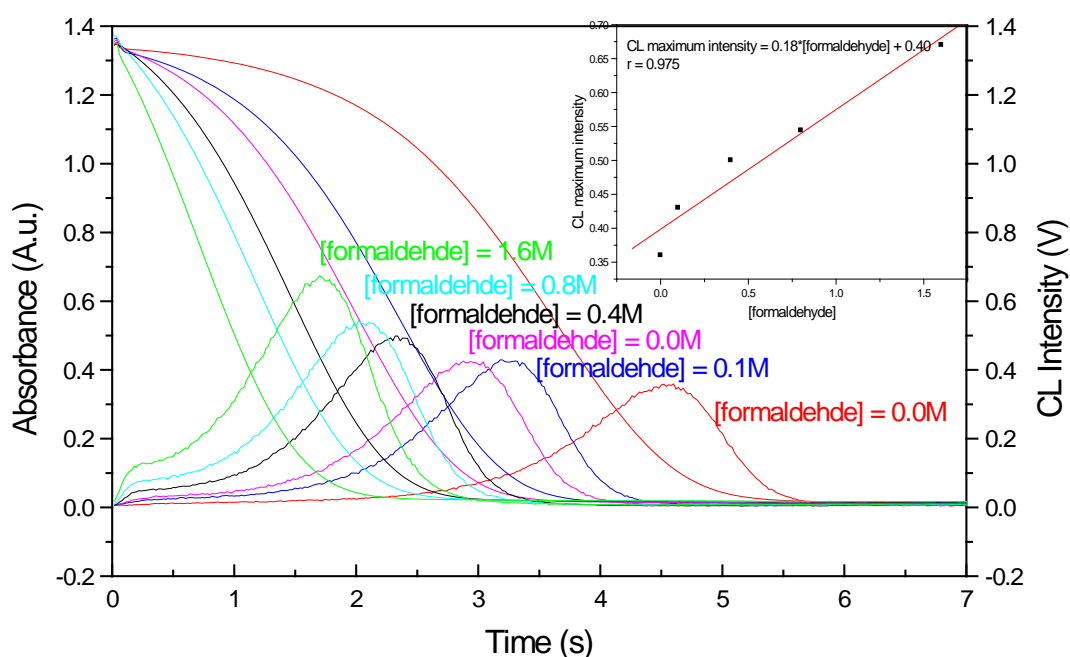


Figure 4.8 Effect of [HCHO] on the kinetic of the reaction and CL signal. Experimental conditions: [OCHCHO] = 0.1M, [MnO₄⁻] = 0.005M, [HCHO] = 0.0 – 1.6 M, Temperature = 25°C, [H₂SO₄] = 2M, Wavelength = 525 nm; HT: 500V.

To understand the involvement of formaldehyde, the reaction kinetic of formaldehyde and acidic potassium permanganate was separately investigated. The experiment was conducted under same experimental conditions.

Figure 4.9 below demonstrates that formaldehyde can also reduce permanganate to Mn(III) intermediate. It depicts the kinetics of the chemiluminescence emission and of the reaction between 0.75M formaldehyde in sulphuric acid medium and 0.01 permanganate.

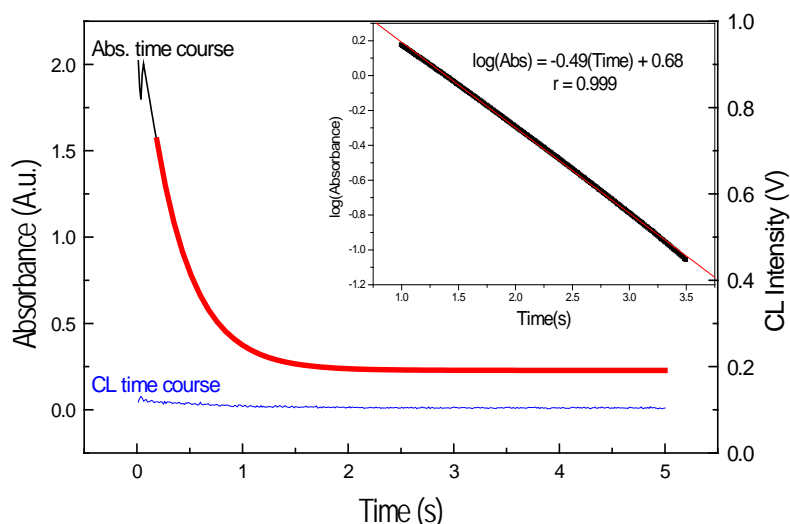


Figure 4.9 Plot comparing CL time course versus absorbance time course for KMnO_4 oxidation reaction of formaldehyde. Experimental conditions: $[\text{HCHO}] = 0.75\text{M}$, $[\text{MnO}_4^-] = 0.02\text{M}$, Temperature = 25°C , $[\text{H}_2\text{SO}_4] = 2\text{M}$, Wavelength = 500 nm ; HT: 800V .

The kinetic measurements were carried out under pseudo-first-order conditions where the formaldehyde was present in a large excess over that of oxidizing agent.

From the results in Figure 4.9, there is clear evidence of reaction between formaldehyde and MnO_4^- ; however, the experiment did not detect any evidence for measurable CL response from the reaction.

These findings of the current study confirm the conclusion that the augmented CL observed when formaldehyde is added in the mixture reaction is associated with the co-oxidation of formaldehyde and glyoxal to generate more Mn(III) intermediate, which then immediately reacts with glyoxal to produce more light.

The oxidation reaction was found first order with respect to MnO_4^- concentration, indicated by the linearity of $\log(\text{absorbance}) - \text{time}$ plots (inset of Figure 4.9) for more than three half-lives of reaction completion.

4.2.2 Manganese(III) oxidation of glyoxal

As mentioned in the second chapter, Mn(III) is believed to be the active oxidizing intermediate species that reacts with glyoxal or organic intermediates in a final reaction to form excited manganese(II) species (Mn(II)^*) that emits light. It is therefore essential to investigate separately, but under the same conditions, the oxidation reaction between Mn(III) and glyoxal in order to evaluate its CL potential.

In addition to permanganate, chemiluminescence has also been detected during reactions with other manganese species, including manganese(III) and 'soluble' manganese(IV) oxi-

dants. Several research groups have detected CL from reactions with Mn(III) species^{218, 221, 393}.

Junghänel and co-workers reported that the oscillating manganese(II)-catalysed Belousov–Zhabotinskii system (i.e. the oxidation of malonic acid with bromate catalysed by the repeated interchange between manganese(II) and manganese(III) evoked a periodic emission of light with a maximum intensity at 630 nm⁵⁷⁷, which they attributed to excited molecular oxygen formed by the recombination of HO₂ radicals.

However, Karavaev et al. subsequently showed that this emission (which they found to be most intense at 680 – 720 nm) was a result of the reduction of manganese(III), and postulated that the emitter was electronically excited Mn(II)³⁹³, noting the similarity of the emission with the corresponding photoluminescence reported by Sveshnikova and Stroganov³⁹⁴.

Lilley et al. detected CL from the oxygenase activity of manganese(II)-activated d-ribulose-1,5-bisphosphate carboxylase/oxidase (Rubisco) and presented evidence that this luminescence emanated from the manganese(II) ion at the active site, due to an electron exchange process involving a transient manganese(III) intermediate⁵⁷⁸.

Similarly, Watanabe et al. found that the oxidation of glyoxal in a tartrate buffer using either a manganese(III)–lactate complex or a combination of hydrogen peroxide and manganese peroxidase, produced an emission of light with maximum intensity at 700–710 nm³⁹⁵.

Using FIA methodology, Zhang and co-workers developed a method for the determination of isoniazid, based on the chemiluminescence reaction with a manganese(III) reagent that was generated on-line by constant-current electrolysis of Mn(II) sulphate in acidic solution²²¹.

The on-line electrogeneration of manganese(III) from manganese(II) has been applied to the chemiluminescence determination of a wide range of analytes²²¹. This approach is not limited to manganese(III); other oxidants such as hypochlorite, hypobromite, silver(II) and cobalt(II), which are either unstable in aqueous solution or undesirable to prepare off-line, have been generated for chemiluminescence reactions in a similar manner^{218, 396}.

As said earlier, in these experiments, the oxidation of glyoxal with and without the addition of enhancers was extended to manganese(III) as CL reagents. The characteristics of the kinetics and the intensity of the CL emission and the kinetics of the reaction were investigated.

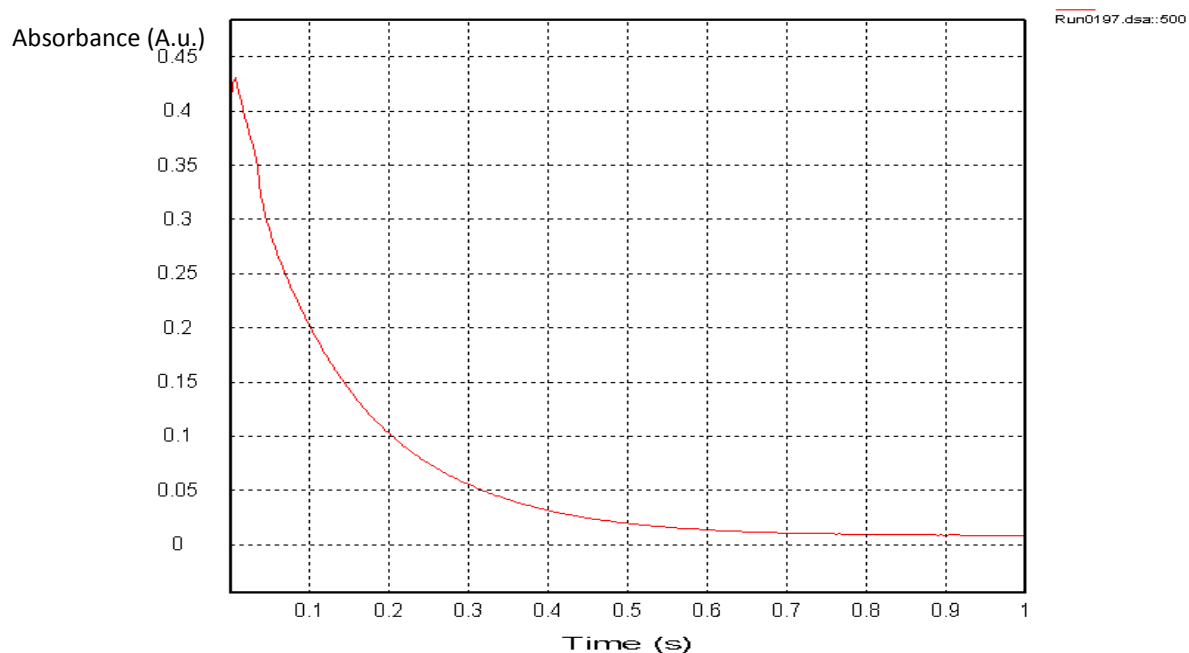


Figure 4.10 Plot of absorbance time course for Mn(III) oxidation reaction of glyoxal. Experimental conditions: $[\text{Mn(III)}] = 0.0025\text{M}$; $[\text{OCHCHO}] = 0.025\text{M}$; $[\text{H}_2\text{SO}_4] = 2\text{M}$; Wavelength = 500 nm; Temperature = 25° C.

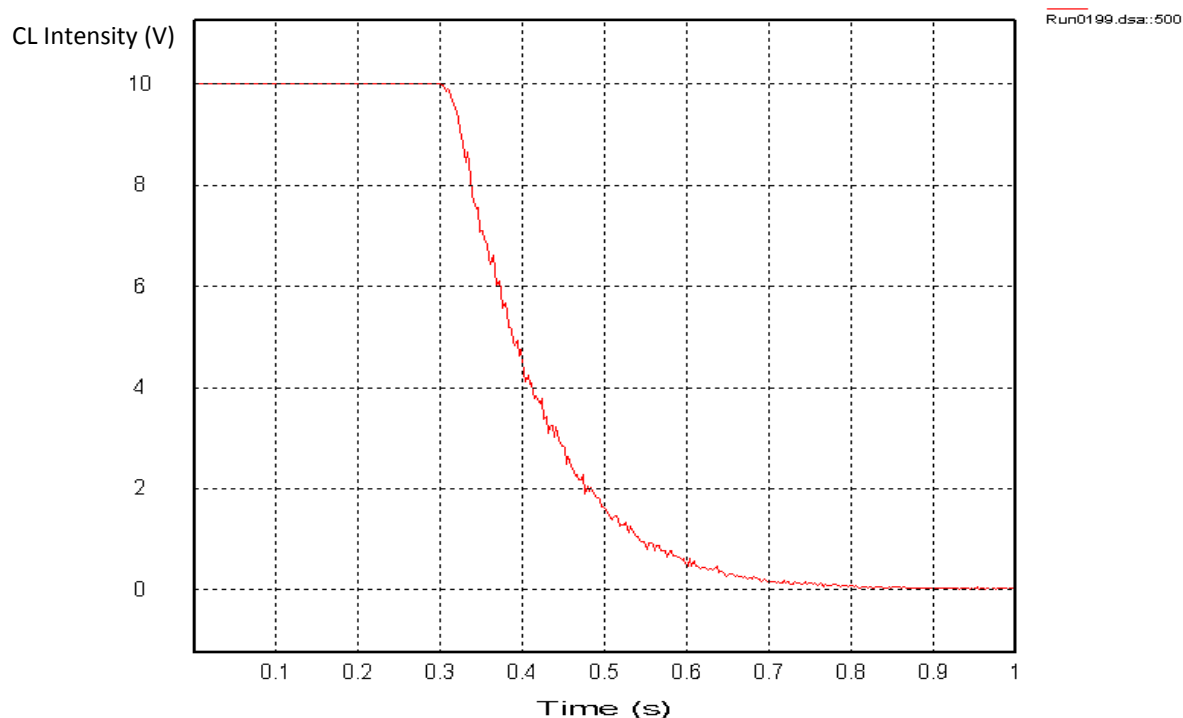


Figure 4.11 Plot of chemiluminescence time course for Mn(III) oxidation reaction of glyoxal. Experimental conditions: $[\text{Mn(III)}] = 0.0025\text{M}$; $[\text{OCHCHO}] = 0.025\text{M}$; $[\text{H}_2\text{SO}_4] = 2\text{M}$; Temperature = 25° C and HT (Fluorescence channel):800V.

The results of the investigation of the kinetics of the manganese(III) oxidation of glyoxal and the kinetics of the chemiluminescence response are given in Figures 4.10 and 4.11, which show typical examples of stopped-flow chemiluminescence and absorbance time courses for the oxidation reactions of glyoxal using Mn(III), respectively.

As expected, stopped-flow experiments demonstrated that glyoxal (dissolved in 2 mol L⁻¹ sulphuric acid) is rapidly and effectively oxidized by Mn(III) under the reaction conditions.

The absorbance time courses (Figures 4.10) indicates half-life ($t_{1/2}$) for the reaction of about 0.1 second. These results confirm the hypothesis suggested earlier about the light-producing pathway that, it is Mn(III) intermediate generated in the course of the reaction that quickly reacts with glyoxal and/or daughter products to yield the CL emission. It has been assumed above that, in the co-oxidation of glyoxal and formaldehyde, under the reaction conditions, formaldehyde does not react with Mn(III) intermediate during the reaction and react only with MnO₄⁻ to accumulate up Mn(III) used in the second step of the reaction.

In order to verify this hypothesis and to evaluate the potential CL enhancement of formaldehyde upon Mn(III) oxidation of glyoxal, the oxidation reaction of Mn(III) of glyoxal with and without formaldehyde was monitored at maximum absorbance of Mn(III) at 500 nm and the CL signals were recorded at its maximum emission.

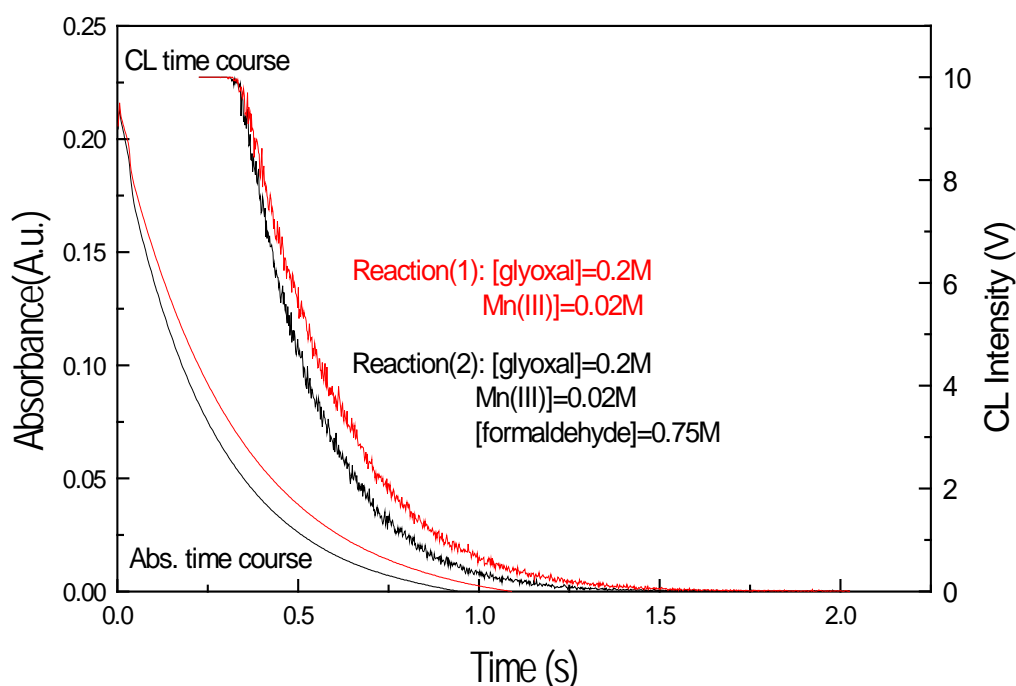


Figure 4.12 Plot comparing chemiluminescence time course versus absorbance time course for Mn(III) oxidation reaction of glyoxal with and without HCHO. Experimental conditions: [HCHO] = 0.75M, [OCHCHO] = 0.2M, [Mn(III)] = 0.02M, Temperature = 25°C, [H₂SO₄] = 2M, Wavelength = 500 nm; HT (Fluorescence channel): 500V.

In Figure 4.12, the absorbance profiles of Mn(III) versus time in the reaction of 0.2M glyoxal with 0.02M Mn³⁺ with and without 0.75M formaldehyde are compared to its corresponding chemiluminescence signal profiles.

The experimental results indicated that the kinetics and the intensity of the chemiluminescence response and the kinetics of reaction were unchanged on addition of formaldehyde to the reaction mixture.

These results confirm the conclusion that formaldehyde does not undergo significant oxidation in the presence on Mn(III) and consequently, formaldehyde is not an enhancer for Mn(III) chemiluminescence oxidation of glyoxal.

To confirm these results, Mn(III) was mixed with formaldehyde to initiate oxidation reaction in the absence of glyoxal. Figure 4.13 shows the stopped-flow results of the oxidation reaction between Mn(III) and formaldehyde and confirm the previous results that formaldehyde remains unreacted in the presence of oxidant Mn(III) under the reaction conditions.

These results clearly demonstrated that there was no or very slow chemical reaction between Mn(III) and formaldehyde.

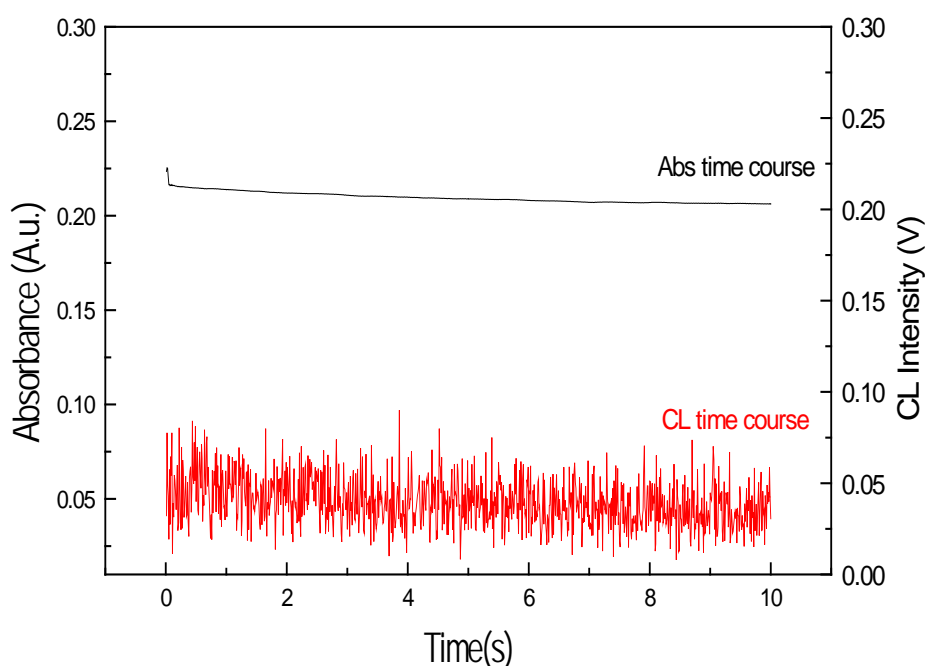


Figure 4.13 Plot comparing CL time course versus absorbance time course for Mn(III) oxidation reaction of formaldehyde. Experimental conditions: [HCHO] = 0.75M, [Mn(III)] = 0.02M, T° = 25°C, [H₂SO₄] = 2M, Wavelength = 500 nm; HT (Fluorescence channel): 800V.

Since it has been shown that formaldehyde does not produce any measurable chemiluminescence either with permanganate or Mn(III), it is reasonable to believe that the reaction

between glyoxal and permanganate in sulphuric medium follows one defined light-producing pathway and the observed chemiluminescence enhancement from formaldehyde in permanganate oxidation of glyoxal is associated with the reaction of formaldehyde with permanganate to generate additional Mn(III) intermediate and more CL emission.

4.2.3 Manganese(IV) oxidation of glyoxal

With Mn(V) and Mn(VI) being highly unstable in acid medium and thus very difficult to monitor, Mn(IV) is the only other possible stable oxidizing intermediate species during acidic MnO_4^- oxidation of glyoxal. Glyoxal can be oxidized by Mn(IV) in an acidic medium, producing a CL signal. As such, under the reaction conditions, Mn(IV) is expected to play an important role into the light-producing pathways of this reaction. In order to elucidate whether or not Mn(IV) plays an essential role into CL reaction of MnO_4^- oxidation of glyoxal, the kinetics of reaction and the kinetics and the intensity of the CL emission were examined.

It has been claimed that manganese(IV) oxidant reacts with many organic compounds to produce an excited manganese(II) species that emits light²¹⁸. It has been suggested that the chemiluminescence that accompanies the reaction of the manganese(IV) reagent with a range of analytes results from a manganese(II) species²¹⁸ and is enhanced by the presence of formaldehyde.

As with many CL reactions with MnO_4^- , the addition of formaldehyde was found to significantly enhance the emission of light^{218, 351}. Soluble manganese(IV) has been used as a CL reagent and this chemistry has been applied to the determination of various inorganic and organic analytes²¹⁸. Brown and co-workers^{218, 351} carried out investigation of CL reactions with soluble manganese(IV). Using flow injection analysis methodology, analytically useful CL responses were obtained from the oxidation of several organic and inorganic compounds.

According to Brown and co-workers²¹⁸ a further fourteen publications have emerged on the use of soluble manganese(IV) as a CL reagent for the determination of various organic compounds, since their initial evaluation. Manganese(IV) concentrations of between 8×10^{-5} M and 1×10^{-3} M have been reported as optimal for detection (4×10^{-4} M most commonly employed). Contrary to the claim of the Australian's, the first published report on Mn(IV) was by Agater in her thesis of 1999. This thesis is available in the University repository. The rate of the light-producing reactions between the soluble Mn(IV) reagent, various analytes and formaldehyde have been examined with stopped-flow experiments^{218, 219, 351}.

In most cases, the chemiluminescence intensity versus time profiles reached a maximum between 0.5 s and 6.0 s after the reaction was initiated, and returned to baseline within 15–70 second^{218, 219, 351}. However, the light-producing reaction between the manganese(IV) reagent and potassium oxalate was found to persist for several minutes³⁵¹.

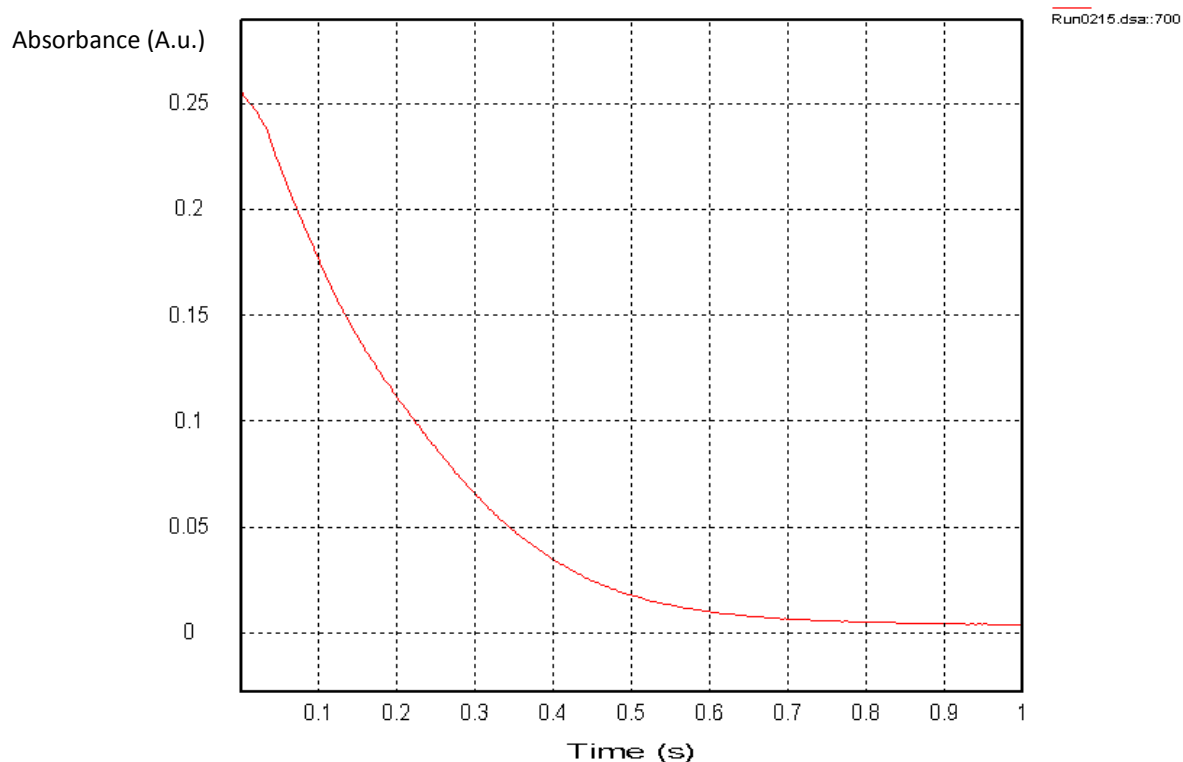


Figure 4.14 Plot of absorbance time course for Mn(IV) oxidation reaction of glyoxal. Experimental conditions: [Mn(IV)] = 0.0025M; [OCHCHO] = 0.025M; [H₂SO₄] = 2M; Wavelength = 400 nm; Temperature = 25° C.

In these experiments, the kinetics and intensity of the CL emission and the kinetics of reaction between glyoxal and Mn(IV) were examined under the reaction conditions relevant to CL emission.

The kinetic measurements were conducted under pseudo- first-order conditions, where glyoxal was present in a large excess (0.025 mol dm⁻³) over that of MnO₄⁻ concentration (0.0025 mol dm⁻³) and at a constant acidic solution of 2.0 mol dm⁻³ (maintained with sulphuric acid).

The results of the investigation of the kinetics of the Mn(IV) oxidation of glyoxal and the kinetics of the CL response are given in Figures 4.14 and 4.15, which show typical examples of stopped-flow CL and absorbance time courses for the oxidation reactions of glyoxal using Mn(III), respectively.

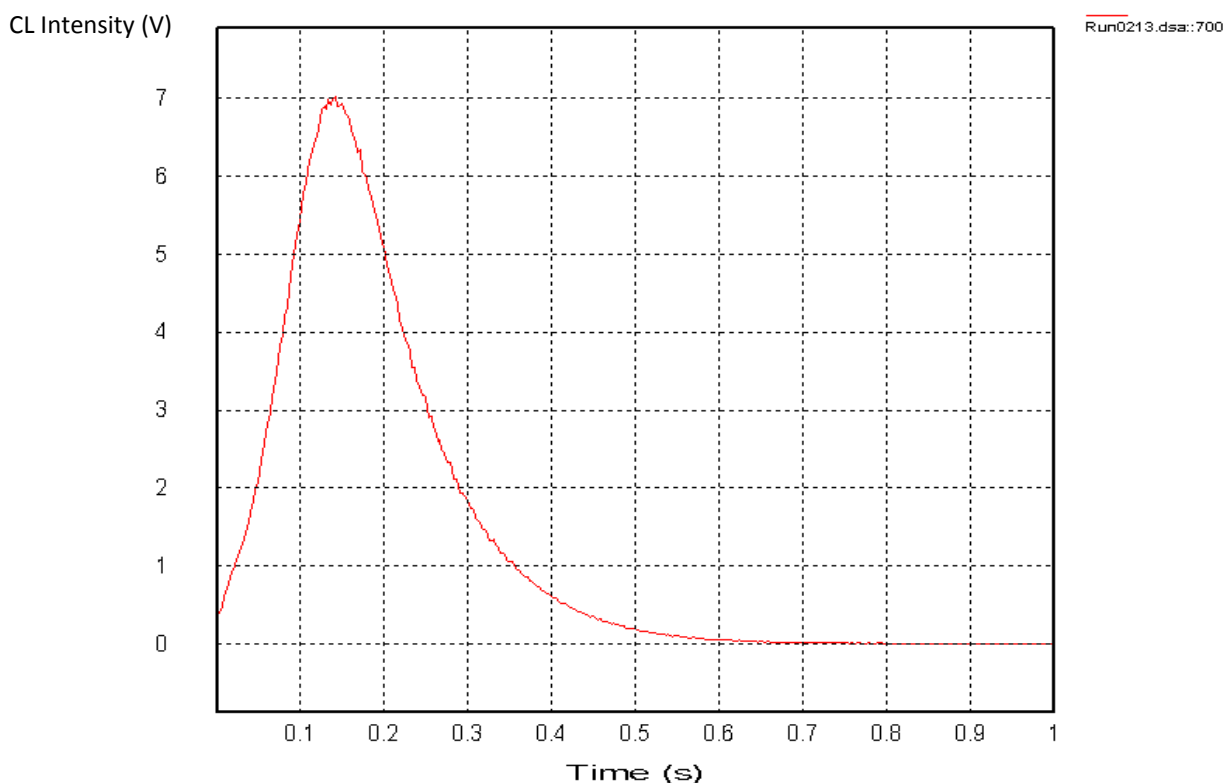


Figure 4.15 Plot of CL time course for Mn(IV) oxidation reaction of glyoxal. Experimental conditions: [Mn(IV)] = 0.0025M; [OCHCHO] = 0.025M; [H₂SO₄] = 2M; Temperature = 25° C and HT (Fluorescence channel): 800V.

As expected, it has been observed from Figure 4.15 that Manganese(IV) reacts quickly with glyoxal to produce light emission in sulphuric acid medium. The absorbance time course (Figure 4.15) indicates half-time ($t_{1/2}$) reaction of about 0.15 second.

It has been demonstrated that all manganese-based oxidants i.e. MnO_4^- , Mn(IV) and Mn(III) yield CL emission in reaction with glyoxal. However, the resultant chemiluminescence intensity versus time profiles (Figures 4.3, 4.11 and 4.15) showed significant differences in the kinetics of CL emission with permanganate, manganese(IV) and manganese(III).

It is interesting to note that both Mn(IV) UV absorbance and CL emission spectra exhibit similar time dependence, as can be seen in the figures 4.14 and 4.15. A comparison of the kinetics of the CL emission and the rate of manganese(IV) disappearance as measured by UV absorption at 400 nm displays a good agreement. These results indicate that the observed CL emission is associated with the oxidation reactions of glyoxal by Mn(IV) oxidant.

Although it is difficult to compare the CL intensities of different oxidants due to the wide range of experimental conditions particularly related to the differences in their stabilities, in these experiments, efforts were made to maintain the same reaction conditions in order to compare their chemiluminescence potentials with glyoxal.

Manganese(IV) and manganese(III) oxidations of glyoxal were found to elicit relatively intense CL over a period of one minute, whereas CL response derived from permanganate oxidation was relatively weak.

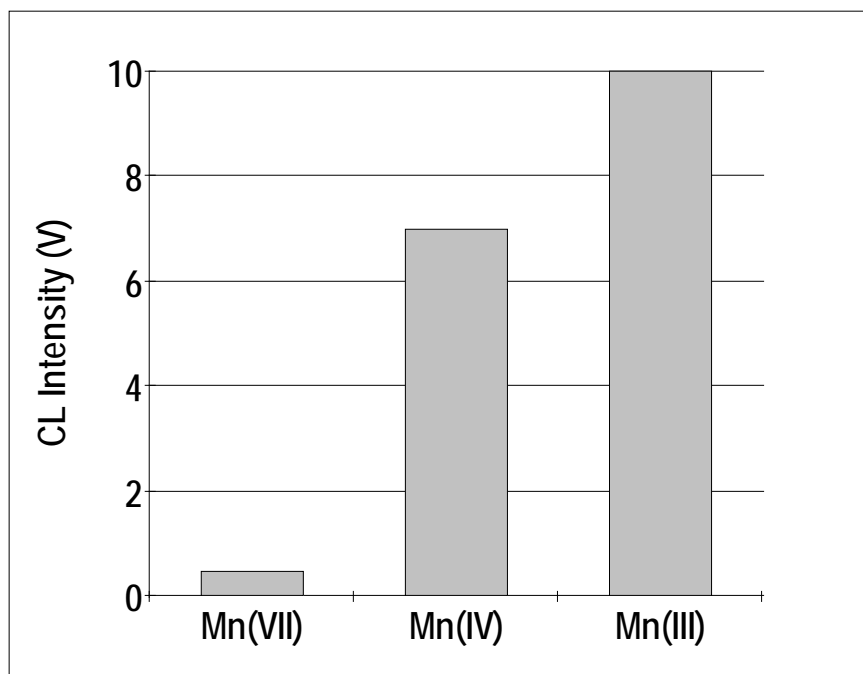


Figure 4.16 Plot comparing CL intensity (peak height) generated by MnO_4^- , Mn(IV) and Mn(III) oxidation reaction of glyoxal. Experimental conditions are the same as above.

Figure 4.16, which compares the CL responses, shows significant differences in the CL intensity (or peak height), which is increased 15-fold for manganese(IV) and more than 20-fold for Mn(III) when compared with that produced by permanganate oxidation.

Comparable responses from glyoxal oxidation by Mn(III) offers a distinct advantage over other chemiluminescence reagents i.e. Mn(IV) and permanganate. From an analytical point of view, although permanganate is presented as the most efficient oxidant for direct liquid phase chemiluminescent processes, Mn(IV) and Mn(III) offer here the advantage of highly sensitive chemiluminescence detection.

It was stated above that Mn(IV) and Mn(III) are the common and relevant redox intermediate species during acidic permanganate oxidation of glyoxal. They both have proved to react with glyoxal in acid medium and produce a significant amount of CL emission.

In order to show their existence and to identify these intermediate species, a detailed investigation of spectral changes occurring during the oxidation of glyoxal by permanganate using the stopped-flow technique including a diode-array detector is essential.

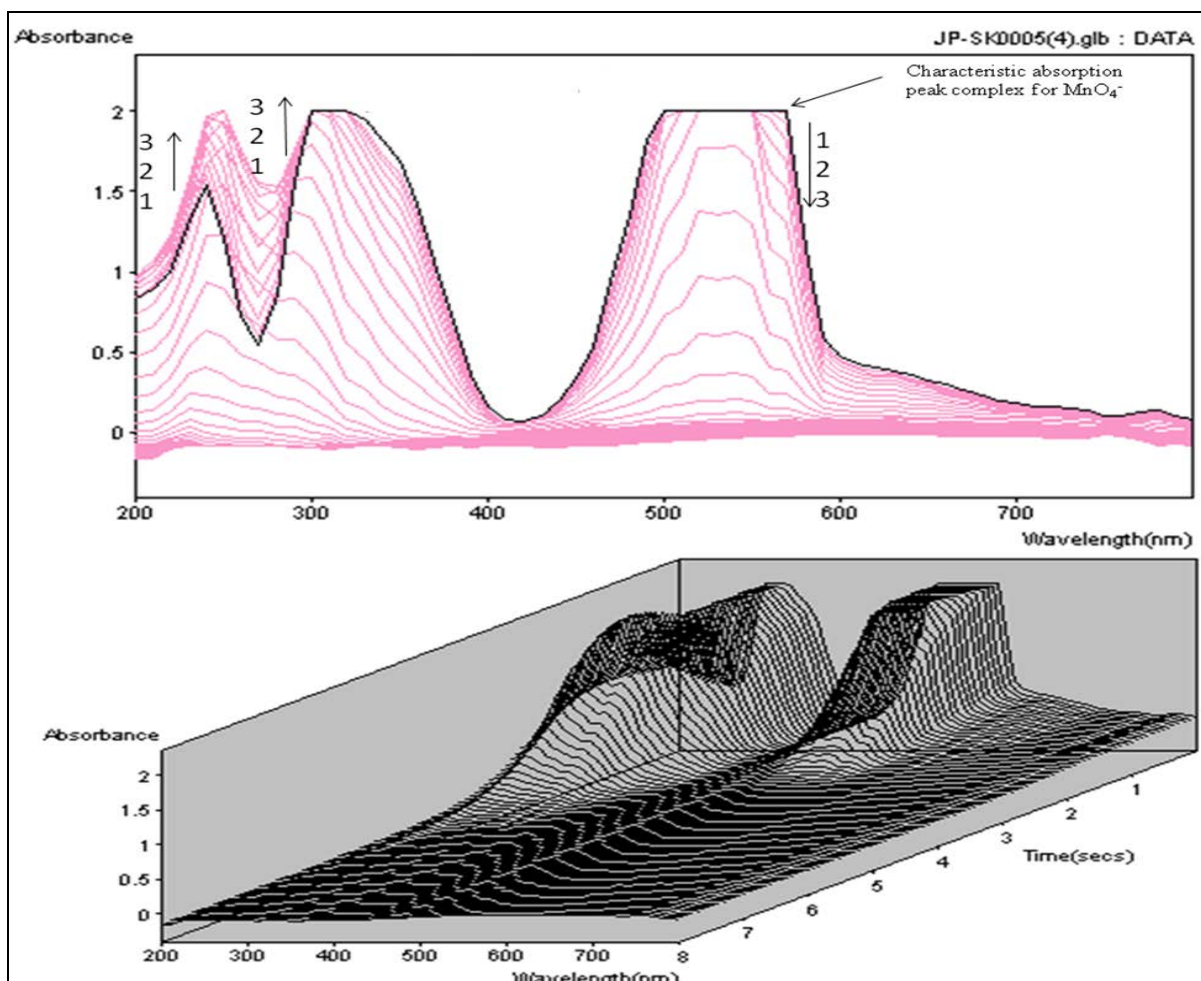


Figure 4.17 (2D) and (3D)-Spectral changes observed upon the reaction of 0.02M MnO_4^- with 0.2M glyoxal acquired over a broad wavelength range (200–800 nm). Reaction conditions: Temperature 25 °C, 2M H_2SO_4 .

Figure 4.17 shows the time-resolved spectrum acquired over a broad wavelength range (200 nm – 800 nm) for the oxidation of 0.2M glyoxal in 2M sulphuric acid medium with 0.02M permanganate at room temperature.

As expected, the absorption intensity in the broad wavelength region 480 to 600 nm (characteristic peak complex for permanganate) decreased gradually as the reaction proceeded, and MnO_4^- concentration decreased.

As mentioned before, it is believed that the overall reaction has more than one step, which are characterized by the generation of Mn(IV) and Mn(III) redox intermediates. As the MnO_4^- peak at ~ 320 nm increases, the spectral changes exhibits a superimposed absorption band on MnO_4^- , for Mn(IV) between 300 and 400 nm, which increased a second after the reaction is initiated and then gradually decreased with time as see in Figure 4.17(3D).

It is difficult to explain this result, as permanganate also has a significant absorbance in this region, but this behaviour might be related to the formation and disappearance of the Mn(IV) intermediate. The observed decrease in Mn(IV) in the course of the reaction could be attributed to the rapid reaction of Mn(IV) with glyoxal and Mn(II) to generate Mn(III).

Between 200 and 300 nm, the absorbance initially increased as the reaction proceeded with a band maximum at 250 nm. This is most likely due to the intermediate organic products produced during glyoxal oxidation.

Again permanganate spectrum also shows some absorbance similarity in this region. Further research needs to be conducted to identify these intermediates produced from the oxidation of glyoxal by permanganate.

Another problem with this permanganate spectral change is that no evidence for increase of absorbance indicating the presence Mn(III) intermediate with its maximum located at 500 nm was seen in these experiments.

This was due to the fact that Mn(III) reacts rapidly with organic substrate and that MnO_4^- absorbance contributes to the Mn(III) absorbance measured at 500 nm (an absorbance maximum for Mn(III)).

Although MnO_4^- spectral change failed to identify the existence of Mn(III) intermediate and since Mn(IV) could be more or less identified on this spectral change, it was essential to look in the spectral change in the course of the reaction between Mn(IV) and glyoxal.

Thus, the changes of spectrum during the oxidation of glyoxal with permanganate were considered to determine whether Mn(III) intermediate is generated during the reaction between Mn(IV) and excess of glyoxal by using the stopped-flow technique. Figure 4.18 depicts the reaction of 0.05M Mn(IV) with 0.5M glyoxal in sulphuric acid medium.

As expected, the absorption intensity in the region 300 and 400 nm (characteristic spectra for Mn(IV)) decreased gradually as the reaction proceeded, and the concentrations decreased.

Here, it is demonstrated by using the stopped-flow technique including a PTM detector that no direct transition from the Mn(IV) to a Mn(II)-like species occurs upon mixing glyoxal with permanganate.

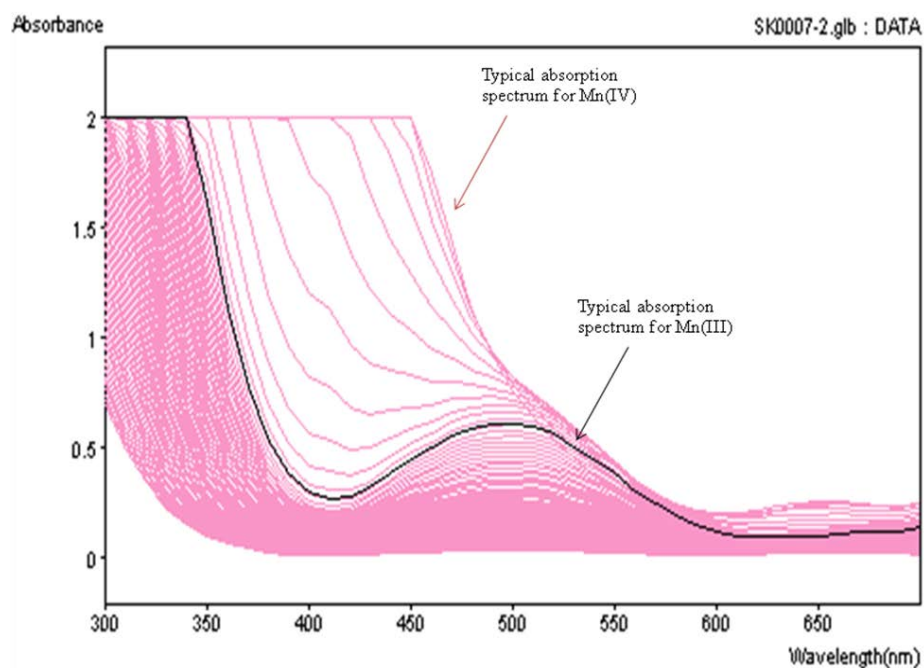


Figure 4.18 (2D)-Spectral changes observed upon the reaction of 0.02M Mn(IV) with 0.2M glyoxal acquired over a broad wavelength range (300–700 nm). Reaction conditions: Temperature 25 °C, 2M H₂SO₄

Figure 4.18 shows two clearly distinct phases in the reaction between 0.02M permanganate with 0.2M glyoxal in sulphuric acid medium. Within the first phase, the absorption intensity in the region 300 and 400 nm, characteristic spectra for Mn(IV)(Figure 3.3), decreased gradually as the reaction proceeded, at the same time the absorbance at the characteristic peak of Mn(III) (500 nm) also increased with time, which closely resembles the Mn(III) spectrum obtained above (Figure 3.2).

This is indicating that Mn(IV) and glyoxal attended the reaction that lead to the generation of Mn(III) intermediate. The first and slower phase of Mn(III) formation was followed by the disappearance of the Mn(III)-typical peak at 500 nm. Mn(III) was formed as long as the spectral features of Mn(III) persisted (see black spectrum).

The fact that manganese(III) did not accumulate and was readily transformed to manganese (II) suggested that it was rapidly reduced either by glyoxal or a reaction product of the system manganese(IV)/glyoxal.

It is generally believed that Mn(III), as the common intermediate species, reacts with the organic substrate in a final elementary reaction to form excited manganese(II) species (Mn(II)*) that emits light.

In order to convince ourselves that the reaction between Mn(III) and glyoxal does not involve any observable intermediate species, the Mn(III) spectral changes for the reaction between excess of glyoxal and Mn(III) were recorded.

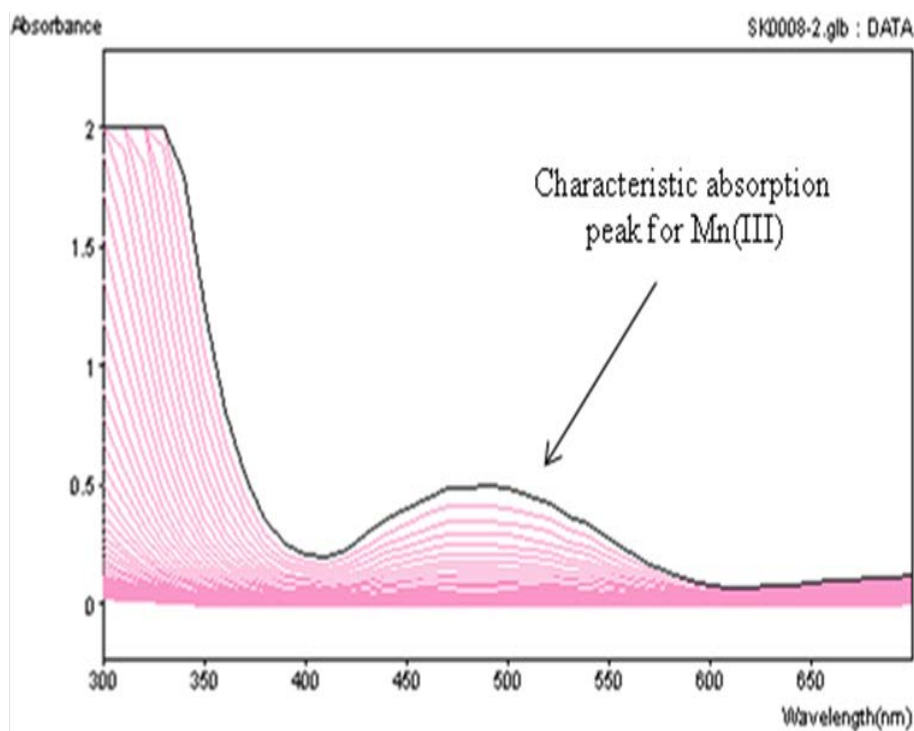


Figure 4.19 (2D)-Spectral changes observed upon the reaction of 0.02M Mn(III) with 0.2M glyoxal acquired over a broad wavelength range (300–700 nm). Reaction conditions: Temperature 25 °C, 2M H₂SO₄

Figure 4.19 demonstrates, as expected, that Mn(III) effectively oxidizes glyoxal and depicts the spectral changes of the reaction of 0.02M Mn(III) with 0.2M glyoxal in sulphuric acid.

Spectroscopically Mn(III) is recognized by a characteristic peaks at 500 nm. The absorption intensity in the wavelength region 480 to 600 nm (characteristic peaks for permanganate) decreased gradually as the reaction proceeded, indicating that permanganate and glyoxal attended the reaction and no evidence of intermediate species was detected.

Returning to the hypothesis at the beginning of this study and taken together, these results confirm our working hypothesis suggested earlier in this section about the light-producing pathway that, it is a Mn(III) intermediate generated during the permanganate and manganese(IV) reactions that react with glyoxal to produce the CL emission.

4.2.4 Dichromate (Cr₂O₇²⁻) oxidation of glyoxal

It is beyond the scope of this study to examine the effect of replacing permanganate with dichromate. However, the acidic dichromate oxidation of glyoxal was considered to look at what might happen to glyoxal CL emission when MnO₄⁻ is replaced with Cr₂O₇²⁻.

The kinetics of oxidation of glyoxal with and without Mn(II) by dichromate was monitored at the dichromate maximum wavelength of 320 nm. The results are summarized in Figure 4.20.

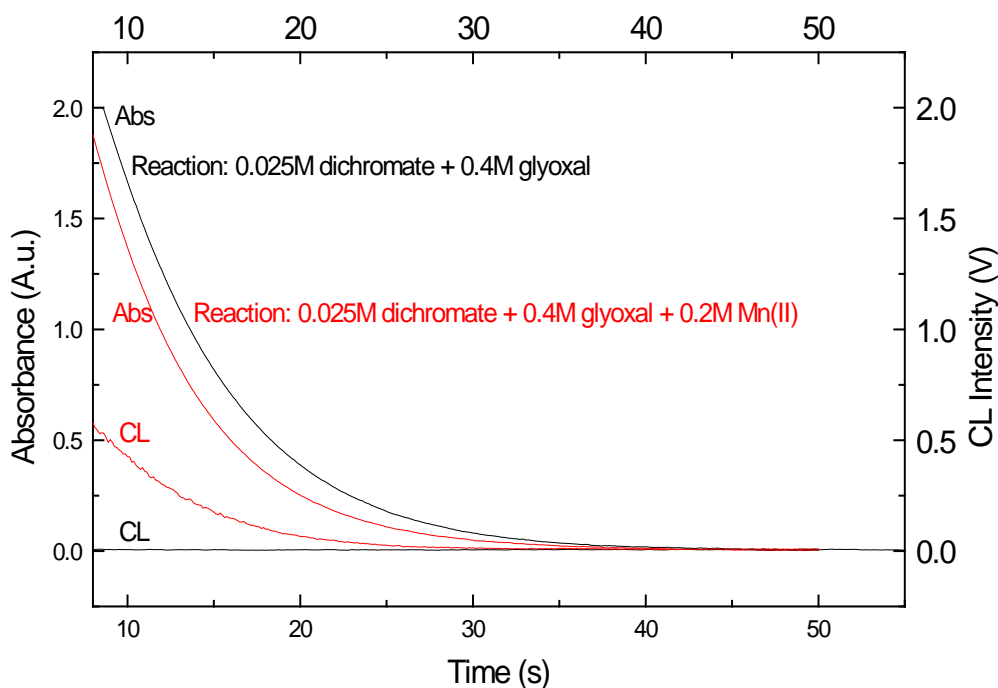


Figure 4.20 Plot comparing CL time course versus absorbance time course for $\text{Cr}_2\text{O}_7^{2-}$ oxidation reaction of glyoxal. Experimental conditions: $[\text{OCHCHO}] = 0.4\text{M}$, $[\text{Cr}_2\text{O}_7^{2-}] = 0.025\text{M}$, $[\text{Mn(II)}] = 0.2\text{M}$, Temperature = 25°C , $[\text{H}_2\text{SO}_4] = 2\text{M}$, Wavelength = 320 nm ; HT (Fluorescence channel): 800V .

The absorbance spectra of the glyoxal/ $\text{Cr}_2\text{O}_7^{2-}$ system showed a rapid consumption of dichromate within 20 first seconds of the reaction, however, no evidence of a measurable CL emission was detected.

Interestingly, the addition of 0.1M Mn(II) into the reaction mixture produced significant chemiluminescence emission intensity. A likely explanation for this is that dichromate reacts with Mn(II) ions to generate Mn(III) which immediately oxidizes glyoxal to produce chemiluminescence emission. The CL emission that has been detected therefore assists in our understanding of the role played by Mn(II) in CL reaction between MnO_4^- and glyoxal.

4.3 Glyoxylic acid (HCOCO_2H) chemiluminescence oxidation reactions

4.3.1 Permanganate oxidation of glyoxylic acid

It was suggested that acidic permanganate oxidation of glyoxal can presumably lead to unstable cyclic ester from which several transient intermediates can be formed (including formic, glyoxylic and oxalic acids) through several oxidative or hydrolysis pathways until carbon dioxide are formed as the final product.

Thus, it was assumed that these organic intermediates are capable of reacting with Mn-based oxidants as well and generating the observed light during the glyoxal CL oxidation.

So far, however, no research has been found that surveyed the chemiluminescence reaction of glyoxylic acid in the presence manganese-based oxidants. Therefore, it was decided to look at and to evaluate the characteristics of the CL process associated with glyoxylic acid oxidation by permanganate, Mn(III) and Mn(IV).

Preliminary experiments indicated that the oxidation reaction and chemiluminescence response are of such rates that it can conveniently be measured using an SX.20 stopped-flow reaction analyzer instrument with both absorbance and fluorescence detection.

4.3.1.1 Effect of glyoxylic acid concentration

Kinetic experiments of oxidation of glyoxylic acid with permanganate were conducted at a constant temperature of 25 °C under dark conditions and in 2.0 mol dm⁻³ sulphuric acid medium. The kinetic measurements were conducted under pseudo- first-order conditions, where glyoxylic acid was present in a large excess over that of oxidant concentration.

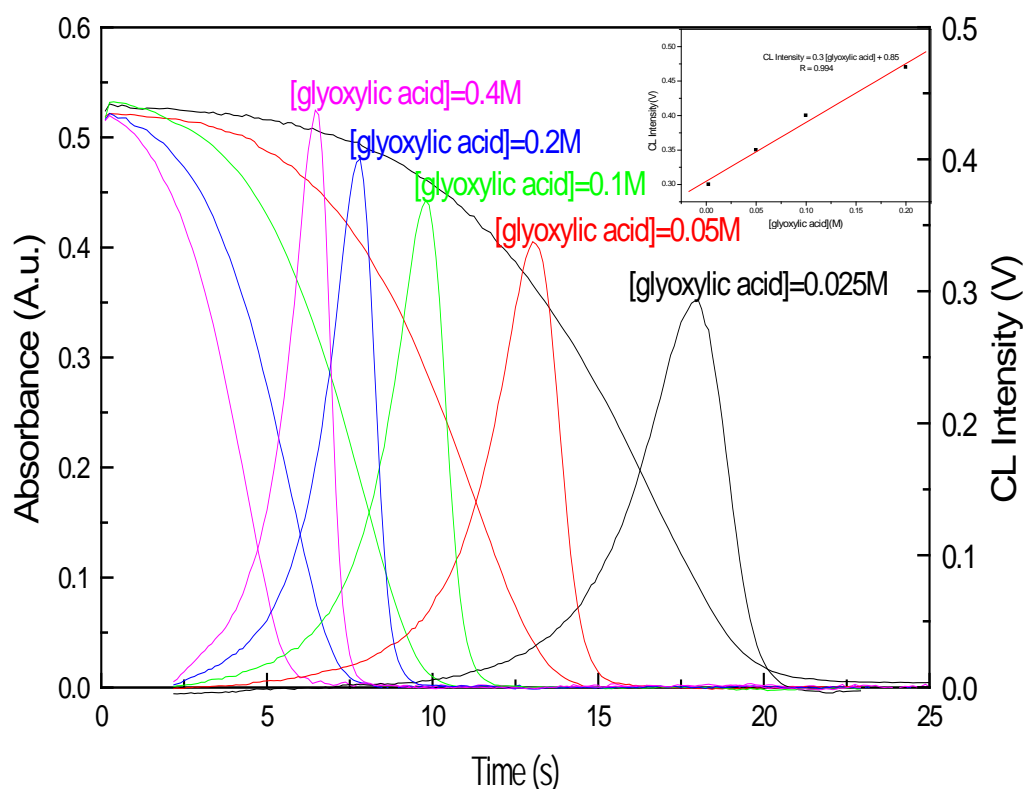


Figure 4.21 Chemiluminescence time course versus absorbance time course for KMnO_4 oxidation of four initial $[\text{HCOCO}_2\text{H}]$. Experimental conditions: $[\text{MnO}_4^-] = 0.0025\text{M}$, $[\text{HCOCO}_2\text{H}] = 0.025, 0.05, 0.10, 0.20$ and 0.40M , Temperature = 25°C, $[\text{H}_2\text{SO}_4]=2\text{M}$; Wavelength = 525 nm and HT (Fluorescence channel): 600V.

Results from experiments designed to assess the rate of reaction and chemiluminescence intensity of glyoxylic acid-permanganate system are summarized in Figure 4.21.

It shows the glyoxylic acid oxidation curves and CL responses, when the initial permanganate concentration was held constant at 0.0025M and the initial glyoxylic acid concentrations were varied between 0.025 and 0.40M.

As expected, stopped-flow experimental results show that glyoxylic acid is rapidly oxidized by MnO_4^- . For example, ~90% of glyoxylic acid is oxidized by 0.0025M Mn(VII) in < 20 seconds. A comparison of the kinetic curves of the CL and the rate of disappearance of MnO_4^- shows that in these curves there is a match in time profile and there is a direct relationship between the maximum intensity of the CL and the rate of oxidation.

It is evident from Figure 4.21 that the effect of varying the glyoxylic acid concentration increased both the reaction rate and CL signal with the increase of [glyoxylic acid].

A plot of the CL intensity versus glyoxylic acid concentration produced a straight line having a correlation coefficient of $R = 0.994$ (inset of Figure 4.21).

The results of this research support the idea that the intensity of the CL emission from organic substrates such as glyoxalyc acid depends on the concentration of the analyte. An implication of this is the possibility that a relationship between chemiluminescence response and analyte concentration can be exploited to develop a CL analytical technique for the determination of glyoxylic acid in different matrices.

4.3.1.2 Effect of permanganate concentration

As with glyoxylic acid, it was hypothesized that as the concentration of MnO_4^- increases, the rate of the reaction and the intensity of the CL emission from that reaction increases.

To test the hypothesis, the MnO_4^- oxidation of glyoxylic acid was carried out in 2.0 moldm⁻³ sulphuric acid medium and at a constant temperature of 25 °C under dark conditions.

Figure 4.22 shows the kinetics of permanganate decay and of the intensity of the CL emission at five different initial MnO_4^- concentrations (0.000625, 0.00125; 0.0025; 0.005 and 0.01M) with a constant initial glyoxylic acid concentration of 0.02M.

Again the results clearly indicated that change in permanganate concentration has little effect on the time of the CL emission but does increase the chemiluminescence intensity.

Thus, the CL response increased as permanganate concentration increased and the maximum intensity of the CL is proportional to the concentration of permanganate.

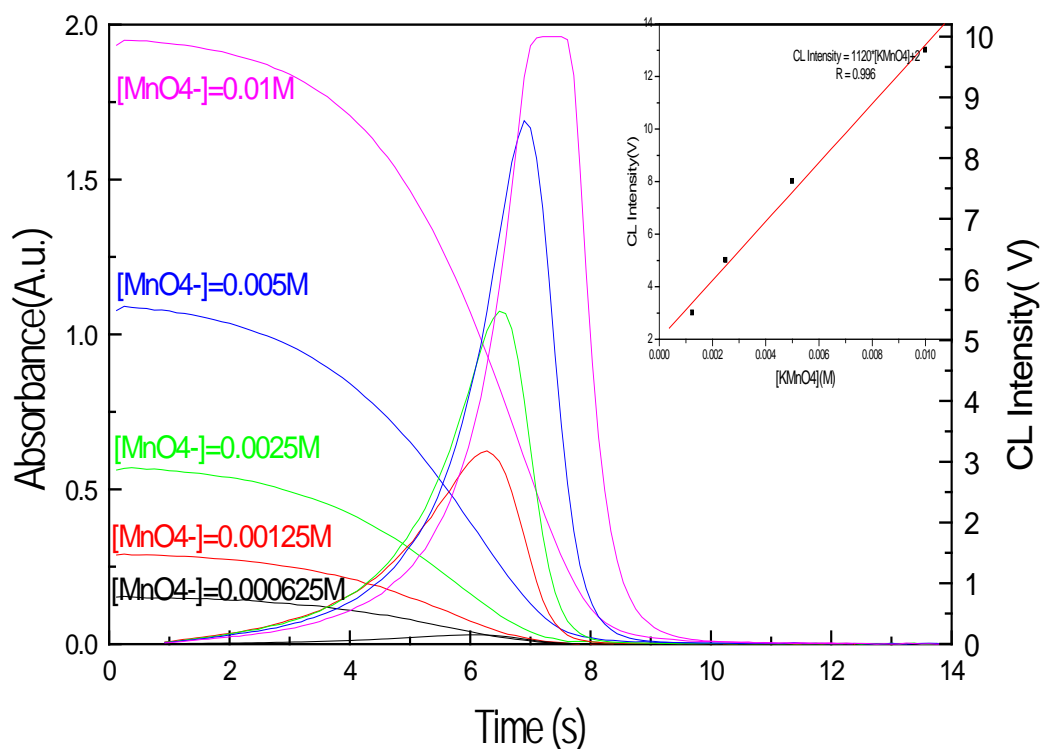


Figure 4.22 Effect of MnO_4^- concentrations on the CL signal vs. time profile. Experimental conditions: $[\text{MnO}_4^-] = 0.00125; 0.0025; 0.005$ and 0.01M , $[\text{HCOCO}_2\text{H}] = 0.02\text{M}$, Temperature = 25°C , $[\text{H}_2\text{SO}_4] = 2\text{M}$; Wavelength = 525 nm and HT (Fluorescence channel): 800V .

Nevertheless, it has conclusively been shown that the permanganate concentration increase the maximum intensity of the chemiluminescence. An implication of these findings for future practice is that both substrate concentration and manganese-based oxidant concentration should be taken into account when assessing the CL response from a chemical reaction.

4.3.2 Manganese(III) oxidation of glyoxylic acid

It has been demonstrated above that manganese(III) is definitely a redox intermediate and glyoxylic acid is a presumed intermediate in the course of the reaction between glyoxal and permanganate. And they have been identified as major contributing factors for the chemiluminescence reaction between permanganate and glyoxal.

To establish whether manganese(III) and glyoxylic acid interact during the reaction to produce light emission, the kinetics of chemiluminescence reaction between manganese(III) and glyoxylic acid was examined.

4.3.2.1 Effect of Mn(III) concentration

In Figure 4.23 the initial glyoxylic acid concentration was held constant at 0.2M and the initial manganese(III) concentrations were varied between 0.00625 and 0.05M .

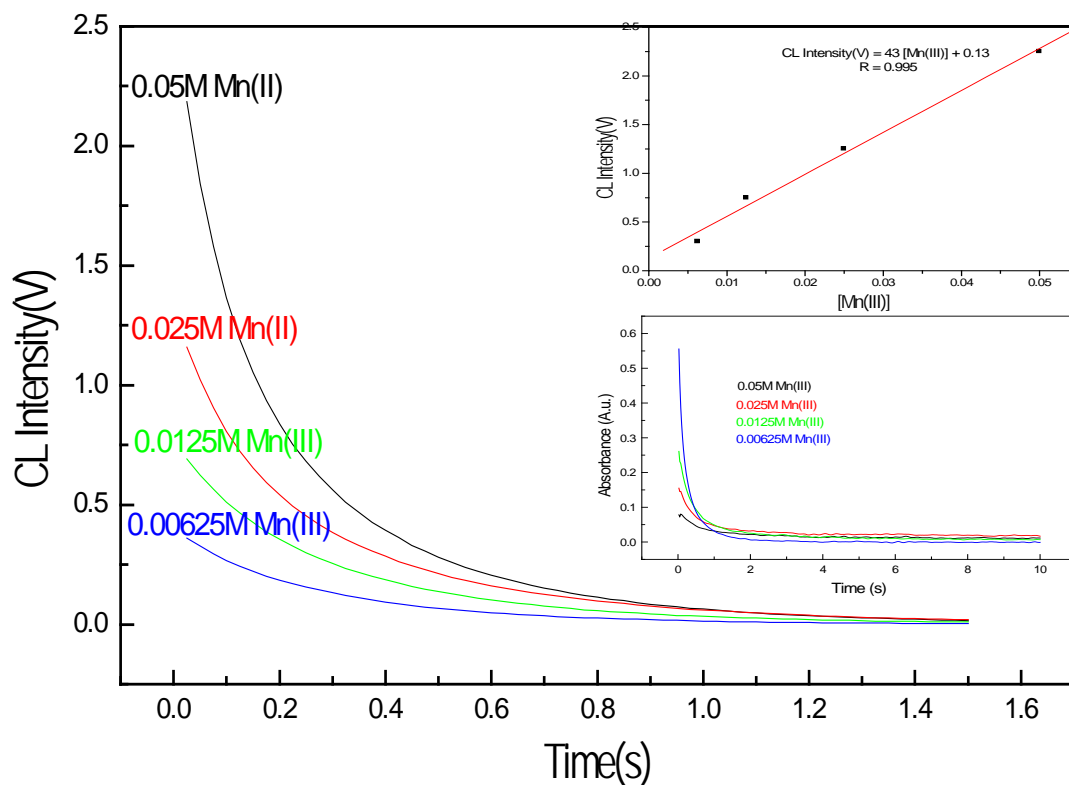


Figure 4.23 Effect of Mn(III) concentrations on the CL response versus time profile. Experimental conditions: $[Mn(III)] = 0.00625; 0.0125; 0.025$ and $0.05M$, $[HCO_2H] = 0.2M$, Temperature = $25^\circ C$, $[H_2SO_4] = 2M$ and HT (Fluorescence channel): $400V$.

As it can be seen from Figure 4.23, the oxidation of glyoxylic acid by manganese(III) was very fast that the maximum of chemiluminescence spectra is within deadtime.

The fact that manganese(III) reacted with glyoxylic acid and elicited intense chemiluminescence emission suggested that manganese(III) and glyoxylic acid are major contributing factors for the chemiluminescence reaction between permanganate and glyoxal.

It was not possible to investigate the dependence of the rate of reaction further because the absorbance of manganese(III) at such low concentrations was too small to be measured accurately. Nevertheless, based on the existing relationship between the kinetics of the chemiluminescence emission and the rate of the reaction, it has been assumed that kinetics of the reaction increased with the increase in manganese(III) concentration.

This study confirms that the intensity of the chemiluminescence response is associated with the manganese(III) concentration, as it can be seen from the figure 4.23 that the chemiluminescence intensity increased with increasing manganese(III) concentration and the plot of chemiluminescence intensity as a function of the initial manganese(III) concentration (inset of Figure 4.23) was linear with a correlation coefficient $R=0.995$.

4.3.2.2 Effect of glyoxylic acid concentration

After oxidant concentration, it was necessary to examine the impact of glyoxylic acid concentration on the kinetics and the intensity of the chemiluminescence emission in the reaction between glyoxylic acid and manganese(III). Thus, the effect of increasing the glyoxylic acid concentration from 0.025 to 0.4M on the chemiluminescence intensity was assessed.

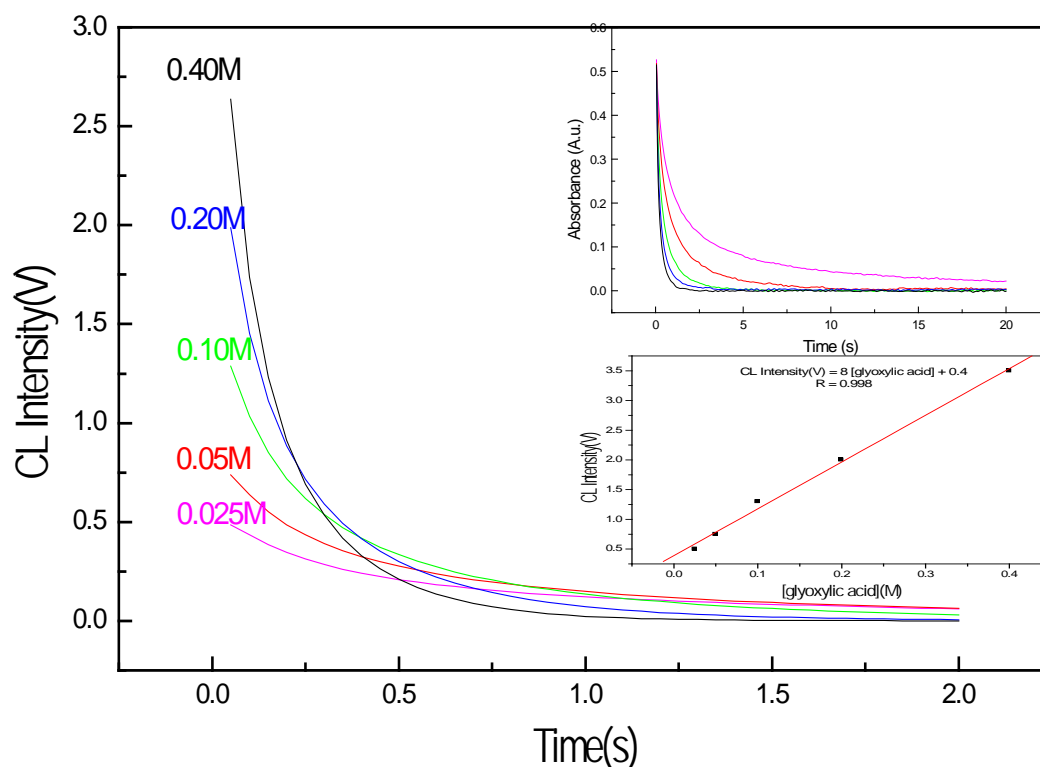


Figure 4.24 Effect of glyoxylic acid concentration on the CL response versus time profile. Experimental conditions: $[\text{HCO}_2\text{H}] = 0.025; 0.05; 0.1; 0.2$ and 0.4M , $[\text{Mn(III)}] = 0.05\text{M}$, Temperature = 25°C , $[\text{H}_2\text{SO}_4] = 2\text{M}$ and HT (Fluorescence channel): 400V .

As it can be seen in Figure 4.24, as the glyoxylic acid concentration increased, the CL signal intensity increased. The plot of CL intensity as a function of the initial glyoxylic acid concentration (inset of Figure 4.24) was linear with a correlation coefficient $R=0.998$.

These findings support our earlier observations, which links the intensity of the CL response and the concentration of the substances participating in the reaction.

4.3.3 Manganese(IV) oxidation of glyoxylic acid

Manganese(IV) has been identified as an intermediate in the experiments above and glyoxylic acid is presumably likely to be formed, as an intermediate in the course of the reaction between glyoxal and permanganate. Manganese(IV) has been suggested as additional major contributing factors for the CL reaction between permanganate and glyoxal.

4.3.3.1 Effect of Mn(IV) concentration

To evaluate the dependence of the intensity of the CL emission on the concentration of Mn(IV), as oxidizing agent, the CL reaction between Mn(IV) and glyoxylic acid was investigated at room temperature and in 2.0 mol L^{-1} sulphuric acid medium.

Thus, the effect of Mn(IV) concentration upon the CL behaviour of glyoxylic acid was examined over the range $0.00125 - 0.02\text{M}$ in acidic solution. The results are shown in Figure 4.25.

The results of this investigation showed that Mn(IV) reacted with glyoxylic acid and produced intense CL emission. The fact that Mn(IV) reacted with glyoxylic acid and elicited intense chemiluminescence emission suggested that Mn(IV) and glyoxylic acid may also be contributing factors for the CL reaction between permanganate and glyoxylic acid.

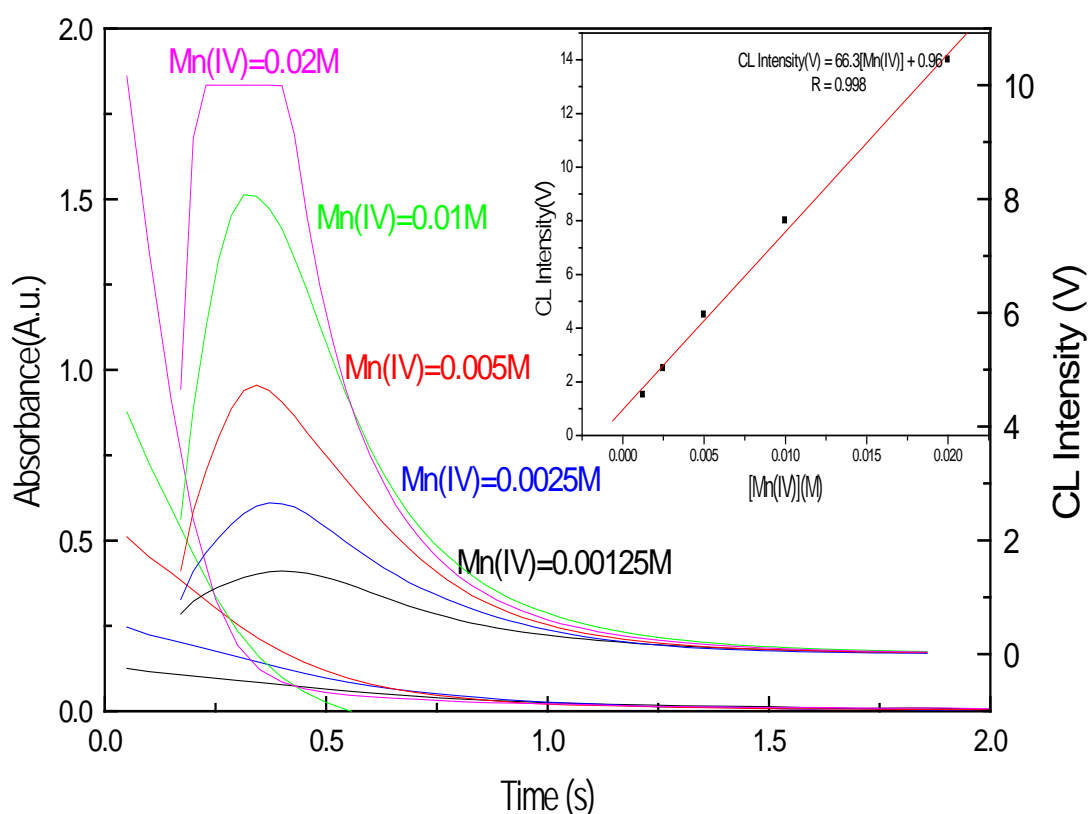


Figure 4.25 Effect of Mn(IV) concentration on the CL response versus time profile. Experimental conditions: $[\text{Mn(IV)}] = 0.00125; 0.0025; 0.005; 0.01$ and 0.02M , $[\text{HCOCO}_2\text{H}] = 0.2\text{M}$, Temperature = 25°C , $[\text{H}_2\text{SO}_4] = 2\text{M}$ and HT (Fluorescence channel): 600V .

It can be seen from Figure 4.25 that as the Mn(IV) concentration increased, the maximum signal intensity increased, and the time to reach the maximum signal decreased. The plot of chemiluminescence intensity as a function of the initial Mn(IV) concentration (inset of Figure 4.25) was linear with a correlation coefficient $R=0.998$.

Once again, the results of this investigation show that the intensity of the chemiluminescence response is directly proportional to the manganese(IV) concentration for conditions of $[\text{HCOCO}_2\text{H}] \gg [\text{MnO}_2]$.

Most importantly is that the relationship between the maximum intensity of the chemiluminescence response and the concentration of Mn(IV) has been established.

4.3.3.2 Effect of glyoxylic acid concentration

The effect of increasing the glyoxylic acid concentration from 0.025 to 0.4M on the CL intensity was investigated.

As it can be seen in Figure 4.26, under reaction conditions of $[\text{glyoxylic acid}] \gg [\text{MnO}_4^-]$, as the glyoxylic acid concentration increased, the maximum signal intensity increased, and the time to reach the maximum signal decreased as well as the rate of reaction. The plot of CL intensity as a function of the initial glyoxylic acid concentration (inset of Figure 4.26) was linear with a correlation coefficient $R=0.995$.

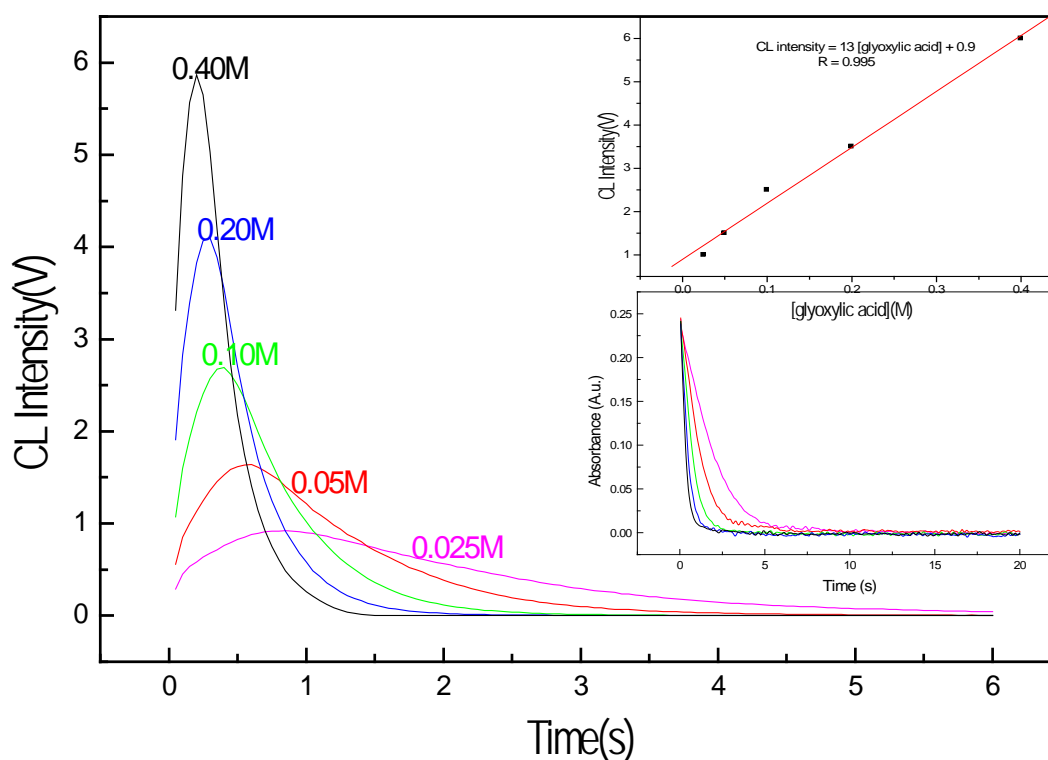


Figure 4.26 Effect of glyoxylic acid concentration on the CL response versus time profile. Experimental conditions: $[\text{HCOCO}_2\text{H}] = 0.025; 0.05; 0.1; 0.2$ and 0.4M , $[\text{Mn(IV)}] = 0.0025\text{M}$, Temperature = 25°C , $[\text{H}_2\text{SO}_4] = 2\text{M}$ and HT (Fluorescence channel): 600V .

Overall, it has been demonstrated that the intensity and the kinetics of the chemiluminescence emission are fundamentally dependent of the kinetics of a chemical reaction – in particular, of the concentration of the substances participating in the reaction.

Thus, these results confirm our working hypothesis for the light-producing mechanism that the observed chemiluminescence emission is associated with the oxidation reaction of Mn(III) intermediate and organic substrate or some organic intermediates. This finding has important implications for developing new chemiluminescence analytical techniques.

4.4 Oxalic acid($\text{H}_2\text{C}_2\text{O}_4$) chemiluminescence oxidation reactions

As already pointed out oxalic acid is presumably a common intermediate in the chemiluminescence reaction of glyoxal and permanganate. As such, it was assumed that oxalic acid was capable of reacting with manganese-based oxidants and generating the observed light during the glyoxal CL oxidation. Therefore, it was reasonable to consider the oxidation reactions between all manganese-based oxidizing agents and oxalic acid, in order to determine whether it contributes to the resultant CL emission from permanganate and glyoxal.

4.4.1 Permanganate oxidation of oxalic acid

With the objective of understanding better the oxalate/permanganate chemiluminescence reaction mechanism, a set of kinetics experiments of this system were performed in sulphuric acid solution at a constant temperature of 25 °C.

He et al⁴⁰³ examined the reaction of acidic potassium permanganate with oxalic acid and reported the determination of oxalate in urine, using FIA methodology. The method was based on the effect of formaldehyde, as enhancer, on the rate of the CL reaction of permanganate with oxalic acid, where the 'peak appearance time' was directly related to the concentration of oxalate and the limit of detection was reported to be 5×10^{-2} M.

This contribution describes for the oxidation of oxalic acid by permanganate with a focus on characterizing the kinetic curves of the CL and kinetic curves for oxalate-Mn(VII) reactions.

Figure 4.27 shows the kinetic curves of the CL emission and the kinetics of the reaction in which the initial $[\text{MnO}_4^-]$ was held constant at 0.0025M and the initial [oxalic acid] were varied between 0.1 and 0.8M.

The results of this study indicate that oxalic acid and MnO_4^- reacted and produced a very weak intensity of the CL emission. The experimental evidence from the absorbance time course indicated half-time of reaction of about 75 seconds.

It can be seen that glyoxal reaction with permanganate is faster than oxalic acid reaction, therefore, returning to the hypothesis at the beginning of this study, it is now possible to state that oxalic acid has not emerged as a major contributing factor for the glyoxal CL emission. But, the possible small involvement of oxalic acid cannot be ruled out.

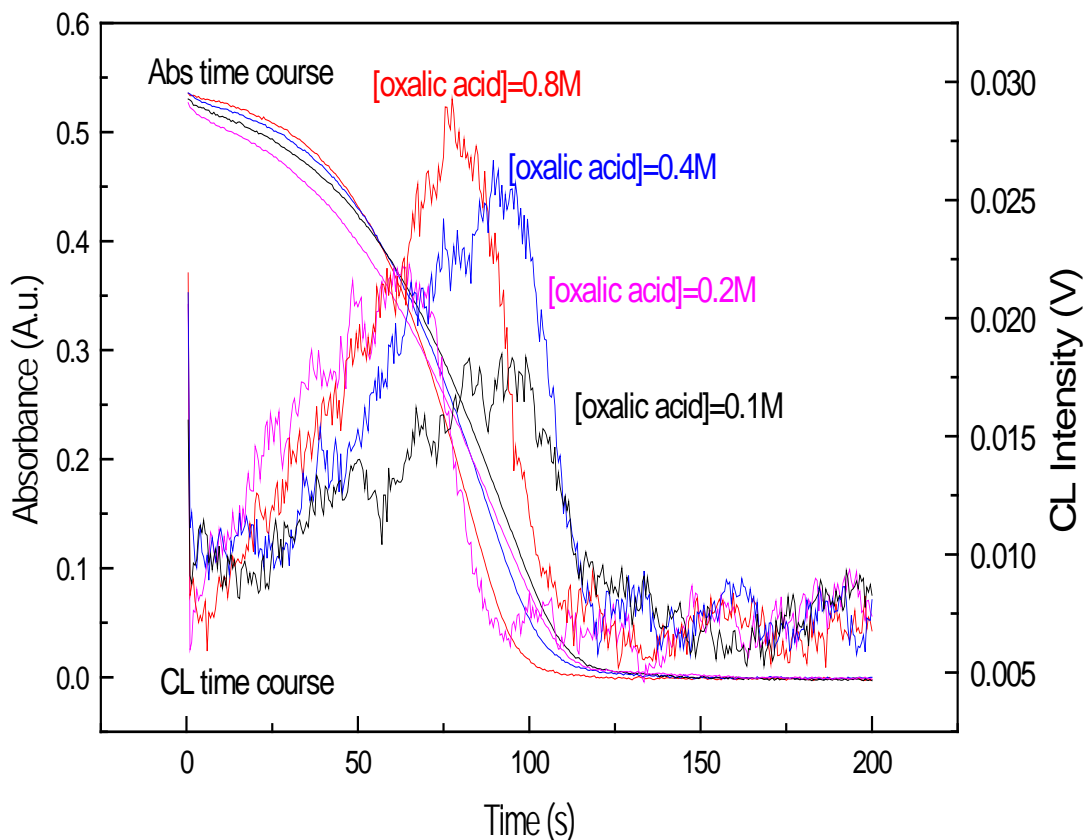


Figure 4.27 Plot comparing chemiluminescence time course versus absorbance time course for MnO_4^- oxidation reaction of oxalic acid. Experimental conditions: $[\text{H}_2\text{C}_2\text{O}_4] = 0.1, 0.2, 0.4$ and 0.8M , $[\text{MnO}_4^-] = 0.0025\text{M}$, Temperature = 25°C , $[\text{H}_2\text{SO}_4] = 2\text{M}$, Wavelength = 525 nm ; HT (Fluorescence channel): 800V .

Contrary to expectations, this study also did not find a significant increase in the intensity of the CL emission, or the rate of reaction as oxalic acid concentration increased. The reason for the weak CL is not clear but it may have something to do with the way for electronically excited state loses its energy as heat rather than as photon of light.

4.4.2 Manganese(III) oxidation of oxalic acid

It was suggested in the previous section that, although the CL reaction between oxalic acid and permanganate occurs on a longer time scale than the glyoxal reaction, the possible involvement of oxalic acid during CL reaction between glyoxal and permanganate cannot be ruled out. The reason for that is that Mn(III) , as oxidizing agent, may react more rapidly with oxalic acid rather than with glyoxal.

Interestingly, the results in Figure 4.28 indicated that Mn(III) reacted rapidly with oxalic within glyoxal and produced a significant chemiluminescence emission. It is possible to hypothesise that this reaction is more likely to occur in the course of the chemiluminescence reaction of glyoxal and permanganate.

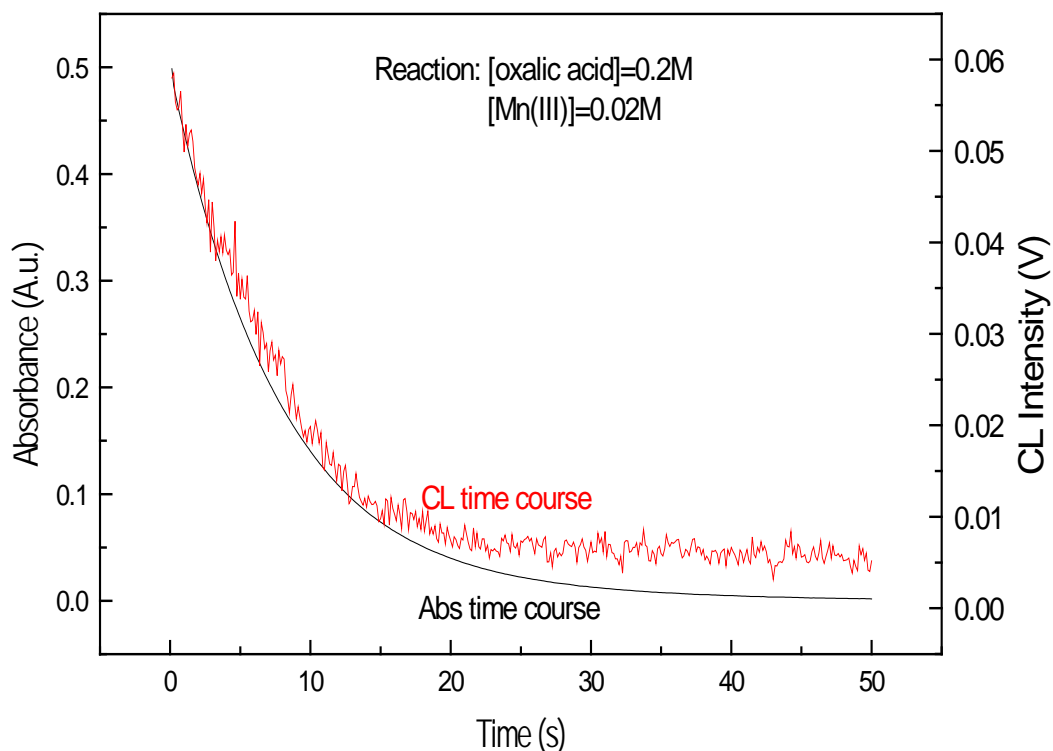


Figure 4.28 Plot comparing CL time course versus absorbance time course for Mn^{3+} oxidation reaction of oxalic acid. Experimental conditions: $[\text{H}_2\text{C}_2\text{O}_4] = 0.2\text{M}$, $[\text{Mn}^{3+}] = 0.02\text{M}$, Temperature = 25°C , $[\text{H}_2\text{SO}_4] = 2\text{M}$, Wavelength = 500 nm; HT (Fluorescence channel): 800V.

Contrary to permanganate, the manganese(III) oxidation of oxalate in sulphuric acid medium was accompanied by the development of an intense CL emission, which can be straightforwardly exploited in analytical measurements.

A comparison of the two results - the kinetic curve of the CL and the UV absorbance of manganese(III) disappearance simply indicates that the development of the CL emission is directly related to the oxidation reaction, which suggests a direct connection between CL and consumption of Mn(III) . This explains why formaldehyde acts as an enhancer.

4.4.3 Manganese(IV) oxidation of oxalic acid

Like Mn(III) , the possibility of Mn(IV) reacting with oxalic acid and producing light during the chemiluminescence reaction of glyoxal and permanganate is very high. It was therefore necessary to look at the reaction between Mn(IV) and oxalic acid.

The findings in Figure 4.29 indicated that the chemiluminescence intensity reached a maximum at 2.5 s after the reaction was initiated and returned to baseline within 10 s. Given this time scale was the same as glyoxal time reaction; it is possible that oxalic acid and Mn(IV) contributed for the glyoxal-permanganate chemiluminescence emission.

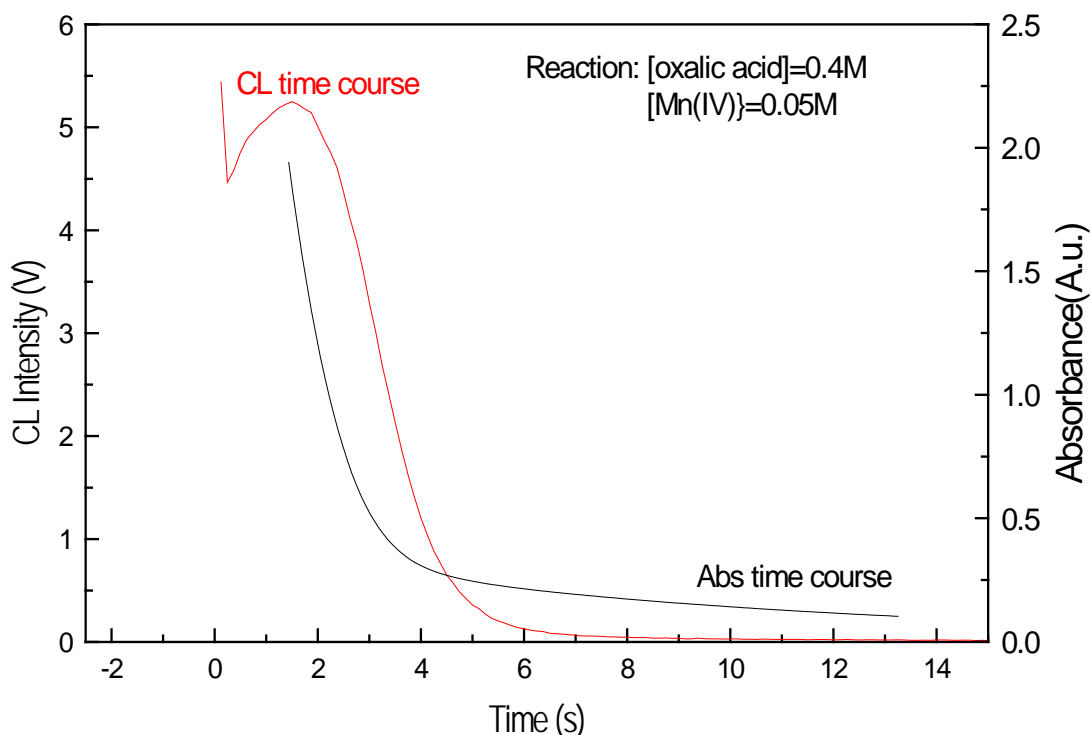


Figure 4.29 Plot comparing CL time course versus absorbance time course for Mn(IV) oxidation reaction of oxalic acid. Experimental conditions: $[\text{H}_2\text{C}_2\text{O}_4] = 0.4\text{M}$, $[\text{Mn(IV)}] = 0.05\text{M}$, Temperature = 25°C , $[\text{H}_2\text{SO}_4] = 2\text{M}$, WL = 400 nm; HT (Fluorescence channel): 800V.

These stopped-flow experimental results also revealed that the oxidation of oxalate by manganese(IV) in sulphuric acid produced greater chemiluminescence signal when compared to the chemiluminescence emissions from oxalate-Mn(III) and oxalate-Mn(VII) systems.

Comparing the two results, CL time curve and absorbance time curve, there appears to be a direct connection between the CL emission and the Mn(IV) consumption.

Returning to the observed CL response from glyoxal/permanganate system, it has been demonstrated that many of the dark reactions that occur during its reaction may affect the overall CL emission.

These effects include the increase in the rate of the reaction and, most importantly, the amplification of the chemiluminescence emission as a result of chemical reaction between one or more enhancers and intermediate products produced in course of the reaction, such as, Mn(III), Mn(IV), glyoxylic acid and oxalic acid.

During the chemiluminescence reaction of glyoxal/permanganate system, the three major oxidants MnO_4^- , Mn(IV) and Mn(III) govern the chemical processes. While MnO_4^- slowly initiates the reaction, a net four (or three)-electron-transfer process occurs initially, followed by reactions between either Mn(IV) or Mn(III) and glyoxal or the organic intermediates, which are manifested by the emission of the chemiluminescence response.

These results are also consistent with our working hypothesis for the light-producing mechanism, as they demonstrated that the observed chemiluminescence emission is enhanced by the addition of reductants such as Mn(II) or formaldehyde, which convert MnO_4^- into Mn(III), thereby suggesting that the Mn(III) is involved in the production of the chemiluminescence emission from the glyoxal or other reactive intermediate products.

4.5 Malic acid chemiluminescence oxidation reactions

In order to test our working hypothesis for the light-producing pathway in permanganate oxidation CL, more complex compounds were considered. In this section the CL reactions between malic acid and manganese-based oxidants, as well as, the effect of initial additions of substances such as glyoxal, pyrogallol, etc. were examined.

4.5.1 Permanganate oxidation of malic acid ($\text{HO}_2\text{CCH}_2\text{CHOHCO}_2\text{H}$)

It has been found that the permanganate oxidation of malic acid elicits fairly intense luminescence. Using an FIA system with the permanganate chemiluminescence method, the determination of malic acid in apple juice and cider was reported by Luo et al⁸⁷ and good agreement was observed with a titration method. However, little is known about malic acid chemiluminescence reaction with different manganese-based oxidants and it is not clear what factors influence the chemiluminescence signal intensity.

This work focuses on characterizing the kinetic curves of the chemiluminescence emission and light-producing pathway.

4.5.1.1 Effect of malic acid concentration

If CL signal intensity is dependent on malic acid concentration, there should be observed an increase in the intensity and the rate of the CL emission during the permanganate oxidation of malic acid.

The effect of malic acid concentration on the CL intensity was investigated. The results are presented in Figure 4.30.

As expected, it can be seen from the Figure 4.30 that the permanganate oxidation of malic acid in acidic solution produces light and the intensity of the luminescence is proportional to the initial concentration of malic acid. At higher concentrations of malic acid e.g. over 0.5M, it is difficult to observe the beginning of the kinetic curve of the chemiluminescence because the reaction rate increases with the increase in malic acid concentration.

These results support the conclusion that the observed chemiluminescence is correlated to the kinetics of reaction and Mn(III) intermediate is involved in light-producing reaction.

However, it is apparent from the inset of Figure 4.30 that absorbance profiles do not display any induction period. This result may be explained by the fact that malic acid oxidation reaction by permanganate is very fast and removes the induction period.

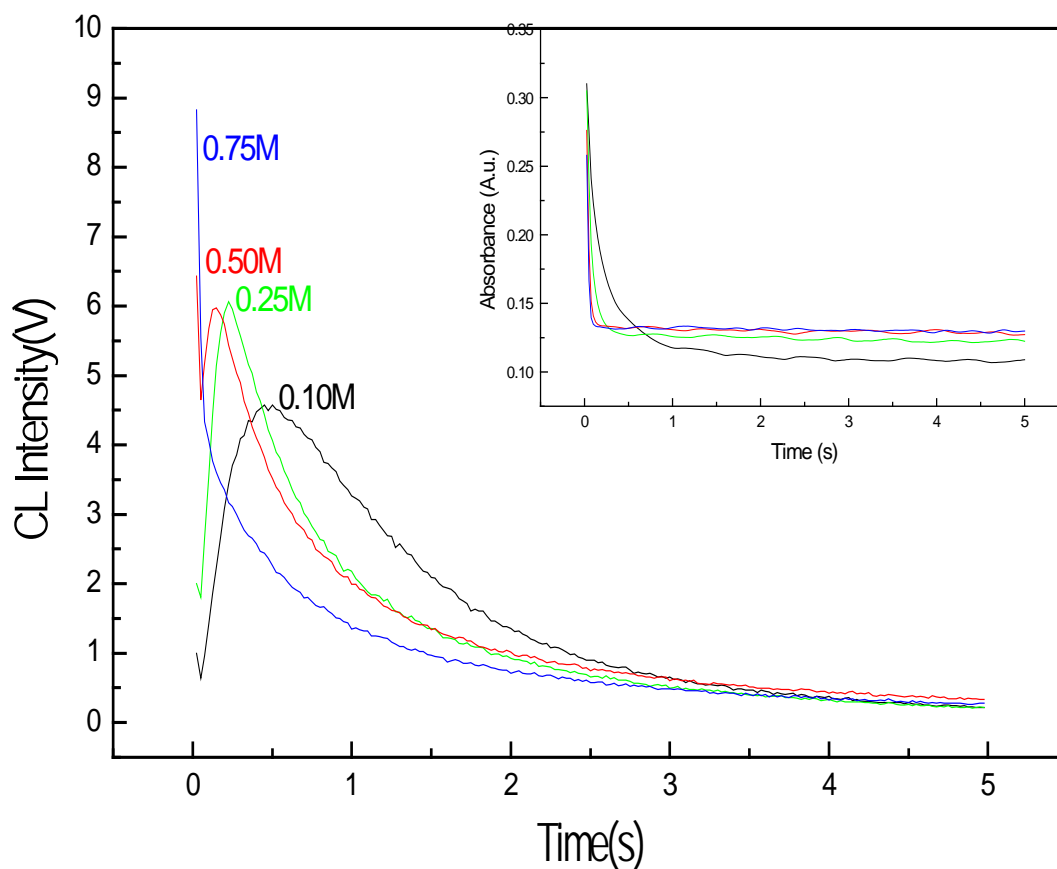


Figure 4.30 Effect of malic acid concentration on the CL response versus time profile. Experimental conditions: $[\text{HO}_2\text{CCH}_2\text{CHOHCO}_2\text{H}] = 0.1; 0.25; 0.5$ and 0.75M , $[\text{MnO}_4^-] = 0.001\text{M}$, Temperature = 25°C , $[\text{H}_2\text{SO}_4] = 2\text{M}$ and HT (Fluorescence channel): 800V .

4.5.1.2 Influence of formaldehyde on malic acid chemiluminescence

It has been demonstrated above that formaldehyde reacts with MnO_4^- to produce Mn(III) intermediate and it is the latter that oxidizes quickly the analyte or its organic intermediates in a final elementary reaction to form an excited manganese(II) species (Mn(II)^*) that emits light and enhances the resulting chemiluminescence signal intensity.

If CL signal intensity is dependent on formaldehyde concentration and formaldehyde enhances the CL emission that accompanies the MnO_4^- oxidation of malic acid, it should be observed an increase in the intensity and the kinetics of the CL emission during the reaction.

Figure 4.31 shows the kinetic curves of the CL emission for several experiments of a series in which the initial concentration of MnO_4^- and malic acid were held constant, namely 0.001M and 0.05M , respectively and the initial [formaldehyde] was varied from 0.1 to 1.0M .

Very low concentration was used for malic acid to slow down the oxidation reaction and ensure a generation of fairly intensity CL emission that allows the investigation of the dependence of the intensity of the CL on various parameters, such as formaldehyde and manganese(II).

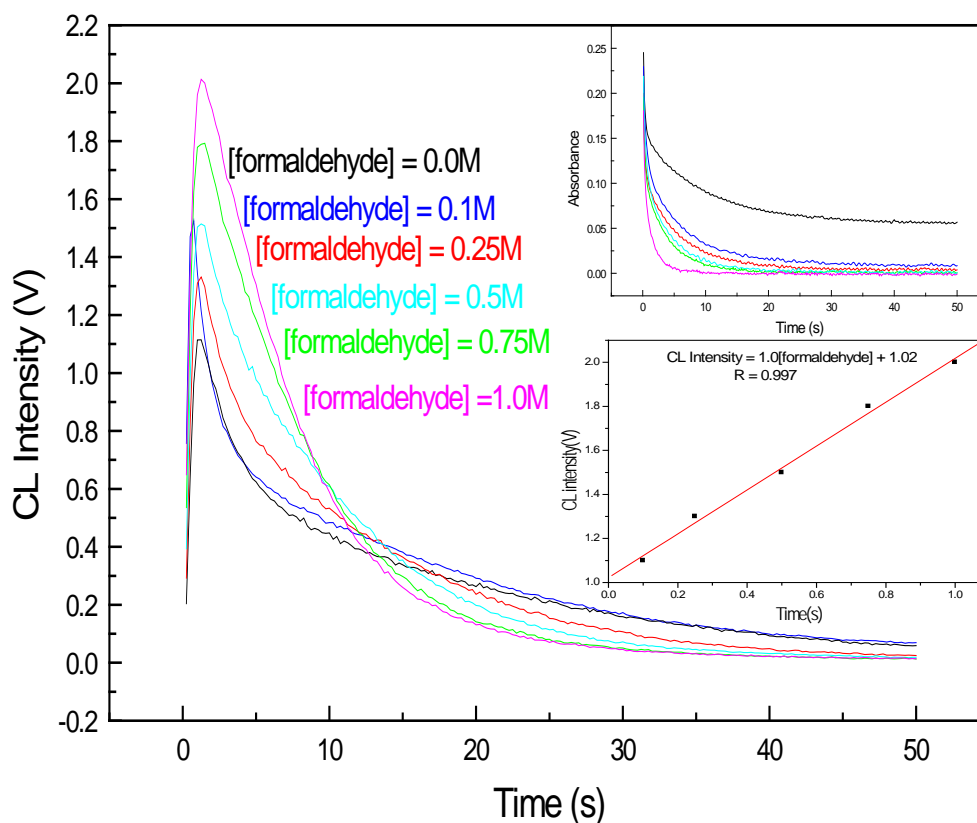


Figure 4.31 Influence of added formaldehyde on the kinetics of the chemiluminescence response versus time profile. Experimental conditions: $[HCHO] = 0.1; 0.25; 0.5; 0.75$ and $1.0M$, $[HO_2CCH_2CHOHCO_2H] = 0.05M$; $[MnO_4^-] = 0.001M$, Temperature = $25^\circ C$, $[H_2SO_4] = 2M$ and HT (Fluorescence channel): $800V$.

As it can be seen in Figure 4.31, the addition of some limiting concentrations of formaldehyde to the reaction mixture leads to an increase in the chemiluminescence signal intensity and a larger amount of formaldehyde corresponds to a higher rate of the reaction.

The results of this investigation show a good correlation between the CL maximum signal intensity and the initial concentrations of formaldehyde.

The plot of the intensity as a function of the initial formaldehyde concentration (inset of Figure 4.31) was linear with a correlation coefficient $R=0.997$.

These results are consistent with the postulate that formaldehyde oxidation speeds up the accumulation of Mn(III) that then undergoes a rapid reduction to form excited manganese(II) species ($Mn(II)^*$) that emits light.

4.5.1.3 Influence of added Mn(II) on malic acid chemiluminescence

Figure 4.32 shows the kinetic curves of the CL emission for several experiments of a series in which the initial concentration of MnO_4^- and malic acid were held constant, namely 0.001M and 0.05M, respectively and the initial $[\text{Mn(II)}]$ was varied from 0.01 to 0.5 M.

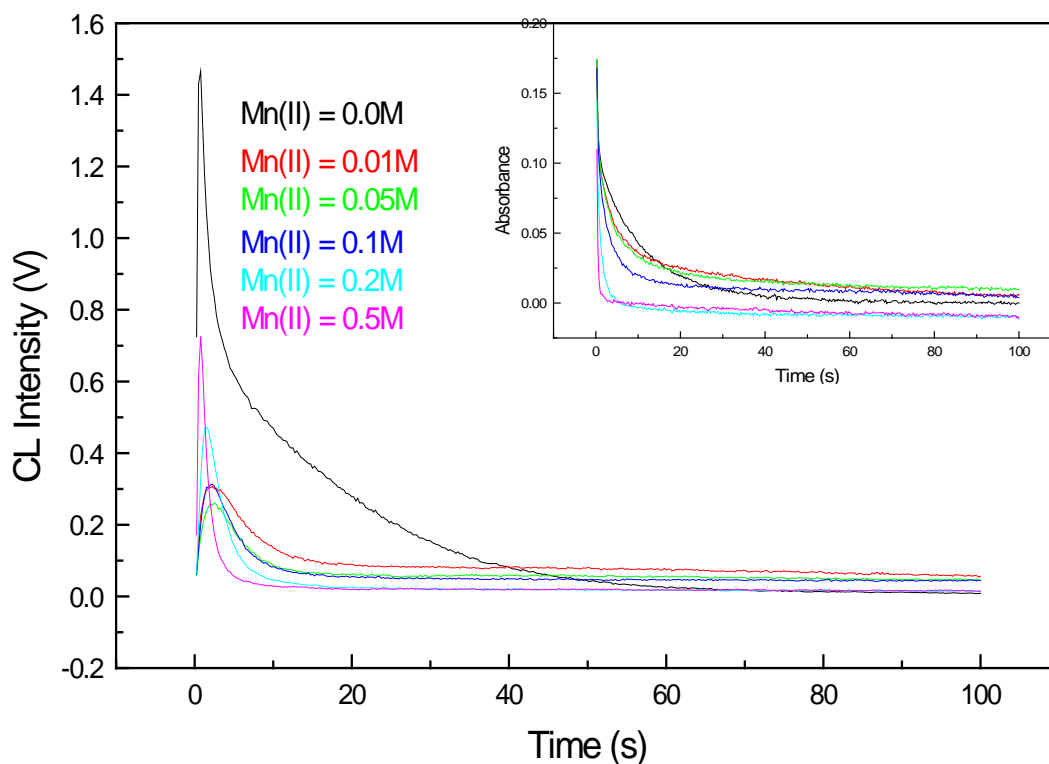


Figure 4.32 Influence of added manganese(II) on the kinetics of the chemiluminescence response versus time profile. Experimental conditions: $[\text{Mn(II)}] = 0.01; 0.05; 0.1; 0.2$ and 0.5 M, $[\text{HO}_2\text{CCH}_2\text{CHOHCO}_2\text{H}] = 0.05\text{M}$; $[\text{MnO}_4^-] = 0.001\text{M}$, Temperature = 25°C , $[\text{H}_2\text{SO}_4] = 2\text{M}$ and HT (Fluorescence channel): 800V .

As it can be seen in Figure 4.32, the addition of some limiting concentrations of Mn(II) to the reaction mixture seems to have no expected effect on the chemiluminescence emission.

The reason for this is not clear but it may have something to do with the lack of the induction period observed for malic acid oxidation by permanganate.

4.5.1.4 Influence of glyoxal on malic acid chemiluminescence

It was hypothesized above that the addition of a new substrate in the system would lead to a change in the intensity of the CL in virtue of the co-oxidation reaction. So far, this assumption has been demonstrated by the addition of formaldehyde in the reaction mixture.

In order to test further the hypothesis, the enhancement experiments have been extended to other organic additives such as glyoxal.

Figure 4.33 shows the kinetic curves of the CL emission for several experiments of a series in which the initial concentration of MnO_4^- and malic acid were held constant, namely 0.001M and 0.01M, respectively and the initial concentration of glyoxal was varied from 0.01 - 0.2 M.

From Figure 4.33, it can be seen that the addition of some limiting concentrations of glyoxal to the reaction mixture leads to an increase in the chemiluminescence signal intensity and a larger amount of glyoxal corresponds to a higher rate of the reaction.

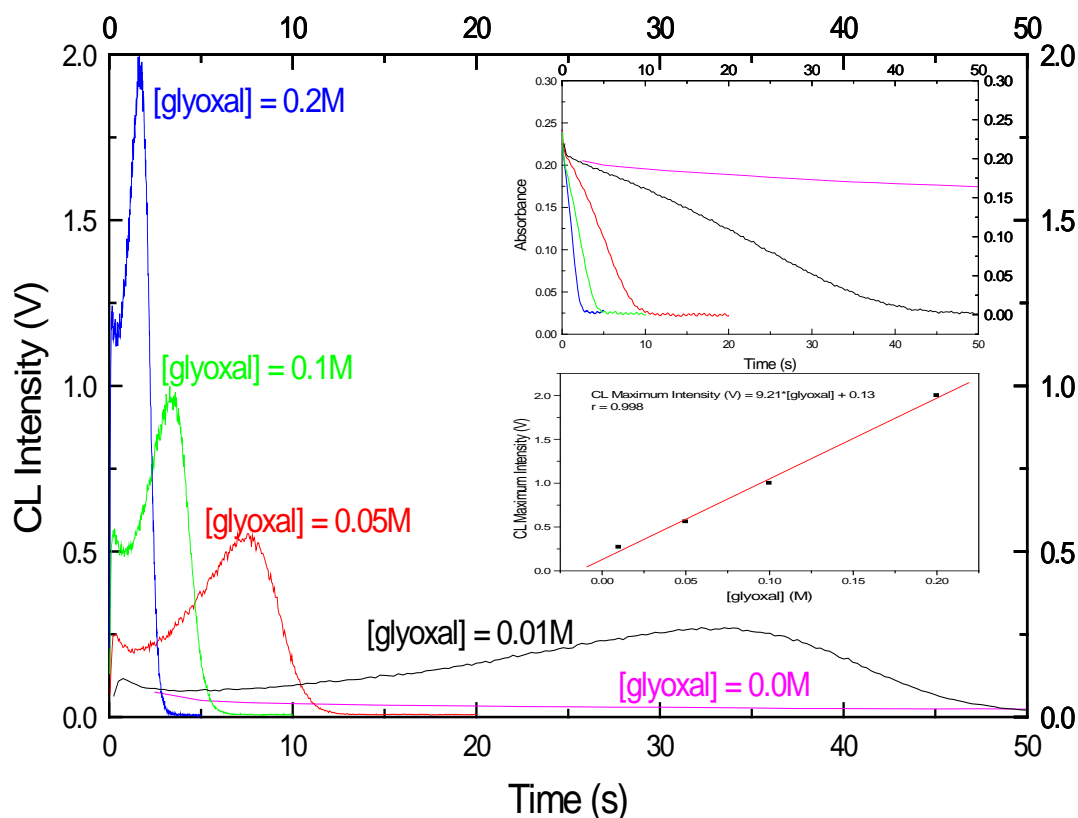


Figure 4.33 Influence of added glyoxal on the kinetics of the chemiluminescence response versus time profile. Experimental conditions: [glyoxal] = 0.1; 0.25; 0.5; 0.75 and 1.0M, $[\text{MnO}_4^-] = 0.001\text{M}$, $[\text{HO}_2\text{CCH}_2\text{CHOHCO}_2\text{H}] = 0.01\text{M}$, $T^\circ = 25^\circ\text{C}$, $[\text{H}_2\text{SO}_4] = 2\text{M}$ and HT (Fluorescence channel): 800V.

The results also show a good correlation between the CL signal intensity and the initial concentrations of glyoxal. The plot of the CL maximum intensity as a function of the initial glyoxal concentration (inset of Figure 4.33) was linear with a correlation coefficient $R=0.998$.

These results are consistent with the postulate that the addition of another reductant in the reaction mixture increases the CL signal intensity.

The observed increase in CL signal intensity is attributed to co-oxidation of malic acid and glyoxal by permanganate to speed up the accumulation of manganese(III) that then undergoes a rapid reduction to form excited manganese(II) species (Mn(II)^*) that emits light.

An implication of this is the possibility that glyoxal could be used as enhancer in malic acid/ MnO_4^- CL system.

4.5.2 Manganese(III) oxidation of malic acid

It was hypothesized that, in the light-producing pathway, malic acid reduces Mn(III) to form excited manganese(II) species that emits light. Therefore, it was essential to separately evaluate the CL reaction of malic acid and Mn(III).

In this set of experiments, the initial concentration of Mn(III) was held constant at 0.05M and the initial concentration of malic acid was varied from 0.05 to 1.0M and the effect of increasing malic acid concentration on chemiluminescence intensity was evaluated.

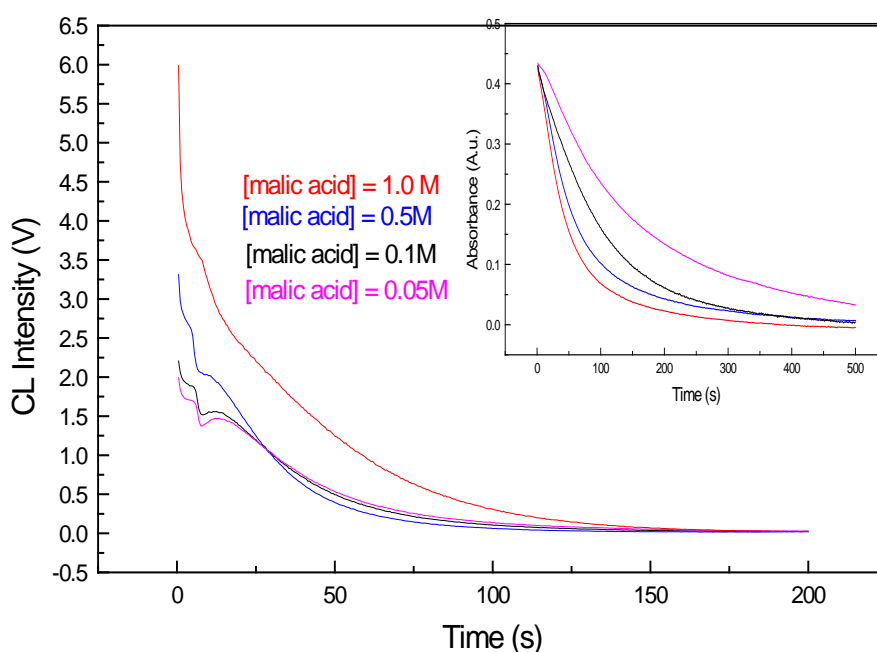


Figure 4.34 Effect of malic acid concentration on the kinetics of CL response versus time profile. Experimental conditions: $[\text{HO}_2\text{CCH}_2\text{CHOHCO}_2\text{H}] = 0.05; 0.10; \text{ and } 1.0\text{M}$, $[\text{Mn(III)}] = 0.05\text{M}$, Temperature = 25°C , $[\text{H}_2\text{SO}_4] = 2\text{M}$ and HT (Fluorescence channel): 800V .

It was found that manganese(III) reacts with malic acid to produce light emission in acid solution. The concentration of the malic acid had a very strong influence on chemiluminescence signal intensity.

The results from experiments demonstrated that as the concentration of malic acid increased, the maximum of CL signal intensity gradually increased, as seen in Figure 4.34.

The results support the involvement of Mn(III) in the light-producing pathway in which it oxidizes malic acid to form excited manganese(II) species that emits light.

For an additional check on the conclusion that the excited Mn(II) is formed by the reduction of Mn(III) intermediate by malic acid, experiments were carried out in which Mn(II) was added into the reaction mixture.

If the excited Mn(II) is formed in a chemical reaction and not as the result of energy transfer, then the addition of Mn(II) should not lead to the CL emission or an enhancement of the CL observed.

Figure 4.35 shows the effect of externally added Mn(II) on the CL response from Mn(III) and malic acid.

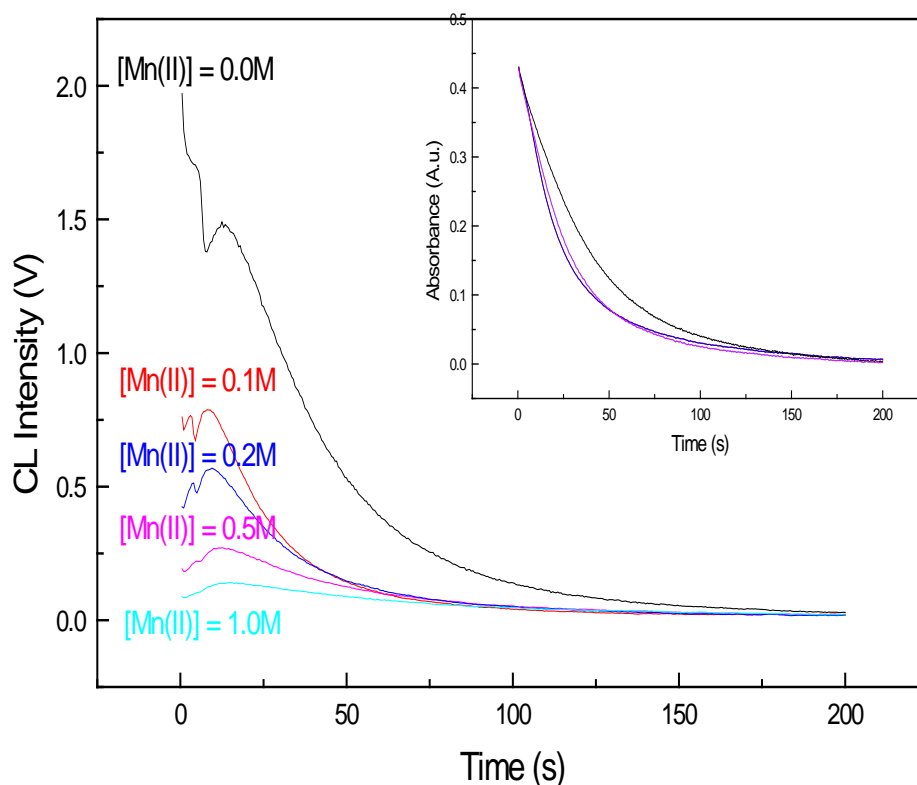


Figure 4.35 Effect of [Mn(II)] on the kinetics of chemiluminescence response versus time profile. Experimental conditions: [Mn(II)] = 0.0; 0.10; 0.20; 0.50 and 1.0M, [Mn(III)] = 0.05M, [HO₂CCH₂CHOHCO₂H] = 0.05M, Temperature = 25°C, [H₂SO₄] = 2M and HT (Fluorescence channel): 800V.

It was found that the addition of various concentrations (0.1 to 1.0M) of Mn(II) to malic acid oxidation by Mn(III) did not lead to the increase of CL emission, as for MnO₄⁻ reaction, but the added Mn(II) lead to the quenching of the CL signal.

One of the more significant findings to emerge from this study is that formaldehyde, as an enhancer, does not participate in the reduction of Mn(III) intermediate, under the reaction

conditions, to form excited manganese(II) species that emits light, due to the slow reaction between Mn(III) and formaldehyde as demonstrated in Figure 4.13.

For additional check on this conclusion, experiments were carried out, in which formaldehyde concentration was varied in the range 0.1 to 0.8M, while 0.05M malic acid and 0.05M Mn(III) concentrations were held constants.

If the formaldehyde is involved in the CL emission resulting from Mn(III) oxidation of malic acid, then the addition of formaldehyde should lead to an enhancement of the CL signal intensity. The results of the experiments are presented in Figure 4.36.

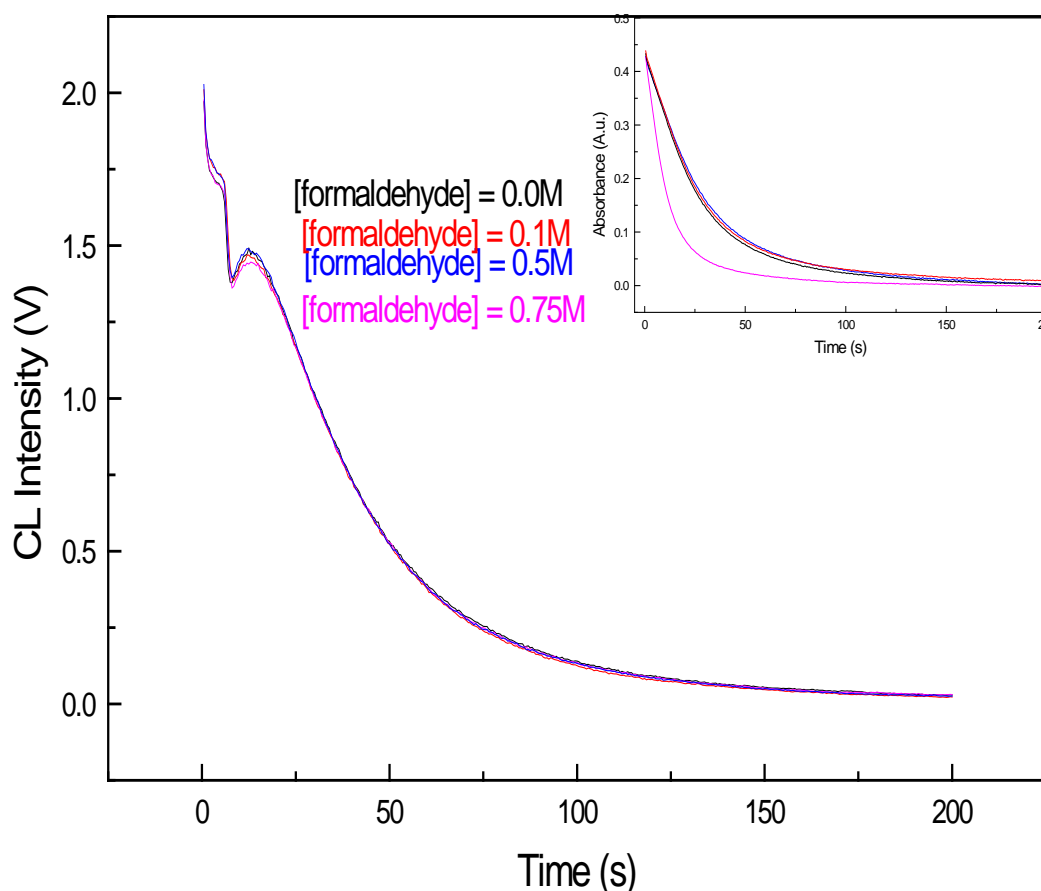


Figure 4.36 Effect of formaldehyde concentration on the kinetics of CL response versus time profile. Experimental conditions: [HCHO] = 0.0; 0.10; 0.20; 0.50 and 0.80M, [Mn(III)] = 0.05M, [HO₂CCH₂CHOHCO₂H] = 0.05M, Temperature = 25°C, [H₂SO₄] = 2M and HT (Fluorescence channel): 800V

The test was successful as it was able to demonstrate that the added formaldehyde concentrations did not lead to the chemiluminescence emission observed.

The addition of formaldehyde to the malic acid-manganese(III) system, where the oxidation of malic acid accompanied by chemiluminescence emission takes place did not lead to an

enhancement of the chemiluminescence emission. The results confirm the hypothesis that, under the reaction conditions, Mn(III) oxidation reaction of formaldehyde is very much slower to illicit a measurable CL response and contribute to the malic acid CL intensity.

4.5.3 Manganese(IV) oxidation of malic acid

After Mn(III) oxidation of malic acid, it was necessary to look at Mn(IV) oxidation of malic acid, as it is likely that that reaction occurs and contributes for malic acid – permanganate chemiluminescence system.

The chemiluminescence profiles obtained by varying the large excess of malic acid concentration in the range 0.005 – 0.1 M are shown in Figure 4.37.

It has been observed that Manganese(IV) reacts with malic acid to produce light emission in acid solution.

The results from experiments demonstrate that as the concentration of malic acid increased, the maximum of chemiluminescence signal intensity increased dramatically. The plot of the CL maximum intensity as a function of the initial malic acid concentration (inset of Figure 4.37) was linear with a correlation coefficient $R=0.962$.

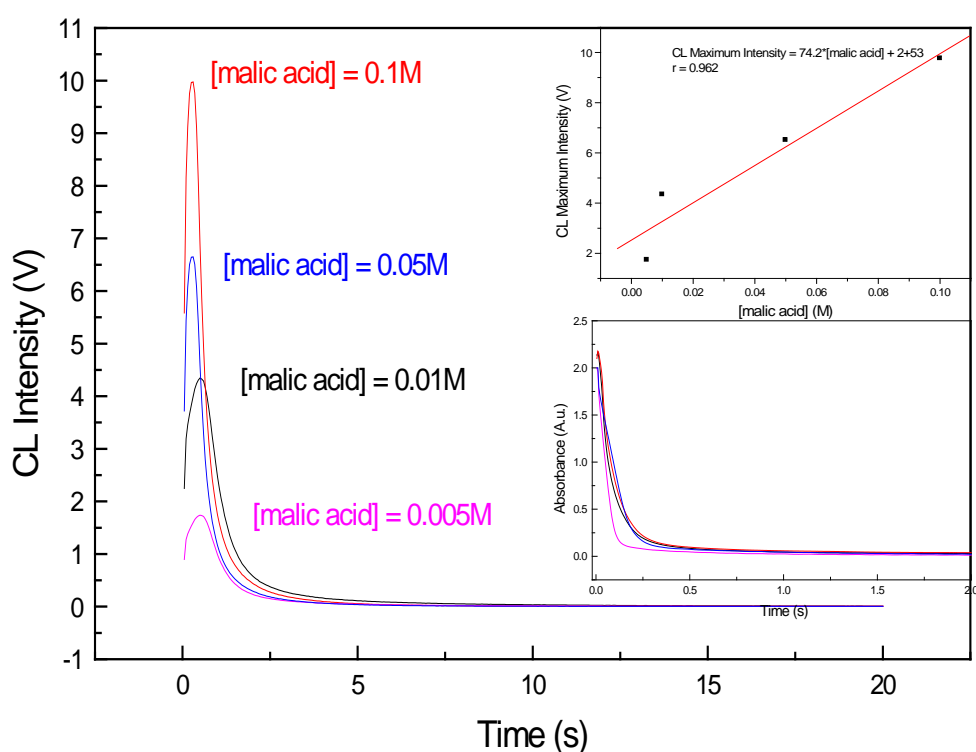


Figure 4.37 Effect of malic acid concentration on the kinetics of CL response versus time profile. Experimental conditions: $[\text{HO}_2\text{CCH}_2\text{CHOHCO}_2\text{H}] = 0.005; 0.01; 0.05; 0.1$ and 0.5M , $[\text{Mn(IV)}] = 0.02\text{M}$, Temperature = 25°C , $[\text{H}_2\text{SO}_4] = 2\text{M}$ and HT (Fluorescence channel): 600V .

These results confirm our working hypothesis for the light-producing pathway that malic acid and others reductants (e.g. formaldehyde, Mn(II), etc.) initiates the reduction of permanganate to generate Mn(III) intermediate, which then reacts with malic acid to form excited Mn(II) species that emit light.

4.6 Metronidazole (C₆H₉N₃O₃) chemiluminescence oxidation reactions

Metronidazole, as a substance test with slower rate of reaction compared with glyoxal, was used to test our working hypothesis for the light-producing pathway in manganese-based chemiluminescence oxidation system.

Metronidazole is an important antibiotic drug largely prescribed in the treatment against anaerobic bacteria and certain parasites. Therefore, a sensitive and selective analytical control for the study of this molecule and its metabolites in biological fluids is necessary.

Despite that acidic MnO₄⁻ CL detection has been used to determine a number of pharmaceutical molecules in commercial formulations, no reported attempt to the determination of metronidazole using CL technique was found and little is known about the light-producing pathway in the reaction between MnO₄⁻ and metronidazole and it is not clear what factors influence the kinetics and the intensity of the CL emission.

In this section the chemiluminescence reactions of metronidazole with manganese-based oxidants are examined and the light-producing pathway hypothesis is tested by predicting the effects of enhancers.

4.6.1 Permanganate oxidation reaction of Metronidazole

The characteristics of the chemiluminescence kinetics of the reaction of permanganate and metronidazole in sulphuric acid medium were investigated.

Kinetic experiments of oxidation of metronidazole with permanganate were conducted at a constant temperature of 25 °C under the reaction conditions relevant to chemiluminescence emission signal exhibition.

As can be expected, the stopped-flow experiments demonstrated in Figure 4.38 that the reaction between metronidazole (dissolved in 2 mol L⁻¹ sulphuric acid) and permanganate was accompanied by the reduction of the permanganate, attendant oxidation of the target compound - metronidazole, and formation of a variety of reaction products.

It is evident from Figure 4.38 that metronidazole is oxidized by permanganate (MnO₄⁻) in sulphuric acid medium and generates a relatively weak chemiluminescence response.

The results revealed that, although, the oxidation of metronidazole by permanganate in sulphuric acid was relatively slow - the absorbance time course indicates half-time ($t_{1/2}$) reaction of 50 seconds and the permanganate reduction efficiency is up to 99.5% within 300 seconds.

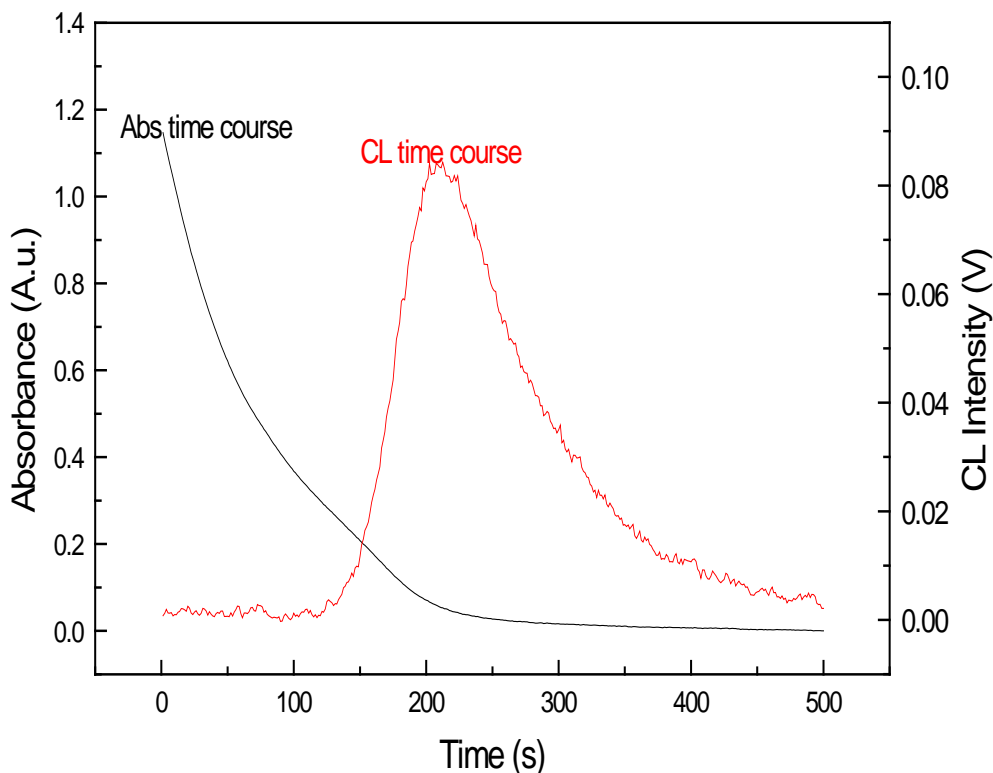


Figure 4.38 Plot comparing CL time course versus absorbance time course for MnO_4^- oxidation reaction of metronidazole. Experimental conditions: $[\text{C}_6\text{H}_9\text{N}_3\text{O}_3] = 0.01\text{M}$, $[\text{MnO}_4^-] = 0.005\text{M}$, Temperature = 25°C , $[\text{H}_2\text{SO}_4] = 2\text{M}$, Wavelength = 525 nm; HT (Fluorescence channel): 800V

4.6.1.1 Effect of formaldehyde concentration on the Chemiluminescence

The hypothesis for the light-producing reaction was tested by predicting the effects of added formaldehyde as enhancer in metronidazole/permanganate system.

As mentioned previously, the presence of formaldehyde increases the emission intensity from reactions with acidic potassium permanganate. In order to investigate the enhancement effects, a series of kinetic runs, monitored at maximum absorbance of KMnO_4 at 525 nm, and the chemiluminescence signal was recorded at its maximum emission, were performed by increasing the concentration of formaldehyde (range: $0.1 - 1.0 \text{ mol dm}^{-3}$) at constant concentrations of other reactants. $[\text{Metronidazole}] = 0.001\text{M}$; $[\text{MnO}_4^-] = 0.005 \text{ mol dm}^{-3}$; $[\text{H}_2\text{SO}_4] = 2.0 \text{ mol dm}^{-3}$ and temperature = 25°C .

Figure 4.39 shows the kinetic curves of the chemiluminescence emission and its corresponding absorbance time courses (inset of Figure 4.39) at four concentrations of formaldehyde. It is characteristic that as the concentration of formaldehyde increases the rate of the reaction increases. Thus, there is a direct relationship between the intensity of the chemiluminescence and the rate of oxidation.

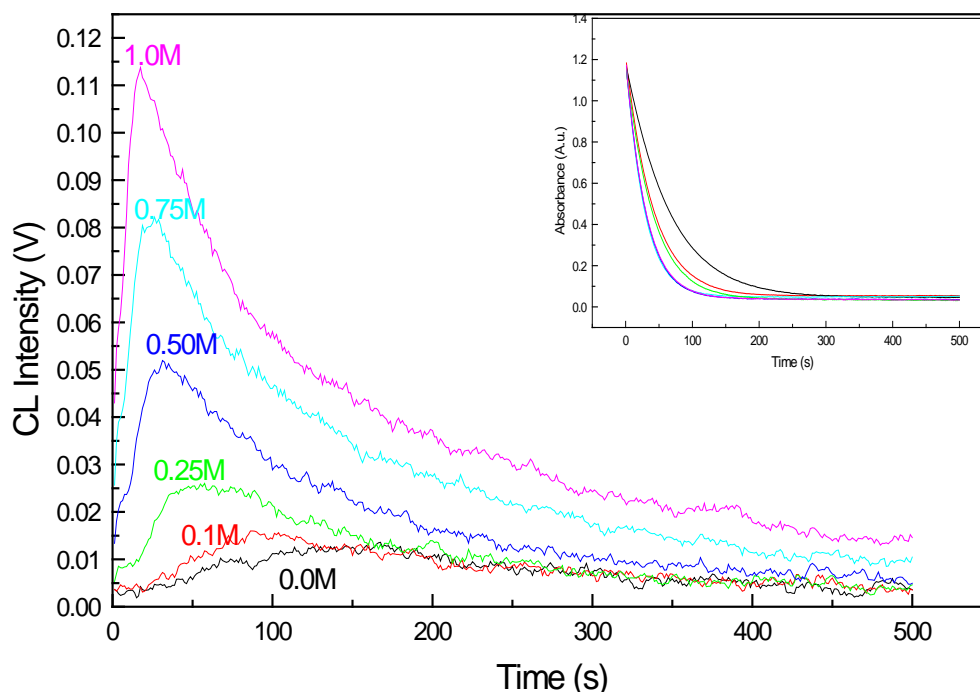


Figure 4.39 Effect of formaldehyde concentration on the kinetics of chemiluminescence response versus time profile and absorbance time course. Experimental conditions: [formaldehyde] = 0.1; 0.25; 0.5; 0.75 and 1.0M, $[\text{MnO}_4^-] = 0.005\text{M}$, $[\text{C}_6\text{H}_9\text{N}_3\text{O}_3] = 0.001\text{M}$, Temperature = 25°C , $[\text{H}_2\text{SO}_4] = 2\text{M}$, Wavelength = 525 nm and HT (Fluorescence channel): 800V.

The results confirm the hypothesis that, under the reaction conditions, formaldehyde increases the CL by increasing the concentration of Mn(III) intermediate, which is rapidly reduced by organic species to form excited manganese(II) species that emits light.

4.6.1.2 Influence of glyoxal concentration on the Chemiluminescence

It was suggested earlier that the addition of a new substrate in a slower and non-CL system would lead to a change in the intensity of the chemiluminescence emission and an increase in the reaction rate.

To test the hypothesis in the metronidazole-permanganate chemiluminescence system, a series of stopped-flow experiments was carried out. In these experiments 0.01M glyoxal was added into the oxidation reaction between 0.001M metronidazole and 0.005M KMnO_4 in sulphuric acid in which no significant chemiluminescence emission was observed.

A comparison of the two results reveals that the introduction of 0.01M glyoxal leads to an enhancement of the intensity of the CL and an increase of the reaction rate.

The resultant chemiluminescence time course and its corresponding absorbance time course presented in Figure 4.40 showed significant differences in the kinetics and the intensity of the chemiluminescence emission with and without glyoxal.

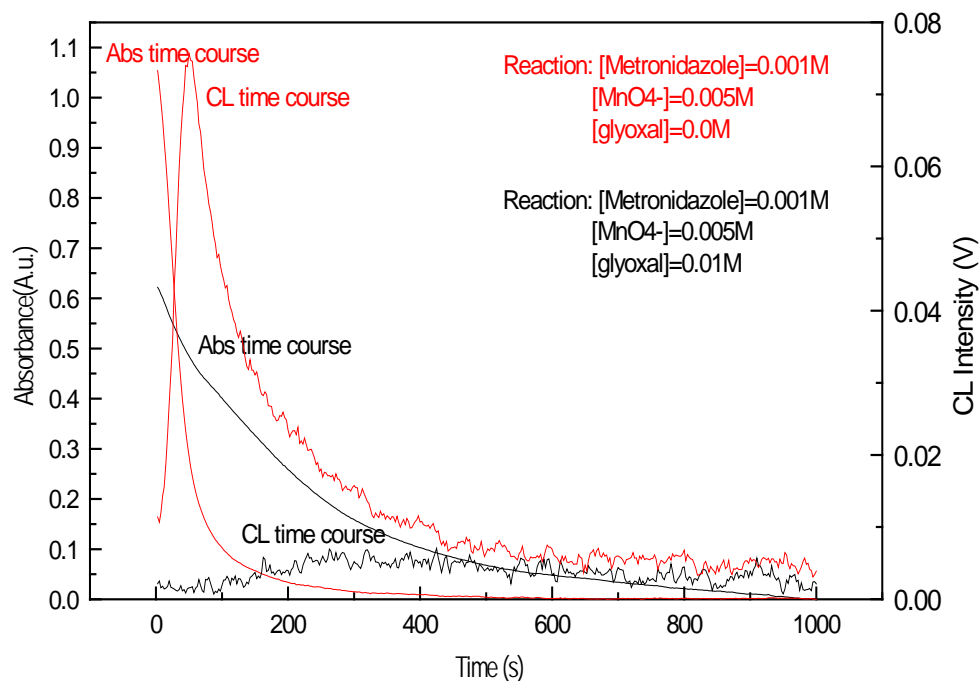


Figure 4.40 Plot comparing CL time course versus absorbance time course for KMnO_4 oxidation reaction of metronidazole with and without glyoxal. Experimental conditions: Wavelength = 525 nm; $[\text{C}_6\text{H}_9\text{N}_3\text{O}_3] = 0.001\text{M}$; $[\text{KMnO}_4] = 0.005\text{M}$; $[\text{OCHCHO}] = 0.01\text{M}$; $[\text{H}_2\text{SO}_4] = 2\text{M}$; Temperature = 25°C .

Again the results of these experiments support the hypothesis that co-oxidation of organic substrates increases the rate of formation of Mn(III) that increases the CL emission.

In order to check whether the order by which a compound is added in a chemiluminescence system has any effect on the reaction rate and on the kinetics and the intensity of the chemiluminescence emission, a series of univariate experiments was carried out.

In these experiments metronidazole was used as enhancer and added into glyoxal-permanganate chemiluminescence system rather than adding glyoxal into metronidazole-permanganate system. Figure 4.41 gives the kinetic curves of the chemiluminescence and the absorbance time courses at four concentrations of metronidazole.

The experimental results indicate that the addition of metronidazole to glyoxal- MnO_4^- CL system leads to an enhancement of the observed chemiluminescence intensity.

As it can be seen in Figure 4.41, a larger amount of metronidazole produces a higher intensity of the chemiluminescence and leads to a higher rate of reaction (inset of Figure 4.41).

The findings of this study suggest that the order by which a compound is added into a system has no significant effects on the resulting chemiluminescence signal intensity, but it is the mixture composition that matters.

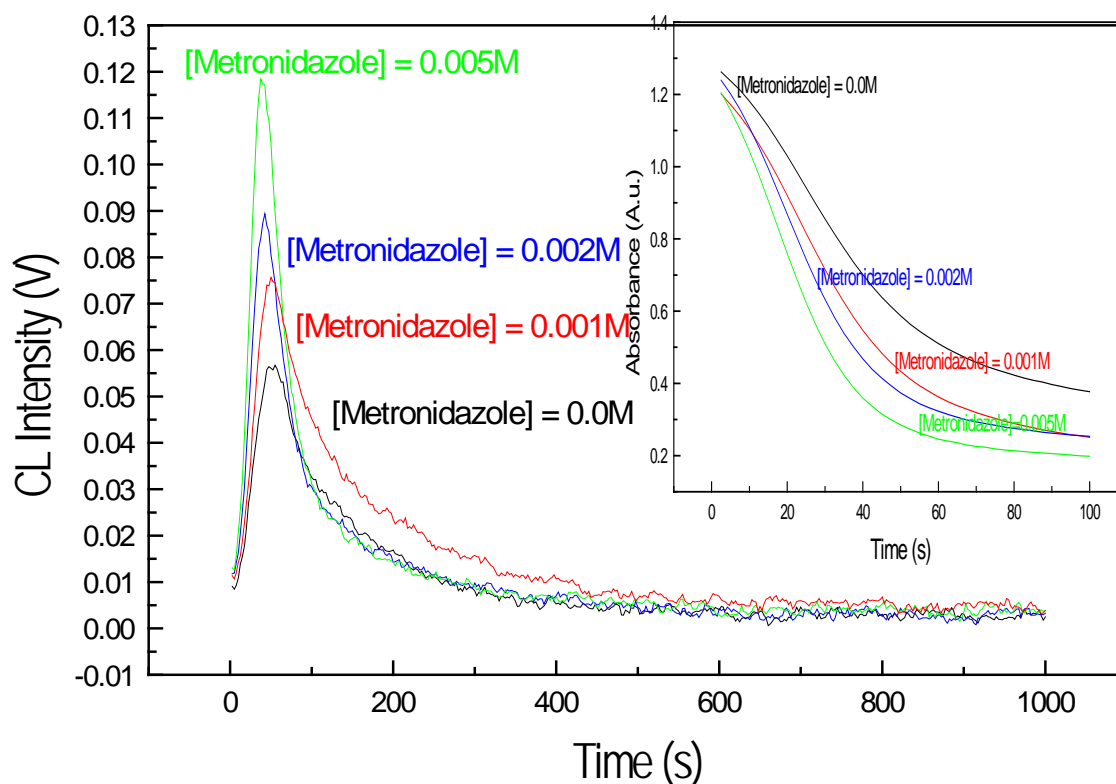


Figure 4.41 Influence of added metronidazole on the kinetics of glyoxal oxidation reaction and chemiluminescence response versus time profile. Experimental conditions: $[C_6H_9N_3O_3] = 0.0; 0.001; 0.002$ and $0.005M$, $[MnO_4^-] = 0.005M$, $[OCHCHO] = 0.01M$, Temperature = $25^\circ C$, $[H_2SO_4] = 2M$, Wavelength = 525 nm and HT (Fluorescence channel): $800V$.

Taken together, these results further support the hypothesis that co-oxidation of organic substrates increases the concentration of manganese(III) that increases the chemiluminescence emission.

4.6.1.3 Influence of pyrogallol ($C_6H_6O_3$) concentration on the CL emission

In her attempt to explain the mechanism of the enhancement, Abdel-Mageed¹⁰ used pyrogallol and gallic acid to enhance permanganate chemiluminescence systems, however, there has been little discussion about light-producing pathway.

In order to test the hypothesis of the light-producing reaction by predicting the effects of pyrogallol as enhancer, a series of kinetic experiments was carried out, in which the initial

concentration of metronidazole and permanganate were held constant at 0.001M and 0.005M, respectively and the initial concentration of pyrogallol was varied in the range 0.0 to 0.001M.

As expected, the experimental results in Figure 4.42 indicate the addition of pyrogallol to metronidazole/permanganate CL system leads to an enhancement of the intensity of chemiluminescence observed. As it can be seen, a larger amount of pyrogallol produces a higher intensity of the CL and leads to a higher rate of reaction (inset of Figure 4.42).

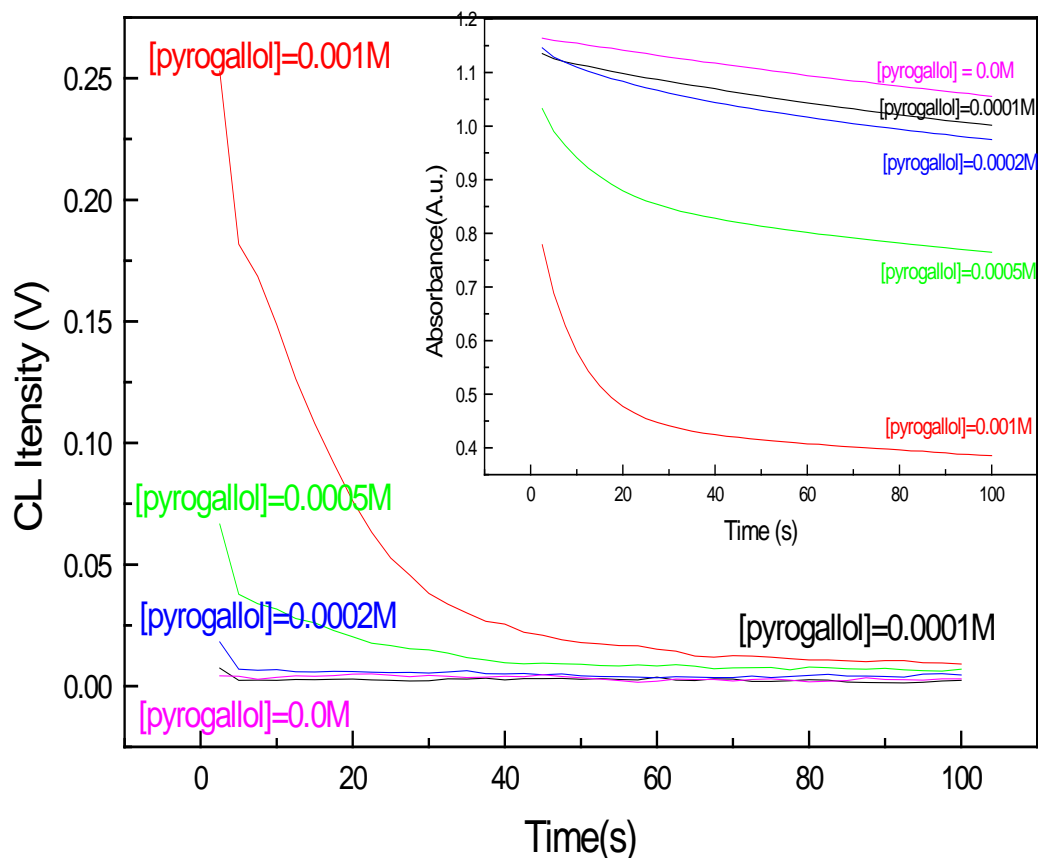


Figure 4.42 Influence of added pyrogallol on the kinetics of metronidazole oxidation reaction and CL response versus time profile. Experimental conditions: $[C_6H_6O_3] = 0.0; 0.0001; 0.0002; 0.0005; \text{ and } 0.001M$, $[MnO_4^-] = 0.005M$, $[C_6H_9N_3O_3] = 0.001M$, Temperature = $25^\circ C$, $[H_2SO_4] = 2M$, Wavelength = 525 nm and HT (Fluorescence channel): $800V$.

To convince ourselves that the order by which pyrogallol and metronidazole is mixed produces similar effects of enhancement on the metronidazole/pyrogallol/ MnO_4^- CL system, a series of kinetic experiments in which metronidazole was added to pyrogallol and MnO_4^- was carried out.

The results in Figure 4.43 show that the addition of metronidazole into pyrogallol oxidation by permanganate leads, as expected, to an enhancement of the chemiluminescence observed and also to an increase of the reaction rate (inset of Figure 4.43).

The observed difference between pyrogallol and metronidazole, as enhancers in this study was not significant.

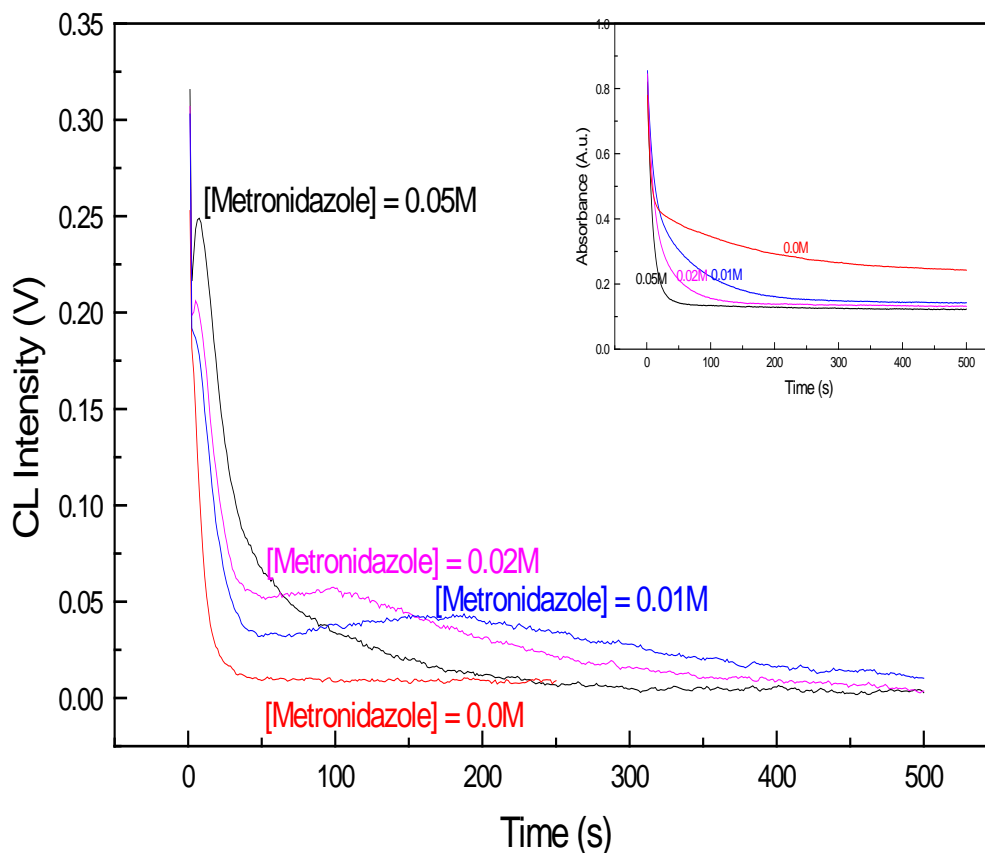


Figure 4.43 Influence of added metronidazole on the kinetics of pyrogallol oxidation reaction and chemiluminescence response versus time profile. Experimental conditions: $[C_6H_9N_3O_3] = 0.0; 0.01; 0.02; \text{ and } 0.05M$, $[MnO_4^-] = 0.005M$, $[C_6H_6O_3] = 0.001M$, Temperature = $25^\circ C$, $[H_2SO_4] = 2M$, Wavelength = 525 nm and HT (Fluorescence channel): $800V$.

Taken together, these results again further support the conclusion that the enhancement in the observed chemiluminescence emission is associated with the co-oxidation of pyrogallol and metronidazole to increases the concentration of Mn(III) that increases the CL emission.

4.6.1.4 Influence of gallic acid concentration on the chemiluminescence

As mentioned earlier, gallic acid has been used by Abdel-Mageed¹⁰ as an enhancer for MnO_4^- CL system, however, there has been little discussion about light-producing pathway.

To test the hypothesis for the light-producing pathway by predicting the effects of gallic acid, as enhancer, a series of kinetic experiments was carried out, in which the initial concentration of metronidazole and MnO_4^- were held constants at $0.001M$ and $0.005M$, respectively and the initial concentration of gallic acid was varied in the range 0.0 to $0.002M$.

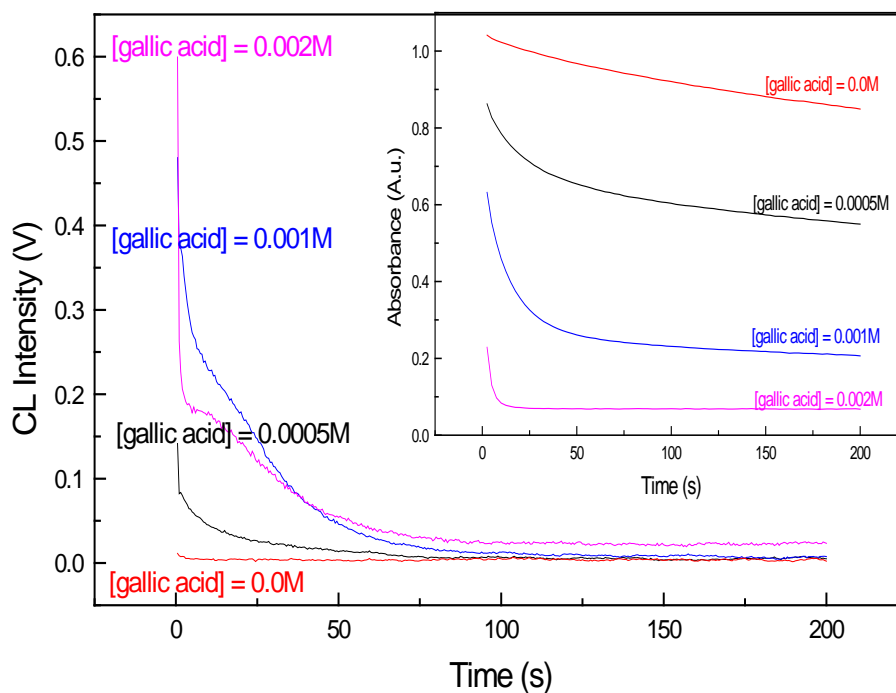


Figure 4.44 Influence of added gallic acid on the kinetics of metronidazole oxidation reaction and CL response versus time profile. Experimental conditions: $[C_7H_6O_5] = 0.0; 0.0005; 0.001$ and $0.002M$, $[MnO_4^-] = 0.005M$, $[C_6H_9N_3O_3] = 0.001M$, Temperature = $25^\circ C$, $[H_2SO_4] = 2M$, Wavelength = 525 nm and HT (Fluorescence channel): $800V$.

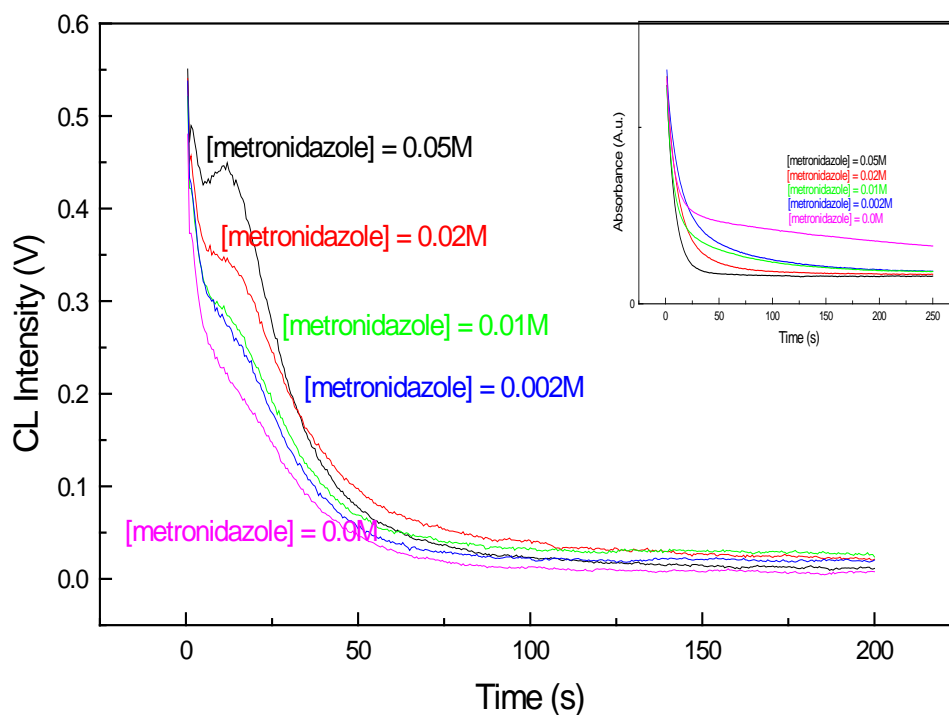


Figure 4.45 Influence of added metronidazole on the kinetics of gallic acid oxidation reaction and CL response versus time profile. Experimental conditions: $[C_6H_9N_3O_3] = 0.002; 0.01; 0.02; \text{ and } 0.05M$, $[MnO_4^-] = 0.005M$, $[C_7H_6O_5] = 0.001M$, $T^\circ = 25^\circ C$, $[H_2SO_4] = 2M$, Wavelength = 525 nm and HT (Fluorescence channel): $800V$.

As expected, the experimental results in Figure 4.44 indicate the addition of gallic acid to metronidazole/permanganate CL system leads to an enhancement of the observed CL signal intensity.

As it can be seen, a larger amount of gallic acid produces a higher intensity of the CL emission and leads to a higher rate of reaction (inset of Figure 4.44).

The addition of metronidazole into gallic acid-permanganate CL system produced similar effect of enhancement as it can be seen in Figure 4.45. The observed difference in between gallic acid and metronidazole, as enhancers in this study was not significant. The reaction rate and the CL signal intensity increased as the concentration of metronidazole increased.

Taken together, these results confirm the conclusion that the enhancement in the observed chemiluminescence emission is associated with the co-oxidation of gallic acid and metronidazole to increases the concentration of Mn(III) that increases the CL emission.

4.6.2 Manganese(III) oxidation of metronidazole

It has been postulated in scheme 4.1 that Mn(III) intermediate reacts with organic substrates and intermediates to form excited Mn(II) species that emit light. To test the hypothesis the reaction between Mn(III) and metronidazole was studied.

If the observed CL emission during the MnO_4^- oxidation of metronidazole follows the light-producing pathway proposed, the reaction of Mn^{3+} and metronidazole should lead to CL emission.

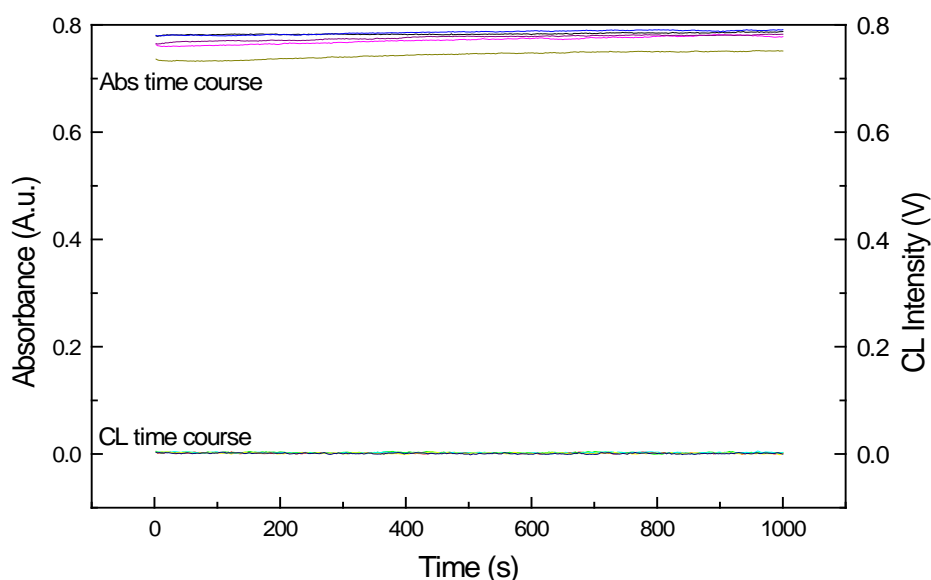


Figure 4.46 Plot comparing chemiluminescence time course versus absorbance time course for Mn(III) oxidation reaction of metronidazole. Experimental conditions: $[\text{C}_6\text{H}_9\text{N}_3\text{O}_3] = 0.002, 0.005, 0.01, 0.05$ and 0.1M , $[\text{Mn(III)}] = 0.05\text{M}$, Temperature = 25°C , $[\text{H}_2\text{SO}_4] = 2\text{M}$, Wavelength = 500 nm ; HT (Fluorescence channel): 800V

To evaluate the chemiluminescence potential of metronidazole-manganese(III) system, a series of univariate experiments were carried out, in which the kinetics of the chemiluminescence reaction between manganese(III) and metronidazole and the dependence of the chemiluminescence signal intensity on metronidazole concentration were examined.

In these experiments, the initial concentration of Mn(III) was held constant at 0.05M while the initial concentration of metronidazole was varied in the range 0.002 to 0.10M and the effects of increasing metronidazole concentration on CL signal intensity were evaluated. The experimental results are presented in Figure 4.46.

It is somewhat surprising that no noticeable chemical reaction and no measurable CL signal were noted in these experimental conditions. No increase of CL emission associated with [metronidazole] increase was detected. This finding was unexpected and would suggest that Mn(III) is not involved in the light-producing pathway. The experimental results are rather controversial, and they are not in good agreement with our working hypothesis for light-producing pathway.

It is difficult to explain this result in relation with the proposed light-producing mechanism, but the observed chemiluminescence emission during metronidazole oxidation by MnO_4^- could be attributed to the reaction between Mn(III) intermediate and organic intermediates formed in the course of the initial reaction in which metronidazole reduces MnO_4^- to Mn(III).

4.6.3 Manganese(IV) oxidation of metronidazole

It was suggested in Scheme 4.1 that Mn(IV) is in rapid equilibrium with Mn^{3+} . Therefore, it was necessary that after Mn(III) failed to react with metronidazole, to examine the reaction between Mn(IV) and metronidazole.

If the reaction between Mn(IV) and metronidazole produces chemiluminescence signal, which would suggest that Mn(IV) could react with organic substrates in two electron transfer process to form directly Mn(II) species that elicits light and the proposed light-producing pathway must be modified.

The oxidation reaction of metronidazole in acidic solution and manganese(IV) was monitored at its maximum absorbance at 400 nm. This reaction was studied over the metronidazole concentration range of 0.005 – 0.1M.).

Contrary to expectations no significant chemical reaction and no measurable chemiluminescence signal were noted under the reaction conditions. Again there was no increase of chemiluminescence emission associated with metronidazole concentration increase. The experimental results are rather controversial, and they are not in good agreement with the light-producing pathway proposed in Scheme 4.1.

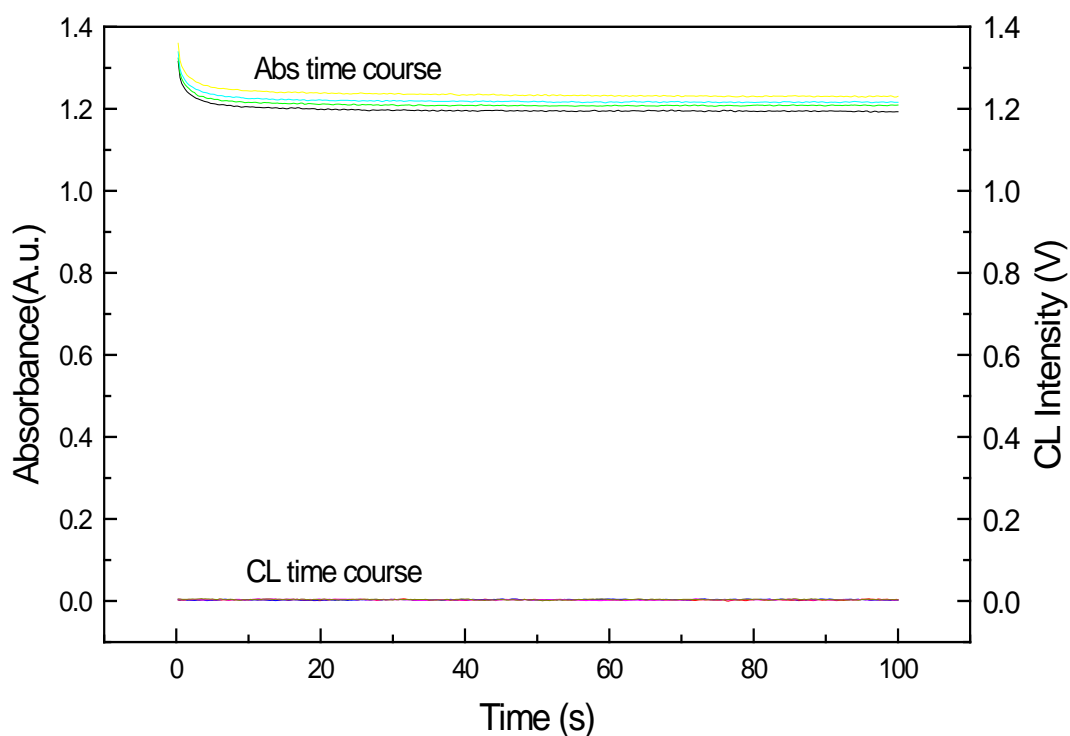


Figure 4.47 Plot comparing chemiluminescence time course versus absorbance time course for Mn(IV) oxidation reaction of metronidazole. Experimental conditions: $[\text{C}_6\text{H}_9\text{N}_3\text{O}_3] = 0.001, 0.005, 0.01, 0.05$ and 0.1M , $[\text{Mn(IV)}] = 0.01\text{M}$, Temperature = 25°C , $[\text{H}_2\text{SO}_4] = 2\text{M}$, Wavelength = 400 nm ; HT (Fluorescence channel): 800V .

A possible explanation for the observed chemiluminescence response during permanganate oxidation of metronidazole might be that organic intermediates (first step products) react successively with Mn(IV) and Mn(III) to form excited manganese(II) species that elicit light. In this case, it is not metronidazole that reacts in the second step of the pathway, but its intermediate formed during the first step process.

4.7 Tetracycline ($\text{C}_{22}\text{H}_{24}\text{N}_2\text{O}_8$) chemiluminescence oxidation reactions

For an additional check on the hypothesis postulated in Scheme 4.1, tetracycline was also used as a substance which for a similar rate of reaction compared to glyoxal.

Tetracycline is an important antibiotic drug for which, a sensitive and selective analytical method for the molecule and its metabolites in biological fluids is necessary. Although acidic potassium permanganate chemiluminescence detection has been used to determine a number of pharmaceutical molecules in commercial tablets, little is known about the light-producing pathway in the reaction between permanganate and tetracycline and it is not clear what factors that influence the kinetics and the intensity of the CL emission.

In this section the CL reactions of tetracycline with manganese-based oxidants are examined and the proposed light-producing pathway tested by predicting the effects of enhancers.

4.7.1 Permanganate oxidation of tetracycline

Li et al.⁵¹⁴ described a rapid and simple flow injection CL procedure for the determination of trace amounts of tetracyclines, which elicited CL with potassium permanganate in hydrochloric acid in the presence of a sensitizer, octylphenyl polyglycol ether.

The response to the concentration of tetracycline was linear in the range of 1.00 to 1000 $\mu\text{g mL}^{-1}$ with a relative standard deviation < 2.3 % for determination of 50.0 $\mu\text{g mL}^{-1}$ of each antibiotic ($n = 11$). The detection limits for tetracycline, oxytetracycline and chlortetracycline were 0.40, 0.52 and 0.60 $\mu\text{g mL}^{-1}$, respectively. The method is suitable for automatic and continuous analysis and has been successfully tested for determination of tetracycline in commercial formulations. The CL intensity was found to be remarkably enhanced when in the presence of octylphenyl polyglycol ether micellar system. So far, however, there has been little discussion about the light-producing reaction of tetracycline.

With the objective of understanding better the reaction mechanism of tetracycline - MnO_4^- CL system, a set of stopped-flow experiments of the system was carried out at a constant temperature of 25 °C.

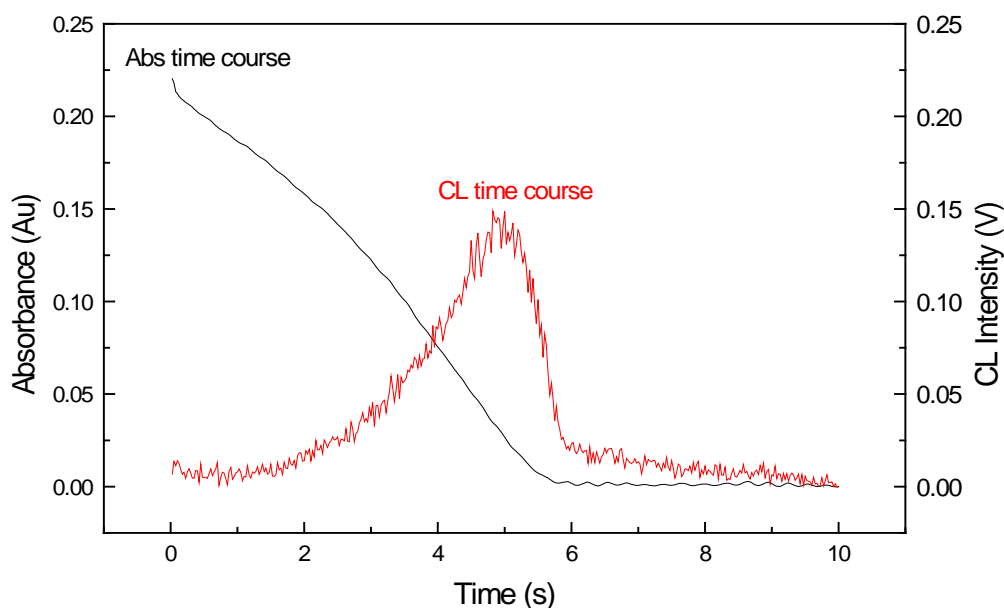


Figure 4.48 Plot comparing CL time course versus absorbance time course for MnO_4^- oxidation reaction of tetracycline. Experimental conditions: $[\text{C}_{22}\text{H}_{24}\text{N}_2\text{O}_8] = 0.01\text{M}$, $[\text{MnO}_4^-] = 0.001\text{M}$, Temperature = 25°C, $[\text{H}_2\text{SO}_4] = 2\text{M}$, Wavelength = 525 nm; HT: 800V.

Figure 4.48 compares the kinetic curves of the chemiluminescence emission and the reaction rate in which 0.001M permanganate and 0.01M tetracycline were reacted.

As was be expected, the stopped-flow experiments demonstrated in Figure 4.48 that tetracycline (dissolved in 2 mol L^{-1} sulphuric acid) is rapidly oxidized by permanganate.

It is believed that the reaction is a result of permanganate reduction, attendant oxidation of the target compound - tetracycline, and formation of a variety of reaction products. It is evident from Figure 4.48 that permanganate oxidation of tetracycline in sulphuric acid medium is accompanied by a chemiluminescence emission.

4.7.1.1 Effect of manganese(II)

It has been previously found that permanganate oxidation of tetracycline in sulphuric acid solution gives off a weak chemiluminescence. However, the addition of Mn(II) salt should lead to an enhancement of the observed chemiluminescence signal intensity with an increase in the reaction rate.

A set of univariate experiments was carried out to test the effect of adding Mn(II) salt on the kinetics of tetracycline CL reaction. The experimental results are presented in Figure 4.49.

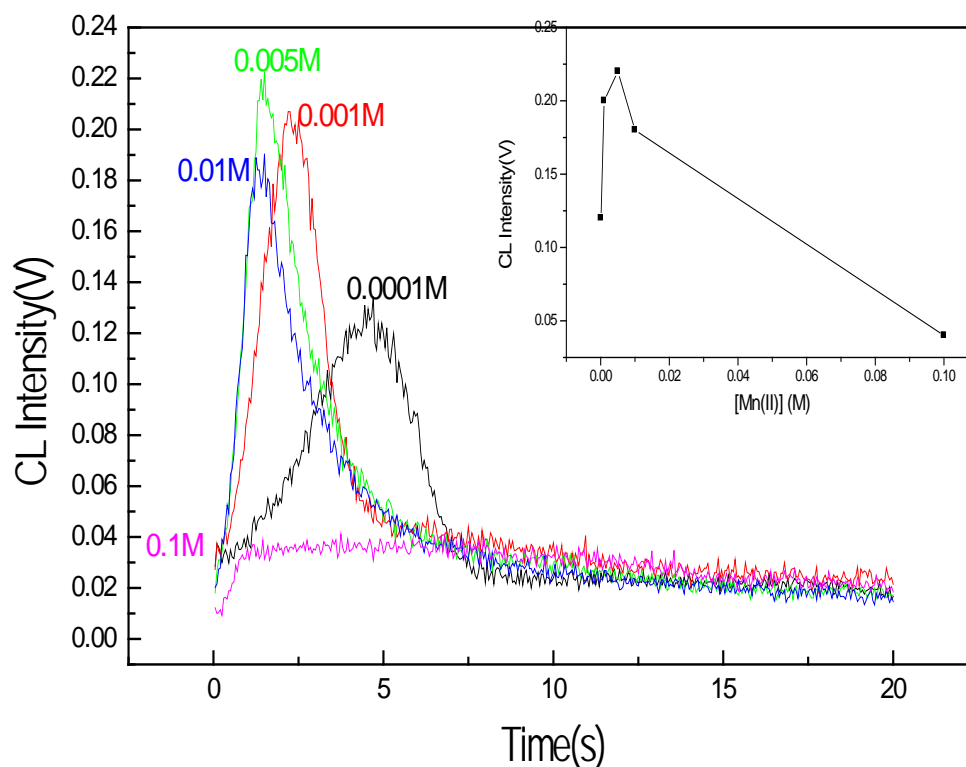


Figure 4.49 Effect of Mn(II) concentrations on the kinetic curves of the chemiluminescence signal. Experimental conditions: $[C_{22}H_{24}N_2O_8] = 0.0005M$, $[MnO_4^-] = 0.001M$, $[Mn(II)] = 0.0001, 0.0005, 0.001, 0.005, 0.01$ and $0.1M$; Temperature = $25^\circ C$, $[H_2SO_4] = 2M$, Wavelength = 525 nm ; HT (Fluorescence channel): $800V$

As it can be seen in Figure 4.49, under the reaction experimental conditions of a large excess of permanganate, the chemiluminescence emission increased sharply as manganese(II) concentration increased up to $0.005M$, then decreased at higher concentrations. Manganese(II) provided a 2-10 fold increase compared to CL response from the reaction without Mn(II).

Thus, the test for the hypothesis was successful, as CL signal intensity increased with the addition of manganese(II) salt. The mechanism of enhancement is thought to involve both autocatalytic role of Mn(II) and CL oxidation reaction between Mn(III) intermediate with tetracycline and some organic intermediates.

However, the quenching of CL intensity could be attributed to light absorption by molecules at higher tetracycline concentrations. It is also possible that the rate of reaction is so fast that some CL is lost in the dead-time.

4.7.1.2 Effect of formaldehyde

As mentioned previously, the presence of formaldehyde increases the CL response from oxidation reactions of many analytes with acidic KMnO_4 ^{77, 96, 110, 125, 126, 145-147, 464, 519}.

To ascertain our working hypothesis for the light-producing mechanism, the addition of formaldehyde in the reaction mixture should increase the observed CL signal intensity with an increase in the reaction rate.

A series of kinetic runs were carried out by increasing the [formaldehyde] from 0.0 – 1.0M at constant concentrations of other reactants. The results are shown in the Figure 4.50.

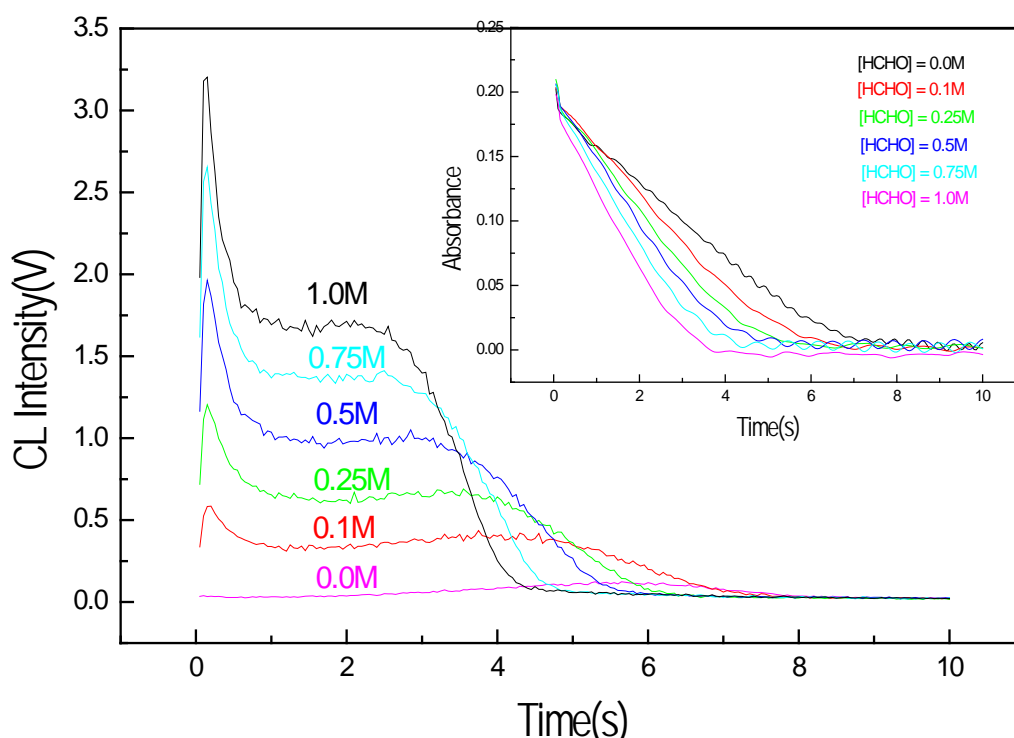


Figure 4.50 Effect of formaldehyde concentration on the kinetic of the reaction and CL signal. Experimental conditions: $[\text{C}_{22}\text{H}_{24}\text{N}_2\text{O}_8] = 0.0005\text{M}$, $[\text{MnO}_4^-] = 0.001\text{M}$, $[\text{HCHO}] = 0.0, 0.1, 0.25, 0.5, 0.75$ and 1.0M ; Temperature = 25°C , $[\text{H}_2\text{SO}_4] = 2\text{M}$, Wavelength = 525 nm ; HT (Fluorescence channel): 800V .

The experimental results in Figure 4.50 show that the addition of formaldehyde to the reaction mixture leads to an increase of the reaction rate and to an enhancement of the observed CL signal intensity. As the initial formaldehyde concentration increased, the maximum of the intensity of the CL signal gradually increased in the concentration range 0.10 – 1.0 mol dm⁻³.

According to the proposed mechanism, the effect of formaldehyde in the CL reaction of tetracycline and MnO₄⁻ is associated with the co-oxidation of formaldehyde and tetracycline to increase the concentration of Mn(III) intermediate and thus the CL emission.

4.7.1.3 Effect of glyoxal

If the observed CL response in the presence of glyoxal is a result of chemical co-oxidation of tetracycline and glyoxal to generate Mn(III) intermediate that forms excited Mn(II) species, then increasing concentrations of glyoxal should lead to an enhancement of the observed CL emission.

To examine the effects of glyoxal as enhancer, a series of univariate experiments were carried out by increasing the glyoxal concentration from 0.0 – 0.4 mol dm⁻³ at constant concentrations of other reactants.

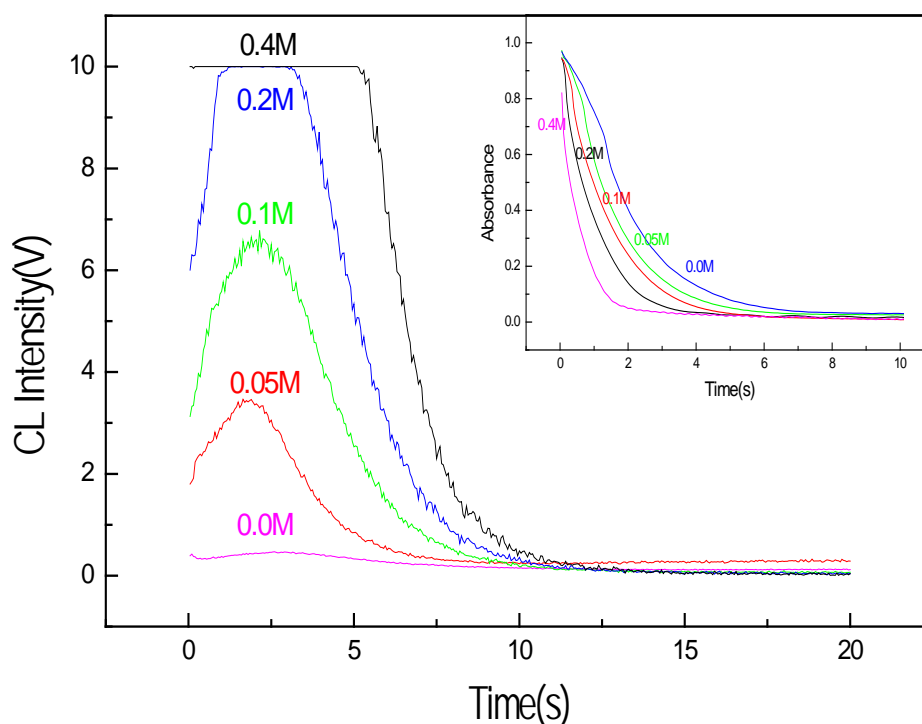


Figure 4.51 Effect of added glyoxal concentration on the kinetic of the reaction and tetracycline CL signal. Experimental conditions: [C₂₂H₂₄N₂O₈] = 0.0005M, [MnO₄⁻] = 0.01M, [OCHCHO] = 0.0, 0.05, 0.1, 0.2 and 0.4M; Temperature = 25°C, [H₂SO₄] = 2M, Wavelength = 525 nm; HT (Fluorescence channel): 800V.

The experimental results in Figure 4.51 show that the addition of glyoxal into the reaction mixture leads to a significant increase in the rate of reaction and to an enhancement of the observed CL signal intensity, which could be useful for developing suitable analytical CL-procedures.

To complement the study of the tetracycline CL potential during oxidation by KMnO_4 , the effect of added tetracycline concentration in glyoxal oxidation reaction was also examined.

A series of univariate experiments was performed, in which the tetracycline initial concentration was varied in the range 0.0 to 0.005M, while holding the initial concentrations of the glyoxal and MnO_4^- constituents constant. The concentration of glyoxal was in excess.

As seen in Figure 4.52, the addition of tetracycline concentration in glyoxal oxidation increased the rate of the reaction with subsequent increase in the CL intensity.

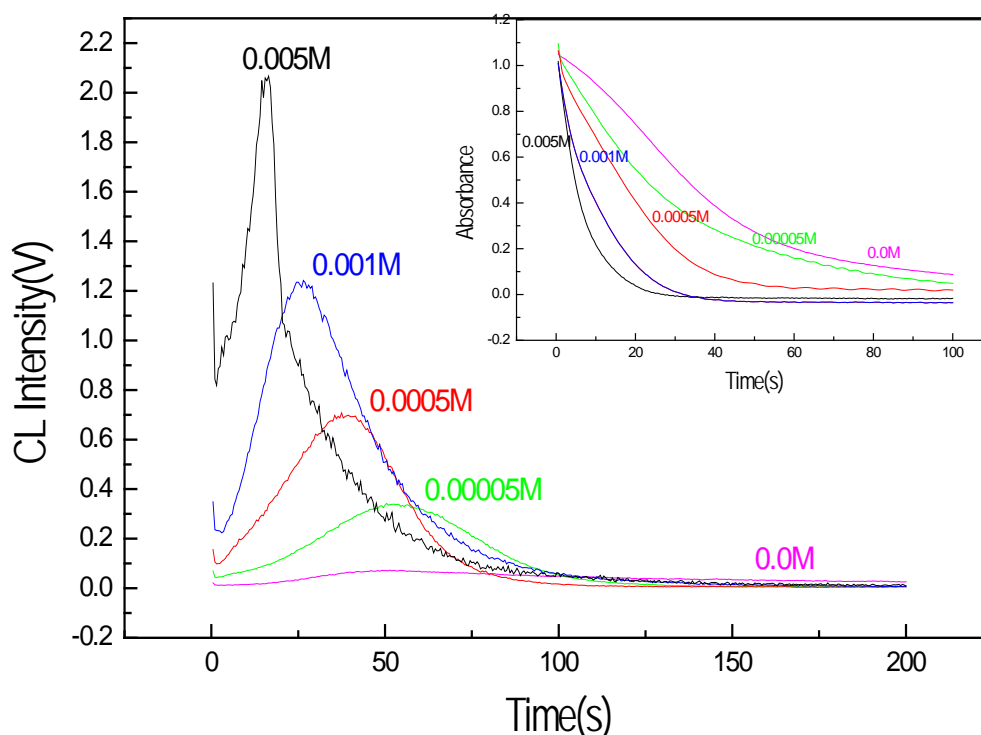


Figure 4.52 Effect of added tetracycline concentration on the kinetic of the reaction and glyoxal chemiluminescence signal. Experimental conditions: $[\text{OCHCHO}] = 0.01\text{M}$, $[\text{MnO}_4^-] = 0.005\text{M}$, $[\text{C}_{22}\text{H}_{24}\text{N}_2\text{O}_8] = 0.0, 0.00005, 0.0005, 0.001$ and 0.005M ; Temperature = 25°C , $[\text{H}_2\text{SO}_4] = 2\text{M}$, Wavelength = 525 nm ; HT (Fluorescence channel): 800V .

4.7.2 Manganese(IV) oxidation of tetracycline

The kinetics of the CL reaction between Mn(IV) and tetracycline were examined. In Figure 4.53, the Mn(IV) absorbance time course (left axis) in the reaction of 0.001M tetracycline with 0.01M Mn(IV) is compared with its corresponding CL time course (right axis).

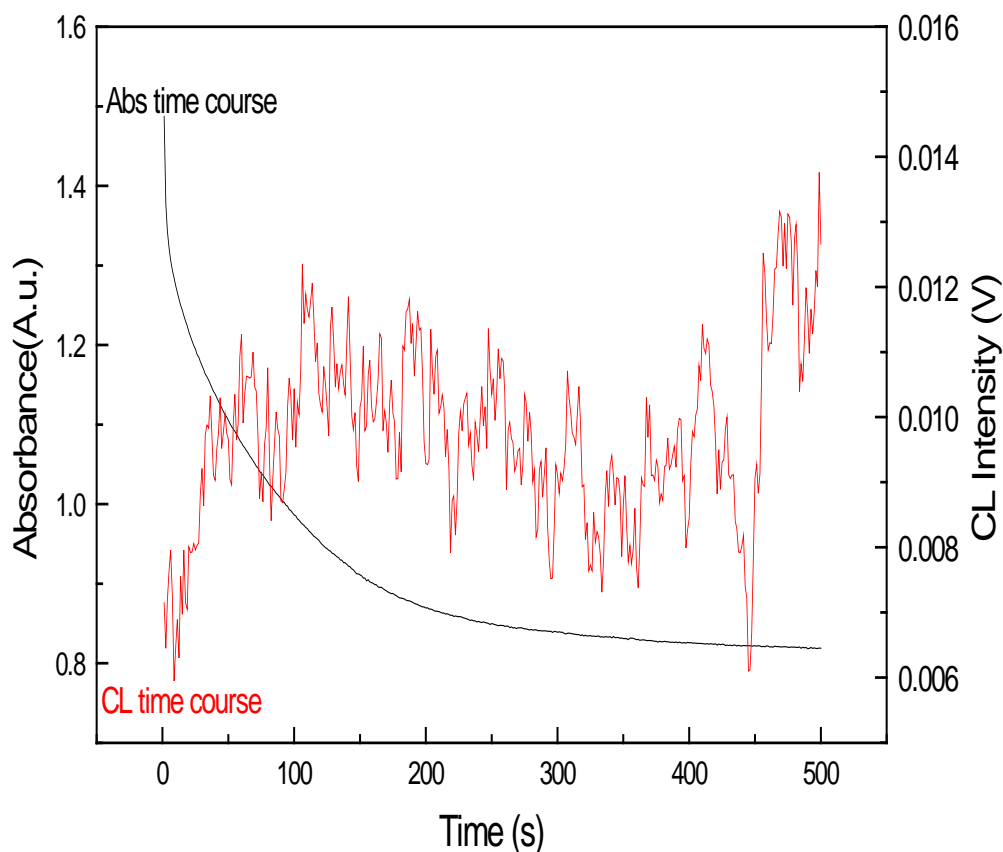


Figure 4.53 Plot comparing CL time course versus absorbance time course for Mn(IV) oxidation reaction of tetracycline. Experimental conditions: $[C_{22}H_{24}N_2O_8] = 0.001M$, $[Mn(IV)] = 0.01M$, Temperature = $25^{\circ}C$, $[H_2SO_4] = 2M$, Wavelength = 400 nm ; HT (Fluorescence channel): $800V$.

It can be seen that, under the reaction conditions, although the tetracycline reacts with manganese(IV), no significant CL emission was observed. The addition of formaldehyde is predicted to lead to an enhancement of the observed CL signal intensity.

As shown in Figure 4.54, it was found that the addition of 0.1 to 1.0M formaldehyde to tetracycline oxidation by manganese(IV) did lead to an enhancement of the observed chemiluminescence signal intensity and to an increase of the reaction rate.

The results support our hypothesis which links the observed CL response with the reaction between Mn(III) intermediate and organic substrate or organic intermediates.

It is thought that formaldehyde and tetracycline undergo a co-oxidation reaction to increase Mn(III) intermediate concentration responsible for the chemiluminescence response.

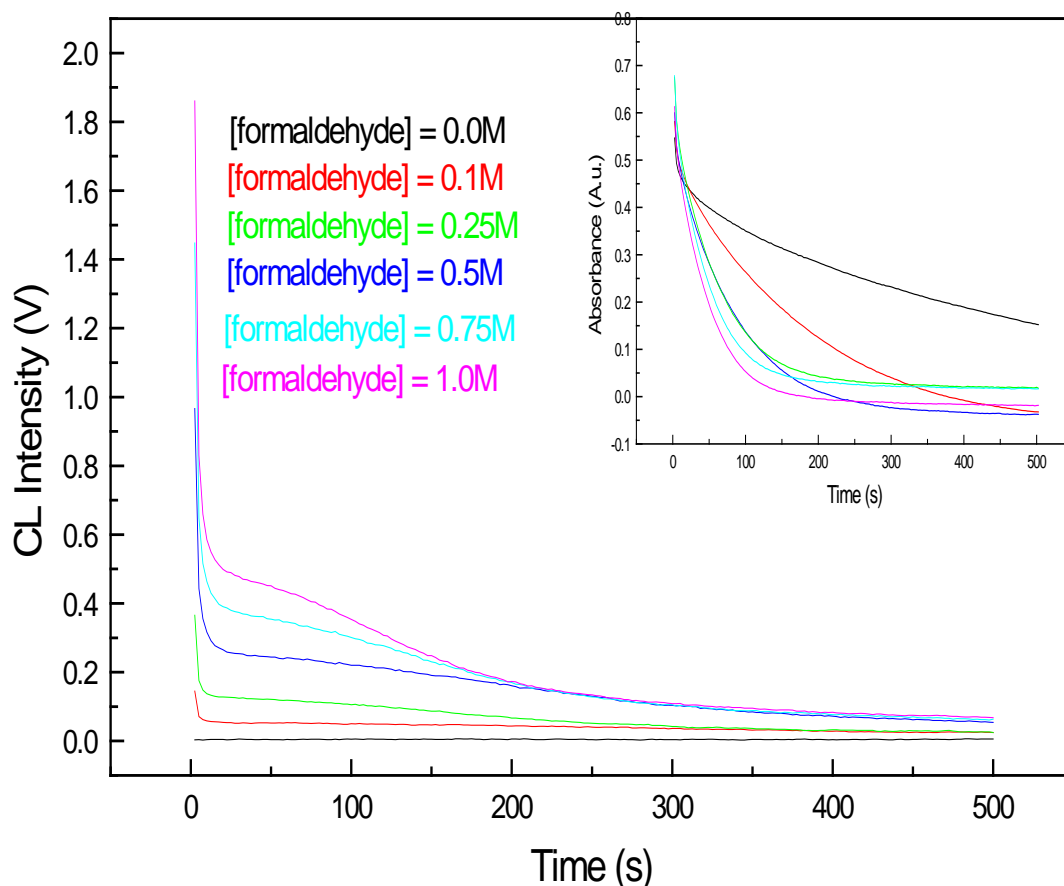


Figure 4.54 Effect of added formaldehyde concentration on the kinetic of the reaction and tetracycline chemiluminescence signal. Experimental conditions: $[C_{22}H_{24}N_2O_8] = 0.0005M$, $[Mn(IV)] = 0.01M$, $[HCHO] = 0.0, 0.1, 0.25, 0.5, 0.75$ and $1.0M$; Temperature = $25^\circ C$, $[H_2SO_4] = 2M$, Wavelength = 400 nm ; HT (Fluorescence channel): $800V$.

4.7.3 Manganese(III) oxidation of tetracycline

For additional check on the conclusion that excited Mn(II) species that emit light are formed by the reaction of Mn(III) intermediate and organic substrate or organic intermediate, univariate experiments were carried out, in which the initial Mn(III) concentration was held constant while the tetracycline concentration was varied in the range of 0.001 to $0.05M$.

The plot of the Mn(III) decay and chemiluminescence emission are given in Figure 4.55. It was found that under the reaction conditions, manganese(III) reacted very slowly with tetracycline and no measurable chemiluminescence signal was detected.

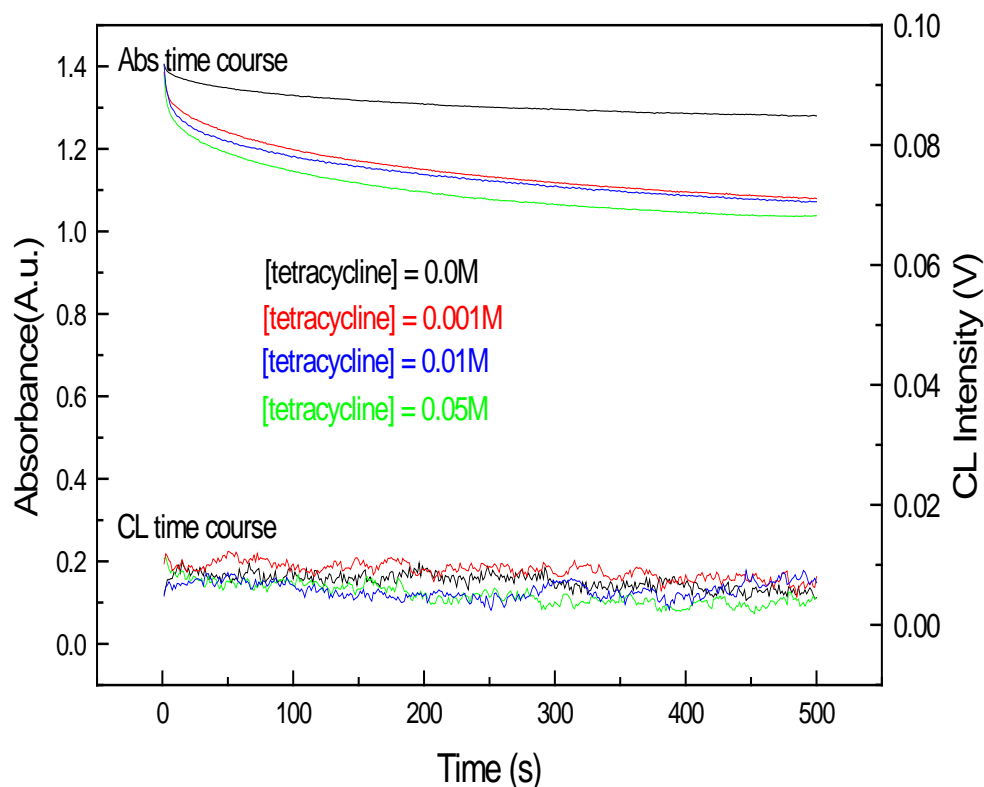


Figure 4.55 Plot comparing chemiluminescence time course versus absorbance time course for Mn(III) oxidation reaction of tetracycline. Experimental conditions: $[\text{C}_{22}\text{H}_{24}\text{N}_2\text{O}_8] = 0.001, 0.01$ and 0.05M , $[\text{Mn(III)}] = 0.05\text{M}$, Temperature = 25°C , $[\text{H}_2\text{SO}_4] = 2\text{M}$, Wavelength = 500 nm ; HT (Fluorescence channel): 800V .

This finding was unexpected although similar to metronidazole and suggests that manganese(III) cannot be responsible for the chemiluminescence. There is, however, another possible explanation for the observed chemiluminescence might be that Mn(III) reacts with organic intermediates to form excited manganese(II) species that emit light.

4.8 Pyridoxine chemiluminescence oxidation reactions

In order to confirm the validity of our working hypothesis for the light-producing pathway further, kinetic characteristics of the chemiluminescence reaction of pyridoxine and manganese-based oxidants, were investigated.

4.8.1 Permanganate oxidation of pyridoxine ($\text{C}_8\text{H}_{11}\text{NO}_3$)

Alwarthan and co-workers⁵⁷⁹ reported the chemiluminescence method using flow injection for the determination of pyridoxine hydrochloride. Its detection limit, linearity and reproducibility were examined. The method was based on the enhancing effect of pyridoxine hydrochloride on the chemiluminescence generated by the oxidation of luminol with hydrogen peroxide in aqueous potassium hydroxide and sodium oxalate.

The chemiluminescence intensity was a linear function of pyridoxine hydrochloride concentration over the range 10 - 250 $\mu\text{g ml}^{-1}$ with a detection limit of 6 $\mu\text{g ml}^{-1}$.

The applicability of the method was demonstrated by the determination of pyridoxine hydrochloride in different tablet formulations and some dietary sources.

This present study examines the oxidation of pyridoxine in sulphuric acid medium by potassium permanganate, Mn(III) and Mn(IV), with a focus on characterizing the kinetic curves of the CL emission and the reaction rates for pyridoxine-Mn(VII), pyridoxine-Mn(III) and pyridoxine-Mn(IV) systems, respectively. Preliminary studies showed that KMnO_4 solution, for example, could react with pyridoxine in the presence of sulphuric acid medium to produce CL emission.

Figure 4.56 compares typical CL emission time course and the rate of MnO_4^- absorbance for the oxidation reaction between 0.005M MnO_4^- and 0.01M pyridoxine. Stopped-flow results revealed that pyridoxine in sulphuric acid medium was rapidly oxidized by MnO_4^- and produced a considerable CL emission for developing suitable analytical CL-procedures.

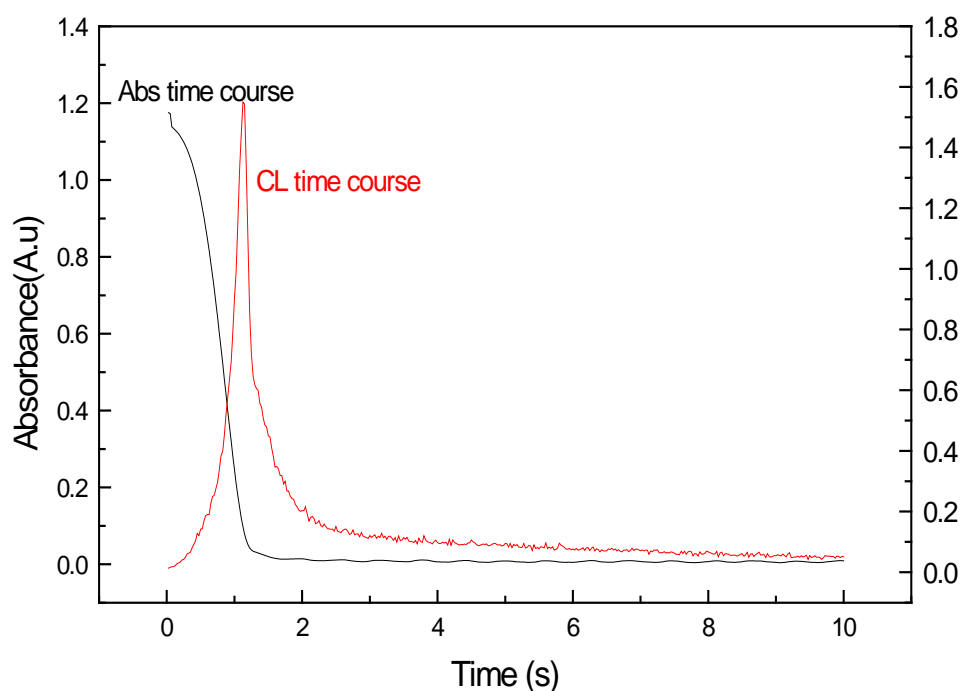


Figure 4.56 Plot comparing CL time course versus absorbance time course for MnO_4^- oxidation reaction of pyridoxine. Experimental conditions: $[\text{C}_8\text{H}_{11}\text{NO}_3] = 0.01\text{M}$, $[\text{MnO}_4^-] = 0.005\text{M}$, Temperature = 25°C , $[\text{H}_2\text{SO}_4] = 2\text{M}$, Wavelength = 525 nm; HT (Fluorescence channel): 800V.

These results also accords with our earlier observations, which showed that there is a connection between chemiluminescence curve and the reaction rate, suggesting that the observed chemiluminescence emission is the direct result of pyridoxine oxidation.

4.8.1.1 Effect of manganese(II)

In relatively weak CL system, it is possible to obtain a high sensitivity in increasing the chemiluminescence signal by introducing manganese salt in the reaction mixture.

Thus, based on these enhancement effects, Mn(II) has been extensively used in the CL analysis of a variety of compounds⁷. However, the evidence for this mechanism of the enhancement is still inconclusive⁷.

In our working hypothesis, it has been suggested that the added Mn(II) salt autocatalysis the reaction in reacting with permanganate to generate Mn(III) intermediate, which is responsible for excited manganese(II) species that emit light. The proposed hypothesis was tested by predicting the effects of Mn(II) during the pyridoxine oxidation reaction – if the added Mn(II) reacts with permanganate to generate more Mn(III) that is responsible for the chemiluminescence emission, it should be observed an increase in the reaction rate and an enhancement of the observed chemiluminescence signal intensity.

A set of experiments has been carried out to evaluate the effect of adding manganese(II) salt on the kinetics of the pyridoxine chemiluminescence reaction. The effects of manganese(II) concentration were examined by increasing Mn(II) concentration over the range 0.0001 to 0.2M and in the presence of 0.005M KMnO_4 , 0.001M pyridoxine and 2M H_2SO_4 at 25°C. The results obtained are presented in Figure 4.57.

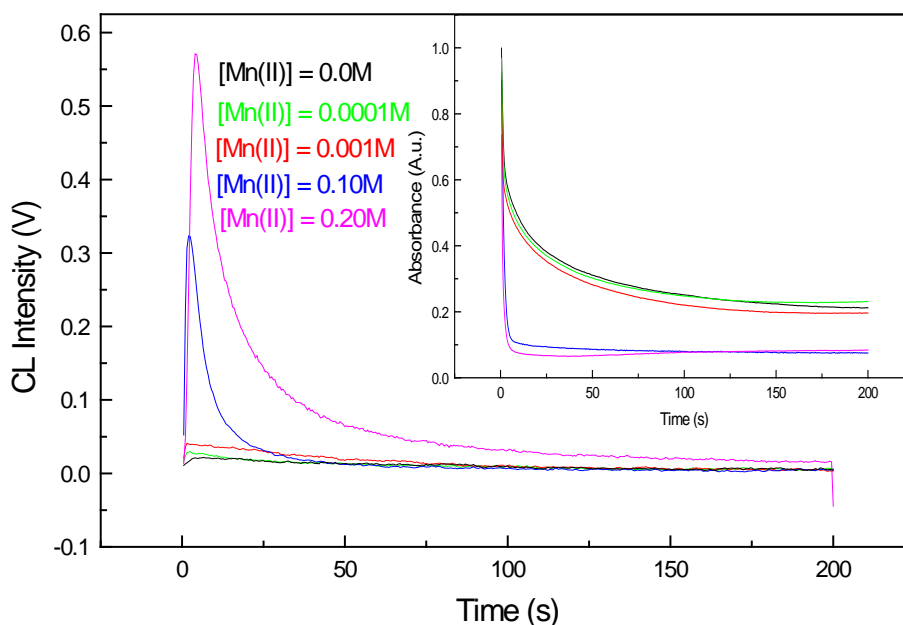


Figure 4.57 Effect of Mn(II) concentrations on the kinetic curves of the CL signal. Experimental conditions: $[\text{C}_8\text{H}_{11}\text{NO}_3] = 0.001\text{M}$, $[\text{MnO}_4^-] = 0.005\text{M}$, $[\text{Mn(II)}] = 0.0, 0.0001, 0.001, 0.1$ and 0.2M ; Temperature = 25°C, $[\text{H}_2\text{SO}_4] = 2\text{M}$, Wavelength = 525 nm; HT (Fluorescence channel): 800V.

As it can be seen in Figure 4.57, the test for the working hypothesis was successful, as it found that, under experimental conditions, the intensity of the CL signal gradually increased as Mn(II) concentration increased up to 0.001M, and then sharply increased from 0.1M. Mn(II) provided a 10 fold increase compared to chemiluminescence response from the reaction without Mn(II).

4.8.1.2 Effect of formaldehyde

It has been previously demonstrated that the presence of formaldehyde increases the CL response from oxidation reaction of many analytes with acidic MnO_4^- ^{77, 96, 110, 125, 126, 145-147, 464, 519}. It is therefore possible to test our working hypothesis for the light-producing reaction, by predicting the enhancement effect of formaldehyde on the CL signal intensity generated during the oxidation reaction between pyridoxine and MnO_4^- . If the observed enhancement effects are a result of a chemical co-oxidation reaction of the added compound, as suggested in our working hypothesis, then the addition of formaldehyde should lead to an enhancement of the observed CL signal intensity.

To evaluate the effects of formaldehyde on the CL emission produced during the MnO_4^- oxidation of pyridoxine, a series of kinetic runs were carried out by increasing the formaldehyde concentration from 0.1 – 1.0 mol dm^{-3} at constant concentrations of 0.005 M KMnO_4 , 0.001 M tetracycline, 2.0 M H_2SO_4 and at 25°C. The results are presented in the Figure 4.58.

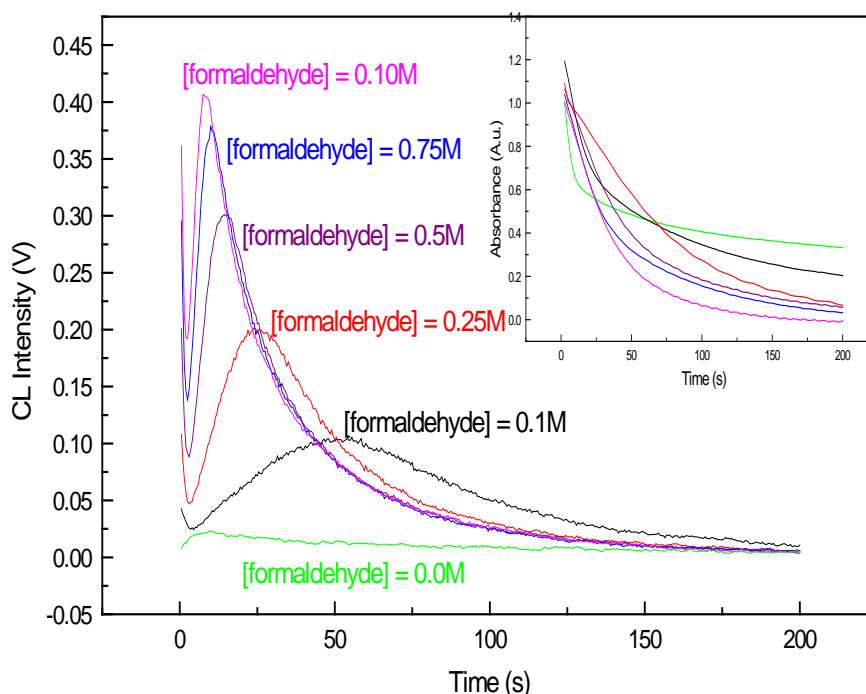


Figure 4.58 Effect of formaldehyde concentration on the kinetics of CL response versus time profile and absorbance time course. Experimental conditions: $[\text{HCHO}] = 0.1; 0.25; 0.5; 0.75$ and 1.0M , $[\text{MnO}_4^-] = 0.005\text{M}$, $[\text{C}_8\text{H}_{11}\text{NO}_3] = 0.001\text{M}$, Temperature = 25°C, $[\text{H}_2\text{SO}_4] = 2\text{M}$ and HT (Fluorescence channel): 800V.

It was found that the addition of formaldehyde lead to an enhancement of the CL signal intensity, suggesting a co-oxidation of formaldehyde to generate Mn(III) intermediate responsible for the CL emission - as the initial formaldehyde concentration increased, the CL maximum signal increased sharply in the concentration range $0.10 - 0.75 \text{ mol dm}^{-3}$.

The results of this investigation show a good correlation between the chemiluminescence signal intensity and the initial concentrations of formaldehyde. The plot of the chemiluminescence intensity as a function of the initial formaldehyde concentration (Graph not given) was linear with a correlation coefficient $R=0.998$.

These findings again confirm our working hypothesis as it confirms the involvement of formaldehyde in the light-producing pathway, according to which formaldehyde participates in the co-oxidation with pyridoxine generate more Mn(III) intermediate that is responsible for the excited manganese(II) species(Mn(II)^*) that emits light.

4.8.2 Manganese(III) oxidation of pyridoxine

Our working hypothesis suggests that Mn(III) intermediate is responsible for the CL emission, as it react rapidly with organic substrate or organic intermediates to form excited manganese(II) species(Mn(II)^*) that emits light. It was therefore essential to test our working hypothesis by examining the oxidation of pyridoxine by Mn(III), with a focus on characterizing the light-producing pathway, the kinetics of the CL emission and the reaction rate.

If a chemical oxidation reaction between Mn(III) and pyridoxine occurs and as it leads to excited Mn(II) species, it should be observed a chemiluminescence emission arises from the reaction and this will confirm the hypothesis for light-producing mechanism.

Stopped-flow experiments revealed that the oxidation of pyridoxine in sulphuric acid medium by Mn(III) illicited intense chemiluminescence. The kinetic curves of the intensity of the CL for four different concentrations of permanganate are given in Figure 4.59.

The test for the hypothesis was successful, as the results showed that the reaction between Mn(III) and pyridoxine was not only accompanied of chemiluminescence emission, but the increase in pyridoxine concentration lead to both an enhancement of the chemiluminescence signal intensity and an increase in the reaction rate (inset of Figure 4.59).

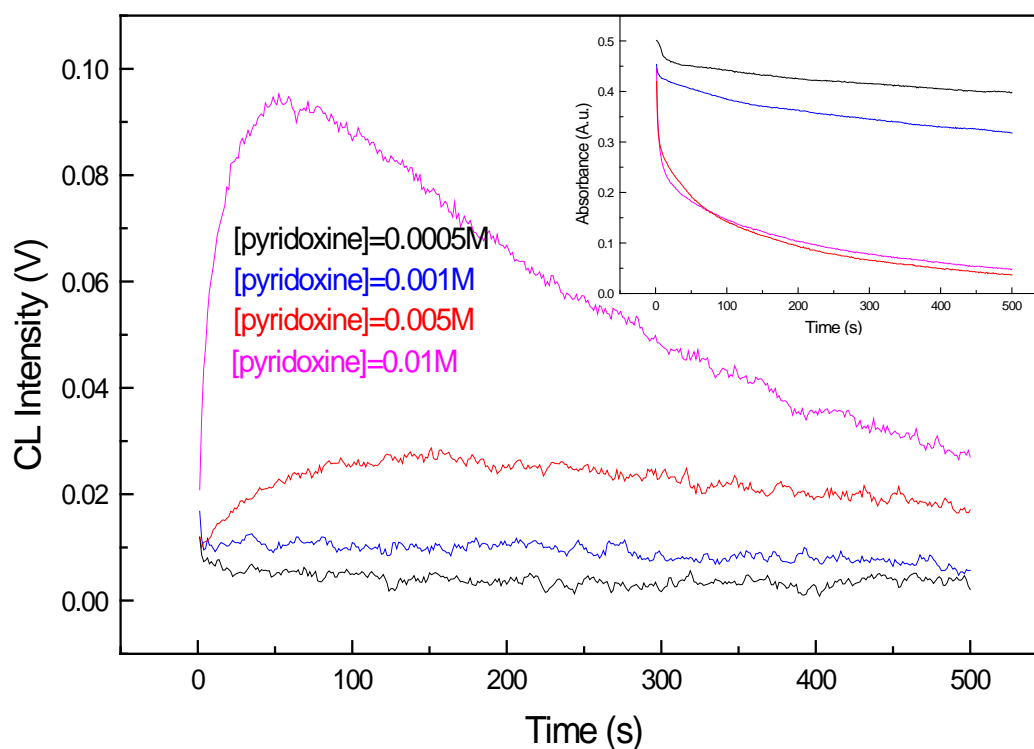


Figure 4.59 Plot of CL time course for Mn(III) oxidation reaction of pyridoxine. Experimental conditions: $[C_8H_{11}NO_3] = 0.0005, 0.001, 0.005$ and $0.01M$ $[Mn(III)] = 0.05M$, Temperature = $25^\circ C$, $[H_2SO_4] = 2M$, Wavelength = 500 nm ; HT (Fluorescence channel): $800V$.

4.8.3 Manganese(IV) oxidation of pyridoxine

Our working hypothesis also suggests that manganese(IV) is in rapid equilibrium with Mn(III) intermediate that is responsible for forming excited manganese(II) species that are responsible for the chemiluminescence emission.

To test the light-producing pathway proposed, the kinetics of CL reaction of pyridoxine with manganese(IV) was examined using a stopped-flow instrument at room temperature.

If the oxidation reaction of pyridoxine with manganese(IV) generates more Mn(III) intermediate, it should be observed more CL emission as pyridoxine concentration increases.

The chemiluminescence profiles obtained by varying the pyridoxine concentration in the range $0.0001 - 0.01M$ are presented in Figure 4.60. The experimental results demonstrated that as the concentration of pyridoxine increased, the CL signal intensity increased.

Again these results support our working hypothesis that manganese(IV) intermediate species react rapidly to generate manganese(III) that produces excited manganese(II) species responsible for the chemiluminescence emission in the course of permanganate oxidation of pyridoxine in sulphuric acid medium.

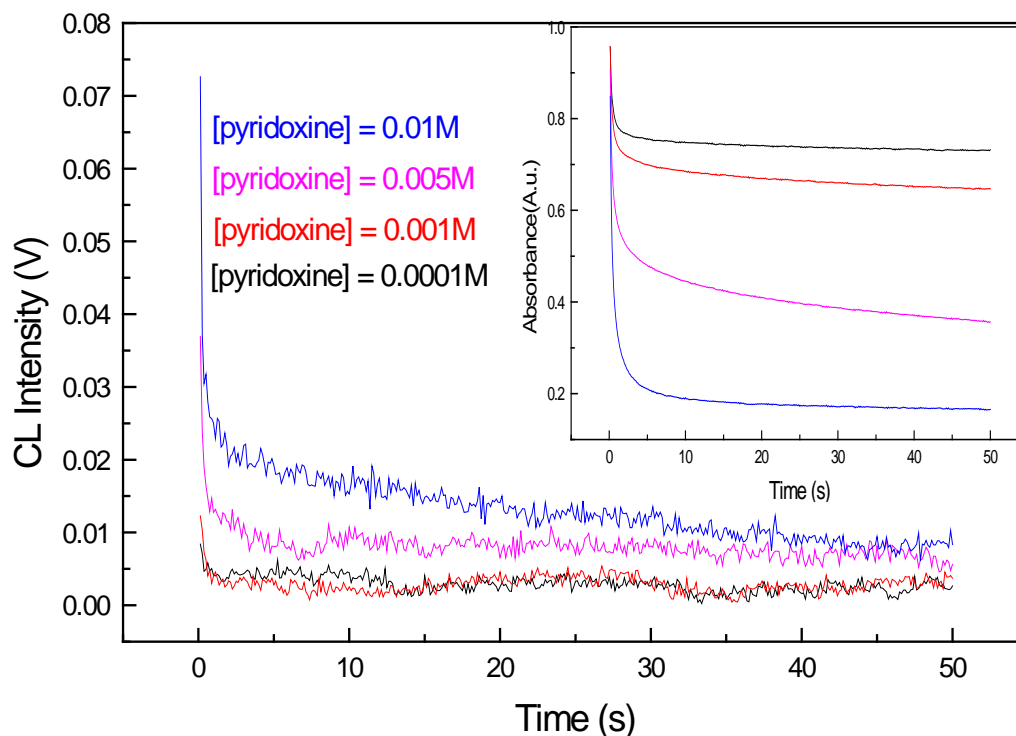


Figure 4.60 Plot of chemiluminescence time course for Mn(IV) oxidation reaction of pyridoxine. Experimental conditions: $[C_8H_{11}NO_3] = 0.0001, 0.001, 0.005$ and $0.01M$ $[Mn(IV)] = 0.01M$, Temperature = $25^\circ C$, $[H_2SO_4] = 2M$, Wavelength = 400 nm ; HT (Fluorescence channel): $800V$.

4.9 Summary

The stopped-flow experiments, involving simultaneous recording of absorbance and emission, reported in this chapter for the first time have confirmed that it is the rate of reaction which determines the profile of the chemiluminescent emission. Most reported analytical methods relate analyte concentration to the maximum observed emission on oxidation of the analyte carried out in a flow system. Under these conditions, even when the concentration of analyte does not limit the total emission, the increase in concentration will increase the rate giving a proportionality, often direct, between analyte concentration and peak height.

The results are also consistent with the hypothesis presented at the start of the chapter that enhancement is a kinetic effect and that, for oxidations by manganese species, reagents which increase the rate of formation of Mn^{3+} , increase the rate of formation of the chemiluminescence.

Other species, such as glyoxal, gallic acid and pyrogallol also show enhancement and this has again been shown to be due to an increase the rate of formation of Mn^{3+} which can then re-

act with the analyte. These enhancers do themselves react with Mn^{3+} , which means that in an analytical method the background response will increase.

Mn^{2+} reacts with permanganate to form Mn^{3+} and thus increases the rate of formation of chemiluminescence and aqueous formaldehyde reduces permanganate to Mn^{3+} without forming Mn^{2+} and thus also increases the rate of formation of chemiluminescence.

With some more complex molecules such as metronidazole and tetracycline, the interpretation is not so simple.

These molecules are not or at least very slowly oxidised by Mn^{3+} . It is possible that a two electron oxidant such as MnO_4^- is required and that the subsequent chemiluminescence arises from an intermediate oxidation product which then reacts with Mn^{3+} .

Having demonstrated the essential features of the mechanism, an attempt was next made to model the reactions in the hope that this will enable predictions to be made. The modelling is discussed in the next chapter.

Chapter 5

Modelling and Mechanism for Manganese Chemiluminescence Reactions

5.1 Introduction

It has been demonstrated in the preceding chapter that the chemiluminescence emission is a product of manganese oxidation processes and kinetics dependent. The core aim of this work is to produce a kinetic model for the chemiluminescent reactions which can then be used to predict chemiluminescence and hence used to design new analytical methods.

However, the chemistry of manganese oxidations is complex. It is well known that permanganate oxidation of organic compounds is necessarily a multistage process where the probably stepwise oxidation of organic compounds involves an overall 5-electron transition ($\text{MnO}_4^- \rightarrow \text{Mn}^{2+}$) in acid solution. Other manganese ions of intermediate oxidation states have also been observed including Mn(IV) and Mn(III). No simple mechanism has been reported in the literature. These mechanisms of manganese oxidation reactions have been covered by a number of published reviews^{329, 332, 580, 581}.

The most comprehensive study of the effect on the kinetics of different reductants with permanganate was probably by Waters and co-workers.³³² It is our view that although publication of kinetic studies of manganese oxidations has continued, none of more recent papers has added much novelty to this. This includes models involving 14 or more steps, which are still unsatisfactory⁵⁸⁰.

No previous kinetic study has included fitting observed chemiluminescence in the model but it was recognised that given the established complexity of the kinetics that only either an approximate model or one of somewhat limited applicability would be possible. Thus, in this work, we have not attempted to establish a full mechanism but rather we have looked for the simplest mechanism which would enable us to predict CL approximately.

As previously mentioned, the approach was that experiments were carried out under pseudo-first order conditions with respect to organic substrate in the hope that oxidation, in each step, is predominantly of original organic species. This does assume, however, that any initial intermediate oxidation products do not react substantially faster than the original compound. Since manganese(VI) and manganese(V) are highly unstable in acid medium and thus very difficult to monitor, they were not included in the mechanism. The same applies to manganese(IV) except where conditions under which it was stabilised have been used.

As for manganese-based chemiluminescence process, it is previously established⁹ that it is the same CL emission that arises from MnO_4^- , MnO_2 and Mn^{3+} oxidations reactions of organic species. The simplest explanation is that manganese-based CL emission is from the Mn^{3+} reduction to Mn^{2+} , although there are at least two other possible explanations.

If CL emission is from $\text{Mn}^{3+} \rightarrow (\text{Mn}^{2+})^* \rightarrow \text{Mn}^{2+}$ pathway, then the second emission step will either be very fast (rate in the range 10^6 - 10^{12} s^{-1}) if there is no change in electron spin like fluorescence or if there is electron spin rearrangement like phosphorescence, then the rate will be slower in the range 1 - 10^6 s^{-1} . The former is much more likely with both ions being high spin. Since Mn^{3+} is in a rapid equilibrium with disproportionation products MnO_2 and Mn^{2+} , there is also the possibility that MnO_2 is involved in the chemiluminescence step but this would not affect the predictions based on our model.

A third possibility is that in the oxidation reaction, an excited CO_2 product is produced which transfers its excess energy to a manganese species that then emits light. This is difficult either to prove or eliminate as the ultimate product of these oxidations will be CO_2 gas. The simplest mechanism is then as follows, where the CL arises from the second step:



It was postulated in the preceding chapter a working hypothesis, which describes the proposed mechanism of “enhanced” chemiluminescence of organic species in manganese systems as a kinetic effect. It was suggested that the mechanism of the chemiluminescence enhancement observed in the presence of a catalyst (Mn(II)) or second reactant (e.g. formaldehyde) arises by virtue of additional chemical reactions of these additives with MnO_4^- . In the former case, producing Mn^{3+} more rapidly by reaction 5.3 and in the latter case producing it more rapidly by parallel reaction 5.1. However, no quantitative data for this mechanism of this chemiluminescence enhancement were given.

Very few studies are available that provide mechanistic information on manganese CL oxidation reactions with various organic compounds. Karavaev et al.³⁹³, for example, demonstrated that the chemiluminescence emission was a result of the chemical reduction of manganese(III), and postulated that the emitter was electronically excited manganese(II).

However, these studies were focused mainly on the chemiluminescence emitting species and the lack of detailed kinetic data on the wide range of organic compounds is an impediment to expanded application of this manganese analytical technology. The meaning for this is that the mechanism such as of “enhanced chemiluminescence” of organic species in manganese systems is not fully characterized.

In this chapter the fit of the kinetic model to the experimental data and its ability to predict the CL of different reactions are evaluated. The kinetic model will allow us to determine whether the manganese CL emission is predictable for a range of organic analytes and the

systems function according to the proposed mechanism. We report here the kinetic fit to the model, mostly with glyoxal and glyoxylic acid systems.

We have not coupled this information with the flow dynamics of a flow injection analysis (FIA) system to describe the analytical response of these systems for the analysis of these organic compounds in a range of samples, although this should be relatively simple.

5.2 Modelling Permanganate Chemiluminescence System

We have used the software Berkeley Madonna v8.3.18 for Windows⁵⁸². Model simulations were run from rate equations with a time step of 20 ms and using the Runge–Kutta method for numerical integration. The experimental data were fitted by changing the three kinetic rate constants either by minimising the root mean square differences of the permanganate concentration or both the permanganate concentration and the CL. A scaling factor for CL intensity was also used since the intensity values are relative rather than absolute.

The kinetic model, as defined by Equations 5.1 to 5.3, was entered into the software for simulation with typical values of k_1 , k_2 and k_3 , to give an output such as that depicted in Figure 5.1. The rate constants k_1 and k_2 are pseudo first order as the organic reductant is in large excess and the value for k_3 is assumed to be simple bimolecular. (Other orders were considered but did not improve the fits to experimental data.) The concentration of MnO_4^- is proportional to the absorbance shown on the left ordinate axis. The concentrations of the other Mn species are shown relative to this, the line at the top of this plot confirming that the total concentration of Mn species is constant as expected. Chemiluminescence output is a separate arbitrary scale shown as the right hand ordinate axis. The shape of the MnO_4^- concentration curve is typical of an autocatalytic reaction such as this and the proposed step mechanism is the simplest that can be proposed for such observed kinetics. Involving three manganese species (MnO_4^- , Mn^{3+} and Mn^{2+}) the intermediate Mn^{3+} could be replaced by MnO_2 , but would still give similar results and would be less compatible with chemical knowledge of these oxidations under acid conditions. The relative concentrations of Mn^{3+} and Mn^{2+} are shown but as these have much lower extinction coefficients than MnO_4^- , it was not possible to observe these experimentally in the case of the MnO_4^- reactions. If the CL arises from an excited Mn^{2+} species, then as explained above, since the decay is likely to be faster than the formation, then the CL signal will be proportional to the rate of reaction of Mn^{3+} , which is in turn proportional to the $[\text{Mn}^{3+}]$. The accuracy of this kinetic model for predicting permanganate CL systems was tested and validated by comparing the model prediction with the experimental data for two representative cases of permanganate oxidation CL systems, in which glyoxylic acid and glyoxal are the main organic reductants in the absence or in the presence of additives such as catalyst manganese(II) or reactant enhancer formaldehyde. The comparison was carried out by fitting the experimental data for permanganate absorbance and comparing the CL profile with the CL experimental data. The obtained results are shown in Figures 5.2 – 5.7.

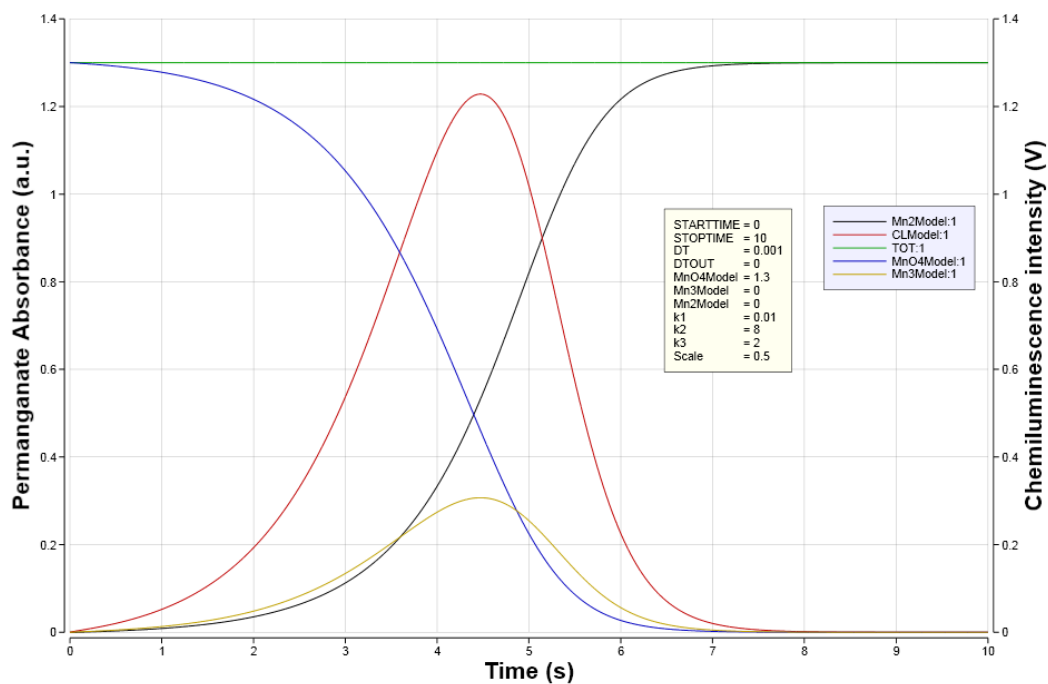


Figure 5.1 Simulation run of proposed kinetic models for permanganate CL oxidations

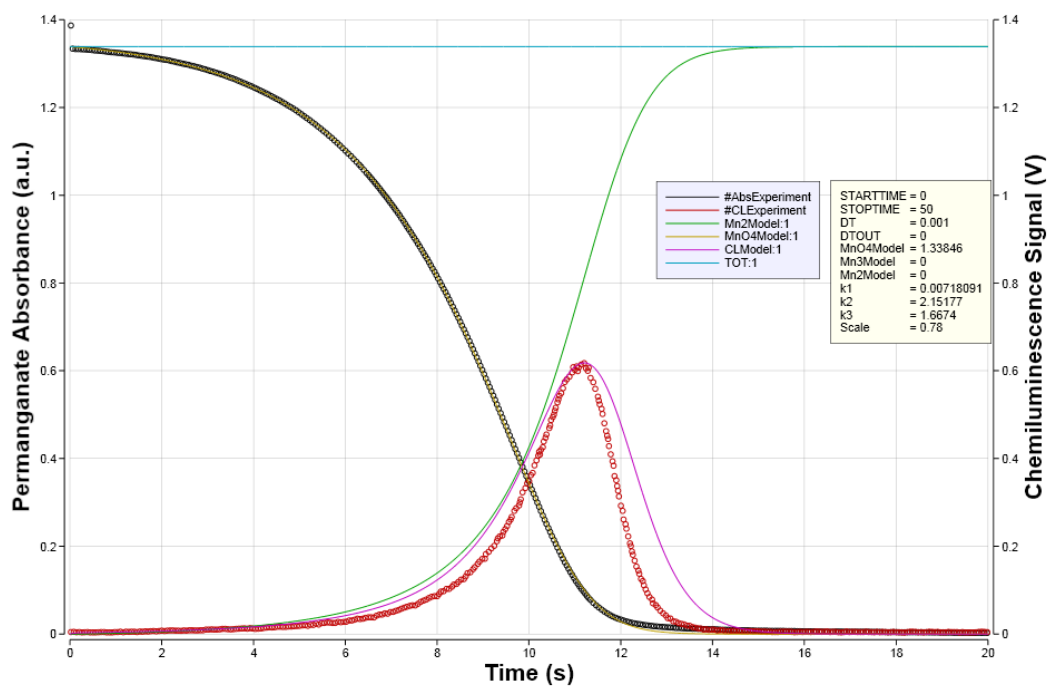


Figure 5.2 Comparison of kinetic model predictions (line curves) and experimental data (circle curves) - CL and absorbance time courses for MnO_4^- oxidation reaction of glyoxylic Acid. Reaction experimental conditions: $[\text{OCHCO}_2\text{H}] = 0.1\text{M}$; $[\text{MnO}_4^-] = 0.005\text{ M}$; $[\text{H}_2\text{SO}_4] = 2\text{M}$; Temperature = 25°C ; Wavelength = 525 nm

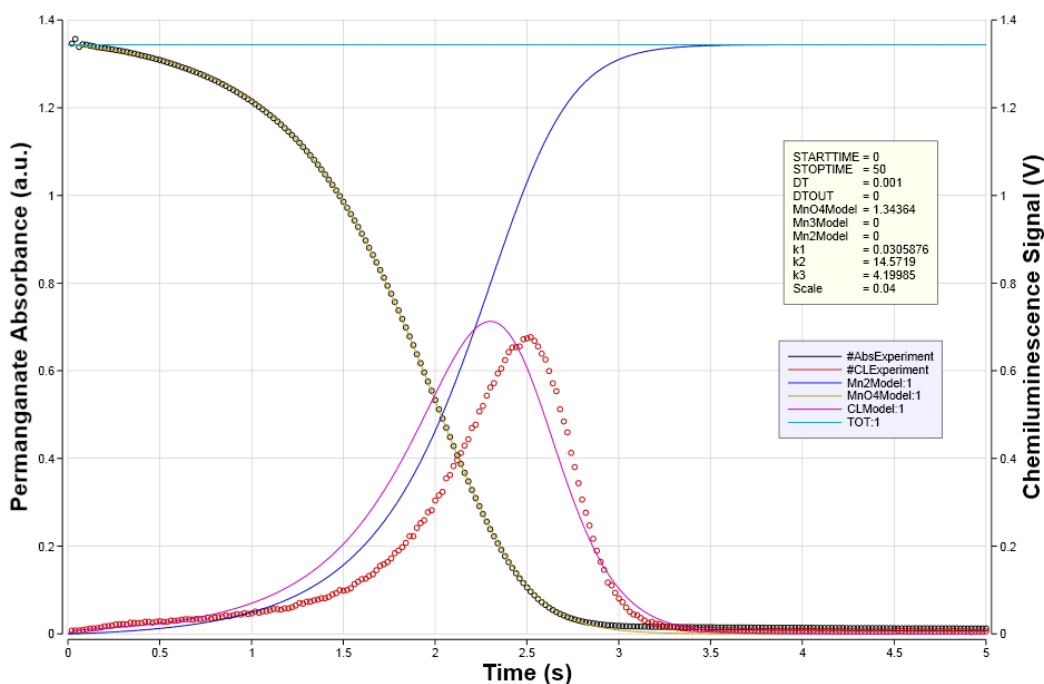
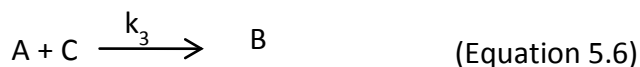
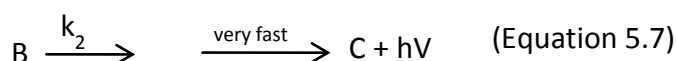


Figure 5.3 Comparison of kinetic model predictions (line curves) and experimental data (circle curves) - CL and absorbance time courses for KMnO_4 oxidation reaction of glyoxal. Reaction experimental conditions: $[\text{OCHCHO}] = 0.2\text{M}$; $[\text{MnO}_4^-] = 0.005\text{ M}$; $[\text{H}_2\text{SO}_4] = 2\text{M}$; Temperature = 25°C ; Wavelength = 525 nm .

In both Figures 5.2 and 5.3, the disappearance of MnO_4^- (it has got a strong absorbance and is easy to measure) follows a sigmoidal curve typical of an autocatalytic reaction, and a good fit to the sigmoidal decay of permanganate is observed. This confirms that the reaction is autocatalytic fitted by the general mechanism:



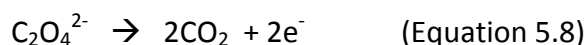
For the chemiluminescence it can be noted that predicted CL profiles are of the observed shape, although the maxima differ by about one second. This provides reasonable support for our model, in which the CL producing step is:



It has been observed that formaldehyde does not react with manganese(III) at an appreciable rate, therefore, the reaction goes no further than this species, and no induction period is observed in the kinetics.

This implies that B in the general mechanism, represents Mn^{3+} and hence C is Mn^{2+} , which confirms the chemical kinetic model as suggested by equations 5.1 – 5.3.

Identifying a mechanism for permanganate oxidations has long provided a challenge. One of the most studied reactions is that of oxalate with MnO_4^- . This is a slow reaction, used in qualitative analysis for many years, for which there can only be very few intermediate organic products before CO_2 .



Micheau and co-workers have suggested a fourteen step mechanism³⁴⁷, but under other conditions, this has been shown not to be valid⁵⁸⁰. The difficulty in kinetics modelling is the complexity of the system along with the limited number of measurements which could be made (usually absorbance) and the difficulty of monitoring organic species.

5.2.1 Rate constants dependence on glyoxal and glyoxylic acid concentrations

In preceding chapter, it was established that both the intensity of the CL signal and the rate of some of the reactions increased as the glyoxal, glyoxylic acid or MnO_4^- concentration increased. In the proposed mechanism, k_1 and k_2 are pseudo first order rate constants and the observed constants should be dependent upon the concentration of organic reductant.

The third proposed step does not involve the reductant and thus this rate constant is predicted to be independent of reductant concentration. To test these predictions, experiments were conducted in which the MnO_4^- concentration for each trial was held constant while the initial organic reductant concentration was varied.

Glyoxal and glyoxylic acid concentrations were chosen to allow the reactions to proceed within a reasonable time frame and produce a measurable CL signal.

The first set of experiments was conducted with an initial permanganate concentration of 0.005M and the initial glyoxal concentration was varied between 0.05 and 0.8M.

The observed reaction rate constants were determined from the kinetic model. Reaction conditions and estimated rate constants are given in Table 5.1 and plots of rate constants versus glyoxal concentration are shown in Figure 5.4.

Table 5.1 Experimental reaction conditions for permanganate oxidation of glyoxal and estimated reaction rate constants.

Non-variables conditions of the reaction	Variables factors: [OCHCHO]/(M)	$k_1(s^{-1})$	$k_2 (s^{-1})$	$k_3 (s^{-1})$
[KMnO ₄] = 0.005M; T° = 25°C; [H ₂ SO ₄]=2M	0.05	0.012	4.80	0.95
[KMnO ₄] = 0.005M; T° = 25°C; [H ₂ SO ₄]=2M	0.10	0.019	8.40	2.00
[KMnO ₄] = 0.005M; T° = 25°C; [H ₂ SO ₄]=2M	0.20	0.031	14.6	4.20
[KMnO ₄] = 0.005M; T° = 25°C; [H ₂ SO ₄]=2M	0.40	0.055	21.7	8.30
[KMnO ₄] = 0.005M; T° = 25°C; [H ₂ SO ₄]=2M	0.80	0.086	34.3	14.0

To estimate the order of the dependence of the pseudo first order rate constants upon glyoxal concentration, the rate constants from the model were plotted versus concentration of glyoxal as a log-log plot in Figure 5.4. If a pseudo first order rate constant, $k_i = k_i' [OCHCHO]^n$, then the plot of $\log(k_i)$ versus $\log([OCHCHO])$ will have a slope of n . The proposed model predicts that the order for k_1 and k_2 will be one and for k_3 will be zero.

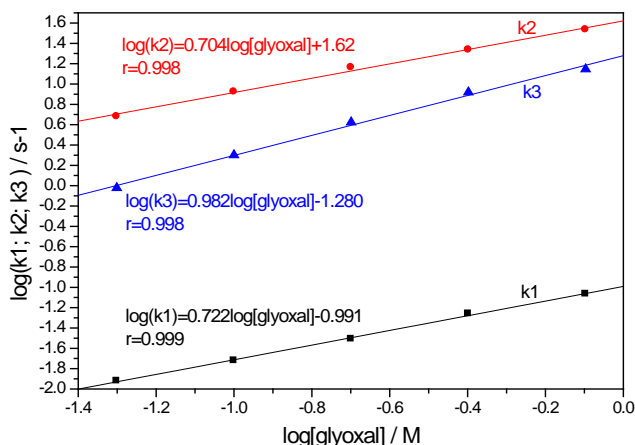
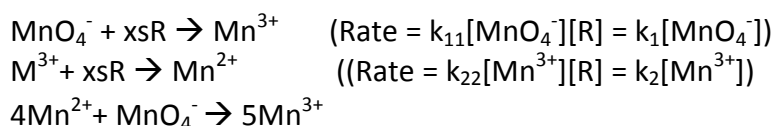


Figure 5.4 Plots and fittings showing the dependence of reaction rate constants (k_1 , k_2 , k_3) on [OCHCHO]. Reaction conditions: [KMnO₄] = 0.005M; Temperature = 25°C; [H₂SO₄]=2M; [OCHCHO]= 0.05 – 0.8M.

As it can be seen from the Table 5.1 above, all three rate constants k_1 , k_2 , and k_3 from the proposed mechanism based on a fit to the absorbance of MnO_4^- increased with increase in the glyoxal concentration. The slopes of the log-log plots give the order in glyoxal concentration. The values 0.72 and 0.70 are in reasonable agreement with that of 1.0 predicted for a second order reaction under pseudo first order conditions.



The dependence of the last reaction upon concentration of reductant (R) is a surprise, as the equation given does not include R. This dependence is close to unity at 0.98. This is clearly a complex reaction involving as it does a four electron change for permanganate. In the model, it has been assumed that the rate determining step is second order (i.e. rate = $k_3[\text{Mn}^{2+}][\text{MnO}_4^-]$). The introduction of a variable order term did not significantly change the fit and was not pursued. The dependence upon R concentration could imply that the reaction does not involve permanganate directly but a reduced species, even MnO_2 which is known to be in a reversible equilibrium with Mn^{2+} to form Mn^{3+} .

The observed fractional-order dependence on glyoxal concentration for k_1 and k_2 , could be due to measurement uncertainty, an incorrect overall mechanism or additional reaction with a partially oxidised species, which reacts more rapidly than glyoxal itself.

In the last case, as glyoxal concentration increases, the proportion of this intermediate will decrease so the increase in the reaction rate will be less than first order as observed.

In the second set of experiments, the initial permanganate concentration was held constant at 0.005M and the initial glyoxylic acid concentration was varied between 0.005 and 0.8M. The initial reaction rate constants were determined from the kinetic model as shown in Figure 5.2. Reaction conditions and estimated rate constants are given in Table 5.2 and plots of log (rate constant) versus log (glyoxal concentration) are shown in Figure 5.5.

Table 5.2 Experimental reaction conditions for permanganate oxidation of glyoxylic acid and estimated reaction rate constants.

Non-variables conditions of the reaction	Variables factors: [OCHCO ₂ H]/(M)	$k_1(\text{s}^{-1})$	$k_2(\text{s}^{-1})$	$k_3(\text{s}^{-1})$
[KMnO ₄] = 0.005M; T° = 25°C; [H ₂ SO ₄]=2M	0.05	0.0040	1.72	1.48
[KMnO ₄] = 0.005M; T° = 25°C; [H ₂ SO ₄]=2M	0.10	0.0072	2.15	1.67
[KMnO ₄] = 0.005M; T° = 25°C; [H ₂ SO ₄]=2M	0.20	0.013	2.53	1.95
[KMnO ₄] = 0.005M; T° = 25°C; [H ₂ SO ₄]=2M	0.40	0.025	2.60	2.51
[KMnO ₄] = 0.005M; T° = 25°C; [H ₂ SO ₄]=2M	0.80	0.050	2.37	3.36

To graphically illustrate the obtained results presented in table 5.2 above, the experimental data of k_1 , k_2 , k_3 of the reactions monitored by visible absorbance were plotted versus glyoxylic acid concentration, again as log-log plots.

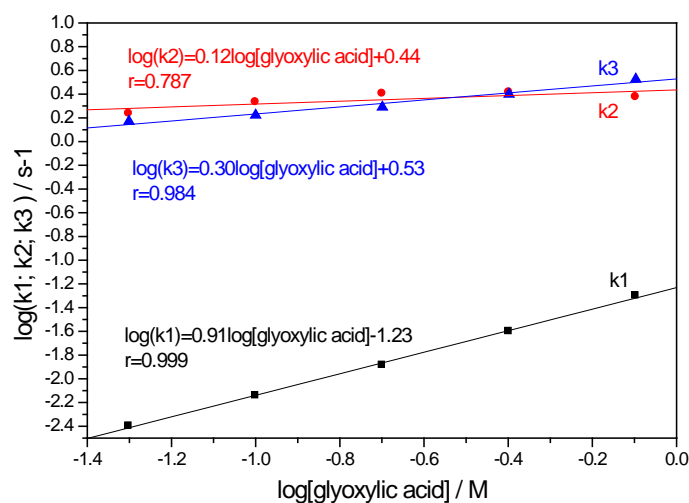


Figure 5.5 Plots and fittings showing the dependence of reaction rate constants (k_1 , k_2 , k_3) on [glyoxylic acid]. Reaction conditions: $[KMnO_4] = 0.005M$; Temperature = $25^\circ C$; $[H_2SO_4] = 2M$; $[OCHCO_2H] = 0.05 - 0.8M$.

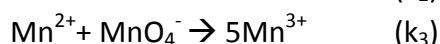
These results are less clear cut than those for glyoxal. The dependence of k_1 upon reductant concentration is 0.91, fitting well with the proposed mechanism. The observed rate constant k_2 , increases only at the lowest concentrations and the dependence upon reductant for k_3 is 0.30.

It is difficult to draw any definite conclusion from these results, although they do imply that the mechanism is more complicated than that proposed and the difference between the two reductants might suggest that the reductant itself has a more significant role that has been assumed.

5.2.2 Rate constants dependence on formaldehyde concentration

In the preceding chapter, it was demonstrated that the addition of a reactant additive such as formaldehyde in the reaction mixture increased the reaction rate and enhanced chemiluminescence emission.

However, the reaction between formaldehyde and permanganate does not exhibit chemiluminescence. This is because the second reaction in the proposed kinetic model either does not occur or is very slow (k_2 very small) but does enhance CL emission signal as the concentration of Mn^{3+} increases through the first reaction.



Therefore, it is expected that the addition of formaldehyde will show simple pseudo first order decay with no induction.

Combining rate constants obtained from glyoxal or glyoxylic acid and formaldehyde oxidations should give a good fit with observed rates from the mixture of reductants. Although there are complications due to the fact MnO_4^- is measured at 525nm while Mn^{3+} has λ_{max} at 500nm (although ϵ much lower), build-up of Mn^{3+} with formaldehyde means the absorbance of Mn^{3+} is significant.

Figures 5.6 and 5.7 show the comparison of numerical computations with the experimental data obtained from acidic permanganate oxidation of glyoxal and glyoxylic acid in the presence of formaldehyde as an enhancer using the proposed chemical kinetic model that accounts the reaction between formaldehyde and permanganate by adding the individual rate constants together .

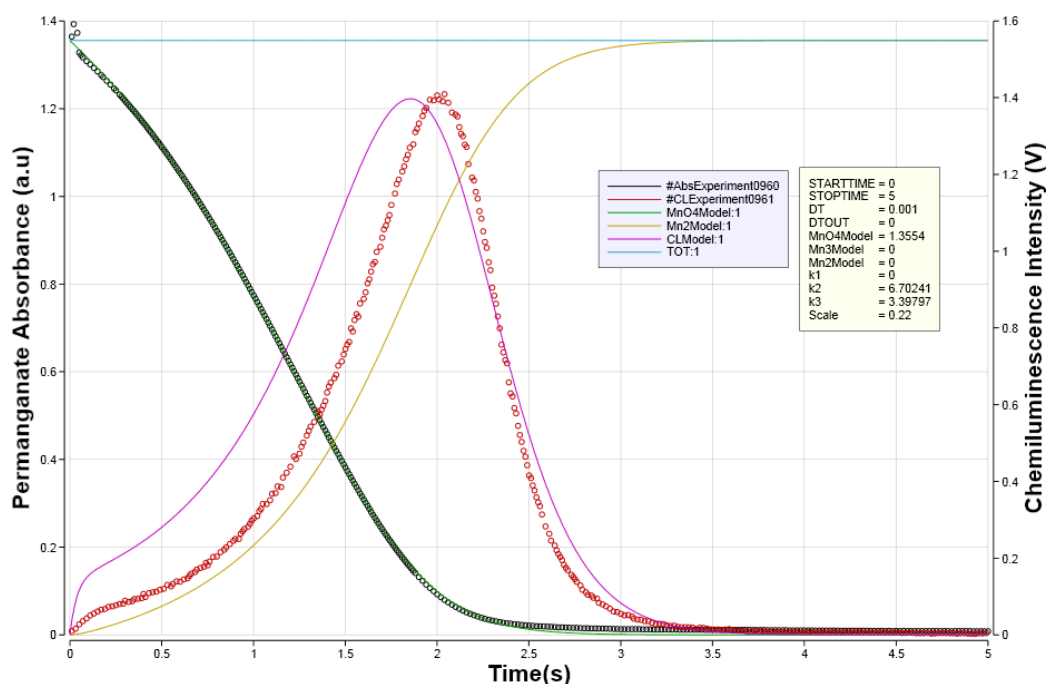


Figure 5.6 Comparison of kinetic model predictions (line curves) and experimental data (circle curves) - Chemiluminescence and Absorbance time courses for KMnO_4 oxidation reaction of glyoxylic acid in the presence of formaldehyde. Reaction experimental conditions: $[\text{HCHO}] = 0.8\text{M}$; $[\text{OCHCO}_2\text{H}] = 0.1\text{M}$; $[\text{KMnO}_4] = 0.005\text{ M}$; $[\text{H}_2\text{SO}_4] = 2\text{M}$; Temperature = 25°C ; Wavelength = 525 nm.

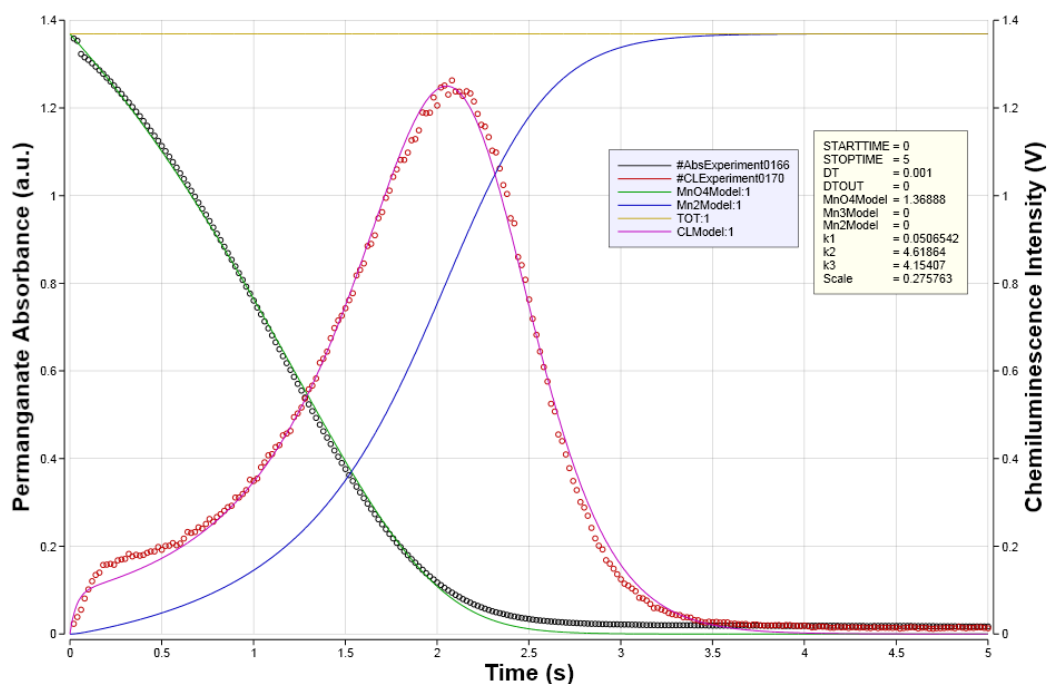


Figure 5.7 Comparison of kinetic model predictions (line curves) and experimental data (circle curves) - CL and absorbance time courses for KMnO_4 oxidation reaction of glyoxal in the presence of formaldehyde as enhancer. Reaction experimental conditions: $[\text{HCHO}] = 0.8\text{M}$; $[\text{OCHCHO}] = 0.1\text{M}$; $[\text{KMnO}_4] = 0.005\text{ M}$; $[\text{H}_2\text{SO}_4] = 2\text{M}$; Temperature = 25° C ; Wavelength = 525 nm .

As expected, the addition of formaldehyde as enhancer increased the reaction rate and the CL response, and both predicted profiles for permanganate consumption and chemiluminescence emission agreed very well with measured profiles. This represents a significant advance in the understanding of the mechanism of the CL enhancement for permanganate oxidation.

Table 5.3 below compares the predicted rate k_1 obtained from the sum of k_1 from permanganate oxidation of formaldehyde and glyoxal, respectively, with the experimental rate k_1 from the mixture of formaldehyde and glyoxal.

Table 5.3 Comparison of predicted rate k_1 with the mixture experimental rate k_1 for permanganate oxidation of glyoxal with and without formaldehyde.

Reaction Conditions	k_1 (s^{-1})
0.005M $KMnO_4$ and 0.1M Formaldehyde only	0.043
0.005M $KMnO_4$ and 0.1M glyoxal only	0.019
Predicted k_1 (0.043 + 0.019)	0.062
Experimental k_1 for 0.005M $KMnO_4$ and 0.1M Formaldehyde and 0.1M glyoxal	0.061
0.005M $KMnO_4$ and 0.2M Formaldehyde only	0.080
0.005M $KMnO_4$ and 0.1M glyoxal only	0.019
Predicted k_1 (0.080 + 0.019)	0.099
Experimental k_1 for 0.005M $KMnO_4$ and 0.2M Formaldehyde and 0.1M glyoxal	0.095
0.005M $KMnO_4$ and 0.4M Formaldehyde only	0.149
0.005M $KMnO_4$ and 0.1M glyoxal only	0.019
Predicted k_1 (0.149 + 0.019)	0.168
Experimental k_1 for 0.005M $KMnO_4$ and 0.4M Formaldehyde and 0.1M glyoxal	0.166
0.005M $KMnO_4$ and 0.8M Formaldehyde only	0.284
0.005M $KMnO_4$ and 0.1M glyoxal only	0.019
Predicted k_1 (0.284 + 0.019)	0.303
Experimental k_1 for 0.005M $KMnO_4$ and 0.8M Formaldehyde and 0.1M glyoxal	0.270
0.005M $KMnO_4$ and 1.6M Formaldehyde only	0.552
0.005M $KMnO_4$ and 0.1M glyoxal only	0.019
Predicted k_1 (0.552 + 0.019)	0.571
Experimental k_1 for 0.005M $KMnO_4$ and 1.6M Formaldehyde and 0.1M glyoxal	0.553

It can be seen from Table 5.3 that the sum of k_1 values for reactions 0.005M $KMnO_4$ and 0.1M formaldehyde only and with 0.1M glyoxal only is the same as for the permanganate oxidation of their mixture. The predicted rate is as expected equal to that expected from a mixture of the experimental rates ($k_1 = 0.061 s^{-1}$ compared with $k_1 = 0.062 s^{-1}$).

A similar experiment was carried out for permanganate oxidation of glyoxylic acid with and without formaldehyde and the obtained results are summarized in Table 5.4.

Table 5.4 Comparison of predicted rate k_1 with the mixture experimental rate k_1 for permanganate oxidation of glyoxylic acid with and without formaldehyde.

Reaction Conditions	k_1 (s^{-1})
0.005M $KMnO_4$ and 0.1M Formaldehyde only	0.0430
0.005M $KMnO_4$ and 0.1M glyoxylic acid only	0.0072
Predicted k_1 (0.043 + 0.0072)	0.0473
Experimental k_1 for 0.005M $KMnO_4$ and 0.1M Formaldehyde and 0.1M glyoxylic acid	0.0486
0.005M $KMnO_4$ and 0.2M Formaldehyde only	0.080
0.005M $KMnO_4$ and 0.1M glyoxylic acid only	0.0072
Predicted k_1 (0.080 + 0.0072)	0.0874
Experimental k_1 for 0.005M $KMnO_4$ and 0.2M Formaldehyde and 0.1M glyoxylic acid	0.0920
0.005M $KMnO_4$ and 0.4M Formaldehyde only	0.149
0.005M $KMnO_4$ and 0.1M glyoxylic acid only	0.0072
Predicted k_1 (0.149 + 0.0072)	0.156
Experimental k_1 for 0.005M $KMnO_4$ and 0.4M Formaldehyde and 0.1M glyoxylic acid	0.158
0.005M $KMnO_4$ and 0.8M Formaldehyde only	0.284
0.005M $KMnO_4$ and 0.1M glyoxylic acid only	0.0072
Predicted k_1 (0.284 + 0.0072)	0.291
Experimental k_1 for 0.005M $KMnO_4$ and 0.8M Formaldehyde and 0.1M glyoxylic acid	0.293
0.005M $KMnO_4$ and 1.6M Formaldehyde only	0.552
0.005M $KMnO_4$ and 0.1M glyoxylic acid only	0.0072
Predicted k_1 (0.552 + 0.0072)	0.56
Experimental k_1 for 0.005M $KMnO_4$ and 1.6M Formaldehyde and 0.1M glyoxylic acid	0.51

This demonstrates the increase in the overall reaction with glyoxal or glyoxylic acid in the presence of formaldehyde. It confirms that reaction with formaldehyde goes only as far as Mn^{3+} . It also confirms that although reaction of formaldehyde with MnO_4^- is slow, it is faster than corresponding reaction (k_1) with glyoxal. The faster reaction explains the increased CL as normally measured in a flow system.

These results confirmed the early conclusion that there is a co-oxidation reaction (or competitive oxidation) of formaldehyde and organic substrate that speeds up the consumption of permanganate, thereby the reaction rate to generate transient manganese(III) intermediate, which is suggested to be a precursor for the observed chemiluminescence process.

The proposed CL enhancement mechanism was studied further by varying the reaction conditions for MnO_4^- oxidations of the mixture of formaldehyde with glyoxal and glyoxylic acid, respectively. Experiments were conducted in which the MnO_4^- as well as glyoxal and glyoxylic acid concentrations for each trial were held constant while the initial formaldehyde concentration was varied.

In this case we expect that the increase in rate constant over the underlying rate constant should be directly proportional to the formaldehyde concentration for k_1 . We expect to see an increase in k_2 because the Mn^{3+} concentration has increased and, in the mechanism as written, no change in k_3 .

Table 5.5 Experimental reaction conditions for permanganate oxidation of glyoxal in the presence of formaldehyde and estimated reaction rate constants.

Non-variables conditions of the reaction	Variables factors [HCHO] / (M)	Rate Constant for Eq. 1		Rate Constant for Eq. 2		Rate Constant for Eq. 3	
		$k_1(s^{-1})$	$k_1(s^{-1})$	$k_2 (s^{-1})$	$k_2(s^{-1})$	$k_3 (s^{-1})$	$k_3(s^{-1})$
			- 0.019		- 8.43		- 2.03
[OCHCHO] = 0.1M; [KMnO ₄]=0.005M; T° = 25°C; [H ₂ SO ₄]=2M	0.0	0.019	0.0	8.43	0.0	2.03	0.0
[OCHCHO] = 0.1M; [KMnO ₄]=0.005M; T° = 25°C; [H ₂ SO ₄]=2M	0.1	0.062	0.043	9.60	1.17	2.37	0.34
[OCHCHO] = 0.1M; [KMnO ₄]=0.005M; T° = 25°C; [H ₂ SO ₄]=2M	0.2	0.095	0.076	10.4	1.97	2.26	0.23
[OCHCHO] = 0.1M; [KMnO ₄]=0.005M; T° = 25°C; [H ₂ SO ₄]=2M	0.4	0.166	0.147	13.8	5.37	2.20	0.17
[OCHCHO] = 0.1M; [KMnO ₄]=0.005M; T° = 25°C; [H ₂ SO ₄]=2M	0.8	0.270	0.251	16.0	7.57	1.97	-0.06
[OCHCHO] = 0.1M; [KMnO ₄]=0.005M; T° = 25°C; [H ₂ SO ₄]=2M	1.6	0.462	0.443	22.6	14.17	1.81	-0.22

A series of experiments was conducted with initial permanganate concentration of 0.005M, initial glyoxal concentration of 0.1M. The initial formaldehyde concentration was varied be-

tween 0.1 and 1.6M. The reaction rate constants were determined from the kinetic model with typical fit shown in Figure 5.7. Reaction conditions and estimated rate constants are given in Table 5.5 and plots of rate constants versus glyoxal concentration are shown in Figure 5.10 above.

To graphically illustrate the obtained results presented in table 5.5 above, the experimental data of k_1 , k_2 , k_3 of the reactions monitored by absorbance were plotted versus formaldehyde concentration.

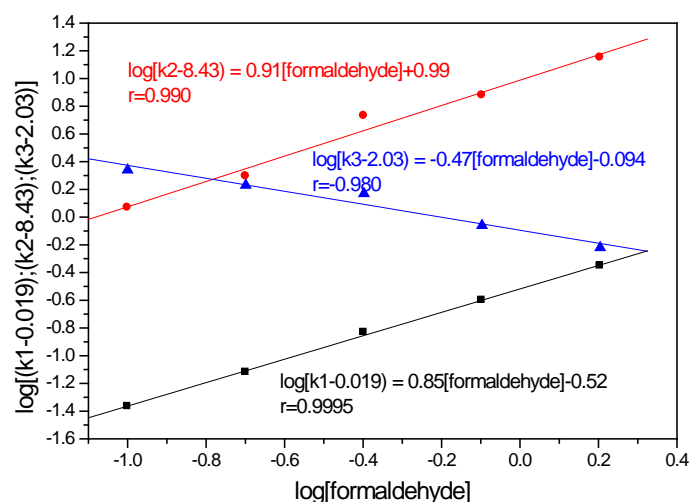


Figure 5.8 Plots and fittings showing the dependence of reaction rate constants (k_1 , k_2 , k_3) on [formaldehyde]. Reaction conditions: [HCHO] = 0.1–1.6M; Temperature = 25°C; [H₂SO₄] = 2M; [OCHCHO] = 0.1M.

It can be seen that for the glyoxal – formaldehyde mixtures, the dependence of rate constant (k_1) upon formaldehyde has an order in formaldehyde concentration of 0.85 close to the predicted unity for a rate which is the sum of two pseudo first order reactions.

The dependence of the observed rate constant (k_2) for the second reaction is also close to unity as the concentration of Mn^{3+} being dependent additionally upon the formaldehyde concentration, increases with the latter. As expected the rate constant (k_3) for the third reaction shows no dependence on formaldehyde concentration.

Similar experiments were also carried out with Glyoxylic acid. The experiments was conducted with initial MnO_4^- concentration of 0.005M, initial glyoxylic acid concentration of 0.1M and as before, the initial formaldehyde concentration was varied between 0.1 and 1.6M. The reaction rate constants were determined from the kinetic model with a typical fit shown in Figure 5.6.

Reaction conditions and estimated rate constants are given in Table 5.6 and plots of rate constants versus glyoxal concentration are shown in Figure 5.9

Table 5.6 Experimental reaction conditions for MnO_4^- oxidation of glyoxylic acid in the presence formaldehyde and estimated rate constants.

Non-variables conditions of the reaction	Variables factors [HCHO]/(M)	Rate Constant for Eq. 1		Rate Constant for Eq. 2		Rate Constant for Eq. 3	
		$k_1(\text{s}^{-1})$	$k_1(\text{s}^{-1}) - 0.0072$	$k_2(\text{s}^{-1})$	$k_2(\text{s}^{-1}) - 2.15$	$k_3(\text{s}^{-1})$	$k_3(\text{s}^{-1}) - 1.67$
[OCHCO ₂ H] = 0.1M; [KMnO ₄]=0.005M; T° = 25°C; [H ₂ SO ₄]=2M	0.0	0.0072	0.0	2.15	0.0	1.67	0.0
[OCHCO ₂ H] = 0.1M; [KMnO ₄]=0.005M; T° = 25°C; [H ₂ SO ₄]=2M	0.1	0.0486	0.0414	4.22	2.07	2.34	0.67
[OCHCO ₂ H] = 0.1M; [KMnO ₄]=0.005M; T° = 25°C; [H ₂ SO ₄]=2M	0.2	0.092	0.0848	4.96	2.81	2.87	1.2
[OCHCO ₂ H] = 0.1M; [KMnO ₄]=0.005M; T° = 25°C; [H ₂ SO ₄]=2M	0.4	0.158	0.1508	6.32	4.17	2.94	1.27
[OCHCO ₂ H] = 0.1M; [KMnO ₄]=0.005M; T° = 25°C; [H ₂ SO ₄]=2M	0.8	0.293	0.2858	7.10	4.95	3.30	1.63
[OCHCO ₂ H] = 0.1M; [KMnO ₄]=0.005M; T° = 25°C; [H ₂ SO ₄]=2M	1.6	0.510	0.5028	9.42	7.27	3.22	1.55

To graphically illustrate the obtained results presented in table 5.6 above, the experimental data of k_1 , k_2 , k_3 of the reactions monitored by absorbance were plotted versus formaldehyde concentration.

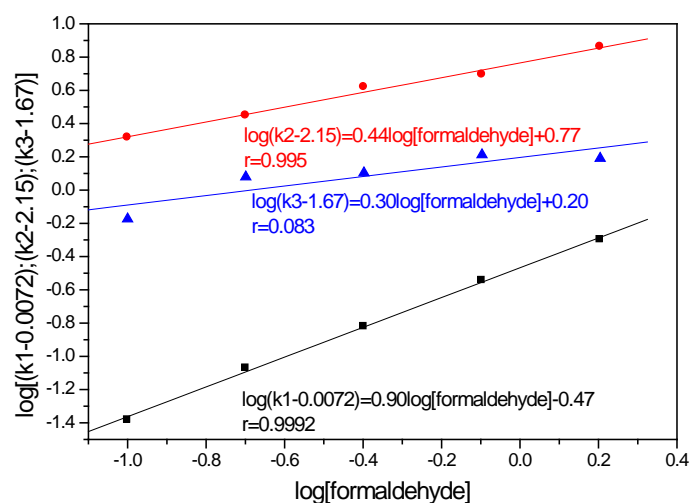
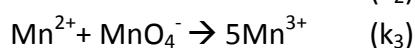
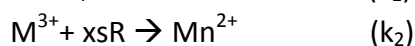


Figure 5.9 Plots and fittings showing the dependence of reaction rate constants (k_1 , k_2 , k_3) on [HCHO]. Reaction conditions: [HCHO] = 0.1–1.6M; Temperature = 25°C; [H₂SO₄] = 2M; [OCHCO₂H] = 0.1M.

Again, it can be seen that for the glyoxylic – formaldehyde mixtures the dependence of k_1 [formaldehyde] has an order in formaldehyde concentration of 0.9 close to the predicted unity for a rate which is the sum of two pseudo first order reactions. The dependence of the observed rate constant (k_2) for the second reaction is 0.4 (as compared to 0.9 for glyoxal) consistent again with the concentration of Mn³⁺ being dependent additionally upon the formaldehyde concentration, increasing with the latter. As expected the rate constant (k_3) for the third reaction shows no dependence on formaldehyde concentration.

5.2.3 Rate constants dependence on manganese(II) concentration

The sigmoidal decay curve for permanganate concentration implies that the reaction is autocatalytic and the proposed mechanism incorporates catalysis by the Mn²⁺ product. It is suggested that manganese(II) reacts with permanganate to yield manganese(III) as a transient intermediate product, which reacts with the organic substrate or/and organic intermediate products in the reaction mixture. Therefore, the equation (k_3) in the proposed chemical model makes the reaction autocatalytic and predicts the suppression of the induction by adding Mn²⁺ in acidic permanganate oxidations.



Given that the CL process is the reaction kinetics dependent and Mn^{3+} is suggested to be the precursor for the observed CL emission in MnO_4^- based CL reactions, the addition of manganese(II) in the reaction mixture should increase the reaction rate of MnO_4^- oxidations by removing the induction period and subsequently increasing the intensity of the CL signal.

Therefore, if the proposed chemical model is correct, the addition of Mn^{2+} should increase the reaction rate of MnO_4^- oxidations in predictable manner. There is a complication that the scale is not MnO_4^- concentration but MnO_4^- absorbance. Thus in fitting, manganese (II) is expressed as the absorbance of an equivalent concentration of MnO_4^- .

As it is reported in the literature for other MnO_4^- oxidations, although initial Mn^{2+} increases the rate of reaction of permanganate, it does not remove the induction as predicted. For example, although conditions are different, Treindl and co-workers⁵⁸³ have found that shape of autocatalytic sigmoidal curve varies not only with Mn^{2+} but also with pH and with phosphate.

Figures 5.10 and 5.11 show the change in MnO_4^- concentration and CL for the permanganate oxidation of glyoxylic acid and glyoxal CL systems in the presence of manganese(II) ions.

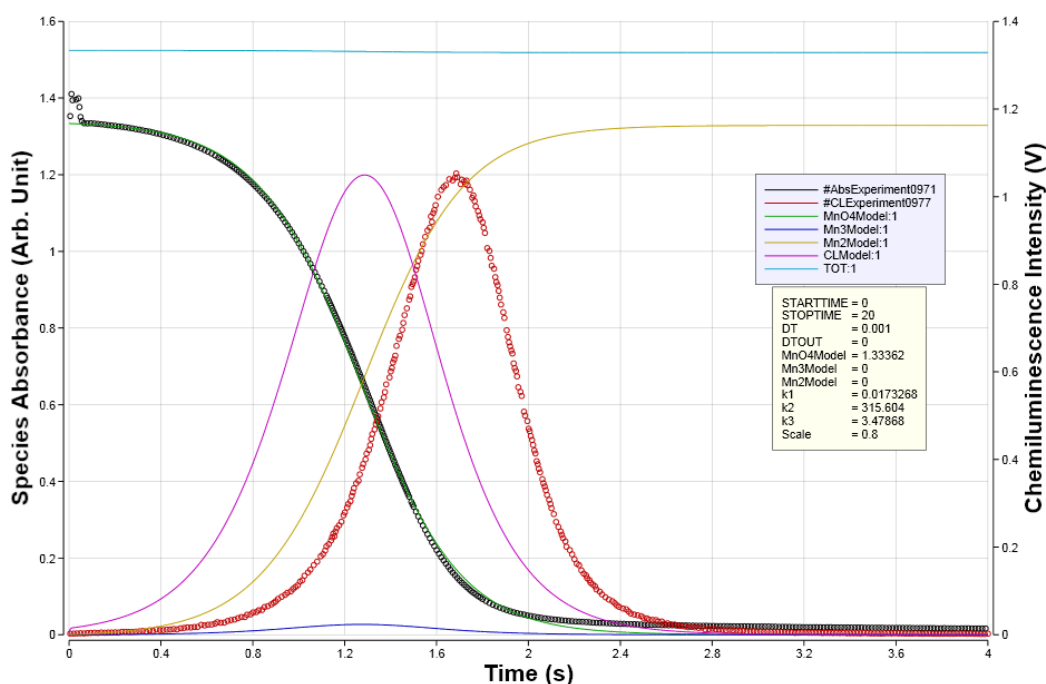


Figure 5.10 Experimental data (circle curves) - CL and Abs time courses for KMnO_4 oxidation reaction of glyoxylic acid in the presence of manganese(II). Fit shown ignores initial Mn(II). Reaction experimental conditions: $[\text{Mn(II)}] = 0.04\text{M}$; $[\text{OCHCO}_2\text{H}] = 0.1\text{M}$; $[\text{KMnO}_4] = 0.005\text{ M}$; $[\text{H}_2\text{SO}_4] = 2\text{M}$; Temperature = 25°C ; Wavelength = 525 nm .

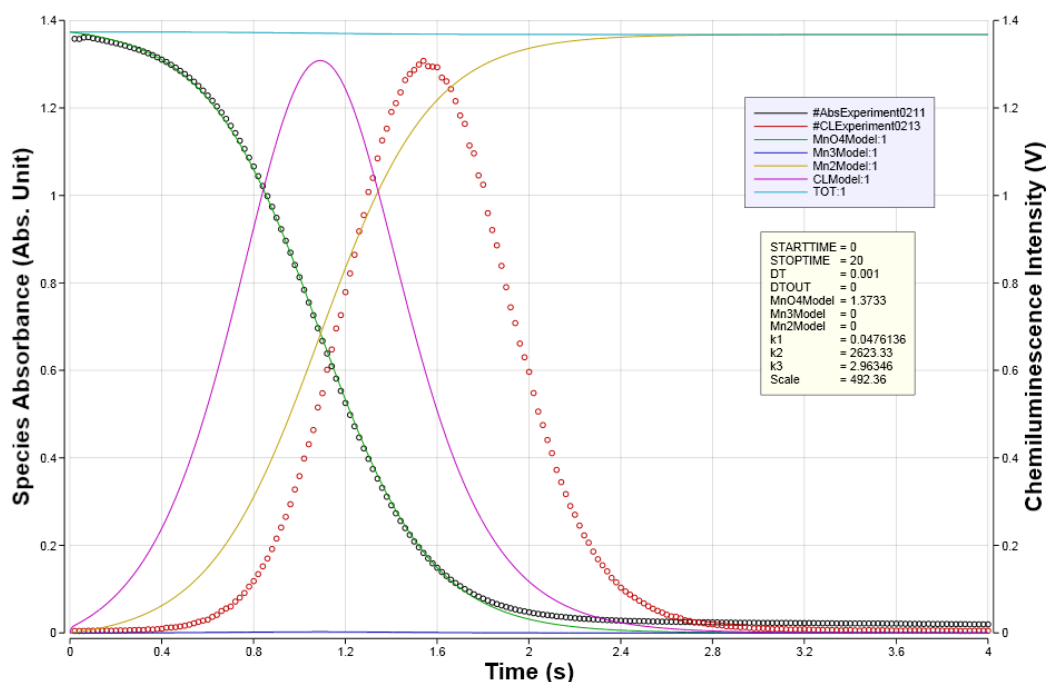
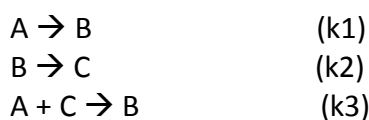


Figure 5.11 Experimental data (circle curves) - CL and Abs time courses for KMnO_4 oxidation reaction of glyoxal in the presence of manganese(II). Fit shown ignores initial Mn(II) . Reaction experimental conditions: $[\text{Mn(II)}] = 0.04\text{M}$; $[\text{OCHCHO}] = 0.1\text{M}$; $[\text{KMnO}_4] = 0.005\text{M}$; $[\text{H}_2\text{SO}_4] = 2\text{M}$; Temperature = 25°C ; Wavelength = 525 nm .

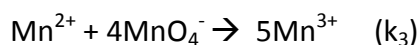
It is apparent from both Figures 5.10 and 5.11 that fit to the MnO_4^- consumption is better than that to the CL profiles. The fit cannot be improved in this simple model and attempts to add other steps whilst retaining the feedback equation (k_3) do not change this.

Whilst Mn^{2+} does increase the reaction rate, it does not remove the induction period as predicted by the model. Initial Mn^{2+} increases the rate of reaction in proportion to its concentration, but at a significantly lower rate than predicted. For every added Mn^{2+} concentration studied ($0.04 - 0.2\text{M}$) an induction period remains at and a three step mechanism of the form below is needed to fit the data.



It can be deduced that from dependence upon glyoxal and glyoxylic acid concentration, that the induction involves the organic reductant. In addition, Mn^{2+} may react not with MnO_4^- but with another intermediate formed more slowly from MnO_4^- . Dependence on Mn(II) initial concentration ($0.04 - 0.2\text{M}$) shows that rate (k_3) does not increase as rapidly as expected and crucially that the sigmoidal shape remains, which would not be expected if initial Mn^{2+} is present at these concentrations relatively to MnO_4^- at 0.005M .

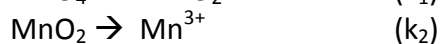
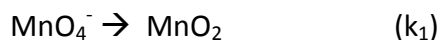
As for the induction period, it is known that Mn^{2+} must be involved as not seen in formaldehyde reaction which goes to Mn^{3+} . It is also known that MnO_4^- is involved because that is what we are measuring. Therefore, it is not as simple as hypothesised equation (k_3);



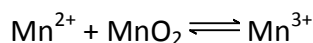
This because the reaction rate did not increase as expected upon addition of Mn^{2+} and the unexpected rate dependent on organic substrate (R) concentration. A possible explanation for the discrepancy between the model and the experimental data is that within reaction 3, there is an additional kinetically important step such as the slow build-up of an intermediate. It has been observed that adding manganese(II) does not suppress the induction period as it would be predicted and the reaction rates are not correct either. This can be attributed to the incorrect reaction mechanism or that the system is complicated by intermediate species that could not be properly accounted for in the global CL MnO_4^- oxidation reaction model.

5.2.4 Complex (alternative) mechanism

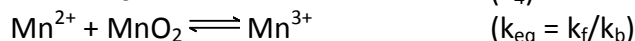
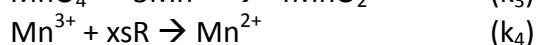
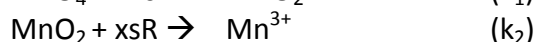
The discrepancy between the model and the experimental data for the resulting CL profile makes clear that considerable work remains to reconcile predictions with experimental measurements. There must be a feedback mechanism which does not involve Mn^{2+} directly. Note that this is contrary to what is generally believed, according to current literature. If it is not Mn^{2+} then could it be Mn^{3+} . Then the chemical kinetic model would be as follows;



It is also known that Mn^{2+} speeds up the reaction, so this must be through pre-equilibrium chemical reaction with MnO_2 as follows;



The reaction $\text{Mn}^{3+} \rightarrow \text{Mn}^{2+}$ will occurs with most reductants but not formaldehyde. However, the reaction with formaldehyde does not show feedback. We believe that this goes to Mn^{3+} and the product spectrum does confirm this. Otherwise, an organic intermediate would be involved in the induction but this will still have to be linked to manganese species. Therefore, the revised mechanism is;



The value of k_{eq} is a constant but only in absence of any other ligands. It is known from literature that many ligands (pyrophosphate is best known) stabilise Mn^{3+} and perhaps the excess of organic substrate (R) also does.

This revised mechanism has too many variables (rate constants k_1, k_2, k_3, k_4, k_f and k_b) to realistically fit to just two kinetic curves. Fits at different concentrations of R should have k_1, k_2 and k_4 with first order dependence and k_3 independent of R with $k_{eq} = k_f/k_b$ possibly dependent but in a consistent way.

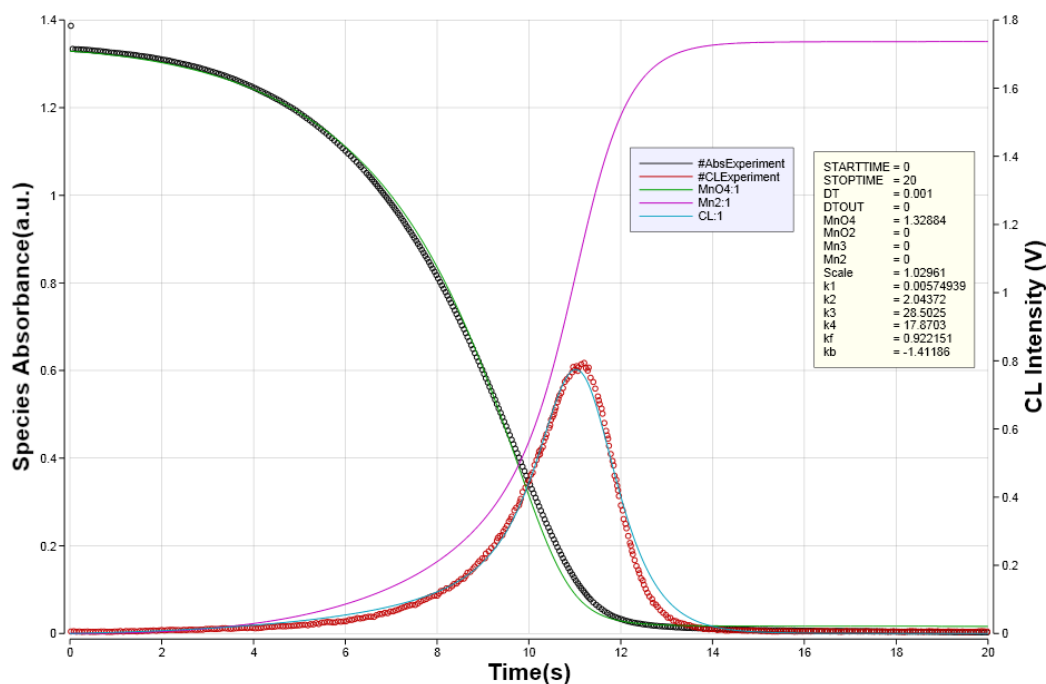


Figure 5.12 Comparison of kinetic model predictions (line curves) and experimental data (circle curves) - CL and Abs time courses for $KMnO_4$ oxidation reaction of glyoxylic acid. Reaction experimental conditions: $[OCHCO_2H] = 0.1M$; $[KMnO_4] = 0.005 M$; $[H_2SO_4] = 2M$; Temperature = $25^\circ C$; Wavelength = $525 nm$.

The accuracy of the revised kinetic model was tested and validated by comparing the model prediction with the experimental data for two representative cases of permanganate oxidation CL systems, in which glyoxylic acid and glyoxal are the main organic reductants in the absence or in the presence of additives such as catalyst manganese(II) or reactant enhancer formaldehyde.

The comparison was carried out by only curve-fitting the data from unreacted permanganate absorbance and then seeing how the CL predicted profile matched the CL experimental data. The obtained results are shown in Figures 5.12 – 5.13.

Figures 5.12 and 5.13 show the comparison of the experimentally measured data with the computed ones using the revised kinetic model for CL oxidations of glyoxal and glyoxylic acid with acidic permanganate.

For both cases, the disappearance of MnO_4^- (as it has got a strong absorbance, and is easy to measure) follows a sigmoidal curve typical of an autocatalytic reaction, and a good fit to the sigmoidal decay of permanganate is observed. This confirms that the reaction can be fitted by the revised mechanism.

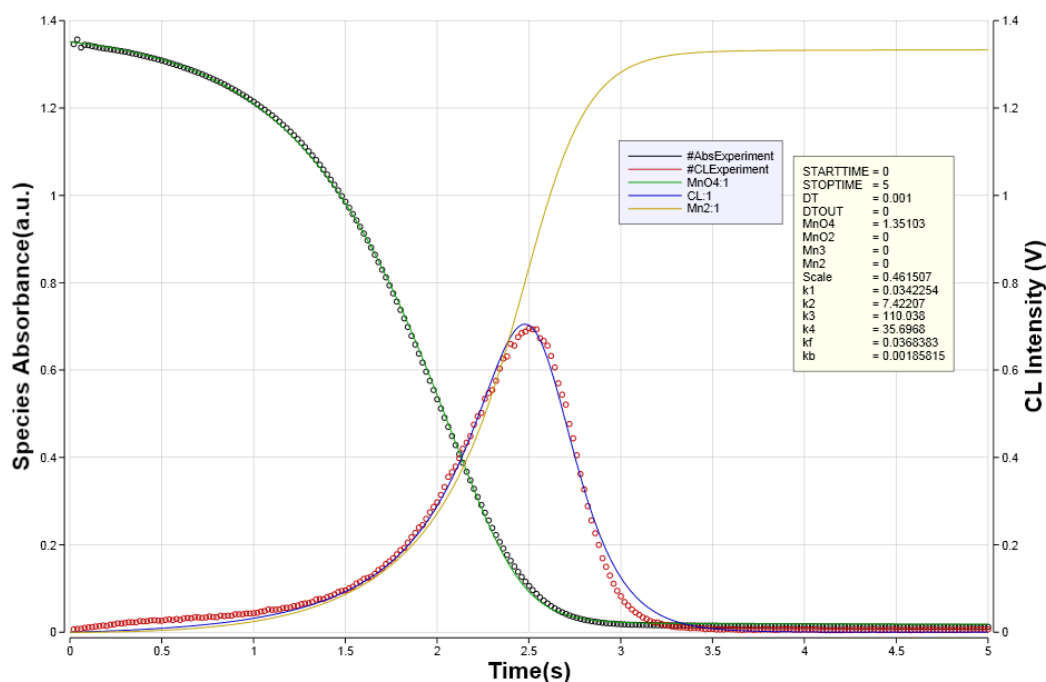


Figure 5.13 Comparison of kinetic model predictions (line curves) and experimental data (circle curves) - CL and Abs time courses for KMnO_4 oxidation reaction of glyoxal. Reaction experimental conditions: $[\text{OCHCHO}] = 0.2\text{M}$; $[\text{KMnO}_4] = 0.005\text{ M}$; $[\text{H}_2\text{SO}_4] = 2\text{M}$; Temperature = 25°C ; Wavelength = 525 nm .

5.2.4.1 Rate Constant Dependence on Glyoxylic Acid Concentration

The accuracy of the revised mechanism above was again tested in varying the reaction conditions for permanganate oxidation of glyoxylic acid. Experiments were conducted in which the permanganate concentration for each trial was held constant while the initial glyoxylic acid concentration was varied. Glyoxylic acid concentrations were chosen to allow the reactions to proceed within a reasonable time frame and produce a measurable CL signal. The set of experiments was conducted with an initial permanganate concentration of 0.005M .

The initial glyoxylic acid concentration was varied between 0.05 and 0.8M . The initial reaction rate constants were determined from the kinetics model as shown in Figure 5.12. Reaction conditions and estimated rate constants are given in Table 5.7 and plots of rate constants versus glyoxylic acid concentration are shown in Figures 5.14 -5.17.

Table 5.7 Experimental reaction conditions for permanganate oxidation of glyoxylic acid and estimated reaction rate constants.

Non-variables conditions of the reaction	[OCHCO ₂ H] / (M)	k ₁ (s ⁻¹)	k ₂ (s ⁻¹)	k ₃ (s ⁻¹)	k ₄ (s ⁻¹)	k _f (s ⁻¹)	k _b (s ⁻¹)
[KMnO ₄] = 0.005M; T° = 25°C; [H ₂ SO ₄] = 2M	0.05	0.003 5	1.32	91.5	26.1	0.012	0.0031
[KMnO ₄] = 0.005M; T° = 25°C; [H ₂ SO ₄] = 2M	0.10	0.006 6	1.60	18.0	4.73	5.0 x 10 ⁻⁵	0.0017
[KMnO ₄] = 0.005M; T° = 25°C; [H ₂ SO ₄] = 2M	0.20	0.012	1.90	10.7	2.60	2.0 x 10 ⁻⁵	0.0005
[KMnO ₄] = 0.005M; T° = 25°C; [H ₂ SO ₄] = 2M	0.40	0.023	1.91	23.6	5.70	0.0018	4.0 x 10 ⁻⁸
[KMnO ₄] = 0.005M; T° = 25°C; [H ₂ SO ₄] = 2M	0.80	0.046	1.90	17.3	3.70	3.0 x 10 ⁻¹⁰	0.026

To graphically illustrate the results presented in table 5.7, the estimated rate constants of the reaction were plotted versus concentration as log-log plots in Figures 5.14 -5.17.

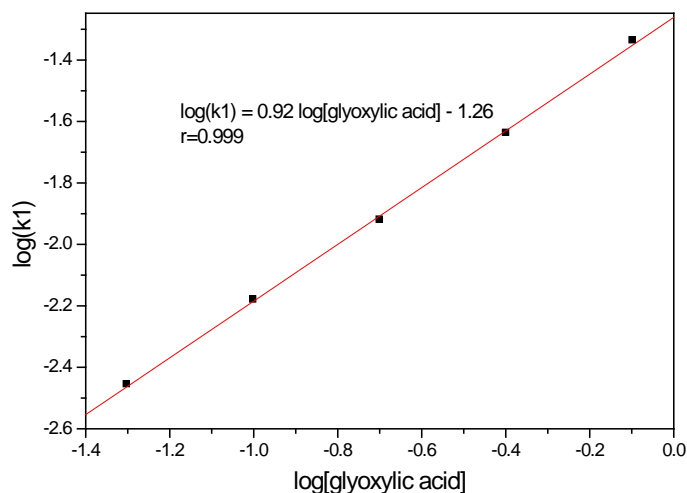


Figure 5.14 Plots and fittings showing the dependence of k_1 on [OCHCO₂H]. Reaction conditions: [KMnO₄] = 0.005M; T° = 25°C; [H₂SO₄] = 2M; [OCHCO₂H] = 0.05 – 0.8M.

As expected, the kinetics of the reaction increased as the glyoxylic acid concentration increased and good fits to MnO_4^- decay were observed using the revised kinetic model.

It was expected that the rate constant k_1 show first order dependence on glyoxylic acid concentration (R) and k_3 independent of [glyoxylic acid]. As expected the plot of rate constant (k_1) versus glyoxylic acid concentration (Figure 5.14) produced a straight line dependence on

glyoxylic acid concentration. The slope of the linear regression for k_1 is approximately one indicating pseudo first order with respect to glyoxylic acid.

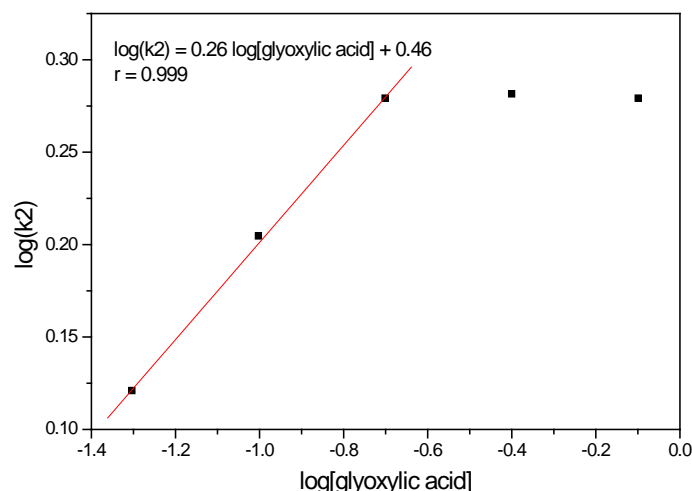


Figure 5.15 Plots and fittings showing the dependence of k_2 on $[\text{OCHCO}_2\text{H}]$. Reaction conditions: $[\text{KMnO}_4] = 0.005\text{M}$; Temperature = 25°C ; $[\text{H}_2\text{SO}_4] = 2\text{M}$; $[\text{OCHCO}_2\text{H}] = 0.05 - 0.8\text{M}$.

It was expected that the rate constant k_2 shows first order dependence on glyoxylic acid concentration (R) and k_3 independent of glyoxylic acid concentration. As expected the plot of rate constant (k_2) versus glyoxylic acid concentration (Figure 5.15) produced a straight line dependence on $[\text{glyoxylic acid}]$ of 0.05 to 0.2M. Above this concentration k_2 become constant possibly due to the reaction saturation.

However, the slope of the linear regression for k_2 shows a fractional-order dependence on glyoxylic acid concentration. A possible explanation is that the reaction k_2 involve a partially oxidised species, which reacts more rapidly than glyoxylic acid. As glyoxylic acid concentration increases, the proportion of this intermediate will decrease so the increase in the reaction rate will be less than first order as observed.

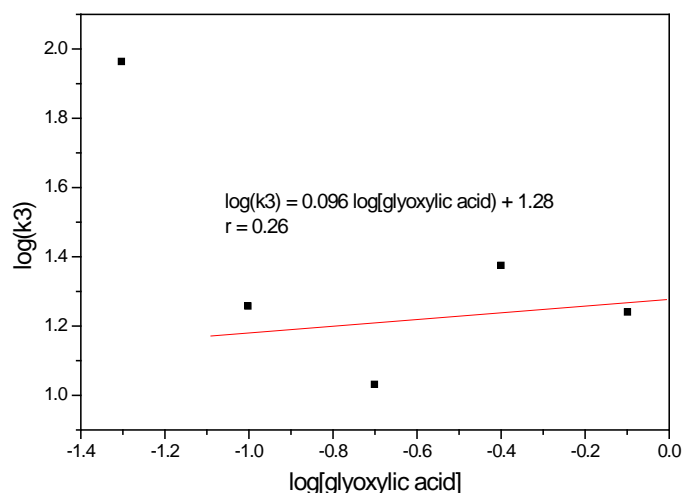


Figure 5.16 Plots and fittings showing the dependence of k_3 on $[\text{OCHCO}_2\text{H}]$. Reaction conditions: $[\text{KMnO}_4] = 0.005\text{M}$; Temperature = 25°C ; $[\text{H}_2\text{SO}_4] = 2\text{M}$; $[\text{OCHCO}_2\text{H}] = 0.05 - 0.8\text{M}$.

The graph in Figure 5.16 represents the plotting of the rate constant (k_3) versus glyoxylic acid concentration. As predicted by the model, the plot of $\log(k_3)$ versus $\log[\text{glyoxylic acid}]$ shows no relationship between k_3 and glyoxylic acid with a correlation coefficient of $r = 0.260$ and slope of 0.096, indicating no dependence on the glyoxylic acid concentration.

The log-log plot (Figure 5.17) of the rate constant (k_4) versus glyoxylic acid concentration showed no dependence upon glyoxylic acid concentration having a slope of 0.01. This rather contradictory result on the dependence of equation 4 on glyoxylic acid concentration could be attributed to partially oxidised species, which reacts more rapidly than glyoxylic acid. Data from the table 5.7 also show that $k_{\text{eq}} = k_f/k_b$ is not dependent upon $[\text{glyoxylic acid}]$.

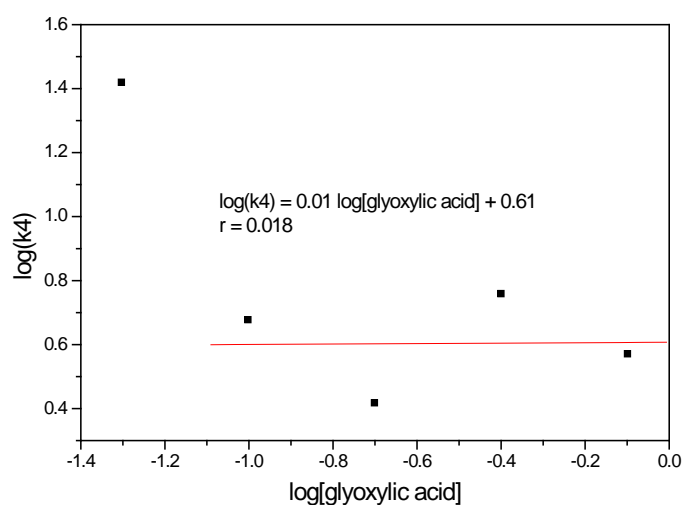


Figure 5.17 Plots and fittings showing the dependence of k_4 on $[\text{OCHCO}_2\text{H}]$. Reaction conditions: $[\text{KMnO}_4] = 0.005\text{M}$; Temperature = 25°C ; $[\text{H}_2\text{SO}_4] = 2\text{M}$; $[\text{OCHCO}_2\text{H}] = 0.05 - 0.8\text{M}$.

5.2.4.2 Rate Constants Dependence on Glyoxal Concentration

The second set of experiments, the effect of glyoxal concentration was investigated using the reaction conditions in which the initial glyoxal concentration in large excess over MnO_4^- , was varied in the range 0.05 to 0.8M and initial permanganate concentration was held constant at 0.005M.

The initial reaction rate constants were determined from the kinetics model as shown in Figure 5.13. Reaction conditions and estimated rate constants are given in Table 5.8 and plots of rate constants versus glyoxylic acid concentration are shown in Figures 5.18 -5.21.

Table 5.8 Experimental reaction conditions for permanganate oxidation of glyoxal and estimated reaction rate constants.

Non-variables conditions of the reaction	[OCHCHO] (M)	k_1 (s ⁻¹)	k_2 (s ⁻¹)	k_3 (s ⁻¹)	k_4 (s ⁻¹)	k_f (s ⁻¹)	k_b (s ⁻¹)
[KMnO ₄] = 0.005M; T° = 25°C; [H ₂ SO ₄] = 2M	0.05	0.011	2.51	3.64	1.10	9.82 x 10 ⁻⁴	26.6 x 10 ⁻⁵
[KMnO ₄] = 0.005M; T° = 25°C; [H ₂ SO ₄] = 2M	0.10	0.019	4.80	7.20	2.0	27.7 x 10 ⁻⁵	1.9 x 10 ⁻⁴
[KMnO ₄] = 0.005M; T° = 25°C; [H ₂ SO ₄] = 2M	0.20	0.037	8.0	12.8	3.04	94.4 x 10 ⁻⁵	6.3 x 10 ⁻⁶
[KMnO ₄] = 0.005M; T° = 25°C; [H ₂ SO ₄] = 2M	0.40	0.050	17.9	11.4	1.42	5.9 x 10 ⁻⁴	1.6 x 10 ⁻⁵
[KMnO ₄] = 0.005M; T° = 25°C; [H ₂ SO ₄] = 2M	0.80	0.67	28.1	29.8	7.23	2.1 x 10 ⁻³	1.7 x 10 ⁻³

To determine the dependence upon glyoxal concentration, log-log plots of the estimated rate constants of the reaction steps were plotted versus concentration as shown in Figures 5.18 - 5.21.

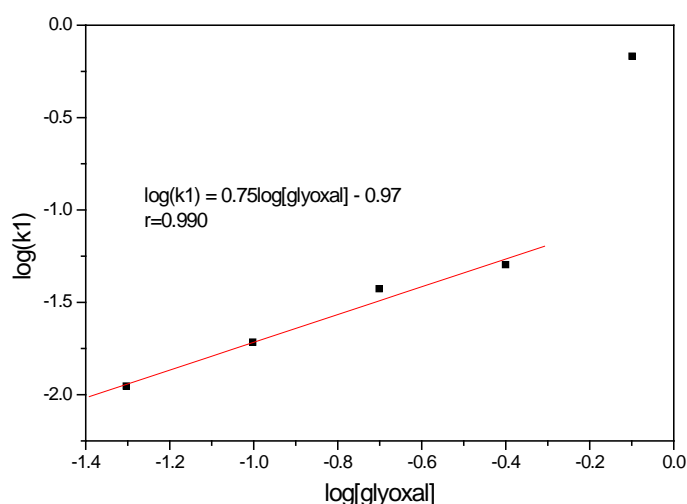


Figure 5.18 Plots and fittings showing the dependence of the rate constant (k_1) on [OCHCHO]. Reaction conditions: [KMnO₄] = 0.005M; T° = 25°C; [H₂SO₄] = 2M; [OCHCHO] = 0.05 – 0.8M.

It was expected that the rate constant k_1 would show first order dependence on glyoxal concentration (R) and k_3 independent of glyoxal. The slope of the linear regression fit for k_1 is approximately one indicating pseudo first order with respect to glyoxal.

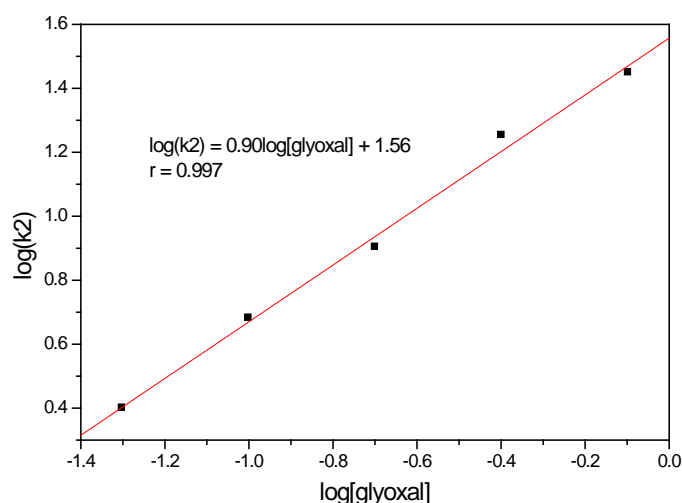


Figure 5.19 Plots and fittings showing the dependence of the rate constant (k_2) on [OCHCHO]. Reaction conditions: $[KMnO_4] = 0.005M$; $T^\circ = 25^\circ C$; $[H_2SO_4] = 2M$; $[OCHCHO] = 0.05 - 0.8M$.

The log-log plot (Figure 5.19) of the rate constant (k_2) versus glyoxal concentration gave a slope of 0.9 consistent with pseudo first order with respect to glyoxal.

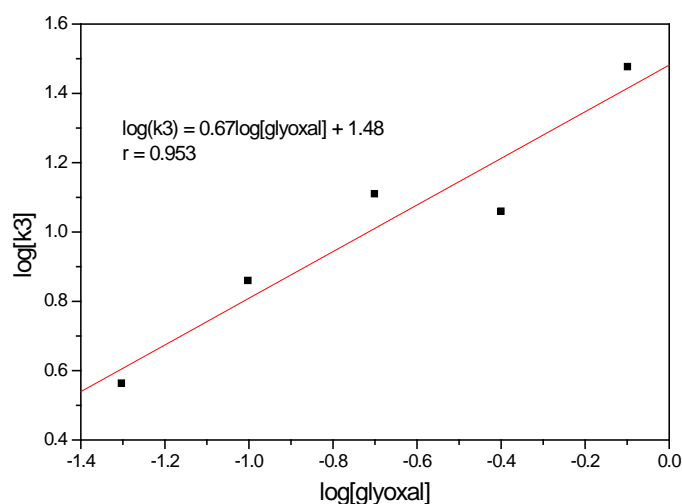


Figure 5.20 Plots and fittings showing the dependence of k_3 on [OCHCHO]. Reaction conditions: $[KMnO_4] = 0.005M$; Temperature = $25^\circ C$; $[H_2SO_4] = 2M$; $[OCHCHO] = 0.05 - 0.8M$.

Contrary to prediction the log-log plot (Figure 5.20) of the rate constant (k_3) versus glyoxal concentration had a slope of 0.67, although the fit was not particularly good.

This rather contradictory result on the dependence of equation 3 on glyoxal concentration could be attributed to possible interference of glyoxal (R) within step 3. For example Mn^{2+} may react not with MnO_4^- but with another intermediate formed more slowly from MnO_4^- .

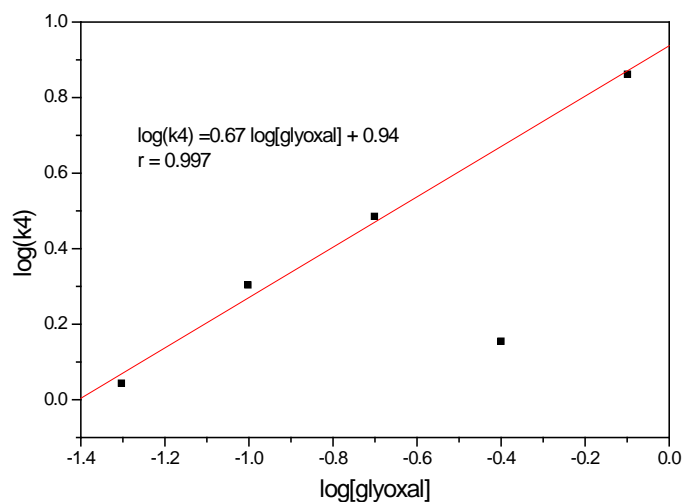


Figure 5.21 Plots and fittings showing the dependence of k_4 on [OCHCHO]. Reaction conditions: $[\text{KMnO}_4] = 0.005\text{M}$; Temperature = 25°C ; $[\text{H}_2\text{SO}_4] = 2\text{M}$; $[\text{OCHCHO}] = 0.05 - 0.8\text{M}$.

The graph in Figure 5.21 represents the log-log plot of the rate constant (k_4) versus glyoxal concentration. Accordingly to expectations, k_4 showed a good dependence upon glyoxal concentration having a slope of 0.67, confirming pseudo first order with respect to glyoxal. Data from the table 5.8 also show that $k_{\text{eq}} = k_f/k_b$ is not dependent upon glyoxal concentration.

5.2.4.3 Rate Constants Dependence on Formaldehyde Concentration

It is expected that the addition of formaldehyde will show simple pseudo first order decay with no induction. As with the simple mechanism, combining rate constants obtained from glyoxal or glyoxylic acid and formaldehyde oxidations should give good fit with mixture.

Figures 5.22 and 5.23 show the comparison of numerical computations with the experimental data obtained from acidic permanganate oxidation of glyoxal and glyoxylic acid in the presence of formaldehyde as an enhancer using the revised chemical kinetic model that accounts the reaction between formaldehyde and MnO_4^- by adding the individual rate constants together.

As expected, the addition of formaldehyde as enhancer increased the reaction rate and the CL response, and both predicted profiles for permanganate consumption and chemiluminescence emission agreed with measured profiles. Table 5.9 below compare predicted rate k_1 obtained from the sum of k_1 from permanganate oxidation of formaldehyde and glyoxal, respectively, with the experimental rate k_1 from the mixture of formaldehyde and glyoxal.

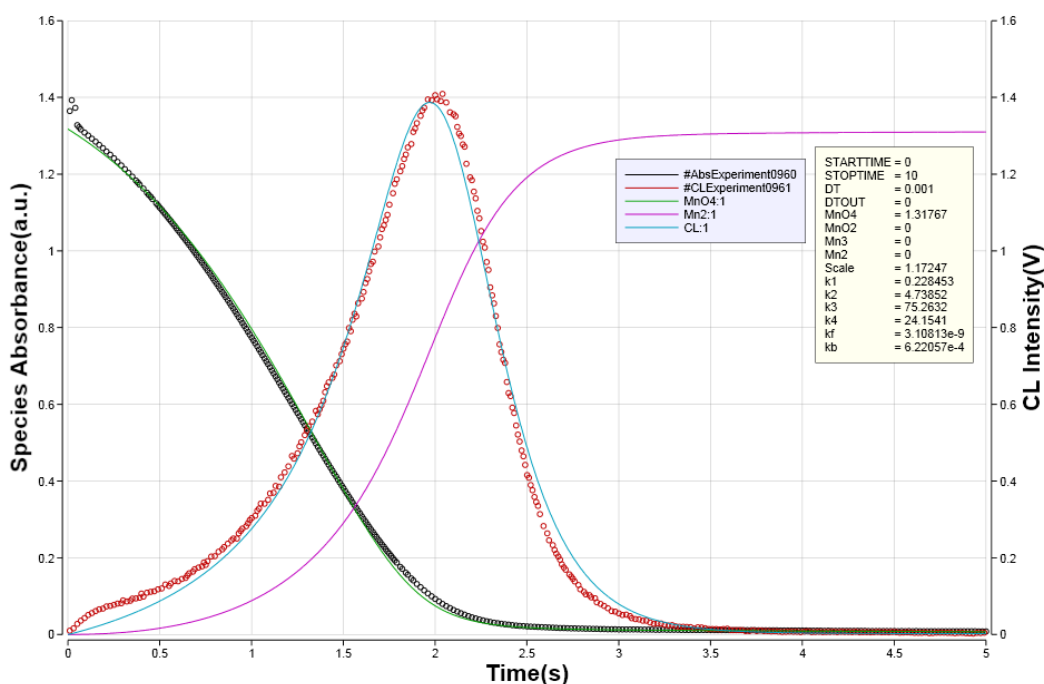


Figure 5.22 Comparison of kinetic model predictions (line curves) and experimental data (circle curves) - CL and Abs time courses for MnO_4^- oxidation reaction of glyoxylic acid in the presence of formaldehyde. Reaction experimental conditions: $[\text{HCHO}] = 0.8\text{M}$; $[\text{OCHCO}_2\text{H}] = 0.1\text{M}$; $[\text{MnO}_4^-] = 0.005\text{ M}$; $[\text{H}_2\text{SO}_4] = 2\text{M}$; $T^\circ = 25^\circ\text{C}$; Wavelength = 525 nm.

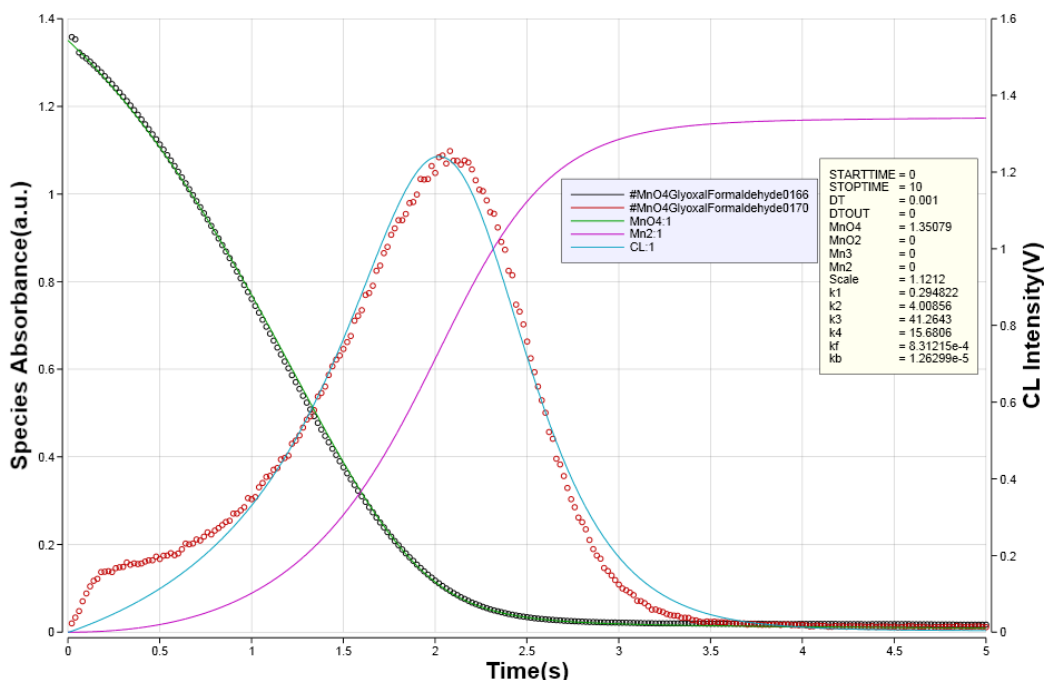


Figure 5.23 Comparison of kinetic model predictions (line curves) and experimental data (circle curves) - CL and Abs time courses for MnO_4^- oxidation reaction of glyoxal in the presence of formaldehyde as enhancer. Reaction conditions: $[\text{HCHO}] = 0.8\text{M}$; $[\text{OCHCHO}] = 0.1\text{M}$; $[\text{MnO}_4^-] = 0.005\text{ M}$; $[\text{H}_2\text{SO}_4] = 2\text{M}$; $T^\circ = 25^\circ\text{C}$; Wavelength = 525 nm.

It can be seen from Table 5.9 that the sum of k_1 values for reactions 0.005M KMnO_4 and 0.1M Formaldehyde only and with 0.1M glyoxal only is the same as of the permanganate oxidation of their mixture. The predicted rate is as expected equal to mixture experimental rate ($k_1 = 0.062 \text{ s}^{-1}$ compared with $k_1 = 0.062 \text{ s}^{-1}$). Similar experiment was carried out for permanganate oxidation of glyoxylic acid with and without formaldehyde and the obtained results are summarized in Table 5.10.

This demonstrates the increase in the overall reaction with glyoxal or glyoxylic acid in the presence of formaldehyde. It confirms that reaction with formaldehyde goes only as far as Mn^{3+} . It also confirms that although reaction of formaldehyde with MnO_4^- is slow, it is faster than corresponding reaction (k_1) with glyoxal. The faster reaction explains the increase CL as normally measured in a flow system.

Table 5.9 Comparison of predicted rate k_1 with the mixture experimental rate k_1 for permanganate oxidation of glyoxal with and without formaldehyde.

Reaction Conditions	$k_1 (\text{s}^{-1})$
0.005M KMnO_4 and 0.1M Formaldehyde only	0.043
0.005M KMnO_4 and 0.1M glyoxal only	0.019
Predicted k_1 (0.043 + 0.019)	0.062
Experimental k_1 for 0.005M KMnO_4 and 0.1M Formaldehyde and 0.1M glyoxal	0.062
0.005M KMnO_4 and 0.2M Formaldehyde only	0.080
0.005M KMnO_4 and 0.1M glyoxal only	0.019
Predicted k_1 (0.080 + 0.019)	0.099
Experimental k_1 for 0.005M KMnO_4 and 0.2M Formaldehyde and 0.1M glyoxal	0.113
0.005M KMnO_4 and 0.4M Formaldehyde only	0.149
0.005M KMnO_4 and 0.1M glyoxal only	0.019
Predicted k_1 (0.149 + 0.019)	0.168
Experimental k_1 for 0.005M KMnO_4 and 0.4M Formaldehyde and 0.1M glyoxal	0.186
0.005M KMnO_4 and 0.8M Formaldehyde only	0.284
0.005M KMnO_4 and 0.1M glyoxal only	0.019
Predicted k_1 (0.284 + 0.019)	0.303
Experimental k_1 for 0.005M KMnO_4 and 0.8M Formaldehyde and 0.1M glyoxal	0.290
0.005M KMnO_4 and 1.6M Formaldehyde only	0.552
0.005M KMnO_4 and 0.1M glyoxal only	0.019
Predicted k_1 (0.552 + 0.019)	0.571
Experimental k_1 for 0.005M KMnO_4 and 1.6M Formaldehyde and 0.1M glyoxal	0.520

Table 5.10 Comparison of predicted rate k_1 with the mixture experimental rate k_1 for permanganate oxidation of glyoxylic acid with and without formaldehyde.

Reaction Conditions	k_1 (s^{-1})
0.005M $KMnO_4$ and 0.1M Formaldehyde only	0.0430
0.005M $KMnO_4$ and 0.1M glyoxylic acid only	0.0069
Predicted k_1 (0.043 + 0.0069)	0.0499
Experimental k_1 for 0.005M $KMnO_4$ and 0.1M Formaldehyde and 0.1M glyoxylic acid	0.0483
0.005M $KMnO_4$ and 0.2M Formaldehyde only	0.080
0.005M $KMnO_4$ and 0.1M glyoxylic acid only	0.0069
Predicted k_1 (0.080 + 0.0069)	0.0874
Experimental k_1 for 0.005M $KMnO_4$ and 0.2M Formaldehyde and 0.1M glyoxylic acid	0.0869
0.005M $KMnO_4$ and 0.4M Formaldehyde only	0.149
0.005M $KMnO_4$ and 0.1M glyoxylic acid only	0.0069
Predicted k_1 (0.149 + 0.0069)	0.156
Experimental k_1 for 0.005M $KMnO_4$ and 0.4M Formaldehyde and 0.1M glyoxylic acid	0.157
0.005M $KMnO_4$ and 0.8M Formaldehyde only	0.284
0.005M $KMnO_4$ and 0.1M glyoxylic acid only	0.0069
Predicted k_1 (0.284 + 0.0069)	0.291
Experimental k_1 for 0.005M $KMnO_4$ and 0.8M Formaldehyde and 0.1M glyoxylic acid	0.283
0.005M $KMnO_4$ and 1.6M Formaldehyde only	0.552
0.005M $KMnO_4$ and 0.1M glyoxylic acid only	0.0069
Predicted k_1 (0.552 + 0.0069)	0.56
Experimental k_1 for 0.005M $KMnO_4$ and 1.6M Formaldehyde and 0.1M glyoxylic acid	0.495

These results confirmed the early conclusion that there is a co-oxidation reaction (or competitive oxidation) of formaldehyde and the organic substrate that speeds up the consumption of permanganate, thereby the reaction rate to generate transient manganese(III) intermediate, which is suggested to be a precursor for the observed chemiluminescence process.

The accuracy of the revised CL enhancement mechanism was tested in varying the reaction conditions for permanganate oxidations of the mixture of formaldehyde with glyoxal and glyoxylic acid, respectively. Experiments were conducted in which the permanganate as well as glyoxal and glyoxylic acid concentrations for each trial were held constant while the initial formaldehyde concentration was varied.

A series of experiments was conducted with initial permanganate concentration of 0.005M, initial glyoxal concentration of 0.1M. The initial formaldehyde concentration was varied between 0.1 and 1.6M. The initial reaction rate constants were determined from the kinetics model as shown in Figure 5.23. Reaction conditions and estimated rate constants are given in Table 5.11 and the plot of rate constant (k_1) versus glyoxal concentration is shown in Figure 5.24.

Table 5.11 Experimental reaction conditions for permanganate oxidation of glyoxal in the presence formaldehyde and estimated reaction rate constants.

Non-variables conditions of the reaction	[HCHO](M)	$k_1(s^{-1})$	$k_2(s^{-1})$	$k_3(s^{-1})$	$k_4(s^{-1})$	$k_f(s^{-1})$	$k_b(s^{-1})$
[OCHCHO] = 0.1M; [KMnO ₄]=0.005M; T° = 25°C; [H ₂ SO ₄]= 2 M	0.0	0.019	4.78	7.20	1.98	9.24 x10 ⁻⁴	9.52 x10 ⁻⁴
[OCHCHO] = 0.1M; [KMnO ₄]=0.005M; T° = 25°C; [H ₂ SO ₄]=2M	0.1	0.056	8.97	2.23	5.5 x 10 ⁻⁶	5.36 x10 ⁻⁴	3.95 x10 ⁻⁹
[OCHCHO] = 0.1M; [KMnO ₄]=0.005M; T° = 25°C; [H ₂ SO ₄]=2M	0.2	0.113	3.83	181	62.2	0.003	5.85 x10 ⁻⁴
[OCHCHO] = 0.1M; [KMnO ₄]=0.005M; T° = 25°C; [H ₂ SO ₄]=2M	0.4	0.163	5.44	17.4	6.64	6.14 x10 ⁻⁴	3.76 x10 ⁻⁴
[OCHCHO] = 0.1M; [KMnO ₄]=0.005M; T° = 25°C; [H ₂ SO ₄]=2M	0.8	0.250	5.66	17.3	7.32	1.10 x10 ⁻⁴	2.96 x10 ⁻⁴
[OCHCHO] = 0.1M; [KMnO ₄]=0.005M; T° = 25°C; [H ₂ SO ₄]=2M	1.6	0.423	5.97	19.0	9.33	6.50 x10 ⁻⁴	4.37 x10 ⁻⁶

To graphically illustrate the obtained results presented in table 5.11 above, the experimental data of $k_1, k_2, k_3, k_4, k_f, k_b$ of the reactions monitored by visible absorbance were plotted versus formaldehyde concentration.

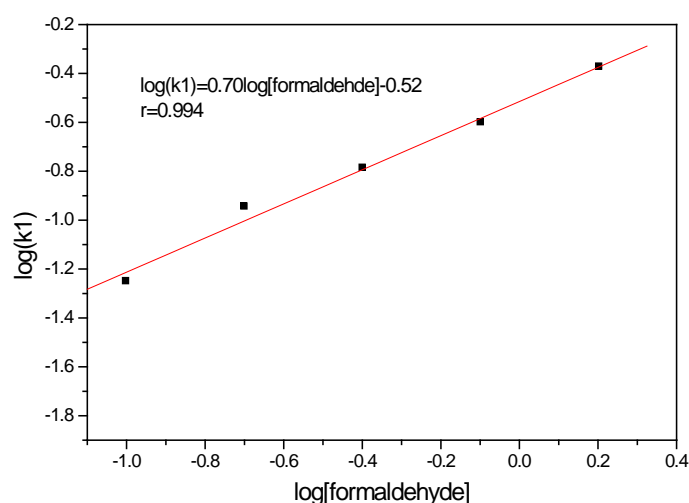


Figure 5.24 Plots and fittings showing the dependence of reaction rate constants (k_1) on [formaldehyde]. Reaction conditions: [HCHO] = 0.1 – 1.6M; Temperature = 25°C; [H₂SO₄] = 2M; [OCHCHO] = 0.1M.

It can be seen that the plot of k_1 versus [formaldehyde] was linear with slope = 0.7, confirming a fractional-order dependence on the formaldehyde concentration. The fractional-order dependence of k_1 on formaldehyde concentration is consistent with triple reduction of permanganate in the first step of the reaction by formaldehyde, glyoxal and manganese(III) to rapidly generate manganese(IV) intermediate. As expected, plots of k_2 , k_3 , k_4 , k_f , k_b versus [formaldehyde] (graphs not displayed) showed no first-order dependence on the formaldehyde concentration.

To confirm the results above, a series of experiments was conducted with initial permanganate concentration of 0.005M, initial glyoxylic acid concentration of 0.1M. The initial formaldehyde concentration was varied between 0.1 and 1.6M. The initial reaction rate constants were determined from the kinetics model as shown in Figure 5.22. Reaction conditions and estimated rate constants are given in Table 5.12 and the plot of rate constant (k_1) versus glyoxal concentration are shown in Figure 5.25.

Table 5.12 Experimental reaction conditions for MnO_4^- oxidation of glyoxylic acid in the presence formaldehyde and estimated reaction rate constants.

Non-variables conditions of the reaction	[HCHO](M)	$k_1(s^{-1})$	$k_2 (s^{-1})$	$k_3 (s^{-1})$	$k_4 (s^{-1})$	$k_f (s^{-1})$	$k_b (s^{-1})$
[OCHCO ₂ H] = 0.1M; [KMnO ₄]=0.005M; T° = 25°C; [H ₂ SO ₄]=2M	0.0	0.069	1.53	147.4	40.6	3.17×10^{-4}	0.0012
[OCHCO ₂ H] = 0.1M;; [KMnO ₄]=0.005M; T° = 25°C; [H ₂ SO ₄]=2M	0.1	0.05	2.53	94.7	27.6	2.46×10^{-4}	1.90×10^{-4}
[OCHCO ₂ H] = 0.1M; [KMnO ₄]=0.005M; T° = 25°C; [H ₂ SO ₄]=2M	0.2	0.092	3.02	56.3	16.5	5.98×10^{-4}	2.38×10^{-4}
[OCHCO ₂ H] = 0.1M; [KMnO ₄]=0.005M; T° = 25°C; [H ₂ SO ₄]=2M	0.4	0.16	3.54	162	54.4	9.6×10^{-4}	1.41×10^{-8}
[OCHCO ₂ H] = 0.1M; [KMnO ₄]=0.005M; T° = 25°C; [H ₂ SO ₄]=2M	0.8	0.28	4.11	44.2	15.3	2.43×10^{-10}	2.03×10^{-4}
[OCHCO ₂ H] = 0.1M; [KMnO ₄]=0.005M; T° = 25°C; [H ₂ SO ₄]=2M	1.6	0.50	4.55	645	264	0.003	0.006

To graphically illustrate the obtained results presented in table 5.12 above, the experimental data of k_1 , k_2 , k_3 , k_4 , k_f , k_b of the reactions monitored by visible absorbance were plotted versus formaldehyde concentration.

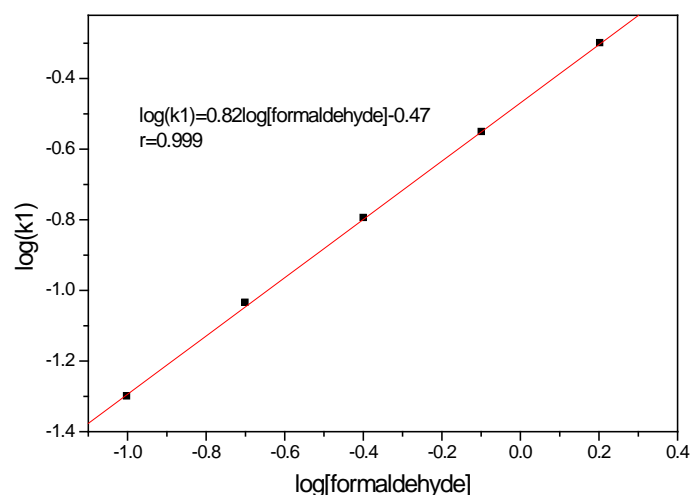


Figure 5.25 Plots and fittings showing the dependence of reaction rate constants (k_1) on [HCHO]. Reaction conditions: [HCHO] = 0.1 – 1.6M; Temperature = 25°C; [H₂SO₄] = 2M; [OCHCO₂H] = 0.1M.

As expected, the plot of k_1 versus [formaldehyde] was linear with slope = 0.82, confirming once again a fractional-order dependence on the formaldehyde concentration. The fractional-order dependence of k_1 on formaldehyde concentration is consistent with triple reduction of permanganate in the first step of the reaction by formaldehyde, glyoxylic acid and manganese(III) to rapidly generate manganese(IV). As expected, plots of k_2 , k_3 , k_4 , k_f , k_b versus [formaldehyde] (graphs not displayed) showed no first-order dependence on the formaldehyde concentration.

5.2.4.4 Rate Constants Dependence on Manganese(II) Concentration

It is well known that the added manganese(II) catalyses various reactions with permanganate in increasing the rate of MnO_4^- oxidations and the chemiluminescence signal intensity. Figures 5.26 and 5.27 show the change in permanganate concentration and chemiluminescence for the permanganate oxidation of glyoxylic acid and glyoxal CL systems in the presence of manganese(II) ions.

Contrarily to simple mechanism, it is apparent from both Figures 5.26 and 5.27 that both the predicted MnO_4^- consumption and CL profiles well represented the experimental data. The accuracy of the revised mechanism was tested by varying the manganese(II) concentration. If the revised chemical model is correct, the addition of Mn^{2+} should increase the reaction rate of MnO_4^- oxidations in predictable manner. It is expected that the added manganese(II) concentration piles up manganese(III) through k_f . The effect of manganese(II) concentration was studied with constant initial concentrations of 0.005M KMnO_4 , 0.2M glyoxal and 2M H_2SO_4 at 25°C, while the initial manganese(II) concentration was varied from 0.04 to 0.2M. The results (the $\log k - \log [\text{Mn}^{2+}]$ profiles) are shown in Figure 5.28 and the derived values of rate constants (k) are provided in Table 5.12.

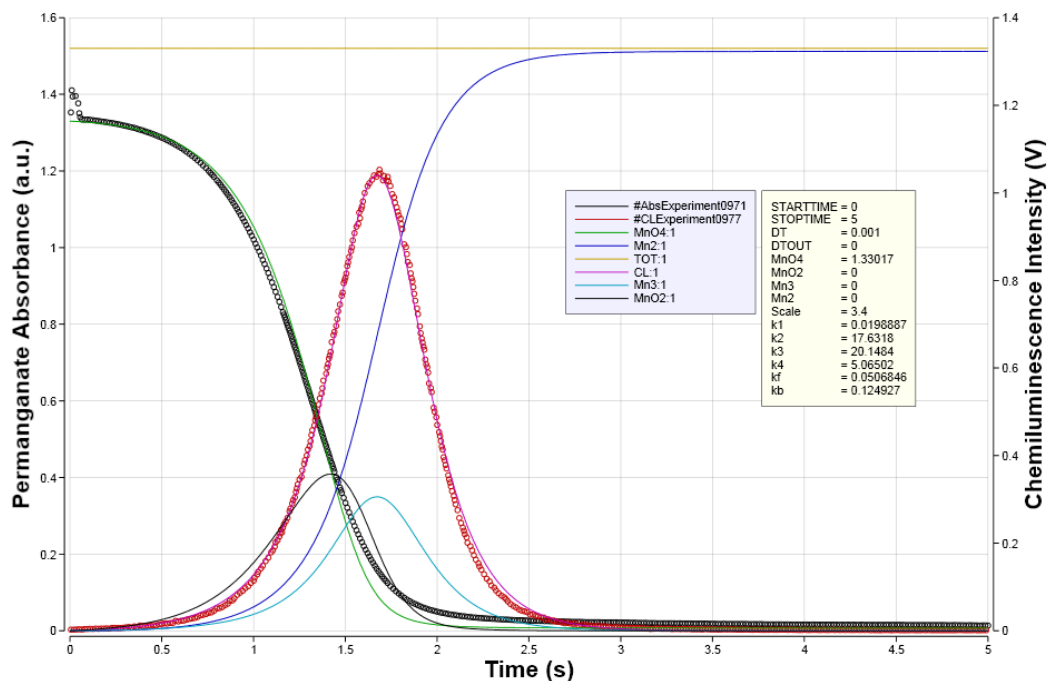


Figure 5.26 Experimental data (circle curves) - CL and Abs time courses for KMnO_4 oxidation reaction of glyoxylic acid in the presence of manganese(II). Fit shown ignores initial Mn(II). Reaction experimental conditions: $[\text{Mn(II)}] = 0.04\text{M}$; $[\text{OCHCO}_2\text{H}] = 0.1\text{M}$; $[\text{KMnO}_4] = 0.005\text{ M}$; $[\text{H}_2\text{SO}_4] = 2\text{M}$; Temperature = 25°C ; Wavelength = 525 nm .

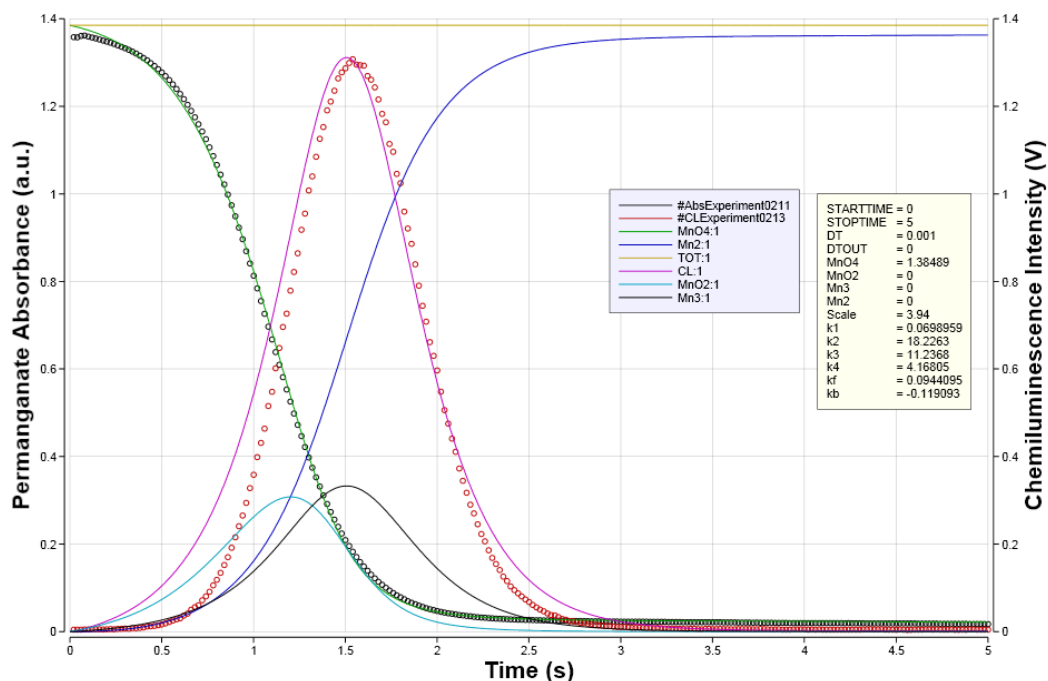


Figure 5.27 Experimental data (circle curves) - CL and Abs time courses for KMnO_4 oxidation reaction of glyoxal in the presence of manganese(II). Fit shown ignores initial Mn(II). Reaction experimental conditions: $[\text{Mn(II)}] = 0.04\text{M}$; $[\text{OCHCHO}] = 0.1\text{M}$; $[\text{KMnO}_4] = 0.005\text{ M}$; $[\text{H}_2\text{SO}_4] = 2\text{M}$; Temperature = 25°C ; Wavelength = 525 nm .

Table 5.12 Experimental reaction conditions for permanganate oxidation of glyoxal in the presence manganese(II) and estimated reaction rate constants.

Non-variables conditions of the reaction	[Mn ²⁺] / (M)	k ₁ (s ⁻¹)	k ₂ (s ⁻¹)	k ₃ (s ⁻¹)	k ₄ (s ⁻¹)	k _f (s ⁻¹)	k _b (s ⁻¹)
[OCHCHO] = 0.1M; [KMnO ₄] = 0.005M; T° = 25°C; [H ₂ SO ₄] = 2M	0.0	0.021	4.32	12.6	4.30	0.35	1.8x10 ⁻⁷
[OCHCHO] = 0.1M; [KMnO ₄] = 0.005M; T° = 25°C; [H ₂ SO ₄] = 2M	0.04	0.054	30.1	7.4	1.31	6.3x10 ⁻⁷	1.12
[OCHCHO] = 0.1M; [KMnO ₄] = 0.005M; T° = 25°C; [H ₂ SO ₄] = 2M	0.08	0.10	49.1	7.30	2.42	0.144	0.160
[OCHCHO] = 0.1M; [KMnO ₄] = 0.005M; T° = 25°C; [H ₂ SO ₄] = 2M	0.10	0.143	44.6	7.70	2.80	0.40	0.120
[OCHCHO] = 0.1M; [KMnO ₄] = 0.005M; T° = 25°C; [H ₂ SO ₄] = 2M	0.20	0.26	34.5	17.0	7.93	2.60	1.2 x10 ⁻⁸
[OCHCHO] = 0.1M; [KMnO ₄] = 0.005M; T° = 25°C; [H ₂ SO ₄] = 2M	0.30	0.513	142	8.30	4.0	4.14	1.1 x10 ⁻⁵

The results in Table 5.12 illustrate some of the established main characteristics of the MnO₄⁻ CL reaction such as the linear enhancement effect of the added Mn(II) on the reaction rates and CL signal intensity. To graphically illustrate the obtained results presented in table 5.12 above, the experimental data of k₁, k₂, k₃, k₄, k_f, k_b of the reactions monitored by UV absorbance were plotted vs. Mn(II) concentration.

Unexpectedly the plot of rate constants (k₁) versus manganese(II) concentration (Figure 25) produced a straight line dependence on manganese(II) concentration having a correlation coefficient of r = 0.999, with a positive slope = 1.10 and a positive intercept indicating first-order dependence on the manganese(II) concentration. This rather contradictory result on the dependence of equation 1 on manganese(II) concentration confirm the manganese(II) autocatalytic role which contributes for the feedback equation.

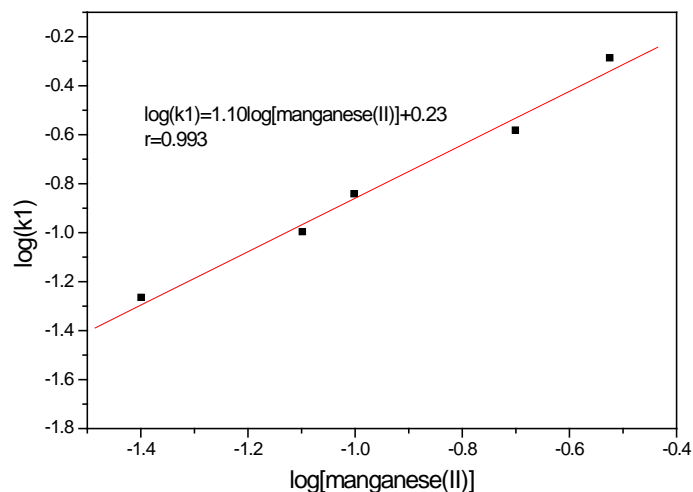


Figure 5.25 Plots and fittings showing the dependence of reaction rate constants (k_1) on $[\text{Mn}^{2+}]$. Reaction conditions: $[\text{Mn}^{2+}] = 0.1 - 1.6\text{M}$; $T^{\circ} = 25^{\circ}\text{C}$; $[\text{H}_2\text{SO}_4] = 2\text{M}$; $[\text{OCHCHO}] = 0.1\text{M}$.

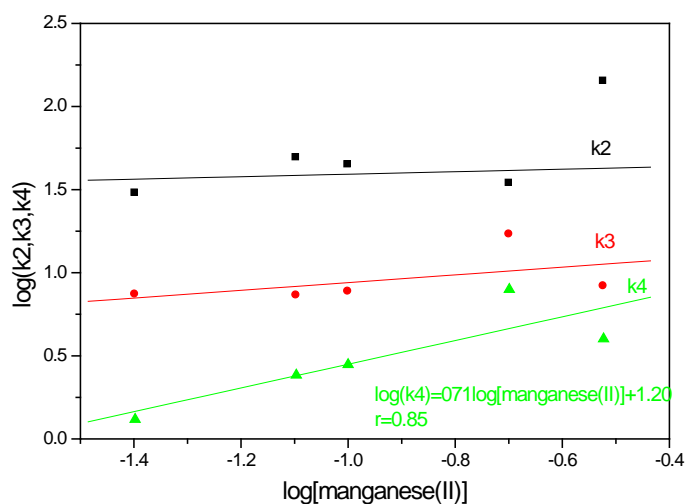


Figure 5.26 Plots and fittings showing the dependence of reaction rate constants (k_2 , k_3 , k_4) on $[\text{Mn}^{2+}]$. Reaction conditions: $[\text{Mn}^{2+}] = 0.1 - 1.6\text{M}$; $T^{\circ} = 25^{\circ}\text{C}$; $[\text{H}_2\text{SO}_4] = 2\text{M}$; $[\text{OCHCHO}] = 0.1\text{M}$.

As expected, rate constants k_2 and k_3 are independent on manganese(II) concentration; however, the plot of k_4 versus manganese(II) concentration shows some dependence on manganese(II) concentration. A possible explanation for this might be that the added manganese(II) concentration reacts with permanganate to form manganese(III) and the rate of the reaction 4.

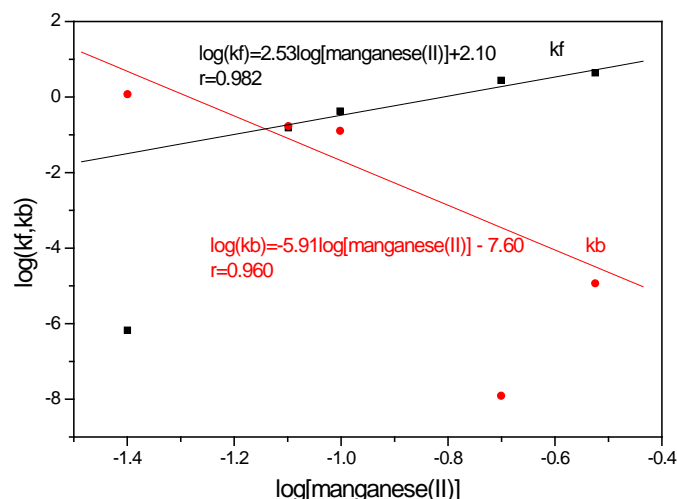


Figure 5.27 Plots and fittings showing the dependence of reaction rate constants (k_f , k_b) on $[\text{Mn}^{2+}]$. Reaction conditions: $[\text{Mn}^{2+}] = 0.1 - 1.6\text{M}$; $T^\circ = 25^\circ\text{C}$; $[\text{H}_2\text{SO}_4] = 2\text{M}$; $[\text{OCHCHO}] = 0.1\text{M}$.

Accordingly to expectations, the plot of rate constants (k_f) versus manganese(II) concentration (Figure 27) produced a straight line dependence on manganese(II) concentration having a correlation coefficient of $r = 0.960$, with a positive slope = 2.5 and a positive intercept indicating first-order dependence on the manganese(II) concentration. As the added manganese(II) concentration increased k_f increased favouring the reaction forward to pile up manganese(III) responsible for the chemiluminescence reaction, while k_b decreased.

The effect of manganese(II) concentration was studied with constant initial concentrations of 0.005M KMnO_4 , 0.2M glyoxal and $2\text{M H}_2\text{SO}_4$ at 25°C , while the initial manganese(II) concentration was varied from 0.04 to 0.2M . The results (the $\log k - \log [\text{Mn}^{2+}]$ profiles) are shown in Figure 5.28 and the derived values of rate constants (k) are provided in Table 5.12.

To visualize further how manganese(II) catalysis the permanganate oxidation to enhance chemiluminescence emission, another series of kinetic runs were carried out with glyoxylic acid by increasing the manganese(II) concentration (range: $0.04 - 0.3 \text{ mol dm}^{-3}$) at constant concentrations of other reactants and reaction factors including $[\text{MnO}_4^-] = 0.05 \text{ mol dm}^{-3}$; $[\text{H}_2\text{SO}_4] = 2.0 \text{ mol dm}^{-3}$ and temperature = 25°C . The experimental results are summarized in Table 5.13 below and derived graphs are shown in Figures 28 - 30.

Table 5.13 Experimental reaction conditions for permanganate oxidation of glyoxylic acid in the presence Mn(II) and estimated reaction rate constants.

Non-variables conditions of the reaction	[Mn ²⁺](M)	k ₁ (s ⁻¹)	k ₂ (s ⁻¹)	k ₃ (s ⁻¹)	k ₄ (s ⁻¹)	k _f (s ⁻¹)	k _b (s ⁻¹)
[OCHCO ₂ H] = 0.1M; [KMnO ₄]=0.005M; T° = 25°C; [H ₂ SO ₄]=2M	0.0	0.007	1.54	67.4	18.4	3.1 x 10 ⁻⁴	0.002
[OCHCO ₂ H] = 0.1M; [KMnO ₄]=0.005M; T° = 25°C; [H ₂ SO ₄]=2M	0.04	0.026	18.2	18.3	6.14	3.6 x 10 ⁻⁵	1.5 x 10 ⁻⁶
[OCHCO ₂ H] = 0.1M; [KMnO ₄]=0.005M; T° = 25°C; [H ₂ SO ₄]=2M	0.08	0.047	56.0	8.76	2.64	0.0052	0.0014
[OCHCO ₂ H] = 0.1M; [KMnO ₄]=0.005M; T° = 25°C; [H ₂ SO ₄]=2M	0.10	0.10	35.5	11.6	3.80	0.0028	5.6 x 10 ⁻⁴
[OCHCO ₂ H] = 0.1M; [KMnO ₄]=0.005M; T° = 25°C; [H ₂ SO ₄]=2M	0.20	0.44	18.8	47.3	21.3	0.0058	0.008
[OCHCO ₂ H] = 0.1M; [KMnO ₄]=0.005M; T° = 25°C; [H ₂ SO ₄]=2M	0.30	0.56	88.2	11.3	4.80	0.0096	0.044

The results in Table 5.13 illustrate some of the established main characteristics of the permanganate chemiluminescence reaction such as the linear enhancement effect of the added manganese(II) on the reaction rates and chemiluminescence signal intensity.

To graphically illustrate the obtained results presented in table 5.13 above, the experimental data of k₁, k₂, k₃,k₄ k_f,k_b of the reactions monitored by UV absorbance were plotted manganese(II) concentration.

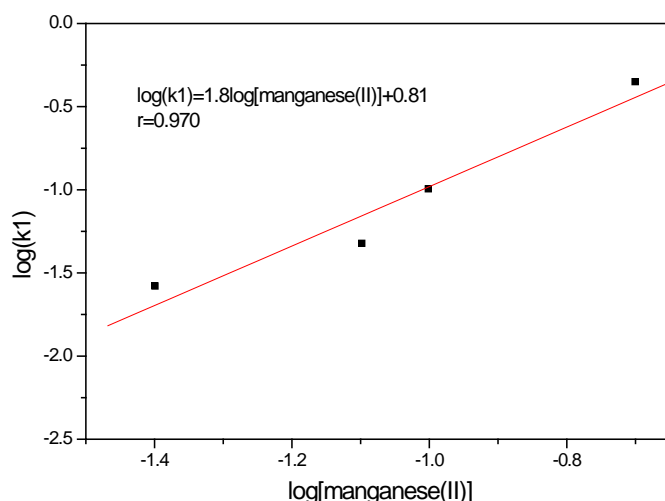


Figure 5.28 Plots and fittings showing the dependence of reaction rate constants (k_1) on $[\text{Mn}^{2+}]$. Reaction conditions: $[\text{Mn}^{2+}] = 0.1 - 1.6\text{M}$; $T^\circ = 25^\circ\text{C}$; $[\text{H}_2\text{SO}_4] = 2\text{M}$; $[\text{OCHCO}_2\text{H}] = 0.1\text{M}$.

Again, the plot of rate constants (k_1) versus manganese(II) concentration (Figure 28) produced a straight line dependence on manganese(II) concentration confirming the dependence of equation 1 on manganese(II) concentration and the manganese(II) autocatalytic role which contributes for the feedback equation.

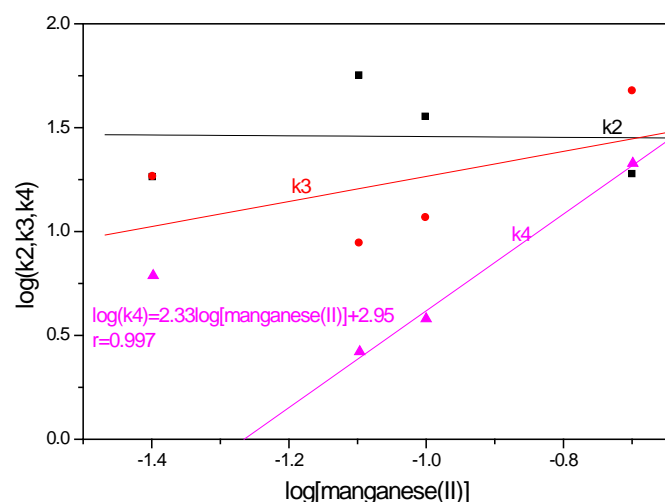


Figure 5.29 Plots and fittings showing the dependence of reaction rate constants (k_2 , k_3 , k_4) on $[\text{Mn}^{2+}]$. Reaction conditions: $[\text{Mn}^{2+}] = 0.1 - 1.6\text{M}$; $T^\circ = 25^\circ\text{C}$; $[\text{H}_2\text{SO}_4] = 2\text{M}$; $[\text{OCHCO}_2\text{H}] = 0.1\text{M}$.

As expected, rate constants k_2 and k_3 are independent on Mn(II) concentration; however, the plot of k_4 versus Mn(II) concentration confirms a dependence on manganese(II) concentration with a possible explanation for this might be that the added Mn(II) concentration reacts with MnO_4^- to pile up Mn(III), which increases the rate of the reaction 4.

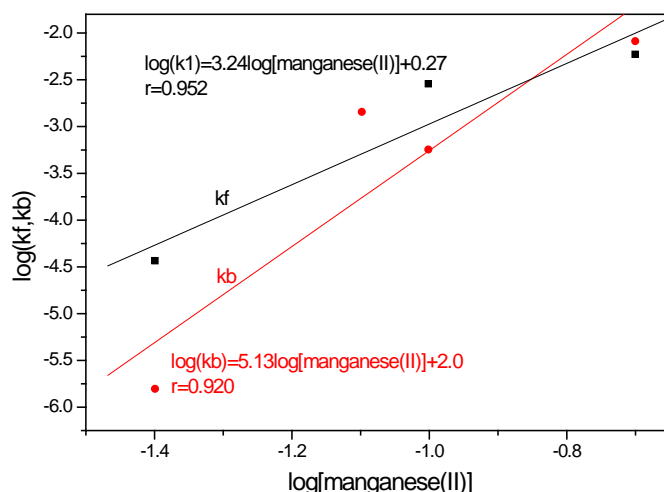


Figure 5.30 Plots and fittings showing the dependence of reaction rate constants (k_f , k_b) on $[\text{Mn}^{2+}]$. Reaction conditions: $[\text{Mn}^{2+}] = 0.1 - 1.6\text{M}$; $T^\circ = 25^\circ\text{C}$; $[\text{H}_2\text{SO}_4] = 2\text{M}$; $[\text{OCHCHO}] = 0.1\text{M}$.

As expected, the plot of rate constants (k_f) versus manganese(II) concentration (Figure 30) produced a straight line dependence on manganese(II) concentration indicating first-order dependence on the manganese(II) concentration. As the added manganese(II) concentration increased k_f increased favouring the reaction forward to pile up manganese(III), however, the plot showed that k_b increased as well.

The results of the chemical kinetic modelling investigation validate the revised mechanism, which has demonstrated to reproduce most of the CL experimental systems. Thus, confirming the hypothesis that the CL emission comes from the last step, which is the rate of formation of manganese(II) (i.e. an excited Mn(II)^* species as suspected).

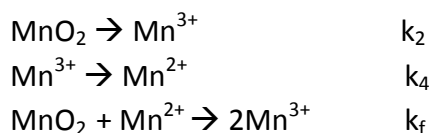
Therefore, the modelling results indicate that the mechanism of permanganate CL reaction, which has been tested against a variety of data from permanganate oxidation of glyoxylic acid and glyoxal experiments can be used to predict CL emission during permanganate CL processes. The kinetic model can also be used to obtain estimates the individual rate constants for permanganate oxidation process and predict the chemiluminescence emission process associated with the reaction.

5.3 Modelling Mn(IV) Chemiluminescence System

Manganese(IV) is generally believed to be an important reactive intermediate product in the permanganate oxidation process, and plays a key role in permanganate CL systems.

It was thus suggested in the preceding chapter that manganese(IV) is an additional major contributing factor for the CL reaction between permanganate and organic substrate, and it was successfully demonstrated that manganese(IV) reacts with organic substrates such as glyoxal and glyoxylic acid to produce a significant and measurable CL emission.

Based on the kinetic experiments obtained from Mn(IV) oxidation reactions over various organic substrates in the preliminary experiments in the precedent chapter, the following predictive model was developed to describe Mn(IV) CL oxidation in acidic solution and under the reaction conditions which stabilise manganese(IV):



This model assumes that organic substrate concentration is in large excess of manganese(IV) to ensure oxidation is of original organic species, unless daughters species react more rapidly, which may be likely. The accuracy of this kinetic model for predicting manganese(IV) CL systems was tested and validated by comparing the model predictions with the present experimental data for manganese(IV) oxidation CL systems.

The model can be used to determine kinetic parameters for manganese(IV) oxidation and chemiluminescence emission process that accompanies the oxidation reaction.

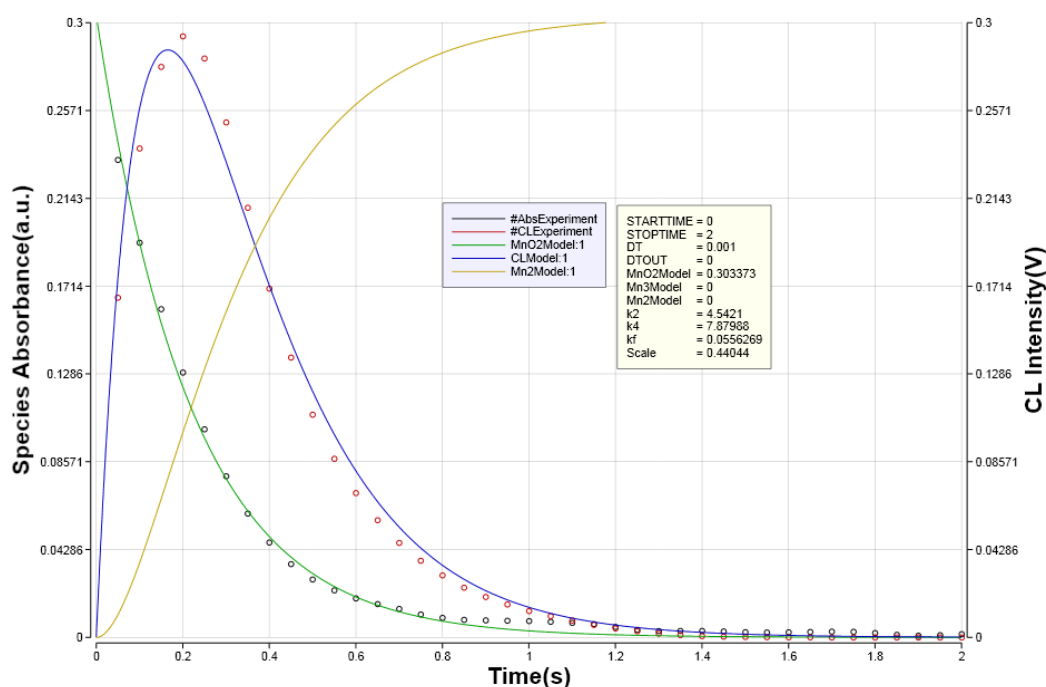


Figure 5.31 Comparison of kinetic model predictions (line curves) and experimental data (circle curves) - CL and Abs time courses for Mn(IV) oxidation reaction of glyoxylic acid. Reaction experimental conditions: [OCHCO₂H] = 0.8M; [Mn(IV)] = 0.0025 M; [H₂SO₄] = 2M; Temperature = 25° C; Wavelength = 400 nm

The results presented in Figure 5.31 show good agreements between model predictions and measurements of CL emission during oxidation of 0.8M glyoxylic acid with 0.0025M Mn(IV).

Both experimental data and model prediction for absorbance time course show >95% glyoxylic acid oxidation is achieved within two minutes and the model predictions fall within one standard deviation of the measured values. Thus, these results indicate that the kinetics model can be used to estimate kinetic parameters of manganese(IV) oxidation of many organic species and also predict the process of the CL emission that accompanies the oxidation reaction. It was hypothesised that the rate of CL emission is proportional to manganese(III) concentration and is the same as that for the change in Mn(II) concentration.

The accuracy of this kinetic model for predicting manganese(IV) CL systems was also tested and validated by investigating the effect of glyoxylic acid concentration using the reaction conditions in which the initial glyoxylic acid concentration in large excess over manganese(IV) was varied in the range 0.025 to 0.8M and manganese(IV) concentration was held constant at 0.0025M. The experimental results are summarized in Table 5.14 below and derived graphs are shown in Figure 32.

Table 5.14 Experimental reaction conditions for manganese(IV) oxidation of glyoxylic acid and estimated reaction rate constants.

Non-variables conditions of the reaction	Variables factors: [OCHCO ₂ H]/(M)	k ₂ (s ⁻¹)	k ₄ (s ⁻¹)	k _f (s ⁻¹)
[Mn(IV)] = 0.0025M; T ^o = 25°C; [H ₂ SO ₄]=2M	0.025	0.55	1.74	0.008
[Mn(IV)] = 0.0025M; T ^o = 25°C; [H ₂ SO ₄]=2M	0.05	0.93	1.35	0.004
[Mn(IV)] = 0.0025M; T ^o = 25°C; [H ₂ SO ₄]=2M	0.10	1.54	1.37	0.009
[Mn(IV)] = 0.0025M; T ^o = 25°C; [H ₂ SO ₄]=2M	0.20	2.38	1.22	0.009
[Mn(IV)] = 0.0025M; T ^o = 25°C; [H ₂ SO ₄]=2M	0.40	3.35	1.16	0.008
[Mn(IV)] = 0.0025M; T ^o = 25°C; [H ₂ SO ₄]=2M	0.80	4.40	1.40	0.005

To graphically illustrate the obtained results presented in table 5.14 above, the experimental data of k₂, k₄ and k_f of the reactions monitored by UV absorbance were plotted versus glyoxylic acid concentration.

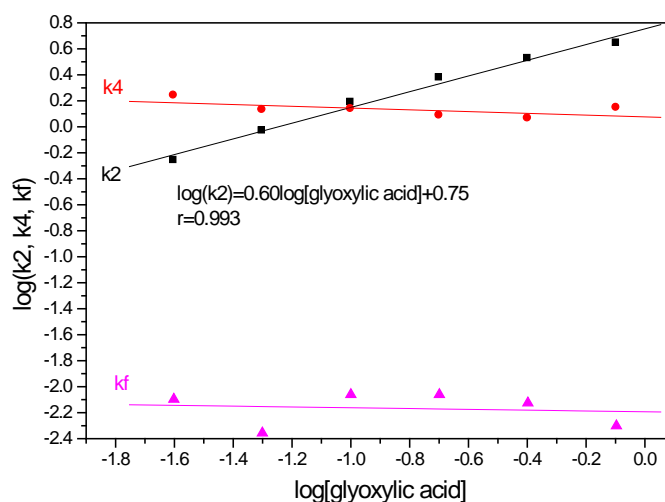


Figure 5.32 Plots and fittings showing the dependence of reaction rate constants (k_2 , k_4 and k_f) on $[\text{OCHCO}_2\text{H}]$. Reaction conditions: $[\text{OCHCO}_2\text{H}] = 0.025 - 0.8\text{M}$; $T^\circ = 25^\circ\text{C}$; $[\text{H}_2\text{SO}_4] = 2\text{M}$; $[\text{Mn (IV)}] = 0.0025\text{M}$.

It was expected that k_2 and k_4 would show first order dependence on glyoxylic acid concentration (R) and k_f would be independent of $[\text{glyoxylic acid}]$. As expected k_2 produced a straight line dependence on glyoxylic acid concentration having a correlation coefficient of $r = 0.993$, with a positive slope = 0.6 indicating a fractional-order dependence on the glyoxylic acid concentration. However, k_4 showed no dependence on the glyoxylic acid concentration.

A possible explanation is that most of glyoxylic acid is used to convert manganese(IV) to manganese(III), which reacts mainly with organic intermediates and which is the light-producing step in this concentration regime.

A good agreement was observed between the obtained numerical values representing the kinetics parameters and the chemiluminescence features, confirming a significant existing positive correlation between the oxidation reaction and the chemiluminescence process. The first-order dependence of rate constant (k_2) on glyoxylic acid concentration is consistent with the second step in the permanganate chemiluminescence reaction. Also these findings of the current study confirm our mechanistic working hypothesis that manganese (IV) oxidation reaction of glyoxylic acid lead to manganese (III) and the light-producing step in permanganate CL system.

5.4 Modelling the Mn(III) Chemiluminescence System

It was hypothesised in the preceding chapter that manganese(III) is a precursor for the observed CL emission in MnO_4^- oxidation reactions.

It has been demonstrated that manganese(III) can react with organic substrates such as glyoxal and glyoxylic acid to produce a significant and measurable chemiluminescence signal.

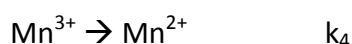
However, contrary to permanganate, under the reaction conditions, the experiments did not find any evidence for the reaction between manganese(III) and formaldehyde or manganese(II). This confirmed our earlier findings that manganese(II) and formaldehyde speed up only the first steps of the permanganate chemiluminescence reaction, which consists with permanganate reduction to generate manganese(III) intermediate.

The data obtained were fitted to exponential equation and the pseudo-first order rate constants (k_{obs}) produced and second order rate constants (k) calculated are shown in Table 5.15. As Table 5.15 shows, no significant difference were found between kinetics parameters and chemiluminescence features obtained from manganese(III) system with and without formaldehyde, confirming earlier results that, under the reaction conditions, the reaction between manganese(III) and formaldehyde is not very significant to make any contribution to the resulting chemiluminescence emission intensity of Mn(III) oxidation of glyoxal in the presence of formaldehyde.

Table 5.15 Rate constants for the $KMnO_4$ and Mn(III) chemiluminescence oxidations of Glyoxal with and without Formaldehyde

Non-variables Conditions of the Reaction	CL Decay		Absorbance change	
	k_{obs} (s^{-1})	k ($s^{-1}M^{-1}$)	k_{obs} (s^{-1})	k ($s^{-1}M^{-1}$)
$[MnO_4^-] = 0.02M$; $[OCHCHO] = 0.2M$; $T^{\circ} = 25^{\circ}C$; $[H_2SO_4] = 2M$	3.57	17.87	2.80	14.0
$[MnO_4^-] = 0.02M$; $[OCHCHO] = 0.2M$; $[H_2CO] = 0.75M$; $T^{\circ} = 25^{\circ}C$; $[H_2SO_4] = 2M$	4.41	22.0	3.60	18.0
$[MnO_4^-] = 0.02M$; $[H_2CO] = 0.75M$ $T^{\circ} = 25^{\circ}C$; $[H_2SO_4] = 2M$	No CL	No CL	0.97	1.30
$[Mn(III)] = 0.02M$; $[OCHCHO] = 0.2M$ $T^{\circ} = 25^{\circ}C$; $[H_2SO_4] = 2M$	4.16	20.8	3.40	17.0
$[Mn(III)] = 0.02M$; $[OCHCHO] = 0.2M$; $[H_2CO] = 0.75M$; $T^{\circ} = 25^{\circ}C$; $[H_2SO_4] = 2M$	3.63	18.2	3.32	16.60
$[Mn(III)] = 0.02M$; $[H_2CO] = 0.75M$; $T^{\circ} = 25^{\circ}C$; $[H_2SO_4] = 2M$	No Reaction	No Reaction	No Reaction	No Reaction

Based on the kinetic experiments obtained from manganese(III) oxidation, reactions with various organic substrates in the preliminary experiments in precedent chapter, the following predictive simplest model was developed to describe manganese(III) CL oxidation in acid solution and under the reaction conditions which stabilise manganese(III). The model can be used to determine kinetic parameters for manganese(III) oxidation and chemiluminescence emission process that accompanies the oxidation reaction.



The accuracy of this kinetic model for predicting manganese(III) CL systems was tested and validated by comparing the model predictions with the present experimental data for manganese(III) oxidation CL systems.

Results presented in Figure 5.33 and 5.34 show reasonably good agreements between model predictions and measurements of CL emission during oxidation of 0.8M glyoxylic acid or 0.5M glyoxal with 0.05M Mn(III), respectively. Both experimental data and model prediction for absorbance time course show >95% glyoxylic acid oxidation is achieved within one minutes and the model predictions fall within less than one standard deviation of the measured values.

Thus, these results indicate that the kinetics model can be used to obtain estimates kinetic parameters of Mn(III) oxidation of many organic species and also predict the process of the CL emission that accompanies the oxidation reaction. The solid line in Figure 5.33, for example, represents the best fit results, where $k_4=8.2 \text{ s}^{-1}$. It was hypothesized that the rate of CL emission is the same as that for the formation of Mn(II) or Mn(III) consumption. In curve fitting CL time course experimental data for this reaction, the rate of the CL decay ($k_4 = 8.3 \text{ s}^{-1}$) is the same as it falls within the standard deviation of the k_4 values obtained from fitting Mn^{3+} consumption.

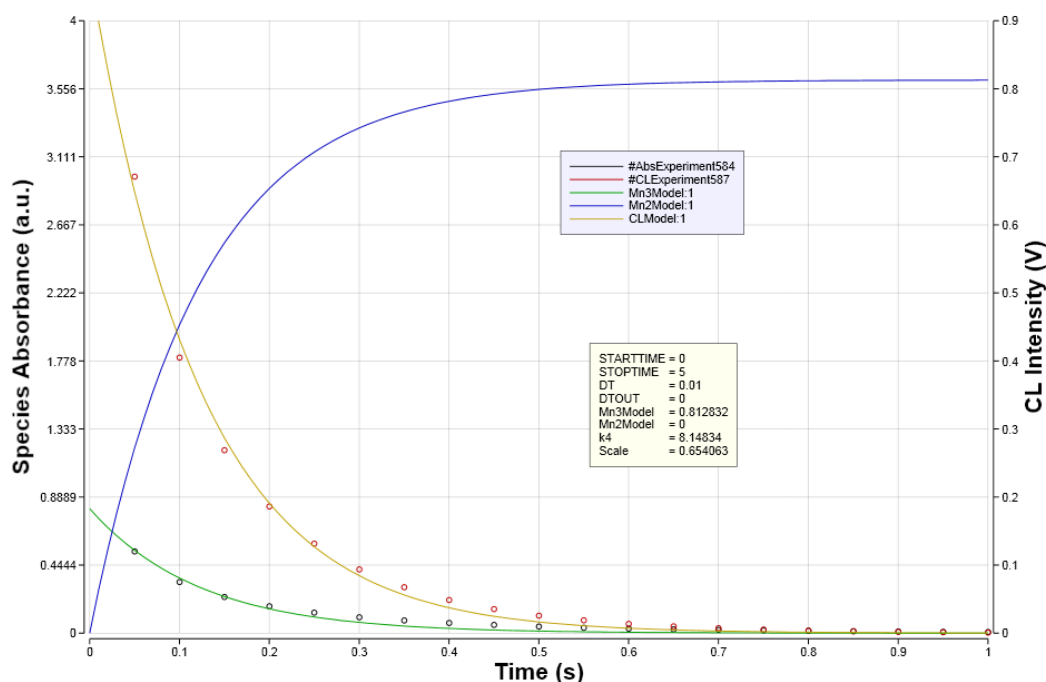


Figure 5.33 Comparison of kinetic model predictions (line curves) and experimental data (circle curves) - CL and Abs time courses for Mn(III) oxidation reaction of glyoxylic acid. Reaction experimental conditions: $[\text{OCHCO}_2\text{H}] = 0.8\text{M}$; $[\text{Mn(III)}] = 0.05 \text{ M}$; $[\text{H}_2\text{SO}_4] = 2\text{M}$; Temperature = 25°C ; Wavelength = 400 nm .

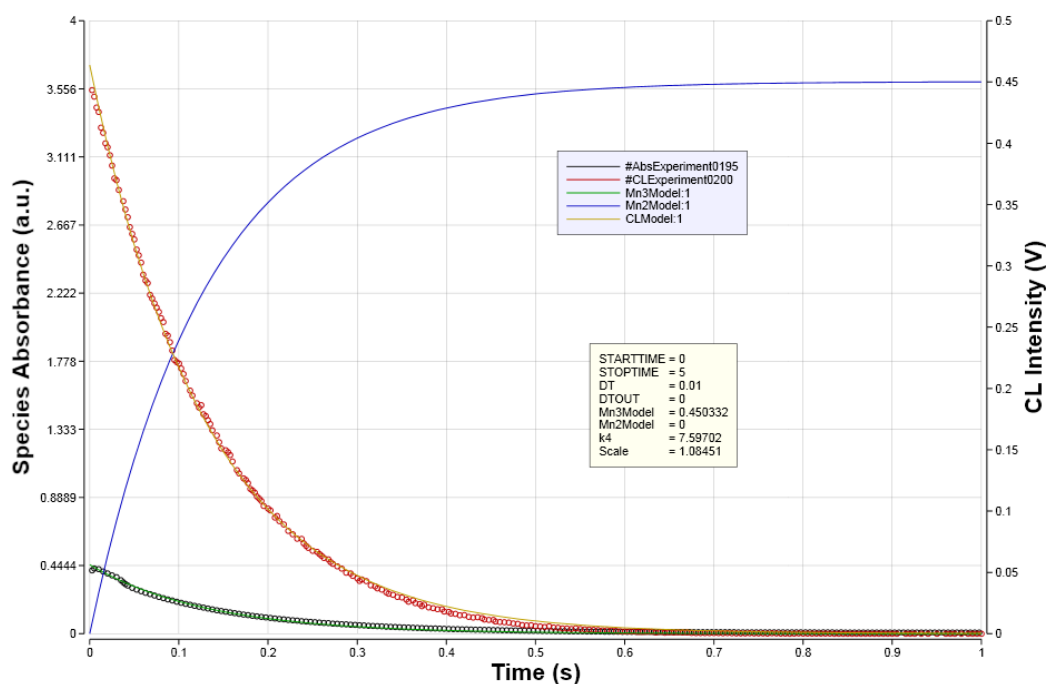


Figure 5.34 Comparison of kinetic model predictions (line curves) and experimental data (circle curves) - CL and Abs time courses for Mn(III) oxidation reaction of glyoxal. Reaction experimental conditions: [OCHCHO] = 0.5M; [Mn(III)] = 0.05 M; [H₂SO₄] = 2M; Temperature = 25° C; Wavelength = 400 nm.

It was also observed in the precedent chapter that the intensity of the chemiluminescence signal and the reaction rate increased with glyoxylic acid or glyoxal concentration (see Figure 4.23). Therefore, to test the kinetic model, a series of kinetic runs were performed, in which the initial concentration of manganese(III) was held constant at 0.05M while the initial glyoxylic acid concentration was varied from 0.025 to 0.8 M. The reaction rate constants (k_4) derived from the disappearance of unreacted Mn(III) are summarised in Tables 5.16.

Table 5.16 Experimental reaction conditions for manganese(III) oxidation of glyoxylic acid and estimated reaction rate constants (k_4).

Non-variables conditions of the reaction	Variables factors: [OCHCO ₂ H]/(M)	k_4 (s ⁻¹)
[Mn(III)] = 0.05M; T° = 25°C; [H ₂ SO ₄] = 2M	0.025	0.26
[Mn(III)] = 0.05M; T° = 25°C; [H ₂ SO ₄] = 2M	0.05	0.41
[Mn(III)] = 0.05M; T° = 25°C; [H ₂ SO ₄] = 2M	0.10	0.80
[Mn(III)] = 0.05M; T° = 25°C; [H ₂ SO ₄] = 2M	0.20	3.45
[Mn(III)] = 0.05M; T° = 25°C; [H ₂ SO ₄] = 2M	0.40	5.15
[Mn(III)] = 0.05M; T° = 25°C; [H ₂ SO ₄] = 2M	0.80	8.20

To determine the dependence upon excess glyoxylic acid concentration log of k_4 of the reactions monitored by visible absorbance were plotted versus log of the glyoxylic acid concentration.

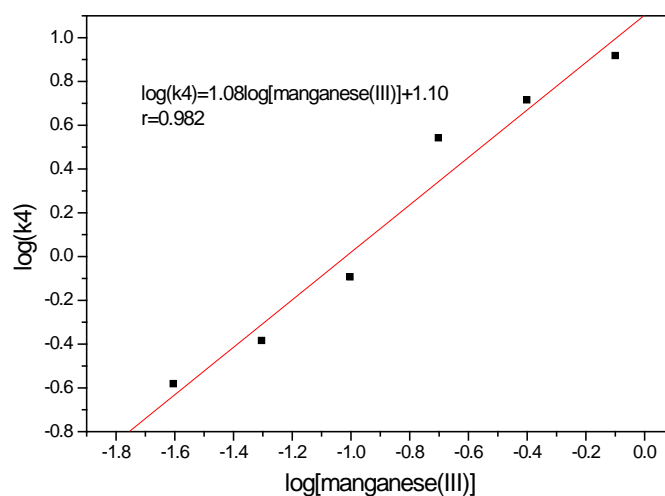


Figure 5.35 Plots and fittings showing the dependence of reaction rate constants (k_4) on $[\text{OCHCO}_2\text{H}]$. Reaction conditions: $[\text{OCHCO}_2\text{H}] = 0.025 - 0.8\text{M}$; $T^\circ = 25^\circ\text{C}$; $[\text{H}_2\text{SO}_4] = 2\text{M}$; $[\text{Mn}^{3+}] = 0.0025\text{M}$.

As expected the rate constant (k_4) showed a first-order dependence on the initial glyoxylic acid concentration, as measured by UV absorbance of the unreacted manganese(III).

In general, a good agreement was observed between obtained numerical values representing the kinetic parameters and the chemiluminescence features, confirming a significant existing positive correlation between the oxidation reaction and the CL process.

The first-order dependence of the rate constant (k_4) on glyoxylic acid concentration is consistent with the single step of the chemiluminescence oxidation reaction between manganese(III) and glyoxylic acid, with excess glyoxylic acid being the limiting chemiluminescence reagent under these reaction conditions. Also these findings of the current study confirm our mechanistic working hypothesis that manganese(III) oxidation reaction of glyoxylic acid is the light-producing step in permanganate chemiluminescence system.

5.5 Reaction Mechanism for Manganese-based Chemiluminescence Systems

The identification of the rate law provides valuable insight into the reaction mechanism, the sequence of elementary steps by which a reaction takes place. The aim of this section is to identify the CL-producing pathway by constructing the rate law that it implies. It has been well demonstrated that manganese-based oxidants, particularly permanganate oxidant is a versatile oxidizing agent and is largely used in chemiluminescence analytical technique and for studying the oxidation kinetics of many organic substrates.

The reaction mechanisms for different organic substrates suggested by various authors are not similar, indicating that a variety of mechanisms are possible, depending upon the nature of the reactive manganese species involved, the reaction conditions and environment, the nature of the organic substrate being oxidised, etc. However, the literature available on manganese-based chemiluminescence contains little information on the kinetics and mechanism resulting in the chemiluminescence process.

Herein, based in the obtained results from the preliminary experiments in the preceding chapter, the reaction of glyoxal and glyoxylic acid with acidic manganese oxidants were selected as case studies for the determination of the kinetics parameters and the chemiluminescence features that characterise the light-producing pathway and the mechanism of the chemiluminescence enhancement in manganese chemiluminescence systems.

This, because they have been found as a perfect representative examples of the relatively fast chemiluminescence reaction between a strong manganese oxidizing agent and an organic analyte. The emission from these particular reactions reaches maximum intensity within a few seconds and display good chemiluminescence signal shape under stopped-flow conditions.

As a preliminary to the understanding of the proposed mechanism of these manganese chemiluminescence reactions, it was essential that the emitting species is definitely known. Thus, all the results obtained in this study can be adequately explained by accepting that the emitting species in manganese-based chemiluminescence reactions was assigned to excited manganese(II) as a result of manganese(III) intermediate product reduction by an organic substrate.

A mechanism consistent with all of kinetics and chemiluminescence emissions observations is given in Figure 5.36 and the Table 5.17 summarizes the reaction steps probed by the kinetics, chemiluminescence emissions and the rate laws that apply to this mechanism for pseudo-first order conditions with organic substrate in large excess.

All of the results including kinetic modelling are consistent with the conclusion that under conditions of a large excess of organic substrate (e.g. glyoxal or glyoxylic acid) over permanganate, the formation of manganese(III) intermediate product is the rate limiting step for the chemiluminescence rise reaction, assuming that, under the reaction conditions in which the ratios of the organic substrate to MnO_4^- are at least 10:1, the oxidation reaction either between permanganate or Mn(III) intermediate product with daughter products is not likely to be significant.

By comparison of the time courses for the chemiluminescence emission and for disappearance of permanganate, it is possible to conclude that permanganate must be converted to an intermediate which then undergoes a chemiluminescence reaction.

Thus, the decrease in permanganate follows a first-order k_1 rate law while the build-up of the chemiluminescence signal intensity and the chemiluminescence signal decay of the intensity of the chemiluminescence emission follow consecutive first-order kinetics.

It has been found that the pseudo-first order rate constants, as measured by visible absorbance of the unreacted permanganate, have first-order dependence on the glyoxylic acid or glyoxal concentration. The first-order dependence of k_1 on the glyoxylic acid or glyoxal concentration is characteristic of the initial step of permanganate conversion to manganese(IV), then manganese(III) intermediate product, which undergoes later a reduction reaction accordingly to k_4 to produce CL emission.

With respect to formaldehyde signal enhancement effect, it was found that formaldehyde does affect the reaction rate and the chemiluminescence rise rate at significantly higher concentrations. The fact that, in a separate experiment and under a similar experimental conditions, no evidence of a reaction was observed between Mn(III) and formaldehyde, suggesting that in the presence of formaldehyde concentration, only the initial stage of the reaction is affected as a result of a direct reaction between permanganate and formaldehyde to form the manganese(IV), then the manganese(III) intermediate.

The comparison of the measured rate constant ($k_{\text{obs}} = 3.60 \text{ s}^{-1}$) for $\text{KMnO}_4^-/\text{Glyoxal}/\text{Formaldehyde}$ system is relatively equal to $\text{Mn(III)}/\text{Glyoxal}/\text{Formaldehyde}$ system ($k_{\text{obs}} = 3.02 \text{ s}^{-1}$), confirming that formaldehyde has no significant effect on manganese(III) oxidation reaction. We understand that in the presence of formaldehyde, there is a competition between formaldehyde and organic substrate to react with MnO_4^- , which increases the overall rate of reaction with subsequent increase in chemiluminescence signal emission.

It was also demonstrated that manganese(II) increases the reaction rate and chemiluminescence emission. Manganese(II) enhancement effect on permanganate chemiluminescence systems can only be explained by permanganate reduction as a result of a back reaction between Mn(II) and MnO_4^- to form manganese(III) intermediate.

The reaction rate constants, as measured by UV absorbance of the unreacted permanganate, have a first-order dependence on the added Mn(II).

Since there is no evidence of a reaction between Mn(II) and a Mn(III) intermediate, under the reaction conditions, the first-order dependence on the added Mn(II) concentration can only be a characteristic of the initial step of MnO_4^- conversion to Mn(IV), then Mn(III) intermediate product, which undergoes later a reduction reaction accordingly to k_4 to produce light.

Therefore, in presence of Mn(II), there is also a predominant catalysis reaction of Mn(II) and MnO_4^- , which results in increasing the reaction overall rate and CL emission.

Table 5.17 Summary of proposed reaction mechanism and approximate rate law

reaction step	excess of organic substrate (S) (e.g. glyoxal or glyoxylic acid)	In the presence of an enhancer additive (e.g. formaldehyde)	In the presence of a catalyst (e.g. Manganese(II))
$\text{MnO}_4^- + \text{xsS} \rightarrow \text{MnO}_2$ (k ₁) Initial step	reaction rate = -k ₁ [MnO ₄ ⁻] slow; not CL	rate = -(k ₁ +k')[MnO ₄ ⁻][HCHO] k ₁ < k' for [HCHO] ≥ 0.8M ; not CL	rate = -(k ₁ +k'')[MnO ₄ ⁻][M(II)] k ₁ < k'' for [Mn(II)] ≤ 0.1M; not CL
$\text{MnO}_2 + \text{xsS} \rightarrow \text{Mn(III)}$ (k ₂)	reaction rate = -k ₂ [MnO ₂] k ₁ < k ₂ ; not CL	-	-
$3\text{Mn(III)} + \text{MnO}_4^- \rightarrow 4\text{MnO}_2$ (k ₃)	reaction rate = -k ₃ [MnO ₄ ⁻][M(III)] ³ not CL	-	-
$\text{Mn(III)} + \text{xsS} \rightarrow \text{Mn(II)} + \text{light}$ (k ₄)	reaction rate = -k ₄ [Mn(III)] fast; CL step	-	-
$\text{MnO}_2 + \text{Mn(II)} \leftrightarrow 2\text{Mn(III)}$ K _{eq} =k _f /k _b	reaction rate = k _f [MnO ₂][M(II)] reaction rate = k _b [M(III)] not CL	-	k _f favoured

The presence of Mn(VI) and Mn(V) could not be demonstrated, as they are highly unstable in acid medium and difficult to measure. However, under the reaction conditions, it is believed that, like permanganate, Mn(IV) is rapidly converted to an Mn(III) intermediate product, either by Mn(II) or a reducing agent.

In acidic solution, permanganate is reduced to Mn(II) and produces chemiluminescence emission if excess of organic reducing agent is present, whereas in the presence of excess permanganate, a possible MnO₂ solid is formed as a result of the oxidation of Mn(II) by MnO₄⁻ with subsequent quenching effect on chemiluminescence intensity.

Taken together, these findings suggest that the role for external addition of Mn(II) and formaldehyde in enhancing chemiluminescence signal emission can be explained by virtue of a chemical reaction with permanganate rather than by virtue of a physical process of solution mixing.

The current findings add substantially to our understanding of manganese-based chemiluminescence systems and its chemiluminescence signal enhancement. It has been well demonstrated that most chemiluminescence responses of organic species, such as glyoxal and glyoxylic acid, in the manganese-based systems result from that the chemical oxidation of these species producing strong reducing intermediates, usually manganese(III) species, which react immediately with an organic substrate to generate excited-state Mn(II)* and lead to light emission.

It is anticipated that this work will lead to a better interpretation of solution CL and hence better design of methods. This can be illustrated by considering recent papers involving CL using permanganate, all of which involve other species usually referred to as enhancers.

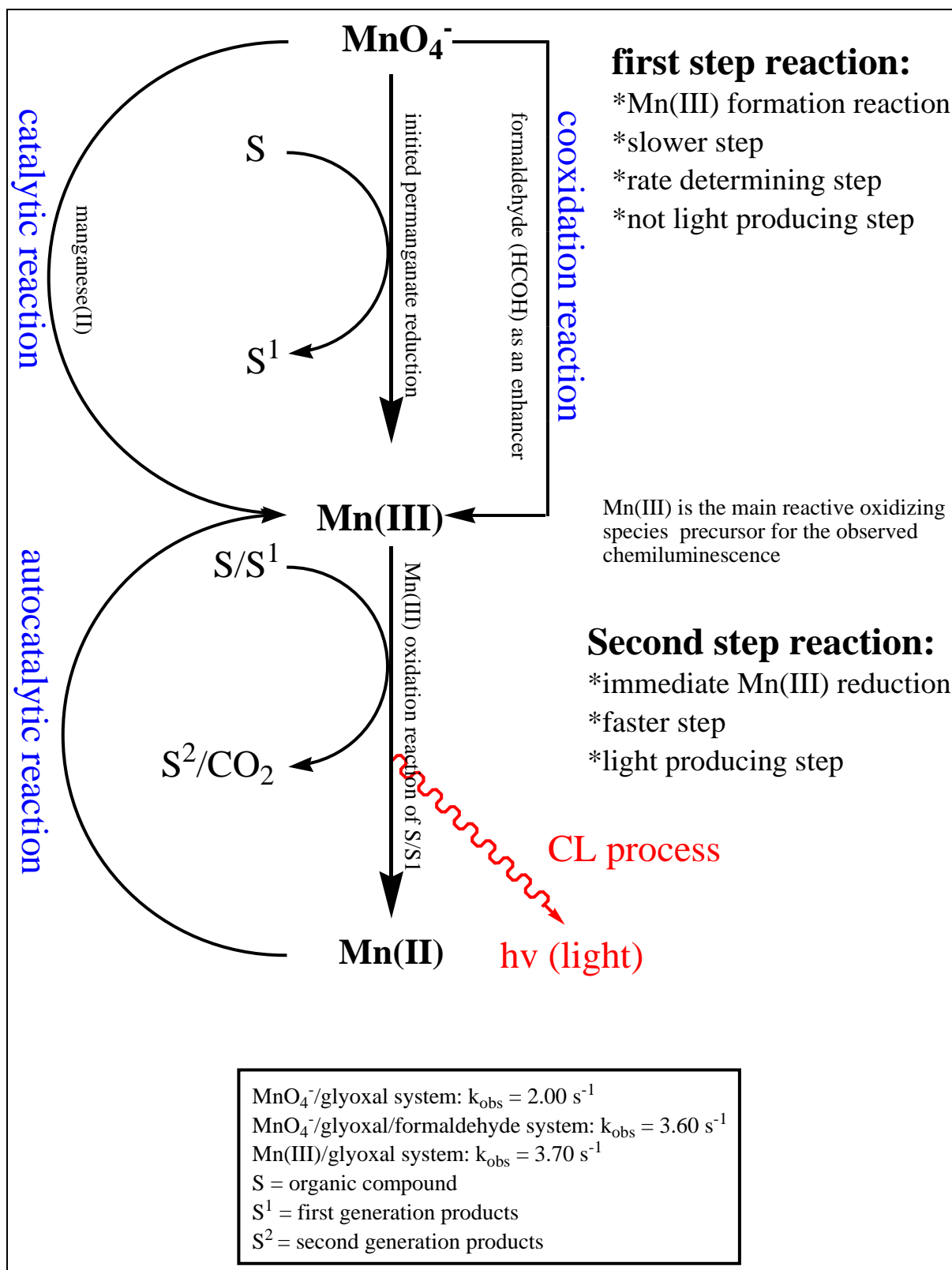
Many of these papers use formaldehyde as an enhancer. In a study of the chemiluminescent oxidation of lipoic acid⁵⁸⁴, a range of potential enhancers were tried including potential energy transfer fluorophores and formaldehyde without explanation as was the use of formaldehyde in catecholamine detection^{424, 585} in another publication. The optimisation of these methods in flow systems were carried out entirely empirically.

There have been some quite detailed studies of the design of flow detection cells using permanganate with and without thiosulphate⁵⁸⁶. Thiosulphate, described as an enhancer, was used to generate Mn²⁺ in situ to increase the rate of oxidation by permanganate^{140, 587} and hence the chemiluminescence. Strangely, this was compared to the addition of Mn²⁺ to permanganate prior to mixing, which in the absence of a reductant is slow and it is not clear why thiosulphate should have any advantage over the direct addition of Mn²⁺, although we have not verified this. What is clear, however, is that the optimisation of the flow cell design should be much easier knowing the rates of the appropriate reactions.

Many reported methods are even more complicated. Chromium(IV), toxic at low levels, has been detected in aqueous solutions using peroxide, permanganate and gallic acid⁵⁸⁸. We have shown that dichromate oxidations in the presence of Mn^{2+} produce Mn^{3+} and hence chemiluminescence and permanganate and peroxide will generate Mn^{3+} . We have also shown that the oxidation of gallic acid by permanganate is rapid, so the observation of chemiluminescence in this mixture is not surprising and would be better understood in terms of the kinetics.

It is reported²¹⁸ that Mn(III) and Mn(IV) oxidations differ markedly in selectivity and sensitivity from permanganate. These differences will undoubtedly be due to the rates of the reactions and again optimisation of flow conditions would be considerably aided by an understanding of the rate constants.

Luminol chemiluminescence is another fertile area for chemiluminescence and published methods again usually include enhancers. In a method for the determination of catecholamines using periodate and luminol, enhancement was observed for gallic acid, acetaldehyde and Manganese(II)⁵⁸⁹. The conditions here are alkaline rather than acidic as studied here, but the generation of oxidising manganese species from periodate and Mn^{2+} is likely.



Scheme 5.1 The proposed mechanism for the enhancement of the observed CL emission during the oxidation reaction of glyoxal by MnO_4^-

Chapter 6

Conclusions

This research has investigated the kinetics of some oxidations by permanganate, manganese(IV) and manganese(III) compounds which exhibit chemiluminescence and thus are of analytical interest. The group has previously suggested that the chemiluminescence from all three reactions has the same origin and that the origin of action of so-called enhancers and sensitizers is kinetic.

An attempt has been made to find a simple kinetic mechanism to fit the decay of the three oxidants with several substrates. The mechanism of permanganate oxidations has been studied for around 150 years without a definitive model and although this work has not solved that problem, using a simple model has enabled us to predict the chemiluminescence emission and explain the observed behaviour of mixtures.

Under the conditions used, the decay of permanganate shows a sigmoidal decay curve characteristic of autoxidation most simply explained by a feedback from Mn^{2+} product after the formation of an intermediate species such as MnO_2 or Mn^{3+} . For the simplest mechanism and the acid conditions used, it has been assumed that this is Mn^{3+} , although the choice does not affect the fit of the model.

In the proposed mechanism, the emission of chemiluminescence is assumed to be at the final stage, which is reduction of Mn^{3+} to Mn^{2+} . Although it is postulated that this involves an excited Mn^{2+} species, this does not affect the validity of the approach and the mechanism would still apply if chemiluminescence involved other species, such as MnO_2 , as MnO_2 , Mn^{3+} and Mn^{2+} are in equilibrium with each other.

Addition of Mn^{2+} is known to increase the rate of permanganate oxidations, but does not remove the induction as predicted by the simple mechanism. An alternative more complex mechanism has been suggested to explain this, although this is not entirely satisfactory. Nevertheless, the observed increase in chemiluminescence matches the change in kinetics as predicted.

The explanation for enhancement as a kinetic effect is clearly demonstrated by aqueous formaldehyde. Formaldehyde is observed to reduce permanganate to Mn^{3+} rather than the more usual Mn^{2+} . This reaction does not exhibit chemiluminescence. The addition of excess formaldehyde in addition to another reductant thus increases the rate of formation of Mn^{3+} and thus the chemiluminescence. The rates of the reaction mixture are in excellent agreement with those observed for the constituent components.

Although it was not possible to prepare MnO_2 (sol) and Mn^{3+} under identical conditions to those used for permanganate oxidations, the kinetic model is applicable to these and the three reactions were shown to be consistent.

Using this kinetic approach it should now be possible to predict the effect of mixtures and of reaction conditions on chemiluminescent reactions of analytical importance. Not only does an understanding of the kinetics and mechanism enable the optimisation of the conditions for chemiluminescence, it also enables the prediction of suitable enhancers. This approach whilst demonstrated for permanganate reactions is clearly much more generally applicable. This is in contrast to the more serendipitous approach used to date.

Future work should involve the extension to other conditions, for example the effect of pH on manganese oxidations, and also other oxidants and reductants.

Bibliographic References

1. I. Kruk, *Environmental Toxicology and Chemistry of Oxygen Species*, Springer-Verlag, 1998.
2. E. N. Harvey, *History of Luminescence from the Earliest Times Until 1900*, American Philosophical Society, 1980.
3. A. K. Campbell, *Chemiluminescence: principles and applications in biology and medicine*, VCH, 1988.
4. A. M. G. Campaña and W. R. G. Baeyens, *Chemiluminescence in Analytical Chemistry*, Marcel Dekker, 2001.
5. J.L. Adcock, N.W. Barnett, J. J.W. Costin, P.S. Francis and S.W. Lewis, *Talanta*, 2005, **67**, 585-589.
6. B. J. Hindson and N. W. Barnett, *Analytica Chimica Acta*, 2001, **445**, 1-19.
7. J. L. Adcock, P. S. Francis and N. W. Barnett, *Analytica Chimica Acta*, 2007, **601**, 36-67.
8. S. Kulmala and J. Suomi, *Analytica Chimica Acta*, 2003, **500**, 21-69.
9. I. B. Agater, (1999). Applications of Permanganate Chemiluminescence to the Analysis of Food Components. Department of Chemical and Biological Sciences. Huddersfield, University of Huddersfield. PhD Thesis: 236.
10. A. Abdel-Mageed, (2002). Development and Mechanistic Study of a Manganese(III) CL Sensor for On-Line Trace Environment and Industrial Analysis. Department of Chemical and Biological Sciences. Huddersfield, University of Huddersfield. PhD Thesis: 178.
11. P. Fletcher, K. N. Andrew, A. C. Calokerinos, S. Forbes and P. J. Worsfold, *Luminescence*, 2001, **16**, 1-23.
12. J. Cepas, M. Silva and D. Pérez-Bendito, *Journal of Chromatography A*, 1996, **749**, 73-80.
13. J. Ishida, T. Yakabe, H. Nohta and M. Yamaguchi, *Analytica Chimica Acta*, 1997, **346**, 175-181.
14. G. H. G. Thorpe and L. J. Kricka, *Methods in Enzymology*, 1986, **133**, 331-353.
15. N. W. Barnett, D. G. Rolfe, T. A. Bowser and T. W. Paton, *Analytica Chimica Acta*, 1993, **282**, 551-557.
16. J. E. Wampler, *Instrumentation: Seeing the Light and Measuring It, in Chemi- and Bioluminescence*, J.G. Burr, ed, Marcel Dekker, New York, 1985.
17. F. Berthold, *Instrumentation for Chemiluminescence Immunoassays, in Luminescence Immunoassay and Molecular Applications*, K. Van Dyke and R. Van Dyke, eds, CRC Press, Boca Raton, 1990.
18. T. Nieman, *Chemiluminescence: Theory and Instrumentation, Overview, in Encyclopedia of Analytical Science*, Academic Press, Orlando, 1995.
19. J. M. Terry, J. L. Adcock, D. C. Olson, D. K. Wolcott, C. Schwanger, L. A. Hill, N. W. Barnett and P. S. Francis, *Analytical Chemistry*, 2008, **80**, 9817-9821.
20. X. A. Conlan, N. Stupka, G. P. McDermott, N. W. Barnett and P. S. Francis, *Analytical Methods*, 2010, **2**, 171-173.
21. Z. Gong, Y. Zhang, H. Zhang and J. Cheng, *Journal of Chromatography A*, 1999, **855**, 329-335.
22. N. W. Barnett, C. E. Lenehan, S. W. Lewis, D. J. Tucker and K. M. Essery, *Analyst* 1998, **123**, 601- 605.
23. N. W. Barnett, S. W. Lewis and D. J. Tucker, *Analytical Chemistry*, 1996, **355**, 591-595.
24. N. W. Barnett, B. J. Hindson and S. W. Lewis, *Analyst*, 2000, **125**, 91-95.
25. J. W. Costin, S. W. Lewis, S. D. Purcell, L. R. Waddell, P. S. Francis and N. W. Barnett, *Analytica Chimica Acta* 2007, **597**, 19-23.
26. C. E. Lenehan, N. W. Barnett, S. W. Lewis and K. M. Essery, *Australian Journal of Chemistry*, 2004, **57**, 1001-1004.
27. R. Su, J. M. Lin, F. Qu, Z. Chen, Y. Gao and M. Yamada, *Analytica Chimica Acta*, 2004, **508**, 11-15.
28. Y. Sun, Y. Tang, H. Yao and Y. Li, *Analytical Sciences*, 2005, **21**, 457-460.
29. W. Cao, J. Yang, C. Sun, Y. Chen and Q. Gao, *Luminescence*, 2005, **20**, 20-24.
30. K. Zhao, J. Shi and Q. Song, *Fenxi Shiyanshi* 2005, **24**, 12-14.
31. Y. Liang, J. Song and S. Zhao, *Xi'an Keji Xueyuan Xuebao*, 2004, **24**, 336-338 349.
32. Z. Zhang and R. Fan, *Fenxi Shiyanshi*, 2007, **26**, 97-99.
33. M. C. Icardo, J. V. G. Mateo, M. F. Lozano and J. M. Calatayud, *Analytica Chimica Acta*, 2003, **499**, 57-69.
34. H. Liu, J. Ren, Y. Hao, P. He and Y. Fang, *Talanta*, 2007, **72**, 1036-1041.
35. H. Paseková, M. Polásek, J. F. Cigarro and J. Dolejšová, *Analytica Chimica Acta*, 2001, **438**, 165-173.
36. D. Zhang, Y. Ma, M. Zhou, L. Li and H. Chen, *Analytical Sciences*, 2006, **22**, 183-186.
37. Y. Sun, Y. Tang, H. Yao and X. Zheng, *Talanta*, 2004, **64**, 156-159.
38. C. Thongpoon, B. Liawruangrath, S. Liawruangrath, R.A. Wheatley and A. Townshend, *Journal of Pharmaceutical and Biomedical Analysis*, 2006, **42**, 277-282.
39. F. A. Aly, N. A. Alarfajj and A. A. Alwarthan, *Talanta*, 1998, **47**, 471-478.
40. Z. Chen, F. Cai, Y. Huang and W. Liu, *Xinan Shifan Daxue Xuebao, Ziran Kexueban*, 2002, **27**, 806-810.

41. J. Wang and H. Xiong, *Fenxi Shiyanshi* 2004, **23**, 9-13.
42. Z. Chen and Y. Huang, *Xinan Shifan Daxue Xuebao, Ziran Kexueban* 2004, **29**, 991-995.
43. D. Zhang, Y. Ma, M. Zhou, Y. Yang, X. Zhou and H. Chen, *Fenxi Shiyanshi* 2006, **25**, 44-47.
44. H. Paseková and M. Polásek, *Talanta*, 2000, **52**, 67-75.
45. X. R. Zhang, W. R. G. Baeyens, G. V. Der Weken, A. C. Calokerinos and K. Imai, *Analytica Chimica Acta*, 1995, **303**, 137-142.
46. S. M. Sultan, A. M. S. Abdennabi and A. d. M. Almuaibed, *Talanta*, 1999, **49**, 1051-1057.
47. S. M. Sultan, Y. A. M. Hassan and A. M. Abulkibash, *Talanta*, 2003, **59**, 1073-1080.
48. A. Townshend, *Analyst* 1990, **115**, 495-500.
49. R. W. Abbott, A. Townshend and R. Gill, *Analyst*, 1987, **112**, 397-406.
50. L. Zhu, M. Feng, X. Wan and J. Lü, *Fenxi Huaxue*, 1996, **24**, 1295-1297.
51. E. Amriott and A. R. J. Andrews, *Journal of Liquid Chromatography & Related Technologies*, 1997, **20**, 311 - 325.
52. J. L. Adcock, N. W. Barnett, J. W. Costin, P. S. Francis and S. W. Lewis, *Talanta*, 2005, **67**, 585-589.
53. J. L. Adcock, P. S. Francis, K. M. Agg, G. D. Marshall and N. W. Barnett, *Analytica Chimica Acta*, 2007, **600**, 136-141.
54. J. Stauff and W. Jaeschke, *Atmospheric Environment* 1975, **9**, 1038-1039.
55. W. Jaeschke, J. Stauff and Ber, *Bunsen-Ges*, 1978, **82**, 1180-1184.
56. F. X. Meixner and W. A. Jaeschke, *International Journal of Environmental Analytical Chemistry*, 1981, **10**, 51-67.
57. W. Jaeschke, R. Schmitt and H. W. Georgii, *Geophysical Research Letters*, 1976, **3**, 517-519.
58. W. Jaeschke and W. Haunold, *WMO Publication Part-II*, 1977, **460**, 193-198.
59. W. Jaeschke, *Atmospheric Environment* 1978, **12**, 715-721.
60. F. Meixner and W. Jaeschke, *Fresenius' Journal of Analytical Chemistry*, 1984, **317**, 343-344.
61. F. X. Meixner, *Journal of Atmospheric Chemistry*, 1984, **2**, 175-189.
62. P. W. West and G. C. Gaeke, *Analytical Chemistry*, 1956, **28**, 1816-1819.
63. M. Ishii, M. Miura and J. Sato, *Bunseki Kagaku*, 1992, **41**, 157-162.
64. H. Meng, F. Wu, Z. He, L. Yuan, Q. Luo and Y. Zeng, *International Journal of Environmental Analytical Chemistry*, 1999, **75**, 299-307.
65. H. Meng, F. Wu, Z. He and Y. Zeng, *Talanta*, 1999, **48**, 571-577.
66. M. Kato, M. Yamada and S. Suzuki, *Analytical Chemistry*, 1984, **56**, 2529-2534.
67. T. G. Climent, J. R. Albert-García and J. M. Calatayud, *Analytical Letters*, 2007, **40**, 629-643.
68. M. Palomeque, J. A. Garcla Bautista, M. Catalá Icardo, J. V. Garcla Mateo and J. Martínez Calatayud, *Analytica Chimica Acta*, 2004, **512**, 149-156.
69. J. R. Albert-García, M. C. Icardo and J. M. Calatayud, *Talanta*, 2006, **69**, 608-614.
70. J. A. Murillo Pulgarin, L. F. Garcia Bermejo and J. A. Rubio Aranda, *Journal of Agricultural and Food Chemistry*, 2005, **53**, 6609-6615.
71. A. Chivulescu, M. Catalá-Icardo, J. V. García Mateo and J. Martínez Calatayud, *Analytica Chimica Acta*, 2004, **519**, 113-120.
72. G. Z. Tsogas, D. L. Giokas, P. G. Nikolakopoulos, A. G. Vlessidis and N. P. Evmiridis, *Analytica Chimica Acta*, 2006, **573-574**, 354-359.
73. J. Michalowski, P. Halaburda and A. Kojlo, *Analytical Letters*, 2000, **33**, 1373 - 1386.
74. W. Cao, X. Mu, J. Yang, W. Shi and Y. Zheng, *Spectrochimica Acta Part A: Molecular and Biomolecular Spectroscopy*, 2007, **66**, 58-62.
75. K. Fujimori, N. Takenaka, H. Bandow and Y. Maeda, *Analytical Communications*, 1998, **35**, 307-308.
76. B. Gómez-Taylor Corominas, J. V. García Mateo, L. Lahuerta Zamora and J. Martínez Calatayud, *Talanta*, 2002, **58**, 1243-1251.
77. K. Fujimori, W. Ma, T. Moriuchi-Kawakami, Y. Shibutani, N. Takenaka, H. Bandow and Y. Maeda, *Analytical Sciences*, 2001, **17**, 975-978.
78. M. Feng, Z. Li, J. Lu and H. Jiang, *Microchimica Acta*, 1997, **126**, 73-76.
79. M. C. Icardo, J. V. G. Mateo and J. M. Calatayud, *Analyst* 2001, 1423-1427.
80. K. Takeuchi and T. Ibusuki, *Kogai* 1984, **19**, 239-248.
81. I. S. Ricart, G. M. Antón-Fos, M. J. Duart, J. V. G. Mateo, L. L. Zamora and J. M. Calatayud, *Talanta* 2007, **72**, 378-386.
82. S. I. Montalvo and J. D. Ingle, *Talanta*, 1993, **40**, 167-172.
83. J. W. Costin, N. W. Barnett, S. W. Lewis and D. J. McGillivray, *Analytica Chimica Acta* 2003, **499**, 47-56.
84. W. Qin, Z. Zhang and C. Zhang, *Analytica Chimica Acta*, 1998, **361**, 201-203.

85. I. B. Agater and R. A. Jewsbury, *Analytica Chimica Acta*, 1997, **356**, 289-294.
86. Y. Huang and Z. Zhang, *Analytical Letter*, 2003, **36**, 2783-2792.
87. K. Luo, K. Wang, B. Peng, X. Yang and H. Li, *Fenxi Ceshi Xuebao*, 1999, **18**, 9-11.
88. X. Wang, J. Wang and N. Yang, *Food Chemistry*, 2007, **102**, 422-426.
89. M. Yaqoob, R. A. Ur, A. Waseem and A. Nabi, *Luminescence*, 2006, **21**, 221-225.
90. Q. Gao, C. Wang and Y. B. 23, *Shipin Gongye Keji* 2002, **23**, 68-69.
91. E. Liu, S. Han, H. Wei, J. Liang, R. Ren and J. Cheng, *Fenxi Kexue Xuebao* 2002, **18**, 207-209.
92. C. Gao, S. Fan and J. Yao, *Fenxi Shiyanshi* 2006, **25**, 38-41.
93. Z. Xie, X. Ouyang, L. Guo, X. Lin and G. Chen, *Luminescence*, 2005, **20**, 231-235.
94. M. Timotheou-Potamia and A. C. Calokerinos, *Talanta*, 2007, **71**, 208-212.
95. T. Slezak, P. S. Francis, N. Anastos and N. W. Barnett, *Analytica Chimica Acta*, 2007, **593**, 98-102.
96. A. Townshend, R. A. Wheatley, A. Chisvertb and A. Salvadorb, *Analytica Chimica Acta*, 2002, **462**, 209-215.
97. Y. Wei, Z. Zhang, Y. Zhang and Y. Sun, *Chromatographia*, 2007, **65**, 443-446.
98. B. Gómez-Taylor Corominas, M. Catalá Icardo, L. Lahuerta Zamora, J. V. García Mateo and J. Martínez Calatayud, *Talanta*, 2004, **64**, 618-625.
99. P. S. Francis, J. W. Costin, X. A. Conlan, S. A. Bellomarino, J. A. Barnett and N. W. Barnett, *Food Chemistry*, 2010, **122**, 926-929.
100. N. Anastos, N. W. Barnett, S. W. Lewis, N. Gathergood, P. J. Scammells and D. N. Sims, *Talanta*, 2005, **67**, 354-359.
101. L. J. Kricka and P. E. Stanley, *Journal of Bioluminescence and Chemiluminescence*, 1996, **11**, 271-288.
102. L. J. Kricka, *Journal of Bioluminescence and Chemiluminescence*, 1988, **2**, 171-171.
103. I. Weeks, *Chemiluminescence Immunoassay*, Elsevier, New York, 1992.
104. J. W. Birks, *Chemiluminescence and Photochemical Reaction Detection in Chromatography*, VCH, New York, 1989.
105. J. G. Burr, *Chemi- And Bioluminescence*, Marcel Dekker, New York, 1985.
106. W. Adam and G. C. (eds.), *Chemical and Biological Generation of Excited States*, Academic Press, New York, 1982.
107. M. A. DeLuce, *Bioluminescence and Chemiluminescence, Methods in Enzymology, LVII*, Academic Press, New York, 1978.
108. J. Wang and S. Thongngamdee, *Analytica Chimica Acta*, 2003, **485**, 139-144.
109. N. T. Deftereos, N. Grekas and A. C. Calokerinos, *Analytica Chimica Acta*, 2000, **403**, 137-143.
110. R. W. Abbott, A. Townshend and R. Gill, *Analyst* 1986, **111**, 635-640.
111. A. A. Alwarthan and A. Townshend, *Analytica Chimica Acta*, 1986, **185**, 329-333.
112. N. W. Barnett, B. J. Hindson, P. Jones and T. A. Smith, *Analytica Chimica Acta*, 2002, **451**, 181-188.
113. N. Pinotsis, A. C. Calokerinos and W. R. G. Baeyens, *Analyst*, 2000, **125**, 1307 - 1311.
114. A. Mitsana-Papazoglou, A. Fragaki, P. Chamosfakidi and A. C. Calokerinos, *Analytica Chimica Acta*, 2000, **410**, 153-157.
115. N. W. Barnett, B. J. Hindson and S. W. Lewis, *Analytica Chimica Acta*, 1998, **362**, 131-140.
116. M. Polásek and M. Jambor, *Talanta*, 2002, **58**, 1253-1261.
117. S. Satienperakul, T. J. Cardwell, S. D. Kolev, C. E. Lenehan and N. W. Barnett, *Analytica Chimica Acta*, 2005, **554**, 25-30.
118. A. Townshend, N. Youngvises, R. A. Wheatley and S. Liawruangrath, *Analytica Chimica Acta*, 2003, **499**, 223-233.
119. J. Du, Y. Li, Y. Tang and J. Lu, *Analytical Letters*, 2002, **35**, 463-472.
120. A. Townshend and R. A. Wheatley, *Analyst*, 1998, **123**, 267-272.
121. S. Fan, Z. Wu, L. Zhang and C. Lv, *Analytical Letters*, 2002, **35**, 1479-1489.
122. N. Deftereos, A. C. Calokerinos and C. E. Efstathiou, *Analyst* 1993, **118**, 627-632.
123. X. Wang, J. Wang and N. Yang, *Food Chemistry*, 2007, **102**, 422-426.
124. S. L. Fan, L. K. Zhang and J. M. Lin, *Talanta*, 2006, **68**, 646-652.
125. A. Townshend, J. A. M. Pulgarín and M. T. A. Pardo, *Analytical and Bioanalytical Chemistry*, 2005, **381**, 925-931.
126. A. Townshend, J. A. Murillo Pulgarín and M. T. Alañón Pardo, *Analytica Chimica Acta*, 2003, **488**, 81-88.
127. N. Anastos, N. W. Barnett, B. J. Hindson, C. E. Lenehan and S. W. Lewis, *Talanta*, 2004, **64**, 130-134.
128. J. A. M. Pulgarín, P. F. López and P. H. Nuño, *Analytical and Bioanalytical Chemistry* 2006, **384**, 423-430.
129. M. Liu, Y. He and J. Lü, *Fenxi Huaxue*, 2005, **33**, 535-537.
130. H. Wei and E. Liu, *Journal of the Chinese Chemical Society(Taipei)* 2005, **52**, 1043-1048.

131. S. Liao, X. Wu and Z. Xie, *Analytica Chimica Acta*, 2005, **537**, 189-195.
132. Y. He, Y. Xue, M. Feng and J. Lü, *Fenxi Huaxue* 1998, **20**, 1136–1138.
133. J. A. Murillo Pulgarín, L. F. García Bermejo and P. F. López, *Analytica Chimica Acta*, 2005, **546**, 60-67.
134. E. B. Liu, H. Q. Wei, X. L. Zhao, X. X. Li and F. X. Jiang, *Chinese Chemical Letters*, 2004, **15**, 1067-1070.
135. B. G. T. Corominas, J. V. G. Mateo, L. L. Zamora and J. M. Calatayud, *Analytical Letter*, 2005, **38**, 499–510.
136. M. Wang, L. Zhao, M. Liu and J. M. Lin, *Spectrochimica Acta Part A: Molecular and Biomolecular Spectroscopy*, 2007, **66**, 1222-1227.
137. M. Yaqoob, A. Waseem and A. Nabi, *Journal of Analytical Chemistry*, 2006, **61**, 917-921.
138. H. Zhou, Z. Zhang, D. He, Y. Hu, Y. Huang and D. Chen, *Analytica Chimica Acta*, 2004, **523**, 237-242.
139. Y. He, J. Du, M. Feng and J. Lu, *Fenxi Shiyanshi*, 1999, **18**, 60–62.
140. P. S. Francis, C. M. Hindson, J. M. Terry, Z. M. Smith, T. Slezak, J. L. Adcock, B. L. Fox and N. W. Barnett, *Analyst*, 2011, **136**, 64-66.
141. G. M. Greenway, A. W. Knight and P. J. Knight, *Analyst*, 1995, **120**, 2549-2552.
142. B. J. Hindson, (2001). The Chemistry, Spectroscopy and Analytical Applications of Certain Chemiluminescent Reactions. School of Biological Chemical Sciences, Faculty of Science Technology, Deakin University, Victoria. PhD Thesis: 344.
143. C. M. Hindson, P. S. Francis, G. R. Hanson, J. L. Adcock and N. W. Barnett, *Analytical Chemistry*, 2010, **82**, 4174-4180.
144. N. Anastos, N. W. Barnett, B. J. Hindson, C. E. Lenehan and S. W. Lewis, *Talanta*, 2004, **64**, 130-134.
145. I. B. Agater, R. A. Jewsbury and K. Williams, *Analytical Communications*, 1996, **33**, 367-369.
146. C. Thongpoon, B. Liawruangrath, S. Liawruangrath, R. A. Wheatley and A. Townshend, *Journal of Pharmaceutical and Biomedical Analysis*, 2006, **42**, 277-282.
147. A. R. J. Andrews and A. Townshend, *Analytical Proceedings*, 1989, **26**, 368-369.
148. T. Slezak, J. M. Terry, P. S. Francis, C. M. Hindson, D. C. Olson, D. K. Wolcott and N. W. Barnett, *Analytical Chemistry*, 2010, **82**, 2580-2584.
149. F. A. Aly, S. A. Al-Tamimi and A. A. Alwarthan, *Journal of AOAC International*, 2000, **83**, 1299-1305.
150. H. Chen, C. Lu, R. Li, G. Guo and J. M. Lin, *Science China Chemistry*, 2010, **53**, 1784-1792.
151. G. Chen, F. Huang, X. Wu, Z. Zhao and J. Duan, *Analytical and Bioanalytical Chemistry*, 2003, **376**, 873-878.
152. J. Adcock, P. Francis and N. Barnett, *Journal of Fluorescence*, 2009, **19**, 867-874.
153. J. Pan and Y. Huang, *Analytical Letters*, 2004, **37**, 2321 - 2335.
154. Y. B. Tsaplev, *Russian Journal of Physical Chemistry(Engl. Transl.)*, 1991, **65**, 420-422.
155. C. Zhu, L. Wang, Y. Li and F. Gao, *Fenxi Huaxue*, 1997, **25**, 387-390.
156. U. Isacsson and G. Wettermark, *Analytica Chimica Acta*, 1974, **68**, 339-362.
157. F. McCapra, *Accounts of Chemical Research*, 1976, **9**, 201-208.
158. E. H. White and B. R. Branchini, *Journal of the American Chemical Society*, 1975, **97**, 1243-1245.
159. E. H. White, M. G. Steinmetz, J. D. Miano, P. D. Wildes and R. Morland, *Journal of the American Chemical Society*, 1980, **102**, 3199-3208.
160. R. S. Chittock, J. M. Hawronskyj, J. Holah and C. W. Wharton, *Analytical Biochemistry*, 1998, **255**, 120-126.
161. O. Shimomura and F. H. Johnson, *Biochemistry*, 1968, **7**, 1734-1738.
162. E. H. White, F. McCapra and G. F. Field, *Journal of the American Chemical Society*, 1963, **85**, 337-343.
163. D. S. Auld, N. T. Southall, A. Jadhav, R. L. Johnson, D. J. Diller, A. Simeonov, C. P. Austin and J. Inglese, *Journal of Medicinal Chemistry*, 2008, **51**, 2372-2386.
164. K. Gleu and W. Petsch, *Angewandte Chemie*, 1935, **48**, 57-59.
165. W. R. Seitz and D. M. Hercules, *Journal of the American Chemical Society*, 1974, **96**, 4094-4098.
166. E. Huntress, L. Stanley and A. Parker, *Journal of the American Chemical Society*, 1934, **56**, 241-242.
167. T. G. Burdo and W. R. Seitz, *Analytical Chemistry*, 1975, **47**, 1639-1643.
168. W. S. Oleniacz, M. A. Pisano, M. H. Rosenfeld and R. L. Elgart, *Environmental Science & Technology*, 1968, **2**, 1030-1033.
169. T. Uzu and S. Sasaki, *Organic Letters*, 2007, **9**, 4383-4386.
170. Z. F. Zhang, H. Cui, C. Z. Lai and L. J. Liu, *Analytical Chemistry*, 2005, **77**, 3324-3329.
171. A. L. Rose and T. D. Waite, *Analytical Chemistry*, 2001, **73**, 5909-5920.
172. L. Harris and A. S. Parker, *Journal of the American Chemical Society*, 1935, **57**, 1939-1942.
173. R. Maskiewicz, D. Sogah and T. C. Bruice, *Journal of the American Chemical Society*, 1979, **101**, 5347-5354.
174. R. Maskiewicz, D. Sogah and T. C. Bruice, *Journal of the American Chemical Society*, 1979, **101**, 5355-5364.
175. J. Z. Guo, H. Cui, S. L. Xu and Y. P. Dong, *The Journal of Physical Chemistry C*, 2007, **111**, 606-611.
176. J. Z. Guo and H. Cui, *The Journal of Physical Chemistry C*, 2007, **111**, 12254-12259.

177. A. Graefe, S. E. Stanca, S. Nietzsche, L. Kubicova, R. Beckert, C. Biskup and G. J. Mohr, *Analytical Chemistry*, 2008, **80**, 6526-6531.
178. P. V. Santacroce, J. T. Davis, M. E. Light, P. A. Gale, J. C. Iglesias-Sanchez, P. Prados and R. Quesada, *Journal of the American Chemical Society*, 2007, **129**, 1886-1887.
179. L. Guerrini, J.V. Garcia-Ramos, C. Domingo and S. Sanchez-Cortes, *Analytical Chemistry*, 2009, **81**, 1418-1425.
180. K. D. Legg and D. M. Hercules, *Journal of the American Chemical Society*, 1969, **91**, 1902-1907.
181. K. D. Legg and D. M. Hercules, *The Journal of Physical Chemistry*, 1970, **74**, 2114-2118.
182. K. D. Legg, D. W. Shive and D. M. Hercules, *Analytical Chemistry*, 1972, **44**, 1650-1655.
183. A. Ma and Z. Rosenzweig, *Analytical Chemistry*, 2004, **76**, 569-575.
184. L.L. Klopff and A.N.Timothy, *Analytical Chemistry*, 1984, **56**, 1539-1542.
185. C. Huber, I. Klimant, C. Krause and O. S. Wolfbeis, *Analytical Chemistry*, 2001, **73**, 2097-2103.
186. J. N. Herron, K. R. Ely and A. B. Edmundson, *Biochemistry*, 1985, **24**, 3453-3459.
187. C. H. Tsai, Chang, J. F. Chiou and T. Z. Liu, *Journal of Agricultural and Food Chemistry*, 2003, **51**, 58-62.
188. L. L. Klopff and T. A. Nieman, *Analytical Chemistry*, 1985, **57**, 46-51.
189. F. H. Beyerlein and R. S. Nicholson, *Analytical Chemistry*, 1972, **44**, 1647-1650.
190. A. Ingvarsson, C. L. Flurer, T. E. Riehl, K. N. Thimmaiah, J. M. Williams and W. L. Hinze, *Analytical Chemistry*, 1988, **60**, 2047-2055.
191. E. F. Muller and J. B. Hyne, *Journal of the American Chemical Society*, 1969, **91**, 1907-1912.
192. C. W. Chen, J. F. Chiou, C. H. Tsai, C. W. Shu, M. H. Lin, T. Z. Liu and L. Y. Tsai, *Journal of Agricultural and Food Chemistry*, 2006, **54**, 9297-9302.
193. D. W. King, W. J. Cooper, S. A. Rusak, B. M. Peake, J. J. Kiddle, D. W. O'Sullivan, M. L. Melamed, C. R. Morgan and S. M. Theberge, *Analytical Chemistry*, 2007, **79**, 4169-4176.
194. M. M. Rauhut, D. Sheehan, R. A. Clarke and A. M. Semsel, *Photochemistry and Photobiology*, 1965, **4**, 1097-1110.
195. M. M. Rauhut, D. Sheehan, R. A. Clarke, B. G. Roberts and A. M. Semsel, *Journal of Organic Chemistry*, 1965, **30**, 3587-3592.
196. T. Kawashima and T. Hasebe, *Analytical Sciences* 1996, **12**, 773-777.
197. C. Marquette and L. Blum, *Analytical and Bioanalytical Chemistry*, 2006, **385**, 546-554.
198. X. Lu and M. Lu, *Fenxi Ceshi Tongbao*, 1992, **11**, 41-43.
199. C. Cunningham, K.F.Tipton and H. B. F. Dixon, *The Biochemical Journal*, 1998, **330**, 939-945.
200. W. R. Seitz, *Review in Analytical Chemistry*, 1981, **13**, 1-58.
201. K. Robards and P. J. Worsfold, *Analytica Chimica Acta*, 1992, **266**, 147-173.
202. A. A. Grinberg and J. Russ, *Chemical and Physical Society* 1920, **52**, 151.
203. H. Kautsky and O. Neitzke, *Z. Physik*, 1925, **31**, 60.
204. R. Audubert, *Transactions of the Faraday Society*, 1939, **35**, 197-204.
205. K. Mizuno, S. Hata and S. Tomioka, *Chemical & Pharmaceutical Bulletin (CPB)*, 1970, **18**, 2588.
206. V. S. Nikolaevsky and A. T. Miroshnikova, *Trudy Moskovskogo obshchestva ispytatelei prirody*, 1972, **39**, 198.
207. J. Stauff and U. Z. Bergman., *The Journal of Physical Chemistry* 1972, **78**, 263-276.
208. J. Stauff, U. Sander and W. Jaeschke, *Chemiluminescence of perhydroxyl-and-carbonateradicals in Chemiluminescence and bioluminescence*, Plenum Press, New York, 1973.
209. V. A. Veselovskii, V. S. Lebedev and T. M. Chernysheva, *Biologicheskie nauki*, 1976, **19**, 24.
210. V. S. Lebedev and I. V. Tsibanova., *Russian Journal of Physical Chemistry*, 1977, **51**, 819.
211. V. S. Lebedev and V. A. Veselovskii., *Biologicheskie nauki*, 1978, **12**, 44.
212. N. A. Ushakova and I. M. Parkhomenko., *Mikrobiologiya* 1980, **49**, 833.
213. M. V. Guse, I. M. Parkhomenko and N. A. Ushakova., *Mikrobiologiya* 1980, **49**, 911.
214. R. W. Abbott and A. Townshend, *Analytical Proceedings*, 1986, **23**, 25-26.
215. J. W. Costin, N. W. Barnett, S. W. Lewis and D. J. McGillivray, *Analytica Chimica Acta*, 2003, **499**, 47-56.
216. B. Gómez-Taylor Corominas, G. M. Antón Fos, J. V. García Mateo, L. Lahuerta Zamora and J. Martínez Calatayud, *Talanta*, 2003, **60**, 623-628.
217. Y. F. Mestre, L. L. Zamora and J. M. Calatayud, *Luminescence* 16 2001, **16**, 213-235.
218. A. J. Brown, P. S. Francis, J. L. Adcock, K. F. Lim and N. W. Barnett, *Analytica Chimica Acta*, 2008, **624**, 175-183.
219. A.J. Brown, C.E. Lenehan, P.S. Francis, D.E. Dunstan and N.W. Barnett, *Talanta*, 2007, **71**, 1951-1957.
220. M. Jáky, L. I. Simándi and V. Y. Shafirovich, *Inorganica Chimica Acta* 1984, **90**, 39.
221. B. Li, Z. Zhang, X. Zheng and C. Xu, *Microchemical Journal*, 1999, **63**, 374-380.

222. X. Chen, C. Zhang and J. Lu, *Fenxi Huaxue* 2000, **28**, 1126–1128.
223. X. N. Chen and S. I. Shen, *Shanxi Daxue Xuebao, Ziran Kexueban* 2001, **24**, 230–233.
224. H. B. Yang and C. X. Zhang, *Fenxi Shiyanshi* 2001, **20**, 43–46.
225. X. Zheng, Z. Zhang and B. Li, *Electroanalysis*, 2001, **13**, 1046–1050.
226. X. I. Chen and C. X. Zhang, *Shaanxi Shifan Daxue Xuebao, Ziran Kexueban* 2003, **31**, 76–78.
227. X. I. Chen, H. Y. Ma and Y. T. Zhang, *Fenxi Kexue Xuebao* 2005, **21**, 636–638.
228. X. A. Chen, S. A. Shen, C. B. Zhang and J. B. Lü, *Fenxi Huaxue* 2002, **30**, 1501–1503.
229. X. Zheng and Z. Zhang, *Analytical Sciences*, 2000, **16**, 1345–1347.
230. H. B. Yang and C. X. Zhang, *Shaanxi Shifan Daxue Xuebao, Ziran Kexueban* 2000, **28**, 71–74.
231. X. Zheng and Z. Zhang, *Sensors and Actuators B: Chemical*, 2002, **84**, 142–147.
232. H. B. Yang, L. Q. Liang and L. L. Lu, *Shihezi Daxue Xuebao, Ziran Kexueban* 2005, **23**, 673–675.
233. E. Wiedemann, *Annalen der Physik und Chemie*, 1888, **34**, 446–463.
234. D. D. A. McQuarrie and J. J. D. Simon, *Physical Chemistry: A Molecular Approach*, University Science Books, 1997.
235. J. R. Lakowicz, *Principles of fluorescence spectroscopy*, Springer London, Limited, 2009.
236. D. H. Stedman and M. E. Fraser, *Analytical Applications of Gas Chemiluminescence, in Chem- and Bioluminescence*, 1985, 439–468.
237. B. A. Ridley and J. Grahek, *Journal of Atmospheric and Oceanic Technology*, 1990, **7**, 307–311.
238. V. H. Regener, *Journal of Geophysical Research (JGR)*, 1964, **69**, 3795–3702.
239. J. A. Hodgson, K. J. Krost, A. E. O’Keeffe and R. K. Stevens, *Analytical Chemistry Acta.*, 1970, **42**, 1795–1803.
240. J. A. Bognar and J. W. Birks, *Analytical Chemistry Acta.*, 1996, 3059–3062.
241. M. Burba, *Zuckerind*, 1996, **121**, 165–173.
242. A. M. Jiménez and M. J. Navas, *Critical Review Analytical Chemistry.*, 1997, **27**, 291–305.
243. J. K. Nelson, R. H. Getty and J. W. Birks, *Journal of the American Chemical Society*, 1983, **55**, 1767–1770.
244. T. G. Chasteen, R. Fall, J. W. Birks, H. R. Martin, R. Glinski and *Journal of Chromatographia*, 1991, **31**, 342–346.
245. D. A. Stiles, A. C. Calokerinos and A. Townshend, *Flame chemiluminescence analysis by molecular emission cavity detection*, Wiley, Chichester; New York, 1994.
246. S. Sass and G. A. Parker, *Journal of Chromatography A*, 1980, 331–349.
247. B. J. Culliford, *The Examination and Typing of Bloodstains in the Crime Laboratory*, US Gov’t Printing Office, Washington DC, 1971.
248. A. G. Hadd, A. Seeber and J. W. Birks, *The Journal of Organic Chemistry*, 2000, **65**, 2675–2683.
249. R. E. Milofsky and J. W. Birks, *Journal of Agricultural and Food Chemistry*, 1991, **113**, 9715–9723.
250. H. P. Chokshi, M. Barbush, R. G. Carlson, R. S. Givens, T. Kuwana and R. L. Schowen, *Biomedical Chromatography*, 1990, **4**, 96–99.
251. G. Orosz, R. S. Givens and R. L. Schowen, *Critical Reviews in Analytical Chemistry*, 1996, **26(1)**, 1–27.
252. G. A. Crespo, G. Mistlberger and E. Bakker, *Journal of the American Chemical Society*, 2011, **134**, 205–207.
253. Y. M. Fang, J. Song, J. Li, Y. W. Wang, H. H. Yang, J. J. Sun and G. N. Chen, *Chemical Communications*, 2011, **47**, 2369–2371.
254. M. M. Richter, *Chemical Reviews*, 2004, **104**, 3003–3036.
255. R. Forster, P. Bertoncello and T. E. Keyes, *Annual Review of Analytical Chemistry* 2009, **2**.
256. A. J. Bard, *Electrogenerated Chemiluminescence*, Marcel Dekker, 2004.
257. W. Y. Lee, *Mikrochim. Acta*, 1997, **127**, 19–39.
258. R. D. Gerardi, N. W. Barnett and S. W. Lewis, *Analytica Chimica Acta*, 1999, **378**, 1–14.
259. F. Jameison, R. I. Sanchez, L. Dong, J. K. Leland, D. Yost and M. T. Martin, *Analytical Chemistry*, 1996, **68(8)**, 1298–1302.
260. N. Tokel and A. J. Bard, *Journal of the American Chemical Society*, 1972, **94** 2862–2863.
261. J. Leland and M. Powell, *Journal of the Electrochemical Society*, 1990, **137**, 3127– 3131.
262. H. White and A. Bard, *Journal of the American Chemical Society*, 1982, **104**, 6891–6895
263. S. D. Kolev and D. I. Mckelvie, in *Comprehensive Analytical Chemistry*, Elsevier, 2008, vol. 54.
264. S. Gaßmann, I. Ibendorf and L. Pagel, *Sensors and Actuators A: Physical*, 2007, **133**, 231–235.
265. P. Tzanavaras, (2008, September 15). Flow Injection Analysis. SciTopics. Retrieved December 18, 2012, from http://www.scitopics.com/Flow_Injection_Analysis.html
266. C. B. Ranger, *Analytical Chemistry*, 2008, **53**, 20A–32A.
267. A. I. Fernando and B. T. Mabel, *Advances in Flow Analysis*, 2008, 1–42.
268. J. Ruzicka and E. H. Hansen, *Analytica Chimica Acta*, 1975, **78**, 145–147.

269. D. P. Tzanavaras, *Flow Injection Analysis - SciTopics*, http://www.scitopics.com/Flow_Injection_Analysis.html Accessed 10 October, 2008.
270. S. D. Kolev and I. D. McKelvie, *Advances in Flow Injection Analysis and Related Techniques*, 54 - Elsevier, http://www.elsevier.com/wps/product/cws_home/716411 Accessed 12 January, 2009.
271. J. Ruzicka and G. D. Marshall, *Analytical Chemistry Acta.*, 1990, **237**, 329-343.
272. K. A. Edwards and A. J. Baeumner, *Analytical Chemistry*, 2006, **78**, 1958-1966.
273. A. C. V. dos Santos and J.C. Masini, *Microchemical Journal*, 2009, **93**, 110-114.
274. W. Laiwattanapaisal, U. Kuananuvat, W. Intharachuti, C. Chinvongamorn, S. Hannongbua and O. Chailapakul, *Talanta*, 2009, **79**, 1104-1110.
275. W. Siangproh, N. Teshima, T. Sakai, S. Katoh and O. Chailapakul, *Talanta*, 2009, **79**, 1111-1117.
276. R. B. Mesquita and A. O. Rangel, *Analytica Chimica Acta* 2009, **648**, 7-22.
277. R. I. Stefan, J. F. van Staden and H. Y. Aboul Enein, *Encyclopedia of Chromatography: Second Edition*, 2005, 1537 - 1540.
278. S. K. Hartwell, K. Grudpan and G. D. Christian, *TrAC Trends in Analytical Chemistry*, 2004, **23**, 619-623.
279. P. Ampan, S. Lapanantnoppakhun, P. Sooksamiti, J. Jakmune, S. Kradtap Hartwell, S. Jayasvati, G. D. Christian and K. Grudpan, *Talanta*, 2002, **58**, 1327-1334.
280. C. C. Oliveira, E. A. G. Zagatto, J. Ruzicka and G. D. Christianb, *Analytical Letters*, 2000, **33**, 929 - 940.
281. W. Som-Aum, S. Liawruangrath and E. H. Hansen, *Analytica Chimica Acta*, 2002, **463**, 99-109.
282. J. Wang, Q. Lin, R. Zhou and B. Xu, *Sensors and Actuators B: Chemical*, 2002, **81**, 248-253.
283. H. Zhu, H. Chen and Y. Zhou, *Analytical Sciences*, 2003, **19**, 289-294.
284. I. Lähdesmäki, C. Beeson, G. D. Christian and J. Ruzicka, *Talanta*, 2000, **51**, 497-506.
285. J. Wang and E. H. Hansen, *Analytica Chimica Acta*, 2001, **435**, 331-342.
286. J. Wang and E. H. Hansen, *TrAC Trends in Analytical Chemistry*, 2003, **22**, 225-231.
287. A. D. Carroll, L. Scampavia, D. Luo, A. Lernmark and J. Ruzicka., *Analyst* 2003, **128**, 1157.
288. A. D. Carroll, L. Scampavia and J. Ruzicka, *Analyst*, 2002, **127**, 1228-1232.
289. Y. Ogata, L. Scampavia, J. Růžička, C. R. Scott, M. H. Gelb and F. Tureček, *Analytical Chemistry*, 2002, **74**, 4702-4708.
290. J. Ruzicka, *Analytica Chimica Acta*, 1995, **308**, 14-19.
291. B. C. Erickson, B. R. Kowalski and J. Ruzicka, *Analytical Chemistry*, 2002, **59**, 1246-1248.
292. N. Spatny, S. J. Haswell and M. Grasserbauer, *Analytical Proceedings*, 1995, **32**, 141-143.
293. A. Cladera, E. Gomez, J. M. Estela and V. Cerda, *Analyst*, 1991, **116**, 913-917.
294. D. H. Chen, M. L. DeCastro and M. Valcarcel, *Analyst*, 1991, **116**, 1095-1111.
295. R. Shi, K. Stein, G. Schwedt and Z. Lebesm, *Unters Forsh A*, 1977, **204**, 99-102.
296. W. R. Wolf and K.K.Stewart, *Analytical Chemistry Acta.*, 1979, **51**, 1201-1205.
297. P. D. Tzanavaras and D. G. Themelis, *Analytica Chimica Acta*, 2007, **588**, 1-9.
298. T. Matsue, A. Aoki, E. Ando and I. Uchida, *Analytical Chemistry*, 2002, **62**, 407-409.
299. E. S. Rudakov, V. L. Loachev and E. V. Zaichuk, *Kinetics and Catalysis*, 1996, **37(4)**, 500-507.
300. B. A. Gorman, N. W. Barnett and R. Bos, *Analytica Chimica Acta*, 2005, **541**, 117-122.
301. Burguera J. L , A Townshend and S. Greenfield, *Analytica Chimica Acta*, 1980, **114**, 209-214.
302. D. W. King, W. J. Cooper, S. A. Rusak, B. M. Peake, J. J. Kiddle, D. W. O'Sullivan, M. L. Melamed, C. R. Morgan and S. M. Theberge, *Analytical Chemistry*, 2007, **79**, 4169-4176.
303. K. Hayashi, S. Sasaki, K. Ikebukuro and I. Karube, *Analytica Chimica Acta*, 1996, **329**, 127-134.
304. P. E. Michel, G. C. Fiaccabrino, N. F. d. Rooij and M. Koudelka-Hep, *Analytica Chimica Acta*, 1999, **392**, 95-103.
305. B. Kuswandi, Nuriman, J. Huskens and W. Verboom, *Analytica Chimica Acta*, 2007, **601**, 141-155.
306. L. J. Kricka and J. Y. Park, in *Chemiluminescence and Bioluminescence*, The Royal Society of Chemistry, 2011, pp. 543-556.
307. Á. Ríos, M. Zougagh and M. Avila, *Analytica Chimica Acta*, 2012, **740**, 1-11.
308. A. G. Crevillén, M. Hervás, M. A. López, M. C. González and A. Escarpa, *Talanta*, 2007, **74**, 342-357.
309. B. F. Liu, M. Ozaki, Y. Utsumi, T. Hattori and S. Terabet, *Analytical Chemistry*, 2003, **75**, 36-41.
310. B. F. Liu, M. Ozaki, H. Hisamoto, Q. Luo, Y. Utsumi, T. Hattori and S. Terabe, *Analytical Chemistry*, 2005, **77**, 573-578.
311. R. Su, J. M. Lin, K. Uchiyama and M. Yamada, *Talanta*, 2004, **64**, 1024-1029.
312. X. Huang and J. Ren, *ELECTROPHORESIS*, 2005, **26**, 3595-3601.
313. M. Amatongchai, O. Hofmann, D. Nacapricha, O. Chailapakul and A. deMello, *Analytical and Bioanalytical Chemistry*, 2007, **387**, 277-285.
314. B. Chance, *The Franklin Institute*, 1940, **229**, 737-766.

315. S.R.Crouch, F. J. Holler, P. K. Notz and P. M. Beckwith, *Applied Spectroscopy Reviews*, 1977, **13**, 165-259.
316. A. Gomez-Henz and D. Perez-Bendito, *Analytica Chimica Acta* 1991, **242**, 147-177.
317. L. M. Sara and A. C. Clark, *Protein Science*, 2009, **18**, 2500-2517.
318. W. C. Cooper, Y. Jin and T. M. Penning, *Journal of Biological Chemistry*, 2007, **282**, 33484-33493.
319. O. V. Moskvina, S. Kaplan, M. A. Gilles Gonzalez and M. Gomelsky, *Journal of Biological Chemistry*, 2007, **282**, 28740-28748.
320. J. A. Murillo Pulgarín, L. F. García Bermejo and J. A. Rubio Aranda, *Analytica Chimica Acta*, 2004, **517**, 111-117.
321. J. A. Murillo Pulgarin, L. F. Garcia Bermejo, J. M. Lemus Gallego and M. N. Sanchez Garcia, *Talanta*, 2008, **74**, 1539-1546.
322. B. E. Chance, N. Harvey, F. Johnson and M. N., *Journal of Cellular and Comparative Physiology*, 1940, **7**, 195-215.
323. W. R. Seitz and M. P. Neary, *Analytical Chemistry*, 2008, **46**, 188A-202a.
324. M. DeLuca and W. D. McElroy, *Biochemistry*, 2002, **13**, 921-925.
325. E. H. White, M. G. Steinmetz, J. D. Miano, P. D. Wildes and R. Morland, *Journal of the American Chemical Society*, 2002, **102**, 3199-3208.
326. Z. N. Pierre, C. R. Field and A. Scheeline, *Analytical Chemistry*, 2009, **81**, 8496-8502.
327. A. G. Hadd, A. L. Robinson, K. L. Rowlen and J. W. Birks, *The Journal of Organic Chemistry*, 1998, **63**, 3023-3031.
328. R. Stewart, *Oxidation by permanganate. In: Wiberg, K.B. (ed.), Oxidation in Organic Chemistry Part A.*, Academy Press, New York., 1965.
329. J. W. Ladbury and C. F. Cullis, *Chemical Reviews*, 2002, **58**, 403-438.
330. A. J. Bard, R. Parsons and J. Jordan, *Standard Potentials in Aqueous Solutions*, IUPAC (Marcel Dekker), USA, New York, 1985.
331. Hazen and Sawyer, *Disinfection Alternatives for Safe Drinking Water*, Van Nostrand Reinhold, New York, 1992.
332. W. A. Waters, *Quarterly Reviews, Chemical Society*, 1958, **12**, 277-300.
333. V. L. Lobachev, E. S. Radakov and E. V. Zaichuk, *Kinetics and Catalysis*, 1997, **38(6)**, 745-761.
334. K. A. Gardner and J. M. Mayer, *Science*, 1995, **269**, 1849-1851.
335. R. H. Ferguson, W. Lerch and J. E. Day, *Journal of the American Chemical Society*, 1931, **53**, 126-137.
336. A. V. Harcourt and W. Esson, *The Royal Institute of Philosophy* 1866, **156**, 193-221.
337. R. W. Fessenden and B. C. Redmon, *Journal of the American Chemical Society*, 1935, **57**, 2246-2249.
338. R. Belcher and T. S. West, *Analytica Chimica Acta* 1952, **6**, 322-332.
339. H. Donganmoya, E. Almeidaneves and N. Coichev, *Talanta*, 1997, **44**, 897-903.
340. H. F. Launer, *Journal of the American Chemical Society*, 1932, **54**, 2597-2610.
341. S. J. Alder and R. M. Noyes, *Journal of the American Chemical Society*, 1955, **77**, 2036-2042.
342. B. Miles and S. K. Nyaruk, *Journal of American Chemical Society*, 1990, **67**, 269-270.
343. M. A. Koupparis and M. I. Karyannis, *Analytica Chimica Acta* 1982, **138**, 303-310.
344. L. I. Simandi and E. Zahonyi-Budo, *Inorganic Chimica Acta*, 1998, **281**, 235-238.
345. G. Lunge and J. H. Smith, *Journal of the Society of Chemical Industry*, 1883, **2**, 463.
346. J. F. PerezBendito, C. Anas and E. Amat, *Colloidal and Interface Science*, 1996, **177**, 288-297.
347. V. Pimenta, D. Lavabre, G. Levy and J. C. Micheau, *The Journal of Physical Chemistry* 1994, **98**, 13294-13299.
348. S. Keki and M. T. Beck, *Reactions Kinetics and Catalysis Letters*, 1991, **44**, 75-77.
349. K. Fujiwara, T. Kashima, B. Tsubatoa, T. Toyoshima, M. Aihara and M. Kiboki, *Chemistry Letters*, 1990, **8**, 1385-1386.
350. T. Fazekas, M. Mrakavrova, A. Nagy and A. Olexova, *Reaction Kinetics and Catalysis Letters* 1990, **42**, 181-188.
351. N. W. Barnett, B. J. Hindson, S. W. Lewis and P. Jones, *Analytica Chimica Acta*, 2001, **126**, 1636-1639.
352. M. A. Ansari and J. C. Graig, *Synthesis Communications*, 1996, **26**, 1789-1792.
353. S. B. Mandal, B. Achari and P. P. G. Dastidar, *Tetrahedron Letters*, 1993, **34**, 1979-1980.
354. G. Davies, *Co-ordination Chemistry Reviews*, 1963, **4**, 199-224.
355. B. S. I. Staff, *Water Quality. Determination of Permanganate Index*, B S I Standards, UK, 1995.
356. S. Dash, S. Patel and B. K. Mishra, *Tetrahedron*, 2009, **65**, 707-739.
357. A. Lapworth and E. N. Mottram, *Journal of the Chemical Society, Transactions*, 1925, **127**, 1628-1631.
358. E. J. Witzmann, W. L. Evans, H. Hass and E. F. Schroeder, *Organic Synthesis Vol. II*, Wiley edn., Wiley, New York, 1943.

359. J. E. Coleman, C. Ricciuti and D. Swern, *Journal of the American Chemical Society*, 1956, **78**, 5342-5345.
360. E. M. Stoddart, F. W. Canter and A. Robertson, *Journal of the Chemical Society (Resumed)*, 1931, 1874-1876.
361. L. I. Simandi and M. Jaky, *Journal of the Chemical Society, Perkin Transactions 2*, 1972, 2326-2330.
362. M. Jaky and L. I. Simandi, *Journal of the Chemical Society, Perkin Transactions 2*, 1972, 1481-1486.
363. M. Jaky, L. I. Simandi, L. Maros and I. Molnar-Perl, *Journal of the Chemical Society, Perkin Transactions 2*, 1973, 1565-1569.
364. L. I. Simandi and J. Miklos, *Journal of the American Chemical Society*, 1976, **98**, 1995-1997.
365. H. Matsubara and S. Nakayama, *Water Research* 1992, **26**, 1471-1478.
366. M. Jaky and J. Szammer, *Journal of Physical Organic Chemistry*, 1997, **10**, 420-426.
367. R. Lindroos-Heinonen and P. O. I. Virtanen, *Finnish Chemical Letters* 1988, **15**, 117-121.
368. M. J. Insausti, M. P. Alvarezmacho and F. Mataperez, *Collection of Czechoslovak Chemical Communications*, 1992, **57**, 2331-2336.
369. P. N. Pande, H. L. Gupta, S. C. Ameta and T. C. Shama, *Physical Chemistry Acta.* , 1981, **22**, 125-128.
370. K. K. Sengupta, A. Sanyal, P. S. Tribendi and S. Sengupta, *Journal of Chemical Research*, 1993, 484-485.
371. G. V. Rao, K. C. Rajanna and P. K. Saiprakash, *Zeitschrift fur Physikalische Chemie (Leipzig)*, 1982, **3**, 622-627.
372. Y. E. Yan and F. W. Schwartz, *Environmental Science & Technology*, 2000, **34**, 2535-2541.
373. P.S. Francis, J.L. Adcock, J.W. Costin, S.D. Purcell, F. M. Pfeffer and N.W. Barnett, *Journal of Pharmaceutical and Biomedical Analysis*, 2008, **48**, 508-518.
374. J. Huclová, D. Šatínský, H. Sklenářová and R. Karlíček, *Analytical and Bioanalytical Chemistry*, 2003, **376**, 448-454.
375. M. C. S. Alonso, L. L. Zamora and J. M. Calatayud, *Talanta*, 2003, **60**, 369-376
376. J. Du, Y. Li and J. Lu, *Analytical Letters*, 2002, **35**, 2295 - 2304.
377. B. Gomez-Taylor Corominas, J. V. Garca Mateo, L. Lahuerta Zamora and J. Martinez Calatayud, *Talanta*, 2002, **58**, 1243-1251.
378. Y. He, F. Nie and J. Lu, *Fenxi Huaxue*, 2001, **29**, 296-298.
379. Z. Wang, Z. Zhang, Z. Fu, D. Chen and X. Zhang, *Journal of Pharmaceutical and Biomedical Analysis*, 2003, **33**, 765-773.
380. M. C. Icardo, M. Misiewicz, A. Ciucu, J. V. García Mateo and J. M. Calatayud, *Talanta*, 2003, **60**, 405-414.
381. M. C. Icardo, J. V. G. Mateo, M. F. Lozano and J. M. Calatayud, *Analytica Chimica Acta*, 2003, **499**, 57-69.
382. B. Gomez-Taylor, M. Palomeque, J. V. Garcia Mateo and J. Martinez Calatayud, *Journal of Pharmaceutical and Biomedical Analysis*, 2006, **41**, 347-357.
383. J. L. Adcock, P. S. Francis, T. A. Smith and N. W. Barnett, *Analyst*, 2008, **133**, 49-51.
384. F. Nie, J. Lu, Y. He and J. Du, *Talanta*, 2005, **66**, 728-733.
385. N. W. Barnett, B. J. Hindson, S. W. Lewis, P. Jones and P. J. Worsfold, *Analyst*, 2001, **126**, 1636-1639.
386. A. G. Alapont, E. A. Giménez, L. L. Zamora and J. M. Calatayud, *Journal of Bioluminescence and Chemiluminescence*, 1998, **13**, 131-137.
387. L. Zhao, B. Li, Z. Zhang and J. M. Lin, *Sensors and Actuators B: Chemical*, 2004, **97**, 266-271.
388. F. Nie, J. Lu, Y. He and J. Du, *Luminescence*, 2005, **20**, 315-320.
389. T. J. Christie, R. H. Hanway, D. A. Paulls and A. Townshend, *Analytical Proceedings*, 1995, **32**, 91-93.
390. Y. He, J. Lu, M. Liu and J. Du, *Analyst*, 2005, **130**, 1032 - 1037.
391. M. Liu, J. Lu, Y. He and J. Du, *Analytica Chimica Acta*, 2005, **541**, 97-102.
392. H. Kunze, H. Ritschel, H. R. Weigt and G. Junghänel, *Zeitschrift fur Chemie*, 1983, **23**, 224-225.
393. A. D. Karavaev, A. I. Voloshin, G. L. Sharipov, V. P. Kazakov and G. A. Tolstikov, *Russian Chemical Bulletin*, 1987, **36**, 1105-1105.
394. E. B. Sveshnikova and A. A. Stroganov, *Optics and Spectroscopy (USSR)*, 1986, **60**, 320-324.
395. W. Takashi, S. Nobuaki, O. Hitomi, H. Yoichi and K. Masaaki, 2001, **268**, 6114-6122.
396. Z. J. Zhang, B. X. Li and X. W. Zheng, *Chinese Journal of Chemistry*, 2003, **21** 1403-1409.
397. Y. Zhang, Z. Zhang, G. Qi, Y. Sun, Y. Wei and H. Ma, *Analytica Chimica Acta*, 2007, **582**, 229-234.
398. S. N. Mogel and B. A. McFadden, *Biochemistry*, 1990, **29**, 8333-8337.
399. R. M. Lilley, X. Wang, E. Krausz and T. J. Andrews, *Journal of Biological Chemistry*, 2003, **278**, 16488-16493.
400. R. O. S. Guerrero, M. C. Icardo, N. G. Benito and J. M. Calatayud, *Analytical Letter*, 2003, **36**, 1039-1049.
401. O. R. Pons, D. M. Gregorio, J. V. G. Mateo and J. M. Calatayud, *Analytica Chimica Acta*, 2001, **438**, 149-156.
402. D. Li, J. Du and J. Lu, *Microchimica Acta*, 2008, **161**, 169-173.
403. Y. He, J. Du, M. Feng and J. Lu, *Fenxi Shiyanshi*, 1999, **18**, 60-62.
404. Y. He, J. Du, M. Feng and J. Lü, *Gaodeng Xuexiao Huaxue Xuebao*, 1999, **20**, 1049-1051.

405. J. Shi, K. Zhao, Q. Song, L. Qu and X. Gong, *Yaowu Fenxi Zazhi* 2004, **24**, 395-397.
406. J. Shi, K. Zhao, X. Gong and Q. Song, *Fenxi Kexue Xuebao* 2006, **22**, 43-45.
407. L. Li, F. Nie, M. Yang, M. Feng and J. Lu, *Shaanxi Shifan Daxue Xuebao, Ziran Kexueban*, 1998, **26**, 65-67.
408. S. Fan, W. Li, X. Wang and J. Wang, *Fenxi Shiyanshi* 2004, **23**, 58-61.
409. T. E. A. Ahmed and A. Townshend, *Analytica Chimica Acta*, 1994, **292**, 169-174.
410. C. Q. Zhu, L. Wang and J. Wu, *Fenxi Shiyanshi*, 1996, **15**, 49-51.
411. C. Xie, C. Liu, W. Chang and H. Li, *Guangpu Shiyanshi* 2004, **21**, 439-441.
412. X. Xu, N. Wang and S. Fan, *Fenxi Shiyanshi*, 2006, **25**, 76-79.
413. X. Xu, Q. Lin, X. He, F. Fu and G. Chen, *Luminescence*, 2010, **25**, 403-408.
414. A. Pawlicov, Z. Aacute, A. Garc, A. Iacute, J. Sahuquillo, I. Garc and J. Nez Calatayud, *Analytical Sciences*, 2006, **22**, 29-34.
415. L. Zhu, M. Feng, X. Wan and J. Lu, *Gaodeng Xuexiao Huaxue Xuebao*, 1996, **17**, 1693-1696.
416. H. Qi, M. L. Yang, M. Feng and J. Lu, *Chemical Research in Chinese Universities*, 1997, **13**, 229-234.
417. Alwarthan, A. Abdul and A. Townshend, *Analytica Chimica Acta*, 1986, **185**, 329-333.
418. Y. Zhu, M. Zhang, M. Li and L. Wang, *Anhui Shifan Daxue Xuebao, Ziran Kexueban* 2002, **25**, 161-163.
419. C.M. Amorim, J.R. Albert-Garcia, M.C. Montenegro, A.N. Araujo and J.M. Calatayud, *Journal of Pharmaceutical and Biomedical Analysis*, 2007, **43**, 421-427.
420. A. Townshend and R. A. Wheatley, *Analyst* 1998, **123**, 1047-1051.
421. H. Li and C. Xie, *Guangpu Shiyanshi*, 2004, **21**, 13-15.
422. J. M. Lin and R. Su, *Bioluminescence & Chemiluminescence*, 2004, 421-424.
423. H. Ikkai, T. Nakagama, M. Yamada and T. Hobo, *Bulletin of the Chemical Society of Japan*, 1989, **62**, 1660-1662.
424. H. W. Wu, M. L. Chen, D. Shou and Y. Zhu, *Chinese Chemical Letters*, 2012, **23**, 839-842.
425. T. Nakagama, M. Yamada and S. Suzuki, *Analytica Chimica Acta*, 1989, **217**, 371-376.
426. M. C. Icardo, M. Misiewicz, A. Ciucu, J. V. G. Mateo and J. M. Calatayud, *Talanta*, 2003, **60**, 405-414.
427. L. Shen, J. Du and J. Lv, *Xi'an Keji Xueyuan Xuebao* 2005, **25**, 198-200 215.
428. J. Shi, K. Zhao, X. Gong and Q. Song, *Fenxi Shiyanshi* 2004, **23**, 46-48.
429. H. Yang, J. Wang and L. Li, *Shihezi Daxue Xuebao, Ziran Kexueban* 2005, **23**, 117-119.
430. Zhujun Zhang, D. He, W. Liu and Y. Lv, *Luminescence*, 2005, **20**, 377-381.
431. Z. Ji, X. Yao and J. Li, *Luminescence*, 2011, **26**, 741-746.
432. X. F. Yang, D. B. Wu and H. Li, *Luminescence*, 2004, **19**, 322-327.
433. D. Wu, X. Yang and H. Li, *Xibei Daxue Xuebao, Ziran Kexueban*, 2005, **35**, 296-298.
434. X. Liu, Z. He, Q. Luo, X. Yu, J. Huang, R. Liu and Y. Zeng, *Fenxi Huaxue*, 1995, **23**, 652-654.
435. M. Yang, L. Li, M. Feng, J. Lü and Z. Zhang, *Fenxi Huaxue*, 2000, **28**, 161-163.
436. Z. Rao, W. Zhang, Q. Li, G. Xie and H. Yang, *Guangpuxue Yu Guangpu Fenxi*, 2004, **24**, 278-280.
437. S. Fan, Z. Wu, L. Zhang, C. Lu and J. Lin, *Fenxi Ceshi Xuebao* 2003, **22**, 87-89.
438. M. Yang, L. Li, M. Feng and J. Lu, *Yaowu Fenxi Zazhi* 1998, **18**, 41-44.
439. S. M. Wabaidur, Z. A. Alothman, S. M. Alam and S. H. Lee, *Spectrochimica Acta Part A: Molecular and Biomolecular Spectroscopy*, 2012, **96**, 221-225.
440. L. Wang, F. Yuan, H. Q. Chen, B. Ling and J. Xu, *Spectrochimica Acta Part A: Molecular and Biomolecular Spectroscopy*, 2012, **91**, 295-300.
441. L. Fang, *Jiangxi Shifan Daxue Xuebao, Ziran Kexueban* 2005, **29**, 393-396.
442. A. Campiglio, *Analytical Letters*, 2001, **34**, 2701-2710.
443. A. Campiglio, *Analytical Letters*, 2002, **35**, 1977-1985.
444. A. Mitsana-Papazoglou, E. G. Sarantonis and A. C. Calokerinos, *Biomedical Chromatography*, 1997, **11**, 67-68.
445. L. N. Li, N. B. Li and H. Q. Luo, *Analytical Sciences* 2005, **21**, 963-966.
446. F. Nie and J. Lu, *Talanta*, 2008, **74**, 1242-1246.
447. H. Sun, L. Li and X. Chen, *Journal of Clinical Laboratory Analysis*, 2007, **21**, 213-219.
448. C. Sun, H. Zhao and Y. Ou, *Fenxi Shiyanshi* 2000, **19**, 60-62.
449. Y. Li and J. Lu, *Shaanxi Shifan Daxue Xuebao, Ziran Kexueban*, 2002, **30**, 79-81.
450. L. Fang, *Chongqing Shifan Daxue Xuebao, Ziran Kexueban* 2006, **23**, 58-60.
451. G. P. McDermott, P. S. Francis, K. J. Holt, K. L. Scott, S. D. Martin, N. Stupka, N. W. Barnett and X. A. Conlan, *Analyst*, 2011, **136**, 2578-2585.
452. A. Nicole, S. W. Lewis, N. W. Barnett and D. N. Sims, *Journal of Forensic Sciences*, 2006, **51**, 45-51.
453. X. Zhu, J. Wang and M. Fu, *Fenxi Shiyanshi* 2004, **23**, 50-53.
454. L. Li, Y. Zhou, M. Feng, J. Lu and L. Jianyan, *Huaxue Fence* 2003, **39**, 406-407.

455. J. L. L. Paz and A. Townshend, *Analytical Communications*, 1996, **33**, 31–33.
456. Y. Xue, Y. He and J. Lu, *Fenxi Shiyanshi*, **18**, 49–51.
457. S. Han, *Microchimica Acta*, 2010, **168**, 169–175.
458. S. A. Al-Tamrah, A. A. Al-Warthan and A. S. Al-Amri, *Journal of Saudi Chemical Society* 1997, **1**, 1–8.
459. L. Li, B. Qin, M. Feng and J. Lu, *Shandong Keji Daxue Xuebao, Ziran Kexueban* 2001, **20**, 25–27.
460. Y. Zhuang and H. Song, *Journal of Pharmaceutical and Biomedical Analysis*, 2007, **44**, 824–828.
461. B. A. Gorman, N. W. Barnett and R. Bos, *Analytica Chimica Acta*, 2004, **541**, 119–124.
462. Z. Rao, Q. Lu, L. Fang, L. She, H. Yan and W. Chen, *Spectroscopy Letters: An International Journal for Rapid Communication*, 2006, **39**, 249–264.
463. E. Wołyniec, J. Karpińska, S. Łosiewska, M. Turkowicz, J. Klimczuk and A. Kojło, *Talanta*, 2012, **96**, 223–229.
464. A. R. J. Andrews and A. Townshend, *Analytica Chimica Acta*, 1989, **227**, 65–71.
465. M. C. S. Alonso, L. L. Zamora and J. M. Calatayud, *Analytica Chimica Acta*, 2001, **438**, 157–163.
466. S. M. Sultan, A. d. M. Almuaibed and A. Townshend, *Fresenius' Journal of Analytical Chemistry*, 1998, **362**, 167–169.
467. X. Wu, J. Duan, H. Chen, D. Chen, F. Huang and G. Chen, *Guangpu Shiyanshi* 2003, **20**, 781–786.
468. J. Manzoori, M. Amjadi and J. Hassanzadeh, *Microchimica Acta*, 2011, **175**, 47–54.
469. L. Wang, B. Ling, H. Chen, A. Liang, B. Qian and J. Fu, *Luminescence*, 2010, **25**, 431–435.
470. C. Fan and Y. Huang, *Xinan Shifan Daxue Xuebao, Ziran Kexueban*, 2005, **30**, 104–107.
471. Y. Wei, Z. J. Zhang, Y. T. Zhang and Y. H. Sun, *Journal of Chromatography B*, 2007, **854**, 239–244.
472. S. Fan, L. Zhang, Z. Wu and J. Lin, *Fenxi Shiyanshi*, 2003, **22**, 48–50.
473. Z. Wu, G. Li, J. Wang, K. Liu, X. Liu and S. Fan, *Huaxue Yanjiu*, 2005, **16**, 87–89.
474. S. He and C. Li, *Zhongguo Xinyao Zazhi* 2006, **15**, 1862–1864.
475. W. Chang, B. Zhang, N. Lu and Y. Ci, *Fenxi Shiyanshi* 1995, **14**, 1–5.
476. S. W. Lewis, P. S. Francis, K. F. Lim, G. E. Jenkins and X. D. Wang, *Analyst*, 2000, **125**, 1869–1874.
477. C. E. Lenehan, N. W. Barnett and S. W. Lewis, *Journal of Automated Methods and Management in Chemistry*, 2002, **24**, 99–103.
478. J. A. Gunn, C. Shelley, S. W. Lewis, T. Toop and M. Archer, *Journal of Analytical Toxicology*, 2006, **30**, 519–523.
479. J. W. Costin, S. W. Lewis, S. D. Purcell, L. R. Waddell, P. S. Francis and N. W. Barnett, *Analytica Chimica Acta*, 2007, **597**, 19–23.
480. A. Campiglio, *Analyst* 1998, **123**, 1053–1056.
481. N. N. Wang, Y. Q. Shao, Y. H. Tang, H. P. Yin and X. Z. Wu, *Luminescence*, 2009, **24**, 178–182.
482. S. A. Al-Tamrah and A. Townshend, *Analytica Chimica Acta*, 1987, **202**, 247–250.
483. K. M. Agg, G. D. Marshall, J. L. Adcock, N. W. Barnett and P. S. Francis, *Analytica Chimica Acta*, 2007, **600**, 136–141.
484. D. W. Percy, J. L. Adcock, X. A. Conlan, N. W. Barnett, M. E. Gange, L. K. Noonan, L. C. Henderson and P. S. Francis, *Talanta*, 2010, **80**, 2191–2195.
485. Y. He, J. Du, M. Feng and J. Lu, *Shaanxi Shifan Daxue Xuebao, Ziran Kexueban*, 1999, **27**, 76–78.
486. L. Wang, *Chem. Anal. (Warsaw)* 2006, **51**, 211–219.
487. W. Cao, J. He, Y. C. Xia, S. Z. Juang and G. Z. Q. Fei, *Luminescence*, 2005, **20**, 238–242.
488. H. Zhang, J. Lue, Y. He and J. Du, *Huaxue Xuebao*, 2005, 210–214.
489. L. Li, X. Chen and H. Sun, *Shanghai Huanjing Kexue*, 2005, **24**, 266–267, 270.
490. Y. Li, C. Zhu and L. Wang, *Anhui Shifan Daxue Xuebao, Ziran Kexueban*, 2001, **24**, 47–48, 56.
491. J. W. Costin, P. S. Francis and S. W. Lewis, *Analytica Chimica Acta*, 2003, **480**, 67–77.
492. N. W. Barnett, B. J. Hindson and S. W. Lewis, *Analytica Chimica Acta*, 1998, **362**, 131–139.
493. C. Yu and B. Liu, *Fangzhi Gaoxiao Jichu Kexue Xuebao*, 2005, **18**, 371–373.
494. W. Liu and Y. Huang, *Xinan Shifan Daxue Xuebao, Ziran Kexueban* 2004, **29**, 415–418.
495. Y. F. Mestre, L. L. Zamora and J. M. Calatayud, *Journal of AOAC International*, 2001, **84**, 13–18.
496. C. Xie and H. Li, *Guangpuxue Yu Guangpu Fenxi* 2004, **24**, 1521–1523.
497. J. Dolejšová, M. Polášek, P. Solich and R. Karliček, *Folia Pharmaceutica Universitatis Carolinae*, 2006, **33**, 67–75.
498. S. Fan, L. Zhang, Y. Wei and J. Lin, *Sepu (Sociedad Española de Precios Únicos)* 2006, **24**, 148–151.
499. Y. Xue, Y. He, M. Feng and J. Lu, *Fenxi Huaxue*, 1999, **27**, 427–429.
500. W. Liu, J. Du and J. Lu, *Fenxi Shiyanshi*, 2004, **23**, 41–43.
501. K. L. Marques, J. L. M. Santos and J. L. F. C. Lima, *Journal of Pharmaceutical and Biomedical Analysis*, 2005, **39**, 886–891.
502. L. Li, M. Yang, M. Feng and J. Lü, *Fenxi Huaxue*, 1998, **26**, 307–309.

503. L. Li, Y. Wu and M. Feng, *Huanjing Yu Jiankang Zazhi*, 2002, **19**, 334-335.
504. C. Xie, H. Li and C. Liu, *Huaxue Yanjiu*, 2004, **15**, 53-55.
505. H. Zhuang, G. Chen and J. Huang, *Faguang Xuebao*, 1999, **20**, 358-362.
506. J. Dolejšová, M. Polášek, P. Solich, R. Karlíček and L. Tůmová, *Czech and Slovak Pharmacy*, 2004, **53**, 145-150.
507. N. W. Barnett, B. J. Hindson and S. W. Lewis, *Analytica Chimica Acta*, 1999, **384**, 151-158.
508. L. Li, M. Yang, Z. Zhang and J. Lu, *Zhongguo Yiyao Gongye Zazhi* 2004, **35**, 425-426.
509. Y. Fuster Mestre, L. Lahuerta Zamora and J. Martínez Calatayud, *Analytica Chimica Acta*, 1999, **394**, 159-163.
510. Y. He, Z. Wang and J. Liu, *Fenxi Shiyanshi*, 2001, **20**, 70-72.
511. C. Xie and H. Li, *Fenxi Shiyanshi*, 2004, **23**, 61-62.
512. E. J. Llorent-Martínez, P. Ortega-Barrales and A. Molina-Díaz, *Analytica Chimica Acta*, 2006, **580**, 149-154.
513. Y. T. Lee and C. Whang, *Journal of Chromatography A*, 1997, **771**, 379-384.
514. Z. Li, M. Feng, J. Lu, Z. Gong and H. Jiang, *Analytical Letter* 1997, **30**, 797-807.
515. S. Zhang, Y. Wu and H. Li, *Fenxi Huaxue* 2001, **29**, 150-153.
516. H. Wei, E. Liu, R. Ren, X. Zhao, X. Li and F. Jiang, *Guangpuxue Yu Guangpu Fenxi* 2005, **5**, pp. 844-847.
517. A. Wasieleczuk, M. C. Icardo, J. V. García Mateo and J. M. Calatayud, *Analytical Letters*, 2004, **37**, 3205-3218.
518. M. Ciborowski, M. C. Icardo, J. V. G. Mateo and J. Martínez Calatayud, *Journal of Pharmaceutical and Biomedical Analysis*, 2004, **36**, 693-700.
519. A. Kojlo, J. Michalowski and E. Wolyniec, *Journal of Pharmaceutical and Biomedical Analysis*, 2000, **22**, 85-91.
520. L. P. Palilis and A. C. Calokerinos, *Analytica Chimica Acta*, 2000, **413**, 175-186.
521. H. Chen, L. Li, M. Zhou and Y. J. Ma, *Chinese Chemical Letters*, 2008, **19**, 203-206.
522. M. Yang, L. Li, M. Feng and J. Lu, *Shaanxi Shifan Daxue Xuebao, Ziran Kexueban*, 1997, **25**, 61-63.
523. H. Liu, Y. Hao, J. Ren, P. He and Y. Fang, *Luminescence*, 2007, **22**, 302-308.
524. L. Li, M. Yang, M. Feng and J. Lu, *Shaanxi Shifan Daxue Xuebao, Ziran Kexueban* 1997, **25**, 67-69.
525. C. Zhu, Y. Li and L. Wang, *Fenxi Shiyanshi* 2001, **20**, 4-6.
526. Y. He and Z. Wang, *Fenxi Shiyanshi* 2002, **21**, 70-72.
527. Z. Li, M. Feng and J. Lu, *Microchemical Journal*, 1998, **59**, 278-283.
528. M. Timotheou-Potamia and A. C. Calokerinos, *Talanta*, 2007, **71**, 208-212.
529. Y. Li and J. Lu, *Analytica Chimica Acta*, 2006, **577**, 107-110.
530. Y. He and J. Lu, *Fenxi Shiyanshi*, 2003, **22**, 67-69.
531. Z. Zhang, H. Cui and M. Shi, *The Journal of Physical Chemistry*, 2006, **8**, 1017-1021.
532. Z. He, X. Liu, Q. Luo, H. Tang, X. Yu, H. Chen and Y. Zeng, *Microchemical Journal*, 1996, **53**, 356-360.
533. N. Omi, M. Ishii, Y. Kato and M. Yamada, *Tetsu to Hagane*, 2003, **89**, 102-107.
534. Q. Gao, S. Fan and Z. Zhang, *Shipin Kexue (Beijing, China)* 2002, **23**, 135-136.
535. W. Li, R. Lin, X. Wang, Y. Lu, Y. Chen and S. Fan, *Henan Shifan Daxue Xuebao, Ziran Kexueban*, 2004, **32**, 65-68.
536. J. Tian, Y. Hu and J. Zhang, *Journal of Environmental Sciences*, 2008, **20**, 252-256.
537. Y. He and J. Lu, *Fenxi Huaxue*, 2002, **30**, 598-600.
538. M. Yamada, T. Nakada and S. Suzuki, *Analytica Chimica Acta*, 1983, **147**, 401-404.
539. S. A. Al-Tamrah, A. Townshend and A. R. Wheatley, *Analyst*, 1987, **112**, 883-886.
540. P. Qu, B. Li and Z. Zhang, *Fenxi Shiyanshi*, 2004, **23**, 19-21.
541. S. Satienperakul, P. Phongdong and S. Liawruangrath, *Food Chemistry*, 2010, **121**, 893-898.
542. F. X. Meixner and W. Jaeschke, *Anal Application of Bioluminescence and Chemiluminescence(Proc Int Symp)* 1979, **3**, 258-271.
543. F. X. Meixner, *Atmospheric Trace Const., (Proceeding Two-Annual Colloquium)*, 1982, **5th** 53-63.
544. K. Takeuchi and T. Ibusuki, *Kogai* 1986, **21**, 177-186.
545. X. Li, H. Qiang, X. Wang, S. Chen and H. Zhao, *Guangpuxue Yu Guangpu Fenxi*, 2004, **24**, 1518-1520.
546. M. Yang, L. Li, J. Lu and Z. Zhang, *Fenxi Huaxue* 2001, **29**, 410-412.
547. I. M. Psarellis, N. T. Deftereos, E. G. Sarantonis and A. C. Calokerinos, *Analytica Chimica Acta*, 1994, **294**, 27-34.
548. A. Waseem, M. Yaqoob and A. Nabi, *Luminescence*, 2007, **22**, 349-354.
549. H. W. Sun, L. Q. Li and X. Y. Chen, *Analytical and Bioanalytical Chemistry*, 2006, **384**, 1314-1319.
550. Z. Zhang, X. Li, X. Wang, S. Chen, B. Song and H. Zhao, *Journal of Rare Earths*, 2006, **24**, 285-288.
551. L. Yi, H. Zhao, S. Chen, L. Jin, D. Zheng and Z. Wu, *Talanta*, 2003, **61**, 403-409.

552. Y. Li and J. Lu, *Luminescence*, 2007, **22**, 326-330.
553. Y. Zhuang, X. Cai, J. Yu and H. Ju, *Journal of Photochemistry and Photobiology A: Chemistry*, 2004, **162**, 457-462.
554. Y. Zhuang, S. Zhang, J. Yu and H. Ju, *Analytical and Bioanalytical Chemistry*, 2003, **375**, 281-286.
555. X. Xiong, Y. Tang, N. Wang and S. Wu, *Fenxi Shiyanshi* 2007, **26**, 80-83.
556. X. L. Wang, S. L. Chen, H. C. Zhao, L. P. Jin and X. Li, *Analytical Letter*, 2005, **38**, 971-979.
557. B. Li, Z. Zhang and L. Zhao, *Analytica Chimica Acta*, 2002, **468**, 65-70.
558. L. Li, Y. Wu, M. Feng and J. Lu, *Fenxi Huaxue*, 2002, **30**, 169-171.
559. M. Yang, L. Li, J. Lu and Z. Zhang, *Zhongguo Yiyao Gongye Zazhi* 2002, **33**, 85-87.
560. L. Li, M. Yang, M. Feng and J. Lu, *Fenxi Shiyanshi* 1997, **16**, 33-35.
561. L. Li, Y. Zhou, X. Tao, M. Feng and J. Lü, *Fenxi Huaxue* 1999, **27**, 1333-1336.
562. Y. Sun, Y. Zhang and Z. Zhang, *Fenxi Ceshi Xuebao* 2006, **25**, 87-89.
563. L. Li, F. Nie, M. Feng and J. Lu, *Shaanxi Shifan Daxue Xuebao, Ziran Kexueban*, 1999, **27**, 73-75.
564. G. H. Wan, H. Cui, H. S. Zheng, J. Zhou, L. J. Liu and X. F. Yu, *Journal of Chromatography B*, 2005, **824**, 57-64.
565. L. Li, M. Yang, M. Feng and J. Lu, *Fenxi Huaxue* 1997, **25**, 1321-1323.
566. L. Li, Y. Zhou, M. Feng and J. Lu, *Shandong Daxue Xuebao, Lixueban* 2002, **37**, 78-79 (83).
567. L. Li, X. Wang, Z. Liu, H. Shi and H. Sun, *Zhongguo Yiyao Gongye Zazhi* 2005, **36**, 638-639.
568. L. Li, M. Yang, M. Feng and J. Lu, *Fenxi Shiyanshi*, 1998, **17**, 5-8.
569. X. Zhu, Y. He, M. Liu, J. Du and J. Lu, *Fenxi Huaxue*, 2004, **32**, 752-754.
570. Y. H. Li and J. R. Lu, *Fenxi Huaxue* 2007, **35**, 743-746.
571. Y. H. He, J. R. Lu, H. G. Zhang and J. X. Du, *Gaodeng Xuexiao Huaxue Xuebao* 2005, **26**, 642-646.
572. F. Nie, X. H. Zhu, Y. H. He and J. R. Lu, *Shaanxi Shifan Daxue Xuebao, Ziran Kexueban* 2004, **32**, 75-77.
573. H. Yang, C. Zhang and C. Hong, *Lihua Jianyan, Huaxue Fence* 2006, **42**, 526-528 530.
574. A. I. Vogel and J. Mendham, *Vogel's textbook of quantitative chemical analysis*, Hardback edn., Prentice Hall, 2000.
575. G. A. Ahmed, A. Fawzy and R. M. Hassan, *Carbohydrate Research*, 2007, **342**, 1382-1386.
576. B. Tonomura, H. Nakatani, M. Ohnishi, J. Yamaguchi-Ito and K. Hiromi, *Analytical Biochemistry*, 1978, **84**, 370-383.
577. H. Kunze, H. Ritschel, H. R. Weigt and G. Junghähnel, *Zeitschrift fur Chemie*, 1983, **23**, 224-225.
578. R. M. Lilley, X. Wang, E. Krausz and T. J. Andrews, 2003, **278**, 16488-16493.
579. A. A. Alwarthan and F. A. Aly, *Talanta*, 1998, **45**, 1131-1138.
580. K. A. Kovács, P. Gróf, L. Burai and M. Riedel, *The Journal of Physical Chemistry A*, 2004, **108**, 11026-11031.
581. J. W. Ladbury and C. F. Cullis, *Chemical Reviews*, 1958, **58**, 403-438.
582. R. Macey and G. Oster, *Berkeley Madonna - Modelling and Analysis of Dynamic System*, Accessed 10/01, 2009.
583. M. Tothova, A. Nagy and L. Treindl, *Chemical Physics Letter*, 1998, 243 - 246.
584. E. Wolyniec, J. Karpinska, S. Losiewska, M. Turkowicz, J. Klimczuk and A. Kojlo, *Talanta*, 2012, **96**, 223-229.
585. H. W. Wu, M. L. Chen, D. Shou and Y. Zhu, *Chinese Chemical Letters*, 2012, **23**, 839-842.
586. J. M. Terry, S. Mohr, P. R. Fielden, N. J. Goddard, N. W. Barnett, D. C. Olson, D. K. Wolcott and P. S. Francis, *Analytical and Bioanalytical Chemistry*, 2012, **403**, 2353-2360.
587. P. S. Francis, C. M. Hindson, J. M. Terry, Z. M. Smith, T. Slezak, J. L. Adcock, B. L. Fox and N. W. Barnett, *Analyst* 2011, **136**, 64-66.
588. S. Kanwal, Q. Ma, W. Dou, G. Wang and X. Su, *International Journal of Environmental Analytical Chemistry*, 2012, **92**, 210-221.
589. Y. C. Chen and W. Y. Lin, *Luminescence*, 2010, **25**, 43-49.